

Alexander García Mariaca

Carbon capture and storage in heavy-duty internal combustion engine vehicles: energy and techno-economic assessment

Director/es

Llera Sastresa, Eva María

<http://zaguan.unizar.es/collection/Tesis>



Universidad de Zaragoza
Servicio de Publicaciones

ISSN 2254-7606

Tesis Doctoral

**CARBON CAPTURE AND STORAGE IN HEAVY-
DUTY INTERNAL COMBUSTION ENGINE
VEHICLES: ENERGY AND TECHNO-ECONOMIC
ASSESSMENT**

Autor

Alexander García Mariaca

Director/es

Llera Sastresa, Eva María

UNIVERSIDAD DE ZARAGOZA
Escuela de Doctorado

Programa de Doctorado en Energías Renovables y Eficiencia Energética

2024



Universidad
Zaragoza

Tesis Doctoral

CARBON CAPTURE AND STORAGE IN HEAVY-DUTY INTERNAL COMBUSTION ENGINE VEHICLES: ENERGY AND TECHNO-ECONOMIC ASSESSMENT

Autor

Alexander García Mariaca

Directora

Eva María Llera Sastresa

UNIVERSIDAD DE ZARAGOZA

Escuela de Ingeniería y Arquitectura

2024

Repositorio de la Universidad de Zaragoza – Zaguan <http://zaguan.unizar.es>

COMPENDIO DE PUBLICACIONES

La presente tesis ha sido elaborada como un compendio de publicaciones en diversas revistas científicas y conferencias académicas, que se listan a continuación:

1. García-Mariaca A, Llera Sastresa Eva. (2024). Techno-economic assessment for the practicability of on-board CO₂ capture in ICE vehicles. *Applied energy*, 376, Part B, 124167. <https://doi.org/10.1016/j.apenergy.2024.124167>
2. García-Mariaca, A., Llera-Sastresa, E., & Moreno, F. (2024). CO₂ capture feasibility by Temperature Swing Adsorption in heavy-duty engines from an energy perspective. *Energy*, 292, 130511. <https://doi.org/10.1016/j.energy.2024.130511>
3. García-Mariaca, A., & Llera-Sastresa, E. (2023). Energy and economic analysis feasibility of CO₂ capture on a natural gas internal combustion engine. *Greenhouse Gases: Science and Technology*, 13(2), 144-159. <https://doi.org/10.1002/ghg.2176>
4. García-Mariaca, A., Llera-Sastresa, E., & Moreno, F. (2022). Application of ORC to reduce the energy penalty of carbon capture in non-stationary ICE. *Energy Conversion and Management*, 268, 116029. <https://doi.org/10.1016/j.enconman.2022.116029>
5. García Mariaca, Alexander and Llera, Eva, (2022) Dynamic CO₂ Capture in a Natural Gas Engine Used in Road Freight Transport. Proceedings of the 16th Greenhouse Gas Control Technologies Conference (GHGT-16) 23-24 Oct 2022, <http://dx.doi.org/10.2139/ssrn.4272013>
6. García-Mariaca, A. Llera-Sastresa, (2021) E. Review on Carbon Capture in ICE Driven Transport. *Energies* (2021), 14, 6865. <https://doi.org/10.3390/en14216865>

AGRADECIMIENTOS

En la realización de esta tesis han intervenido de manera directa e indirecta muchas personas e instituciones, cuyo valioso aporte hizo posible su culminación. Por tanto, deseo expresar mis más sinceros agradecimientos a cada uno de ellos:

A mi directora, Eva María Llera Sastresa, por abrirme las puertas para continuar con mis estudios. Su asesoramiento, dedicación, sabiduría y apoyo incondicional me han permitido alcanzar logros que antes creía inalcanzables. Además, su calidad humana me ha permitido disfrutar de este viaje desde el inicio.

A Francisco Moreno, cuyos aportes y conocimientos hicieron posible el desarrollo de esta tesis. A los miembros del grupo de investigación Energía y CO₂, por sus asesoramientos, ayuda, apoyo y amistad brindada durante la realización de esta tesis. A Santiago y José Luis que sin su ayuda no hubiese sido posible iniciar mi doctorado.

Al programa de estudios de doctorado para Iberoamericanos Universidad de Zaragoza - Santander por financiar mis primeros dos años de doctorado. Asimismo, agradezco al Ministerio de Ciencia y Tecnología de Colombia por la financiación final de mis estudios de doctorado.

A mi esposa, Laura Irene Cortes Piraquive, la responsable de que este viaje haya sido posible en el extranjero. Con su amor, apoyo, paciencia y ayuda en todos los aspectos de la vida, me permite cada día cumplir mis metas y objetivos. Su constante ánimo y dedicación han sido fundamentales en este camino.

A mi madre, Edilma Mariaca Herrera, por darme la vida, por inculcarme el estudio como camino de vida y por todo el amor que siempre me ha brindado. A mis hermanos, Nana, Mijohn y Henner, por su amor y apoyo, y a mis sobrines, Mona, Pipe, Pancho, Flaco y Criito, por su alegría y cariño.

Por último, al ser más importante de mi vida **Nicolas Antonio García Cortes** por ser la fuerza y mi razón de vivir ¡Te amo hasta el infinito por infinito!

ABSTRACT

The freight and passenger road transport will have to continue using combustion-based technologies in the medium and long term since electrification is still far from being a reality in this sector. Using onboard CO₂ capture and storage (CCS) systems could be a feasible option to reduce CO₂ emissions generated by this sector. Furthermore, if the captured CO₂ is used as raw material for producing synthetic fuels, the industry sector can use these again, thus reducing dependence on fossil fuels and generating added value to CO₂. However, CO₂ capture and storage in mobile sources currently present several challenges. Among them are the high energy consumption of traditional CCS systems, the limited space to install an onboard CCS system into a vehicle, and the difficulty that the CCS system would have in adapting to the various operating conditions of internal combustion engines (ICE).

Based on the above, the first part of this thesis consisted of identifying the CO₂ capture technique that best adapts to the operating characteristics of a heavy-duty internal combustion vehicle (HD-ICEV). As a result of the review of publications and patents, it was determined that post-combustion CO₂ capture techniques are the most suitable; in this way, the engine is not modified and, therefore, does not affect its operating conditions. Specifically, the most appropriate techniques are temperature swing adsorption (TSA) and amine-scrubbing absorption. The advantage of these techniques is that both can use the waste heat contained in the exhaust gases in their processes. Furthermore, an energy balance on typical engines used in freight and passenger road transport shows that the waste heat contained in the exhaust gases (EG) can be used for CO₂ desorption and by producing mechanical energy by integrating some additional system. This would allow partial or total coverage of the energy needs of the CCS system.

This thesis opts to hybridize the CCS system with an organic Rankine cycle (ORC) to take advantage of the waste heat contained in the EG. This decision is based on the level of development of this technology and the ability of the ORC to adapt to the different operating conditions of an ICE. The following steps in this thesis were to select natural gas HD-ICEs (to use the methane produced from the captured CO₂) that operate in vehicles used for freight and passenger road transport. These HD-ICE were simulated using the AVL software. The simulations were conducted under four engine loads and in the entire rpm range of each engine, obtaining the temperature, pressure, and composition of the EG for each established condition. Subsequently, the inlet pressures of each ORC device were determined based on the inlet pressure calculation in the expander. This process yielded the required mass flows of the working fluid and cooling air, as well as the thermal efficiency of the ORC, which reached maximum values of 12.5% in both engines. The results also indicate that the ORC can supply the CCS

system, which operates using TSA, with up to 60% of the power needed operating at a carbon capture rate (CCR) of 90% and an engine load of 25%.

Once it was established that the ORC avoids excessive penalties over the ICE due to the operation of the CCS system, a comprehensive energy assessment of the CCS-ORC system using three different sorbents (PPN-6-CH₂-DETA, MOF-74-Mg, and active carbon) was performed. This energy evaluation is carried out at 70 and 100% CCR. Furthermore, this analysis made it possible to determine the areas of the heat exchangers that make up the CCS-ORC system, which facilitates the sizing of the system and the estimation of the space necessary for its installation in the vehicles selected for the study. The results show a penalty in engine power induced by the CCS-ORC system between 1.9% with MOF-74-Mg and 23.5% with activated carbon at 100% CCR, translating into a maximum increase of 6.14% in engine fuel consumption to cover this penalisation. Finally, the maximum energy consumption of the CO₂ capture process is 631 kJ/kgCO₂, 10% lower than that reported in the literature for TSA.

After completing the energy analysis and equipment sizing, the techno-economic evaluation of the proposed CCS-ORC system is conducted. For this evaluation, the TSA device is designed, and the capital and operational expenditures are estimated, as well as the net present value and the cost of CO₂ abatement (CAC). In addition, a sensitivity analysis is carried out to determine the size of the engine necessary so that the return on investment is achieved within the vehicle lifespan, and it is evaluated what the CO₂ tax should be so that the integration of the CCS-ORC system is profitable in the same period. The CAC obtained for the CCS-ORC system is less than €35/tCO₂ at 100% CCR. Additionally, with engines of displacement volume greater than 18 and 21 L, the CAC of the CCS-ORC system is zero at 100% and 70% CCR, respectively. It was also determined that a CO₂ emission tax greater than €71/tCO₂ allows the initial investment of the CCS-ORC system payback within the lifespan of the HD-ICEV for all sorbents evaluated at 100% CCR.

In the last part of this research and to cover the two most promising CO₂ capture techniques for the transportation sector, the CCS-ORC system was designed using the absorption technique, specifically amine-scrubbing. For this study, an energy and economic evaluation of a CCS-ORC system similar to those previously developed was conducted. This analysis is carried out by comparing the performance of a primary and a tertiary amine. The results show that the CCS-ORC system operating with the primary amine at 30 wt% achieved a maximum CO₂ capture rate of 66%, with a penalty on engine power of only 10%. On the other hand, the economic analysis revealed that the CCS system with the primary amine and without ORC is 31.8% cheaper than a hydrogen fuel cell bus and 26% cheaper than a battery electric bus. Finally, it was determined that tertiary amines present poor performance results due to their low reaction rate.

According to the results of the two techniques studied to capture CO₂ in HD-ICEV, temperature swing adsorption requires less thermal energy for CO₂ desorption than amine-scrubbing. Therefore, the ORC has more waste heat from the exhaust gases with temperature swing adsorption than with amine-scrubbing, thus producing more mechanical energy to supply the CCS system energy demand. This allows higher CO₂ capture rates to be achieved with adsorption than with amine scrubbing for the same penalty on the engine. The results also show that the CCS-ORC system can operate under the different operating conditions of an ICE without a significant penalty. In addition, the CO₂ abatement cost obtained by integrating the CCS-ORC system in a heavy vehicle is lower than that of other CCS system applications. These promising results suggest that, with further development and research in this area, CO₂ capture is a strategy that should be implemented, thus contributing to the decarbonization of this energy-intensive sector.

RESUMEN

El transporte por carretera de mercancías y viajeros tendrá que seguir utilizando tecnologías basadas en la combustión a medio y largo plazo, ya que la electrificación aún está lejos de ser una realidad en este sector. El uso de sistemas de captura y almacenamiento de CO_2 (CAC) a bordo podría ser una opción viable para reducir las emisiones de CO_2 generadas por este sector. Además, si el CO_2 capturado se utiliza como materia prima para producir combustibles sintéticos, la industria podrá volver a utilizarlos, reduciendo así la dependencia de los combustibles fósiles y generando valor añadido al CO_2 . Sin embargo, la captura y almacenamiento de CO_2 en fuentes móviles presenta actualmente varios desafíos. Entre ellos se encuentran el alto consumo de energía de los sistemas CAC tradicionales, el espacio limitado para instalar un sistema CAC a bordo en un vehículo y la dificultad que tendría el sistema CAC para adaptarse a las diversas condiciones de funcionamiento de los motores de combustión interna.

Con base en lo anterior, la primera parte de esta tesis consistió en identificar la técnica de captura de CO_2 que mejor se adapta a las características de funcionamiento de un vehículo pesado con motor de combustión interna. Como resultado de la revisión de publicaciones y patentes se determinó que las técnicas de captura de CO_2 en postcombustión son las más adecuadas, de esta forma no se modifica el motor de combustión interna y por tanto no afecta las condiciones de operación de este. En concreto, las técnicas más apropiadas son la adsorción por oscilación de temperatura y la absorción por lavado de aminas. La ventaja de estas técnicas es que ambas pueden utilizar el calor residual contenido en los gases de escape en sus procesos. Además, un balance de energía hecho en motores típicos usados en el transporte de mercancías y pasajeros muestra que el calor residual contenido en los gases de escape puede ser utilizado para la desorción de CO_2 y para la producción de energía mecánica por medio de la integración de algún sistema adicional. Esto permitiría cubrir parcial o totalmente las necesidades energéticas del sistema de CAC.

Esta tesis opta por hibridar el sistema CAC con un ciclo orgánico Rankine (COR) para aprovechar el calor residual contenido en los gases de escape. Esta decisión se basa en el nivel de desarrollo de esta tecnología y la capacidad del COR para adaptarse a las diferentes condiciones de operación de un motor de combustión interna. Los siguientes pasos de esta tesis fueron seleccionar motores de gas natural (para utilizar el metano producido a partir del CO_2 capturado) que operen en vehículos utilizados para el transporte por carretera de mercancías y pasajeros. Estos motores fueron simulados utilizando el software AVL. Las simulaciones se realizaron bajo cuatro cargas de motor y en todo el rango de rpm de cada motor, obteniendo la temperatura, presión y composición de los gases de escape para cada condición establecida. Posteriormente, las presiones de entrada de cada dispositivo del COR se determinaron con base en el cálculo de la presión de entrada en el expansor. Este proceso proporcionó los caudales máxicos

requeridos de fluido de trabajo y aire de refrigeración, así como la eficiencia térmica del COR, que alcanzó valores máximos del 12.5% en ambos motores. Los resultados también indican que el COR puede suministrar al sistema CAC, que funciona mediante adsorción por oscilación de temperatura, hasta el 60% de la potencia necesaria para una tasa de captura de CO₂ del 90% con una carga en el motor del 25%.

Una vez que se estableció que el COR evita penalizaciones excesivas sobre el motor de combustión interna debido a la operación del sistema CAC se realizó una evaluación energética integral del sistema CAC-COR utilizando tres sorbentes diferentes (PPN-6-CH₂-DETA, MOF-74-Mg, y carbón activo). Esta evaluación energética se realiza al 70 y 100% de tasa de captura de CO₂. Además, este análisis permitió determinar las áreas de los intercambiadores de calor que componen el sistema CAC-COR, lo que facilita el dimensionamiento del sistema y la estimación del espacio necesario para su instalación en los vehículos seleccionados para el estudio. Los resultados muestran una penalización en la potencia del motor inducida por el sistema CAC-COR entre un 1.9% con MOF-74-Mg y un 23.5% con carbón activado al 100% de tasa de captura de CO₂, lo que se traduce en un aumento máximo del 6.14% en el consumo de combustible del motor para cubrir esta penalización. Finalmente, el consumo máximo de energía del proceso de captura de CO₂ es de 631 kJ/kgCO₂, un 10% menor que lo reportado en la literatura para adsorción por oscilación de temperatura.

Luego de realizar el análisis energético y el dimensionamiento de los equipos, se realiza la evaluación tecno-económica del sistema CAC-COR propuesto. Para esta evaluación se diseña el dispositivo adsorción por oscilación de temperatura y se estiman los costes de inversión y operación, así como el valor presente neto y el costo de abatimiento de CO₂. Además, se realiza un análisis de sensibilidad para determinar el tamaño del motor necesario para que el retorno de la inversión se logre dentro de la vida útil del vehículo, y se evalúa cuál debe ser el impuesto al CO₂ para que la integración del sistema CAC-COR sea rentable en el mismo período de tiempo. El costo de abatimiento de CO₂ obtenido para el sistema CAC-COR es inferior a 35 €/tCO₂ al 100% de tasa de captura de CO₂. Además, con motores de volumen de desplazamiento superior a 18 y 21 L, el costo de abatimiento de CO₂ del sistema CAC-COR es cero al 100% y 70% de tasa de captura de CO₂, respectivamente. También se determinó que un impuesto a las emisiones de CO₂ superior a 71 €/tCO₂ permite recuperar la inversión inicial del sistema CAC-COR dentro de la vida útil del vehículo de trabajo pesado para todos los sorbentes evaluados al 100% de tasa de captura de CO₂.

En la última parte de esta investigación y para cubrir las dos técnicas de captura de CO₂ más prometedoras para el sector del transporte, se diseñó el sistema CAC-COR utilizando la técnica de absorción, específicamente el lavado de aminas. Para este estudio se realizó una evaluación energética y económica de un sistema CAC-COR similar a los desarrollados previamente. Este análisis se lleva a cabo comparando el rendimiento de una amina primaria y una terciaria. Los

resultados muestran que el sistema CAC-ORC operando con la amina primaria al 30% en peso logró una tasa de captura de CO₂ máxima del 66%, con una penalización en la potencia del motor de solo el 10%. Por otro lado, el análisis económico reveló que el sistema CAC con la amina primaria y sin COR es un 31.8% más barato que un autobús de pila de combustible de hidrógeno y un 26% más barato que un autobús eléctrico de batería. Finalmente, se determinó que las aminas terciarias presentan malos resultados de rendimiento debido a su baja velocidad de reacción.

Según los resultados de las dos técnicas estudiadas para capturar CO₂ en vehículos pesados, la adsorción por oscilación de temperatura requiere menos energía térmica para la desorción del CO₂ que el lavado de aminas. Por lo tanto, el ciclo orgánico Rankine tiene más calor residual de los gases de escape con adsorción por oscilación de temperatura que con el lavado de aminas, produciendo así más energía mecánica para suplir la demanda energética del sistema CAC. Esto permite lograr tasas de captura más altas con adsorción que con el lavado de aminas, para una misma penalización sobre el motor. Los resultados también muestran que el sistema CAC-COR es energéticamente capaz de operar bajo las diferentes condiciones de operación de un motor de combustión interna sin una gran penalización. Aunado a esto, el costo de abatimiento de CO₂ obtenido al integrar el sistema CAC-ORC en un vehículo pesado es menor que el de otras aplicaciones de sistemas CAC. Estos resultados prometedores sugieren que, con un mayor desarrollo e investigación en esta área, la captura de CO₂ es una estrategia que debería implementarse, contribuyendo así a la descarbonización de este sector de uso intensivo de energía.

CONTENTS

COMPENDIO DE PUBLICACIONES	i
AGRADECIMIENTOS	ii
ABSTRACT	iii
1. INTRODUCTION, OBJECTIVES AND METHODOLOGY	1
1.1 INTRODUCTION AND JUSTIFICATION	1
1.2 OBJECTIVES AND METHODOLOGY.....	5
2. CARBON CAPTURE ON MOBILE SOURCES	9
2.1 CARBON CAPTURE IN THE MARITIME SECTOR	9
2.2 CARBON CAPTURE ON INTERNAL COMBUSTION ENGINES VEHICLES	11
2.3 CCS-SYSTEM: FIRST ENERGY AND SIZING ASSESSMENT	13
2.3.1 Results	16
2.4 SUMMARY	17
2.5 PUBLISHED PAPER.....	17
3. WASTE HEAT RECOVERY TO MEET THE ENERGY DEMANDS OF A CCS SYSTEM IN AN HD-ICEV.	48
3.1 ENGINE SIMULATIONS.....	49
3.2 ORC DESIGN	51
3.3 CARBON CAPTURE AND STORAGE (CCS) SYSTEM	53
3.4 SIMULATION PROCEDURE	54
3.5 RESULTS	54
3.6 DYNAMIC OPERATION OF THE CCS-ORC SYSTEM	56
3.7 SUMMARY	58
3.8 PUBLISHED PAPERS	58
4. CARBON CAPTURE IN HD-ICEV BY ADSORPTION	79
4.1 CCS-ORC SYSTEM CONFIGURATION AND DESIGN	79
4.1.1 Heat exchangers	81
4.1.2 Sorbent selection	81
4.1.3 CO ₂ compression and storage process	81
4.1.4 Assumptions and procedures in the simulations	81
4.2 RESULTS AND ANALYSIS	82
4.2.1 Heat transfer areas and WF and cooling mass flows	82

4.2.2 Energy analyses	84
4.2.3 Weight and volume of the CCS-ORC system	88
4.3 ANALYSES.....	89
4.4 SUMMARY	90
4.5 PUBLISHED PAPER.....	91
5. SIZING AND TECHNO-ECONOMIC ASSESSMENT OF A CCS-ORC SYSTEM BY ADSORPTION.....	110
5.1 METHODOLOGY	110
5.1.1 Description of CCS-ORC system and assessment conditions.....	110
5.1.2 Heat exchanger sizing.....	110
5.1.3 Design of the TSA device	113
5.1.4 Economic assessment.....	114
5.2 SIZING AND TECHNO-ECONOMIC ASSESSMENT RESULTS	115
5.2.1 Heat exchanger sizing.....	115
5.2.2 TSA device design	116
5.2.3 Tecno-economic assessment.....	117
5.3 SENSITIVITY ANALYSIS	120
5.4 SUMMARY	121
5.5 PUBLISHED PAPER.....	122
6 CARBON CAPTURE IN HD-ICEV BY ABSORPTION	137
6.1 SIMULATION DESCRIPTION OF THE CCS-ORC SYSTEM	137
6.2 ABSORPTION RESULTS.....	139
6.3 ORC AND ENERGY ANALYSIS.....	141
6.4 ECONOMIC ANALYSIS.....	142
6.5 SUMMARY AND COMPARISON	144
6.6 PUBLISHED PAPER.....	145
7 CONCLUSIONS, SCIENTIFIC CONTRIBUTIONS AND FUTURE RESEARCH AND ENDEAVOURS.....	161
7.1 CONCLUSIONS.....	161
7.2 SCIENTIFIC CONTRIBUTIONS.....	164
7.3 FUTURE RESEARCH ENDEAVOURS.....	166
BIBLIOGRAPHY	174
ANNEXES.....	193

List of Figures

Figure 1. Worldwide CO ₂ emission from transport and global electric car sales...	3
Figure 2. Transport sector CO ₂ emissions in 2022 by subsectors and vehicle type.	3
Figure 3. Reboiler heat duty.....	10
Figure 4. Amine-scrubbing CO ₂ capture cost in the maritime sector.	11
Figure 5. CCR values obtained with several sorbents.....	12
Figure 6 Mass and energy chart of the CCS system for its operation into an ICE.	14
Figure 7. Remaining heat, ORC power output, CO ₂ compression power output and maximum CCR obtained in each engine.....	17
Figure 8. Performance curves of the engines at full engine load.	50
Figure 9. Fuel energy distribution obtained in the engines used in the simulations.	50
Figure 10. Behaviour of the exhaust gas temperatures and mass flow at partial engine loads.....	51
Figure 11. ORC system layout proposed.....	52
Figure 12. Total and cooling heat required by the TSA process.	53
Figure 13. ORC behaviour: a) 25% of engine load and b) engine loads above 25%.	54
Figure 14. Air cooling and C ₅ H ₁₀ mass flows obtained from ORC simulations...	55
Figure 15. Permeability behaviour in the entire rpm range and at partial engine loads.....	55
Figure 16. Percentage of parasitic loads covered by the ORC-X under partial engine loads.....	56
Figure 17. Actual torque and speed for the M936G engine.....	56
Figure 18. Power penalisation, fuel mass and CO ₂ mass flow increase in dynamic conditions.	57
Figure 19. Initial and final engine power due to the CCS system operation in the WHTC.....	58
Figure 20. Energy and mass flows and CCS-ORC system configuration.	80
Figure 21. C ₅ H ₁₀ mass flow obtained for the two CCRs in both engines at the entire rpm range and engine loads.	84
Figure 22. Cooling mass flow obtained for the two CCRs in both engines at the entire rpm range and engine loads.	84
Figure 23. Parasitic loads covered by the ORC at 70% of CCR in the F1C engine.	85
Figure 24.Parasitic loads covered by the ORC at 100% of CCR in the F1C engine.	85
Figure 25.Parasitic loads covered by the ORC at 70% of CCR in the M936G engine.....	86
Figure 26. Parasitic loads covered by the ORC at 100% of CCR in the M936G engine.....	86

<i>Figure 27. Power percentage required by the CCS system operating in the M936G engine.....</i>	<i>87</i>
<i>Figure 28. Power percentage required by the CCS system operating in the F1C engine.....</i>	<i>87</i>
<i>Figure 29. Average percentage weight of the components of the CCS-ORS system</i>	<i>89</i>
<i>Figure 30. Energy consumption of the CO₂ capture process obtained for the study cases.....</i>	<i>90</i>
<i>Figure 31. CCS-ORC system schematic layout.</i>	<i>111</i>
<i>Figure 32. Cross-sectional view of TSA device</i>	<i>113</i>
<i>Figure 33. NPV calculated at 10 years of CCS-ORC system for the whole sorbent, CCR and engines.....</i>	<i>120</i>
<i>Figure 34. CCS-ORC system carbon abatement cost calculated for each sorbent, CCR, and engine.....</i>	<i>120</i>
<i>Figure 35. Payback sensitivity analysis: a) 100 CCR and b) 70 CCR</i>	<i>121</i>
<i>Figure 36. CAC sensitivity analysis for engine size</i>	<i>121</i>
<i>Figure 37. layout of the CCS-ORC system with amine-scrubbing.....</i>	<i>139</i>
<i>Figure 38. CCRs for MEA and MDEA over the entire rpm range and at partial engine loads.....</i>	<i>140</i>
<i>Figure 39. Heat duty in stripper and CO₂ mass captured with the amine selected</i>	<i>140</i>
<i>Figure 40. Solvent mass flow and regeneration.</i>	<i>140</i>
<i>Figure 41. Air and working fluid mass flows in the ORC</i>	<i>141</i>
<i>Figure 42. ORC efficiency over the entire engine rpm range and engine load conditions.</i>	<i>142</i>
<i>Figure 43. Percentage of power penalized of the engine by the CCS system with and without ORC.</i>	<i>142</i>
<i>Figure 44. Total and percentage weight of each item included in the CAPEX..</i>	<i>143</i>

List of Tables

Table 1. Engine Technical specifications.	14
Table 2. Sorbent physical properties used in the simulations.	15
Table 3. Available heat in the EG at low, medium, and full engine load and regeneration heat at 90% of CCR for each sorbent	16
Table 4. Power produced by the ORC at low, medium, and full engine loads in each engine.....	16
Table 5. Volume calculations for each sorbent and engine.	17
Table 6. Technical specifications of the study engines	49
Table 7. Parameter values used in the calculation of the inlet pressure to the ORC-X.....	52
Table 8. Equipment conditions in ORC simulations	53
Table 9. Simulation restriction parameters.....	54
Table 10. Heat exchanger areas obtained from ORC simulations.....	55
Table 11. Average percentage penalty of the CCS system over the engines power with and without ORC.....	56
Table 12. Speed variable values taken for actualising the engine speed in the WHTC.....	57
Table 13. Parameters and conditions used in the ORC simulations.	80
Table 14. U for the heat exchangers used in the CCS system.	81
Table 15. ΔT and design conditions of the heat exchangers in the CCS-ORC system simulations	82
Table 16. Heat exchangers areas obtained in the simulations.	83
Table 17. Sorbent mass and volume at 25% of EL and maximum RPM for 30 min of operation of CCS-ORC system.....	88
Table 18. Total and percentage increase of fuel mass in the engines to cover the operation of the CCS-ORC system at 75% of EL, 8 hours of operation and maximum torque.....	90
Table 19. Correlation to obtain the Nusselt number in the shell side.....	111
Table 20. Correlation to obtain the Nusselt number in the annular section. ...	112
Table 21. Sorbent properties and temperature conditions used in the heat transfer mathematical model.	113
Table 22. CAPEX cost correlations and parameters	115
Table 23. OPEX cost correlations and parameters.....	115
Table 24. β , number and length of tubes for the heat exchangers operating in the CCS-ORC system in the M936G engine.....	116
Table 25. β , number and length of tubes for the heat exchangers operating in the CCS-ORC system in the F1C engine.....	116
Table 26. Sizing of the TSA device operating in the CCS-ORC system at 100% of CCR.....	116
Table 27. Sizing of the TSA device operating in the CCS-ORC system at 70% of CCR.....	117

Table 28. CAPEX results of the CCS-ORC system operating in the m936G engine.	117
Table 29. CAPEX results of the CCS-ORC system operating in the F1C engine.	117
Table 30 CAPEX including the initial purchase of the vehicle.....	118
Table 31. OPEX [k€/year] for the CCS-ORC systems	119
Table 32. Incomes and Profits obtained for integrating a CCS-ORC system in a heavy-duty vehicle.	119
Table 33. Thermodynamic conditions of the fluids in the simulations.....	138
Table 34. Amine properties at 313 K and 30wt%.	139
Table 35. Heat exchangers areas obtained in the simulations	141
Table 36. CO ₂ capture equipment installation costs CAPEX.....	143
Table 37. Initial purchase value of a bus	144

NOMENCLATURE

Variable	Units	Description
β_ω	-	Angular velocity ratio
β	m ² /m ³	Area density
BEV	-	Battery Electric Vehicles
B	-	Baffles
CAPEX	€	Capital expenditure
CAC	€	Carbon abatement cost
CCS	-	Carbon Capture and Storage
CCR	%	Carbon Capture rate
C'	m	Clearance between tubes
CNG	-	Compressed natural gas
CI	-	Compression ignition
Z	-	Compressibility factor
h	W/m ² K	Convection heat transfer coefficient
HE-CO ₂ -C	-	CO ₂ cooling heat exchanger
CO ₂ -con	-	CO ₂ condenser
CO ₂ -com	-	CO ₂ compressor
C ₅ H ₁₀	-	Cyclopentane
f	-	Darcy friction factor
ρ	kg/m ³	Density
S_D	m	Diagonal pitch
D	m	Diameter
V_d	m ³	Displacement volume
β_{vol}	-	Displacement volume ratio
μ	Ns/m ²	Dynamic viscosity
EB	-	Electric batteries
η	%	Efficiency
EL	%	Engine load
D_e	m	Equivalent diameter
EU	-	European Union
EG	-	Exhaust gases
HE-EG1	-	Exhaust gas cooling heat exchanger 1
HE-EG2	-	Exhaust gas cooling heat exchanger 2
Fr	-	Froude number
u	m/s	Flow speed
g	m/s ²	Gravity
\dot{Q}	W	Heat
HE	-	Heat exchanger
HD-ICEV	-	Heavy-duty internal combustion engine vehicles
HFCB	-	Hydrogen fuel cell batteries
ICE	-	Internal Combustion Engine
R	J/kgK	Ideal gas constant
ICEV	-	Internal Combustion Engine Vehicle
Ja	-	Jacob number
h_{fg}	J/kg	Latent heat of vaporization
q	-	Loading Capacity
S_L	m	Longitudinal pitch
LHV	J/kg	Lower Heating Value
m	kg	Mass
\dot{m}	kg/s	Mass flow
MDEA	-	Methyldiethanolamine
MEA	-	Monoethanolamine
NPV	€	Net present value
q_s	J/m ²	Nucleate boiling heat
Nu	-	Nusselt number

OPEX	-	Operational Expenditures
ORC-C	-	ORC condenser
ORC-E	-	ORC evaporator
ORC-H	-	ORC heater
ORC-P	-	ORC pump
ORC-X	-	ORC expander
ORC	-	Organic Rankine Cycle
U	W/m ² K	Overall heat coefficient
\dot{W}	W	Parasitic loads
\dot{W}	W	Power
Pr	-	Prandtl number
P	Pa, bar	Pressure
$\dot{Q}_{reg-sorb}$	W	Regeneration sorbent heat
Re	-	Reynolds number
RWA	-	Rotary Wheel Adsorbed
T_{sat}	°C	Saturation temperature
Sc	-	Schmidt number
\dot{Q}_{sen}	W	Sensible heat
ΔH_{des}	J/molCO ₂	Adsorption heat
SI	-	Spark Ignition
c_p	J/kgK	Specific heat
$G_{s,f}$	-	Surface-fluid combination
σ	N/m	Liquid surface tension
TSA	-	Temperature Swing Adsorption
k	W/mK	Thermal conductivity
S_T	m	Transverse pitch
P_t	m	Tube pitch
\bar{X}	%	Vapour mass fraction
V	m ³	Volume
$\beta_{\eta v}$	-	Volumetric efficiency product
WF	-	Working fluid
WHTC	-	World Harmonized Transient Cycle

1. INTRODUCTION, OBJECTIVES AND METHODOLOGY

1.1 INTRODUCTION AND JUSTIFICATION

The International Energy Agency reports a continual rise in energy consumption annually [1]. Regrettably, this uptick correlates with heightened CO₂ emissions released into the atmosphere, primarily stemming from the electricity and heat production sectors (41.4%) and transportation (24.5%) [2]. This increase in CO₂ emissions poses a significant challenge to meeting the European Union's goal of having an economy with zero net greenhouse gas emissions [3], thereby restring global temperature increase to below 2°C established in the Paris Agreement [4].

Addressing this challenge, the European Union (EU) has promoted renewable energies, energy efficiency enhancements, and fuel substitution policies [5]. Despite these efforts, these measures have not been enough to reduce CO₂ from the main energy-intensive sectors [6]. Nonetheless, several technologies are being developed to tackle this problem. One of the most promising is carbon capture and storage (CCS) technologies; these technologies have undergone extensive research in recent years to be used mainly in power plants and other energy-intensive sectors such as iron and glass producers [7–9], which are large CO₂ emitters worldwide. Until 2023, 41 commercial CCS facilities are in operation, with an additional 26 under construction and 325 projects in various stages of

development; collectively, these facilities can capture 1% of total CO₂ emissions by 2023 [10].

CCS technologies are considered to have great potential for reducing CO₂ emissions from energy-intensive sectors [11,12]. The CCS systems allow CO₂ to be separated from a gas stream before or after a combustion process [13]. The most studied CO₂ capture technique used in CCS systems is amine scrubbing [14]. This method has been widely used since the 1930s to clean natural gas during extraction, making it relatively easy to implement for exhaust gases from stationary applications [15]. However, the significant energy penalty associated with amine scrubbing has driven researchers to develop alternative technologies to improve carbon capture rates (CCR), reduce energy penalties, and adapt to various CO₂ emission sources. Notable among these new developments are membranes, which are still in the experimental phase [16], as well as pressure, vacuum and temperature swing adsorption techniques. Many of these CO₂ capture methods have already undergone experimental research in pilot plant applications [17–19].

On the other hand, current technological advancements aimed at reducing CO₂ emissions within the transport sector are primarily centred on four key areas: i) the use of alternative fuels, such as biofuels, compressed natural gas (CNG), liquefied petroleum gas, and H₂ [20,21]; ii) the fuel consumption reduction, through by using eco-driving technologies [22,23]; the reduction of driving resistances [24]; harnessing of waste heat flows through Organic Rankine Cycles (ORC) or Thermo-Electric Generators [25–28], and iii) advancements in electric powertrains that produce zero CO₂ emissions in its operation [29]. The EU has decided to prohibit the sale of internal combustion vehicles (ICEV) in the European Union from 2035 unless they operate on synthetic fuels [30].

Nevertheless, as depicted in Figure 1, worldwide CO₂ emissions from the transport sector continue to rise, reaching 7.98 Gt in 2022, despite the exponential increase in electric car sales [31,32]. Consequently, these technologies have been insufficient to reduce CO₂ emissions from this sector, despite electric vehicles gaining ground between passenger vehicles [33]. However, electrification is still far from reality in heavy-duty internal combustion engine vehicles (HD-ICEV) [34], responsible for 31% of the total CO₂ emission in the transport sector (Figure 2) [35]. This is primarily due to the low energy density and high weight of their batteries, which result in limited ranges in those HD-ICEV [36], joined to the absence of an adequate charging infrastructure [37]. Moreover, significant technical and economic challenges are still associated with recycling battery electric vehicles (BEVs), particularly high-voltage lithium-ion batteries [38] even these batteries not only increase environmental toxicity and cause global warming (due to the material extraction for their manufacture and final disposal of the

batteries) but induce pulmonary and neurological diseases in people involved in the production chain [39].

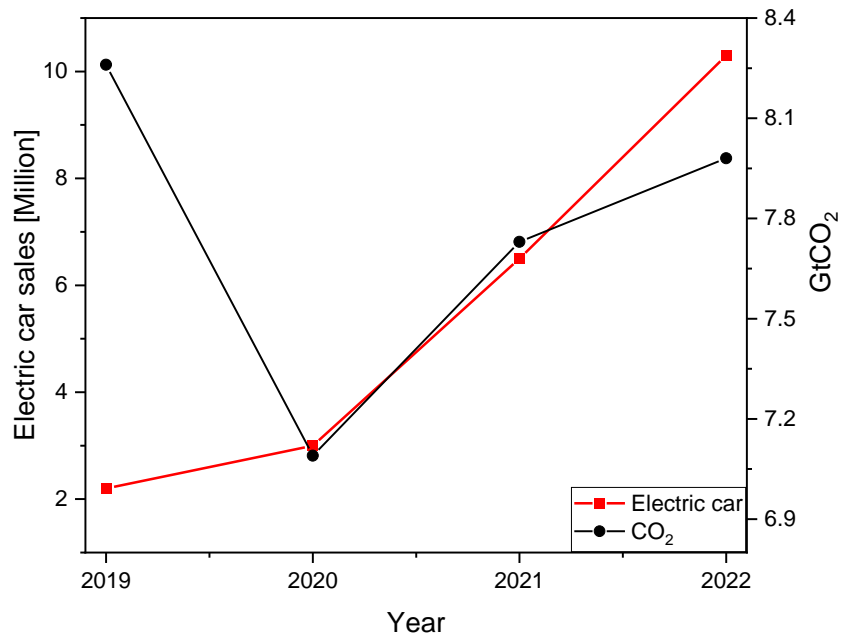


Figure 1. Worldwide CO₂ emission from transport and global electric car sales (source [31,32]).

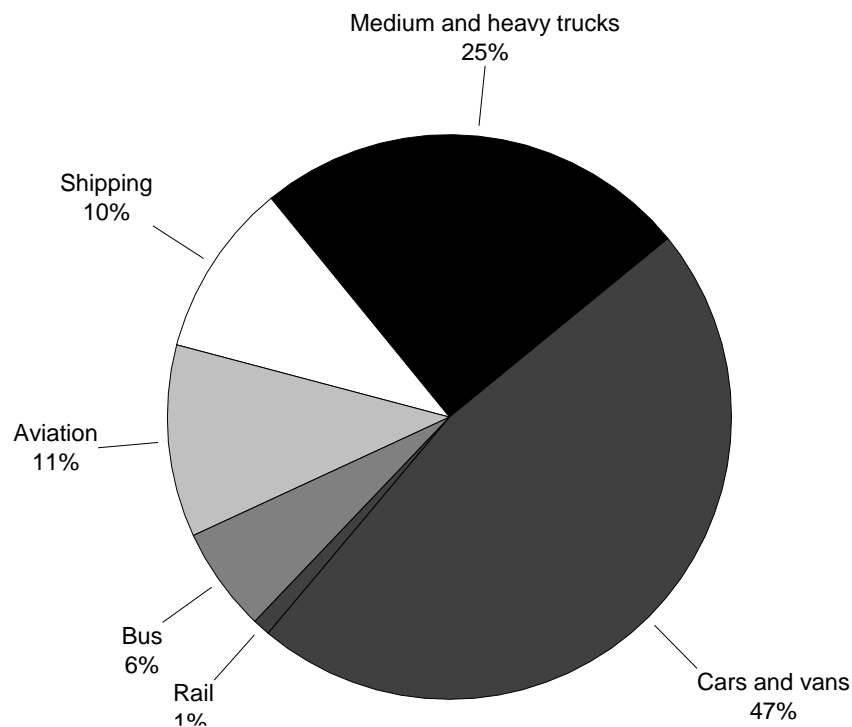


Figure 2. Transport sector CO₂ emissions in 2022 by subsectors and vehicle type. (Adapted from [35]).

Given the preceding insights, the road transport sector of goods and passengers must continue operating with ICE in the medium term [40], and therefore, it must consider integrating alternative technological innovations, such as CCS technologies, in order to achieve a significant CO₂ reduction [41]. However, the integration of these kinds of technologies into an HD-ICEV poses several

challenges for its operation, such as variations of the mass flow and concentration of species in the exhaust gases due to acceleration, decelerations, and vary in the engine load, as well as constraints on available space for hosting the necessary devices and ancillaries. Additionally, in pursuing a decarbonized and circular economy within the transportation sector, captured CO₂ could be utilized as a raw material for producing fuels such as synthetic methane [42–47]. This approach would not require additional infrastructure costs, as the existing natural gas networks could be used for synthetic methane distribution [48–50], allowing these fuels to be used in ICEV again. Therefore, an integrated CCS system in an HD-ICEV fuelled with synthetic methane could be an excellent way to keep existing ICEVs in the market under near-zero CO₂ emissions scenarios and without relying on fossil fuels [51–53].

In recent years, research has been carried out on CCS systems in mobile sources (vehicles and ships) propelled with ICEs to address these challenges. These studies have assessed various aspects, including the energy consumption of CCS systems employing different solvents and sorbents [54–64], economic implications of CCS system implementation [65,66], the technical feasibility of integrating CCS systems [67–70], enhancing of sorbent material properties to CO₂ capture on board [71], and CCR evaluations with several sorbents under stationary conditions and without regeneration [63,72,73]. These research works reveal that absorption is the predominant CO₂ capture technique in the maritime sector, while adsorption is favoured in road transport. Additionally, they highlight that CO₂ storage represents the most energy-intensive process, contingent upon the CO₂ capture rate (CCR). Consequently, some researchers have proposed hybrid solutions integrating an Organic Rankine Cycle (ORC) with CCS systems [74,75].

The key concept behind hybridizing an ORC with a CCS system is utilising the waste heat in the exhaust gases to generate mechanical energy. By doing so, the ORC can either fully or partially supply the mechanical energy needed for the CCS system's operation; this integration minimizes the power the engine supplies to the CCS system, thereby optimizing overall energy efficiency. The ORC is a well-developed technology that has been extensively studied through experimental [76–80], simulation and modelling investigations [81–85], design of their devices [86], and techno-economic assessments [87]. These studies have found that the ORC requires low maintenance costs, is highly safe, and offers flexibility to adapt to different residual heat sources.

The literature review reveals that there has been increasing interest in CO₂ capture in mobile sources in recent years, mainly in trucks (HD-ICEV). However, all of the studies published before the development of this thesis focused on CCS-ORC systems operating on a single ICE operating condition, which does not

accurately fit the current operating conditions of ICEVs. Therefore, these research works do not show an objective mapping of the energy behaviour of the CCS-ORC system operation. Hence, their implications at energy and techno-economic levels, which are key factors in determining their feasibility, are unknown until the day, leading to biased conclusions and the inability to extrapolate their results.

In this vein, the lack of information and poor development of CCS-ORC systems integrated into HD-ICEV are the main motivations for elaborating the present thesis. Hence, this thesis proposes and performs an energy and techno-economic assessment of a CCS-ORC system integrated into natural gas heavy-duty internal combustion engines. These assessments involve operating the ICE at partial loads and across the entire rpm range. This approach makes it possible to describe the behaviour of the CCS-ORC system more realistically and thereby assess its technical feasibility. By exploring all these aspects, this thesis aims to fill the knowledge gap in this field, offering the heavy transport sector an additional alternative to reduce its carbon footprint and improve its environmental sustainability.

1.2 OBJECTIVES AND METHODOLOGY

The main objective of this thesis is to design and evaluate the energy and techno-economic feasibility of a carbon capture and storage (CCS) system integrated into a natural gas heavy-duty internal combustion engine vehicle. This integration aims to address the current gap in knowledge regarding the operational requirements and performance characteristics of such systems, thereby paving the way for subsequent experimental validation. By thoroughly investigating the energy consumption, cost implications, and potential operational challenges of the CCS system, this research provides a comprehensive framework to guide future developments in this field. Otherwise, the heavy transport sector could not face the stringent CO₂ emission reduction targets for 2050. Therefore, innovations like the one proposed in this thesis contribute to expanding academic knowledge and technical understanding and support broader environmental goals to mitigate climate change.

The main objective of this thesis is divided into four specific objectives. These specific objectives are comprehensively explained below and are individually addressed in separate chapters. Each chapter thoroughly explores the methodologies employed and the results obtained.

Objective 1: Identify the CO₂ capture techniques most compatible with the operating characteristics of a heavy-duty internal combustion vehicle, considering factors such as energy consumption, operating costs, and technology readiness level.

The primary purpose of this objective is to deepen the understanding of the CO₂ capture methods and techniques that have reached a high degree of

development and techno-economic feasibility to discern both their advantages and limitations for their practical application within the transportation sector. Subsequently, a comprehensive review of existing patents and research works addressing CO₂ capture, and storage systems integrated into vehicles will be conducted. This research process will allow previously proposed solutions to be compiled and analysed, and the most promising technologies and lessons learned from previous experiences will be identified.

This exhaustive analysis will serve as a basis for defining the most appropriate methods and techniques for CO₂ capture and storage in mobile sources, considering their technical effectiveness and practical feasibility in an actual application context. By thoroughly understanding the available options and selecting the most appropriate ones, a solid foundation will be laid for the design, energy evaluation and economic feasibility of the CO₂ capture system proposed in this thesis.

To accomplish this objective, the completion of three tasks is required: (1-a) Identify all the CO₂ capture technologies able to adapt to the several engine operations; (1-b) Gather and filter information about all the carbon capture systems in mobile sources published until the date and (1-c) select the most advanced and that best suits technology to recover waste heat from the exhaust gases coming from internal combustion engines.

Objective 2: Evaluate the energy feasibility of hybridizing a waste heat recovery system, which utilizes the thermal energy from internal combustion engine's exhaust gases, with a CO₂ capture and storage system.

One of the main limitations of implementing a CO₂ capture and storage system is its high energy consumption. However, in the case of internal combustion engines, approximately 30% of the fuel energy is contained in the exhaust gases. This energy is currently not used and could be key to mitigating the energy demand of the CO₂ capture and storage system.

Hence, this specific objective aims to evaluate the energy hybridisation between a waste heat recovery system and a CO₂ capture and storage system, both integrated into a heavy-duty internal combustion engine. In such a way, this energy evaluation will determine whether the waste energy recovery system can fully or partially supply the power demand of the CO₂ storage system, especially the CO₂ storage stage, which is the most energy-intensive process. This analysis will also consider the thermal energy processes involved in the hybrid system, such as CO₂ desorption and the necessary cooling stages. All of this will be designed to always seek a configuration of the studied systems that is as practical and simple as possible, which will be achieved by using of optimisation of thermal flows.

To achieve this goal, three tasks must be completed: (2-a) Modelling heavy-duty internal combustion engines to determine the thermodynamic conditions of the exhaust gases; (2-b) Selecting, designing, and modelling a waste heat recovery system that can operate with the exhaust gases waste heat; and (2-c) Conducting an energy evaluation of the hybridization of the waste heat utilization system with a carbon capture system.

Objective 3: Evaluate the energy behaviour of a CO₂ capture and storage system hybridised with an organic Rankine cycle integrated into a heavy-duty internal combustion engine operating at various engine loads and in the entire rpm range.

Integrating a CO₂ capture and storage system into a heavy-duty vehicle with an internal combustion engine is crucial for several reasons. First, such a system must be able to adapt to the various engine operating conditions, which vary considerably depending on engine load and rpm. This adaptability is essential to ensure that the CO₂ capture and storage system does not significantly compromise vehicle performance.

On the other hand, the configuration of the CO₂ capture and storage system is essential for its optimal operation. Consequently, it must maximize the use of the thermal resources available in the exhaust gases to release the captured CO₂, thus improving the process's efficiency. Energy production through the ORC is a key component in this configuration, as it takes advantage of waste heat to generate useful energy, thus covering the system's energy demand.

The CO₂ capture system design also considers size and weight, ensuring its feasibility and practicality for integration into heavy-duty vehicles. So, a well-conceived design will allow a harmonious integration of the capture system with the vehicle, taking advantage of waste energy to maximize its efficiency and capture the greatest amount of CO₂ possible without affecting engine performance.

For this objective, the tasks that should be accomplished are (3-a) dimensioning the carbon capture system hybridised with the waste heat recovery system; (3-b) performing the energy evaluation of the system proposed under different engine operating conditions; and (3-c) Determining the penalty of the system proposed over the engine performance.

Objective 4: Perform a techno-economic assessment of a CO₂ capture system integrated into a heavy-duty internal combustion engine vehicle.

With the preliminary design of the carbon capture and storage system established, a techno-economic analysis is carried out. This analysis evaluates the capital expenditures (CAPEX) associated with the devices that comprise the CO₂

capture and storage system, allowing the identification of the most expensive components. In addition, the operational expenditures (OPEX) that the system could incur are estimated. This approach calculates whether the CAPEX and OPEX can be a payback through the benefits derived from the reduction of CO₂ emissions, the improvement of energy efficiency, and possible economic incentives.

The entire techno-economic assessment will consider the lifespan of a heavy-duty internal combustion engine vehicle. This will determine how economically feasible it is to integrate a CO₂ capture and storage system in this type of vehicle, providing a comprehensive view of the feasibility of implementing carbon capture technologies in the transportation sector.

The tasks to be carried out in this objective are (4-a) determining the CAPEX and OPEX of the system proposed; (4-b) Calculating payback and carbon abatement cost of the system proposed; and (4-c) making a sensitivity analysis of scenarios where the transport sector must pay carbon taxes.

2. CARBON CAPTURE ON MOBILE SOURCES

Capturing CO₂ from mobile sources, mainly ships and internal combustion engine (ICE) vehicles, faces numerous challenges, such as space limitations to house the devices that compound the carbon capture and storage (CCS) system since the mass of CO₂ produced is three times higher than the fuel consumed for an ICE. On the other hand, the CCS operations must be able to adapt to the actual operation of ICE, in which constant changes in engine load and rpm (i.e., rapid acceleration and deceleration) cause sudden changes in mass and temperature in the exhaust gases. Finally, the operation of the CCS system requires additional energy, which penalizes the primary source of energy production, in this case, the ICE. This forces fuel consumption to increase and, consequently, generates higher CO₂ emissions, thus reducing net CO₂ capture and increasing the operating cost of mobile sources that would integrate CCS systems into its operations.

Following this, a detailed review of patents and literature is conducted to determine the most suitable method for carrying out CO₂ capture in mobile sources. The subsequent sections present the latest advancements in CO₂ capture within the maritime sector and ICE Vehicles (ICEVs), accompanied by an energy and sizing assessment of a CCS system integrated into an ICE operating at partial engine loads. Through this review and assessment, the aim is to pinpoint the knowledge gap that this research endeavours to address.

2.1 CARBON CAPTURE IN THE MARITIME SECTOR

Shipping is the most energy-efficient mode of transportation [88], contributing around 2% to global greenhouse gas emissions [89]. Based on this, in 2018, the

International Maritime Organization set a target of reducing CO₂ emissions by at least 50% by 2050 [90]. So, implementing Carbon capture and storage (CCS) technologies seems to be a promising avenue for achieving this target [91] because internal combustion engines that operate on ships work at constant load and rotational speed, producing a quasi-constant concentration and flue gas mass flow, facilitating the integration of CCS technologies.

The research endeavours in the maritime sector have directed their attention towards simulating CO₂ capture processes using amine scrubbing, with MEA, Pz, and NH₃ being the most employed amines [54,60,62,65,92]. All these studies agree that, for this type of technology to be integrated into ships, it is necessary to know two key variables. These are the energy consumption in the reboiler, which provides the thermal energy for the regeneration of the amine-solution and the CO₂ release, and the CO₂ capture cost. Further, these variables depend on several parameters, highlighting the carbon capture rate (CCR), the amine concentration in the solution, and the CO₂ compression pressure for its storage.

Figure 3 shows that the higher the amine concentration in the solution, the lower the heat duty in the reboiler. It is also evidenced that the CO₂ capture with MEA at 30 wt% presents a higher heat duty than Pz at 30 wt% due to the higher absorption heat of MEA than the Pz, regardless of the engine's fuel. Finally, this figure shows that the NH₃ requires 3 times less solvent in the solution and 2.5 times less heat duty to achieve a CCR of 90% than with MEA and Pz.

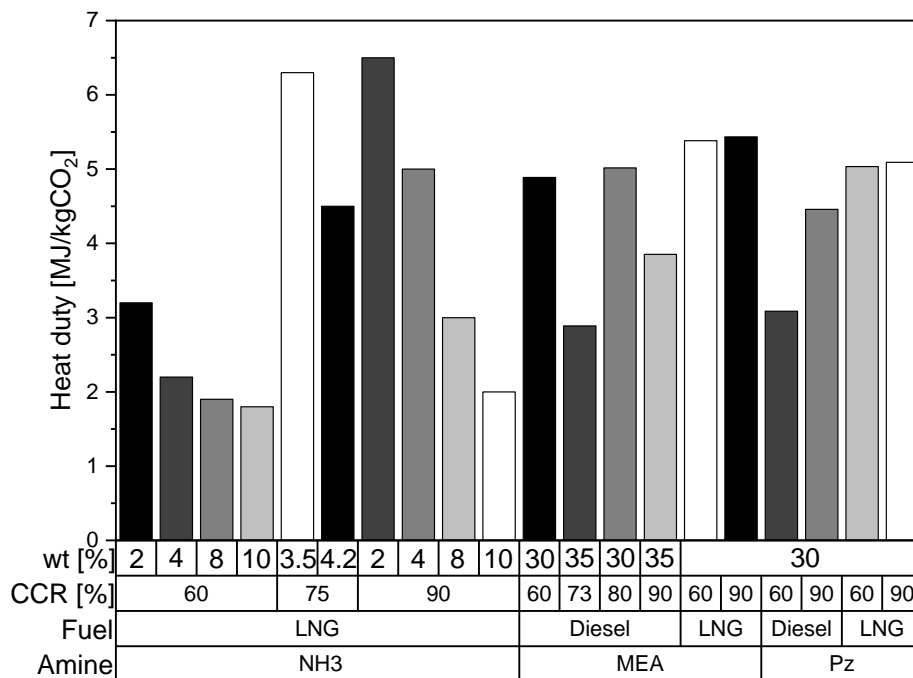


Figure 3. Reboiler heat duty (own elaboration, sources [54,60,62,65,92]).

Figure 4 shows the CO₂ capture costs reported in the literature. A decreasing trend is evident in the CO₂ capture cost as the CCR and the amine concentration

in the solution increase. Of the amines studied, Pz, at 90% of CCR, has the most affordable cost for ships with engines fueled with LNG. Regarding the capital expenditure required for installing an amine-scrubbing facility to operate onboard ships, Fang et al. [93] found that this can amount to 710000 USD/MW. Other studies with amine-scrubbing have shown that tropical atmospheric conditions perform better than arctic conditions in the operation of an amine-scrubbing facility [61] since more waste heat from the EG is recovered, leading to a high CO₂ capture.

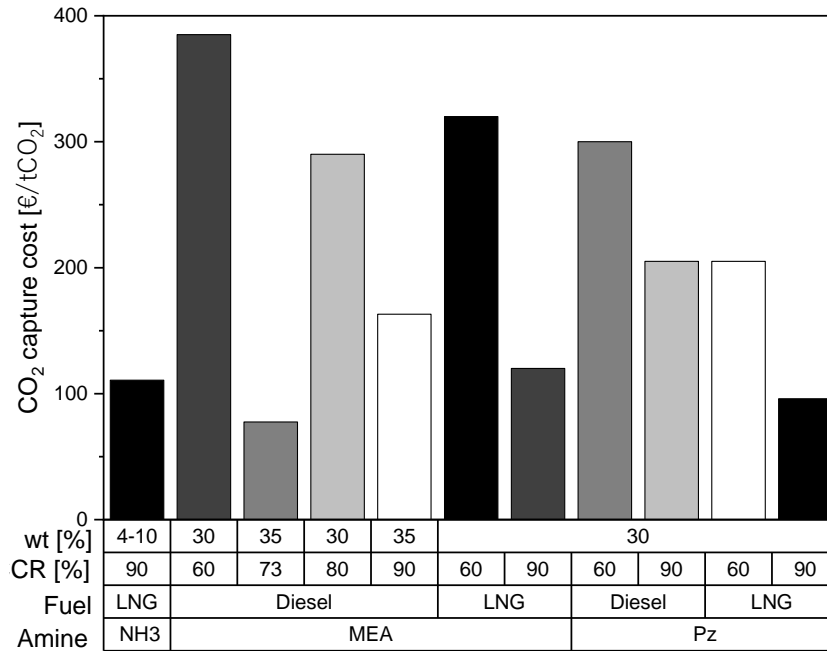


Figure 4. Amine-scrubbing CO₂ capture cost in the maritime sector (own elaboration, sources [54,60,62,65,92]).

2.2 CARBON CAPTURE ON INTERNAL COMBUSTION ENGINES VEHICLES

Integrating CCS systems in vehicles is especially challenging due to the limited space available for storing the CO₂ captured and installing additional devices required for this purpose. Moreover, the extra energy consumption necessary for the operation of the CCS system could be a ballast to the ICE [94]. However, several research works and patents have been conducted on different CO₂ capture methods, such as oxyfuel combustion and post-combustion.

According to these works, oxyfuel combustion could be conducted by membranes installed in the intake manifold, which separate the O₂ from the air [95]. However, the membranes are still underdeveloped to be a real application in ICE. On the other hand, supplying a stream of O₂ from an air separation unit is more feasible for oxy-fuel combustion in ICE. Experimental tests developed on engines show an increase of the indicated work of 7.8% with a 40% O₂ in the intake manifold and thermal efficiency of 42% with an EGR of 5% [96–98].

Amine-scrubbing and temperature, pressure or vacuum swing adsorption are the primary techniques used for CO₂ capture in ICEV. Several patents [99–101] and research works [63,69] have been developed regarding amine-scrubbing, outstanding the experimental tests developed by the Aramco company, where they have achieved up to 50% of CCR with an amine-solution of 30 wt% [70].

Adsorption has been studied more extensively than amine-scrubbing for capturing CO₂ in ICEVs. Several research works have evaluated the CO₂ capture capacity of different sorbents in spark ignition (SI) and compression ignition (CI) engines [58,59,72,73,102–106]. The experimental tests were conducted with a sorbent bed installed in the exhaust gas pipe. As is depicted in Figure 5, the Zeolite X13 has the best performance with CCR values above 60%, independent of the kind of fuel or ICE used. The sorbents impregnated with MEA obtained a CCR similar to that of zeolite X13. Both results stem from the high CO₂ loading of zeolite X13 and MEA, which improves CO₂ capture when impregnated in sorbents.

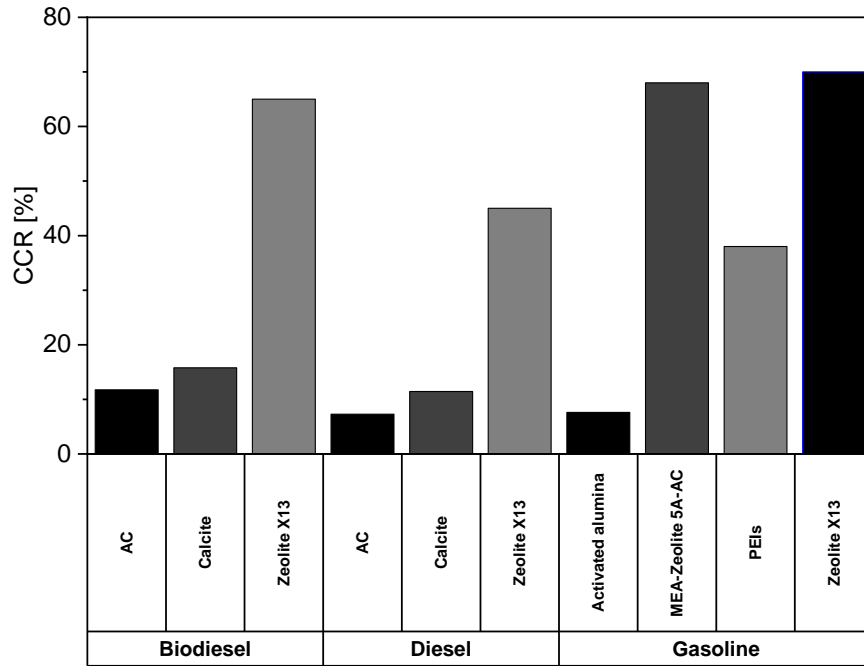


Figure 5. CCR values obtained with several sorbents (own elaboration, sources [58,59,72,73,102–106]).

The first complete study of the energy behaviour of the CCS system integrated into a CI-ICE was performed by Sharma and Maréchal [74]. The CCS system proposed by them operates by temperature swing adsorption (TSA) with PPN-6-CH₂-TETA as sorbent, a rotary wheel adsorbed (RWA) for the TSA processes, an ORC, and a heat pump to supply CCS system energy requirements. The assumptions are a CCR of 90%, an engine operation of 8 h, and a fuel consumption of 50 L for a CO₂ production of 117 kg of CO₂. The main result shows that achieving the CCR established without affecting the engine performance is possible, i.e., the heat and power required for the CCS system operation are obtained by harnessing the EG waste heat. They also showed the thermal

requirements in the adsorption and desorption process and the energy demands in the CO₂ storage stage for the first time. However, this study assumed a constant engine operation, far from the actual engine operating conditions.

As discussed, absorption in the maritime sector and adsorption in ICEV predominate as CO₂ capture techniques. However, only two works on post-combustion (one with adsorption and the other with TSA) consider sorbent or amine regeneration and CO₂ storage. Nevertheless, none of these works was performed under dynamic conditions, partial engine loads or varying rpm, which differ significantly from the actual operation of an ICE, at least of an HD-ICEV. Consequently, research works regarding practical and operational issues need to be improved to advance and close this knowledge gap.

Following the review, a clear trend indicates that integrating CCS systems is more feasible in HD-ICEVs. These vehicles offer more useful space for locating auxiliary equipment and storing CO₂. Moreover, the exhaust gas produced by an HD-ICE contains more waste heat, which can be harnessed to meet a CCS system's thermal and power demands. This minimizes the impact on engine performance caused by CCS system operation and presents minor spatial integration challenges.

Regarding the CO₂ capture technique, this thesis leans towards temperature swing adsorption (TSA) because it requires less energy for regeneration than amine solutions. Specifically, the adsorption heat value of several sorbents, including metal-organic frameworks, porous polymer networks, zeolites, and activated carbons, is less than -50 kJ/mol_{CO₂} [107]. In contrast, the absorption heat for commonly used amine solutions exceeds this value [108]. Furthermore, adsorption can be carried out in fixed beds with short time intervals during the CO₂ adsorption and desorption processes, which allows maintaining a CCR. This behaviour contrasts amine-scrubbing, which holds a constant flow rate and, therefore, cannot adjust to variations in exhaust gas flow and CO₂ concentrations produced during the regular operation of ICEs. Based on all of this, an initial energy assessment and spatial requirements for integrating a CCS system into a mobile source utilizing TSA as a CO₂ capture technique are presented below.

2.3 CCS-SYSTEM: FIRST ENERGY AND SIZING ASSESSMENT

Two representatives turbocharged, four-stroke, water-cooled natural gas ICE (one for road and one for maritime transport) are chosen for the energy assessment. Table 1 presents a summary of the technical specifications of these engines. The CCS system uses TSA for CO₂ capture. The TSA processes are sorbent heating, CO₂ desorption, sorbent cooling, and CO₂ adsorption. For the first two processes, EG waste heat is used. The remaining thermal energy in the EG is

transformed into mechanical energy through an ORC, which powers the CO₂ compression stage. Figure 6 shows the proposed CCS system.

Table 1. Engine Technical specifications.

	BUS (M936G) [111]	Ship (W9L46DF) [112]
Architecture	In-line 6-cylinder	In-line 9-cylinder
Displacement volume [L]	7.7	867.6
Brake Power [kW]	222 at 1950 rpm	10305 at 600 rpm
Specific Fuel Consumption [g/kWh]	194 at 1950 rpm and 100% engine load	165 at 600 rpm and 75% engine load

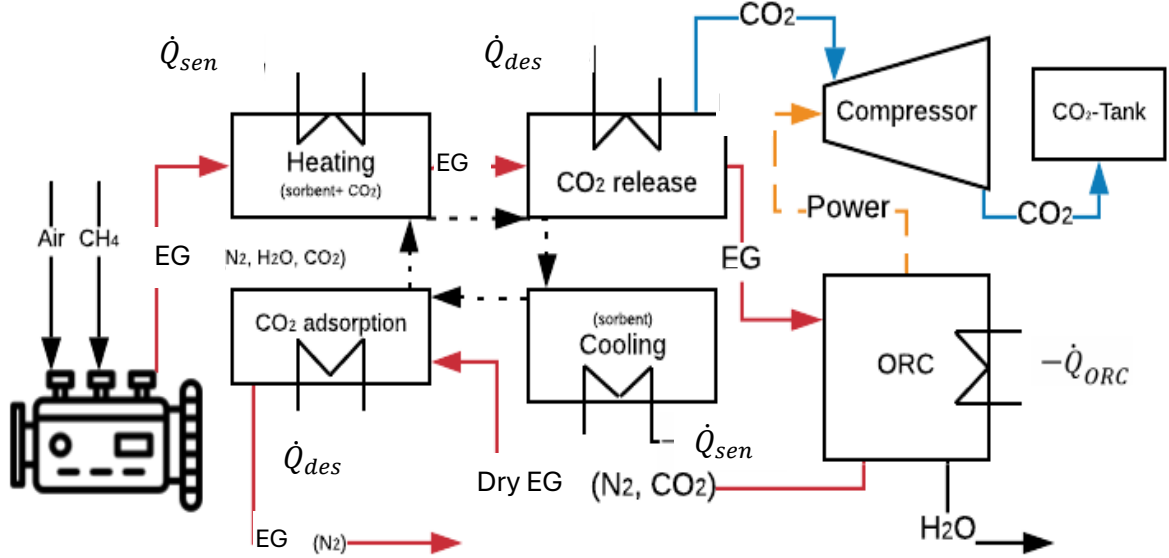


Figure 6 Mass and energy chart of the CCS system for its operation into an ICE.

The calculations required for the energy assessment are based on a 90% CCR, engines fuelled with methane undergoing stoichiometric combustion, and considering only CO₂, H₂O, and N₂ as EG species. Further, three sorbents were selected for this first approach, PPN-6-CH₂-DETA, MOF-74-Mg, and Zeolite-X13 (PPN, MOF and Z13 onwards), to determine better performance. The energy analysis for the M936G engine involves three EG temperature scenarios representing low, medium, and high engine loads (600, 700, and 800 K) [109,110]. Meanwhile, the energy analysis for the maritime engine W9L46DF is conducted at 75% of the engine load with an EG temperature of 700 K. If the CCS system does not get to operate at a CCR of 90% without energy penalties, the highest CCR for each sorbent will be calculated, following the same procedure developed previously. Finally, with the results obtained, the CO₂ volume stored and the sorbent volume in the TSA process will be calculated.

The available thermal energy in the EG is calculated at the turbocharged outlet of the SI-ICE using Equation 1. The EG specific heat (c_p) is obtained from the EG composition using Equation 2, the difference temperature (ΔT_l) represents the difference between the EG temperature at the turbocharged outlet and the reference temperature (25 °C). The regeneration heat for the sorbents ($\dot{Q}_{reg-sorb}$)

is the sum of the sensible heat (\dot{Q}_{sen}) and the desorption heat (\dot{Q}_{des}), Equations 3 and 4. The loading capacity (q) and the ΔH_{des} are shown in Table 2. the ΔT_2 in the \dot{Q}_{sen} considers desorption and adsorption temperatures of 150 and 30 °C, respectively. According to the literature, 150 °C is the most suitable temperature because it guarantees the greatest amount of CO₂ desorption without sorbent degradation [107,113]. At the same time the adsorption temperature selected is 30 °C since the exhaust gas is 99% dry at this temperature, which is ideal for sorbents because they lose CO₂ adsorption capacity with exposure to wet exhaust gases [114].

Table 2. Sorbent physical properties used in the simulations [107,115–118].

Sorbent	Adsorption Heat (ΔH_{ads}) [kJ/molCO ₂]	Loading Capacity (q) [kgCO ₂ /kg _{sorbent}]	Selectivity CO ₂ /N ₂	Specific Heat (c_p) [kJ/kgK]	*Density (ρ) [kg/m ³]
PPN	-45.33	0.2354	>10.000	0.985	805
MOF	-37.4	0.27808	209	0.896	914.9
Z13	-49.72	0.176	17.46	1.07	1360
AC	-25	0.132	11	1.062	1040

*Crystallographic density

$$\dot{Q}_{EG} = \dot{m}_{EG} c_{p-EG} \Delta T_1 \quad (1)$$

$$c_{p-EG} = x_{CO_2} c_{p-CO_2} + x_{N_2} c_{p-N_2} + x_{H_2O} c_{p-H_2O} \quad (2)$$

$$\dot{Q}_{reg-sorb} = \dot{Q}_{des} + \dot{Q}_{sen} \quad (3)$$

$$\dot{Q}_{reg} = CCR x_{CO_2} \dot{m}_{EG} \Delta H_{des} + c_{p-CO_2} CCR x_{CO_2} \dot{m}_{EG} \Delta T_2 + c_{p-ads} \frac{CCR x_{CO_2} \dot{m}_{EG}}{q} \Delta T_2 \quad (4)$$

Subsequently, the power consumption of the CO₂ compressor is determined utilizing the software ASPEN Plus, whose values are 3.16 and 1029.9 kW for the M936G and the W9L46DF engines, respectively. Meanwhile the power output of the ORC (\dot{W}_{out}) is calculated using Equation 5. This equation incorporates the remaining heat in the EG (\dot{Q}_{rem}) as defined by Equation 6, considering an ORC cycle efficiency (η_{ORC}) of 20% [82,119].

$$\dot{W}_{out} = \eta_{ORC} \dot{Q}_{rem} \quad (5)$$

$$\dot{Q}_{rem} = \dot{Q}_{EG} - \dot{Q}_{reg} \quad (6)$$

The space requirements for the CCS system are determined in terms of volume. The CO₂ will be stored as a liquid at 75 bar and 29.35 °C; resulting in a CO₂ density (ρ_{CO_2-L}) of 762.6 kg/m³ under these conditions. The process begins by calculating the mass of CO₂ to be stored (m_{CO_2}), assuming an 8-hour operation, i.e. 28800 s (Equation 7). As was mentioned before, the TSA process comprises four stages (Figure 6), each expected to run for 30 minutes. Therefore, the sorbent mass (m_{sor}) is divided by 4 (Equation 8), and the sorbent volume (V_{sor}) is calculated using Equation 9. Finally, the CO₂ volume (V_{CO_2}) is determined using Equation 10, and the approximate total volume of the CCS system is obtained by summing the volumes of CO₂ and sorbent.

$$m_{CO_2} = 28800 CCR x_{CO_2} \dot{m}_{EG} \quad (7)$$

$$m_{sor} = \frac{m_{CO_2}}{4q} \quad (8)$$

$$V_{sor} = \frac{m_{sor}}{\rho_{sor}} \quad (9)$$

$$V_{CO_2} = \frac{m_{CO_2}}{\rho_{CO_2-L}} \quad (10)$$

2.3.1 Results

The findings presented in Table 3 indicate that the heat available in the EG is sufficient to regenerate the sorbent in the TSA process for all temperatures in both engines. This margin increases as the ΔT rises. Similarly, the remaining heat in the EG and the output power in the ORC have the same behaviour, as seen in Table 4. Further, when the ORC operates at an EG temperature of 800 K, it generates enough power to meet the consumption requirements of the CO₂ compressor with the CCS system employing MOF-74-Mg as sorbent. However, in other scenarios, the power generated by the ORC proves insufficient to satisfy the demands of the CO₂ compressor.

Table 3. Available heat in the EG at low, medium, and full engine load and regeneration heat at 90% of CCR for each sorbent

Engine	EG Mass Flow [kg/s]	Sorbent	Regeneration Heat 90% of CCR [kW]	Available Heat in the EG [kW]		
				600 K	700 K	800 K
M936G	0.03772	PPN	11.2			
		MOF	7.3	13.4	18.5	23.7
		Z13	10.1			
W9L46DF	12.3	PPN	2737.5			
		MOF	2240.5	NA	6021.4	NA
		Z13	3291.5			

Table 4. Power produced by the ORC at low, medium, and full engine loads in each engine.

Engine	M936G			W9L46DF		
Sorbent	PPN	MOF	Z13	PPN	MOF	Z13
\dot{W}_{out} at 600 K [kW]	0.434	1.219	0.661	NA	NA	NA
\dot{W}_{out} at 700 K [kW]	1.448	2.233	1.675	656.8	756.2	545
\dot{W}_{out} at 800 K [kW]	2.492	3.277	2.719	NA	NA	NA

Figure 7 depicts the maximum CCR with which the ORC can cover the total power demand of the CO₂ compressor for each sorbent in both engines, given an EG temperature of 700 K. The maximum CCR values achieved without the need to draw power from the engine to compress the CO₂ and therefore without affecting its performance are 73, 68 and 64% with MOF, PPN and Z13, respectively. Finally, the estimated total volume of the CCS system is obtained using the sorbents that performed better in the energy analysis (PPN and MOF).

As detailed in Table 5, the volume values obtained are less than 0.3 m³ for the M936G engine and less than 100 m³ for the W9L46DF engine.

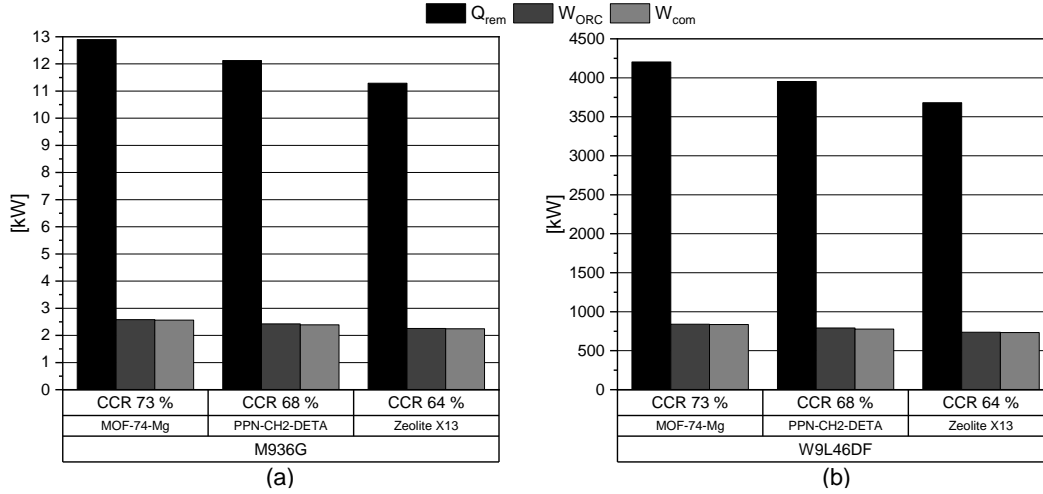


Figure 7. Remaining heat, ORC power output, CO₂ compression power output and maximum CCR obtained in each engine.

Table 5. Volume calculations for each sorbent and engine.

Engine	M936G		W9L46DF	
Sorbent	PPN	MOF	PPN	MOF
CO ₂ Mass (68% of CCR) [kg]	28.0	28.0	9116.0	9116.0
Sorbent mass [kg]	118.8	100.5	38726	32782
Sorbent density [kg/m ³]	805.00	914.88	805.00	914.88
Sorbent Volume [m ³]	0.148	0.110	48.106	35.832
CO ₂ Volume stored [m ³]	0.147	0.147	47.815	47.815
Total volume [m ³]	0.295	0.257	95.922	83.647

2.4 SUMMARY

The combination of a CCS system that uses TSA as a CO₂ capture technique and an ORC for efficiency improvement is a promising alternative for CO₂ capture and storage in mobile sources. This hybridization theoretically allows optimal integration of the CCS system into an HD-ICEV without compromising engine performance, as it harnesses the EG waste heat to meet its energy demands. However, a detailed understanding of the CCS-ORC system is necessary to assess this promising application objectively. Therefore, the detailed design of these systems and their corresponding energy and techno-economic assessments will be addressed in the following chapters of this thesis, thereby establishing the feasibility of this application.

2.5 PUBLISHED PAPER

Finally, all the details, findings and conclusions of this study have been included in an article published in the journal "energies", which has the following reference:

- García-Mariaca, A.; Llera-Sastresa, E. Review on Carbon Capture in ICE Driven Transport. *Energies* 2021, 14, 6865. <https://doi.org/10.3390/en14216865>

Review

Review on Carbon Capture in ICE Driven Transport

Alexander García-Mariaca ¹  and Eva Llera-Sastresa ^{2,*} 

¹ Escuela de Ingeniería y Arquitectura, University of Zaragoza, María de Luna s/n, 50018 Zaragoza, Spain; 808497@unizar.es

² Department of Mechanical Engineering, CIRCE Research Institute, University of Zaragoza, María de Luna s/n, 50018 Zaragoza, Spain

* Correspondence: ellera@unizar.es

Abstract: The transport sector powered by internal combustion engines (ICE) requires novel approaches to achieve near-zero CO₂ emissions. In this direction, using CO₂ capture and storage (CCS) systems onboard could be a good option. However, CO₂ capture in mobile sources is currently challenging due to the operational and space requirements to install a CCS system onboard. This paper presents a systematic review of the CO₂ capture in ICE driven transport to know the methods, techniques, and results of the different studies published so far. Subsequently, a case study of a CCS system working in an ICE is presented, where the energy and space needs are evaluated. The review reveals that the most suitable technique for CO₂ capture is temperature swing adsorption (TSA). Moreover, the sorbents with better properties for this task are PPN-6-CH₂-DETA and MOF-74-Mg. Finally, it shows that it is necessary to supply the energy demand of the CCS system and the option is to take advantage of the waste heat in the flue gas. The case study shows that it is possible to have a carbon capture rate above 68% without affecting engine performance. It was also found that the total volume required by the CCS system and fuel tank is 3.75 times smaller than buses operating with hydrogen fuel cells. According to the review and the case study, it is possible to run a CCS system in the maritime sector and road freight transport.

Keywords: CO₂ emissions; carbon capture; internal combustion engine; mobile sources; TSA



Citation: García-Mariaca, A.; Llera-Sastresa, E. Review on Carbon Capture in ICE Driven Transport. *Energies* 2021, 14, 6865. <https://doi.org/10.3390/en14216865>

Academic Editors: Aristide Ghiliani and José Carlos Magalhães Pires

Received: 26 August 2021

Accepted: 19 October 2021

Published: 20 October 2021

Publisher's Note: MDPI stays neutral with regard to jurisdictional claims in published maps and institutional affiliations.



Copyright: © 2021 by the authors. Licensee MDPI, Basel, Switzerland. This article is an open access article distributed under the terms and conditions of the Creative Commons Attribution (CC BY) license (<https://creativecommons.org/licenses/by/4.0/>).

1. Introduction

The global necessity of maintaining economic growth produces an increase in energy consumption. Despite the efforts in decoupling both issues, this indicator continues to grow, being the industry, transport and residential sectors the major contributors with 79.1% of the total energy consumption in 2017 [1]. Electricity and heat production and the transport sector produced the highest CO₂ emissions, at 41.4% and 24.5%, respectively [2].

To achieve the Paris agreement objective to limit the increase of the global temperature under 2 °C [3], the European Union (EU) has promoted renewable energies, energy efficiency, and fuel substitution policies [4]. These measures have allowed expanding technological innovations to reduce the CO₂ in the energy, construction, industry, agriculture, and transport sectors.

Up to date, the technological innovations to reduce CO₂ emissions in the transport sector revolve around four topics: the use of alternative fuels, such as biofuels, natural gas (NG), liquefied petroleum gas (LPG), and H₂ [5,6]; the reduction of the fuel consumption is achieved through the enhanced engine thermal efficiency [7], by using eco-driving technologies [8,9]; the optimization of the engine energy-balance, transforming waste heat flows through Organic Rankine Cycles (ORC) or Thermo-Electric Generators (TEG) [10–13], the reduction of driving resistances [14], and the development of powertrains powered by electricity. The advantage of these vehicles (fuel cell vehicles and electric vehicles) is that they are CO₂ zero-emission options, unlike the previously mentioned technologies.

These technologies have been insufficient to reduce the CO₂ emissions from this sector, as is shown in Figure 1. However, the EU expects a substitution of internal combustion

engine vehicles (ICEv) by electric vehicles (EVs) in urban transport from 2030, and it will be anticipated CO₂ free city logistics in major urban centres by 2050 [15]. Nevertheless, EVs are far from replacing the engine combustion vehicles used in road freight transport due to low energy density and high weights in their batteries that result in low ranges [16]. On the other hand, according to the United States Environmental Protection Agency (US EPA), lithium-ion batteries not only increase environmental toxicity and cause global warming (due to the material extraction for its manufacture and final disposal of the batteries) but induce pulmonary and neurological diseases in people involved in the production chain [17].

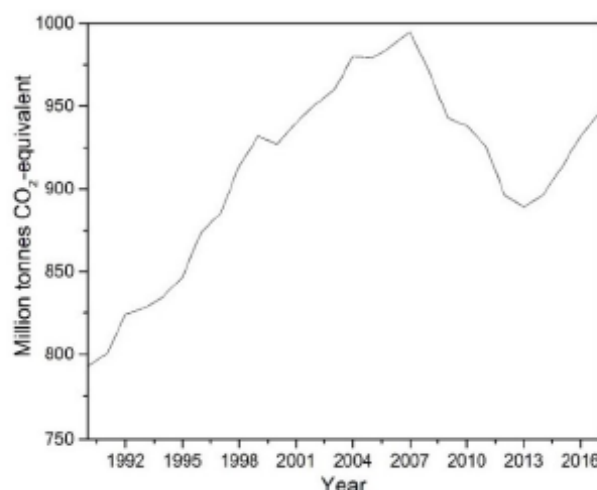


Figure 1. CO₂ emissions from the transport sector in Europe (source [18]).

Therefore, if the transport sector wants to be fully CO₂ zero-emission, technological innovations used in other sectors must be considered to apply in road freight transport. The carbon capture and storage (CCS) technologies have been widely explored, but only some have the potential to capture the CO₂ produced by ICEv used in road freight transport. CCS systems have been primarily used in power plants because they are the predominant source emitter of CO₂ [19]. Until 2019, there were 19 large-scale CCS projects in operation, 4 installations are about to start, and 28 others are in various stages of development, with an estimated CO₂ capture of 96 Mton per year [20], corresponding to 0.3% of the total CO₂ emissions for 2017. In addition, 100 smaller-scale projects are currently ongoing [21].

The existing CCS systems have been adjusted to the nominal operation of power plants, almost always in a stationary mode. Therefore, in the selection of a CCS system for its implementation in an ICE driven vehicle (ship or truck), adaptation to the typical operating characteristics of the transport sector, such as variations of the mass flow and concentration of species in the FG due to acceleration, decelerations, and engine loads, must be considered. Where applicable, the use of CCS technologies in the transport sector should be coupled with a fuel that produces near-zero particle emissions, not to affect the operation of the selected capture method.

In addition, the selection of a CCS system to operate in the transport sector will depend on the end-use of the CO₂ captured onboard. The possibility to produce synthetic methane to be subsequently used as fuel in the internal combustion engine (ICE) should be contemplated if a decarbonized and circular economy is pursued. The generation of synthetic methane combining electrolytic H₂ from renewable electricity and CO₂ captured from an existing source is a promising Power-to-Gas (PTG) technology due to its versatility [22–27] and the possibility of being integrated into the current NG supply and distribution system [28]. In addition, as several studies have shown [29,30], the vehicles

that operate with this kind of fuel produce less noise and near-zero particulate matter. Integration of CO₂ capture in synthetic methane fuelled engines would close the circle and move the ICE vehicle sector towards CO₂ emission neutrality, which will counteract the problems noted above [31–33]. To sum up, the integration of CCS in the transport sector could be an excellent way to keep the existing ICE in the market under the upcoming near-zero CO₂ emissions scenarios with zero presence of fossil fuels.

This paper aims to ascertain which CCS technology already tested in power plants best adapts to the operational characteristics of an ICE used in maritime and road freight transport. First, a short review of the CCS technologies used in power plants is presented. Then, a review of patents and research studies on the CCS systems and techniques in the transport sector is conducted. Finally, a case study is developed to anticipate the energy and space requirements of the CCS system integrated into commercial ICEs for maritime and road freight transport. This paper tries to contribute to the state of the art of CCS with a critical and comprehensive analysis of the possibility of performing CO₂ capture in mobile sources.

2. Carbon Capture and Storage

CCS refers to many technologies that capture CO₂ at some stage of a combustion process or an industrial process that produces CO₂ as waste [34–36]. In the first case, the CO₂ capture can be carried out after the combustion process (post-combustion, oxy-combustion and chemical looping combustion) or before the combustion process (pre-combustion), as represented in Figure 2 [37]. The higher the partial pressure of CO₂ in the gas, the better the efficiency of adsorption or absorption of CO₂ [38,39].

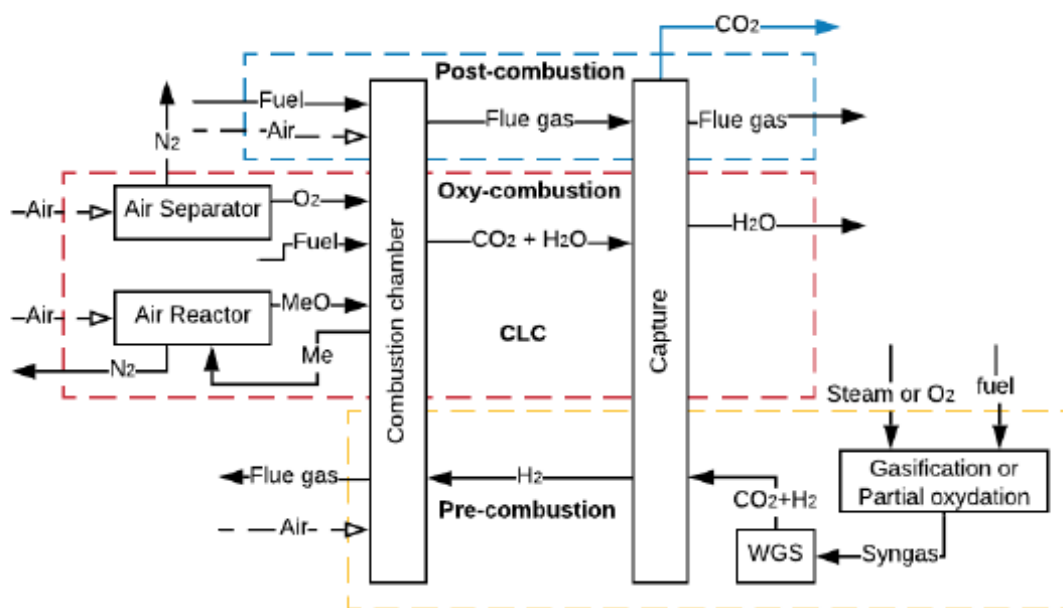


Figure 2. CCS methods (adapted from [37]).

In post-combustion, the capture occurs at a CO₂ low partial pressure, while capturing through oxy-combustion, pre-combustion and chemical looping combustion (CLC), whose aim is to increase the CO₂ concentration in the flue gas (FG), allows a higher partial pressure of CO₂ in the gas. However, to increase the CO₂ concentration, it is necessary to use additional equipment such as reactors or air separator units (ASU), which requires a large amount of power, thus decreasing the overall efficiency of the process [40].

In mobile sources as ICE driven ships and vehicles, the CO₂ capture could be done by the three CCS methods shown in Figure 2. However, the CO₂ capture in post-combustion is the predominant method by the nature of the powertrain used in this sector. According to Wang et al. [41], the main techniques that could be applied for CO₂ capture in maritime transport are amine-absorption, temperature swing adsorption (TSA), cryogenisation and membrane processes. On the other hand, according to Sullivan and Sivak [42], the most promising CO₂ capture technologies for the freight transport sector are amine-absorption and TSA. A short review of these techniques used in CCS is presented below.

2.1. Amine-Absorption

CO₂ capture by amine-absorption is the most mature and economical technology available today used in power plants [43]. According to Joel et al., Salazar et al. and MacDowell et al. [37,44,45], the installation consists of two interconnected columns. In the first column or absorber, the amine absorbs the CO₂ from the FG in a counter-current reactor at temperatures between 40 and 60 °C and pressures around 1 bar. The clean FG leaves the absorber from the top, while the solution rich in CO₂ is pumped from the bottom to the second column or stripper, where it is heated at temperatures between 80 and 120 °C with steam coming from the reboiler at 2 bars of pressure. This reaction breaks the chains between the CO₂ and the amine, and the CO₂ is released while the amine remains clean. Then, CO₂ is compressed and stored, and the lean solution is repumped to the absorber in a cycling process, as shown in Figure 3 [46,47].

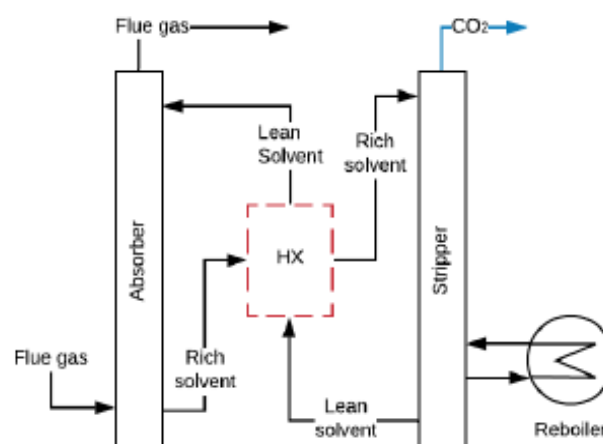


Figure 3. CCS capture with solvents (adapted from [48,49]).

Absorption by amines causes a reduction of approximately 10 points in the overall efficiency of a power plant (there are still no experimental data of mobile sources) [50,51]. This reduction is caused by the vapour extracted in the turbine during the regeneration process and the energy consumed by pumping and compression (parasitic loads), as shown in Figure 3 [52,53]. The required properties of amines to be used in mobile sources should be low absorption heat, to lessen energy requirements, and high CO₂ loading capacity (q), to minimize amine mass in the CO₂ capture. Table 1 shows some amines with suitable characteristics for the capture of CO₂ in mobile sources.

Table 1. Amine main properties at 300 K, with great potential to be used in mobiles sources.

Solvent	Rate Constant Reaction [m ³ /kmol·s]	Absorption Heat (ΔH_{abs}) [kJ/mol _{CO2}]	Loading Capacity (<i>q</i>)		Amine in the Solution [wt%]
			[mol _{CO2} /mol _{amine}]	[mol _{CO2} /L _{amine}]	
Ethanolamine (MEA)	8400 [54]	−88.91 [55]	0.59 [56]	9.77	30
Diethanolamine (DEA)	1340 [54]	−70.44 [55]	0.61 [56]	6.32	30
Ammonia (NH ₃)	7500 [57]	−65.5 [58]	0.4 [59–61]	16	2.5
Piperazine (Pz)	53,700 [62]	−80.58 [56]	0.81 [56,63]	10.34	30
Methyl diethanolamine (MDEA)	11.15 [64]	−52.51 [56]	0.74 [65]	6.51	30

Main problems with the amine-absorption include the degradation in operation at high temperatures and the need to make the FG free of acid emissions (SO₂ and NO_x) and particulate matter [66,67]. The amines are chemically unstable and highly corrosive in the presence of oxygen. Due to their high viscosity, aqueous amine solutions at a maximum concentration of 40 wt% [55] are used. One should not forget that amines are toxic to aquatic organisms and react with NO_x producing carcinogenic compounds that affect human health [68,69].

2.2. Adsorption

The adsorption process is based on an intermolecular relationship among surface forces in solids and gases, largely dependent on the temperature, partial pressure, surface force and adsorbent pore sizes [46,70]. Several materials have an excellent potential for this process, i.e., Activated Carbon (AC), zeolites, alumina, silica adsorbent, carbon nanotubes, porous polymer networks (PPNs), metal-organic frameworks (MOFs) and others [71–74]. Furthermore, materials can be improved with the impregnation of amine sorbents [75]. The adsorption process cannot be used if there are high concentrations of CO₂ in the FG because of the general low *q* of the sorbent, as shown in Table 2, but it is adequate for concentrations under 20% [76].

Table 2. Properties of materials used in adsorption.

Sorbent	Adsorption Heat (ΔH_{ads}) [kJ/mol _{CO2}]	Loading Capacity (<i>q</i>)		Selectivity CO ₂ /N ₂	Specific Heat (<i>c_p</i>) [kJ/kgK]	* Density (<i>ρ</i>) [kg/m ³]
		[kg _{CO2} /kg _{adsorbent}]	** [mol _{CO2} /L _{adsorbent}]			
Polyethylenimine/silica (PEI/HMS) [77]	−95.04	0.059		−	1.81	−
PPN-6-CH ₂ -TETA [73,78]	−48.22	0.06	1.21	>10,000	0.985	883.8
PPN-6-CH ₂ -DETA [73,78]	−45.32	0.112	2.04	>10,000	0.985	805
PEI-PS-50 [79]	−70.4	0.1276		−	1.65	−
Zeolite (13X) [80,81]	−49.72	0.176	2.6	17.46	1.07	1430
MOF-74-Mg [73,78]	−37.4	0.2284	4.75	209	0.896	914.9

* Crystallographic density. ** Calculated with a 50 % of the crystallographic density.

One of the techniques with the most significant potential to capture CO₂ in ICEv is adsorption. Specifically, the TSA technique is the most suitable process due to the high thermal energy available in the FG in ICEv. TSA is a cyclic process that has four stages, as shown in Figure 4. Initially, the CO₂ adsorption occurs at low temperatures (approximately 30 °C). Then, the sorbent bed is heated until the desorption temperature (around 150 °C). Thereafter, at this temperature, the sorbent releases the retained CO₂. Finally, the bed is cooled to start another cycle of adsorption [82–85]. In general, the main limitations of this process are the reduction in the adsorption capacity when the FG stream is wet due to

the hydrophilic character of the materials [86] and the low q (Table 2), which necessitates a large amount of material to achieve more quantities of captured CO_2 . However, the adsorption process can be adapted to several operation conditions because of its flexibility to configure the reactors [86–88].

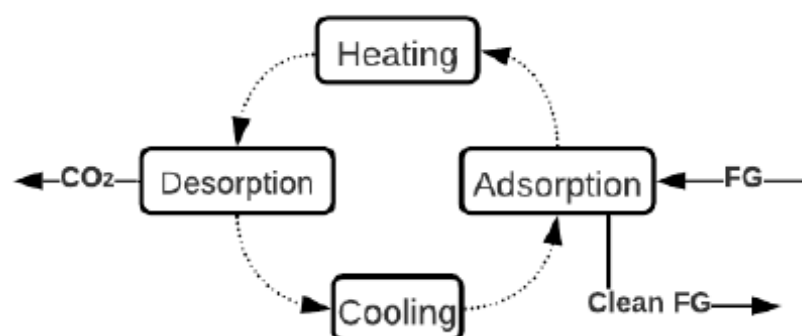


Figure 4. General description of TSA Process (adapted from [82]).

2.3. Carbonate Looping

Carbonate Looping (CL), represented in Figure 5, has been widely investigated for CO_2 capture, and CO_2 captures up to 90% have been experimentally achieved [89]. The process involves reacting the FG with CaO at $650\text{ }^\circ\text{C}$ and atmospheric pressure to obtain calcium carbonate CaCO_3 and FG without CO_2 [90]. The CaCO_3 is carried to a second reactor where it is calcined at temperatures above $900\text{ }^\circ\text{C}$ with pure oxygen, fuel and CO_2 , and regenerate sorbent (CaO) is produced [90,91]. This technology is very advantageous because it can also work for thermal energy storage. The calcination of solid CaCO_3 with concentrated solar energy produces CO_2 and CaO , which are stored for subsequent use [92]. However, this process requires high levels of energy consumption in the ASU to supply pure O_2 .

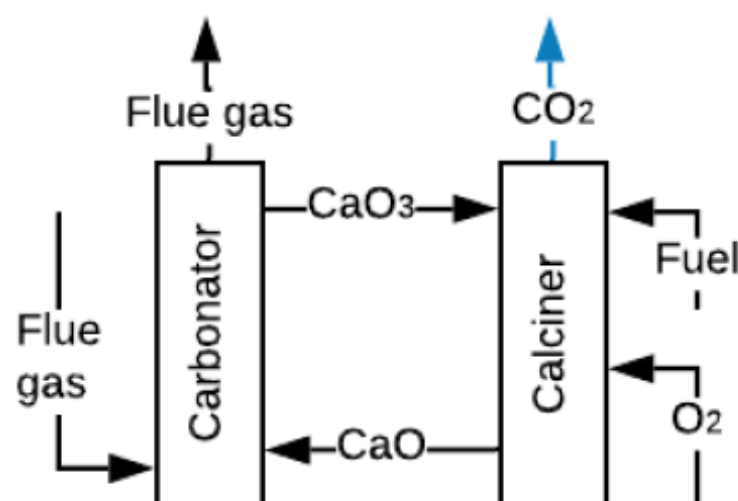


Figure 5. Scheme of the CL process (adapted from [90]).

2.4. Membranes

CO₂ capture with membranes is a concept developed in the nineteen-eighties and includes benefits such as being a compact, flexible and modular solution, as well as ease of maintenance and operation [93,94]. The involved mechanisms are solution/diffusion, adsorption/diffusion, molecular sieve, and ionic transport [46,95]. Figure 6a shows a gas absorption membrane contactor. In this membrane, the CO₂ mass diffuses across the membrane and absorbs into the absorbent [96]. These membranes are usually composed of commercial polymers that absorb the CO₂ from the FG. Figure 6b shows the gas separation membranes. In these membranes, the CO₂ (in the FG at high pressure) diffuses through the membrane pores faster than other components [46]. Membranes that work under the separation principle are manufactured with ceramics, polymers, and blends of both materials [46,97].

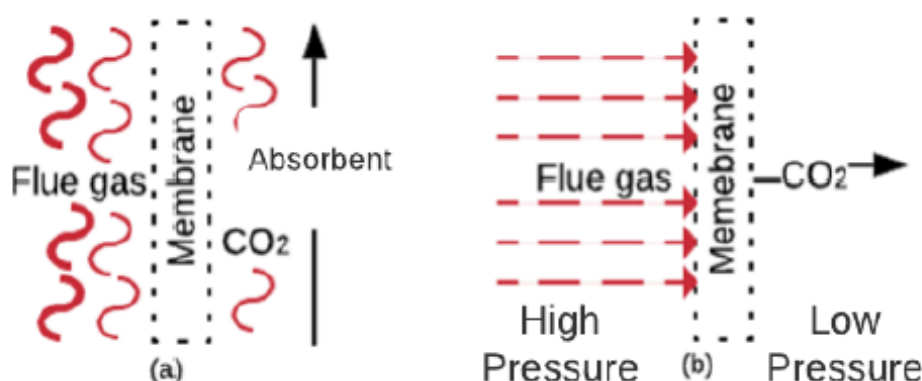


Figure 6. (a) Gas absorption membrane contactor, (b) separation membrane (adapted from [46,95]).

Several studies have tested the use of advanced materials, such as graphene, as fillers in a polymer matrix for separation [98] or have shown that a cascade configuration for compressors improved the energy consumption by achieving an increase in the efficiency of 3.8% with 70% CO₂ separation in real-sized power plants [99]. Mathematical simulations of multi-stage membrane networks for coal-fired power plants [100] have shown that the optimal configuration is a three-stage configuration with a 98% rate of CO₂ capture.

As this technology is in its first stage of implementation, the only applications have occurred at a lab-scale, so that the behaviour at a pilot-scale and full scale remains unknown [66]. Ongoing research is attempting to overcome the capture ratio, which cannot attain good values in only one membrane stage if the concentration of CO₂ is high. For example, for a typical concentration of a coal power plant of approximately 15%, multiple stages of membranes are required, increasing the operational cost [101,102]. However, compared to the absorption process with MEA-scrubbing, membranes are still not competitive, as they need 2.3 times the cost of the operation, according to Jafari et al. [103]. Therefore, several authors have suggested that reducing the price of the membranes would have a significant impact due to the large area required to deal with typical gas flows [104].

2.5. Other Forms for CCS

There are other methods for CO₂ capture that could be excellent alternatives to the previously described methods if the experimental stages are completed. Cryogenic CO₂ capture has been able to accomplish a CO₂ capture of approximately 99.99% [105]. Song et al. [106] describe seven methods (cryogenic packed bed, external cooling loop cryogenic carbon capture, anti-sublimation, cryogenic distillation, controlled freezing zone, cryoCell process and Stirling cooler system) for processing. The main problem with the cryogenic process is the high energy consumption required to keep the temperatures or to increase the

pressures [106], and complications for the CO₂ depositions over the heat transfer surface below its triple point (517 kPa and 56.6 °C) [107]. The bio-fixation of CO₂ with microalgae for biodiesel production is a method that takes advantage of the high photosynthesis rate of microalgae. The process consists of passing the FG through a microalgae crop in the presence of solar radiation so that the microalgae capture the CO₂. Moreover, this process is advantageous because it could be used in parallel with wastewater treatment and thus could result in a double benefit [108].

3. CCS in the Transport Sector

The applicability of the CO₂ capture techniques in mobile sources, specifically in ships and ICE vehicles, faces several challenges, such as space limitations, natural conditions of operation (i.e., rapid acceleration and deceleration), energy requirements for additional devices, low concentrations of CO₂ and low pressures in the FG [42]. In particular, the CO₂ captured (as liquid) storage requires a tank three times larger than the fuel tank because the CO₂ production in mass is three times higher for a mobile source that operates with diesel or gasoline [41]. Several studies of CCS systems mounted in ships and ICEv with the CO₂ capture techniques have been developed previously. These approaches have been conducted from different perspectives, such as economic evaluations, operational conditions, simulations, and experimental oxy-fuel-combustion in ICE, pre-combustion, and even CO₂ bio-fixation. The following sections are focused on the state of the art in CO₂ capture from mobile sources as shown in patents and literature sources.

3.1. Maritime Sector

Shipping is the most efficient mode of transportation from the energy point of view [109], and their GHG emissions represent approximately 2% of global emissions [110]. In 2018, the International Maritime Organization (IMO) established a reduction of at least 50% CO₂ by 2050 as an objective [111]. CCS is an excellent way to achieve this goal, in addition to other technologies to reduce CO₂ emissions, such as hull air lubrication and wind-assist [112]. Furthermore, CO₂ capture in ships is operationally advantageous, as engine loads and velocity are usually constant. These conditions produce constant concentration and FG mass flow (suitable for amine-absorption), and there is available space to install CCS systems. Moreover, it has also thought to perform research into storing the CO₂ in the Liquefied Natural Gas (LNG) tank when it is empty, taking advantage of the temperature and pressure conditions for the LNG storage. It would allow higher cargo space on the ship and, thus, more economic benefits of the CCS system. Table 3 summarises the recently published studies about CCS in the maritime sector reviewed in the following paragraphs.

Table 3. Main results of CO₂ capture in the maritime sector.

Ref.	Method	CO ₂ Technique	Detail	Analysis	Main Results
[113]	Postcombustion	Amine-absorption	MEA at 30 wt% CCR 90%	Economic	€ 73 per ton of captured CO ₂
[114]	Postcombustion	Amine-absorption	MEA at 30 wt% Pz at 30 wt% CCR 60 and 90%	Technical and economic	Pz is 34% more economical than MEA Desorption pressure with Pz at 5 bar Desorption pressure with MEA at 2 bar CO ₂ storage at 11 bar
[115]	Postcombustion	Amine-absorption	MEA at 35 wt% CCR 73 and 90%	Economic	77.5 €/ton CO ₂ at 73% of CCR 163 €/ton CO ₂ at 90% of CCR

Table 3. Cont.

Ref.	Method	CO ₂ Technique	Detail	Analysis	Main Results
[116]	Postcombustion	Amine-absorption	MEA at 35 wt%	Technical and economic	CCR 93% Operational costs decrease when investment is lower than 710,000 USD/MW and the CO ₂ emission tax per unit mass is higher than 32 USD/ton
[117]	Postcombustion	CL	NaOH and CaO	Technical and economic	CCS system requires 24 m ² Operating cost increment of 10.6 and selling the CaCO ₃ of 6.8%
[118]	Postcombustion	Amine-absorption	NH ₃ at 3.5 and 4.1 wt% CCR of 75%	Energy	Reboiler energy consumption is 6.3 and 4.5 MJ/kg CO ₂ at 3.5 and 4.2 wt% of NH ₃
[119]	Postcombustion	Amine-absorption	NH ₃ between 4 and 10 wt% CCR 90%	Energy	Reboiler energy consumption decrease 28.5% for 4% of NH ₃
[120]	Postcombustion	CL	NaOH and CaO	Technical	NaOH flow rate required was 12.52 tons/day CCR of 20%
[121]	Postcombustion	Amine-absorption	MEA at 35 wt%	Energy	CCR of 56.5% tropical conditions
[122]	Postcombustion	Amine-absorption	MDEA at 22% and Pz at 8%	Technical	CCR of 12.2% for 2030 CCR of 34.8% for 2040 CCR of 68.35% for 2050
[123]	Postcombustion	CL	NaOH and CaO	Life cycle	CCR of 37% Life cycle cost is 40% minor than the base configuration
[124]	Pre-combustion	Electromethanol	Hymethship	Life cycle	Reduction of 98% of GWP20 and GWP100
[125]	Postcombustion	Adsorption	K ₂ CO ₃ raw and on an alumina base and support	Technical	CCR of 43% with K ₂ CO ₃ supported on an alumina base
[126]	Postcombustion	Adsorption	K ₂ CO ₃ supported on porous alumina	Energy	CCR of 30% with K ₂ CO ₃ supported on an alumina base Carbonation and regeneration temperatures are 60 and 120 °C, respectively

The maritime sector has focused on investigations on simulations of CO₂ capture employing amine-scrubbing, being the MEA, the Pz, and NH₃ the amines more used [113–115,118,119]. These research works evaluated mainly the CO₂ capture costs and the heat duty in the reboiler varying the CCR, the amine concentration in the solution, the pressure of CO₂ compression, among other variables. As shown in Figure 7, the higher the amine concentration in the solution, the lower the heat duty in the reboiler. It can be explained because there is an increase in the CO₂ loading in the solution, and therefore, there is a lower mass flow of solution for the same CCR, which produces a decrease in required heat duty in the reboiler.

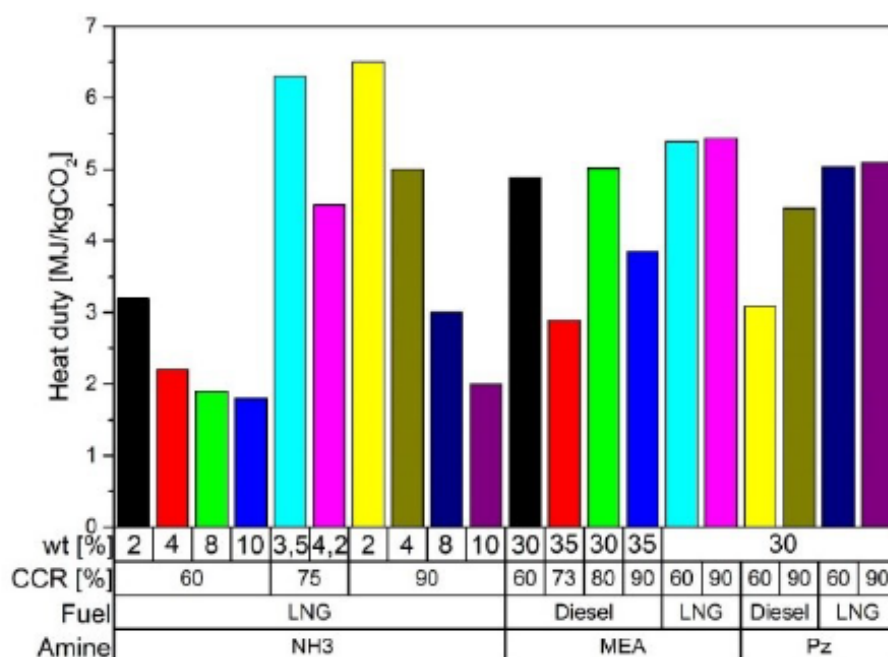


Figure 7. Heat duty in the reboiler (own elaboration from sources [113–115,118,119]).

Figure 7 also leads to predict that an increase of the CCR produces a rise in the heat duty in the reboiler. The absorption heat rules this behaviour because if more CO₂ is captured, it will need more energy in the stripper to clean the solution. Consequently, the CO₂ capture with MEA at 30 wt% presents a higher heat duty than Pz at 30 wt% due to the higher absorption heat of MEA than the Pz. The influence of the fuel is also represented in Figure 7, and it can be found that with Pz at 30 wt%, heating requirements are higher for an ICE fuelled with LNG than an ICE fuelled with diesel because there is less CO₂ emission in an ICE fuelled with LNG. Finally, the gathered results show that the NH₃ requires 3 times less solvent in the solution and 2.5 times less heat duty to achieve a CCR of 90%.

Regarding the CO₂ capture costs summarized in Figure 8, there is a decreasing tendency as the CCR and the amine concentration in the solution increase. The most affordable CO₂ capture cost is with Pz at 90% of CCR and with the engine fuelled with LNG, the value found is close to 100€ per ton of CO₂. It is also observed that the CO₂ capture cost with diesel is the costliest, mainly due to the higher price of this fuel relative to LNG. Fang et al. [116] also found that a ship operation with a CCR of 93% in the CCS system required an investment of 710,000 USD/MW.

Stec et al. [121] showed the influence of atmospheric conditions in the amine-absorption with MEA at 30%. The results show that CCR ranges from 31.4% in arctic conditions to 56.5% in tropical conditions. The higher CCR under tropical conditions can be explained as more waste heat from the FG is recovered, leading to a high CO₂ capture. In addition, Lee et al. [122] studied the scenarios of CO₂ reduction established by the IMO (45% 2030, 55% 2040 and 70% 2050) [113]. The simulation considered a blend MDEA at 22 wt% and Pz at 8 wt% as amines in the CCS system. The results show a reduction of CO₂ in the maritime sector of 12.2, 34.8 and 68.3% in 2030, 2040 and 2050, respectively. These values of CO₂ reduction are lower in 2030 and 2040, but in 2050, the CO₂ reduction value is barely lower than that established by the IMO.

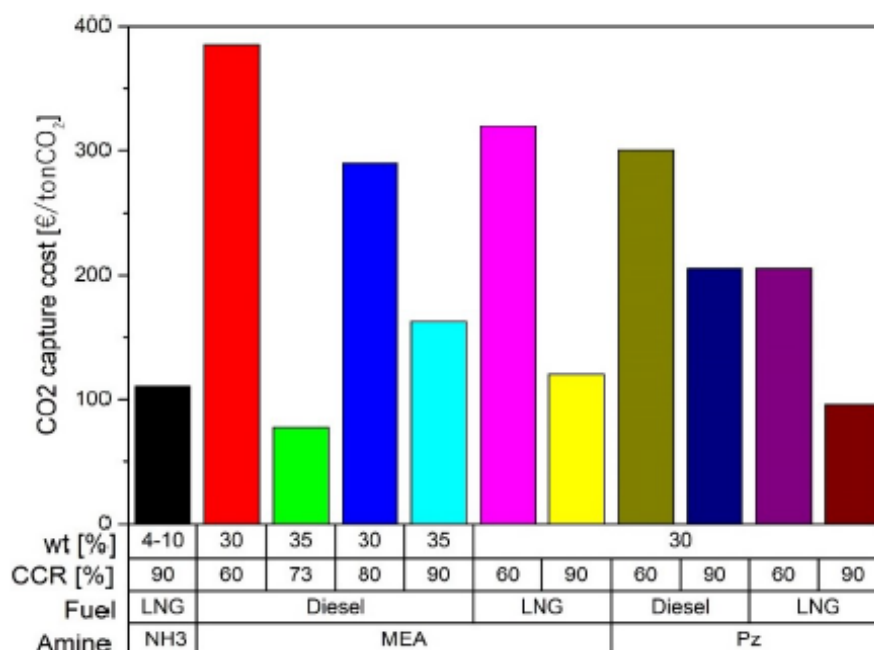


Figure 8. CO₂ capture cost using amine-scrubbing in the maritime sector (own elaboration from sources [113–115,118,119]).

The second technique dealt with in the literature to capture CO₂ in the maritime sector is the CL. Research shows that it is possible to obtain a CCR between 20 and 55.6% [117,120,123]. The operational costs of a ship with a CCS system would suffer an increase of 10.6% that can be reduced to 6.8% after selling the CaCO₃ produced in the CO₂ capture process [117]. However, the life cycle costs can be reduced by 40% compared to a ship without a CCS system [123]. The third technique used in the maritime sector is the adsorption with K₂CO₃ supported on an alumina base. Some experimental tests were carried out with a synthetic composition of FG of a marine diesel engine, obtaining a maximum CCR of 43% using a sorbent with a 3.6 wt% of K₂CO₃, making the carbonation and regeneration processes at 60 and 120 °C, respectively [125,126]. Finally, the last method of CO₂ capture in the maritime sector found in the literature is proposed by Malmgren et al. [124]. It consists in capturing the CO₂ onboard, transporting it to the port, processing it to convert into methanol, and then processing this into the ship through a precombustion process to obtain H₂ (as a fuel of ICE). The life cycle assessment shows that it is possible to reduce climate change variables GWP20 and GWP100 by 98% and the particulate matter by 88% compared to a ship without the CCS system.

The research works found in the literature show that the CO₂ capture in the maritime sector is done chiefly using amine-scrubbing. This inclination in research could be due to the high industrial development that this type of CO₂ capture technology has and the high availability of space on ships for its installation. In addition, a consensus in using waste heat from the FG to supply the energy required by the CCS system was found. Additionally, for the ships that operate with LNG, it is developed to take advantage of the available heat cooling to liquefy the CO₂ captured. According to the review, it is clear that the CO₂ reduction established by the IMO cannot be achieved without a CCS system in the ships. Finally, it is necessary to develop experimental tests to verify all the information provided by the authors, thus trying to close the gap and make the CCS systems in the maritime sector reality.

3.2. Internal Combustion Engines Vehicles (ICEv)

The CCS in vehicles is especially challenging due to the space available for installing devices and store the CO₂ and the additional energy consumption of the system required for CO₂ capture [42]. In this section, a review of patents and research summarized in Table 4 is conducted, focusing on the CO₂ capture techniques and procedures and the extra components in the CCS system to operate.

Table 4. Main results of CO₂ capture in ICEv.

Ref.	Method	CO ₂ Technique	Detail	Analysis	Main Results
[127]	Oxy-fuel combustion	ICRC	O ₂ and water injection	Modelling	Demonstration
[128]	Oxy-fuel combustion	ICRC	SI-ICE, fuel C ₃ H ₈ , 2000 rpm, 40% of O ₂	Performance	Increase in the indicated work of 7.8%
[129]	Oxy-fuel combustion	ICRC	SI-ICE, fuel C ₃ H ₈ , 2000 rpm, 45% of O ₂	Performance	2% reduction in the indicated work
[130–132]	Oxy-fuel combustion	Intake charge EGR and CO ₂	SI-ICE, fuel CH ₄ , 35.4% of O ₂ %	Performance	IMEP: 9.6 bar
[133]	Oxy-fuel combustion	Intake charge and CO ₂	CI-ICE, Fuel diesel	Performance simulation	40 kW of brake power with a CO ₂ fraction 72%, O ₂ ratio 1.5 compression ratio 22
[134]	Oxy-fuel combustion	ICRC	SI-ICE	Performance simulation	EGR 5% Thermal efficiency 42% CFR 26.4%
[135]	Oxy-fuel combustion	ICRC with EGR 60%	SI-ICE fuel C ₃ H ₈	Performance	Indicated work is increased by 7.8%.
[136]	Post-combustion	Amine-absorption	CI-ICE, fuel diesel, MEA 30 wt%, DMEA 30 wt%, NH ₃ 30 wt%	Energy	CCR of 90% regeneration energy 2.2 kWh with MEA CCR of 80% regeneration energy 0.7 kWh with NH ₃ CCR of 90% regeneration energy 1.1 kWh with DMEA
[137]	Post-combustion	Adsorption Absorption	Ford F-250 and Toyota Camry's	Technical	Ford CCR 10%, solid sorbent Toyota CCR 25%, solvent
[138]	Post-combustion	Absorption	Volvo heavy-duty truck	Technical	CCR 40%
[139]	Post-combustion	Adsorption	CI-ICE, fuel diesel and Biodiesel, AC and Calcite as sorbents	Technical	Diesel operation: CCR 11.45% with calcite and CCR 7.29% with AC Biodiesel operation: CCR 15.79% with calcite and CCR 11.76% with AC
[140–142]	Post-combustion	Adsorption	CI-ICE, fuel diesel and blends of KOMA, orange oil, acetone, ethanol or butanol, sorbent AC and Zeolite X13	Technical	Maximum CCR 65% with zeolite X13 CI-ICE fuelled with KOMA, orange oil and methanol
[143]	Post-combustion	Adsorption	CI-ICE, fuel diesel, Sorbent Zeolite X13	Technical	CCR 45%

Table 4. Cont.

Ref.	Method	CO ₂ Technique	Detail	Analysis	Main Results
[144]	Post-combustion	Adsorption	SI-ICE, fuel gasoline, sorbent blend of MEA, zeolite 5A and AC	Technical	CCR 68%
[145]	Post-combustion	Adsorption	SI-ICE, fuel gasoline, sorbent zeolite X13	Technical	CCR 70%
[146]	Post-combustion	Adsorption	SI-ICE, fuel gasoline, sorbent PElS	Technical	CCR 38%
[147]	Post-combustion	Adsorption	SI-ICE, fuel gasoline, sorbent activated alumina	Technical	CCR 7.6%
[148]	Post-combustion	TSA	CI-ICE, fuel diesel, ORC implementation, Sorbent PPN-6-CH ₂ TEFA, CCR 90%	Simulation	It is possible a CCS system operating in CI-ICE for road freight transport without affecting the engine performance
[149]	Post-combustion	absorption Adsorption	Synthetic FG, NaOH and Ca(OH) ₂	Technical	With NaO CCR 100% for 70 min
[150]	Post-combustion	H ₂ Injection	Heavy duty vehicle, Membranes	Simulation	CCR 75%
[151]	Post-combustion	H ₂ Injection RWGS	SI-ICE, fuel CH ₄ operating at 2000 and	Technical	CCR 3.88%
[152]	Bio-fixation	Microalgae	CI-ICE, fuel diesel and biodiesel	Technical	No reported some parameter of CO ₂ reduction

The CCS methods used in ICEv, as found in the literature, are oxy-fuel combustion and post-combustion. According to several patents, oxy-fuel combustion could be conducted by membranes installed in the intake manifold, which separate the O₂ from the air [153–155]. Perovskite membranes can perform this separation of O₂ from the air, but these membranes require high temperatures (approximately 800 °C) to obtain an adequate oxygen flow for the combustion process [156]. This technique is not suitable for ICE because the admission system will need high-temperature materials and a robust cooling system to increase the O₂ density, resulting in higher costs of the ICEv.

Another form to achieve oxy-fuel combustion in ICE's is including an internal combustion Rankine cycle (ICRC). This cycle involves injecting fuel, O₂, and water vapour (to limit the peak temperature in the combustion process) to obtain only CO₂ and water in the FG [127–135]. The experimental tests developed on the engines working in oxy-fuel combustion evaluated the performance and emissions parameters varying the EGR, O₂ concentration, the charge temperature in the intake manifold, compression ratio, among other variables. Obtained results show an increase of the indicated work of 7.8% with a 40% O₂ in the intake manifold and thermal efficiency of 42% with an EGR of 5%. There is a decrease in the total hydrocarbons and CO emissions using wet EGR and an increase of O₂ in the intake charge, and the NO_x emissions present a reduction using wet EGR.

The second CCS method used in ICEv is the post-combustion capture.

Although membranes and microalgae bio-fixation techniques can also be found in the literature, absorption and adsorption are primary methods to capture CO₂. Research

works and patents with amine-scrubbing (absorption) are few. The patents describe how the CCS system would operate in an ICE [157–159]. These patents present new designs of scrubbers, configuration of the reactors, use of elements as TEG's or ORC to take advantage of the waste heat of the FG to supply the system energetically. There is also research and private development with amine scrubbing. The study evaluated experimentally three primary amines at 30 wt% achieving a maximum CCR of 90% with regeneration energy corresponding to the 58% of the energy contained in the FG [136]. However, the regeneration energy of the amines was obtained by energy balance, and it did not consider the energy losses associated with the transformation of thermal energy to mechanical energy. Finally, the company Saudi Aramco has developed two CCS systems by absorption. The first is a solvent system assembled underneath a Toyota Camry's chassis, achieving a CO₂ capture of 25% [137]. The second prototype of the CCS system developed in 2019 uses a solvent based on amino acids, and it was installed at the top of a Class 8 Volvo heavy-duty truck. The company reported a CCR of 40% of this system was achieved [138].

The adsorption has been more investigated than amine-scrubbing to capture CO₂ in ICEv. Several research works have evaluated different sorbents in SI-ICE and CI-ICE. The experimental tests were carried out with a sorbent bed installed in the exhaust gas pipe [139–147]. Figure 9 shows the results of CCR obtained by these investigations. As can be seen in this figure, the Zeolite X13 has the best performance with CCR values above 60% independent on the kind of ICE used. The sorbents impregnated with MEA also had an excellent performance regarding CCR, showing values close to the obtained by the zeolite X13. Both results are a consequence of the high CO₂ loading of zeolite X13 and MEA, which improves CO₂ capture when impregnated in sorbents.

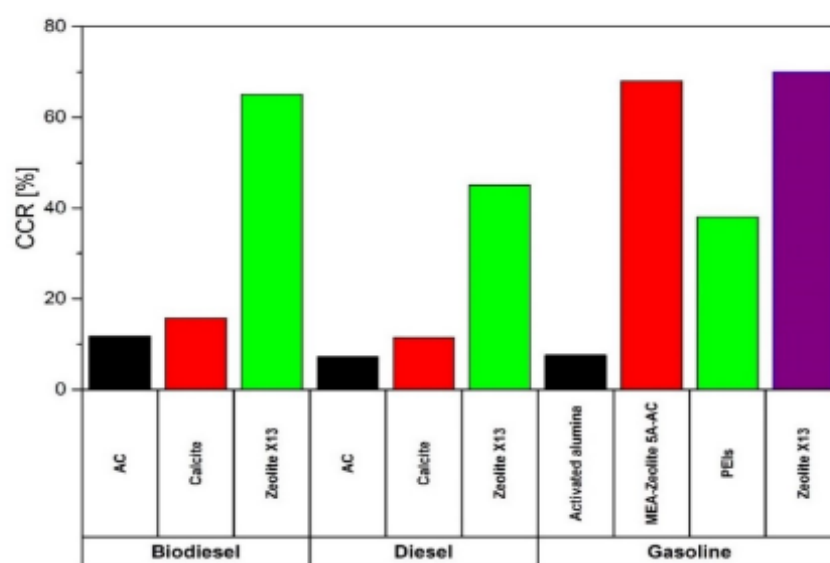


Figure 9. Reported CCR values with several sorbents (own elaboration from sources [139–147]).

It also was found a patent and a private development of CCS systems by adsorption in ICEv by the company Saudi Aramco. According to its website [137], the CCS system by adsorption (2011) consisted of integrating a solid sorbent into a Ford F-250 pickup truck, achieving a captured 10% of the CO₂ emissions. The patent considers using the thermal energy from the FG to regenerate the sorbent and the thermal energy in the cooling engine system to compress the CO₂ [160].

A complete study of the CCS system was performed by Sharma and Maréchal [148]. They made simulations of a TSA system with PPN-6-CH₃ TETA as sorbent, a rotary wheel

adsorbed for the process of regeneration of the sorbent and desorption of the CO_2 , an ORC, and heat pump for the energy requirements, and a CCR of 90%. The CO_2 captured comes from a delivery truck that consumes 50 L of diesel and produces 117 kg of CO_2 during 8 h of operation. The results show that it is possible to conduct the CO_2 capture only with the energy supply by the FG. Although it is a comprehensive study, it does not consider the rpm and load engine variations, which could affect the performance of the CCS system proposed.

Devices that allow the use of solvents or sorbents for CO_2 capture are also reported [149,161]. These devices achieve a CCR of 100% for periods of 70 min. However, it then drops to zero after 220 min of operation. Another CO_2 capture technique proposed in post-combustion is the use of a high flux MFI-Alumina Hollow Fibers membrane. According to the simulations performed by Pera et al. [150], up to 75% CO_2 can be captured with a 95% purity if a cascade of two hollow-fibre units is used.

Bio-fixation with microalgae or injection of H_2 into the FG to produce methane through a reverse water-gas shift (RWGS) to use it again as a fuel in the engine have been also studied [151,152]. Despite being novel techniques, these techniques reported a low CCR and methane conversion. However, they are still far from being well developed to be considered in the short term.

This section has summarized the most important results obtained in the investigations related to the capture of CO_2 in ICEv. As can be seen, patents on post-combustion by adsorption and absorption and oxi-fuel combustion with membranes were found. Regarding research works, experimental tests were carried out on post-combustion by adsorption, oxi-fuel combustion and bio-fixation. Simulations of post-combustion by adsorption and absorption and oxi-fuel combustion and membranes were also conducted.

Although there is a greater variety in CO_2 capture techniques, only two works on post-combustion (one with adsorption and the other with TSA) consider the sorbent or amine regeneration and the CO_2 storage. According to these works, the CO_2 capture and storage could be done without affecting ICE performance. However, these works were performed under stationary conditions, and they did not consider variables such as the rpm and engine load in which a road freight transport vehicle would operate. The sorbents with the best results are sorbent impregnated with MEA, Zeolite X13 and PPN's as sorbents. On the other hand, several research works developed interesting concepts of the CCS system on ICEv. However, these concepts are still impractical because the ICEv would need some modifications, such as additional tanks, reactors, fuel injection systems, and other devices.

4. Case Study

The transport sector of long distances will continue operating with the conventional combustion processes to obtain power. On this basis and considering the current developments in CCS technologies, there are significant opportunities to implant these technologies in ICE once the main challenges related to the operational characteristics have been overcome. After the review conducted in this paper, the TSA method is shown as the most suitable for CO_2 capture in ICEv, but some research regarding practical and operational issues is lacking. This section estimates the energy and space requirements to install such a CCS system without affecting the engine's performance.

4.1. Engine Selection

Two commercial engines used for road (bus) and maritime transport (ship) operating with CNG or LNG are selected. The engines are four-stroke, water cooling, turbo charged with aftercooler and multipoint fuel injection. Table 5 summarizes the main technical information of the engines.

Table 5. Technical specifications of engines.

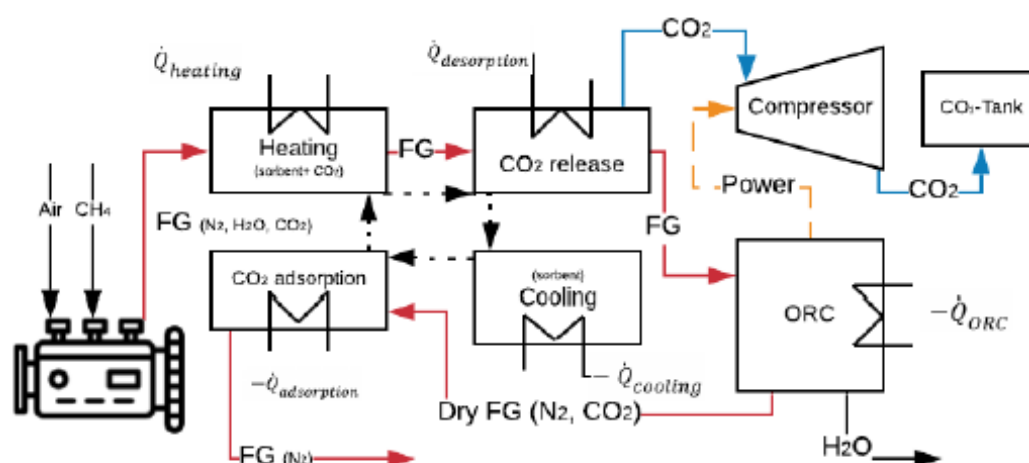
Engine	BUS (M936G) [162]	Ship (W9L46DF) [163]
Architecture	In-line 6-cylinder engine	In-line 9-cylinder engine
Intake	Wastegate Turbocharged with Aftercooler	Turbocharged with Aftercooler
Injection	Multipoint—Stoichiometric combustion	Multipoint
Displacement volume [L]	7.7	867.6
Brake Power [kW]	222 at 1950 rpm	10,305 at 600 rpm
Fuel Consumption [kg/km]	0.361 at average velocity of 20.75 km/h [164]	NA
Specific Fuel Consumption [g/kWh]	194 at 1950 rpm and 100% engine load	165 at 600 rpm and 75% engine load

4.2. Sorbent Selection

The sorbents selected for the case study should have low regeneration energy and high q and CO_2/N_2 selectivity. From the data in Table 2, the sorbents with the best values of the properties mentioned above are: PPN-6- CH_2 -DETA, MOF-74-Mg, and Zeolite-X13.

4.3. CCS System Description

As previously set, a CCS system with TSA for the CO_2 capture operating in an ICE is considered. The CCS system will use the residual heat from the FG to increase the sorbent temperature and CO_2 desorption. The remaining thermal energy in the FG is transformed into mechanical energy to produce power for the CO_2 compression using an ORC. The ORC is one of the most studied and developed methods for that purpose [165]. In addition, this process produces the FG cooling, thus reducing the required power to finish cooling the sorbent, which is necessary for the adsorption process of CO_2 . Figure 10 shows the sketch of the CCS system proposed.

**Figure 10.** Mass and energy balance of the CCS system proposed to operate in ICE.

Initially, the CCS system will be considered to work with a CCR of 90%. Suppose the CCS system does not get to operate at a CCR of 90% without energy penalties. In that case, the highest CCR for each sorbent will be calculated, following the same procedure developed previously. Finally, with the results obtained before, the CO₂ volume stored and the sorbent volume in the TSA process will be calculated. Calculations are described in the following sections.

4.4. Energy Balance

It is assumed that the engines will be fuelled with CH₄ with a stoichiometric combustion process (air-fuel ratio of 17.13). The species in the FG will be only CO₂, H₂O and N₂. The energy analysis for the engine M936G will take three temperatures corresponding at low, medium, and high engine loads as reported in research works (600, 700 and 800 K) for turbocharged SI-ICE [166,167]. The energy analysis for the maritime engine W9L46DF is done at 75% of engine load and 700 K FG temperature. Finally, the reference temperature taken for the calculations is 300 K. The mass fractions of the species in the FG and specific heats at the evaluated temperatures (obtained from the software EES) are listed in Table 6.

Table 6. Mass fraction and c_p at the evaluated temperatures of the FG.

Species	Mass Fraction (x) [%]	c_p at 600 K [kJ/kgK]	c_p at 700 K [kJ/kgK]	c_p at 800 K [kJ/kgK]
CO ₂	0.1514	1.075	1.126	1.168
H ₂ O	0.1239	1.954	2.08	2.147
N ₂	0.7245	1.075	1.098	1.122

The available thermal energy is calculated at the turbine outlet of the SI-ICE (Equation (1)). As can be seen in this equation, it is necessary to obtain the FG mass flow, which is the sum of the air and fuel mass at the engine inlet. In the marine engine, this value is brought by the datasheet and, in the engine, it is the product of the fuel consumption per the average velocity (see Table 5). In addition, it is necessary to obtain the specific heat of the FG (c_{p-FG}) (Equation (2)). Finally, the difference temperature (ΔT) is the difference between the FG temperature in the turbine outlet and the reference temperature.

$$\dot{Q} = \dot{m}_{FG} c_{p-FG} \Delta T \quad (1)$$

$$c_{p-FG} = x_{CO_2} c_{p-CO_2} + x_{N_2} c_{p-N_2} + x_{H_2O} c_{p-H_2O} \quad (2)$$

The regeneration heat for the sorbents ($\dot{Q}_{reg-sorb}$) is the sum of the sensible heat (\dot{Q}_{sen}) and the desorption heat (\dot{Q}_{des}) (Equations (3) and (4)). The ΔT in the \dot{Q}_{sen} takes into account a desorption temperature of 150 °C reported in the literature as a suitable temperature for the sorbents [73,168], and it is assumed an adsorption temperature of 30 °C. The desorption heat of the sorbents is taken from Table 2. Table 7 shows the results found.

$$\dot{Q}_{reg-sorb} = \dot{Q}_{des} + \dot{Q}_{sen} \quad (3)$$

$$\dot{Q}_{reg-sorb} = 0.9 x_{CO_2} \dot{m}_{FG} \Delta H_{des} + c_{p-CO_2} 0.9 x_{CO_2} \dot{m}_{FG} \Delta T + c_{p-ads} \frac{0.9 x_{CO_2} \dot{m}_{FG}}{q} \Delta T \quad (4)$$

Table 7. Regeneration heat at 90% of CCR for each sorbent and available heat in the FG at low, medium, and full engine load.

Engine	FG Mass Flow [kg/s]	Sorbent	Regeneration Heat for a CCR 90% [kW]	Available Heat [kW]		
				600 K	700 K	800 K
M936G	0.03772	PPN-6-CH ₂ -DETA	11.2	13.4	18.5	23.7
		MOF-74-Mg	7.3			
		Zeolite X13	10.1			
W9L46DF	12.3	PPN-6-CH ₂ -DETA	2737.5	NA	6021.4	NA
		MOF-74-Mg	2240.5			
		Zeolite X13	3291.5			

Finally, the energy analysis is completed obtaining the power consumption to compress the CO₂. To obtain this, firstly, the power output of the ORC (\dot{W}_{out}) (Equation (5)) is calculated. This equation takes the remaining heat in the FG (\dot{Q}_{rem}) (Equation (6)), and an ORC cycle efficiency of 20%, that according to the literature, is the average value of ORC cycle efficiency working in ICE [169,170]. Tables 8 and 9 show the results of the \dot{Q}_{rem} and \dot{W}_{out} for each sorbent at the different evaluation temperatures.

$$\dot{W}_{out} = \eta_{ORC} \dot{Q}_{rem} \quad (5)$$

$$\dot{Q}_{rem} = \dot{Q}_{FG} - \dot{Q}_{reg} \quad (6)$$

Table 8. Remaining heat in the FG at low, medium, and full engine load for both engines.

Engine	M936G			W9L46DF		
	PPN-6-CH ₂ -DETA	MOF-74-Mg	Zeolite X13	PPN-6-CH ₂ -DETA	MOF-74-Mg	Zeolite X13
\dot{Q}_{rem} at 600 K [kW]	2.169	6.094	3.303	NA	NA	NA
\dot{Q}_{rem} at 700 K [kW]	7.238	11.163	8.373	3283.9	3780.9	2729.9
\dot{Q}_{rem} at 800 K [kW]	12.460	16.385	13.594	NA	NA	NA

Table 9. Power output of the ORC at low, medium, and full engine load for both engines.

Engine	M936G			W9L46DF		
	PPN-6-CH ₂ -DETA	MOF-74-Mg	Zeolite X13	PPN-6-CH ₂ -DETA	MOF-74-Mg	Zeolite X13
\dot{W}_{out} at 600 K [kW]	0.434	1.219	0.661	NA	NA	NA
\dot{W}_{out} at 700 K [kW]	1.448	2.233	1.675	656.8	756.2	545
\dot{W}_{out} at 800 K [kW]	2.492	3.277	2.719	NA	NA	NA

The power consumption of the CO₂ compressor (\dot{W}_{com}) is obtained using the software ASPEN Plus. The simulation conditions are 1 bar, 150 °C (desorption temperature) at the inlet, 75 bar at the outlet. The compressor has an isentropic efficiency of 0.85 (Equation (7)).

$$\dot{W}_{com} = \frac{0.9 * x_{CO_2} * \dot{m}_{FG} (h_2 - h_1)}{\eta_s} \quad (7)$$

The same calculation procedure is performed to estimate the maximum CCR that the CCS system could reach. However, it is not realistic to consider FG temperatures above or equal to 800 K during the engine performance at partial loads. In this case, a conservative temperature of 700 K for flue gases is considered. Table 9 shows the results obtained for each sorbent and engine.

4.5. Space Requirement

The space requirements for the CCS system are obtained in volume terms. The CO₂ will be stored as a liquid at 75 bar and 25 °C, under these conditions, the CO₂ density (ρ_{CO_2-L}) is 762.6 kg/m³. The procedure starts obtaining the CO₂ mass that will be stored. For this, it is assumed an operation of 8 h (Equation (8)). As shown in Figure 4, the TSA process is divided into four stages, and it is assumed that each stage will operate for 30 min. The sorbent mass and volume are calculated based on the previous assumptions (Equations (9) and (10)). Finally, the CO₂ volume is obtained (Equation (11)), and the total volume of the CCS system is the sum of the CO₂ and sorbent volumes (Equation (12)).

$$m_{CO_2} = 28800 CCR x_{CO_2} \dot{m}_{FG} \quad (8)$$

$$m_{sor} = \frac{m_{CO_2}}{4q} \quad (9)$$

$$V_{sor} = \frac{m_{sor}}{\rho_{sor}} \quad (10)$$

$$V_{CO_2} = \frac{m_{CO_2}}{\rho_{CO_2-L}} \quad (11)$$

$$V_T = V_{sor} + V_{CO_2} \quad (12)$$

4.6. Results

Following the methodology described in the previous section, the quantities of remaining heat in the FG, the maximum CCR, ORR power, CO₂ compression power, CO₂ volume to store, and the CCS system's total volume are estimated.

4.6.1. Energy Results

The results in Table 7 show that the available heat in the FG would be enough to regenerate the sorbent in the TSA process for all temperatures in both engines. This margin increases with the rise of the ΔT . Similarly, the remaining heat in the FG and the output power in the ORC have the same behaviour, as can be seen in Tables 8 and 9.

The power consumptions of the CO₂ compressor (\dot{W}_{com}) are 3.159 and 1029.9 kW for the M936G and the W9L46DF engines, respectively. Contrasting the results in Table 9 with the results of \dot{W}_{com} , it can be seen that the power output in the ORC working at an FG temperature of 800 K can cover the power consumption for the CO₂ compressor with the CCS system using MOF-74-Mg as sorbent. In the other cases, the ORC cannot produce the power required to compress the CO₂ under the FG temperatures and the established CCR. Moreover, the ICE in a vehicle will never continuously be operated at 100% of engine load. For that reason, we proceed to obtain the maximum CCR for each sorbent in both engines at 700 K of FG temperature that allows covering the CO₂ compression without using additional energy from the ICE.

As shown in Figure 11, the sorbent MOF-74-Mg can achieve a CCR of 73% in both engines without affecting the engine's performance. The sorbent PPN-6-CH₂-DETA reaches 68% of CCR. Finally, the Zeolite X13 obtained a CCR of 64%. However, with this last result, the CO₂ purity is 94.6%, while with the other sorbents, the CO₂ purity is higher than 99.5%.

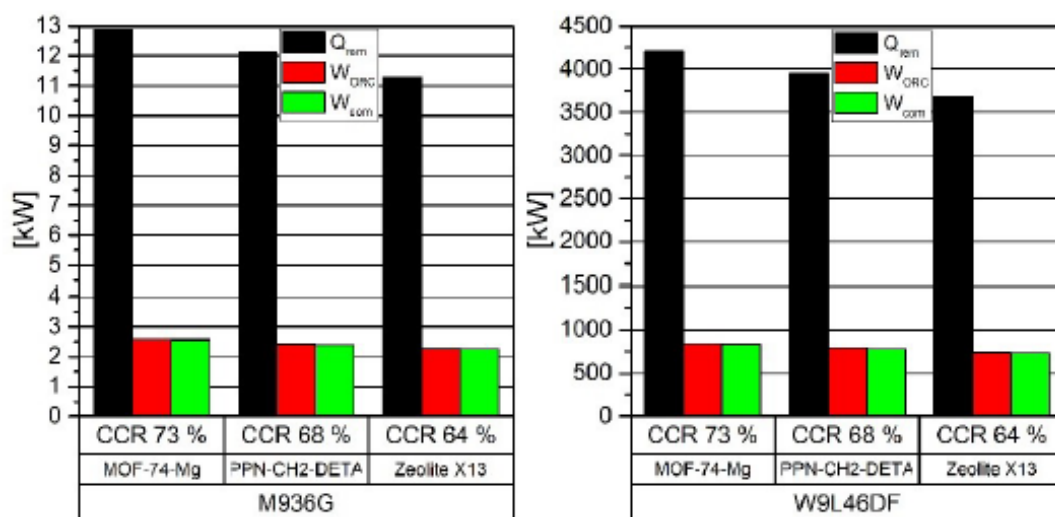


Figure 11. Remaining heat, ORC power, CO₂ compression power and maximum CCR in the engines.

4.6.2. Space Results

As mentioned before, the selected sorbents are PPN-6-CH₂-DETA and MOF-74-Mg due to high selectivity that allow a CO₂ purity greater than 99.5%. In addition, the lowest CCR obtained of both sorbents will be used to compare the final volume resulting. Table 10 shows the results obtained.

Table 10. Volume calculations for adsorption materials.

Engine	M936G		W9L46DF	
Sorbent	PPN-CH ₂ -DETA	MOF-74-Mg	PPN-CH ₂ -DETA	MOF-74-Mg
CO ₂ Mass (68% of CCR) [kg]	28.0	28.0	9116.0	9116.0
CO ₂ loading [kgCO ₂ /kg _{ads}]	0.235	0.278	0.235	0.278
Sorbent mass [kg]	118.8	100.5	38726	32782
Sorbent density [kg/m ³]	805.00	914.88	805.00	914.88
Sorbent Volume [m ³]	0.148	0.110	48.106	35.832
CO ₂ Volume stored [m ³]	0.147	0.147	47.815	47.815
Total volume [m ³]	0.295	0.257	95.922	83.647

5. Discussion

PPN-6-CH₂-DETA and MOF-74-Mg as sorbents in TSA resulted into a CCR above 68% in both engines without affecting the engine performance. These results are mainly a consequence of the low regeneration heat of the sorbents. Therefore, there is still high thermal energy in the FG when it enters the ORC, producing more power output to cover the power required to compress the CO₂ potentially.

Regarding sorbent selection, selectivity plays an important role in the CO₂ purity obtained at the end of the process. For this reason, Zeolite X13 is discarded from the other sorbents studied in the following step because it achieves a CO₂ purity of 94.6%, which is minor in 5 points than the other sorbents. The purification of CO₂ captured when Zeolite X13 in TSA is used requires additional energy that the engine could not provide.

In a potential application, the FG must be dried completely as far as the selected sorbents lose CO₂ uptake capacity. Then, it is expected that an additional cooling system will be required, which could imply parasitic loads not considered in this research. A comprehensive simulation of the integration of the CCS system and engine, which involves cooling and drying of the FG should be done. However, this is out of the scope of this paper.

The CCS system volume obtained with TSA for a CCR of 68% is approximately 0.3 m³ for the M936G engine (0.295 and 0.257 m³ with PPN-6-CH₂-DETA and MOF-74-Mg, respectively). This engine usually operates in buses or trucks, allowing the CCS system to be mounted on the vehicle roof. It would not differ from other vehicles working with hydrogen fuel cells. For example, the Toyota Sora Bus uses hydrogen tanks that required 6 m³ [171]. If the same bus used two CCS systems with MOF-74-Mg to achieve a CCR of 100%, the CCS system only would require 0.6 m³, and added the volume of the fuel tank the global volume (CCS system and fuel tank) would be of 1.6 m³ approximately, which is 3.75 times smaller. Therefore, the values obtained in this research show that installing a CCS with TSA is practical in road freight transport.

In the marine engine, the mass of the sorbent is close to 40 tons, and the CCS volume is 90 m³. These are small values for ships because they usually have a large capacity of cargo and volume. The CCS system with TSA is presented as an excellent alternative to reduce CO₂ emissions in the maritime sector.

Space requirements were obtained by considering the crystallographic density as it was impossible to obtain reliable and comparable bulk density data. Table 11 shows the values of the total volume assuming a bulk density as half of the crystallographic density. It is observed that the total volume has an increase of 50% with PPN-6-CH₂-DETA and 43% with MOF-74-Mg in both engines. However, these values continue being lower than for the commercial vehicle previously mentioned and for a cargo ship.

Table 11. Volume calculations for adsorption materials with bulk density.

Engine	M936G		W9L46DF	
	PPN-CH ₂ -DETA	MOF-74-Mg	PPN-CH ₂ -DETA	MOF-74-Mg
CO ₂ Mass (68% of CCR) [kg]	28.0	28.0	9116.0	9116.0
CO ₂ loading [kgCO ₂ /kg _{ads}]	0.235	0.278	0.235	0.278
Sorbent mass [kg]	118.8	100.5	38,726	32,782
Sorbent density [kg/m ³]	402.5	457.44	402.5	457.44
Sorbent Volume [m ³]	0.295	0.220	96.213	71.664
CO ₂ Volume stored [m ³]	0.147	0.147	47.815	47.815
Total volume [m ³]	0.442	0.366	144.028	119.479

6. Conclusions

A review of the CO₂ capture in mobile sources and a case study to evaluate the potential of CCS systems to reduce the CO₂ produced by ICE were made in this study. According to the detailed review presented here, the patents describe the devices or procedures used to carry out the CO₂ capture. At the same time, research works show experimental tests or simulations of CO₂ capture.

The choice of these two capture methods is based on the performance of the typical engines used in each sector and the available space for additional devices. As the ICE

in a ship regularly operates at a constant regime (rpm and engine load), the continuous variation in the FG mass flow is not expected. This behaviour allows amine scrubbing to be more suitable for this operation. In addition, the cargo ships count with ample space available for the installation of devices required for a CCS system.

On the contrary, the ICEs mounted in road transport vehicles work with variable accelerations and available space to install the required equipment of a CCS system is scarce. For this case, adsorption is shown as the best option because it is a regenerative cyclical process that adapts to different mass flows of exhaust gases. In addition, according to the results obtained in the case study, it could require less space than other commercial vehicles using other CO₂ reduction technologies.

The review shows that the research works have a higher level of development in the maritime sector than in the road transport sector. In addition, it was observed that the amine-absorption technology is the most used in the marine transport sector, and adsorption is preferable in the ICEv. Therefore, the TSA and amine-absorption are the most suitable pre-existing CCS technologies for CO₂ capture for mobile sources due to their well-developed technology and low energy requirements. However, experimental reports on CO₂ capture in ICEv lack information about the experimental conditions, such as engine load, RPM, and the energy of regeneration of the sorbent or solvent.

The results obtained in the case study show the first approximation of a CCS system operating with TSA and an ORC to take advantage of the thermal energy of the FG produced by ship engines. Regarding road freight transport, the results obtained in the case study show a big difference from the study done by Sharma and Maréchal (the most complete study so far). They report that it is possible to obtain a 90% CO₂ capture without affecting the engine performance. The results found in the present case study show that it is possible to achieve this CCR but with sorbent MOF74-Mg at 800 K of FG temperature. However, taking a high FG temperature is not realistic because the engine operates at different engine loads and rpm. The best result obtained in the present case study is 73% of CCR with a temperature corresponding to the medium engine load. Nevertheless, the development of several studies contributes to close the gap to achieve the CO₂ reduction targets established by the European Union for the ICE driven transport sector.

CNG and LNG are the fuels that should be used by the mobile source with operating a CCS system. First, these fuels produce less CO₂ emissions than an ICE fuelled with diesel or gasoline, allowing a higher autonomy in terms of CO₂ storage. Second, the CNG or LNG could be obtained from methanation with the CO₂ and hydrogen produced from RES, and thus keep the door open to a sustainable and circular transport system centred on ICE.

A system that uses the TSA technique for CO₂ capture was theoretically evaluated. According to the results, it is possible to obtain a CCR of 73% and a small volume to operate a CCS system without any supply of additional energy with TSA and MOF-74-Mg as sorbent at a medium engine load condition.

This paper highlights that capture in mobile sources can be developed with available technology, opening opportunities for CO₂ capture in road freight and maritime transport. However, research must continue until a suitable commercial technology is demonstrated to reduce the CO₂ in the atmosphere.

Future research works must give detailed information on the behaviour of the CCS system at partial engines loads and at several rpm conditions, the reduction in engine performance due to backpressure caused by the installation of additional devices in the exhaust pipe, as well as the increase in fuel consumption due to the additional weight of the CCS systems installed in the vehicles. According to US EPA, each 45 kg of extra weight in vehicles originates a 1% increase in the fuel consumption, although this affects smaller vehicles more (less than 2720 kg of weight) than larger ones such as buses or trucks [172,173]. In addition, it is necessary to do detailed research on the degradation of sorbent due to the impact of minor species present in the FG as NO_x and unburned hydrocarbons. Finally, research on energy demands and economic and environmental life

cycle assessments is required to conclude the viability of installing a CCS system in mobile sources.

Author Contributions: Conceptualization, A.G.-M. and E.L.-S.; methodology, A.G.-M. and E.L.-S.; software, A.G.-M.; validation, A.G.-M. and E.L.-S.; formal analysis, A.G.-M. and E.L.-S.; investigation, A.G.-M. and E.L.-S.; resources, A.G.-M.; data curation, A.G.-M.; writing—original draft preparation, A.G.-M. and E.L.-S.; writing—review and editing, A.G.-M. and E.L.-S.; supervision, E.L.-S. All authors have read and agreed to the published version of the manuscript.

Funding: This research received no external funding.

Institutional Review Board Statement: Not applicable.

Informed Consent Statement: Not applicable.

Data Availability Statement: The data will be made available at reasonable request from the corresponding author.

Acknowledgments: A part of this study was developed thanks to the support of the Scholarships for Iberoamerican Doctoral Students granted by the Universidad de Zaragoza—Santander Universidades, the CIRCE Research Institute, and the aid by the Research Groups of the Aragon Government (I46_17R).

Conflicts of Interest: The authors declare no conflict of interest.

Abbreviations

The following abbreviations are used in this manuscript

\dot{Q}_{des}	Desorption Heat
$\dot{Q}_{reg-sorb}$	Sorbent Regeneration Heat
\dot{Q}_{rem}	Remaining Heat in the FG
\dot{Q}_{sen}	Sensible Heat
\dot{W}_{com}	CO ₂ Compressor Power
\dot{W}_{out}	ORC Power Output
ΔH_{abs}	Absorption Heat
ΔH_{ads}	Adsorption Heat
c_p	Specific Heat
ΔT	Difference Temperature
AC	Activate Carbon
ASU	Air Separator Units
CCS	CO ₂ Capture and Storage
CL	Carbonate Looping
CLC	Chemical Looping Combustion
DEA	Diethanolamine
EU	European Union
EVs	Electric Vehicles
FG	Flue gas
ICE	Internal Combustion Engines
ICEv	Internal Combustion Engine Vehicles
ICRC	Internal Combustion Rankine Cycle
IMO	International Maritime Organization
LNG	Liquified Natural Gas
LPG	Liquefied Petroleum Gas
MDEA	Methyl Diethanolamine
MEA	Ethanolamine
MOFs	Metal-Organic Frameworks
NG	Natural Gas

ORC	Organic Rankine Cycle
PPNs	Porous Polymer Networks
PTG	Power to Gas
Pz	Piperazine
RWGS	Reverse Water-Gas Shift
TEG	Thermo-Electric Generators
TSA	Temperature Swing Adsorption
US-EPA	United States Environmental Protection Agency
q	CO ₂ Loading Capacity
x	Mass Fraction
ρ	Density

References

- IEA Total Final Consumption (TFC) by Sector, World 1990–2017. Available online: [https://www.iea.org/data-and-statistics?country=WORLD&fuel=Energy%20consumption&indicator=Total%20final%20consumption%20\(TFC\)%20by%20sector](https://www.iea.org/data-and-statistics?country=WORLD&fuel=Energy%20consumption&indicator=Total%20final%20consumption%20(TFC)%20by%20sector) (accessed on 27 November 2019).
- Bellocchi, S.; De Falco, M.; Gambini, M.; Manno, M.; Stilo, T.; Vellini, M. Opportunities for power-to-Gas and Power-to-liquid in CO₂-reduced energy scenarios: The Italian case. *Energy* **2019**, *175*, 847–861. [CrossRef]
- Hof, A.F.; den Elzen, M.G.J.; Admiraal, A.; Roelfsema, M.; Germaat, D.E.H.J.; van Vuuren, D.P. Global and regional abatement costs of Nationally Determined Contributions (NDCs) and of enhanced action to levels well below 2 °C and 1.5 °C. *Environ. Sci. Policy* **2017**, *71*, 30–40. [CrossRef]
- European Commission. *A Clean Planet for all A European Long-Term Strategic Vision for a Prosperous, Modern, Competitive and Climate Neutral Economy*; European Commission: Luxembourg, 2018; Volume 773, p. 114.
- Tamborra, M. European Commission, DG Research. 2006. Available online: <https://www.iccr.org/> (accessed on 27 November 2019).
- Akram, M.; Ali, U.; Best, T.; Blakey, S.; Finney, K.N.; Pourkashanian, M. Performance evaluation of PACT Pilot-plant for CO₂ capture from gas turbines with Exhaust Gas Recycle. *Int. J. Greenh. Gas Control* **2016**, *47*, 137–150. [CrossRef]
- Leach, F.; Kalghatgi, G.; Stone, R.; Miles, P. The scope for improving the efficiency and environmental impact of internal combustion engines. *Transp. Eng.* **2020**, *1*, 100005. [CrossRef]
- Huang, Y.; Ng, E.C.Y.; Zhou, J.L.; Surawski, N.C.; Chan, E.F.C.; Hong, G. Eco-driving technology for sustainable road transport: A review. *Renew. Sustain. Energy Rev.* **2018**, *93*, 596–609. [CrossRef]
- Fafoutellis, P.; Mantouka, E.G.; Vlahogianni, E.I. Eco-driving and its impacts on fuel efficiency: An overview of technologies and data-driven methods. *Sustainability* **2021**, *13*, 226. [CrossRef]
- Agudelo, A.E.; Garcia-Contreras, R.; Agudelo, J.R.; Armas, O. Potential for exhaust gas energy recovery in a diesel passenger car under European driving cycle. *Appl. Energy* **2016**, *174*, 201–212. [CrossRef]
- Merkisz, J.; Fuc, P.; Lijewski, P.; Ziolkowski, A.; Wojciechowski, K.T. The Analysis of Exhaust Gas Thermal Energy Recovery Through a TEG Generator in City Traffic Conditions Reproduced on a Dynamic Engine Test Bed. *J. Electron. Mater.* **2015**, *44*, 1704–1715. [CrossRef]
- Arsie, L.; Cricchio, A.; Pianese, C.; Ricciardi, V.; De Cesare, M. Modeling analysis of waste heat recovery via thermo-electric generator and electric turbo-compound for CO₂ reduction in automotive SI engines. *Energy Procedia* **2015**, *82*, 81–88. [CrossRef]
- Sprouse, C.; Depcik, C. Review of organic Rankine cycles for internal combustion engine exhaust waste heat recovery. *Appl. Therm. Eng.* **2013**, *51*, 711–722. [CrossRef]
- Kühlwein, J. Driving Resistances of Light-Duty Vehicles in Europe: Present Situation, Trends and Scenarios for 2025. *Communications* **2016**, *49*, 847129–102.
- European Commission. *Roadmap to a Single European Transport Area—Towards a Competitive and Resource Efficient Transport System*; European Commission: Brussels, Belgium, 2011.
- EV-Volumes—The Electric Vehicle World Sales Database. Available online: <https://www.ev-volumes.com/news/global-bev-ph-ev-sales-for-2019/> (accessed on 29 November 2019).
- Amarakoon, S.; Smith, J.; Segal, B. *Lithium-ion Batteries and Nanotechnology for Electric Vehicles*; EPA 744-R-12-001; US Environmental Protection Agency: Washington, DC, USA, 2012.
- European Environmental Agency. *Greenhouse Gas Emissions from Transport in Europe—European Environment Agency*; European Environmental Agency: København, Denmark, 2018; pp. 1–7.
- Wang, D.; Li, S.; Liu, F.; Gao, L.; Sui, J. Post combustion CO₂ capture in power plant using low temperature steam upgraded by double absorption heat transformer. *Appl. Energy* **2018**, *227*, 603–612. [CrossRef]
- New Wave of CCS Activity: Ten Large-Scale Projects Announced—Global CCS Institute. Available online: <https://www.globalccsinstitute.com/news-media/press-room/media-releases/new-wave-of-ccs-activity-ten-large-scale-projects-announced/> (accessed on 17 February 2020).
- International Energy Agency. *20 Years Carbon Capture Storage*; OECD: Paris, France, 2016. [CrossRef]

22. Evely, V.; Gebreegziabher, T. A Review of Projected Power-to-Gas Deployment Scenarios. *Energies* **2018**, *11*, 1824. [\[CrossRef\]](#)
23. Llera, E.; Romeo, L.M.; Bailera, M.; Osorio, J.L. Exploring the integration of the power to gas technologies and the sustainable transport. *Int. J. Energy Prod. Manag.* **2018**, *3*, 1–9. [\[CrossRef\]](#)
24. Streibel, M.; Nakaten, N.; Kempka, T.; Kühn, M. Analysis of an integrated carbon cycle for storage of renewables. *Energy Procedia* **2013**, *40*, 202–211. [\[CrossRef\]](#)
25. Kühn, M.; Nakaten, N.; Streibel, M.; Kempka, T. CO₂ geological storage and utilization for a carbon neutral “power-to-gas-to-power” cycle to even out fluctuations of renewable energy provision. *Energy Procedia* **2014**, *63*, 8044–8049. [\[CrossRef\]](#)
26. Götz, M.; Lefebvre, J.; Mörs, F.; McDaniel Koch, A.; Graf, F.; Bajohr, S.; Reimert, R.; Kolb, T. Renewable Power-to-Gas: A technological and economic review. *Renew. Energy* **2016**, *85*, 1371–1390. [\[CrossRef\]](#)
27. Rönsch, S.; Schneider, J.; Matthischke, S.; Schlüter, M.; Götz, M.; Lefebvre, J.; Prabhakaran, P.; Bajohr, S. Review on methanation—From fundamentals to current projects. *Fuel* **2016**, *166*, 276–296. [\[CrossRef\]](#)
28. Hagos, D.A.; Ahlgren, E. *A State-of-the Art Review on the Development of CNG/LNG Infrastructure and Natural Gas Vehicles (NGVs)*; Chalmers University of Technology: Göteborg, Sweden, 2017.
29. Osorio-Tejada, J.L.; Llera-Sastresa, E.; Scarpellini, S. A multi-criteria sustainability assessment for biodiesel and liquefied natural gas as alternative fuels in transport systems. *J. Nat. Gas Sci. Eng.* **2017**, *42*, 169–186. [\[CrossRef\]](#)
30. Osorio-Tejada, J.L.; Llera-Sastresa, E.; Scarpellini, S. Liquefied natural gas: Could it be a reliable option for road freight transport in the EU? *Renew. Sustain. Energy Rev.* **2017**, *71*, 785–795. [\[CrossRef\]](#)
31. Kalghatgi, G.; Levinsky, H.; Colket, M. Future transportation fuels. *Prog. Energy Combust. Sci.* **2018**, *69*, 103–105. [\[CrossRef\]](#)
32. Horvath, S.; Fasihi, M.; Breyer, C. Techno-economic analysis of a decarbonized shipping sector: Technology suggestions for a fleet in 2030 and 2040. *Energy Convers. Manag.* **2018**, *164*, 230–241. [\[CrossRef\]](#)
33. Mikulić, H.; Ridjan Skov, I.; Dominković, D.E.; Wan Alwi, S.R.; Manan, Z.A.; Tan, R.; Duić, N.; Hidayah Mohamad, S.N.; Wang, X. Flexible Carbon Capture and Utilization technologies in future energy systems and the utilization pathways of captured CO₂. *Renew. Sustain. Energy Rev.* **2019**, *114*, 109338. [\[CrossRef\]](#)
34. Boot-Handford, M.E.; Abanades, J.C.; Anthony, E.J.; Blunt, M.J.; Brandani, S.; Mac Dowell, N.; Fernández, J.R.; Ferrari, M.C.; Gross, R.; Hallett, J.P.; et al. Carbon capture and storage update. *Energy Environ. Sci.* **2014**, *7*, 130–189. [\[CrossRef\]](#)
35. Belaissaoui, B.; Le Moullec, Y.; Willson, D.; Favre, E. Hybrid membrane cryogenic process for post-combustion CO₂ capture. *J. Memb. Sci.* **2012**, *415–416*, 424–434. [\[CrossRef\]](#)
36. Voldsund, M.; Gardarsdottir, S.O.; De Lena, E.; Pérez-Calvo, J.F.; Jamali, A.; Berstad, D.; Fu, C.; Romano, M.; Roussanaly, S.; Anantharaman, R.; et al. Comparison of technologies for CO₂ capture from cement production—Part 1: Technical evaluation. *Energies* **2019**, *12*, 559. [\[CrossRef\]](#)
37. MacDowell, N.; Florin, N.; Buchard, A.; Hallett, J.; Galindo, A.; Jackson, G.; Adjiman, C.S.; Williams, C.K.; Shah, N.; Fennell, P. An overview of CO₂ capture technologies. *Energy Environ. Sci.* **2010**, *3*, 1645–1669. [\[CrossRef\]](#)
38. Sipőcz, N.; Hernandez-Nogales, A.; Gonzalez-Salazar, M.A.; Shisler, R.; Lissianski, V. Low temperature CO₂ capture for near-term applications. *Energy Procedia* **2013**, *37*, 1228–1238. [\[CrossRef\]](#)
39. Hu, Y.; Yan, J. Characterization of flue gas in oxy-coal combustion processes for CO₂ capture. *Appl. Energy* **2012**, *90*, 113–121. [\[CrossRef\]](#)
40. Olajire, A.A. CO₂ capture and separation technologies for end-of-pipe applications—A review. *Energy* **2010**, *35*, 2610–2628. [\[CrossRef\]](#)
41. Wang, H.; Zhou, P.; Wang, Z. Reviews on current carbon emission reduction technologies and projects and their feasibilities on ships. *J. Mar. Sci. Appl.* **2017**, *16*, 129–136. [\[CrossRef\]](#)
42. Sullivan, J.M.; Sivak, M. *Carbon Capture in Vehicles: A Review of General Support, Available Mechanisms, and Consumer Acceptance Issues*; University of Michigan, Ann Arbor, Transportation Research Institute: Ann Arbor, MI, USA, 2012.
43. Echevarria Huaman, R.N. A Review on: CO₂ Capture Technology on Fossil Fuel Power Plant. *J. Fundam. Renew. Energy Appl.* **2015**, *5*. [\[CrossRef\]](#)
44. Joel, A.S.; Wang, M.; Ramshaw, C. Modelling and simulation of intensified absorber for post-combustion CO₂ capture using different mass transfer correlations. *Appl. Therm. Eng.* **2015**, *74*, 47–53. [\[CrossRef\]](#)
45. Salazar, J.; Diwekar, U.; Joback, K.; Berger, A.H.; Bhowan, A.S. Solvent selection for post-combustion CO₂ capture. *Energy Procedia* **2013**, *37*, 257–264. [\[CrossRef\]](#)
46. Mondal, M.K.; Balsora, H.K.; Varshney, P. Progress and trends in CO₂ capture/separation technologies: A review. *Energy* **2012**, *46*, 431–441. [\[CrossRef\]](#)
47. Jonshagen, K.; Sipőcz, N.; Genrup, M. A Novel Approach of Retrofitting a Combined Cycle with Post Combustion CO₂ Capture. *J. Eng. Gas Turbines Power* **2011**, *133*, 1–7. [\[CrossRef\]](#)
48. Xue, B.; Yu, Y.; Chen, J.; Luo, X.; Wang, M. A comparative study of MEA and DEA for post-combustion CO₂ capture with different process configurations. *Int. J. Coal Sci. Technol.* **2017**, *4*, 15–24. [\[CrossRef\]](#)
49. Zhai, R.; Liu, H.; Wu, H.; Yu, H.; Yang, Y. Analysis of integration of MEA-based CO₂ capture and solar energy system for coal-based power plants based on thermo-economic structural theory. *Energies* **2018**, *11*, 1284. [\[CrossRef\]](#)
50. Goto, K.; Yogo, K.; Higashii, T. A review of efficiency penalty in a coal-fired power plant with post-combustion CO₂ capture. *Appl. Energy* **2013**, *111*, 710–720. [\[CrossRef\]](#)

51. Eldardiry, H.; Habib, E. Carbon capture and sequestration in power generation: Review of impacts and opportunities for water sustainability. *Energy Sustain. Soc.* **2018**, *8*, 6. [\[CrossRef\]](#)
52. Hanak, D.P.; Biliyok, C.; Manovic, V. Efficiency improvements for the coal-fired power plant retrofit with CO₂ capture plant using chilled ammonia process. *Appl. Energy* **2015**, *151*, 258–272. [\[CrossRef\]](#)
53. Borhani, T.N.; Wang, M. Role of solvents in CO₂ capture processes: The review of selection and design methods. *Renew. Sustain. Energy Rev.* **2019**, *114*, 109299. [\[CrossRef\]](#)
54. Sada, E.; Kumazawa, H.; Butt, M.A. Gas absorption with consecutive chemical reaction: Absorption of carbon dioxide into aqueous amine solutions. *Can. J. Chem. Eng.* **1976**, *54*, 421–424. [\[CrossRef\]](#)
55. Kim, Y.E.; Lim, J.A.; Jeong, S.K.; Yoon, Y.L.; Bae, S.T.; Nam, S.C. Comparison of carbon dioxide absorption in aqueous MEA, DEA, TEA, and AMP solutions. *Bull. Korean Chem. Soc.* **2013**, *34*, 783–787. [\[CrossRef\]](#)
56. El Hadri, N.; Quang, D.V.; Goetheer, E.L.V.; Abu Zahra, M.R.M. Aqueous amine solution characterization for post-combustion CO₂ capture process. *Appl. Energy* **2017**, *185*, 1433–1449. [\[CrossRef\]](#)
57. Derks, P.W.J.; Versteeg, G.F. Kinetics of absorption of carbon dioxide in aqueous ammonia solutions. *Energy Procedia* **2009**, *1*, 1139–1146. [\[CrossRef\]](#)
58. Qin, F.; Wang, S.; Kim, I.; Svendsen, H.F.; Chen, C. Heat of absorption of CO₂ in aqueous ammonia and ammonium carbonate/carbamate solutions. *Int. J. Greenh. Gas Control.* **2011**, *5*, 405–412. [\[CrossRef\]](#)
59. Qi, G.; Wang, S.; Yu, H.; Wardhaugh, L.; Feron, P.; Chen, C. Development of a rate-based model for CO₂ absorption using aqueous NH₃ in a packed column. *Int. J. Greenh. Gas Control.* **2013**, *17*, 450–461. [\[CrossRef\]](#)
60. Yang, N.; Yu, H.; Li, L.; Xu, D.; Han, W.; Feron, P. Aqueous Ammonia (NH₃) Based Post Combustion CO₂ Capture: A Review. *Oil Gas Sci. Technol.* **2014**, *69*, 931–945. [\[CrossRef\]](#)
61. Yu, H.; Morgan, S.; Allport, A.; Cottrell, A.; Do, T.; Wardhaugh, J.M.G.L.; Feron, P. Results from trialling aqueous NH₃ based post combustion capture in a pilot plant at Munmorah power station: Desorption. *Chem. Eng. Res. Des.* **2012**, *89*, 753–758. [\[CrossRef\]](#)
62. Bishnoi, S.; Rochelle, G.T. Absorption of carbon dioxide into aqueous piperazine: Reaction kinetics, mass transfer and solubility. *Chem. Eng. Sci.* **2000**, *55*, 5531–5543. [\[CrossRef\]](#)
63. Chen, X.; Rochelle, G.T. Aqueous piperazine derivatives for CO₂ capture: Accurate screening by a wetted wall column. *Chem. Eng. Res. Des.* **2011**, *89*, 1693–1710. [\[CrossRef\]](#)
64. Singto, S.; Supap, T.; Idem, R.; Tontiwachwuthikul, P.; Tantayanon, S. The Effect of Chemical Structure of Newly Synthesized Tertiary Amines Used for the Post Combustion Capture Process on Carbon dioxide (CO₂): Kinetics of CO₂ Absorption Using the Stopped-Flow Apparatus and Regeneration, and Heat Input of CO₂ Regeneration. *Energy Procedia* **2017**, *114*, 852–859. [\[CrossRef\]](#)
65. Ali, B.S.; Aroua, M.K. Effect of piperazine on CO₂ loading in aqueous solutions of MDEA at low pressure. *Int. J. Thermophys.* **2004**, *25*, 1863–1870. [\[CrossRef\]](#)
66. Wang, Y.; Zhao, L.; Otto, A.; Robinius, M.; Stolten, D. A Review of Post-combustion CO₂ Capture Technologies from Coal-fired Power Plants. *Energy Procedia* **2017**, *114*, 650–665. [\[CrossRef\]](#)
67. Conway, W.; Yang, Q.; James, S.; Wei, C.C.; Bown, M.; Feron, P.; Puxty, G. Designer amines for post combustion CO₂ capture processes. *Energy Procedia* **2014**, *63*, 1827–1834. [\[CrossRef\]](#)
68. Thompson, J.; Matin, N.; Liu, K. Solubility and Thermodynamic Modeling of Carcinogenic Nitrosamines in Aqueous Amine Solvents for CO₂ Capture. *Energy Procedia* **2017**, *114*, 1038–1044. [\[CrossRef\]](#)
69. Kimura, H.; Kubo, T.; Shimada, M.; Kitamura, H.; Fujita, K.; Suzuki, K.; Yamamoto, K.; Akai, M. Environmental Risk Assessment of MEA and its Degradation Products from Post-combustion CO₂ Capture Pilot Plant: Drafting Technical Guidelines. *Energy Procedia* **2017**, *114*, 6490–6500. [\[CrossRef\]](#)
70. Kumar, S.; Srivastava, R.; Koh, J. Utilization of zeolites as CO₂ capturing agents: Advances and future perspectives. *J. CO₂ Util.* **2020**, *41*, 101251. [\[CrossRef\]](#)
71. Lu, C.; Bai, H.; Wu, B.; Su, E.; Hwang, J.F. Comparative study of CO₂ capture by carbon nanotubes, activated carbons, and zeolites. *Energy Fuels* **2008**, *22*, 3050–3056. [\[CrossRef\]](#)
72. Hinkov, I.; Lamari, F.D.; Langlois, P.; Dicko, M.; Chilver, C.; Pentchev, I. Carbon dioxide capture by adsorption (review). *J. Chem. Technol. Metall.* **2016**, *51*, 609–626.
73. Verdegaa, W.M.; Wang, K.; Sculley, J.P.; Wriedt, M.; Zhou, H.C. Evaluation of Metal-Organic Frameworks and Porous Polymer Networks for CO₂-Capture Applications. *ChemSusChem* **2016**, *9*, 636–643. [\[CrossRef\]](#)
74. Yu, P.; Luo, Z.; Wang, Q.; Fang, M.; Zhou, J.; Wang, W.; Liang, X.; Cai, W. Activated carbon-based CO₂ uptake evaluation at different temperatures: The correlation analysis and coupling effects of the preparation conditions. *J. CO₂ Util.* **2020**, *40*, 101214. [\[CrossRef\]](#)
75. Veneman, R.; Kamphuis, H.; Brilman, D.W.F. Post-combustion CO₂ capture using supported amine sorbents: A process integration study. *Energy Procedia* **2013**, *37*, 2100–2108. [\[CrossRef\]](#)
76. Hasan, M.M.E.; Baliban, R.C.; Elia, J.A.; Floudas, C.A. Modeling, simulation, and optimization of postcombustion CO₂ capture for variable feed concentration and flow rate. 2. Pressure swing adsorption and vacuum swing adsorption processes. *Ind. Eng. Chem. Res.* **2012**, *51*, 15665–15682. [\[CrossRef\]](#)
77. Zhang, W.; Liu, H.; Sun, Y.; Cakstins, J.; Sun, C.; Snape, C.E. Parametric study on the regeneration heat requirement of an amine-based solid adsorbent process for post-combustion carbon capture. *Appl. Energy* **2016**, *168*, 394–405. [\[CrossRef\]](#)

78. Huck, J.M.; Lin, L.C.; Berger, A.H.; Shahrak, M.N.; Martin, R.L.; Bhowan, A.S.; Haranczyk, M.; Reuter, K.; Smit, B. Supporting Information: Evaluating different classes of porous materials for carbon capture. *Energy Environ. Sci.* **2014**, *7*, 4132–4146. [\[CrossRef\]](#)
79. Quang, D.V.; El Hadri, N.; Abu-zahra, M.R.M. Reduction in the regeneration energy of CO₂ capture process by impregnating amine solvent onto precipitated silica. *Eur. Sci. J.* **2013**, *9*, 82–102.
80. Won, W.; Lee, S.; Lee, K.S. Modeling and parameter estimation for a fixed-bed adsorption process for CO₂ capture using zeolite 13X. *Sep. Purif. Technol.* **2012**, *85*, 120–129. [\[CrossRef\]](#)
81. Al Mousa, A.; Abouelnasr, D.; Loughlin, K.F. Saturation loadings on 13X (faujasite) zeolite above and below the critical conditions Part II: Unsaturated and cyclic hydrocarbons data evaluation and modeling. *Adsorption* **2015**, *21*, 321–332. [\[CrossRef\]](#)
82. Hedin, N.; Andersson, L.; Bergström, L.; Yan, J. Adsorbents for the post-combustion capture of CO₂ using rapid temperature swing or vacuum swing adsorption. *Appl. Energy* **2013**, *104*, 418–433. [\[CrossRef\]](#)
83. Creamer, A.E.; Gao, B. Carbon-based adsorbents for postcombustion CO₂ capture: A critical review. *Environ. Sci. Technol.* **2016**, *50*, 7276–7289. [\[CrossRef\]](#) [\[PubMed\]](#)
84. Raganati, F.; Chirone, R.; Ammendola, P. CO₂ Capture by Temperature Swing Adsorption: Working Capacity as Affected by Temperature and CO₂ Partial Pressure. *Ind. Eng. Chem. Res.* **2020**, *59*, 3593–3605. [\[CrossRef\]](#)
85. Song, C.; Kansha, Y.; Fu, Q.; Ishizuka, M.; Tsutsumi, A. Reducing energy consumption of advanced PTSA CO₂ capture process: Experimental and numerical study. *J. Taiwan Inst. Chem. Eng.* **2016**, *64*, 69–78. [\[CrossRef\]](#)
86. Zanco, S.E.; Joss, L.; Hefti, M.; Gazzani, M.; Mazzotti, M. Addressing the Criticalities for the Deployment of Adsorption-based CO₂ Capture Processes. *Energy Procedia* **2017**, *114*, 2497–2505. [\[CrossRef\]](#)
87. Marx, D.; Joss, L.; Hefti, M.; Mazzotti, M. Temperature Swing Adsorption for Postcombustion CO₂ Capture: Single- and Multicolumn Experiments and Simulations. *Ind. Eng. Chem. Res.* **2016**, *55*, 1401–1412. [\[CrossRef\]](#)
88. Dhoke, C.; Zaabout, A.; Cloete, S.; Amini, S. Review on Reactor Configurations for Adsorption-Based CO₂ Capture. *Ind. Eng. Chem. Res.* **2021**, *60*, 3779–3798. [\[CrossRef\]](#)
89. Ströhle, J.; Junk, M.; Kremer, J.; Galloy, A.; Epple, B. Carbonate looping experiments in a 1 MWth pilot plant and model validation. *Fuel* **2014**, *127*, 13–22. [\[CrossRef\]](#)
90. Perejón, A.; Romeo, L.M.; Lara, Y.; Lisbona, P.; Martínez, A.; Valverde, J.M. The Calcium-Looping technology for CO₂ capture: On the important roles of energy integration and sorbent behavior. *Appl. Energy* **2016**, *162*, 787–807. [\[CrossRef\]](#)
91. Alonso, M.; Rodríguez, N.; González, B.; Grasa, G.; Murillo, R.; Abanades, J.C. Carbon dioxide capture from combustion flue gases with a calcium oxide chemical loop. Experimental results and process development. *Int. J. Greenh. Gas Control.* **2010**, *4*, 167–173. [\[CrossRef\]](#)
92. Ortiz, C.; Romano, M.C.; Valverde, J.M.; Binotti, M.; Chacartegui, R. Process integration of Calcium-Looping thermochemical energy storage system in concentrating solar power plants. *Energy* **2018**, *155*, 535–551. [\[CrossRef\]](#)
93. Ahmad, J.; Rehman, W.U.; Deshmukh, K.; Basha, S.K.; Ahamed, B.; Chidambaram, K. Recent Advances in Poly (Amide-B-Ethylene) Based Membranes for Carbon Dioxide (CO₂) Capture: A Review. *Polym. Technol. Mater.* **2019**, *58*, 366–383. [\[CrossRef\]](#)
94. Turi, D.M.; Ho, M.; Ferrari, M.C.; Chiesa, P.; Wiley, D.E.; Romano, M.C. CO₂ capture from natural gas combined cycles by CO₂ selective membranes. *Int. J. Greenh. Gas Control.* **2017**, *61*, 168–183. [\[CrossRef\]](#)
95. Sifat, N.S.; Haseli, Y. A critical review of CO₂ capture technologies and prospects for clean power generation. *Energies* **2019**, *12*, 4143. [\[CrossRef\]](#)
96. Khaisri, S.; deMontigny, D.; Tontiwachwuthikul, P.; Jiratananon, R. Comparing membrane resistance and absorption performance of three different membranes in a gas absorption membrane contactor. *Sep. Purif. Technol.* **2009**, *65*, 290–297. [\[CrossRef\]](#)
97. Norahim, N.; Yaisanga, P.; Faungnawakij, K.; Charinpanitkul, T.; Klaysom, C. Recent Membrane Developments for CO₂ Separation and Capture. *Chem. Eng. Technol.* **2018**, *41*, 211–223. [\[CrossRef\]](#)
98. Fernández-Barquín, A.; Casado-Coterillo, C.; Etxeberria-Benavides, M.; Zufiga, J.; Irabien, A. Comparison of Flat and Hollow-Fiber Mixed-Matrix Composite Membranes for CO₂ Separation with Temperature. *Chem. Eng. Technol.* **2017**, *40*, 997–1007. [\[CrossRef\]](#)
99. Franz, J.; Schiebahn, S.; Zhao, L.; Riensche, E.; Scherer, V.; Stolten, D. Investigating the influence of sweep gas on CO₂/N₂ membranes for post-combustion capture. *Int. J. Greenh. Gas Control.* **2013**, *13*, 180–190. [\[CrossRef\]](#)
100. Arias, A.M.; Mussati, M.C.; Mores, P.L.; Scenna, N.J.; Caballero, J.A.; Mussati, S.F. Optimization of multi-stage membrane systems for CO₂ capture from flue gas. *Int. J. Greenh. Gas Control.* **2016**, *53*, 371–390. [\[CrossRef\]](#)
101. Favre, E. Carbon dioxide recovery from post-combustion processes: Can gas permeation membranes compete with absorption? *J. Memb. Sci.* **2007**, *294*, 50–59. [\[CrossRef\]](#)
102. Zhao, L.; Riensche, E.; Blum, L.; Stolten, D. Multi-stage gas separation membrane processes used in post-combustion capture: Energetic and economic analyses. *J. Memb. Sci.* **2010**, *359*, 160–172. [\[CrossRef\]](#)
103. Jafari, M.; Ghasemzadeh, K.; Amiri, T.Y.; Basile, A. Comparative Study of Membrane and Absorption Processes Performance and their Economic Evaluation for CO₂ Capturing from Flue Gas. *Gas Process. J.* **2019**, *7*, 37–52.
104. Zhao, L.; Weber, M.; Stolten, D. Comparative investigation of polymer membranes for post-combustion capture. *Energy Procedia* **2013**, *37*, 1125–1134. [\[CrossRef\]](#)
105. Yousef, A.M.; El-Maghlany, W.M.; Eldrainy, Y.A.; Attia, A. New approach for biogas purification using cryogenic separation and distillation process for CO₂ capture. *Energy* **2018**, *156*, 328–351. [\[CrossRef\]](#)

106. Song, C.; Liu, Q.; Deng, S.; Li, H.; Kitamura, Y. Cryogenic-based CO₂ capture technologies: State-of-the-art developments and current challenges. *Renew. Sustain. Energy Rev.* **2019**, *101*, 265–278. [\[CrossRef\]](#)
107. Berger, A.H.; Hoeger, C.; Baxter, L.; Bhowan, A.S. Evaluation of Cryogenic Systems for Post Combustion CO₂ Capture. In Proceedings of the 14th Greenhouse Gas Control Technologies Conference, Melbourne, Australia, 21–26 October 2018; pp. 1–8.
108. Razzak, S.A.; Ali, S.A.M.; Hossain, M.M.; deLasa, H. Biological CO₂ fixation with production of microalgae in wastewater—A review. *Renew. Sustain. Energy Rev.* **2017**, *76*, 379–390. [\[CrossRef\]](#)
109. Christodoulou, A.; Gonzalez-Aregall, M.; Linde, T.; Vierth, L.; Cullinane, K. Targeting the reduction of shipping emissions to air. *Marit. Bus. Rev.* **2019**, *4*, 16–30. [\[CrossRef\]](#)
110. Roussanal, S.; Jakobsen, J.P.; Hognes, E.H.; Brunsvold, A.L. Benchmarking of CO₂ transport technologies: Part I—Onshore pipeline and shipping between two onshore areas. *Int. J. Greenh. Gas Control.* **2013**, *19*, 584–594. [\[CrossRef\]](#)
111. IMO Energy Efficiency and the Reduction of GHG Emissions from Ships. Available online: <http://www.imo.org/en/MediaCentre/HotTopics/GHG/Pages/default.aspx> (accessed on 10 June 2020).
112. Comer, A.B.; Chen, C.; Rutherford, D. *Relating Short-Term Measures to IMO's Minimum 2050 Emissions Reduction Target*; International Council on Clean Transportation: Washington, DC, USA, 2018.
113. Van den Akker, J. *Carbon Capture Onboard LNG-Fueled Vessels*; Delft University of Technology: Delft, The Netherlands, 2017.
114. Feenstra, M.; Monteiro, J.; van den Akker, J.T.; Abu-Zahra, M.R.M.; Gilling, E.; Goetheer, E. Ship-based carbon capture onboard of diesel or LNG-fuelled ships. *Int. J. Greenh. Gas Control.* **2019**, *85*, 1–10. [\[CrossRef\]](#)
115. Luo, X.; Wang, M. Study of solvent-based carbon capture for cargo ships through process modelling and simulation. *Appl. Energy* **2017**, *195*, 402–413. [\[CrossRef\]](#)
116. Fang, S.; Xu, Y.; Li, Z. Joint generation and demand-side management for shipboard carbon capture and storage system. *Conf. Rec. Ind. Commer. Power Syst. Tech. Conf.* **2019**, *2019*, 1–8. [\[CrossRef\]](#)
117. Fang, S.; Xu, Y.; Li, Z.; Ding, Z.; Liu, L.; Wang, H. Optimal Sizing of Shipboard Carbon Capture System for Maritime Greenhouse Emission Control. *IEEE Trans. Ind. Appl.* **2019**, *55*, 1. [\[CrossRef\]](#)
118. Awoyomi, A.; Patchigolla, K.; Anthony, E.J. CO₂/SO₂ emission reduction in CO₂ shipping infrastructure. *Int. J. Greenh. Gas Control.* **2019**, *88*, 57–70. [\[CrossRef\]](#)
119. Awoyomi, A.; Patchigolla, K.; Anthony, E.J. Process and Economic Evaluation of an Onboard Capture System for LNG-Fueled CO₂ Carriers. *Ind. Eng. Chem. Res.* **2020**, *59*, 6951–6960. [\[CrossRef\]](#)
120. Zhou, P.; Wang, H. Carbon capture and storage—Solidification and storage of carbon dioxide captured on ships. *Ocean Eng.* **2014**, *91*, 172–180. [\[CrossRef\]](#)
121. Stec, M.; Tatarczuk, A.; Iluk, T.; Szul, M. Reducing the energy efficiency design index for ships through a post-combustion carbon capture process. *Int. J. Greenh. Gas Control.* **2021**, *108*, 103333. [\[CrossRef\]](#)
122. Lee, S.; Yoo, S.; Park, H.; Ahn, J.; Chang, D. Novel methodology for EEDI calculation considering onboard carbon capture and storage system. *Int. J. Greenh. Gas Control.* **2021**, *105*, 103241. [\[CrossRef\]](#)
123. Triviza, N.L.; Rentzelas, A.; Theotokatos, G. Impact of carbon pricing on the cruise ship energy systems optimal configuration. *Energy* **2019**, *175*, 952–966. [\[CrossRef\]](#)
124. Malmgren, E.; Brynolf, S.; Fridell, E.; Grahn, M.; Andersson, K. The environmental performance of a fossil-free ship propulsion system with onboard carbon capture—A life cycle assessment of the HyMethShip concept. *Sustain. Energy Fuels* **2021**, *5*, 2753–2770. [\[CrossRef\]](#)
125. Balsamo, M.; Erto, A.; Lancia, A.; Di Natale, F. Carbon dioxide capture from model marine diesel engine exhaust by means of K₂CO₃-based sorbents. *Chem. Eng. Trans.* **2016**, *52*, 415–420. [\[CrossRef\]](#)
126. Erto, A.; Balsamo, M.; Paduano, L.P.; Lancia, A.; Di Natale, F. Utilization of alumina-supported K₂CO₃ as CO₂-selective sorbent: A promising strategy to mitigate the carbon footprint of the maritime sector. *J. CO₂ Util.* **2018**, *24*, 139–148. [\[CrossRef\]](#)
127. Bilger, R.W.; Wu, Z. Carbon capture for automobiles using internal combustion rankine cycle engines. *J. Eng. Gas Turbines Power* **2009**, *131*, 1–4. [\[CrossRef\]](#)
128. Yu, X.; Wu, Z.; Fu, L.; Deng, J.; Hu, Z.; Li, L. Study of combustion characteristics of a quasi internal combustion rankine cycle engine. *SAE Tech. Pap.* **2013**. [\[CrossRef\]](#)
129. Yu, X.; Wu, Z.; Wang, C.; Deng, J.; Hu, Z.; Li, L. Study of the combustion and emission characteristics of a quasi ICRC engine under different engine loads. *SAE Tech. Pap.* **2014**. [\[CrossRef\]](#)
130. Van Blarigan, A.C.; Seiser, R.; Chen, J.Y.; Cattolica, R.; Dibble, R.W. Working fluid composition effects on methane oxycombustion in an SI-engine: EGR vs. CO₂. *Proc. Combust. Inst.* **2013**, *34*, 2951–2958. [\[CrossRef\]](#)
131. Van Blarigan, A.; Kozarac, D.; Seiser, R.; Cattolica, R.; Chen, J.-Y.; Dibble, R. Experimental Study of Methane Fuel Oxycombustion in a Spark-Ignited Engine. *J. Energy Resour. Technol.* **2014**, *136*, 012203. [\[CrossRef\]](#)
132. Van Blarigan, A.; Kozarac, D.; Seiser, R.; Chen, J.Y.; Cattolica, R.; Dibble, R. Spark-ignited engine NO_x emissions in a low-nitrogen oxycombustion environment. *Appl. Energy* **2014**, *118*, 22–31. [\[CrossRef\]](#)
133. Li, X.; Peng, Z.; Ajmal, T.; Aitouche, A.; Mobasheri, R.; Pei, Y.; Gao, B.; Wellers, M. A feasibility study of implementation of oxy-fuel combustion on a practical diesel engine at the economical oxygen-fuel ratios by computer simulation. *Adv. Mech. Eng.* **2020**, *12*, 1–13. [\[CrossRef\]](#)
134. Yu, X.; Wu, Z. Simulation on Effect of EGR on Oxy-fuel IC Engine.pdf. *Appl. Mech. Mater.* **2012**, *130*, 790–795. [\[CrossRef\]](#)

135. Wu, Z.J.; Yu, X.; Fu, L.Z.; Deng, J.; Li, L.G. Experimental study of the effect of water injection on the cycle performance of an internal-combustion Rankine cycle engine. *Proc. Inst. Mech. Eng. Part D J. Automob. Eng.* **2014**, *228*, 580–588. [CrossRef]
136. Kumar, P.; Rathod, V.; Parwani, A.K. Experimental investigation on performance of absorbents for carbon dioxide capture from diesel engine exhaust. *Environ. Prog. Sustain. Energy* **2021**, *40*, e13651. [CrossRef]
137. Aramco Capturing Carbon on the Move. Available online: <https://www.aramco.com/en/creating-value/technology-development/transport-technologies/mobile-carbon-capture#> (accessed on 19 February 2021).
138. Al-Meshari, A.A.; Muhaish, E.I.; Aleidan, A.A. Carbon Capture: Saudi Aramco's Carbon Management Program. *J. Pet. Technol.* **2014**, *66*, 72–74. [CrossRef]
139. Subramanian, T.; Sonthalia, A.; Varuvel, E.G. Effect of calcite/activated carbon-based post-combustion CO₂ capture system in a biodiesel-fueled CI engine—An experimental study. *Energy Sources Part A Recovery Util. Environ. Eff.* **2018**, *41*, 1972–1982. [CrossRef]
140. Thiagarajan, S.; Edwin Geo, V.; Martin, L.J.; Nagalingam, B. Carbon dioxide (CO₂) capture and sequestration using biofuels and an exhaust catalytic carbon capture system in a single-cylinder CI engine: An experimental study. *Biofuels* **2018**, *9*, 659–668. [CrossRef]
141. Thiagarajan, S.; Varuvel, E.G.; Martin, L.J.; Beddhanan, N. Mitigation of carbon footprints through a blend of biofuels and oxygenates, combined with post-combustion capture system in a single cylinder CI engine. *Renew. Energy* **2019**, *130*, 1067–1081. [CrossRef]
142. Thiagarajan, S.; Geo, V.E.; Martin, L.J.; Nagalingam, B. Combined effect of fuel-design and after-treatment system on reduction of local and global emissions from CI engine. *Environ. Technol.* **2019**, *40*, 2802–2812. [CrossRef]
143. Saravanan, S.; Kumar, C.R. Carbon Dioxide Capture using Adsorption Technology in Diesel Engines. *Int. J. Renew. Energy Res.* **2020**, *10*, 1614–1620.
144. Ajith Kumar, P.S.; Varghese, A.; Vaishanth, S.S.; Balaji, G. Development and test of a new carbon capture system using Zeolite with addition of Activated carbon and Monoethanolamine for IC engines. *IOP Conf. Ser. Mater. Sci. Eng.* **2020**, *912*. [CrossRef]
145. Kumar, R. Experimental Investigations on CO₂ Recovery from Engine Exhaust Using Adsorption Technology. *SAE Tech. Pap.* **2019**. [CrossRef]
146. Kaushal, A.; Ahirwar, R.; Vardhan, A. Investigation of CO₂ Capturing Capacity of Solid Adsorbents (PEIs) Polyethylenimines from Automotive Vehicle Exhausts System for 4-Stroke SI Engine. *Bonfring Int. J. Ind. Eng. Manag. Sci.* **2018**, *8*, 31–35. [CrossRef]
147. Rajdurai, M.S.; Rao, A.H.S.; Kamalakkannan, K. CO₂ Capture Using Activated Alumina in Gasoline Passenger Vehicles. *Fuel* **2016**, *140*, 4300RPM.
148. Sharma, S.; Maréchal, F. Carbon Dioxide Capture from Internal Combustion Engine Exhaust Using Temperature Swing Adsorption. *Front. Energy Res.* **2019**, *7*, 143. [CrossRef]
149. Ahmed, S.F.; Atilhan, M. Evaluating the Performance of a Newly Developed Carbon Capture Device for Mobile Emission Sources. *J. Energy Resour. Technol.* **2017**, *139*, 1–8. [CrossRef]
150. Pera-Titus, M.; Alshehri, A.; Nicolas, C.H.; Roumégoux, J.P.; Miachon, S.; Dalmon, J.A. Nanocomposite MFI-alumina membranes: High-flux hollow fibers for CO₂ capture from internal combustion vehicles. *Ind. Eng. Chem. Res.* **2009**, *48*, 9215–9223. [CrossRef]
151. Bradley, T.; Knackstedt, C.; Jambor, E. Reducing Effective Vehicle Emissions through the Integration of a Carbon Capture and Sequestration System in the CSU EcoCAR Vehicle. *SAE Tech. Pap.* **2016**. [CrossRef]
152. Telles, E.C.; Yang, S.; Vargas, J.V.C.; Ordóñez, J.C.; Mariano, A.B.; Chagas, M.B.; Davis, T. Stationary compression ignition internal combustion engines (CI-ICE) CO₂ capturing via microalgae culture using a mini-photobioreactor. In Proceedings of the 2015 IEEE Conference on Technologies for Sustainability (SusTech), Ogden, UT, USA, 30 July–1 August 2015; pp. 209–215. [CrossRef]
153. Hamad, E.Z.; Al-sadat, W.I. Apparatus and Method for Oxy-Combustion of Fuels in Internal Combustion Engines. US 2013/0247886 A1, 8 November 2013.
154. Hamad, E.Z.; Al-sadat, W.I. Apparatus and Method for Oxy-Combustion of Fuels in Internal Combustion Engines. US 2017/0074213 A1, 7 May 2017.
155. Hamad, E.Z.; Al-sadat, W.I. Apparatus and Method for Oxy-Combustion of Fuels in Internal Combustion Engines. US 10,280,877 B2, 7 May 2019.
156. Athayde, D.D.; Souza, D.F.; Silva, A.M.A.; Vasconcelos, D.; Nunes, E.H.M.; Da Costa, J.C.D.; Vasconcelos, W.L. Review of perovskite ceramic synthesis and membrane preparation methods. *Ceram. Int.* **2016**, *42*, 6555–6571. [CrossRef]
157. Myers, B.A.; Ihms, D.W. Vehicle System to Separate and Store Carbon Dioxide from Engine Exhaust. US 8,480,798B1, 9 July 2013.
158. Myers, B.A.; Ihms, D.W. Heat Exchanger Equipped with Thermal Electric Device for Engine Exhaust Carbon Dioxide Collection System. US 9,267,415B2, 23 February 2016.
159. Younes, M.V.; Hamad, E.Z. Integrated Method of Driving a CO₂ Compressor of a CO₂-Capture System Using Waste Heat from an Internal Combustion Engine on Board a Mobile Source. US 9,222,480B2, 29 December 2015.
160. Hamad, E.Z.; Al-sadat, W.I. Reversible Solid Adsorption Method and System Utilizing Waste Heat for on-Board Recovery and Storage of CO₂. WO 2012/100149A1, 20 January 2012.
161. Hamad, E.Z. Liquid, Slurry and Flowable Powder Adsorption/Absorption Method Utilizing Waste Heat for on-Board Recovery And Storage of CO₂ from Motor Vehicle Internal Combustion Engine Exhaust Gases. US 2016/0059180A1, 8 November 2016.

162. Mercedes-Benz Citaro NGT Technical Information. Available online: https://www.mercedes-benz-bus.com/content/dam/mbo/markets/common/buy/services-online/download-technical-brochures/images/content/regular-service-buses/citaro-ngt/MB-NGT-2-ES-09_17.pdf (accessed on 8 February 2020).
163. Wärtsilä. *Wärtsilä 46DF Product Guide*; Wärtsilä, Marine Solutions: Vaasa, Finland, 2019.
164. Revista Viajeros Prueba: Mercedes-Benz Citaro NGT. Available online: <https://www.revistaviajeros.com/noticia/9877/prueba-mercedes-benz-citaro-ngt> (accessed on 7 May 2021).
165. Talebizadehsardari, P.; Ehyaei, M.A.; Ahmadi, A.; Jamali, D.H.; Shirmohammadi, R.; Eyvazian, A.; Ghasemi, A.; Rosen, M.A. Energy, exergy, economic, exergoeconomic, and exergoenvironmental (5E) analyses of a triple cycle with carbon capture. *J. CO₂ Util.* **2020**, *41*, 101258. [CrossRef]
166. Einewall, P.; Tunestal, P.; Johansson, B. Lean Burn Natural Gas Operation vs. Stoichiometric Operation with Egr and a Three Way Catalyst. *SAE Tech. Pap.* **2005**, *21*, 343–362. [CrossRef]
167. Zhang, Q.; Xu, Z.; Li, M.; Shao, S. Combustion and emissions of a Euro VI heavy-duty natural gas engine using EGR and TWC. *J. Nat. Gas Sci. Eng.* **2016**, *28*, 660–671. [CrossRef]
168. Jiang, N.; Shen, Y.; Liu, B.; Zhang, D.; Tang, Z.; Li, G.; Fu, B. CO₂ capture from dry flue gas by means of VPSA, TSA and TVSA. *J. CO₂ Util.* **2020**, *35*, 153–168. [CrossRef]
169. Scaccabarozzi, R.; Tavano, M.; Invernizzi, C.M. Comparison of working fluids and cycle optimization for heat recovery ORCs from large internal combustion engines. *Energy* **2018**, *158*, 396–416. [CrossRef]
170. Shu, G.; Li, X.; Tian, H.; Liang, X.; Wei, H.; Wang, X. Alkanes as working fluids for high-temperature exhaust heat recovery of diesel engine using organic Rankine cycle. *Appl. Energy* **2014**, *119*, 204–217. [CrossRef]
171. Corporation, T.M. Toyota Unveils FC Bus Concept—Sora. Available online: <https://global.toyota/en/detail/19063778> (accessed on 11 June 2020).
172. US Department of Energy Gas Mileage Tips. Available online: <https://www.fueleconomy.gov/feg/driveHabits.jsp> (accessed on 15 February 2021).
173. Casadei, A.; Broda, R. *Impact of Vehicle Weight Reduction on Fuel Economy for Various Vehicle Architectures*; The Aluminum Association, Inc.: Arlington, VA, USA, 2008.

3. WASTE HEAT RECOVERY TO MEET THE ENERGY DEMANDS OF A CCS SYSTEM IN AN HD-ICEV.

As evidenced in the previous chapter, the strategic utilization of exhaust gas waste heat, which contains about 30% of the fuel's energy [120] is crucial to successfully integrating a CCS system into an HD-ICEV. Among the available technologies for harnessing the waste heat from exhaust gases coming from ICE, the ORC stands out as the most promising technology. This is due to its mature development, low maintenance costs, high safety, and adaptability to various residual heat sources [81–83,87,121–123]. However, implementing an ORC on board an ICEV poses several challenges that have yet to be solved. In addition to the impact on the exhaust gas back pressure and the intrinsic engine operating conditions [84], the system's added weight raises specific fuel consumption by roughly 2 g/kWh at low rpm [76].

Although the previous chapter used an ORC thermal efficiency to determine the amount of energy that can be recovered from the EG, this first approach does not accurately reflect the actual operating conditions of an ICE. It was based on three temperatures for the same mass flow of the EG, which is quite different from the actual operation of an ICE, where the temperature and mass flow of EG vary with each rpm and engine load condition leading to changes in the ORC's

performance. Therefore, a deeper analysis must be conducted, considering an engine's most realistic operating conditions.

This chapter presents a more thorough analysis of harnessing waste heat using ORC and explores how it can reduce the energy consumption of a CCS system. This chapter will begin by simulating two ICEs of different sizes commonly used in road transport. The objective is to determine the actual thermodynamic conditions of exhaust gases under various operating parameters of the ICE. Based on the results from engine simulations, an ORC will be designed to evaluate its possible dimensions and the power it could generate. Moreover, an energy analysis will be carried out, correlating the power output from the ORC with the power required by a CCS system. This analysis will provide a more detailed understanding of the power penalty imposed by the CCS system on the ICE. Finally, a dynamic analysis will be performed to assess the energy behaviour of the CCS system under varying conditions.

3.1 ENGINE SIMULATIONS

Two stoichiometric natural gas four-stroke turbocharger spark-ignition engines (SI-ICE) with different displacement volumes (V_d) were selected to perform the simulations [124,125]. The simulations were conducted using AVL BOOST software. The theoretical models used in each engine are the simplified model of boost pressure to obtain the air mass flow, the Woschni heat transfer model for the heat transfer in the cylinders, the Heywood, Patton, Nitschke model for the friction, and the Re-analogy for the heat transfer in the engine ducts. Air at standard conditions and a lower heating value (LHV) of the CNG of 48351 kJ/kg were taken as inlet parameters [126–128]. Table 6 shows the engine's technical specifications.

Table 6. Technical specifications of the study engines

Engine	M936G [111]	F1C [125]
Architecture	In-line 6-cylinder engine	In-line 4-cylinder engine
Injection	Multipoint	Multipoint
Valves per cylinder:	4	4
Bore [mm]	110	96
Stroke [mm]	135	104
Displacement volume [cm ³]	7700	3000
Connecting Rod Length [mm]	250	220
Compression ratio	17	12.5
Maximum boost pressure ratio	2	1.5
Firing Order	1-5-3-6-2-4	1-3-4-2
Combustion duration [CAD]	57	58
Star of combustion BTDC [CAD]	18	19
Torque [Nm]	1200 at 1600 rpm	350 at 1500 rpm

Figure 8 compares each engine's simulation results and performance curves [111,125]. The maximum error obtained is 3.39% in both BP and torque and 4.4% in BSFC for the M936G engine. On the other hand, the F1C engine has a

maximum error of 5.36% in BP and Torque. The highest values in the errors in the F1C engine regarding the M936G engine could be due to its smaller size, which makes it more sensitive to the values in the parameters and models used in the simulation. However, these low errors and the fuel energy distribution (Figure 9) indicate that the models and parameters used in the simulation accurately represent the selected engines' behaviour, consistent with those reported in the literature [129,130].

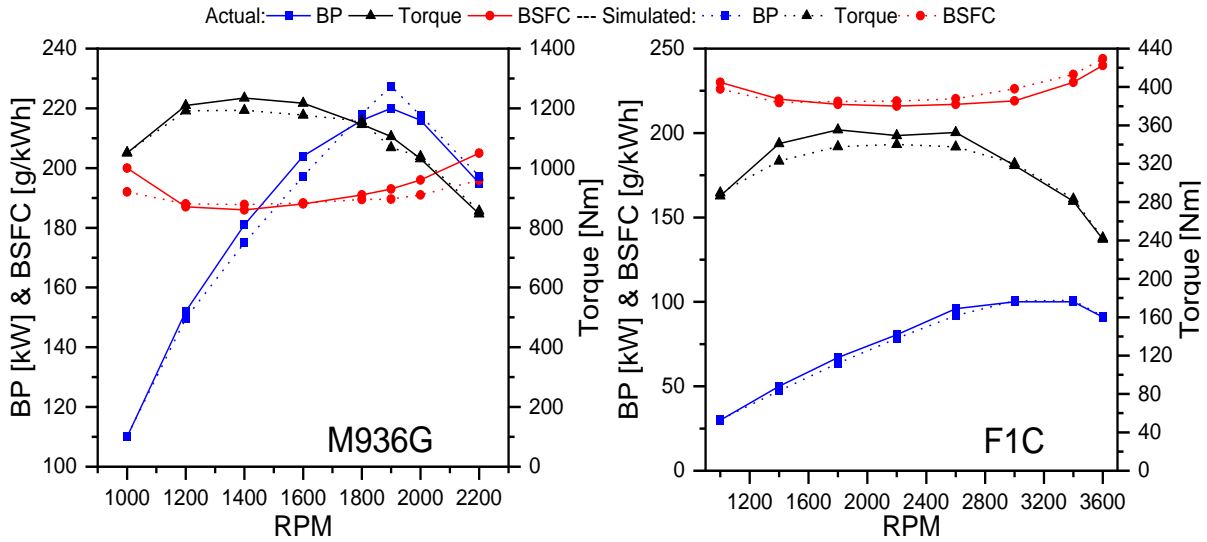


Figure 8. Performance curves of the engines at full engine load.

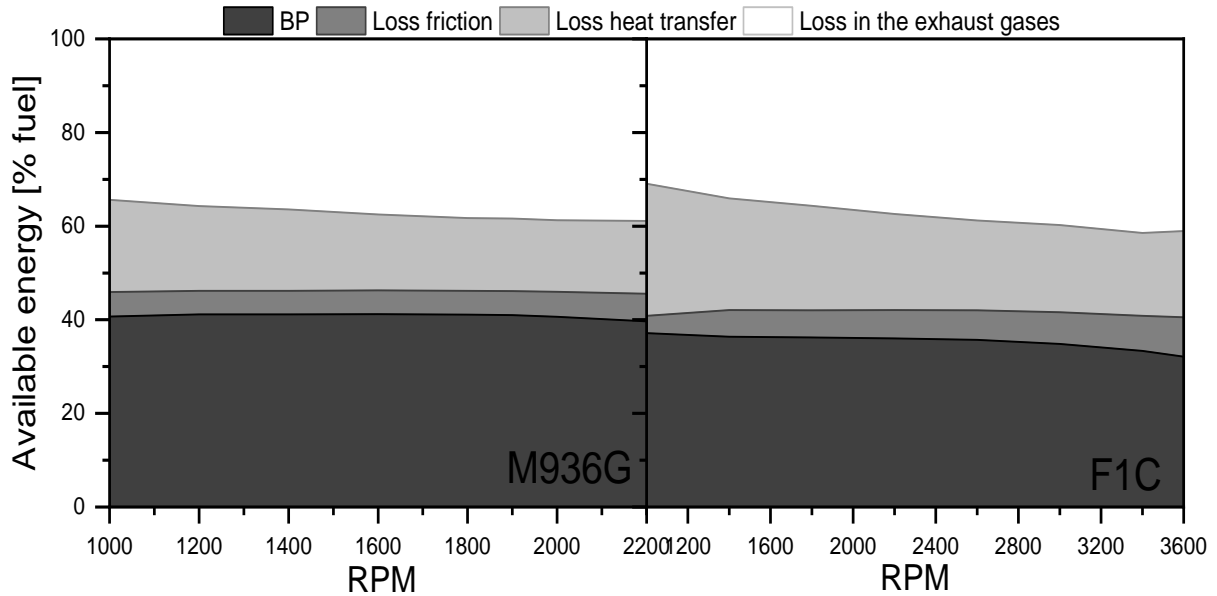


Figure 9. Fuel energy distribution obtained in the engines used in the simulations.

The thermodynamic conditions of the exhaust gas obtained from the simulations indicate that the pressure fluctuates between 1.07 and 1.11 bar. Moreover, the species concentration consistently reflects stoichiometric combustion, with mass fractions of 15.2% CO_2 , 12.4% H_2O , and 72.4% N_2 across all engine loads and the entire range rpm for both engines. Figure 10 shows that

the exhaust gas temperatures and mass flow increase in tandem with the engine load and rpm rise, a trend consistent with findings reported in the literature [109,110].

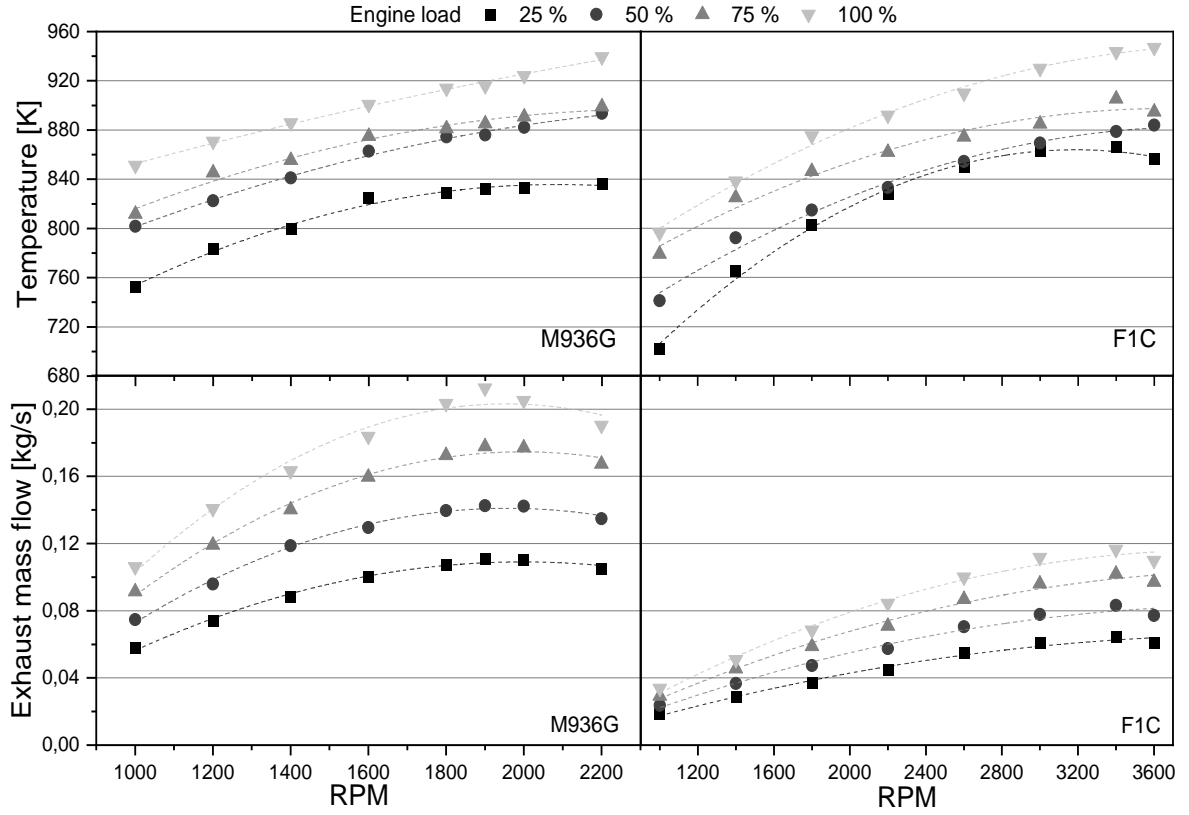


Figure 10. Behaviour of the exhaust gas temperatures and mass flow at partial engine loads.

3.2 ORC DESIGN

Figure 11 illustrates the layout of the proposed ORC system. In this design, the first heat input comes from CO₂ after its compression in the CCS system; this is harnessed in the heat exchanger (HE) ORC-H to preheat the working fluid (WF). The waste heat of the exhaust gases is the second heat input in the ORC, and it is used to evaporate the WF in the HE called ORC-E. The remainder of the ORC devices are an expander (ORC-X), a pump (ORC-P), and a condenser (ORC-C). This configuration is chosen for its cost-effectiveness and simplicity [131]. Cyclopentane (C₅H₁₀) is selected as the working fluid due to its thermal stability at temperatures up to 350 °C [132], but also because of the excellent performance results in previous ORC research works performed on ICE [133]. Its minimal environmental impact, low toxicity, and non-corrosive nature make it a favourable choice [82].

The ORC was designed using the concept of permeability, defined as the ratio of the working fluid (WF) mass flow to the pressure difference between the expander inlet and outlet (ΔP) [80], as expressed in equation 11. The inlet pressure for the ORC-X is determined using Equation 12, developed by Fatigati et al. [78,80,134]. This equation establishes a relationship between the WF inlet

conditions in the pump and in the expander through three dimensionless variables: $\beta_{\eta v}$, which represents the product of the volumetric efficiencies of the pump and the expander; β_{Vol} , the ratio between the displacement volume of the pump and the inlet volume of the expander and β_{ω} , the ratio between the angular velocity of the pump and the expander. To solve this, the WF is treated as an ideal gas at the expander inlet, necessitating the determination of the compressibility factor (Z) and the ΔT_{SH} value, which is the superheat temperature value of the working fluid. Table 7 presents the assumed values, from the literature, to calculate the maximum inlet pressure for the ORC-X.

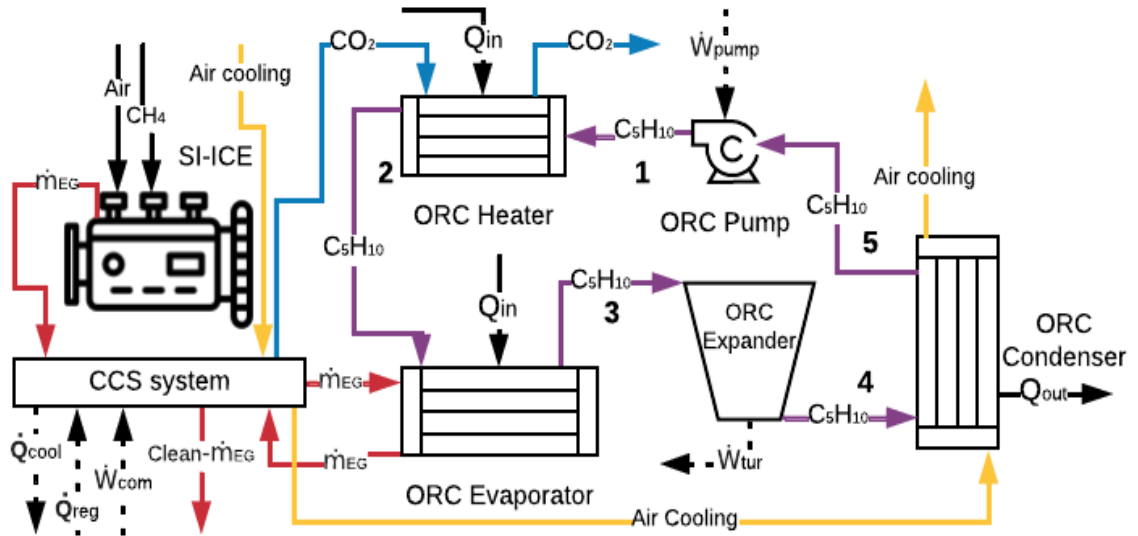


Figure 11. ORC system layout proposed.

$$\alpha = \frac{\dot{m}_{WF}}{\Delta P} \quad (11)$$

$$P_{in,ex} = ZR(T_{sat} + \Delta T_{SH})\rho_{pmp,in}\beta_{\eta v}\beta_{Vol}\beta_{\omega} \quad (12)$$

Table 7. Parameter values used in the calculation of the inlet pressure to the ORC-X

Variable	Value	Unit
Compressibility factor (Z)	0.96	NA
Ideal gas constant (R)	0.1186	kJ/kgK
T_{sat} at 25% of engine load	457.3	K
ΔT_{SH} at 25% engine load	0	K
ΔT_{SH} at 50% engine load	37	K
ΔT_{SH} at 75% engine load	81	K
ΔT_{SH} at 100% engine load	124	K
WF density at 1 bar ($\rho_{pmp,in}$)	735.3	kg/m ³
Expander volumetric efficiency ($\eta_{vol,exp}$)	0.45 [78]	NA
Pump volumetric efficiency ($\eta_{vol,pump}$)	0.8	NA
Volumetric efficiency product ($\beta_{\eta v}$)	0.36	NA
Displacement volume ratio (β_{Vol})	0.76	NA
Angular velocity ratio (β_{ω})	0.2	NA

The calculated maximum ORC-X inlet pressure is 20.96 bar. This value allows the establishment of the inlet pressures for each device. These values incorporate the pressure drops observed in experimental tests for each device [134]. Table 8 shows

the values of the pressures and different parameters considered for each device in the simulations, such as efficiencies, convection heat transfer coefficient (h), and overall heat coefficient (U). Finally, the ORC thermal efficiency is calculated using Equation 13.

$$\eta_{th-ORC} = \frac{\dot{W}_{exp} - \dot{W}_{c-air} - \dot{W}_{pump}}{\dot{Q}_{EG} + \dot{Q}_H} \quad (13)$$

Table 8. Equipment conditions in ORC simulations

Device	Parameter	Unit	Value	State	Fluid
ORC-C	Inlet pressure	Bar	1.5	Vapour	C ₅ H ₁₀
	U [135].	W/m ² K	500 - Condensation	NA	Air- C ₅ H ₁₀
ORC-P	Inlet pressure	Bar	1	Saturated liquid	C ₅ H ₁₀
	Isentropic efficiency	NA	0.55	NA	
ORC-H	Inlet pressure	Bar	24.9	Compressed liquid	C ₅ H ₁₀
	U [135].	W/m ² K	150 - Liquid-Gas	NA	C ₅ H ₁₀ - CO ₂
ORC-E	Inlet pressure	Bar	22.9	Compressed liquid	C ₅ H ₁₀
			70 - Liquid-Gas		
	h [135].	W/m ² K	3000 - Phase change	NA	C ₅ H ₁₀ - EG
			35 - Gas-Gas		
ORC-X	Inlet pressure	Bar	20.9	Vapour	C ₅ H ₁₀

3.3 CARBON CAPTURE AND STORAGE (CCS) SYSTEM

The thermal power consumption of the CCS system is related to the stages that the sorbent undergoes in the TSA process (cooling, adsorption, heating, and desorption). The heat calculations for each TSA stage are done following procedures outlined in Section 2.3, utilizing the properties of the sorbent PPN-6-CH₂-DETA and a CCR of 90%. The CCS system's power consumption is only associated with CO₂ compression developed in the storage stage; this is simulated for a rise in the pressure from 1 to 75 bar with a CO₂ initial temperature of 30 °C and isentropic efficiency of 70% for the compressor. Finally, the cooling heat (\dot{Q}_{cool}) is assumed to be the same as the sorbent regeneration heat ($\dot{Q}_{reg-sorb}$). Figure 12 presents the values obtained of the \dot{Q}_{cool} and $\dot{Q}_{reg-sorb}$

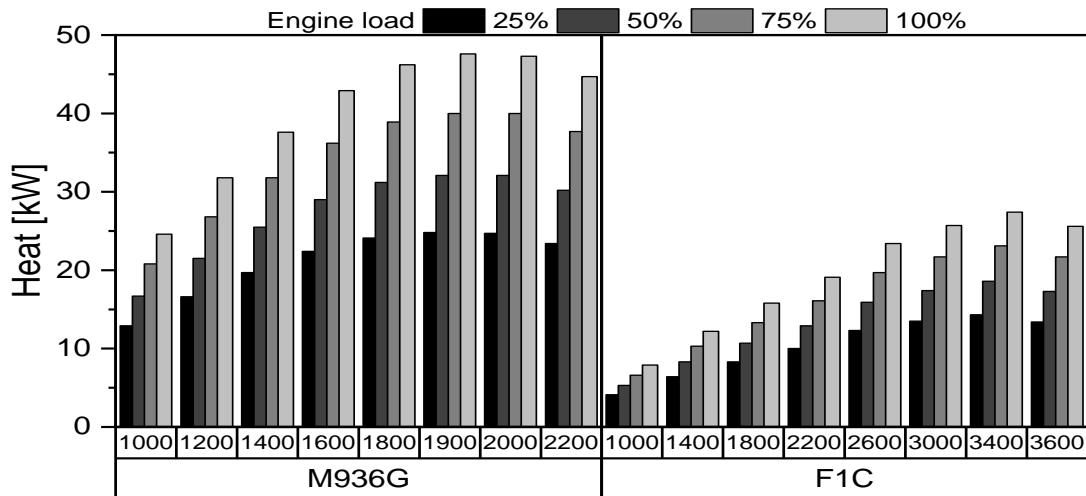


Figure 12. Total and cooling heat required by the TSA process.

3.4 SIMULATION PROCEDURE

The simulation considers the following assumptions: (i) there are no mass losses in pipes, devices, and connections; (ii) there are no pressure drop losses in pipes; (iii) negligible heat losses in pipes; (iv) EG do not change phase-and non-corrosive during the heat transfer; (v) steady-state conditions in the simulations; (vi) inlet cooling air at standard conditions (vii) counter-flow type heat exchangers are simulated. The temperature differentials (ΔT) between the hot and cold fluids within the heat exchangers are detailed in Table 9. Figure 13 illustrates the operational characteristics of the Organic Rankine Cycle (ORC) at both minimum and maximum engine loads. Each simulation verifies that the C_5H_{10} temperature at the evaporator outlet does not exceed $345^\circ C$ (it is thermally stable up to $350^\circ C$). With these assumptions and restrictions, the areas of the heat exchangers are first obtained, and then these areas are kept constant for all engine conditions. Subsequently, the mass flow of C_5H_{10} and cooling air, the pump's power consumption, the power production of the ORC-X, and the heat flux of all heat exchangers are obtained.

Table 9. Simulation restriction parameters

Heat exchanger	Engine load	ΔT between hot and cold fluid [$^\circ C$] [136]	C_5H_{10} outlet Temperature [$^\circ C$]
ORC-C	All	5	≤ 48.87
ORC-E	25	10	184.15
	50 to 100	10	$184.15 > T < 350$
ORC-H	All	10	$48.87 < T < 184.15$

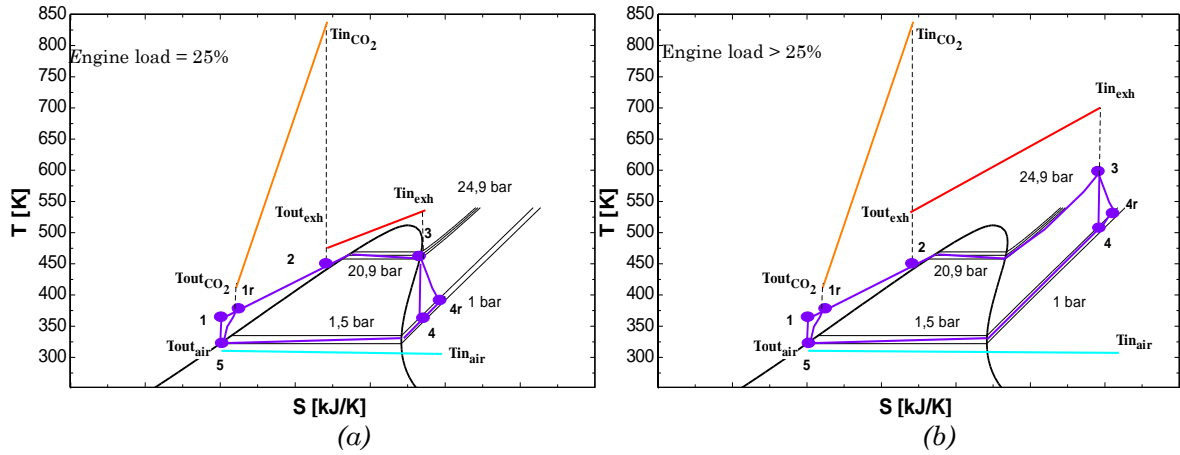


Figure 13. ORC behaviour: a) 25% of engine load and b) engine loads above 25%.

3.5 RESULTS

Table 10 summarises the magnitudes and variations of the ORC heat exchanger areas obtained in the simulations at partial engine loads. On the other hand, The ORC thermal efficiency has an average value of 13% in the M936G engine and 12% in the F1C engine. Moreover, it is observed that the highest values of the ORC thermal efficiency are at the lowest engine load. This behaviour occurs since the permeability, fan, and pump powers have the lowest values due to the

lowest mass flow of cooling air and C_5H_{10} present at this point, as is shown in Figures 14 and 15. The areas and the ORC thermal efficiency are comparable to those found in the literature for an ORC operating at partial engine loads [74,79,81,84,134,137–140]

Table 10. Heat exchanger areas obtained from ORC simulations.

Engine	Heat Exchanger	Area [m ²]	Variation [%]	Total area [m ²]
M936G	ORC-C	1.817	-0.5	7.098
	ORC-H	0.083	-4.6	
	ORC-E	5.198	-0.7	
F1C	ORC-C	0.853	-7.6	2.039
	ORC-H	0.030	-4.7	
	ORC-E	1.156	1.0	

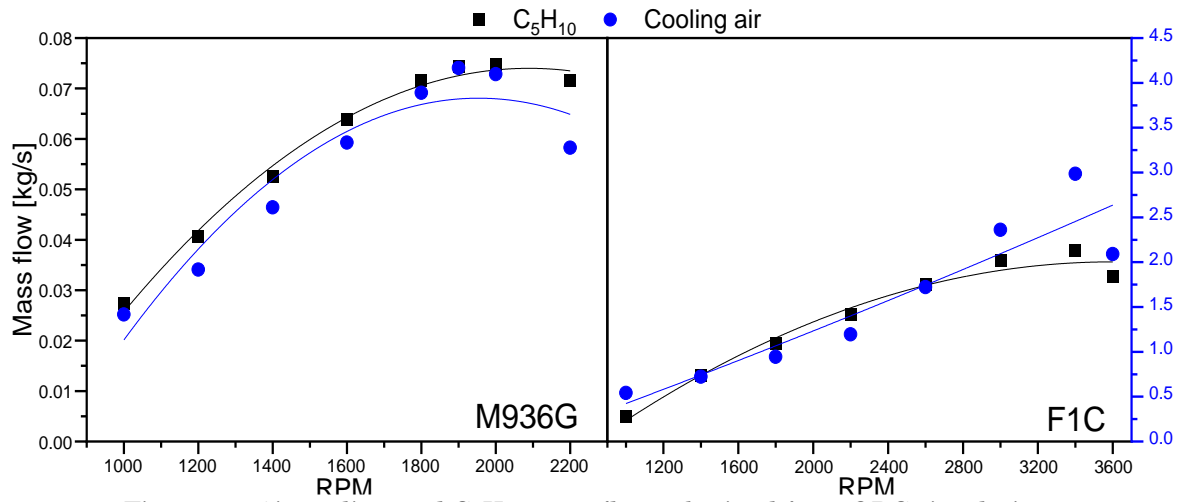


Figure 14. Air cooling and C_5H_{10} mass flows obtained from ORC simulations.

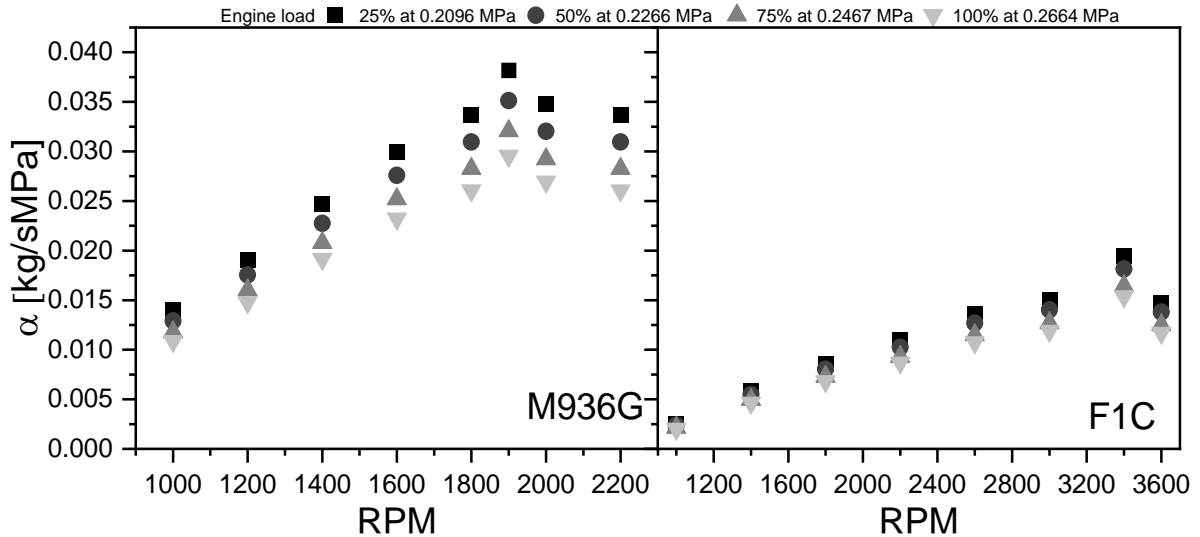


Figure 15. Permeability behaviour in the entire rpm range and at partial engine loads

Figure 16 shows that under the ORC configuration proposed in this research, the ORC can partially cover the CCS system's parasitic loads in any load engine condition. Specifically, on the M936G engine, the ORC can offset between 42% and 76% of the parasitic loads at 1000 to 2200 rpm, respectively. In the F1C, the

highest parasitic load covered by the ORC is 61% at 3400 rpm and 23% at 1000 rpm. Table 11 shows that the average power percentage produced by the ICE consumed by the CCS-ORC system remains below 8.84% for the F1C engine and 5.71% for the M936G engine. However, parasitic loads increase by up to 10% without integrating the ORC into the CCS system.

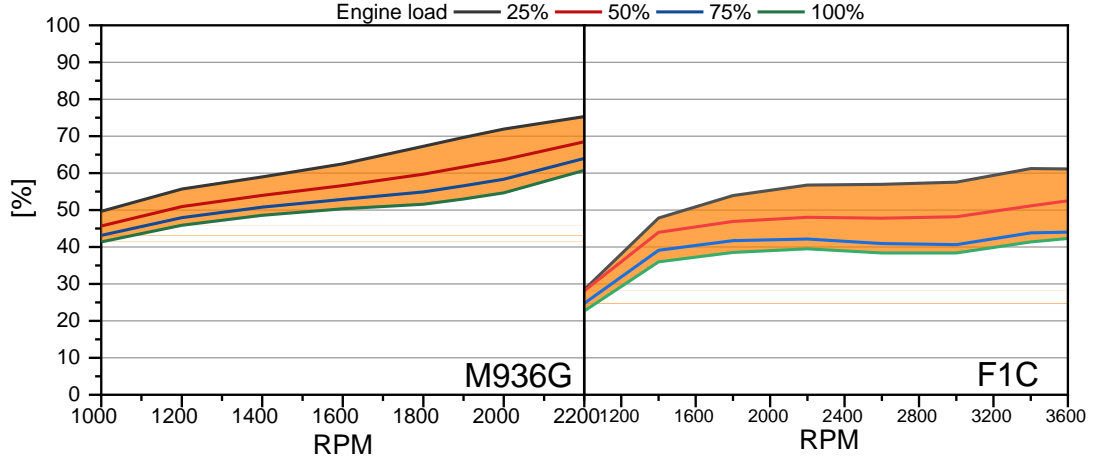


Figure 16. Percentage of parasitic loads covered by the ORC-X under partial engine loads.

Table 11. Average percentage penalty of the CCS system over the engines power with and without ORC.

Engine load [%]	M936G		F1C	
	With ORC [%]	Without ORC [%]	With ORC [%]	Without ORC [%]
25	5.71	15.84	8.84	18.86
50	4.30	10.14	6.52	12.05
75	3.82	8.24	6.01	9.96
100	3.59	7.29	5.44	8.66

3.6 DYNAMIC OPERATION OF THE CCS-ORC SYSTEM

The World Harmonized Transient Cycle (WHTC) is employed to evaluate the CCS-ORC system's operation under dynamic conditions. Equations 14 and 15 determine the actual engine speed and torque values [141]. Table 12 lists the values of the parameters involved in Equation 14. Figure 17 depicts the actual speed and torque the M936G engine attained.

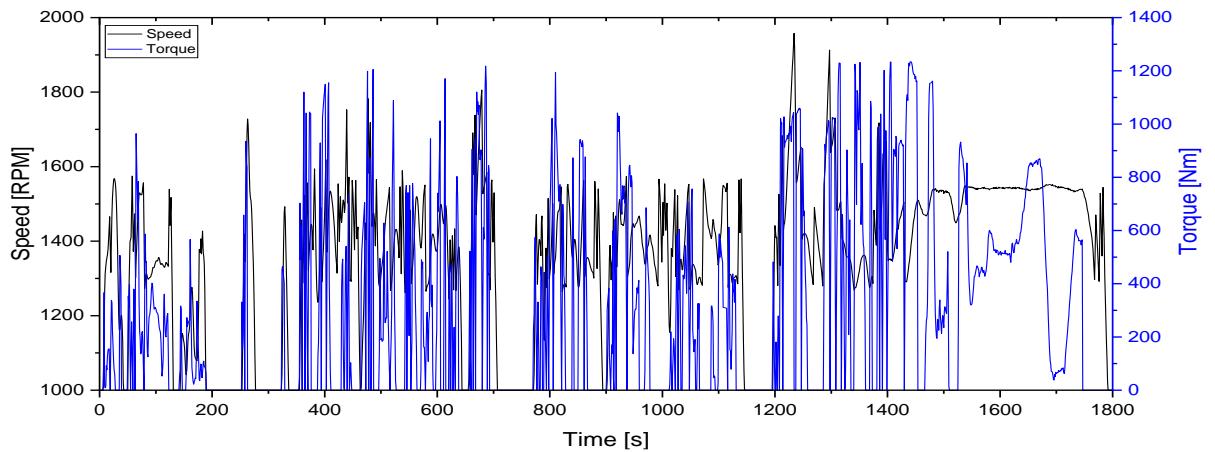


Figure 17. Actual torque and speed for the M936G engine

$$n_{act} = n_{norm} (0.45 n_{lo} + 0.45 n_{pre} + 0.1 n_{hi} - n_{idle}) 2.0327 + n_{idle} \quad (14)$$

$$T_{act} = \frac{\%T T_{max}}{100} \quad (15)$$

Table 12. Speed variable values taken for actualising the engine speed in the WHTC.

Variable	Unit	Value
n_{lo}	RPM	1045.3
n_{pre}	RPM	1552.4
n_{hi}	RPM	1213.6
n_{idle}	RPM	1000
n_{95h}	RPM	2095

After acquiring the torque and speed values corresponding to the WHTC points, the polynomial functions for each speed and load condition of the engine are calculated for the main variables of the CO₂ capture process (required power by the CCS system and CO₂ and fuel mass flows) based on the previous results obtained in ASPEN +; these polynomial functions have a coefficient of determination (R²) greater than 99%. After that, using these polynomial functions, the main variables of the CO₂ capture process are calculated for each WHTC point. This procedure is made in the following form: for a WHTC engine load $\leq 25\%$, it uses the polynomial function of 25% of the engine load of the main variables of the CO₂ capture process, and so on until 100% engine load. Finally, this process is done entirely by iterating until the error between the final captured CO₂ and the previous iteration is less than 0.1%. Figure 18 illustrates the outcomes obtained.

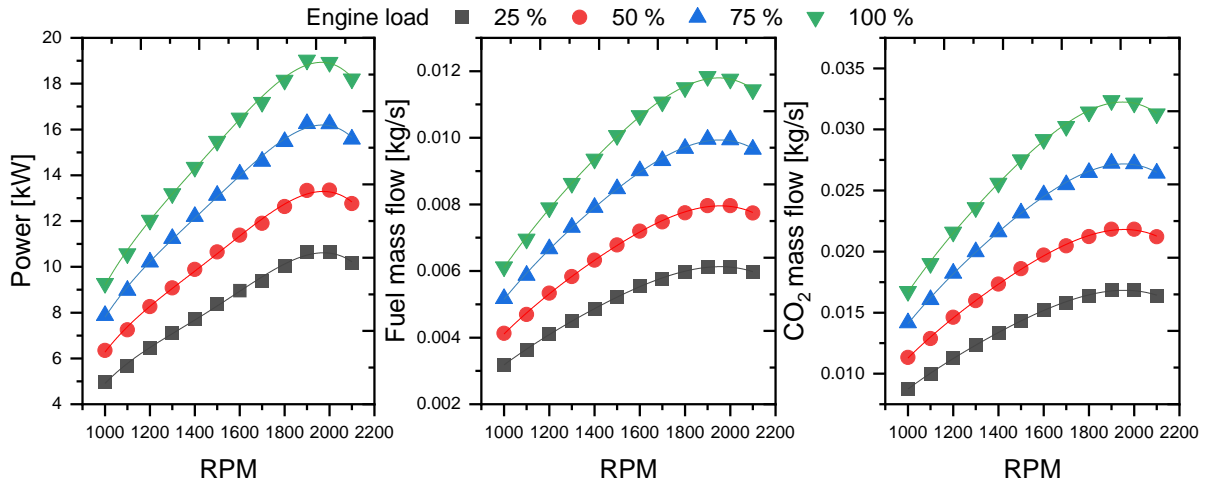


Figure 18. Power penalisation, fuel mass and CO₂ mass flow increase in dynamic conditions.

Due to integrating the CCS-ORC system into the ICEV, the engine's BP must increase by 4.93% throughout the WHTC cycle, as seen in Figure 19. This provokes a rise in the fuel mass of 10.03%, which is quite positive since studies indicate that CCS systems could have penalties of up to 10% [142]. This increase means that the brake specific fuel consumption of the engine goes from 374.6 g/kWh to 395.9 g/kWh.

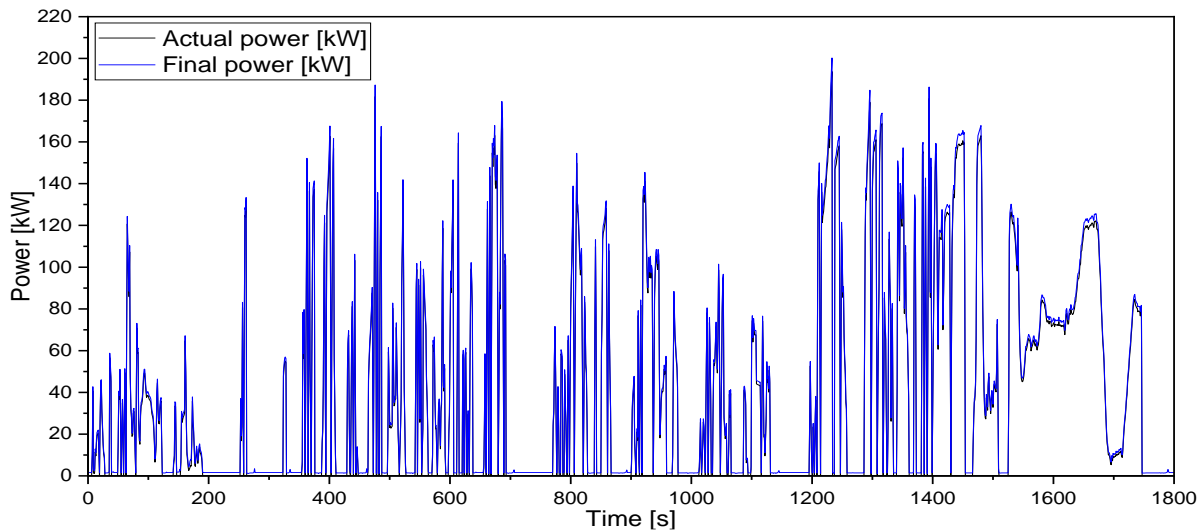


Figure 19. Initial and final engine power due to the CCS system operation in the WHTC

3.7 SUMMARY

The results confirm that the exhaust gases can meet all thermal energy demands of the CCS system. Regarding the ORC, its efficiency at partial engine loads does not present higher variations, and its power production reduces between 3.9 and 13.9 % the penalisation of the CCS system imposed over the engine (depending on the engine load and size). However, the proposed ORC configuration can only take advantage of some of the thermal energy available in the exhaust gases at high engine loads. Hence, the ORC operation must be optimised to improve its performance, thus enhancing its power production and reducing the penalisation provoked by the CCS system over the engine performance. This key factor and a deep energy analysis will be carried out in the next chapter of this thesis.

3.8 PUBLISHED PAPERS

Finally, all the details, findings, and conclusions of this study have been included in two publications. The first is in an article published in the journal *Energy Conversion and Management*, and the second one is in the Proceedings of the 16th Greenhouse Gas Control Technologies Conference (GHGT-16), held in Lyon, France, from 23 to 24 October 2022.

- García-Mariaca, A., Llera-Sastresa, E., & Moreno, F. (2022). Application of ORC to reduce the energy penalty of carbon capture in non-stationary ICE. *Energy Conversion and Management*, 268, 116029. <https://doi.org/10.1016/j.enconman.2022.116029>
- García Mariaca, Alexander and Llera, Eva, Dynamic CO₂ Capture in a Natural Gas Engine Used in Road Freight Transport (August 30, 2022). Proceedings of the 16th Greenhouse Gas Control Technologies Conference (GHGT-16) 23-24 Oct 2022, <http://dx.doi.org/10.2139/ssrn.4272013>



Application of ORC to reduce the energy penalty of carbon capture in non-stationary ICE

Alexander García-Mariaca^{a,*}, Eva Llera-Sastres^b, Francisco Moreno^b

^a Escuela de Ingeniería y Arquitectura, University of Zaragoza, María de Luna s/n, Zaragoza 50018, Spain

^b Department of Mechanical Engineering and CIRCE Research Institute, University of Zaragoza, María de Luna s/n, Zaragoza 50018, Spain

ARTICLE INFO

Keywords:

Organic rankine cycle
Carbon capture and storage
Temperature swing adsorption
CO₂ emissions
Internal combustion engines

ABSTRACT

The electrification of productive activities cannot be considered the only strategy for a low-carbon economy, and sectors such as road freight and passenger transport will have to continue using technologies based on combustion in the medium and long term. It is expected that sustainable synthetic fuels and CO₂ capture and storage technologies (CCS) can help to reduce greenhouse emissions. However, the occupation of spaces and the energy penalty of the capture are handicapped in smaller facilities, such as conventional combustion engine vehicles, and determine its technical and economic viability. In this paper, AVL boost and Aspen + softwares simulations are performed to analyze the feasibility of using an Organic Rankine Cycle (ORC) to supply the power consumption of an on-board CCS system coupled to an internal combustion engine (ICE) operating at partial engine loads and over the whole rpm range. Two spark-ignition engines of different sizes, fueled with CH₄, have been modelled, and temperature swing adsorption is selected as a viable method for the CCS system, assuming a carbon capture rate of 90 %. Results show that the ORC reduces between 3.9 and 13.9 % the penalization of the CCS system over the engine power, keeping it under 8.84 % in the small engine and 5.71 % in the large engine. It can be concluded that an ORC-CCS hybridized system is energy feasible for the operation of an ICE working at partial loads in the entire rpm.

1. Introduction

In 2020, the transport sector generated 8222 MtCO₂, 24.45 % of the worldwide emissions of CO₂ [1], with the shares shown in Fig. 1. Passenger cars are the higher CO₂ emitters, but the ongoing electrification of this sector is expected to reduce CO₂ emissions [2,3]. On the contrary, road freight and passenger transport, which jointly contributed almost equally to passenger cars, will continue using internal combustion engines (ICE) over the short and medium-term as electric vehicles are not totally feasible for those regular transport services [4].

Meanwhile, strategies must follow several staggered schemes to lower CO₂ emissions in ICE. Firstly, the reduction of the driving resistances [6] and the use of eco-driving technologies [7,8]. Secondly, the enhancement of the engine thermal efficiency [9], and the implementation of Organic Rankine Cycles (ORC) to take advantage of the waste heat flows in the exhaust gases and the engine coolant [10–12]. Thirdly, the use of alternative fuels such as natural gas (NG) [13,14], or synthetic fuels [15], and, in an unavoidable step, the CO₂ capture and

storage.

Synthetic fuels are suitable substitutes for fossil fuels as they behave similarly in ICEs. Moreover, the carbon footprint can be minimized if renewable sources or captured CO₂ are considered in their production. Although it is not the scope of this paper, the ultimate idea is to capture the CO₂ to use it as a raw material in producing synthetic natural gas through a Power-to-Gas process that would later be used as fuel.

According to the literature, some research on carbon capture and storage (CCS) systems has been applied to the maritime sector and road freight transport [16–19]. These research works have opted for the use of amine absorption and temperature swing adsorption (TSA) as CO₂ capture techniques. Nevertheless, there is a lack of knowledge of energy requirements to run additional devices in non-stationary conditions.

Some of these referred works have proposed organic Rankine Cycles (ORC) to supply the energy required by the CCS system. The ORC is a well-developed system having low maintenance cost, high safety and flexibility that allows adapting to different residual heat sources [20–26]. However, implementing an ORC on board an ICE vehicle presents several challenges yet to be solved. In addition to the impact on

Abbreviations: η^{th} , ORC Thermal Efficiency; CAD, Crank Angle Degree.

* Corresponding author.

E-mail address: alexander.garcia@unizar.es (A. García-Mariaca).

<https://doi.org/10.1016/j.enconman.2022.116029>

Received 8 April 2022; Received in revised form 27 June 2022; Accepted 18 July 2022

Available online 30 July 2022

0196-8904/© 2022 Elsevier Ltd. All rights reserved.

Abbreviations			
ΔH_{ads}	Adsorption Heat	ICE	Internal Combustion Engines
AF	Air-Fuel ratio	q	Loading Capacity
BORC	Basic Organic Rankine Cycle	LHV	Lower Heating Value
BP	Brake Power	x	Mass Fraction
BSFC	Brake-specific Fuel Consumption	NG	Natural Gas
BMEP	Break Mean Effective Pressure	ORC	Organic Rankine Cycle
CCS	Carbon Capture and Storage	ORC-C	ORC Condenser
CCR	Carbon Capture Rate	ORC-E	ORC Evaporator
C ₅ H ₁₀	Cyclopentane	ORC-X	ORC Expander
ρ	Density	ORC-H	ORC Heater
dv	Displacement Volume	ORC-P	ORC Pump
\dot{m}_{EG}	Exhaust Gases' Mass Flow	α	Permeability
IMEP	Indicated Mean Effective Pressure	RPM	Revolution per Minute
ICEV	Internal Combustion Engine Vehicle	SI	Spark Ignition
		c_p	Specific Heat
		TSA	Temperature Swing Adsorption

the exhaust gas back pressure and the intrinsic engine operating conditions [27], the system's additional weight increases specific fuel consumption at low rpm of approximately 2 g/kWh [28]. Other research studies have established which type of expansion device could be selected according to the engine's power output. For engines with power greater than 100 kW, turbines are more appropriate. Scroll expanders are recommended for engines between 10 and 100 kW, and single-screw expanders are suggested [29]. On the other hand, experimental results show that the ORC efficiency can vary between 1 and 7 % [29,30], while simulation results show that the ORC efficiency reaches 12 % [31]. Research works have also been carried out on the design and control of evaporators and condensers in transient operation [32,33], as well as the determination of mathematical expressions that, using a mass balance, allow relating the pump inlet conditions and the expander inlet conditions [30,34].

Although there are several studies of ORCs operating under transient conditions, no literature considers ORC-CCS systems working on engines operating in the entire rpm range at partial engine loads. Therefore, this paper aims to assess whether the waste thermal energy in the exhaust gases can provide the thermal energy necessary for the desorption

process in the CO₂ capture process and whether an ORC system can supply the mechanical energy for the CO₂ compression in the storage process. All the above under the multiple operating conditions (partial engine loads) of an ICEV. To this end, the feasibility of operating a CCS system by TSA integrated with the ORC under these conditions is evaluated, which has not been previously shown by other research works.

In order to obtain the exhaust gases' composition and thermal conditions under the entire range of rpm and engine loads, it was necessary to develop an engine model using the geometric and operational parameters of real engines with the software AVL BOOST. Afterwards, an ORC is simulated with the software Aspen Plus considering the CCS energy requirements and the exhaust gases' conditions obtained in the model engine.

2. Internal combustion engine modelling

2.1. Engine selection

Since gaseous synthetic fuels are expected to support the future of the ICE engines, natural gas engines will be included in the ORC-CCS system

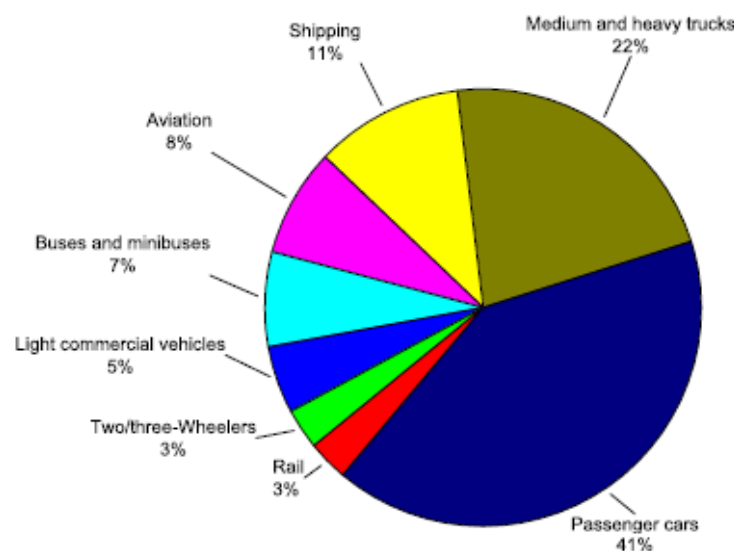


Fig. 1. Transport sector CO₂ emissions worldwide in 2020 by subsector. (Adapted from [5]).

under study. Further, two four-stroke turbochargers spark-ignition engines (SI-ICE) with different displacement volumes (dv) are selected to compare the ORC behaviour under different conditions. The engines selected are a FIC engine manufactured by FPT industrial with a dv of 3000 cc, used in the VAN Iveco Daily, and a M936G engine manufactured by Mercedes Benz with a dv of 7700 cc, which is used in trucks, and buses. Both engines are with stoichiometric combustion [35,36]. Table 1 lists the specifications of the engines.

2.2. Parameters and assumptions

To analyze the ORC-CCS behaviour, the temperature, pressure, mass flow, and composition of the exhaust gases of the SI-ICE fuelled with CH₄ operating at partial loads of the engine and throughout the rpm range must be known. For this purpose, both engines were modelled with the software AVL BOOST (see Fig. 2). The theoretical models used to simulate the thermodynamic and mechanical processes in the engine are the simplified model of boost pressure to obtain the air mass flow, the Woschni heat transfer model for the heat transfer in the cylinders, the Heywood, Patton, Nitschke model for the friction, and the re-analysis for the heat transfer in the engine ducts. Air at standard conditions and a lower heating value (LHV) of the NG of 48351 kJ/kg were taken as inlet parameters. [39–41].

2.3. Model adjustment

The model adjustment was carried out at the maximum torque and BP points. To this end, the fuel mass flow is obtained from the brake-specific fuel consumption, and the air mass flow is set in the simulations using the AF ratio [36,37]. The simulations are set up, changing parameters such as cylinder wall temperatures and friction coefficients in each iteration until the minimum error of the performance parameters (BP, torque, and BSFC) in the selected points. It is verified that the values show centred combustion and an energy balance within a reasonable range for each iteration. Once the simulation models and parameters are configured, the performance variables for each engine's range of rpm are estimated. Finally, simulations are carried out to obtain the performance curves at partial engine loads (25, 50, and 75 %).

2.4. Model validation

The results obtained in the simulations are compared with the

performance curves for each engine given by the manufacturers [36,37]. As can be seen in Fig. 3, the simulations carried out in the software for both engines present maximum errors of 3.39 % in the BP and Torque and 4.4 % in the BSFC in the M936G engine, while the maximum error obtained in BP and Torque in the FIC engine is 5.36 %. The most significant error in the FIC engine regarding the M936G engine could be originated from its smaller size, making it more susceptible to the values in the parameters and models assumed in this engine. However, these low errors in the simulations reveal that the assumed models and parameters represent the behaviour of the selected engines with good precision. Moreover, these values of errors are in concordance with the reported in the literature [42].

2.5. Energy fuel distribution

The fuel energy distribution is mapped from the simulation results (Fig. 4), showing that the fuel energy is mostly distributed in the BP and the exhaust gases with values between 35 and 40 % in the entire rpm range, in agreement with the literature data [43]. This amount of thermal energy in the exhaust gases could be exploited to increase the thermal efficiency of ICE or cover the energy duties of a CCS system. This last would be achieved by hybridizing an ORC and a CCS system using TSA as a CO₂ capture technique.

2.6. Simulation results

The engine simulations were done to get the temperature, pressure, mass flow and species concentration of the exhaust gases at the outlet catalyzer and thus to know the input parameters in the ORC simulations. The results show that the exhaust gas pressure ranges between 1.07 and 1.11 bar, and the species concentration corresponds to stoichiometric combustion in all engine loads and the entire rpm range in both engines.

Figs. 5 and 6 show the exhaust gases' resulting temperatures and mass flows. The temperatures range between 700 and 950 K, which aligns with the literature [44,45]. The increase in engine speed leads to a rise in charge, which results in high energy available for combustion, and a reduction of the residence time of the charge in the combustion chamber, among other things, which leads to an increase in the exhaust gas temperature. As expected, both engines' highest exhaust gas mass flow is at the maximum power and the minimum at the lowest rpm (Fig. 6). Table 2 summarises the minimum and the maximum exhaust gas flows obtained in the simulations in both engines.

3. ORC-CCS Integrated system

As stated, the main objective of this study is to analyze the feasibility of an ORC operating at partial engine loads to supply the energy demand of a CCS system. For this study, a CCS system by TSA is selected as it is the most suitable CO₂ capture technique because of the amount of thermal energy available in the exhaust gases after the catalyzer [46]. This CCS system requires a heat source for the desorption process, a cooling system for adsorption, and a compression system for CO₂ storage. As shown in Figs. 4, 5, and 6, the exhaust gases could cover the thermal demand of the CCS system as it could take advantage of the remaining heat in the exhaust gases in an ORC to supply total or partially the cooling and compression mechanical energy demand of the CCS system. Consequently, the engine performance penalization due to the CCS system operation could be counterbalanced. Fig. 7 shows the ORC-CCS system proposed and the different involved flows.

3.1. ORC design

As Fig. 7 shows, the ORC used in the simulations is a modified basic ORC (BORC) [47] that includes two heat sources due to the coexistence with the CCS system. The selected working fluid in the ORC is cyclopentane (C₅H₁₀). This organic fluid is selected not only because it is

Table 1
Technical specifications of the FIC and M936G engines.

Engine	M936G [37]	FIC [36,38]
Architecture	In-line 6-cylinder engine	In-line 4-cylinder engine
Aspiration method	Turbocharged with Aftercooler	Turbocharged with Aftercooler
Injection	Multipoint	Multipoint
Valves per cylinder	4	4
Bore [mm]	110	96
Stroke [mm]	135	104
Displacement volume [cm ³]	7700	3000
Connecting Rod Length [mm]	250	220
Compression ratio	17	12.5
Maximum boost pressure ratio	2	1.5
Firing Order	1-5-3-6-2-4	1-3-4-2
Combustion duration [CAD]	57	58
Star of combustion BTDC [CAD]	18	19
Air-fuel ratio (AF)	Stoichiometric combustion [16.75]	Stoichiometric combustion [16.75]
Brake Power [kW]	222 at 1950 rpm	100 at 3500 rpm
Torque [Nm]	1200 at 1600 rpm	350 at 1500 rpm

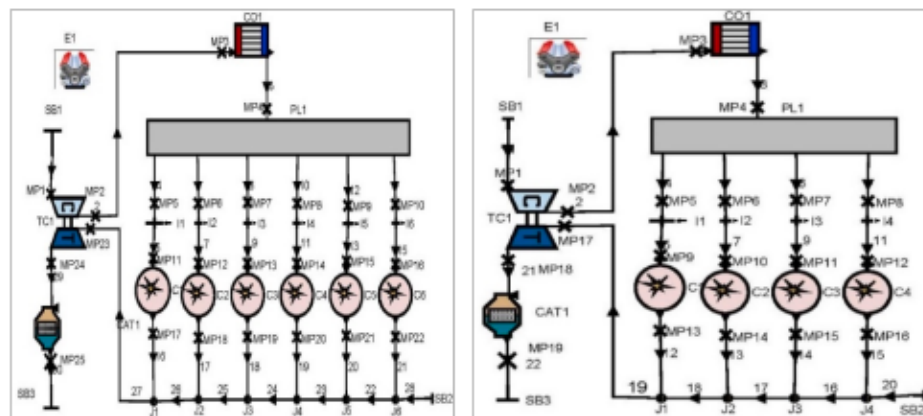


Fig. 2. Configuration of the SI-ICE in the software AVL BOOST a) M936G engine b) F1C engine.

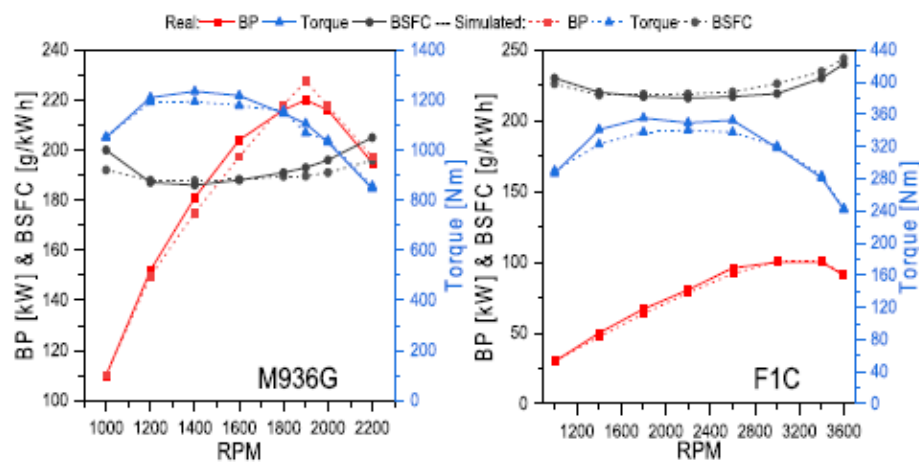


Fig. 3. Real and simulated performance curves of the engines at full engine load.

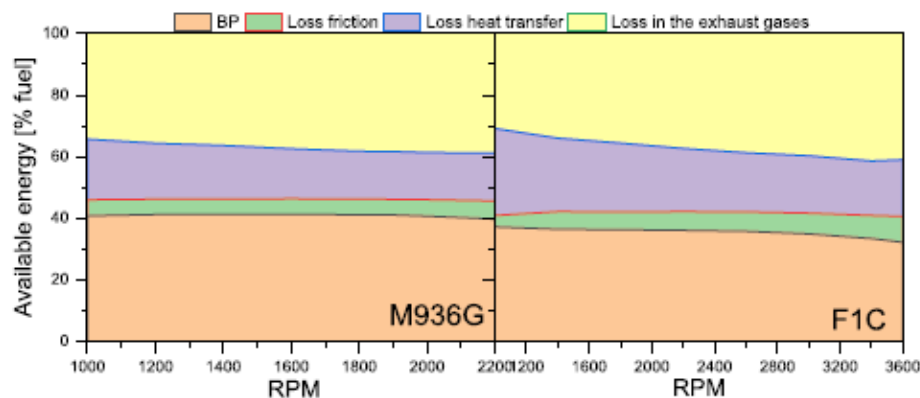


Fig. 4. Fuel energy distribution in the turbocharger SI-ICE's used in the simulation.

thermally stable at temperatures up to 623 K [48], but the excellent performance results in previous ORC research works performed on ICE [49]. Another extensive factor is that C_6H_{10} has a limited environmental

impact, low toxicity, and is non-corrosive [50].

The first heat input to the ORC is provided by CO_2 after the compression process. It is used to preheat the C_6H_{10} in the heat

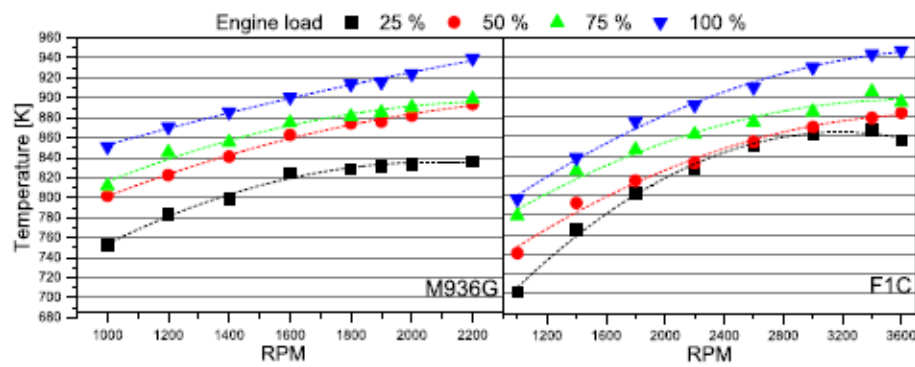


Fig. 5. Exhaust gases' temperatures at partial engine loads.

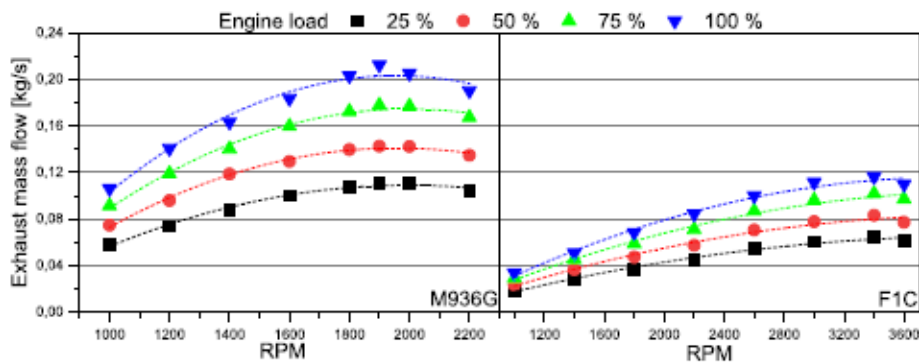


Fig. 6. Exhaust gases' mass flows at partial engine loads.

Table 2
Minimum and maximum exhaust gas flow obtained in the simulations.

Engine	M936G	M936G	F1C	F1C
RPM	1000	1900	1000	3400
Engine load [%]	25	100	25	100
Exhaust gases flow [kg/s]	0.058	0.213	0.018	0.119

exchanger (ORC-H). The waste heat of the exhaust gases is the second heat input in the ORC, and it is used to evaporate the C_5H_{10} in the heat exchanger called ORC-E). The rest of the ORC presents a conventional system, i.e., an expander (ORC-X), a pump (ORC-P), and a condenser (ORC-C), as it is the less expensive and simplest configuration.

The ORC design was performed using the concept of permeability which is the ratio of the working fluid mass flow and the pressure difference between the expander inlet and outlet (ΔP). This parameter indicates the capacity of a plant to be crossed by the working fluid [34], equation (1).

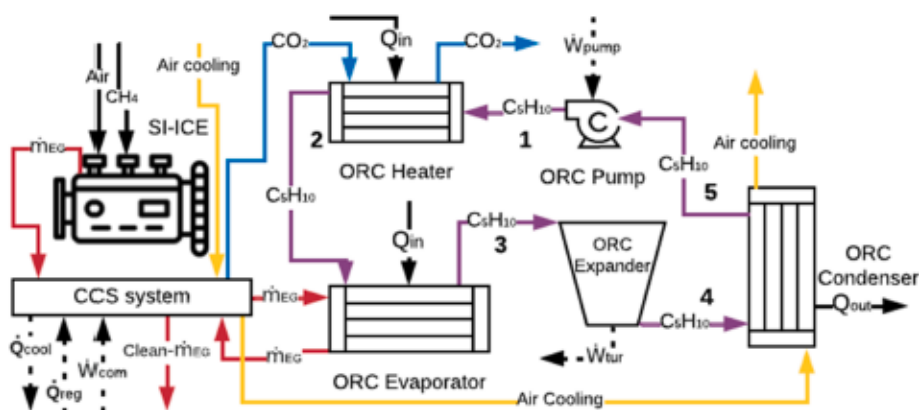


Fig. 7. Diagram configuration of the BORC.

$$\alpha = \frac{\dot{m} \dot{V}}{\Delta P} \quad (1)$$

The outlet pressure is assumed as 1.5 bar. The ORC-X inlet pressure is obtained by using the equation developed by Fatigati et al. [30], equation (2),

$$P_{in,ex} = ZR(T_{sat} + \Delta T_{SH})\rho_{pmp,in}\beta_{pmp}\beta_{vol}\beta_{ex} \quad (2)$$

This equation relates the inlet conditions of the working fluid to the pump and the expander through three dimensionless variables: β_{pmp} , the product of the volumetric efficiencies of the pump and the expander; β_{vol} , the ratio between the displacement volume of the pump and the inlet volume of the expander and β_{ex} , the ratio between the angular velocity of the pump and the expander. As the working fluid is treated as an ideal gas at the inlet of the expander, it is necessary to obtain the value of the compressibility factor (Z) and ΔT_{SH} value, which is the superheat temperature value of the working fluid. Table 3 shows the values assumed and taken from the literature for calculating the maximum inlet pressure in the ORC-X.

In this study, equation (2) is a function only of the saturation temperature of the working fluid because all other parameters are assumed to be constant. On this basis, a saturation temperature of the working fluid 60 K lower than the exhaust gas temperature after the CO₂ desorption process at 25 % engine load and 1000 rpm (the lowest thermal energy point) is taken. At this value, the inlet pressure at the ORC-X is 20.96 bar.

Once the maximum pressure for the expander's inlet is obtained, inlet pressures are established for each device. The pressure drop values in the devices were taken from the literature [51]. Table 4 shows the values of the pressures and parameters considered for each device in the simulations.

3.2. Carbon capture and storage (CCS) system

This study considers the thermal and mechanical energy consumption of a CCS system with TSA as the technique of CO₂ capture. The sorbent selected for the CCS thermal energy calculations is PPN-6-CH₂-DETA; the selection of this sorbent is mainly due to its low adsorption heat and higher loading capacity (q). Table 5 presents the main sorbent properties. The mechanical energy consumption is only associated with the power required to compress the CO₂ in the storage stage. The integration of the CCS system in the vehicle is considered using a rotary wheel adsorber, which is located in the turbocharged outlet, as is shown in the research work developed by Sharma and Maréchal [17].

3.2.1. Outlets and inputs heat in the CCS system

The heat input to the ORC evaporator is the heat remaining in the exhaust gases at the outlet of the CCS system. The total heat (\dot{Q}_{total}) given up by the exhaust gases to the CCS system is the sum of the sensible heat (Equation (3)) and the sorbent desorption heat (Equation (4)). In order

Table 3
Parameter values for the calculation of the inlet pressure to the ORC-X.

Variable	Value	Unit
compressibility factor (Z)	0.73	NA
R	0.1186	kJ/kgK
T_{sat} at 25 % of engine load	457.3	K
ΔT_{SH} at 25 % engine load	0	K
ΔT_{SH} at 50 % engine load	37	K
ΔT_{SH} at 75 % engine load	81	K
ΔT_{SH} at 100 % engine load	124	K
$\rho_{pmp,in}$ at 1 bar (saturated liquid)	735.3	kg/m ³
$\eta_{vol,pmp}$	0.45 [30]	NA
$\eta_{vol,pump}$	0.8 [30]	NA
β_{ex}	0.36	NA
β_{vol}	1 [30]	NA
β_{pmp}	0.2 [30]	NA

Table 4
Equipment conditions for ORC simulations.

Equipment	Parameter	Unit	Value	State	Fluid
ORC-C	Inlet pressure	bar	1.5	Vapour	C ₆ H ₁₀
	Overall heat transfer coefficient	W/m ² K	500	Condensation	Air-C ₆ H ₁₀
ORC-P	Inlet pressure	bar	1	Saturated liquid	C ₆ H ₁₀
	Isentropic efficiency	NA	0.55	NA	
ORC-H	Inlet pressure	bar	24.9	Compressed liquid	C ₆ H ₁₀
	Overall heat transfer coefficient	W/m ² K	150	Liquid-Gas	C ₆ H ₁₀ - CO ₂
ORC-E	Inlet pressure	bar	22.9	Compressed liquid	C ₆ H ₁₀
	Overall heat transfer coefficient	W/m ² K	70	Liquid-Gas	C ₆ H ₁₀ - Exhaust gas
ORC-X	Inlet pressure	bar	20.9	Vapour	C ₆ H ₁₀
	Isentropic efficiency	NA	0.65	NA	

Table 5
Main properties of the sorbent PPN-6-CH₂-DETA [53,54].

Adsorption Heat (ΔH_{des}) [kJ/mol _{CO₂}]	Loading Capacity (q) [kg _{CO₂} /kg _{sorbent}]	Selectivity CO ₂ /N ₂	Specific Heat ($c_{p,sorbent}$) [kJ/kgK]	*Density (ρ) [kg/m ³]
-45.32	0.2354	greater than 10,000	0.985	805

*Crystallographic density.

to obtain both heats, a 90 % CO₂ capture rate (CCR) is set. A ΔT of 423 K is taken as the difference between the desorption temperature [53], and 303 K is assumed as the CO₂ sorption temperature. Given that it is a TSA process, the cooling heat (\dot{Q}_{cool}) is assumed to be the same as the total (\dot{Q}_{total}). Fig. 8 presents the values obtained.

The inlet heat in the ORC Heater is given up by the CO₂ after the compression process in the CCS system. The parameter required for the model to calculate this heat is the CO₂ outlet temperature after the compression process. The CO₂ compression process is then simulated. Pressures from 1 to 75 bar with a CO₂ initial temperature of 303 K and isentropic efficiency of 70 % for the compressor are considered. The result obtained for every engine load condition and rpm in both engines is 328.5 K.

$$\dot{Q}_{sens} = c_{p-CO_2} 0.9x_{CO_2} \dot{m}_{EG} \Delta T + c_{p-sorbent} \frac{0.9x_{CO_2} \dot{m}_{EG}}{q} \Delta T \quad (3)$$

$$\dot{Q}_{des} = 0.9x_{CO_2} \dot{m}_{EG} \Delta H_{des} \quad (4)$$

$$\dot{Q}_{total} = \dot{Q}_{des} + \dot{Q}_{sens} \quad (5)$$

3.3. Simulation procedure

The simulation considers the following assumptions: (i) there are no mass losses in pipes, devices, and connections; (ii) there are no pressure drop losses in pipes; (iii) heat losses in pipes are negligible; (iv) Exhaust gases do not change phase and non-corrosive during the heat transfer; (v) steady-state conditions in the simulations; (vi) inlet cooling air at standard conditions (vii) counter-flow type heat exchangers are

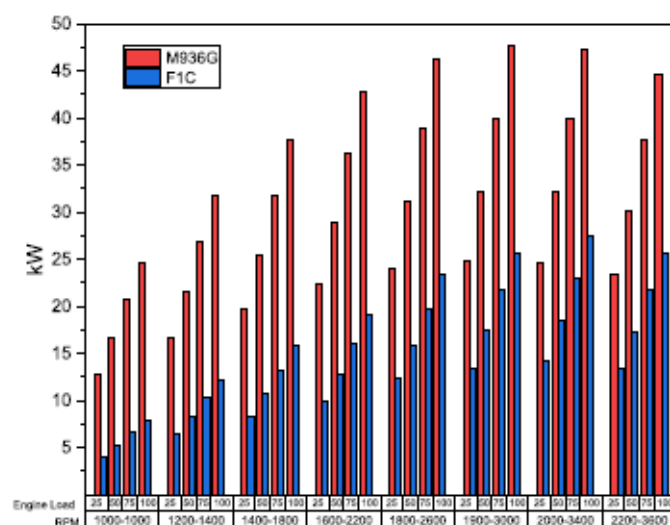


Fig. 8. Total and cooling heat in the CGS system by engine.

simulated. The temperature differences between the hot and cold fluid in the heat exchangers of the simulations (ΔT) are listed in Table 6. The iterative procedure to get the heat exchangers areas and performance values of the ORC at partial engine loads are described below.

At the lowest rpm and 25 % engine load, the cooling air mass flow, the C_5H_{10} mass flow. The evaporator and heater areas are obtained, fulfilling the parameters listed in Table 6. Fig. 9 (a) represents the behaviour at this point. After, at the lowest rpm and 100 % engine load and keeping the heater and evaporator areas and the C_5H_{10} mass flow obtained in the previous step. The evaporator area is found again, verifying that the C_5H_{10} temperature at the evaporator outlet does not overcome 618 K (it is thermally stable up to 623 K). If necessary, the cooling air mass flow and the condenser area are set again. Fig. 9 (b) represents the behaviour at this point.

Subsequently, at rpm where BP is maximum, and 25 % engine load and keeping the heater and evaporator areas obtained in the previous steps and setting a cooling air mass flow, The C_5H_{10} mass flow and the condenser area are obtained. Finally, at the same rpm but at 100 % engine load and taking the heat exchangers areas and the C_5H_{10} mass flow obtained previously, it is proceeded to verify the maximum temperature of the C_5H_{10} . The procedure described before is repeated until the variation of the heat exchanger areas is less than 1 %. Once the heat exchanger areas are obtained, the pump's power consumption, the power production of the ORC-X, and the heat flux of all heat exchangers in the rest of the engine operational points are found.

Table 6
Simulation parameters.

Heat exchanger	Engine load	ΔT between hot and cold fluid [K] [55]	C_5H_{10} outlet Temperature [K]
ORC-C	All	5	≤ 322.02
ORC-E	25	10	457.3
	50 to 100	10	457.3 > T less than 623.15
ORC-H	All	10	322.02 < T less than 195.87

4. Results

4.1. Heat exchanger areas

Table 7 summarises the magnitudes and variations of the ORC heat exchanger areas obtained in the simulations at partial engine loads. The areas are comparable to those found in the literature for an ORC operating at partial engine loads [17,56,57]. The area variations in the rest of the operational points for the M936G engine has a maximum value of -0.5, -4.6, and -0.7 % in the condenser, heater, and evaporator, respectively. While for the F1C engine, the maximum variation in the condenser, heater, and evaporator areas are -7.6, -4.7, and -1%, respectively. The highest condenser area variation between the engines obeys that the F1C engine covers a broader rpm range than the M936G engine. However, these results ensure that ORC heat exchangers will always meet the parameters established in the simulations.

4.2. ORC thermal efficiency and mass flows of cooling air and C_5H_{10} in the ORC

The ORC thermal efficiency is calculated using equation (6). The cooling air power (W_{c-air}) is obtained from commercial fans [58], which fulfils the air mass flows obtained in the simulations for both engines. Fig. 10 shows that ORC thermal efficiency has an average value of 13.06 % in the M936G engine and 12.04 % in the F1C engine. Moreover, it is observed that the highest values of the ORC thermal efficiency are at the lowest engine load. This behaviour occurs since the fan and the pump powers have the lowest values when mass flow cooling air, and C_5H_{10} presents the minimum values, e.i., at the lowest rpm (see Fig. 11). As expected, both flows increase with engine rpm leading to an increase in the thermal energy because of a rise in the exhaust gases' mass flow and temperature, as seen in Figs. 5 and 6.

$$\eta_{th-ORC} = \frac{W_{net} - W_{c-air} - W_{pump}}{Q_{EG} + Q_{CO2}} \quad (6)$$

Another factor affecting the ORC thermal efficiency is the increasing permeability value found for each rpm. As shown in Fig. 12, the permeability increases with increasing rpm as it is a function of the superheat temperature and the mass flow rate of the working fluid (variables that increase with engine load and rpm). This behaviour reduces the working fluid's ability to go through the plant, which

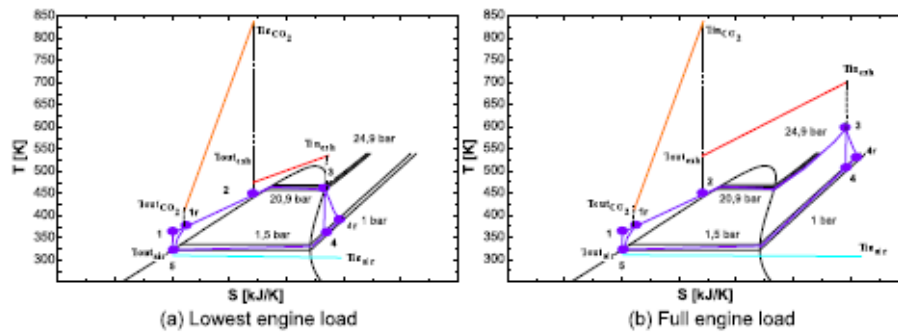


Fig. 9. ORC cycle behaviour.

Table 7

Heat exchanger areas obtained in the ORC simulations.

Engine	Heat Exchanger	Area [m ²]	Variation [%]	Total area [m ²]
M936G	ORC-C	1.817	-0.5	7.098
	ORC-H	0.083	-4.6	
	ORC-E	5.198	-0.7	
F1C	ORC-C	0.853	-7.6	2.039
	ORC-H	0.030	-4.7	
	ORC-E	1.156	1.0	

decreases the performance of the ORC-X, affecting the thermal efficiency.

4.2.1. Power expander

Fig. 13 shows the power output in the ORC-X obtained in the simulations. It is directly related to the available heat in the exhaust gases since they present the highest values at full engine load and the lowest at lower rpm engine. Under the configuration proposed in this research, the ORC in any load engine condition can cover the CCS system's parasitic loads. It can be seen more clearly in Fig. 14, where the ORC working on the M936G engine can supply up to a 76 % of the parasitic loads at 2200 rpm, and the lowest parasitic load power covered by the ORC is 42 % at 1000 rpm at 100 % of engine load. In the F1C, the highest

parasitic load power covered by the ORC is 61 % at 3400 rpm at 25 % of engine load, and the lowest is 23 % at 1000 rpm at 100 % of engine load.

5. Analysis

5.1. ORC analysis

Unfortunately, it is impossible to compare a study with similar characteristics to this one because this is the first study that evaluates the energy requirements of a CCS system with a hybridized ORC on board an ICEV operating at partial loads and in the whole rpm range. However, it is possible to compare the ORC performance, as several studies in the literature evaluate ORCs at different load conditions and engine rpm. Table 8 summarises the main findings of the performance and heat exchanger areas of the ORC from this study and of other authors with engines of similar power and size.

As summarised in Table 8, the thermal efficiency shows values between 12 and 13 % in the simulation-based studies, while this efficiency decreases up to 8 percentage points in the experimental studies. The high results of thermal efficiency found in the simulation are due to the different assumptions, among them, high isentropic efficiencies and the neglected heat losses in the lines and equipment. However, the power obtained by the expander in the present study is in the range of its counterpart.

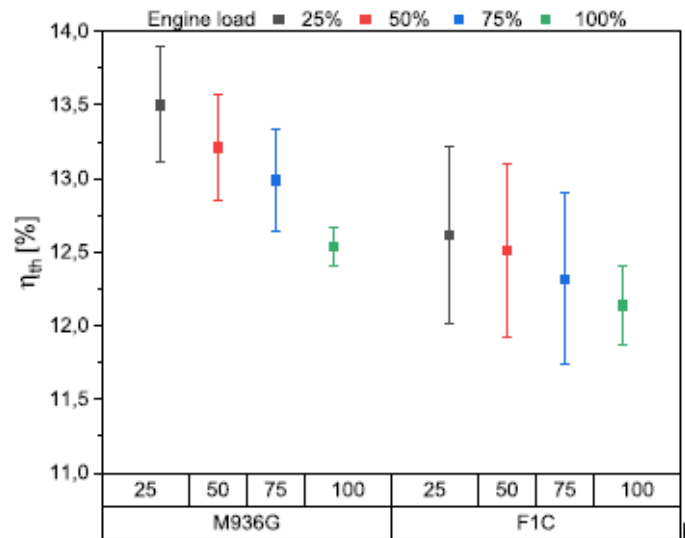


Fig. 10. Thermal efficiency variations of the ORC at all rpm and engine loads.

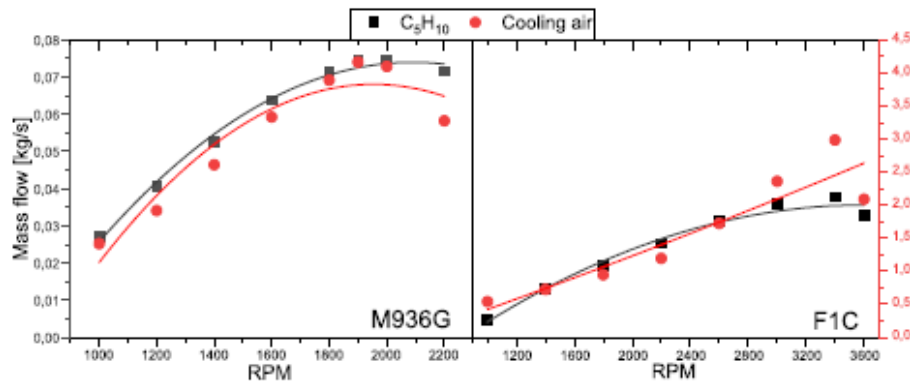


Fig. 11. C_3H_{10} and air cooling mass flows obtained in the ORC simulations.

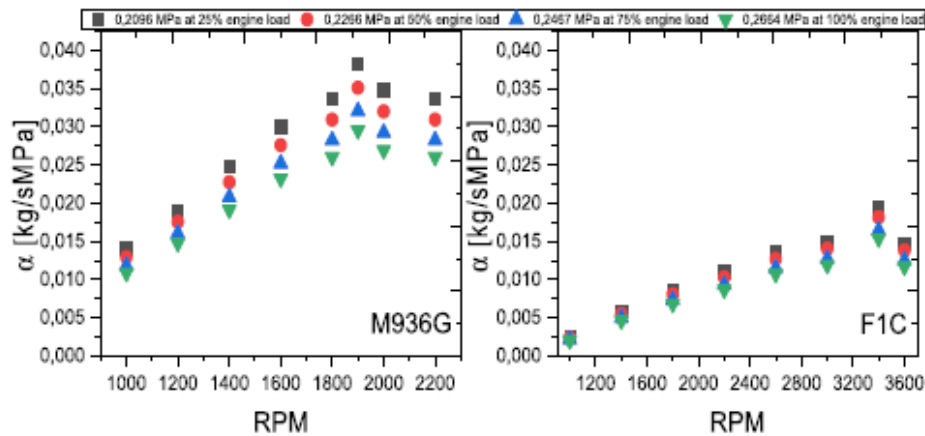


Fig. 12. Permeability in the entire rpm range and at partial engine loads.

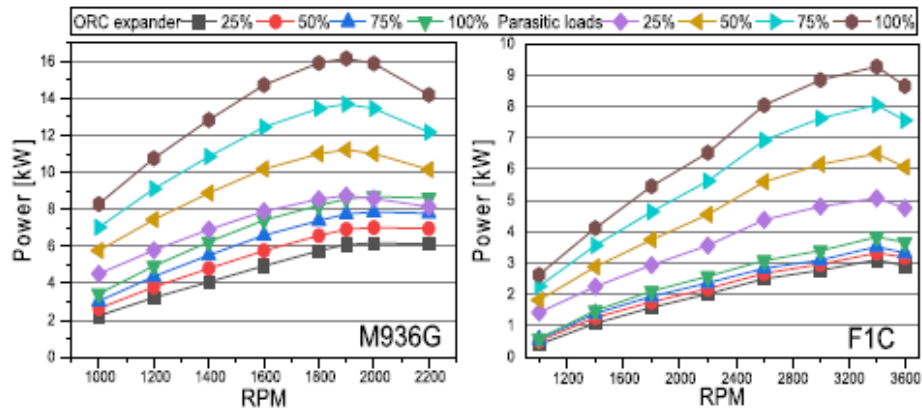


Fig. 13. Outlet power ORC-X and parasitic loads were obtained in the ORC simulations.

Regarding the heat exchanger areas of the evaporator and condenser, they are between 54 and 64 % lower than their counterparts which is a consequence of the design of the ORC proposed in this research being conditioned to the point of lower heat transfer given by the exhaust gases (25 % engine load and 1000 rpm in both engines). This produces a low working fluid mass flow that limits the condenser's size. However,

the condenser in the M936G engine is only 4 % higher than its experimental counterpart. Finally, the difference in results between the present research and those found in the literature is also due to the different working fluids used in the ORC operation.

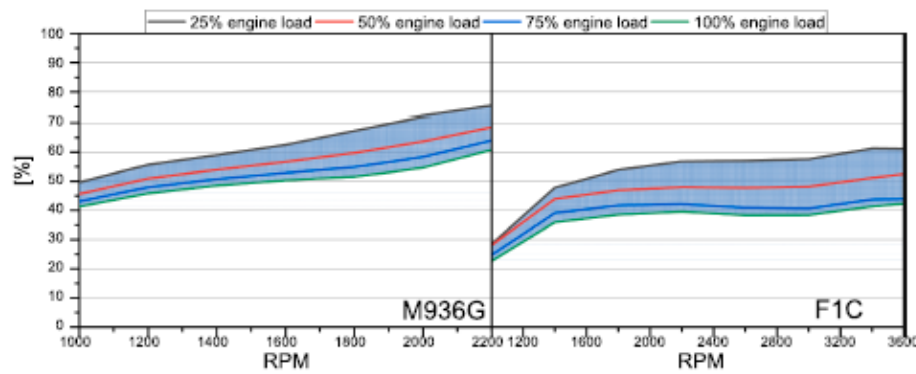


Fig. 14. Percentage of parasitic load power covered by the ORC-X under partial engine loads.

Table 8

Comparison of ORC performance results and heat exchange areas between this study and the literature.

Research work	Type of study	Volume [L], Cylinders, maximum engine power [kW]	Condition test: (rpm, Engine load)	Working fluid	ORC efficiency [%]	ORC Power [kW]	ORC-X Power [kW]	ORC-E [m ²]	ORC-C [m ²]
[51]	Exp	3 – 4-130	NF, NF	R245fa	12 max 4 min	0.55	0.72		4
[30]	Exp	3 – NF - NF	1500	R245fa	4.5 max	2.7 max			
[31]	Sim	3.3 – 4-130	1500, 50 to 100 %	R245fa	12.3	2.46	3.8	2.7	2.5
[27]	Mod	3 – 4 – 12-127,2	2175–3325, 12 loads conditions	R1233zd(E)		5.4 max 0.34 min		2 max 1.35 min	0.23 max 0.17 min
This study	Sim	3 – 4-100	1000–3600, 25 to 100 %	C ₆ H ₁₀	12–12.5	3.7 max 0.4 min	4.4 max 0.5 min	1.15	0.85
[59]	Mod	8 – 6 - NF	1200–2200, 20–100 %	R123	11.8 max 11.3 min		11.5 max 7.5 min		
[22]	Sim	NF – 6-258,3	1500, 5 load conditions	R245fa	11	26 max 10 min		2.38	6.38
[60]	Sim	NF, 6, 258,3	1500, 5 load conditions	R245fa	9.4 max	14.5		8.49	5.18
[29]	Exp	NF – 6-258,3	1800–1900, 56–100 %	R123	7 max 1 min	10 max 2 min		12	1.2
This study	Sim	7,7 – 6-220	1000–2200, 25–100 %	C ₆ H ₁₀	12.5–13.5	8.6 max 2.2 min	11 max 3 min	4.3	1.25

5.2. Energy analysis

The results show that the energy contained in the exhaust gases fully covers the TSA process's heat needs. The excess can be transformed into mechanical energy through an ORC. Depending on the engine and its operating condition, the organic cycle can produce between 22 and 76 % of the power required to cover the parasitic loads.

The additional power demand of the parasitic loads of the process must be taken from the engine, reducing the power output. However, as seen in Table 9, the average percentage of power taken from the engine by the ORC-CCS system for the parasitic loads does not exceed 8.84 % in the F1C engine and 5.71 % in the M936G engine. This table also presents

Table 9

Percentage average penalization of the CCS system over the engines power with and without ORC.

Engine load [%]	M936G		F1C	
	With ORC [%]	Without ORC [%]	With ORC [%]	Without ORC [%]
25	5.71	15.84	8.84	18.86
50	4.30	10.14	6.52	12.05
75	3.82	8.24	6.01	9.96
100	3.59	7.29	5.44	8.66

the average percentage of power required by the CCS without using the ORC at each partial load of the engine. It is observed that the CCS system using the ORC reduces the penalizes over the engine from 8.66 % at 100 % engine load up to 18.86 % at 25 % engine load in the F1C engine, and the M936G engine, it is reduced from 7.29 % at 100 % engine load up to 15.84 % at 25 % engine load. The ORC-ICE system's hybridization allows penalty values in line with those reported in the literature on CCS systems used in conventional applications [61].

It is observed that the worst performance results of the CCS system occurs for the smallest engine size. The lower exhaust gas mass flow of the smaller engine prevents the ORC from delivering more power to meet the energy demands of the CCS system. However, as thermal efficiency is quite similar in any load engine condition for both engines, the higher penalization of the CCS system over the engine is not because of the ORC operation but because of the CO₂ compression power.

On the other hand, if the European Commission extends CO₂ emission rights to the transport sector, this will increase the price of fuels, which will trigger an increase in the price of the final consumer's fuels. For this reason, assuming a 90 % CO₂ capture with the current average CO₂ price of 70 €/tCO₂, the transport sector will avoid paying 166,906.6 billion euros per year. Therefore, the design and implementation of on-board CCS systems for ICEVs as proposed here can also be justified from an economic perspective.

6. Conclusions

The paper discusses the energy feasibility of using carbon capture and storage system hybridized with an Organic Rankine Cycle to CO₂ capture on board in natural gas spark-ignition ICEs used in passenger and road freight transport. The operation at partial engine loads in the entire rpm of two commercial ICE vehicles of different sizes has been analyzed to reproduce the typical behaviour of an engine as close to reality as possible.

As the results confirm, the exhaust gases can cover all thermal energy demands in the CCS system. Regarding the ORC, it is evident that the ORC efficiency at partial engine loads does not present higher variations, and its power production reduces between 3.9 and 13.9 % the penalization of the CCS system over the engine (depending on the engine load and the engine size). These results corroborate that implementing an ORC as a complement to a CCS system is theoretically feasible from the energy point of view. However, it is essential to develop simulations or experimental tests that consider variables such as the back pressure and heat losses in the devices, among others. For instance, the literature indicates that the back pressure caused by the ORC is between 100 and 200 mbar [29]. Suppose the back pressure caused by the CCS system is included. In that case, the value of this parameter will increase and, consequently, the engine's fuel consumption [62], resulting in a decrease in the engine's thermal efficiency, making the CCS-ORC system economically unviable.

On the other hand, the results of the ORC heat exchange areas are between 2.04 m² for the small engine and 7.1 m² for the large engine. Although the areas found in this research work are in the same order of magnitude as those found in the literature, there is a significant difference, mainly in the evaporator area, which is approximately 60 % smaller than the evaporator areas provided in the literature. This variation is due to many factors. The most important is the amount of mass flow of the working fluid, which is related to the permeability, which establishes the ideal thermodynamic conditions of entry of the working fluid into the expander, and, therefore, the saturation temperature achieved in the evaporator.

The present research is still in the first phase and requires joint efforts to reach real applications. There are several open lines of research and future developments. Among others, the optimization of operational points to reduce the heat exchangers surface, the evaluation of several sorbents, the backpressure in the engine caused by the CCS and ORC systems and how they influence the ORC-ICE system's global performance.

The presented modelling and calculation procedures can be used in other sectors where ICE is used, for instance, industrial plants, even where more stability in the engine operating conditions appears. This paper aspires to cover the gap in theoretical-based studies that extend ORCs and CCS systems in less investigated sectors with these technologies, producing greater energy efficiency and reducing CO₂ emissions worldwide.

CRedit authorship contribution statement

Alexander García-Mariaca: Conceptualization, Methodology, Software. Eva Llera-Sastres: Methodology, Writing – original draft, Supervision, Writing – review & editing. Francisco Moreno: Supervision, Software, Validation, Writing – review & editing.

Declaration of Competing Interest

The authors declare that they have no known competing financial interests or personal relationships that could have appeared to influence the work reported in this paper.

Data availability

Data will be made available on request.

References

- [1] IEA. Data & Statistics - IEA 2021. <https://www.iea.org/data-and-statistics/data-browser/?country=WORLD&fuel=CO2%20emissions&indicator=CO2BySector> (accessed November 14, 2021).
- [2] Sullivan JM, Sivak M. Carbon capture in vehicles: a review of general support, available mechanisms, and consumer acceptance issues. University of Michigan Transportation Research Institute; 2012.
- [3] Li Z, Khajepour A, Song J. A comprehensive review of the key technologies for pure electric vehicles. Energy 2019;182:824–39. <https://doi.org/10.1016/j.energy.2019.06.077>.
- [4] Kalghatgi G. Is it really the end of internal combustion engines and petroleum in transport? Appl Energy 2018;225:965–74. <https://doi.org/10.1016/j.apenergy.2018.05.076>.
- [5] Statista. Global transport CO₂ emissions breakdown 2020 | Statista 2020. <http://www.statista.com/statistics/1185535/transport-carbon-dioxide-emissions-breakdown/> (accessed November 14, 2021).
- [6] Kuhlwein J, Berlin B, Brunsel J, San J, Washington FJ. Driving Resistances of Light-Duty Vehicles In Europe: Present Situation, Trends, And Scenarios For 2025. 2016.
- [7] Huang Y, Ng EY, Zhou JL, Surawski NC, Chan EFC, Hong G. Eco-driving technology for sustainable road transport: A review. Renew Sustain Energy Rev 2018;93:596–609. <https://doi.org/10.1016/j.rser.2018.05.030>.
- [8] Fafoutellis P, Mantouka EG, Vlahogianni EI. Eco-driving and its impacts on fuel efficiency: An overview of technologies and data-driven methods. Sustainability 2021;13:226. <https://doi.org/10.3390/su13010226>.
- [9] Leach F, Kalghatgi G, Stone R, Miles P. The scope for improving the efficiency and environmental impact of internal combustion engines. Transportation Engineering 2020;1:100005. <https://doi.org/10.1016/j.treng.2020.100005>.
- [10] Agudelo AF, García-Contreras R, Agudelo JR, Armas O. Potential for exhaust gas energy recovery in a diesel passenger car under European driving cycle. Appl Energy 2016;174:201–12. <https://doi.org/10.1016/j.apenergy.2016.04.092>.
- [11] Merikiz J, Puc P, Lijewski P, Ziolkowski A, Wojciechowski KT. The Analysis of Exhaust Gas Thermal Energy Recovery Through a TEG Generator in City Traffic Conditions Reproduced on a Dynamic Engine Test Bed. J Electron Mater 2015;44:1704–15. <https://doi.org/10.1007/s11664-014-3522-6>.
- [12] Spruce C, Depcik C. Review of organic Rankine cycles for internal combustion engine exhaust waste heat recovery. Appl Therm Eng 2013;51:711–22. <https://doi.org/10.1016/j.applthermaleng.2012.10.017>.
- [13] Osorio-Tejada JL, Llera-Sastres E, Scarpellini S. Liquefied natural gas: Could it be a reliable option for road freight transport in the EU? Renew Sustain Energy Rev 2017;71:785–95. <https://doi.org/10.1016/j.rser.2016.12.104>.
- [14] Osorio-Tejada JL, Llera-Sastres E, Scarpellini S. A multi-criteria sustainability assessment for biodiesel and liquefied natural gas as alternative fuels in transport systems. J Nat Gas Sci Eng 2017;42:169–86. <https://doi.org/10.1016/j.jngse.2017.02.046>.
- [15] Ramirez A, Sarathy SM, Gascon J. CO₂ Derived E-Fuels: Research Trends, Misconceptions, and Future Directions. Trends in Chemistry 2020;2:785–95. <https://doi.org/10.1016/j.trechm.2020.07.005>.
- [16] Wang H, Zhou P, Wang Z. Reviews on current carbon emission reduction technologies and projects and their feasibility on ships. J Mar Sci Appl 2017;16:129–36. <https://doi.org/10.1007/s11804-017-1413-y>.
- [17] Sharma S, Maréchal F. Carbon Dioxide Capture From Internal Combustion Engine Exhaust Using Temperature Swing Adsorption. Front Energy Res 2019;7:1–12. <https://doi.org/10.3389/fenrg.2019.00143>.
- [18] García-Mariaca A, Llera-Sastres E. Review on Carbon Capture in ICE Driven Transport. Energies (Basel) 2021;14:6865. <https://doi.org/10.3390/en14216865>.
- [19] Kumar P, Rathod V, Parwani AK. Experimental investigation on performance of adsorbents for carbon dioxide capture from diesel engine exhaust. Environmental Progress & Sustainable Energy 2021;e13651. <https://doi.org/10.1002/ep.13651>.
- [20] Hoang AT. Waste heat recovery from diesel engines based on Organic Rankine Cycle. Appl Energy 2018;231:138–66. <https://doi.org/10.1016/j.apenergy.2018.09.022>.
- [21] Ringler J, Seifert M, Guyotot V, Hübner W. Rankine Cycle for Waste Heat Recovery of IC Engines. SAE Int J Engines 2009;1:67–76.
- [22] Lin S, Zhao L, Deng S, Ni J, Zhang Y, Ma M. Dynamic performance investigation for two types of ORC system driven by waste heat of automotive internal combustion engine. Energy 2019;169:958–71. <https://doi.org/10.1016/j.energy.2018.12.092>.
- [23] Scaccabarozzi R, Tavano M, Invernizzi CM, Martelli E. Comparison of working fluids and cycle optimization for heat recovery ORCs from large internal combustion engines. Energy 2018;158:396–416. <https://doi.org/10.1016/j.energy.2018.06.017>.
- [24] Bombarda P, Invernizzi CM, Pietra C. Heat recovery from Diesel engines: A thermodynamic comparison between Kalina and ORC cycles. Appl Therm Eng 2010;30:212–9. <https://doi.org/10.1016/j.applthermaleng.2009.08.006>.
- [25] Feng Y, Hung TC, Zhang Y, Li B, Yang J, Shi Y. Performance comparison of low-grade ORCs (organic Rankine cycles) using R245fa, pentane and their mixtures based on the thermoeconomic multi-objective optimization and decision makings. Energy 2015;93:2018–29. <https://doi.org/10.1016/j.energy.2015.10.065>.

- [26] Shi L, Shu G, Tian H, Deng S. A review of modified Organic Rankine cycles (ORCs) for internal combustion engine waste heat recovery (ICE-WHR). *Renew Sustain Energy Rev* 2018;92:95–110. <https://doi.org/10.1016/j.rser.2018.04.023>.
- [27] di Battista D, di Bartolomeo M, Villante C, Cipollone R. On the limiting factors of the waste heat recovery via ORC-based power units for on-the-road transportation sector. *Energy Convers Manage* 2018;155:68–77. <https://doi.org/10.1016/j.enconman.2017.10.091>.
- [28] di Battista D, Mauriello M, Cipollone R. Waste heat recovery of an ORC-based power unit in a turbocharged diesel engine propelling a light duty vehicle. *Appl Energy* 2015;152:109–20. <https://doi.org/10.1016/j.apenergy.2015.04.088>.
- [29] Zhang YQ, Wu YT, Xia GD, Ma CF, Ji WN, Liu SW, et al. Development and experimental study on organic Rankine cycle system with single-screw expander for waste heat recovery from exhaust of diesel engine. *Energy* 2014;77:499–508. <https://doi.org/10.1016/j.energy.2014.09.034>.
- [30] Fatigati F, di Battista D, Cipollone R. Permeability effects assessment on recovery performances of small-scale ORC plant. *Appl Therm Eng* 2021;196:117331. <https://doi.org/10.1016/j.applthermaleng.2021.117331>.
- [31] Badescu V, Aboaltabooq MHK, Pop H, Apostol V, Prisecaru M, Prisecaru T. Design and operational procedures for ORC-based systems coupled with internal combustion engines driving electrical generators at full and partial load. *Energy Convers Manage* 2017;139:206–21. <https://doi.org/10.1016/j.enconman.2017.02.046>.
- [32] Carraro G, Pili R, Lazzaretto A, Haglind F. Effect of the evaporator design parameters on the dynamic response of organic Rankine cycle units for waste heat recovery on heavy-duty vehicles. *Appl Therm Eng* 2021;198:117496. <https://doi.org/10.1016/j.applthermaleng.2021.117496>.
- [33] Grelet V, Reiche T, Lemort V, Nadri M, Dufour P. Transient performance evaluation of waste heat recovery rankine cycle based system for heavy duty trucks. *Appl Energy* 2016;165:878–92. <https://doi.org/10.1016/j.apenergy.2015.11.004>.
- [34] Fatigati F, di Bartolomeo M, di Battista D, Cipollone R. Experimental and Numerical Characterization of the Sliding Rotary Vane Expander Intake Pressure in Order to Develop a Novel Control-Diagnostic Procedure. *Energies (Basel)* 2019;12(10):1970. <https://doi.org/10.3390/en12101970>.
- [35] Kai H, Michael B, Marko W. The New Mercedes-Benz Medium Duty Commercial Natural Gas Engine. *MTZ Worldw* 2014;75:4–11. <https://doi.org/10.1007/s38313-014-0251-4>.
- [36] Iveco company. IVECO DAILY technical information 2015. https://www.iveco.com/Denmark/Documents/Configurator/Brochure/Dailyvan_DK.pdf (accessed February 8, 2020).
- [37] Mercedes-Benz. Citaro NGT technical information 2017:16. https://www.mercedes-benz-bus.com/content/dam/mbo/markets/common/buy/services-online/download-technical-brochures/images/content/regular-service-buses/citaro-ngt/MB-NGT-2-ES-09_17.pdf (accessed February 8, 2020).
- [38] CNH Industrial. CNH Industrial Newsroom : FPT Industrial F1A and F1C Engines for the New IVECO Daily “Bluepower” 2017. <https://media.cnhindustrial.com/EU/ROPE/FPT-INDUSTRIAL/fpt-industrial-f1a-and-f1c-engines-for-the-new-iveco-daily-bluepower-/s/ff84bc56-fd41-452d-b4a5-2d5216ff3a3f> (accessed June 22, 2020).
- [39] Obols J, Soleri D, Dioc N, Moreau M. Potential of concomitant injection of CNG and gasoline on a 1.6L gasoline direct injection turbocharged engine. *SAE Technical Papers* 2011. <https://doi.org/10.4271/2011-01-1995>.
- [40] Yontar AA, Doğu Y. Effects of equivalence ratio and CNG addition on engine performance and emissions in a dual sequential ignition engine. *Int J Engine Res* 2020;21:1067–82. <https://doi.org/10.1177/1468087419834190>.
- [41] López JJ, Novella R, Gomez-Soriano J, Martinez-Hernandez PJ, Rampanarivo F, Libert C, et al. Advantages of the unscavenged pre-chamber ignition system in turbocharged natural gas engines for automotive applications. *Energy* 2021;218:119466. <https://doi.org/10.1016/j.energy.2020.119466>.
- [42] Nikzadfar K, Shamekhi AH. Investigating the relative contribution of operational parameters on performance and emissions of a common-rail diesel engine using neural network. *Fuel* 2014;125:116–28. <https://doi.org/10.1016/j.fuel.2014.02.021>.
- [43] Heywood JB. Internal combustion engine fundamentals. vol. 1. McGraw-Hill Book Company; 1988. 10.1016/s1350-4789(10)70041-6.
- [44] Einewall P, Tunestal P, Johansson B. Lean burn natural gas operation vs. stoichiometric operation with EGR and a three way catalyst. *SAE Technical Papers* 2005. <https://doi.org/10.4271/2005-01-0250>.
- [45] Zhang Q, Xu Z, Li M, Shao S. Combustion and emissions of a Euro VI heavy-duty natural gas engine using EGR and TWC. *J Nat Gas Sci Eng* 2016;28:660–71. <https://doi.org/10.1016/j.jngse.2015.12.015>.
- [46] Ben-Mansour R, Abuelaymen A, Qasem NAA. Thermal design and management towards high capacity CO₂ adsorption systems. *Energy Conversion and Management* 2020;212. 10.1016/j.enconman.2020.112796.
- [47] Peris R, Navarro-Esbrí J, Molés F. Bottoming organic Rankine cycle configurations to increase Internal Combustion Engines power output from cooling water waste heat recovery. *Appl Therm Eng* 2013;51:364–71. <https://doi.org/10.1016/j.applthermaleng.2013.08.016>.
- [48] Invernizzi CM, Bonalumi D. Thermal stability of organic fluids for Organic Rankine Cycle systems. *Elsevier Ltd* 2017. <https://doi.org/10.1016/B978-0-08-100510-1.00005-3>.
- [49] Invernizzi CM, Iora P, Manzolini G, Lasala S. Thermal stability of n-pentane, cyclopentane and toluene as working fluids in organic Rankine engines. *Appl Therm Eng* 2017;121:172–9. <https://doi.org/10.1016/j.applthermaleng.2017.04.038>.
- [50] Scaccabarozzi R, Tavano M, Invernizzi CM. Comparison of working fluids and cycle optimization for heat recovery ORCs from large internal combustion engines. *Energy* 2018. <https://doi.org/10.1016/j.energy.2018.06.017>.
- [51] Fatigati F, di Bartolomeo M, di Battista D, Cipollone R. Experimental characterization of a hermetic scroll expander operating in an ORC-based power unit bottoming an internal combustion engine. *AIP Conference Proceedings*, vol. 2191, American Institute of Physics Inc.; 2019. 10.1063/1.5138802.
- [52] Matthias Kind and Holger Martin. *VDI Heat Atlas*. Second. Berlin: Springer; 2010. 10.1007/978-3-540-77877-6.
- [53] Verdegalm WM, Wang K, Sculley JP, Wriedt M, Zhou HC. Evaluation of Metal-Organic Frameworks and Porous Polymer Networks for CO₂-Capture Applications. *ChemSusChem* 2016;9:636–43. <https://doi.org/10.1002/cssc.201501464>.
- [54] Huck JM, Lin LC, Berger AH, Shahrak MN, Martin RL, Bhowan AS, et al. Supporting Information: Evaluating different classes of porous materials for carbon capture. *Energy Environ Sci* 2014;7:4132–46. <https://doi.org/10.1039/c4ee02636e>.
- [55] A. Kayode Coker. *Ludwig's Applied Process Design for Chemical and Petrochemical Plants*. 4th ed. 2015. 10.1016/B978-0-7506-8524-5.00017-3.
- [56] Badescu V, Aboaltabooq MHK, Pop H, Apostol V, Prisecaru M, Prisecaru T. Avoiding malfunction of ORC-based systems for heat recovery from internal combustion engines under multiple operation conditions. *Appl Therm Eng* 2019;150:977–86. <https://doi.org/10.1016/j.applthermaleng.2019.01.046>.
- [57] Capata R, Piras G, Benato A, Turunen-Saarela T. Condenser Design for On-Board ORC Recovery System. *Applied Sciences (Basel)* 2021;11(14):6356. <https://doi.org/10.3390/app11146356>.
- [58] Ebm-papst. Axial fans 2021. <https://www.ebmpapst.com/de/en/products/axial-fans.html> (accessed November 23, 2021).
- [59] Shu G, Zhao M, Tian H, Wei H, Liang X, Huo Y, et al. Experimental investigation on thermal OS/ORC (Oil Storage/Organic Rankine Cycle) system for waste heat recovery from diesel engine. *Energy* 2016;107:693–706. <https://doi.org/10.1016/j.energy.2016.04.062>.
- [60] Yu G, Shu G, Tian H, Wei H, Liu L. Simulation and thermodynamic analysis of a bottoming Organic Rankine Cycle (ORC) of diesel engine (DE). *Energy* 2013;51:281–90. <https://doi.org/10.1016/j.energy.2012.10.054>.
- [61] Lara Y, Romeo LM, Lisbona P, Espatolero S, Escudero AL. Efficiency and Energy Analysis of Power Plants with Amine-Impregnated Solid Sorbents CO₂ Capture. *Energy Technology* 2018;6:1649–59. <https://doi.org/10.1002/ente.201700806>.
- [62] Singh N, Rutland CJ, Foster DE, Narayanaswamy K, He Y. Investigation into different DPF regeneration strategies based on fuel economy using integrated system simulation. *SAE Technical Paper* 2009:2009-01-1275. <https://doi.org/10.4271/2009-01-1275>.



16th International Conference on Greenhouse Gas Control Technologies, GHGT-16

23rd -27th October 2022, Lyon, France

Dynamic CO₂ Capture in a Natural Gas Engine Used in Road Freight Transport

Alexander García-Mariaca^{a*}, Eva Llera Sastresa^b

^a *Escuela de Ingeniería y Arquitectura, University of Zaragoza, María de Luna s/n, Zaragoza, 50018, Spain*

^b *Department of Mechanical Engineering and CIRCE Research Institute, University of Zaragoza, María de Luna s/n, Zaragoza, 50018, Spain*

Abstract

This paper presents the results of the dynamic CO₂ capture on a turbocharged natural gas spark ignition engine usually used in passenger and freight vehicles operating under the test condition of the world harmonised transient cycle (WHTC). The CO₂ capture and storage (CCS) system uses temperature swing adsorption (TSA) as a technique of CO₂ capture. The sorbent selected for the CO₂ adsorption is the PPN-6-CH₂-DETA which the regeneration process is carried out using the heat in the exhaust gases from the engine. Additionally, an ORC is hybridised in the CCS system to supply the energy demand of the CO₂ compression and cooling processes. The results show that the CCS system operation in the engine entails a 10% increase in fuel consumption, producing a rise in the engine brake power of 4.93%. Moreover, for 8 hours of operation, the TSA system would take up 0.2 m³ plus 0.43 m³ for the CO₂ storage as a liquid, and assuming a volume of 1 m³ of the devices, the total volume of the CCS system is 1,63 m³. These results make the CCS system highly competitive with other CO₂ reduction technologies, such as hydrogen fuel cells requiring high installation volumes.

Keywords: Carbon Capture and Storage; Temperature Swing Adsorption; Internal Combustion Engine; WHTC; dynamic operation

Nomenclature

BP	Brake power
CCR	CO ₂ carbon rate
CCS	CO ₂ capture and storage
CNG	Compressed natural gas
EG	Exhaust gases
ICE	Internal combustion engine
ICEV	Internal combustion engine vehicle
ORC	Organic Rankine cycle
TSA	Temperature swing adsorption
WF	Working fluid

* Corresponding author. Email address: alexander.garcia@unizar.es

1. Introduction

In 2019 the transport sector emitted 8222 MtCO₂, representing 24.45% of the total CO₂ emissions [1]. In order to mitigate global CO₂ emissions, the road freight and passenger transport sector has discouraged the use of diesel as fuel and promoted the use of alternative fuels like natural gas (compressed or liquified). However, it is still necessary to incorporate CO₂ capture and storage (CCS) technologies that allow an additional and challenging reduction. Moreover, it is noteworthy the high potential that could have the CO₂ captured from this source for manufacturing e-fuels and, in a circular perspective achieving a transport sector with near-zero CO₂ emissions.

One of the technologies most developed recently to reduce CO₂ emissions into the atmosphere from the energy and industrial sectors is CO₂ capture systems. The most researched CO₂ capture technique is amine scrubbing [2]. This technique of CO₂ capture is well known because it has been widely used since the 1930s to clean natural gas in the extraction process [3], whereby its use has been relatively easy to implant in exhaust gases of stationary applications. However, the energy penalty of using an amine scrubbing plant has led researchers to develop other technologies to improve carbon capture rates, reduce the energy penalty and that those being able to adapt to the operation of other CO₂ emission sources. Of these new developments, the following stand out: membranes, which are still in the experimental phase [4], and adsorption swing by pressure, electrical or temperature. Many of these CO₂ capture techniques already have experimental research in pilot plant applications [5,6].

Temperature swing Adsorption (TSA) has an excellent potential to be used in the transport sector (maritime and land), as it can be adapted to the operating characteristics of their internal combustion engines (ICE) without generating large penalties for their ICEs [7]. According to studies, it can use the same heat from exhaust gas for its desorption process. Even the remaining heat can be used in a waste heat recovery system for electricity production and thus supply the power demand in the CO₂ storage process [8].

There is scarce research on using CCS systems in the maritime sector [9–11] and very few in the road transport sector [12,13]. The experimental works published about CCS systems in internal combustion engine vehicles (ICEV) have been focused on evaluating several sorbents under stationary conditions and without regeneration [14–16]. On the other hand, simulations research works have opted to implement organic cycles Rankine that take advantage of the waste thermal energy from the exhaust gas to produce the power required for its operation and compress the CO₂ [7,12]. Despite that, these studies also were performed assuming stationary conditions, bringing relevant information about the energy requirements and size of the devices of a CCS system working on an ICEV, so there is a lack of research on the behaviours of the CCS system operating on ICEV under dynamic engine conditions.

This research work aims to evaluate a CCS system onboard with TSA as a CO₂ capture technique, operating in dynamic conditions of a turbocharged spark-ignition ICEV fuelled with natural gas used in road freight and passenger transport. The TSA will take advantage of the waste heat from the exhaust gases in the sorbent regeneration process. The remaining heat in the exhaust gas will enter the ORC to produce mechanical power, thus supplying power to the components involved in the CCS system. The operation engine was simulated under stationary conditions in the entire range of rpm at four engine loads, and the software AVL-boost was used to accomplish this purpose. The CCS-ORC system was modelled in the software Aspen Plus, and simulations were carried out to determine the heat exchanger surfaces and the energy requirements of the CCS system. The sorbent used in the simulations was PPN-6-CH₂-DETA due to its remarkable water stability, ultra-high selectivity for CO₂, exceptional adsorption capacity, and low regeneration energy. This sorbent is suitable for CO₂ capture from the exhaust gases coming from an ICEV [17]. The main parameter assumed in this simulation is a CO₂ capture rate (CCR) of 90%. World Harmonized Transient Cycle (WHTC) was further included in simulations to test the performance of the CCS system under dynamic conditions, with realistic variable mass fuel and brake power engine as it occurs in a transport service. Polynomial regressions from the stationary simulations were used to evaluate each point of the WHTC cycle.

2. Method

2.1. Engine and CO₂ capture storage system

A turbocharged compressed natural gas (CNG) spark ignition internal combustion engine frequently used in passenger and freight transport has been selected for the analysis. This engine was simulated in the software AVL boost under four engine load conditions (25, 50, 75 and 100%) in the entire range of engine speed (from 1000 to 2000 rpm) and with stoichiometric conditions to obtain the performance curve at these conditions, and validate the results of the simulations. The main engine characteristics and the parameters used in the simulation are shown in the studies [8,13].

The CCS system uses TSA as a CO₂ capture technique. The system includes a rotary wheel adsorber (RWA) to develop the process of CO₂ capture by TSA (adsorption, heating desorption, and cooling). The sorbent selected is PPN-6-CH₂-DETA, which has a high CO₂ selectivity (>10000) [18], low adsorption heat (45.32 kJ/molCO₂) [18], and can withstand small amounts of water, which leads to a lower cooling requirement of the exhaust gases, which triggers a reduction in the CCS system penalty by cooling [7]. Also, the CCS system has been hybridised with an ORC, whose design was made following the procedure developed by Fatigat [19,20]. The working fluid (WF) used in the ORC is cyclopentane which was selected due to its excellent performance in previous research works on ORC in ICE [21].

Finally, the CCS stores the captured CO₂ by compressing it until it reaches the liquid phase to reduce its volume and thus facilitate its storage. This condition at 75 bar and 29.3 °C is achieved. The CCR established in the simulations is 90%, and the WF mass flow is set up at the lowest engine load condition for each rpm to operate in the following engine load conditions. The entire CCS-ORC system is designed to be located on the vehicle roof. Thus its carrying capacity is not affected. Figure 1 shows the CCS-ORC system description and its location on the bus. All ORC and CCS simulations were performed in Aspen Plus software. The main ORC operating values and the areas of the ORC and CCS heat exchangers obtained in the simulations are shown in Table 1[8].

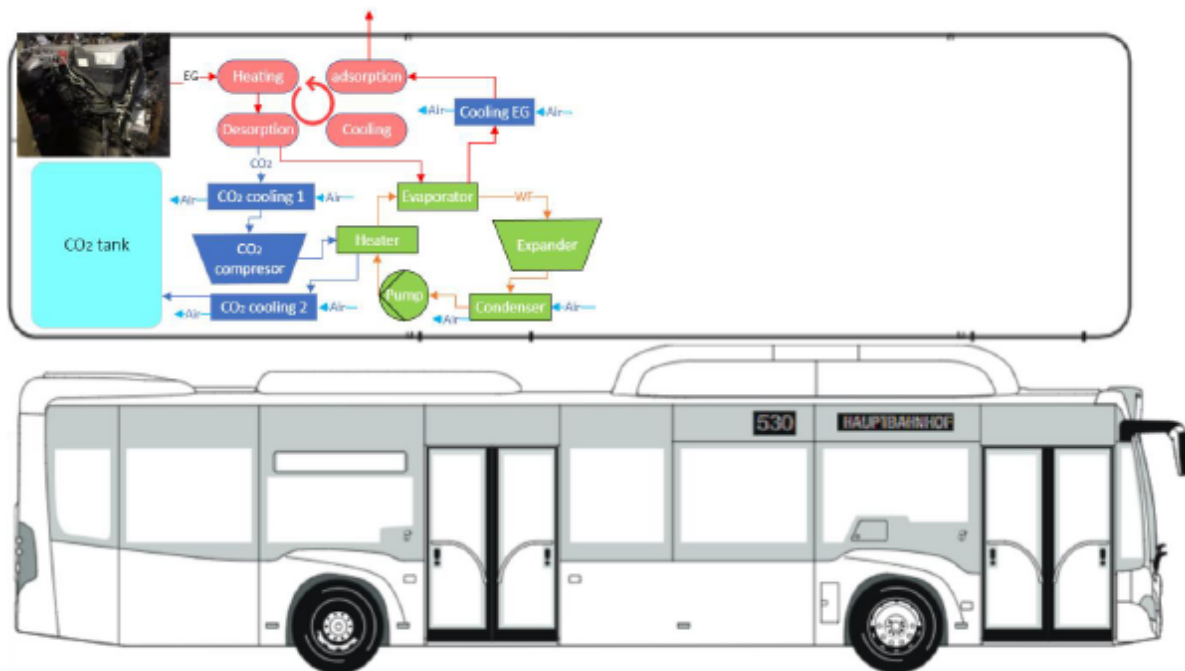


Figure 1. CCS-ORC system configuration on the vehicle roof

Table 1. Main parameter of the ORC [8].

Variable or device	Unit	Value
ORC low pressure	bar	1
ORC high pressure	bar	24.9
ORC condenser	m ²	1.817
ORC Evaporator	m ²	5.198
ORC heater	m ²	0.083

2.2. Procedure

The calculation of the variables of increase in engine brake power (BP), fuel consumption and mass of CO₂ captured due to the operation of the CCS-ORC system under dynamic conditions is carried out using the WHTC cycle. This cycle contains 1800 s, parameterised by points of speed and load values (in terms of torque) set as normalised values. Based on the above, the first procedure is to obtain the actual values for the speed engine following the procedure developed in [22] (equation 1), which requires the calculation of other ICE speeds. In this equation, n_{lo} is the lowest engine speed, where the power is 55 % of maximum power, n_{idle} is the idle speed, $n_{95\%}$ is the highest speed where the power is 95% of maximum power, n_{pref} is the engine speed, where the maximum torque integral is 51% of the whole integral, n_{hi} is the highest speed where the power is 70% of maximum power [22]. The values required for calculating the different speeds are summarised in Table 2. The actual torque calculation is done using equation 2. Figure 22 shows the actual speed and torque obtained for the M936G engine.

$$n_{act} = n_{norm}(0.45n_{lo} + 0.45n_{pre} + 0.1n_{hi} - n_{idle})2.0327 + n_{idle} \quad (1)$$

$$T_{act} = \frac{\%T \cdot T_{max}}{100} \quad (2)$$

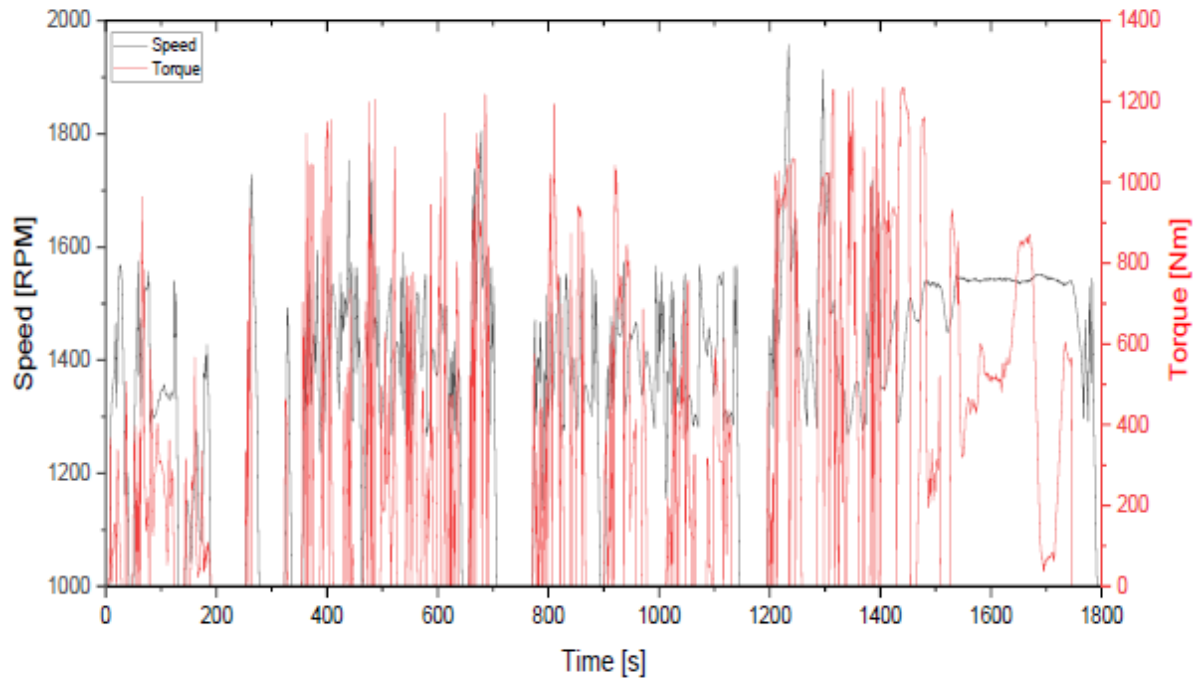
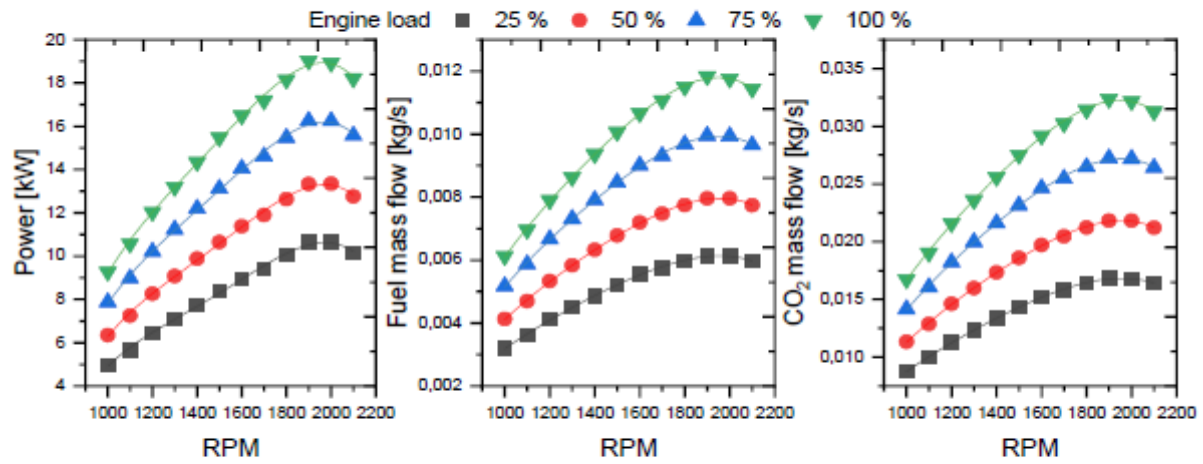


Figure 2. Actual Speed and torque for the M936G engine

Table 2. Values of speed variables taken for actualising the engine speed in the WHTC.

Variable	Unit	Value
n_{lo}	RPM	1045.3
n_{pre}	RPM	1552.4
n_{hi}	RPM	1213.6
n_{idle}	RPM	1000
n_{oth}	RPM	2095

Once the torque and speed values of the WHTC points have been obtained, it proceeds to find the polynomial functions from the results obtained in ASPEN of the variables CO₂ capture process for each engine load condition and engine speed. With these equations, it is possible to calculate the increases in the torque (brake power), fuel mass flow (specific brake fuel consumption) and captured CO₂ emission. Figure 3 shows the results obtained from these variables obtained in the simulations.

Figure 3. Power penalisation, fuel mass flow and CO₂ mass flow captured obtained in the simulations of the CCS-ORC system in ASPEN.

These polynomial functions are always obtained according to each point's engine load and speed, as shown in equation 3, and they have a coefficient of determination (R^2) greater than 99%. Subsequently, an algorithm which calculates the additional engine power required for the operation of the CCS system is developed, as well as the fuel mass flow and the CO₂ mass flow emitted based on actual speed and torque for each point of the WHTC. This process is done by iterating until the error between the final captured CO₂ and the previous iteration is less than 0.1%.

$$\text{Variable (CO}_2, m_f \text{ and Power)} = f(\text{speed, torque})_{act} \quad (3)$$

3. Results

As a consequence of the installation of the CCS-ORC system, the engine must provide the power that the ORC cannot supply to the CCS system, as shown in Figure 3. This increase in engine power throughout the WHTC cycle is 4.93 %, as seen in Figure 4. As a consequence of this rise in engine power, fuel and CO₂ mass flows increase, as shown in Figures 5 and 6. The initial fuel consumption of the engine increased 10.03%, adjusting the brake-specific fuel consumption of the engine from 374.6 g/kWh to 395.9 g/kWh, which represents an increase of 5.67%. Consequently, the CO₂ mass flow captured suffered an increase of 9.14%.

As observed in the results shown previously, the operation of the CCS-ORC system presents a penalty on the engine power on average less than 10%, which is quite positive since studies indicate that the traditional CCS systems could have penalties of up to 10 % [23]. However, the engine penalty values do not take into account at this stage of the research the additional weight of the systems, which can be close to 500 kg between the different CCS-ORC devices (heat exchangers, pumps, fans, expanders, pipes, etc.). Moreover, If it takes 30 min to perform a single TSA cycle,

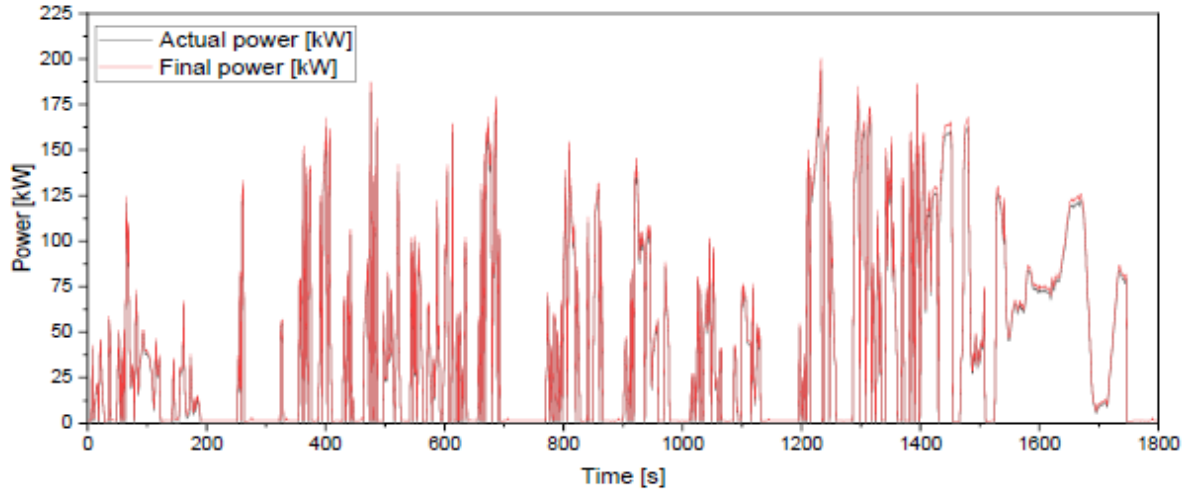


Figure 5. Actual and final engine power in the WHTC.

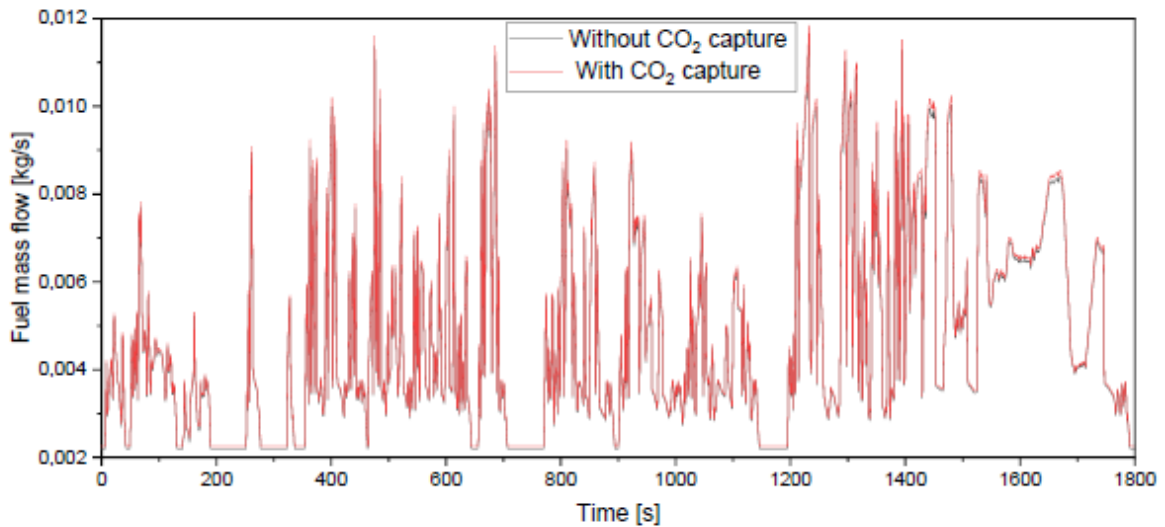


Figure 4. Fuel mass flow with and without CO₂ capture in the WHTC

the estimated weight of the sorbent is 168 kg, which must be added to the device's weight.

In addition, there is also a loss engine power because of the back pressure exerted by the CO₂ capture system (sorbent and ORC). This topic must be studied to establish the total losses in engine power. However, these preliminary results show an encouraging panorama regarding the installation of CO₂ capture systems working with TSA and powered by ORC due to it achieving a high CCR (90%) in a dynamic operation of a freight and passenger vehicle with a low engine power penalisation.

Regarding the space needs of the CCS-ORC system, it is estimated that the devices occupy 1 m^3 and add 500 kg of weight. On the other hand, the sorbent material needs 0.2 m^3 , corresponding to 160 kg, and the CO_2 stored has a volume of 0.43 m^3 with a weight of 326 kg of CO_2 for an operation of 8 hours. That is to say that the estimated weight of the CCS-ORC system is 1000 kg and needs an installation volume of 1.63 m^3 , which could be localised on the vehicle roof, as shown in Figure 1.

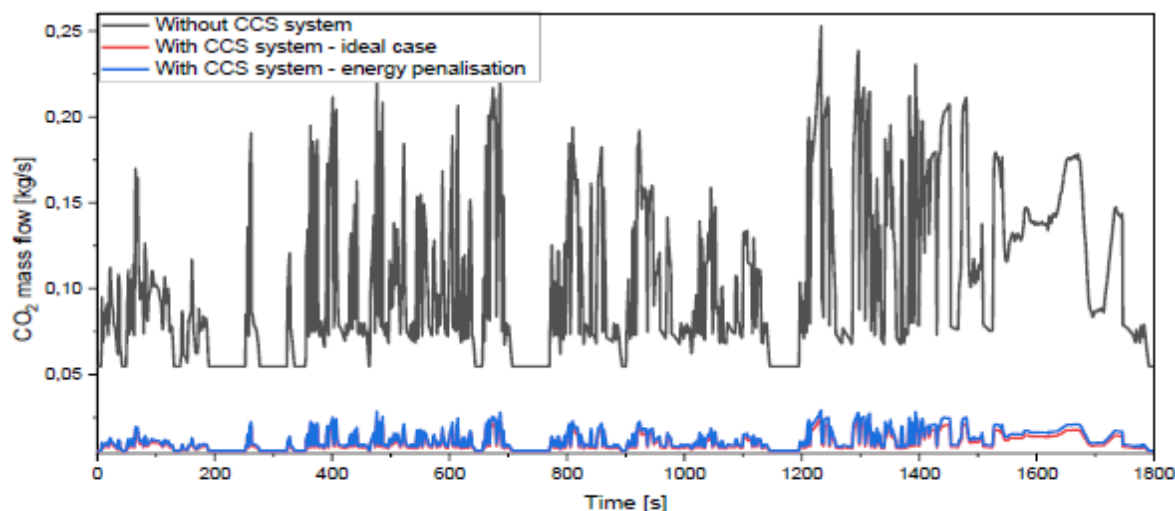


Figure 6. Actual and final CO_2 mass flow capture in the WHTC

Conclusions

- Implementing a CCS-ORC system produces an increase in engine power of 4.93%, leading to an increase in fuel consumption of 10%. This increase in fuel consumption would lead to a rise in the operating cost of the transport sector, which would be compensated if the transport sector must pay for CO_2 emission permits. On the other hand, sorbents as metal-organic frameworks must be evaluated. They have a lesser adsorption heat, and their use could reduce engine penalisation and fuel consumption.
- The installation of the CCS-ORC system on the vehicle's roof is feasible because it only requires a volume of 1.63 m^3 of space for an 8-hour operation. This figure can be compared with other CO_2 reduction technologies in the transport sector. For instance, the CCS-ORC system proposed has a volume of 5.5 times less than a hydrogen fuel cell bus.
- Despite the promising results obtained, care must be taken since this study does not consider either the thermal inertia of the system or incorporate polynomial functions for engine losses lower than 25%, which affects the results obtained in this study. Going to the experimental field and evaluating an engine with a CCS-ORC system is necessary.

References

- [1] IEA. Data & Statistics - IEA 2021. <https://www.iea.org/data-and-statistics/data-browser/?country=WORLD&fuel=CO2%20emissions&indicator=CO2BySector> (accessed November 14, 2021).
- [2] Romeo LM, Bolea I, Escosa JM. Integration of power plant and amine scrubbing to reduce CO_2 capture costs. *Appl Therm Eng* 2008;28:1039-46.
- [3] Wu Y, Xu J, Mumford K, Stevens GW, Fei W, Wang Y. Recent advances in carbon dioxide capture and utilisation with amines and ionic liquids. *Green Chemical Engineering* 2020;1:16-32.
- [4] Demir H, Aksu GO, Gulbalkan HC, Keskin S. MOF Membranes for CO_2 Capture: Past, Present and Future. *Carbon Capture Science & Technology* 2022;2:100026.

- [5] Verougstraete B, Schoukens M, Suteus B, vanden Haute N, de Vos Y, Rombouts M, et al. Electrical swing adsorption on 3D-printed activated carbon monoliths for CO₂ capture from biogas. *Sep Purif Technol* 2022;299:121660.
- [6] Mdletshe Z, Msomi V, Nemraoui O. Experimental investigation of the adsorbents using pressure and thermal swing for adsorption and desorption. *Results in Engineering* 2022;15:100513.
- [7] García-Mariaca A, Llera-Sastresa E. Review on Carbon Capture in ICE Driven Transport. *Energies (Basel)* 2021;14:6865.
- [8] García-Mariaca A, Llera-Sastresa E, Moreno F. Application of ORC to reduce the energy penalty of carbon capture in non-stationary ICE. *Energy Convers Manag* 2022;268:116029.
- [9] Decarre S, Berthiaud J, Butin N, Guillaume-Combecave JL. CO₂ maritime transportation. *International Journal of Greenhouse Gas Control* 2010;4:857–64.
- [10] Fang S, Xu Y, Li Z, Ding Z, Liu L, Wang H. Optimal Sizing of Shipboard Carbon Capture System for Maritime Greenhouse Emission Control. *IEEE Trans Ind Appl* 2019;55:1–1.
- [11] Erto A, Balsamo M, Paduano LP, Lancia A, di Natale F. Utilization of alumina-supported K₂CO₃ as CO₂-selective sorbent: A promising strategy to mitigate the carbon footprint of the maritime sector. *Journal of CO₂ Utilization* 2018;24:139–48.
- [12] Sharma S, Maréchal F. Carbon Dioxide Capture From Internal Combustion Engine Exhaust Using Temperature Swing Adsorption. *Front Energy Res* 2019;7:1–12.
- [13] García-Mariaca A, Llera-Sastresa E. Energy and economic analysis feasibility of CO₂ capture on a natural gas internal combustion engine. *Greenhouse Gases: Science and Technology* 2022.
- [14] Saravanan S, Kumar CR. Carbon Dioxide Capture using Adsorption Technology in Diesel Engines. *International Journal of Renewable Energy Research* 2020;10:1614–20.
- [15] Subramanian T, Sonthalia A, Varuvel EG. Environmental Effects Effect of calcite / activated carbon-based post- combustion CO₂ capture system in a biodiesel- fueled CI engine — An experimental study. *Energy Sources, Part A: Recovery, Utilisation, and Environmental Effects* 2018;41:1972–82.
- [16] Kumar P, Rathod V, Parwani AK. Experimental investigation on performance of absorbents for carbon dioxide capture from diesel engine exhaust. *Environ Prog Sustain Energy* 2021:e13651.
- [17] Dechuan Zhao, Chunlong Kong, Hongbin Du, Yonggang Yan, Zhiyong Wang, Hai-Long Jiang, et al. A molecular-templating strategy to polyamine-incorporated porous organic polymers for unprecedented CO₂ capture and separation. *Sci China Mater* 2019;62:448–54.
- [18] Verdegem WM, Wang K, Sculley JP, Wriedt M, Zhou HC. Evaluation of Metal-Organic Frameworks and Porous Polymer Networks for CO₂-Capture Applications. *ChemSusChem* 2016;9:636–43.
- [19] Fatigati F, di Battista D, Cipollone R. Permeability effects assessment on recovery performances of small-scale ORC plant. *Appl Therm Eng* 2021;196:117331.
- [20] Fatigati F, di Bartolomeo M, di Battista D, Cipollone R. Experimental characterisation of a hermetic scroll expander operating in an ORC-based power unit bottoming an internal combustion engine. *AIP Conf Proc*, vol. 2191, American Institute of Physics Inc.; 2019.
- [21] Invernizzi CM, Iora P, Manzolini G, Lasala S. Thermal stability of n-pentane, cyclo-pentane and toluene as working fluids in organic Rankine engines. *Appl Therm Eng* 2017;121:172–9.
- [22] Stein J. Informal document No. 12, 43rd GRPE session. 2002.
- [23] Escudero AI, Espatolero S, Romeo LM, Lara Y, Paufique C, Lesort AL, et al. Minimisation of CO₂ capture energy penalty in second generation oxy-fuel power plants. *Appl Therm Eng* 2016;103:274–81. <https://doi.org/10.1016/j.applthermaleng.2016.04.116>.

4. CARBON CAPTURE IN HD-ICEV BY ADSORPTION

Continuing with the research, the next step involves conducting an energy analysis of a CCS-ORC system employing temperature swing adsorption (TSA). The aim of this analysis is to quantify, through simulations, the power penalty induced by the operation of the CCS-ORC system over the engine. This requires detailed knowledge of the heat transfer and areas of the heat exchangers, as well as the power production of the ORC expander, pumps, and compressors. These parameters are evaluated for each rpm and partial engine load.

For this, a new operation scheme of the ORC is applied, aimed at enhancing power output at the high engine load points. In addition, a much more detailed sizing of the CCS-ORC system is carried out, including heat exchanger areas, volumes and weight of the primary devices that make up the CCS-ORC system. Finally, the energy consumption cost of CO₂ capture for the proposed system is determined. This exhaustive energy analysis is essential to evaluate the feasibility of implementing the adsorption capture system compared to other available technologies. The comprehensive procedure and outcomes obtained from this novel study are detailed below.

4.1 CCS-ORC SYSTEM CONFIGURATION AND DESIGN

The CCS-ORC system was configured using all the available waste heat sources. This configuration also has an analysis Pinch to reduce the energy requirement in the cooling processes and effectively manage the energy through

heat exchangers involved in the configuration. A RWA is assumed to develop the TSA processes [143]. The advantage of this device is that it is possible to do the TSA cycle in less than 90 s [144], which drives to small equipment sizes. The TSA processes are heating the sorbent, CO₂ desorption, cooling the sorbent, and CO₂ adsorption [144]. The heating and desorption processes harness the waste heat of the EG. Air at standard conditions is used for the cooling and adsorption processes.

As shown in Chapter 3, the ORC takes advantage of two waste heat sources: the remaining heat of the EG after the RWA and the heat contained in the CO₂ after its compression. Four additional heat exchangers complete the CCS system to dry the exhaust gases and cool the CO₂. Figure 20 shows, with different colours, each energy and mass flow operating in the several devices and their arrangement. Additionally, on this occasion, the WF in the ORC will always be saturated vapour at the ORC-X inlet; this allows more mass of the WF to circulate through the ORC (as is shown in Figure 13a), thus taking advantage of more waste heat and, therefore, producing more power output at high engine loads. The ORC operational pressures were obtained following the procedure shown in Chapter 3. For these new simulations, the U and h are actualized to get a more realistic operation of the ORC. These values are shown in Table 13.

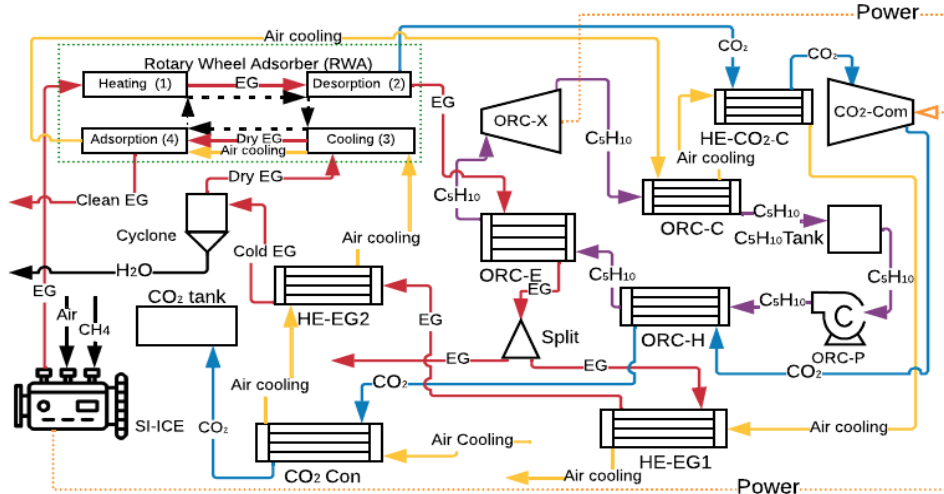


Figure 20. Energy and mass flows and CCS-ORC system configuration.

Table 13. Parameters and conditions used in the ORC simulations.

Device	Parameter	Unit	Value	State	Fluid
ORC-C	Inlet pressure	bar	1.5	Vapour	C ₅ H ₁₀
	U [135]	W/m ² K	120→Condensation	NA	Air-C ₅ H ₁₀
ORC-P	Inlet pressure	bar	1	Saturated liquid	C ₅ H ₁₀
	Isentropic efficiency [145]	NA	0.55	NA	
ORC-H	Inlet pressure	bar	24.9	Compressed liquid	C ₅ H ₁₀
	U [135,146]	W/m ² K	100→Liquid-Gas	NA	C ₅ H ₁₀ -CO ₂
ORC-E	Inlet pressure	bar	22.9	Compressed liquid	C ₅ H ₁₀
	h [135]	W/m ² K	70→Liquid-Gas	NA	C ₅ H ₁₀ -EG
			35→Gas-Gas		
ORC-X	Inlet pressure	bar	20.9	Vapour	C ₅ H ₁₀
	Isentropic efficiency [147]	NA	0.65	NA	

4.1.1 Heat exchangers

As seen in Figure 20, the CCS system has four heat exchangers. The first of them serves to reduce the CO₂ temperature after the desorption process (HE-CO₂-C), the second one is used to condensate the CO₂ (CO₂-con), the third one is used as the primary stage for cooling the EG (HE-EG1), and the last heat exchanger (HE-EG2) completes the cooling and drying process of the exhaust EG. Notably, these heat exchangers utilise the same air cooling that flows through the RWA and the ORC. This information is summarised in Table 14. The simulations consider a U of 100 W/m²K corresponding to a cooling process in a compact heat exchanger [135,146,148].

Table 14. U for the heat exchangers used in the CCS system [135,146,148].

Heat exchanger	Process	Fluids	U [W/m ² K]
HE-CO ₂ -C	Cooling	CO ₂ – Air	100
CO ₂ -Con			
HE-EG1	Cooling	Air – EG	
HE-EG2	Dry		

4.1.2 Sorbent selection

Three sorbents have been chosen for the CCS-ORC simulations: PPN-6-CH₂-DETA, MOF-74-Mg, and activated carbon (AC onwards). PPN and MOF sorbents are notable due to their ultra-high selectivity for CO₂, low desorption energy and exceptional adsorption capacity, all of which are favourable physical properties for CO₂ capture. On the other hand, AC, a commercially available sorbent, boasts a deficient desorption energy, and numerous studies have demonstrated its efficacy as a CO₂ sorbent material [115,116,149]. Table 2 shows the properties of each sorbent. The desorption and adsorption temperatures used in the simulations are presented in Chapter 2.

4.1.3 CO₂ compression and storage process

Simulations consider the storage of CO₂ as a liquid at 75 bar and a temperature of 29.35 °C. However, variations in CO₂ pressure occur across different sorbents due to impurities such as N₂ in the CO₂ stream (due to the selectivity). Consequently, the CO₂ pressure with PPN is 75 bar, with MOF is 77.9 bar and with AC is 85.73 bar. The CO₂ compressor (CO₂-Com onwards) is attributed an assumed isentropic efficiency of 65%. The proposed CCS-ORC system configuration involves three stages to attain the CO₂ storage temperature. Initially, cooling is achieved in HE-CO₂-C using air as a cooling fluid before entering the CO₂ compressor. Subsequently, CO₂ is further cooled in ORC-H using C₅H₁₀ as the cooling fluid. Finally, the last cooling stage occurs in CO₂-con, employing air again.

4.1.4 Assumptions and procedures in the simulations

The following assumptions are considered in the CCS-ORC system simulations: (i) there are no pressure, heat and mass losses in pipes, devices, and

connections; (ii) EG are non-corrosive during the heat transfer; (iii) steady-state conditions in the simulations and (iv) heat exchangers are simulated in counter-flow type. Simulations are performed at 25, 50, 75 and 100% of engine load, in the entire rpm range and at 70 and 100% of CCR. For both CCR conditions, the areas were determined at maximum engine torque, fulfilling the design condition of each heat exchanger and meeting the selected ΔT between the hot and cold fluid in each heat exchanger, as seen in Table 15. The values for the cooling, heating, adsorption and desorption heat developed in the RWA introduced for each simulation are listed in Annexes A, B, C, and D. These values are calculated using equations 16 to 18. The ΔT in these equations is 120 °C, obtained as the difference between desorption temperature and EG drying temperature.

Table 15. ΔT and design conditions of the heat exchangers in the CCS-ORC system simulations

Heat exchanger	ΔT between hot and cold fluid [°C] [148]	Fluids	Design condition of the heat exchanger
ORC-C	5	C ₅ H ₁₀ -Air	C ₅ H ₁₀ outlet as saturated liquid
ORC-E	20	C ₅ H ₁₀ -EG	C ₅ H ₁₀ outlet as saturated vapour
ORC-H	20	C ₅ H ₁₀ -CO ₂	-
HE-CO ₂ -C	3	Air-CO ₂	-
CO ₂ -Con	4	CO ₂ -Air	CO ₂ outlet as saturated liquid
HE-EG1	3	EG-Air	-
HE-EG2	3	EG-Air	EG outlet at 30°C

$$\dot{Q}_{heating} = CCR x_{CO_2} \dot{m}_{EG} \Delta T \left(c_{p-CO_2} + \frac{c_{p-CO_2}}{q} \right) \quad (16)$$

$$\dot{Q}_{cooling} = \frac{c_{p-CO_2} CCR x_{CO_2} \dot{m}_{EG} \Delta T}{q} \quad (17)$$

$$\dot{Q}_{desorption/adsorption} = CCR x_{CO_2} \dot{m}_{EG} \Delta H_{des} \quad (18)$$

The areas were always controlled and verified using equation 19, whose value must always be equal to or greater than zero in each simulation. This method enables us to determine the power consumption of the ORC-P and the CO₂ compressor, the power production of the ORC-X, the air mass flow of the fan employed for cooling the CCS-ORC system, the WF mass flow in the ORC and the heat flux of all heat exchangers in the whole of the engine operational points.

$$A_{difference} = \left(\frac{A_{Tmax} - A_{current}}{A_{Tmax}} \right) 100\% \quad (19)$$

4.2 RESULTS AND ANALYSIS

4.2.1 Heat transfer areas and WF and cooling mass flows

Table 16 shows the values of the areas of the heat exchangers of the CCS-ORC system obtained in the simulations. The areas found for the ORC-E and ORC-C heat exchangers are greater at 70% CCR than 100% CCR. This discrepancy arises from the higher WF mass flow achieved at 70% CCR due to the increased heat available in the EG after the desorption process compared to 100% CCR. On the

contrary, the HE-EG1, HE-EG2, ORC-H, HE-CO₂-C and CO₂-C areas are lower for the lower CCR, caused by a smaller mass flow of EG and CO₂.

Table 16. Heat exchangers areas obtained in the simulations.

Engine	Sorbent	CCR	ORC-C [m ²]	ORC-E [m ²]	ORC-H [m ²]	HE-CO ₂ -C [m ²]	CO ₂ -Con [m ²]	HE-EG1 [m ²]	HE-EG2 [m ²]	Total [m ²]
M936G	MOF	70	17.90	8.17	0.59	0.67	1.87	18.36	11.58	59.13
	PPN		16.53	8.16	0.57	0.67	1.82	18.74	10.18	56.68
	AC		16.71	7.95	0.63	0.73	1.96	17.99	10.25	56.21
	MOF	100	15.61	7.66	0.75	0.95	2.54	25.37	13.02	65.91
	PPN		13.77	7.59	0.72	0.95	2.46	25.30	11.20	62.01
	AC		13.97	7.17	0.79	1.05	2.64	24.23	11.31	61.16
F1C	MOF	70	9.56	4.27	0.31	0.35	0.98	9.61	6.12	31.19
	PPN		8.84	4.27	0.30	0.35	0.96	9.81	5.38	29.91
	AC		8.93	4.16	0.33	0.38	1.02	9.41	5.42	29.66
	MOF	100	8.36	4.02	0.50	2.54	1.33	13.30	6.88	36.93
	PPN		7.92	4.01	0.39	0.50	1.30	13.34	6.40	33.86
	AC		7.51	3.79	0.42	0.55	1.38	12.72	5.99	32.35

During MOF operation, there is an area increase of 2.5% in the CO₂-Con at 70% of CCR and 2.7% at 100% of CCR compared to the PPN operation. This difference is due to the lower selectivity of the MOF-74-mg relative to PPN-6-CH₂-DETA, resulting in a CO₂ mass flow with impurities of N₂, changing the heat transfer parameters and producing this increase. A similar trend is observed with the AC sorbent, which exhibits the lowest selectivity among the three sorbents. Finally, the HE-EG2 area presents an average increase of 11.2% during MOF operation compared to PPN and AC operations across the two CCRs and engines. This result is because, in MOF operation, the cooling air mass flow is the lowest obtained due to the lowest heat of cooling and adsorption heat required by the CCS-ORC system with this sorbent.

Figure 21 illustrates that in all instances, a greater mass flow of C₅H₁₀ is attained at 70% CCR compared to 100% CCR. This is attributed to higher heat in the EG after the sorbent's heating and desorption process at this CCR. In this line, MOF operation always presents a higher C₅H₁₀ mass flow than the PPN and AC operation because of its lower desorption heat than the other evaluated sorbents. On the other hand, Figure 22 depicts that the cooling air mass presents its highest values at a CCR of 100%. These results are due to the increased CO₂ mass for condensing and the higher cooling requirements in the RWA. This also means that cooling air mass flow with PPN and AC operation is higher than with MOF operation, irrespective of engine load and rpm, because of the lowest desorption heat of this latter.

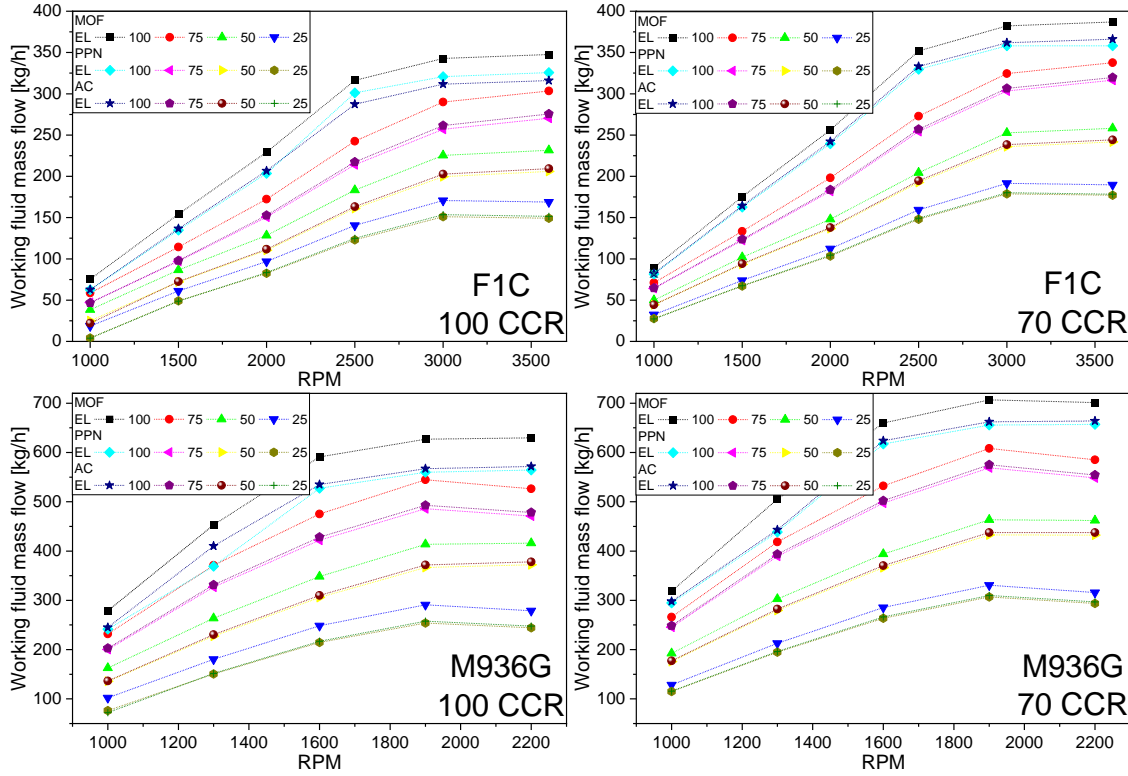


Figure 21. C_5H_{10} mass flow obtained for the two CCRs in both engines at the entire rpm range and engine loads.

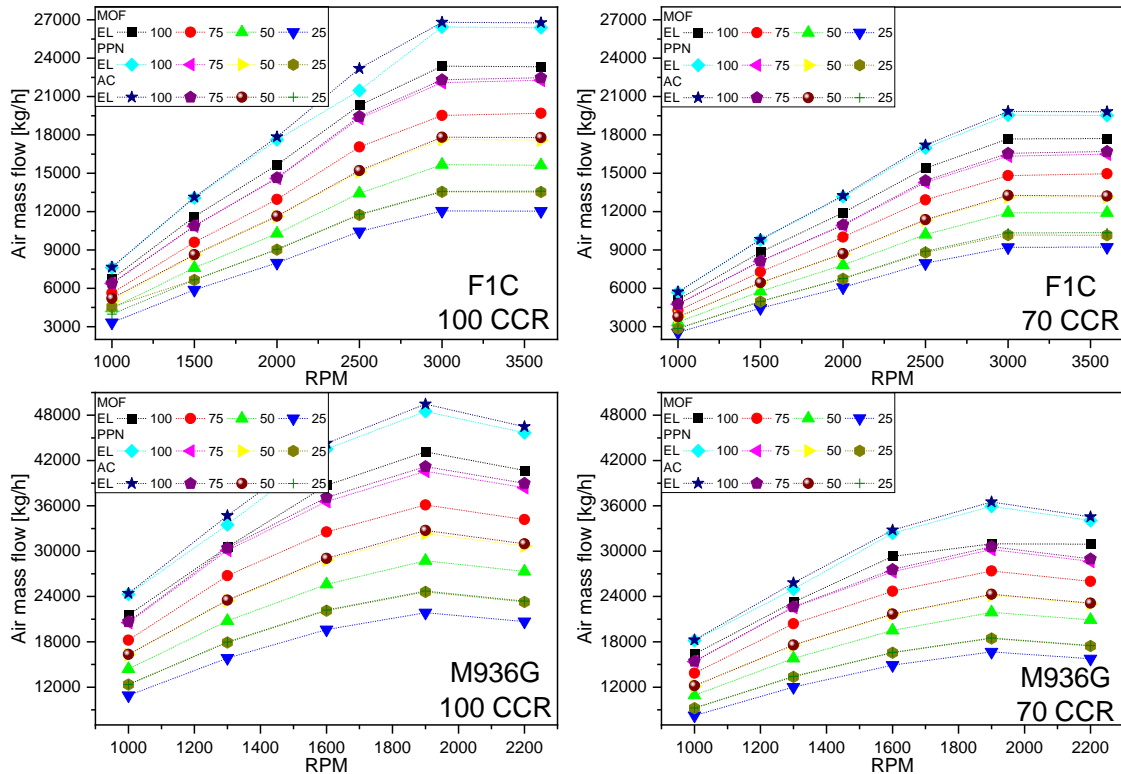


Figure 22. Cooling mass flow obtained for the two CCRs in both engines at the entire rpm range and engine loads.

4.2.2 Energy analyses

Figure 23 shows that in the F1 engine at 70% of CCR and with MOF operation, the parasitic loads are offset by power generated in the ORC-X at 100% engine

load, starting from 2000 rpm; at 75% engine load, the ORC-X covers the parasitic loads from 2800 rpm and at 50% engine load, from 3200 rpm onwards. During PPN operation, the ORC-X generates sufficient power to compensate for the parasitic loads at 100% and 75% of the engine load, starting from 2400 and 3600 rpm, respectively. However, the parasitic loads are only partially compensated at 25% of EL at 70% of CCR and 100% of CCR with any sorbent, as is shown in Figure 24, due to the high power required to achieve the CO₂ storage conditions.

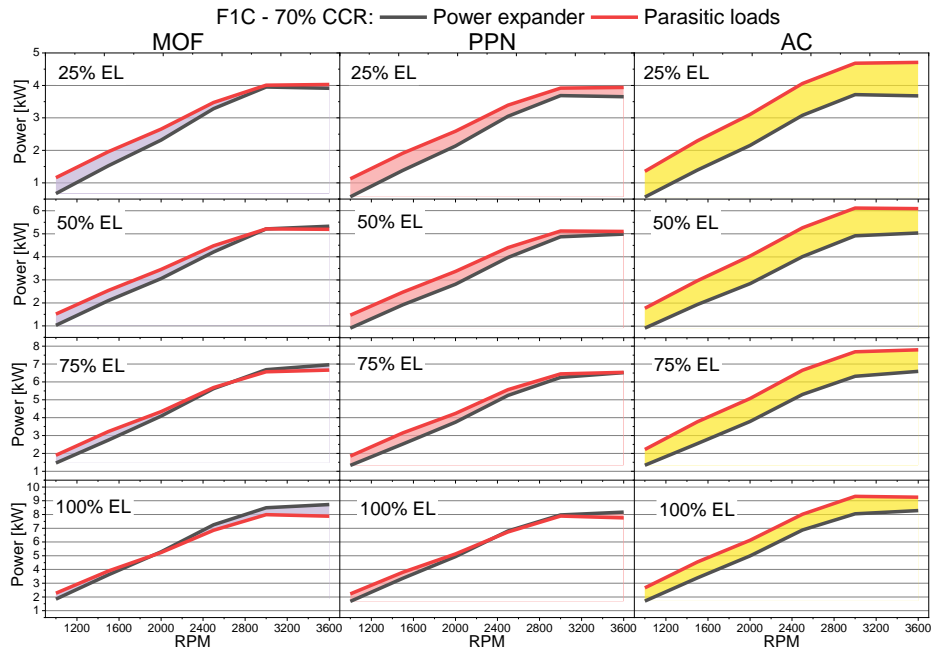


Figure 23. Parasitic loads covered by the ORC at 70% of CCR in the F1C engine.

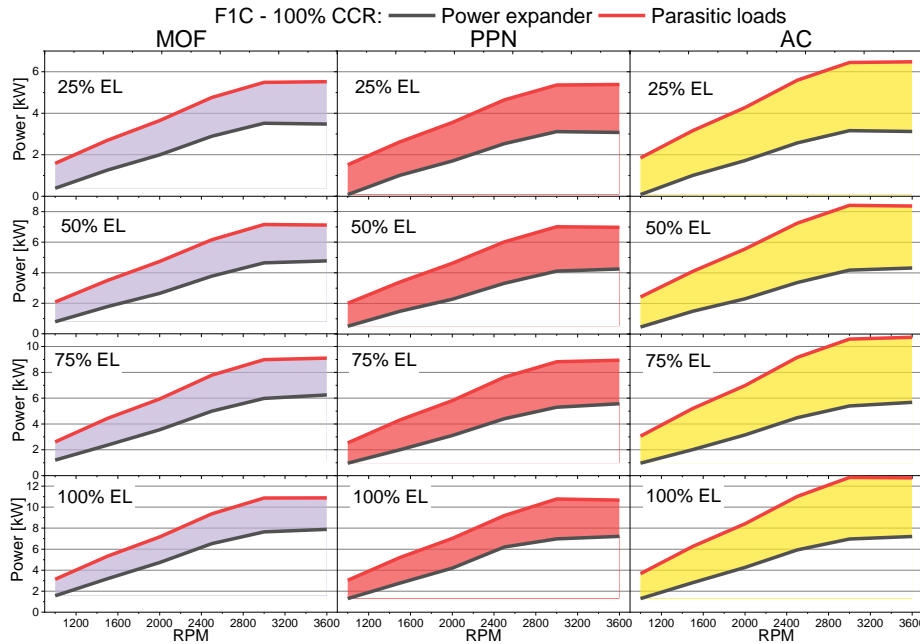


Figure 24. Parasitic loads covered by the ORC at 100% of CCR in the F1C engine.

In the M946G engine with the CCS-ORC system operating at a 70% CCR (Figure 25) in MOF operation, the parasitic loads are compensated for at 100%

engine load starting from 1500 rpm, at 75% of the engine load from 1700 rpm, and at 50% of the engine load from 2000 rpm. During PPN operation, at 100% of the engine load, the parasitic loads are covered from 2000 rpm, and for the rest of the engine loads and rpm, the parasitic loads are partially covered. Figure 26 illustrates a similar pattern across all the sorbents studied at a CCR of 100% to the behaviour observed in the F1C case.

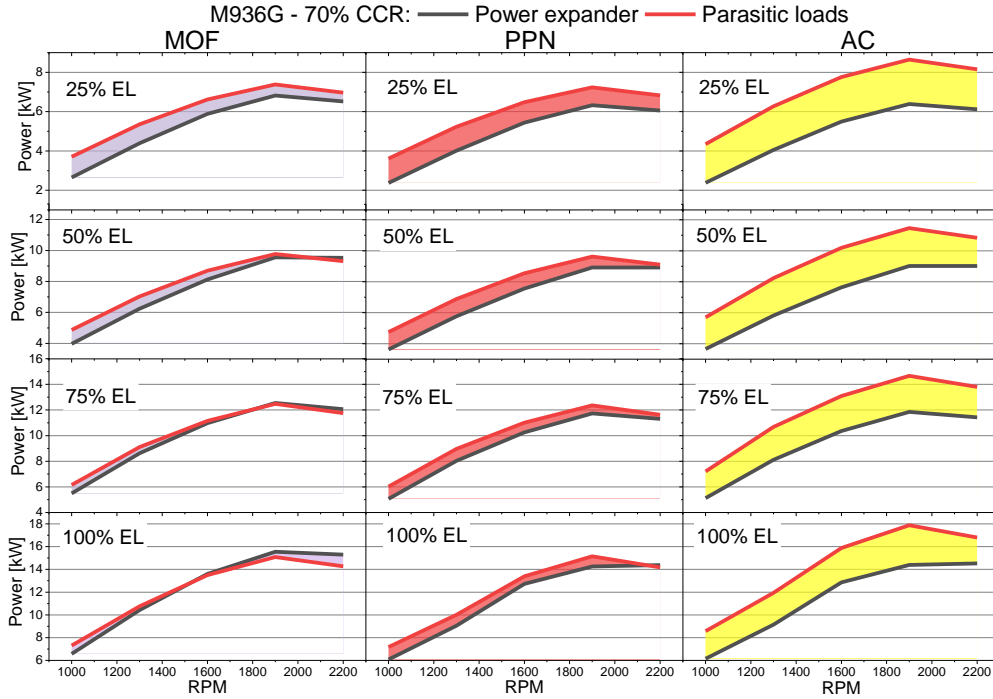


Figure 25. Parasitic loads covered by the ORC at 70% of CCR in the M936G engine.

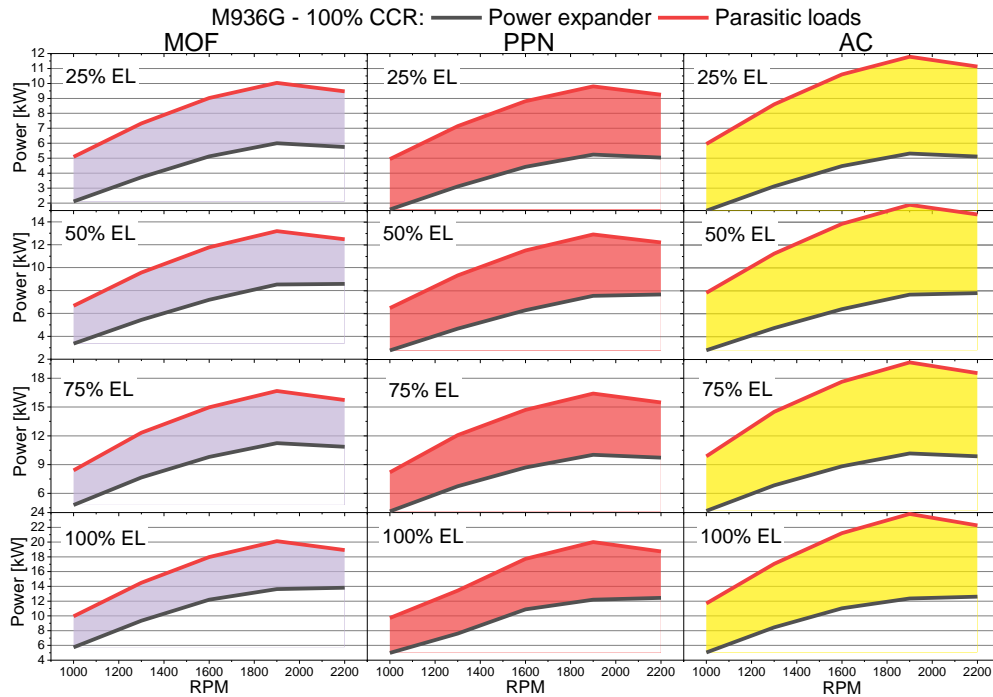


Figure 26. Parasitic loads covered by the ORC at 100% of CCR in the M936G engine.

Figures 27 and 28 depict the percentage of engine power utilized by the CCS-ORC system across various rpm and engine load conditions, sorbents, and selected CCRs. As can be seen in these figures, the most significant impact on the engine performance occurs at 25% of the engine load regardless of the sorbent, CCR, or engine rpm since the engine power output is at its lowest point during this load condition. Consequently, the penalty percentage imposed by the CCS system on the engines is magnified. However, this penalty diminishes as engine load increases; even the ORC system can deliver excess power, as with MOF operation at a 70% CCR. As expected, the CCS-ORC system's penalty percentage on engine performance follows the AC operation > PPN operation > MOF operation sequence. Also, the CCS system has a more significant penalty on the smaller engine, irrespective of the sorbent used.

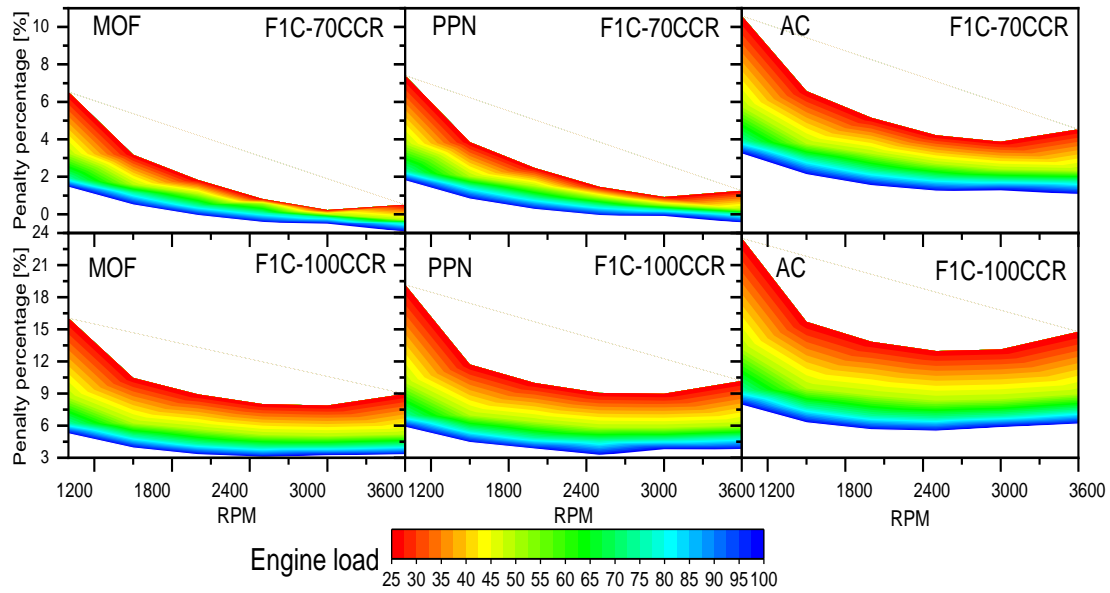


Figure 27. Power percentage required by the CCS system operating in the M936G engine.

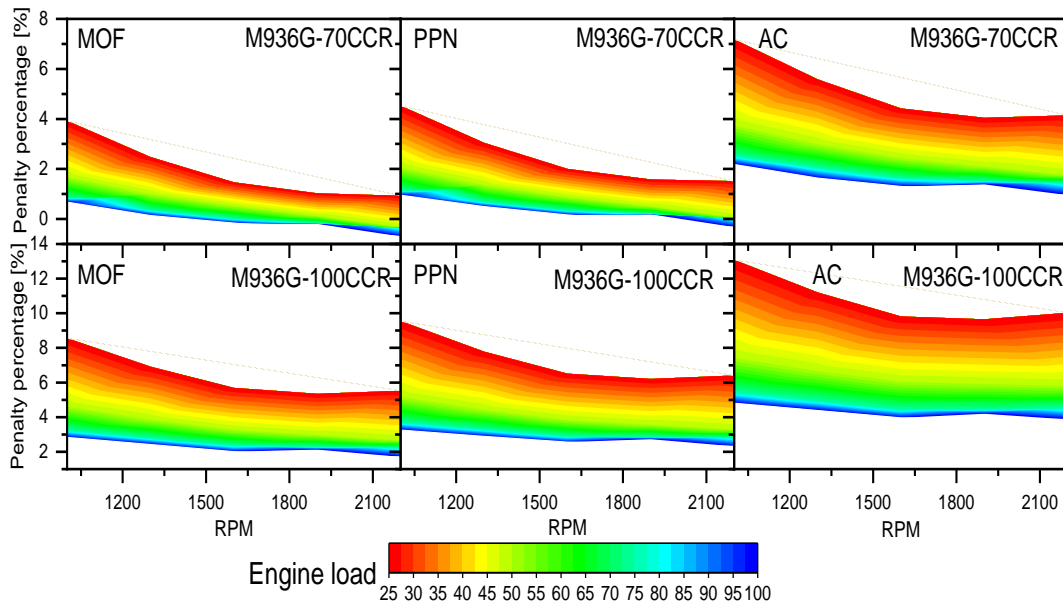


Figure 28. Power percentage required by the CCS system operating in the F1C engine.

4.2.3 Weight and volume of the CCS-ORC system

The limited space within an ICEV poses a notable challenge when installing a CCS-ORC system. Hence, it becomes imperative to ascertain the volume and weight constraints associated with such a system. The calculation procedure for this purpose entails assuming a CCR of 100% for both engines, an 8-hour operation with 48 cycles of desorption and adsorption, and an engine load of 75% at the maximum torque rpm. Subsequently, the weight and volume of commercial compressors that meet the mass flow of CO₂ obtained in both engines are taken [150]. Following this, the volume of the heat exchangers is calculated based on an area density (β) of 100 m²/m³ and the corresponding weight is extrapolated from analogous studies [77]. Finally, the weight of the tanks and ancillary systems associated with the CCS-ORC system is estimated at 200 kg for the M936G engine and 120 kg for the F1C engine.

Table 17. Sorbent mass and volume at 25% of EL and maximum RPM for 30 min of operation of CCS-ORC system.

Engine	M936G			F1C		
Sorbent	MOF	PPN	AC	MOF	PPN	AC
Exhaust mass [kg]		4610.07			2417.76	
CO ₂ mass captured [kg]		710.13			373.16	
CO ₂ volume [m ³]		0.93			0.49	
Sorbent mass (RWA weight) [kg]	53.2	62.9	112.1	28	33.0	58.9
*Sorbent Volume (RWA volume) [m ³]	0.116	0.156	0.224	0.061	0.082	0.118
CO ₂ compressor weight [kg] [150]		540			276	
CO ₂ compressor volume [m ³] [150]		0.366			0.183	
ORC-E weight [kg] [151]			127.8			
ORC-E volume [m ³] [151]			0.03			
Heat exchangers volume [m ³] [77]	0.66	0.62	0.61	0.35	0.34	0.32
Heat exchangers weight [kg] [77]	257	241.8	238.5	135.7	132.1	126.2
**Weight of CCS-ORC system [kg]	1178	1172.5	1218.4	687.4	688.9	708.9
Total Volume of CCS-ORC system [m ³]	2.11	2.11	2.17	1.11	1.12	1.14

*Calculated with 50% of the crystallographic density.

** Without the CO₂ mass

Table 17 shows that the average weight and volume of the CCS-ORC system obtained are 1200 kg and 2.11 m³ for the M936G engine vehicle and 695 kg and 1.12 m³ for the F1C engine vehicle. This table also observes that CO₂ loading governs this evaluation since the highest sorbent mass and volume values found are for AC, whose CO₂ loading is the lowest of the sorbents studied. Figure 29 shows that the CO₂ compressor is the equipment exerting the greatest influence on the total weight of the CCS-ORC system in both ICEVs. Conversely, the heat exchangers, the RWA, and the tanks and auxiliaries exhibit comparable weight contributions across both engines. Notably, the ORC-E exhibits a higher proportional weight in the F1C engine than the M936G; this disparity arises from using the same expander for both cases. The decision to use the same ORC-E in both ICEVs is due to its volume barely representing 2.7% of the total volume of the CCS-ORC system, and it has a good performance with the mass flows of the WF obtained in both engines [77].

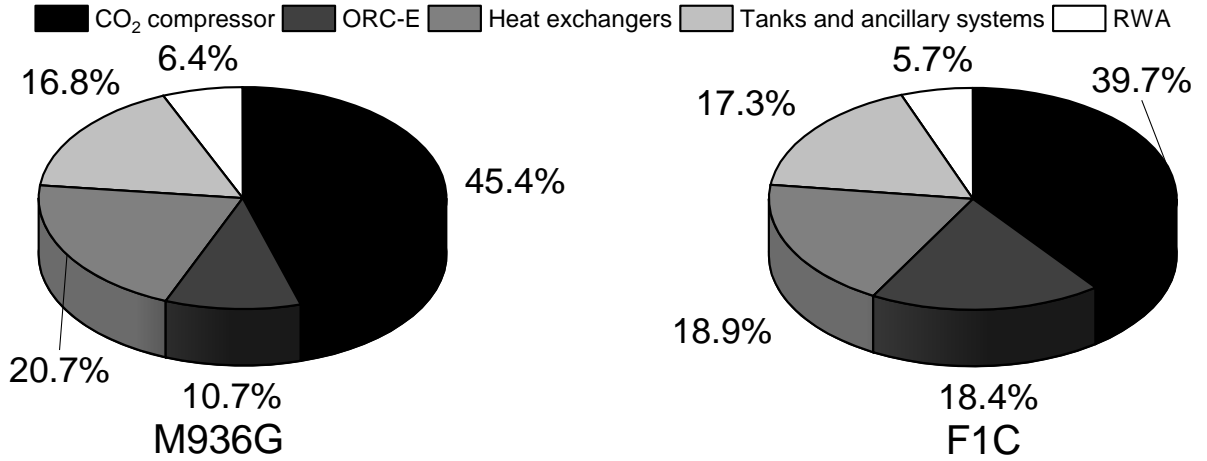


Figure 29. Average percentage weight of the components of the CCS-ORS system

4.3 ANALYSES

The findings reveal that the volume occupied by the CCS-ORC system with a CCR of 100% amounts to merely 3.4% of the total volume of a bus employing the M936G engine, while for a vehicle equipped with an F1C engine, the space allocated for the CCS-ORC system constitutes 10.2% of the vehicle's total volume. Therefore, integrating the CCS-ORC system into a heavy-duty vehicle appears technically feasible since it barely affects its workspace. Notably, these proportions are even 15.6% lower than the volume of an electric battery in a heavy vehicle[152].

Nevertheless, the engine must increase fuel consumption to offset the parasitic loads the ORC fails to address and not for the extra weight that entails integrating the CCS-ORC system into the ICEV [153]. This extra mass fuel is quantified using Equation 20, where η_{com} is the combustion efficiency and η_{th} is the engine's thermal efficiency. These parameters are obtained from the engine simulations, whose values are listed in Annexes E and F. The results are presented in Table 18, revealing, as anticipated, the highest increase in fuel mass occurring at 100% CCR, particularly evident during AC operation. However, at 70% of CCR, the rise in the fuel mass with the MOF and PPN sorbents is almost marginal. This highlights that maximum energy consumption is observed with a CCR of 100% in the F1C engine at 25% engine load and the lowest engine rpm (Figure 30). These findings align with those reported by Kim et al. [64]. Additionally, in the literature, the energy consumption values for TSA, PSA and VSA are higher than 700 kJ/kgCO₂ at 90% of CCR [113,154] and, with amine-scrubbing, are higher than 2500 kJ/kgCO₂ [155,156].

$$m_{fuel} = \frac{28800 (PL - \dot{W}_{ORC-net})}{\eta_{com} \eta_{th} LHV} \quad (20)$$

Table 18. Total and percentage increase of fuel mass in the engines to cover the operation of the CCS-ORC system at 75% of EL, 8 hours of operation and maximum torque.

Engine	mass fuel [kg]	CCR [%]	PPN		MOF		AC	
			mass fuel [kg]	Increase mass fuel [%]	mass fuel [kg]	Increase mass fuel [%]	mass fuel [kg]	Increase mass fuel [%]
M936G	136.30	70	0.71	0.52	0.13	0.09	2.96	2.17
		100	7.04	5.17	6.09	4.47	10.22	7.5
F1C	259.54	70	1.38	0.53	0.31	0.12	4.95	1.91
		100	10.87	4.19	9.37	3.61	15.94	6.14

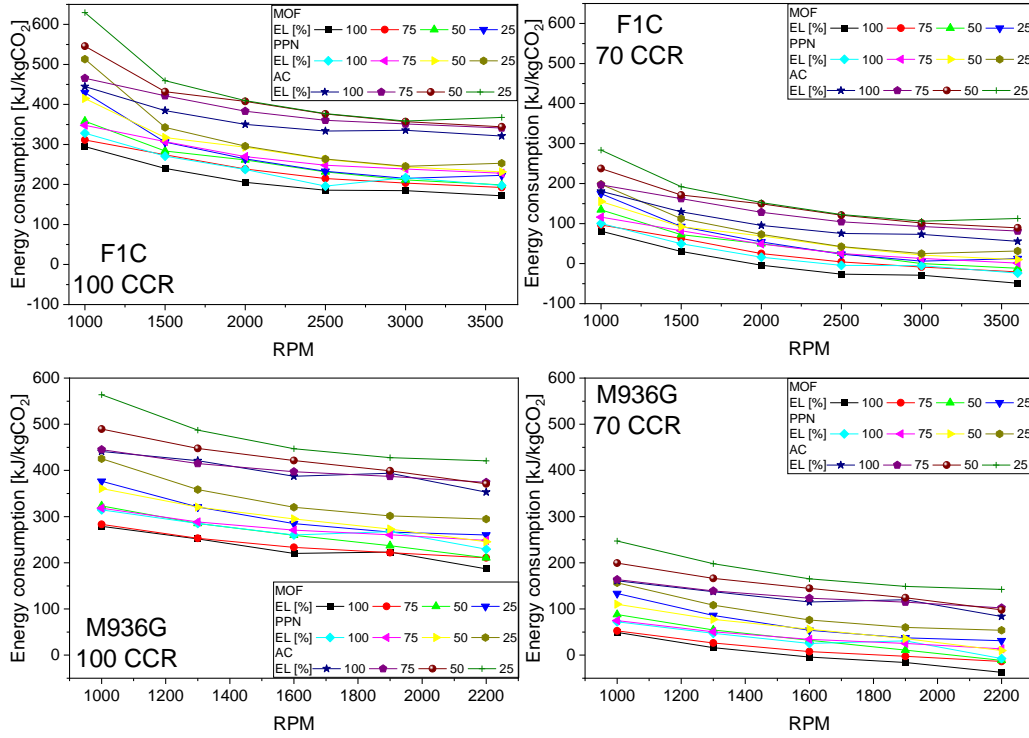


Figure 30. Energy consumption of the CO₂ capture process obtained for the study cases.

4.4 SUMMARY

The results indicate that, among the variables analysed (type of sorbent and engine size), the type of sorbent most significantly affects the behaviour of the CCS-ORC system, with AC performing the worst primarily due to its lower selectivity. On the other hand, with ORC optimisation, greater harnessing of the EG waste heat is achieved, reducing the penalty that the CCS system imposes on the ICE at high engine loads. This leads to the proposed CCS-ORC system requiring almost 15% less energy for CO₂ capture than other studies. Consequently, the energy assessment in this chapter establishes that the proposed CCS-ORC system is energy feasible for its integration into an HD-ICEV, as its maximum average penalty is less than 10% with a CCR of 100%, regardless of engine size. Therefore, in the next chapter, a techno-economic assessment must be performed to determine the complete feasibility of the CCS-ORC system.

4.5 PUBLISHED PAPER

Finally, all the details, findings, and conclusions of this study have been included in an article published in the journal *Energy*.

- García-Mariaca, A., Llera-Sastresa, E., & Moreno, F. (2024). CO₂ capture feasibility by Temperature Swing Adsorption in heavy-duty engines from an energy perspective. *Energy*, 292, 130511. <https://doi.org/10.1016/j.energy.2024.130511>

Energy 292 (2024) 130511



CO₂ capture feasibility by Temperature Swing Adsorption in heavy-duty engines from an energy perspective

Alexander García-Mariaca^{a,*}, Eva Llera-Sastresa^b, Francisco Moreno^c

^a Energy and CO₂ Group, Department of Mechanical Engineering, Aragon Institute of Engineering Research (I3A), University of Zaragoza, Zaragoza 50018, Spain

^b Department of Mechanical Engineering and CIRCE Research Institute, University of Zaragoza, María de Luna s/n, Zaragoza, 50018, Spain

^c Department of Mechanical Engineering, University of Zaragoza, Zaragoza 50018, Spain

ARTICLE INFO

Handling editor: Krzysztof (K.J.) Ptasiński

Keywords:

Carbon capture and storage
CO₂ emissions
Internal combustion engines
Temperature swing adsorption
Organic rankine cycle

ABSTRACT

This study made an energy performance analysis and an estimate of the volume and weight of an innovative carbon capture and storage (CCS) system by temperature swing adsorption (TSA) hybridised with an organic Rankine cycle (ORC) working with the waste heat contained in the exhaust gases of a natural gas engine. To achieve this, two varying-sized engines are simulated across the entire rpm range and under partial engine loads. Subsequently, energy simulations are conducted at two CO₂ capture rates (OCR) and employing three sorbents (MOF-74-Mg, PPN-6-CH₃-DETA and activated carbon) to compare the CCS-ORC performance. Results demonstrate the viability of installing CCS-ORC systems in heavy-duty vehicles since they require less than 6 % of the total volume of the studied vehicles. The engine power penalty induced by the CCS-ORC system varies from 1.9 % with MOF-74-Mg to 23.5 % with activated carbon at 100 % of OCR, leading to a maximum 6.14 % rise in engine fuel consumption. Finally, the maximum CO₂ capture process energy consumption is 631 kJ/kgCO₂, 9.9 % lower than the literature reported for TSA. Based on these promising results, applying the hybridised system presented in this paper for CO₂ capture in sectors that use heavy-duty engines is a strategy to implement.

1. Introduction

Despite the continuous advances in emerging technologies, such as battery vehicles and hydrogen fuel cells, to achieve near-zero CO₂ emissions in freight and passenger road transport, these developments remain insufficient due to their short autonomies, overweight and poor chain supply development, among others [1–3]. For these reasons, this sector continues to use internal combustion engines (ICE) for its propulsion. Nevertheless, to reduce its carbon footprint, it has chosen to migrate from diesel to sustainable fuels such as natural gas (NG) [4,5]. Even though NG is not a renewable fuel, it is expected to facilitate the energy transition of this sector towards a sustainable energy system, as was established by the European Commission in 2022 [6].

However, this sector must achieve CO₂ emissions close to zero; for this reason, existing technologies such as carbon dioxide capture, storage, and utilisation (CCSU) technologies should be explored. Further, if any CO₂ capture technology is combined with technologies such as power-to-gas (PtG) that operate with renewable energy sources to produce synthetic methane, it would promote a circular economy around the captured CO₂ since this would be used as raw material to

manufacture E-fuels [7]. Another advantage of this proposal is that the well-developed infrastructure of the NG could be used for methane transport and supply to the vehicles, so the supply chain would not be a drawback in this type of proposal.

CCSU technologies have been demonstrated mainly for their use in power plants, steel, and cement industries, which are the main emitters of CO₂ [8]. However, in recent years, research works have been carried out on CO₂ capture in mobile sources (vehicles and ships) propelled with traditional ICEs. Several issues have been evaluated in these works: the energy consumption of the CCS system operating with different solvents and sorbents [9–15], the economic impact of the implementation of CCS systems [16–18], the technical feasibility of implementing the CCS systems [19–23]. Also, the properties of the sorbents have been improved to achieve better CO₂ capture on board [24]. These research works show that the most widely used CO₂ capture techniques have been absorption in the maritime sector and adsorption in road transport. They have also found that CO₂ storage is the process that consumes the most energy, and it depends on the CO₂ capture rate (OCR), which is why some authors have hybridised an ORC to the CCS system [25–27]. The ORC takes waste heat from the engine's exhaust gases to produce power, thus offsetting the energy demand in the CO₂ storage process.

* Corresponding author.

E-mail address: alexander.garcia@unizar.es (A. García-Mariaca).

<https://doi.org/10.1016/j.energy.2024.130511>

Received 16 November 2023; Received in revised form 16 January 2024; Accepted 27 January 2024

Available online 30 January 2024

0360-5442/© 2024 The Authors. Published by Elsevier Ltd. This is an open access article under the CC BY-NC-ND license (<http://creativecommons.org/licenses/by-nc-nd/4.0/>).

Abbreviations

Adsorption Heat ΔH_{ads}
 Angular velocity ratio β_w
 Area calculated at maximum torque A_{Tmax}
 Area current $A_{current}$
 Carbon Capture and Storage CCS
 Capture, Storage, and Utilisation CCSU
 Combustion efficiency η_{com}
 Compressibility factor Z
 CO₂ capture rate CCR
 CO₂ cooling heat exchanger HE-CO₂-C
 CO₂ condenser CO₂-con
 CO₂ compressor CO₂-com
 Cyclopentane C₅H₁₀
 Density ρ
 Displacement volume d_v
 Displacement volume ratio β_{Vol}
 Engine load EL
 Exhaust gases EG
 Exhaust gas cooling heat exchanger 1 HE-EG1
 Exhaust gas cooling heat exchanger 2 HE-EG2
 Expander volumetric efficiency $\eta_{vol,exp}$
 Greenhouse gas emissions GHE
 Ideal gas constant R
 Internal Combustion Engine ICE

Loading Capacity q
 Lower Heating Value LHV
 Mass flow \dot{m}
 Mass fraction x
 Natural gas NG
 ORC condenser ORC-C
 ORC evaporator ORC-E
 ORC heater ORC-H
 ORC pump ORC-P
 ORC expander ORC-X
 Organic Rankine Cycle ORC
 Parasitic Load PL
 Power-to-Gas PtG
 Revolutions per minute Rpm
 Rotary Wheel Adsorber RWA
 Saturation temperature T_{sat}
 Specific heat c_p
 Pump volumetric efficiency $\eta_{vol,pump}$
 Temperature Swing Adsorption TSA
 Thermal efficiency η_{th}
 Overall heat coefficient U
 Volumetric efficiency product β_{vp}
 Working Fluid WF
 Working fluid density $\rho_{pmp,in}$

Despite the increased literature on this topic in recent years, most of these research works have been carried out with the ICE operating in a single operating condition, which is suitable for the maritime sector. However, it is far from the actual ICE operation used in freight and passenger road transport vehicles, where the engine must change rpm and engine load constantly to adjust to the required slope or speed, which produces a variation in the mass flow and temperature of the exhaust gases (transient state). These variations affect the performance of any CCS system that could operate in this kind of vehicle due to the variation of the waste heat available in the exhaust gases.

As evidenced in the previous paragraph, there is not enough information in the literature about CCS-ORC systems operation on heavy-duty vehicles whose ICE operates in a transient state. This lack of information is due to the difficulty of obtaining results through simulations of ICE operating in a transient state because of the large number of variables that affect its behaviour. In the same way, experimental tests require a significant investment, which is not easy to assume by a research centre. A way to approach the transient state operation of an ICE through simulations is by sweeping many engines operating conditions, both in rpm and engine load, which would allow knowing the several input conditions of exhaust gases into the CCS-ORC system. With this and through the evaluation of different sorbents, it would establish the CO₂ capture rate (CCR), the energy behaviour, and the first sizing of a CCS-ORC system able to adapt to operate to several operation conditions of an engine.

In this vein, the first objective of this research is to carry out an energy evaluation of a CCS-ORC system designed to capture the CO₂ contained in the exhaust gases of a NG engine operating in several loads and rpm of the engine. For this, two engines (used in freight and passenger road transport and with different displacement volumes) operating at four engine loads in the entire engine rpm are simulated to determine the exhaust gases' temperature, pressure, and composition conditions. The intention of this after the fact is to know if engine size affects the behaviour of the CCS-ORC system. Subsequently, a CCS-ORC system working with temperature swing adsorption (TSA) is simulated. Three sorbents (PPN-6-CH₂-DETA, MOF-74Mg and activated carbon)

Table 1
 Technical specifications of the F1C and M936G engine.

Engine	M936G [30]	F1C [29,31]
Architecture	In-line 6-cylinder engine	In-line 4-cylinder engine
Aspiration method	Turbocharged with Aftercooler	
Injection	Multipoint	
Valves per cylinder:	4	
Bore [mm]	110	96
Stroke [mm]	135	104
Displacement volume [cm ³]	7700	3000
Connecting Rod Length [mm]	250	220
Compression ratio	17	12.5
Maximum boost pressure ratio	2	1.5
Firing Order	1-5-3-6-2-4	1-3-4-2
Combustion duration [deg]	57	58
Star of combustion BTDC	18	19
[CAD]		
Brake Power [kW]	222 at 1950 rpm	100 at 3500 rpm
Torque [Nm]	1200 at 1600 rpm	350 at 1500 rpm

and two CCRs (70 and 100 %) are used in the simulations. The aim is to establish the sensibility of the CCS-ORC system to different sorbents and capture rates regarding the energy balance. The second objective of this research is to size and quantify the volume and weight of the CCS-ORC system, thus determining how its installation can affect the useful space of the heavy-duty vehicle. For this, the heat exchange areas of the CCS-ORC system are calculated, and the volume and mass of the sorbent required in an operation of 8 h are estimated. All this work outlines for the first time a mapping of the energy consumption and the dimension of the CCS-ORC system able to adapt to operate in several loads and rpm of the engine, which expands the knowledge paving the way to use CCS in mobile sources as a valuable strategy to mitigate climate change.

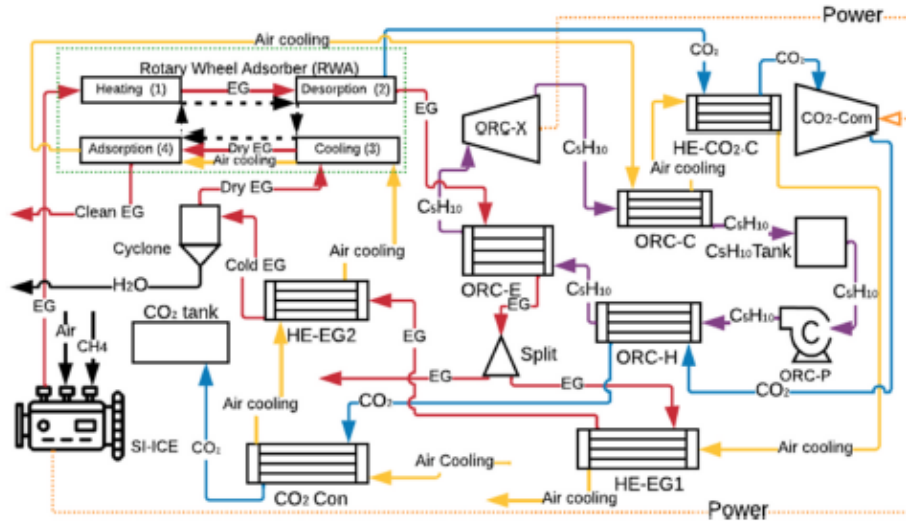


Fig. 1. CCS-ORC system configuration.

2. Methodology

The engine simulations are done in the software AVL boost, and the CCS-ORC system simulations are performed in the software ASPEN +. The following subsections show the procedure developed in this study.

2.1. Engine selection and simulation

Two four-stroke turbochargers natural gas spark-ignition engines with different displacement volumes (d_v) are selected for the energy analyses proposed below. These engines are used frequently in passenger and freight road transport. The engines selected are the M936G engine manufactured by Mercedes Benz with a d_v of 7700 cc and an F1C engine manufactured by FPT Industrial with a d_v of 3000 cc, both engines working with stoichiometric combustion [28,29]. Table 1 lists the specifications of the engines.

The energy simulations for the CCS-ORC system require temperature, pressure, mass flow, and composition of the exhaust gases as input parameters. Both engines are modelled using the software AVL BOOST and values of these parameters are obtained at four partial engine loads (25, 50, 75 and 100 %) in the entire rpm range. The theoretical models used

in the engine are the Woschni heat transfer model for the heat transfer in the cylinders, the simplified model of boost pressure to obtain the air mass flow, the Re-analogy for the heat transfer in the engine ducts and the Heywood, Patton, Nitschke model for the friction. In addition, air at standard conditions (25 °C and 1 atm) and a lower heating value (LHV) of the NG of 48351 kJ/kg were taken as inlet parameters [32–34]. The engine performance results obtained in the engine models and the accuracy between those, and the actual performance curves of the engines provided by the manufacturers [29,30] can be found in previous research [27]. The exhaust gas conditions are also obtained, which are required as input parameters in the CCS-ORC system simulations. These values are consigned in Appendix A and B, the temperature, pressure and mass flow for each species of exhaust gases are shown there. Finally, the mass fraction of the engine exhaust gases obtained in the engine model simulations is 15.4, 12.6 and 72 % for the CO_2 , H_2O and N_2 , respectively.

2.2. CCS-ORC system

2.2.1. CCS-ORC system configuration

The CCS-ORC system was configured using all the high-temperature

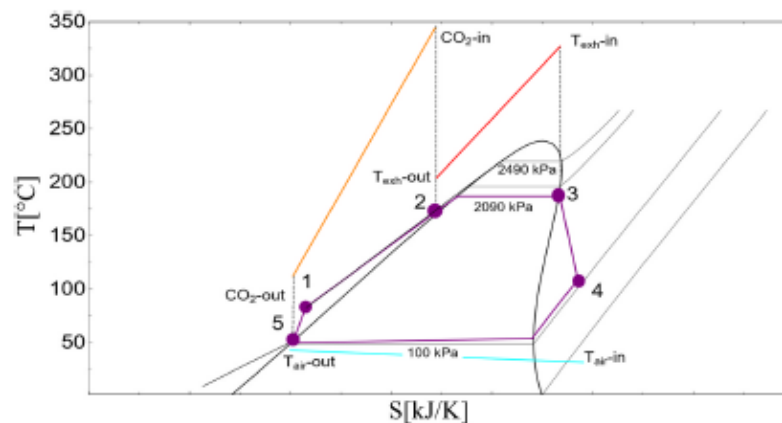


Fig. 2. T-S diagram for the ORC.

Table 2

Input parameters for the calculation of the fluid pressure at the ORC-X inlet.

Variable	Value	Unit
Compressibility factor (Z)	0.96	NA
Ideal gas constant (R)	0.1186	kJ/kgK
Saturation temperature (T_{sat})	186.15	°C
WF density at 1 bar ($\rho_{pump,0}$)	735.3	kg/m ³
Expander volumetric efficiency ($\eta_{vol,exp}$)	0.45 [41]	NA
Pump volumetric efficiency ($\eta_{vol,pump}$)	0.8	NA
Volumetric efficiency product (β_{vol})	0.36	NA
Displacement volume ratio (β_{pda})	0.76	NA
Angular velocity ratio (β_a)	0.2	NA

heat sources to get the most straightforward possible configuration. Moreover, a reduction of 78.1 % for the cooling processes was obtained through a Pinch analysis. Fig. 1 shows the final configuration of all systems integrating the CCS-ORC system proposed for this study.

A rotary wheel adsorber (RWA) is used for the adsorption process (enclosed in green dotted line). The TSA process consists of four stages (black dot lines), represented in Fig. 1. The charged sorbent is heated to a desorption temperature in the first stage so that the CO₂ is released from the sorbent [35] in the second stage. The heat required for these stages is extracted from the exhaust gases coming from the engine exhaust. In the third stage, the sorbent is cooled to the adsorption temperature and is prepared to adsorb CO₂ from the dry exhaust gases in the fourth stage. Air at standard conditions is used for cooling in the last stages.

A basic ORC [36] with two heat sources is integrated into the system to provide the mechanical energy required to compress the CO₂. One source is heat remaining in the exhaust gases after the RWA, and the second is the heat produced in the CO₂ compression. Four additional heat exchangers complete the CCS system to dry the exhaust gases and cool the CO₂. Fig. 1 shows with a different colours each of the flows operating in the systems (exhaust gases - red, CO₂ - blue, air cooling - yellow and ORC working fluid - purple) and the heat exchangers and devices arrangement.

2.2.2. ORC design and working fluid selection

The ORC's working fluid (WF) is cyclopentane (C₅H₁₀). This organic fluid was selected because of the excellent performance results in previous research performed on ORC in ICE [37,38]. On the other hand, C₅H₁₀ has a limited environmental impact and low toxicity, is non-corrosive [39], has a low decomposition rate and is thermally stable at temperatures up to 350 °C despite its high flammability despite its high flammability and has a low decomposition rate [40], making it safe for use in this kind of application.

Fig. 2 shows the TS diagram of the thermodynamic states of the WF along the ORC. The ORC circuit begins with preheating the WF in the heat exchanger (ORC-H), thanks to the heat produced during the compression of the CO₂ (1–2 process). Afterwards, the WF is vaporised in the heat exchanger (ORC-E), taking the exhaust gases' waste heat after CO₂ desorption (2–3 process). After, WF flows through an expander (ORC-X) to produce power (3–4 process). Finally, the WF is condensing in the heat exchanger (ORC-C) (4–5 process), and pumping (ORC-P) to begin the cycle again (5–1 process).

The ORC operational pressures were obtained following the procedure developed by Fatigati et al. [41,42] which is based on the permeability concept (equation (1)). Assuming a pressure of 1.5 bar at the outlet of the ORC-X and the inlet pressure in the ORC-X is obtained using equation (2). The meaning of the three dimensionless variables of equation (2) is explained in Ref. [41], and Table 2 shows the used values.

$$\alpha = \frac{\dot{m}_{WF}}{\Delta P} \quad (1)$$

$$P_{in,ex} = ZRT_{in} \rho_{pump,in} \beta_{vol} \beta_{pda} \beta_a \quad (2)$$

Table 3

Parameters and conditions for ORC simulations.

Device	Parameter	Unit	Value	State	Fluid
ORC-C	Inlet pressure	Bar	1.5	Vapour	C ₅ H ₁₀
	U [44]	W/m ² K	120 → Condensation	NA	Air-C ₅ H ₁₀
ORC-P	Inlet pressure	Bar	1	Saturated liquid	C ₅ H ₁₀
	Isentropic efficiency [46]	NA	0.55	NA	
ORC-H	Inlet pressure	Bar	24.9	Compressed liquid	C ₅ H ₁₀
	U [44,45]	W/m ² K	100 → Liquid-Gas	NA	C ₅ H ₁₀ - C
ORC-E	Inlet pressure	Bar	22.9	Compressed liquid	C ₅ H ₁₀
	h [44]	W/m ² K	70 → Liquid-Gas 2000 → Phase change 35 → Gas-Gas	NA	C ₅ H ₁₀ - Exhaust gas
ORC-X	Inlet pressure	Bar	20.9	Vapour	C ₅ H ₁₀
	Isentropic efficiency [47]	NA	0.65	NA	

Table 4

Overall heat coefficients for the heat exchangers used in the ORC [44,45,48].

System	Heat exchanger	Process	Fluids	U [W/m ² K]
CCS	HE-CO ₂ -C	Cooling	CO ₂ - Air	100
	CO ₂ -Con			
	HE-EG1	Cooling	Air - Exhaust gases	
	HE-EG2	Dry		

The ORC-X inlet pressure obtained following the described procedure is 20.9 bar; at this pressure, the WF saturation temperature is 184.15 °C. This temperature fits with the critical operation condition in the ORC-E, which is at 25 % engine load and 1000 rpm in the FIC engine (the lowest thermal energy); at this point, the inlet exhaust gases in the ORC-E has a temperature of 222 °C, so it fulfils with ΔT established for its operation (see Table 6). From this, the inlet pressures of the ORC devices are subsequently set from this value. The devices' pressure drops, the heat transfer coefficient (h) and the overall heat transfer coefficient (U) values are taken from the literature [43–45]. Table 3 shows the parameter values for each device and fluid conditions in the simulations.

2.2.3. Heat exchangers

As seen in Fig. 1, the CCS system has four heat exchangers. The first of them serves to reduce the CO₂ temperature after the desorption process (HE-CO₂-C), the second one is used to condensate the CO₂ (CO₂-con), the third one is used as a first cooling stage of the exhaust gases (HE-EG1), and the last heat exchanger (HE-EG2) finishes cooling and drying the exhaust gases. These heat exchangers utilise the same air cooling that flows through the RWA and the ORC. This information is summarised in Table 4. An overall heat transfer coefficient of 100 W/m²K corresponding to a cooling process in a compact heat exchanger [44,45,48] is considered.

2.2.4. Rotary wheel adsorber (RWA)

The four TSA processes (adsorption, heating, desorption and cooling) are performed on an RWA (green dot lines Fig. 1). This technology operates with VeloxothermTM, developed by Inventys [49]. The advantage of this device is that it is possible to do the TSA cycle in less than 90 s [35], which drives to small equipment sizes. In the simulations, the cooling and heating of the sorbent in the RWA are made by indirect

Table 5

Main physical properties of the sorbents used in the simulations [50,51,53,54].

Sorbent	Adsorption Heat (ΔH_{ads}) [kJ/mol _{CO₂}]	Loading Capacity (q) [kg _{CO₂} /kg _{sorbent}]	Selectivity CO ₂ /N ₂	Specific Heat (c_p) [kJ/kgK]	Density (ρ) [kg/m ³]
PPN-6-CH ₂ -DETA	-45.33	0.2354	>10.000	0.985	805
MOF-74-Mg	-37.4	0.27808	209	0.896	914.9
Activated carbon	-25	0.132	11	1.062	1040

^a Crystallographic density.

contact with air at standard conditions (25 °C and 1 bar) and with the exhaust gases coming from the engine, respectively.

2.2.5. Sorbent selection

Three sorbents are selected for the CCS-ORC simulations: PPN-6-CH₂-DETA (PPN onwards), MOF-74-Mg (MOF onwards), and activated carbon (AC onwards). PPN and MOF sorbents present an ultra-high selectivity for CO₂, exceptional adsorption capacity, and low desorption energy, which are suitable physical properties for CO₂ capture (see Table 5) [26,50,51]. AC is a commercial sorbent with ultra-low desorption energy, and several studies have shown that it can be used as a sorbent [52–54].

According to the literature, the suitable desorption temperature that guarantees the greatest amount of CO₂ desorption without sorbent degradation is 150 °C [51] which was chosen in the simulations. On the other hand, the adsorption temperature selected is 30 °C since the exhaust gas is 99 % dry at this temperature, which is ideal for sorbents because they lose CO₂ adsorption capacity with wet exhaust gases [55].

2.2.6. CO₂ compression and storage process

Simulations consider the storage of CO₂ as a liquid. According to the CO₂ Mollier diagram, the thermodynamic conditions established in the simulations to do this are a CO₂ pressure of 75 bar and a temperature of 29.35 °C. Regarding the pressure, the CO₂ pressure changed for each sorbent in the simulations due to the impurities of N₂ in the CO₂ stream (due to the selectivity). Consequently, the CO₂ pressure with PPN is 75 bar, with MOF is 77.9 bar and with AC is 85.73 bar; these pressures were calculated using the Dalton Law. The simulations assume an isentropic efficiency of 65 % for the CO₂ compressor (CO₂-Com onwards). The proposed CCS-ORC system configuration has three stages to achieve the CO₂ storage temperature. The first one is done in the HE-CO₂-C using air as cooling fluid before entering the CO₂ compressor. After, the CO₂ is cooled in the ORC-H using the C₅H₁₀ as a cooling fluid. The last cooling stage is done in the CO₂-con using atmospheric air as a cooling fluid (See Fig. 1).

2.3. Energy simulations of the CCS-ORC system

The energy analysis of the CCS-ORC system aims to quantify by simulations the penalty over the engine in power terms that would induce their operation. Thus, it is necessary to know the heat and areas of the heat exchangers and the power consumption of the expander, pumps and compressors. All of this is per each rpm and engine load condition. The following shows the assumptions and the procedure developed in the simulations.

2.3.1. Assumptions

The following assumptions are considered in the CCS-ORC system simulations: (i) there are no mass losses in pipes, devices, and connections; (ii) there are no pressure drop losses in the pipes; (iii) heat losses in

Table 6

 ΔT and requirements of the heat exchangers in the CCS-ORC system simulations.

Heat exchanger	ΔT between hot and cold fluid [°C] [48]	Fluids	Design condition of the heat exchanger
ORC-C	5	C ₅ H ₁₀ -Air	C ₅ H ₁₀ outlet as saturated liquid
ORC-E	20	C ₅ H ₁₀ -Exhaust gases	C ₅ H ₁₀ outlet as saturated vapour
ORC-H	20	C ₅ H ₁₀ -CO ₂	–
HE-CO ₂ -C	3	Air-CO ₂	–
CO ₂ -Con	4	CO ₂ -Air	CO ₂ outlet as saturated liquid
HE-EG1	3	Exhaust gases-Air	–
HE-EG2	3	Exhaust gases-Air	Exhaust gases outlet at 30 °C

pipes are negligible; (iv) exhaust gases are non-corrosive during the heat transfer; (v) steady-state conditions in the simulations; (vi) inlet air for cooling at standard conditions; (vii) heat exchanger are simulated in counter-flow type.

2.3.2. Procedure in simulations

Simulations are performed for two CCR conditions (70 and 100 %), at 25, 50, 75 and 100 % of engine load and in the entire rpm range. For both CCR conditions, the areas of the heat exchangers of the CCS-ORC system must first be known. These areas were determined at maximum engine torque. The cooling air mass flow is obtained when the sorbent is cooled at 30 °C and are fulfil the design condition is reached of the heat exchanger and the selected ΔT (from the literature) between the hot and cold fluid in each heat exchanger is met (see Table 6).

The ORC cycle was simulated so that the WF at the ORC-X outlet was always saturated vapour (see Fig. 2), which fixes the maximum mass flow of the WF for each engine condition in the simulations, thus obtaining the maximum power production. Also, the values for the heating, cooling, desorption and adsorption heat developed in the RWA are introduced for each simulation (Appendix C, D, E and F). These values are calculated using equations (3)–(5). The ΔT in these equations is 120 °C, which is obtained as the difference between desorption temperature (150 °C) and exhaust gas drying temperature (30 °C).

$$\dot{Q}_{heating} = CCR_{XCO_2} \dot{m}_{EG} \Delta T \left(c_{p-CO_2} + \frac{c_{p-CO_2}}{q} \right) \quad (3)$$

$$\dot{Q}_{cooling} = \frac{c_{p-CO_2} CCR_{XCO_2} \dot{m}_{EG} \Delta T}{q} \quad (4)$$

$$\dot{Q}_{desorption/adsorption} = CCR_{XCO_2} \dot{m}_{EG} \Delta H_{des} \quad (5)$$

This procedure allows us to calculate the power consumption of the ORC-P and the CO₂ compressor, the power production of the ORC-X, the air mass flow of the fan used to cool the CCS-ORC system, the WF mass flow in the ORC and the heat flux of all heat exchangers in the rest of the engine operational points.

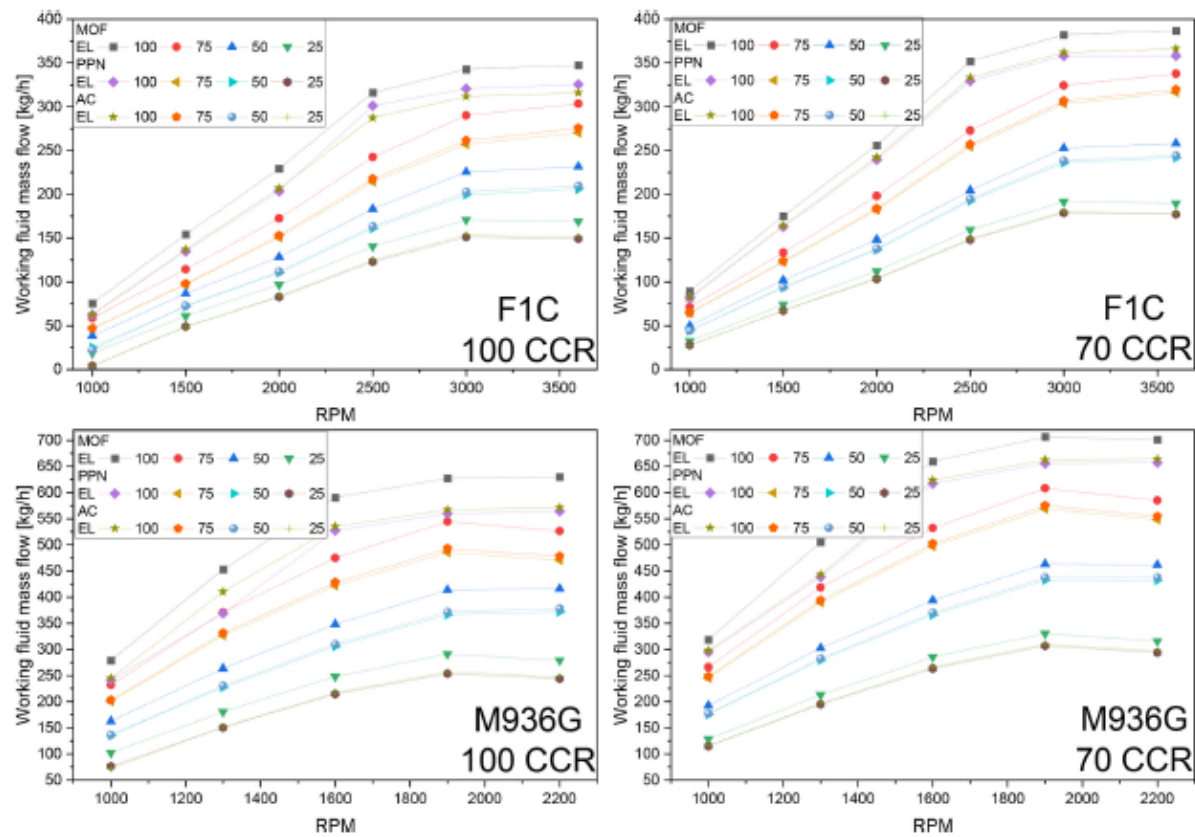
As is expected, for the other simulation points, the values of the areas of heat exchangers change. At thermal operating conditions higher than maximum torque, these areas are equal to the calculated since the software controls this by increasing the cooling flow or limiting the WF flow. By contrast, at lower thermal points than the maximum torque, the heat exchanger areas present a lower value, which is good since if a larger area is required, this would indicate that the heat transfer process could not develop properly. The areas always were controlled and verified using equation (6), whose value must always be equal to or greater than zero.

$$A_{difference} (\%) = \left(\frac{A_{Tmax} - A_{current}}{A_{Tmax}} \right) 100 \quad (6)$$

Table 7

Heat exchangers areas obtained in the simulations.

Engine	Sorbent	CCR	ORC-C [m ²]	ORC-E [m ²]	ORC-H [m ²]	HE-CO ₂ -C [m ²]	CO ₂ -Con [m ²]	HE-EG1 [m ²]	HE-EG2 [m ²]	Total [m ²]
M936G	MOF	70	17.90	8.17	0.59	0.67	1.87	18.36	11.58	59.13
	PPN	70	16.53	8.16	0.57	0.67	1.82	18.74	10.18	56.68
	AC	70	16.71	7.95	0.63	0.73	1.96	17.99	10.25	56.21
	MOF	100	15.61	7.66	0.75	0.95	2.54	25.37	13.02	65.91
	PPN	100	13.77	7.59	0.72	0.95	2.46	25.30	11.20	62.01
	AC	100	13.97	7.17	0.79	1.05	2.64	24.23	11.31	61.16
F1C	MOF	70	9.56	4.27	0.31	0.35	0.98	9.61	6.12	31.19
	PPN	70	8.84	4.27	0.30	0.35	0.96	9.81	5.38	29.91
	AC	70	8.93	4.16	0.33	0.38	1.02	9.41	5.42	29.66
	MOF	100	8.36	4.02	0.50	2.54	1.33	13.30	6.88	36.93
	PPN	100	7.92	4.01	0.39	0.50	1.30	13.34	6.40	33.86
	AC	100	7.51	3.79	0.42	0.55	1.38	12.72	5.99	32.35

Fig. 3. C₅H₁₀ Mass flow under the two CCR conditions and over the entire rpm range.

3. Results and analysis

This section presents the results obtained from the simulations of the CCS-ORC system. Initially, the results of the operational parameters of the CCS-ORC system (heat exchanger areas and fluid mass flows) are presented. Then, energy performance as power production and consumption by the devices and the penalisation over the engine by the CCS-ORC system operation is presented. Finally, the mass and volume of the sorbent for an ICEv operation of 8 h are quantified to establish the required weight and volume in the RWA and the volume of the heat exchangers to get the spatial dimension of the CCS-ORC system.

3.1. Heat exchanger areas

Table 7 shows the values of the heat exchanger areas of the CCS-ORC system that are obtained in the simulations. Both engines' heat exchanger areas of the CCS-ORC system show similar trends. The results show that the ORC-E and ORC-C heat exchanger areas are larger for a 70 % CCR than a 100 % CCR. For the ORC-E and ORC-C exchangers, it can be explained because of the higher WF mass flow needed to take advantage of the heat in the exhaust gases. This remaining heat is higher due to a lower heat requirement in the heating and desorption processes at 70 % of CCR. On the contrary, the HE-EG1, HE-EG2, ORC-H, HE-CO₂-C and CO₂-C areas are lower for the lower CCR, caused by a smaller mass flow of exhaust gases and CO₂.

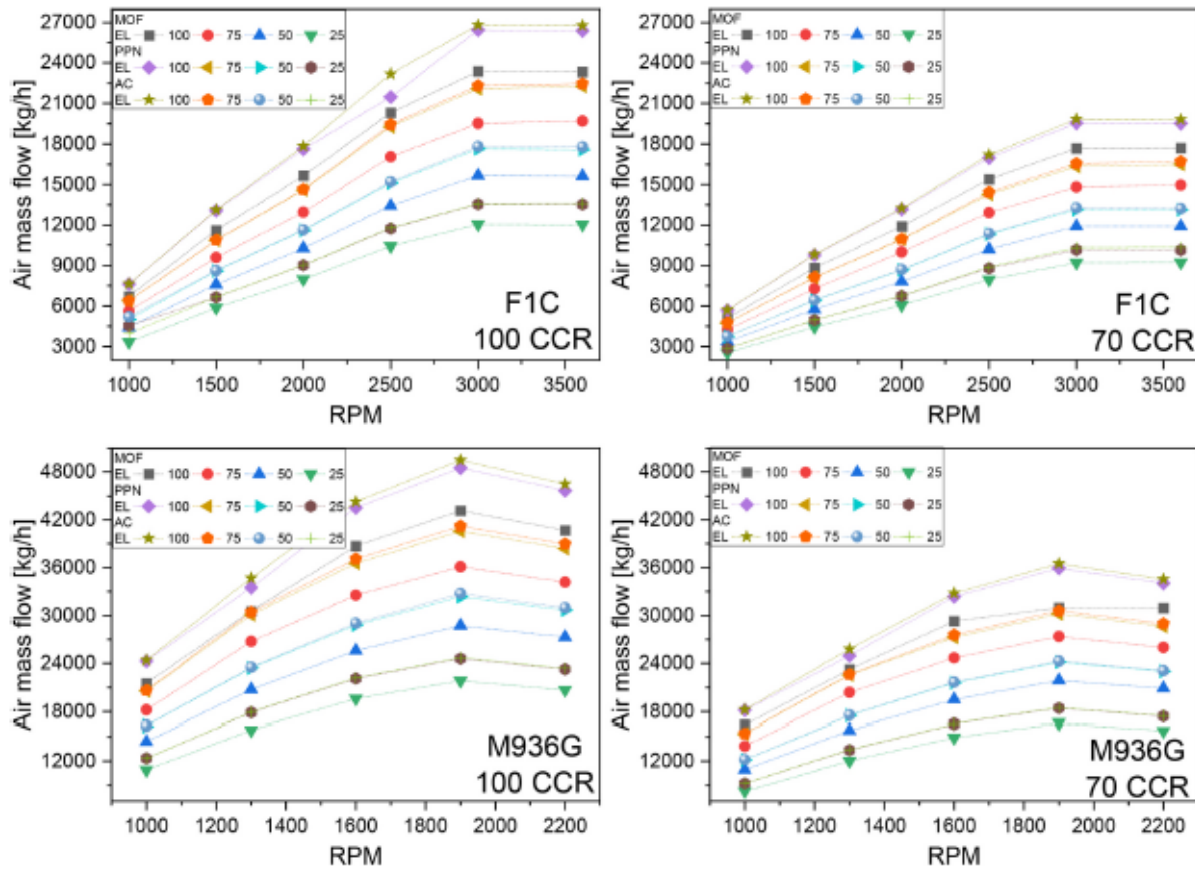


Fig. 4. Cooling air mass flows in the CO₂-Con, the RWA, the ORC-C, the HE-CO₂-C and the HE-EG1 in the entire F1C and M936G engine rpm.

The effect of the sorbent in the heat exchanger areas of the CCS-ORC system can be seen in the CO₂-Con. For instance, with MOF operation, there is a difference between the heat exchanger areas of 2.5 % at 70 % of CCR and 2.7 % at 100 % of CCR regarding PPN operation. This difference is due to the selectivity of the sorbent. The MOF-74-mg has a lower selectivity than the PPN-6-CH₂-DETA, which makes the CO₂ mass flow contain impurities of N₂ which change the heat transfer parameters producing an increase in the area of the CO₂-Con. This same behaviour can be seen with the AC sorbent, whose selectivity is the lowest of the three sorbents.

Finally, the area of the HE-EG2 is, on average, 11.2 % greater with MOF operation regarding PPN and AC operation both for the two CCRs and the two engines. This result is because, in MOF operation, the cooling air mass flow is the lowest obtained due to the lowest heat of cooling and adsorption with this sorbent, which produces that this heat exchanger requires a larger area.

3.2. Mass flows of C₅H₁₀ and air

Fig. 3 shows the C₅H₁₀ mass flows in the ORC simulations. It can be seen a higher C₅H₁₀ mass flow in 70 % CCR than in 100 % CCR in both engines and with all sorbents at the highest engine load (EL). It can be explained as in the 70 % CCR case, less heat from the exhaust gases in the sorbent's heating and desorption process is consumed mainly due to less sorbent and CO₂ mass involved in the processes. However, as mentioned before, this rise in the WF mass flow increases the heat exchanger areas of the ORC-E and ORC-C, regarding the CCS-ORC system operation at 100 % of

CCR.

Considering sorbents, the MOF operation always presents a higher C₅H₁₀ mass flow than the PPN and AC operation. This result is because the heating and desorption heat with MOF operation is less than the PPN operation. At the same time, the difference between MOF and AC operation is due to the higher selectivity of the MOF-74-mg regarding the AC that involves a fewer mass of the sorbent and, hence, a low heating heat.

Fig. 4 shows the cooling air mass that flows through the CO₂-Con, the HE-EG2, the RWA, the ORC-C, the HE-CO₂-C and the HE-EG1 on both SI-ICE, both CCRs and for the three sorbents. It can be seen that the highest cooling air mass flow values appear at a CCR of 100 %. These results are due to more CO₂ mass for condensing and more demand for cooling the RWA since higher heat is consumed from the exhaust gases in the RWA at 100 % of CCR than at 70 % of CCR. For this reason, the air mass flow with PPN and AC operation is higher than with MOF operation under whatever engine load and rpm because of its lowest desorption heat.

3.3. Energy consumption of the CCS system devices

Understanding the power usage of the different devices within the CCS-ORC system is crucial for quantifying power losses. This section presents the findings regarding the power generated by the ORC-X and the power consumed by parasitic loads, which include the combined power from the CO₂-com, the ORC-P, and the air fan utilised in the cooling processes (Equation (7)). The power consumption of the air fan is determined by selecting fans from the EBMPAPST company's online

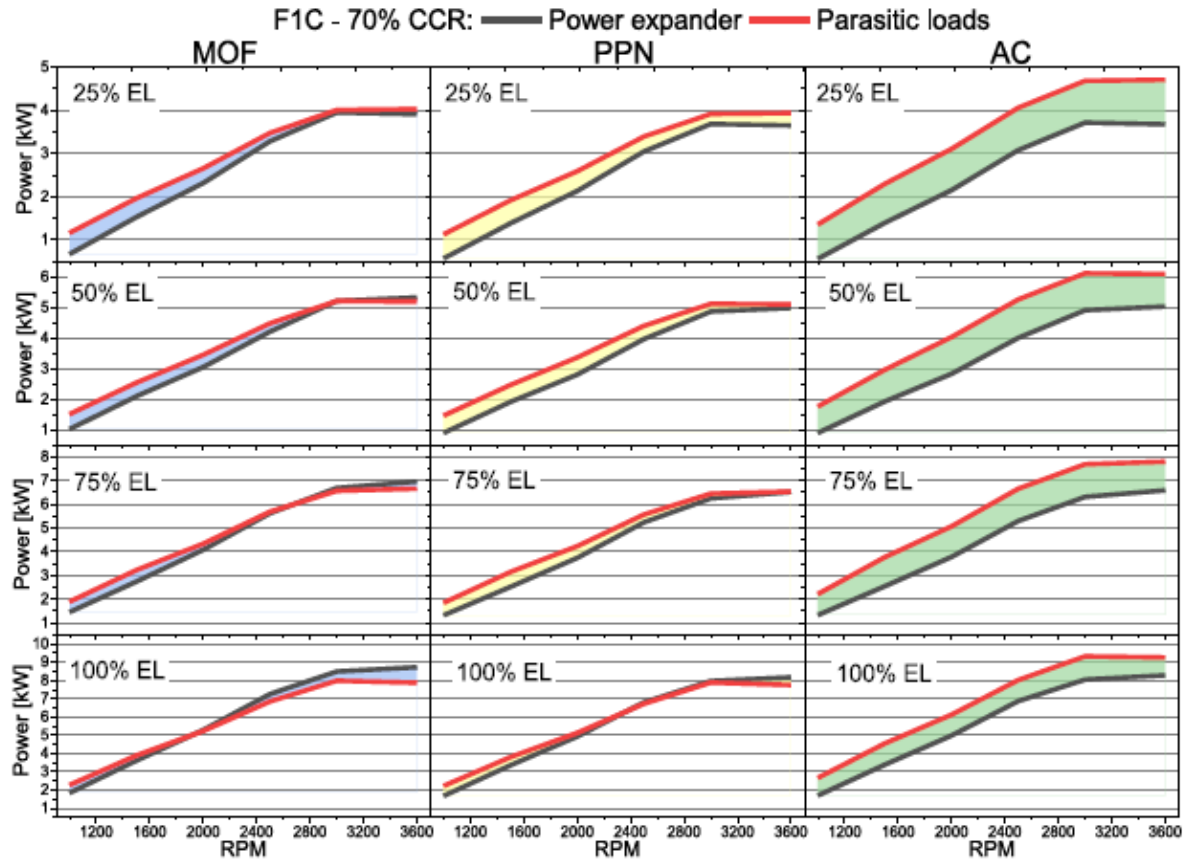


Fig. 5. Power production by the ORC and parasitic loads by the CCS-ORC system in the F1C engine.

catalogue [51] that align precisely with the simulated air mass. Additionally, the section presents the percentage of engine power utilised by the CCS system due to its operation.

$$W_{\text{parasitic loads}} = W_{\text{pump}} + W_{\text{compressor}} + W_{\text{fan}} \quad (7)$$

3.3.1. Power production and parasitic loads in the CCS-ORC system

The following figures show the difference between the power produced by the ORC-X and the parasitic loads of the CCS-ORC system at 70 and 100 % CCR in both engines and for all sorbents. Fig. 5 shows the parasitic loads power consumption and power production of the ORC-X at 70 % of CCR with all sorbents in the engine F1C. There can be seen that with MOF operation, the parasitic loads are covered by power produced in the ORC-X at 100 % of the engine load from 2000 rpm; at 75 % of the engine load, the ORC-X covers the parasitic loads from 2800 rpm, and at 50 % of the engine load, the parasitic loads are covered from 3200 rpm.

During PPN operation, the ORC-X generates sufficient power to compensate for the parasitic loads at 100 % and 75 % of the engine load, starting from 2400 to 3600 rpm, respectively. However, in the case of AC operation, the parasitic loads are never fully compensated due to the elevated pressure needed for CO₂ liquefaction. The lower AC selectivity primarily causes this limitation. Furthermore, when utilising any sorbent, the power generated by the ORC-X is unable to meet the requirements of the parasitic loads at 25 % of the engine load. The main reason for this is that, under this specific engine load condition, the exhaust gases contain the lowest level of thermal energy.

Fig. 6 shows the difference between the power produced by the ORC-X and the parasitic loads of the CCS-ORC system at 100 % CCR in the F1C engine with all sorbents. With this condition, the CCS-ORC system can not cover the parasitic loads with any sorbent. This behaviour was anticipated because, as the CCR increases, the mass flow of the working fluid (WF) in the ORC decreases, resulting in lower power production by the ORC-X. Additionally, the power consumption of the CO₂ compressor rises due to the increased mass of CO₂ being captured.

In the M946G engine at a 70 % CCR (Fig. 7) in MOF operation, the parasitic loads are covered at 100 % of the engine load from the maximum torque (1500 rpm), 75 % of the engine load from 1700 rpm, and 50 % of the engine load from maximum power (2000 rpm). With PPN operation at 100 % of the engine load, the parasitic loads are covered from 2000 rpm and in the rest of the engine loads, the parasitic loads are not covered. Fig. 8 depicts a similar trend with all the sorbents studied at a CCR of 100 %, resembling the behaviour observed in the F1C case.

3.3.2. Engine power percentage consumed by the CCS system

Figs. 9 and 10 show the power percentage required from the engines to operate the CCS-ORC system across various rpm and engine load conditions, sorbents, and selected carbon capture rates (CCRs). These figures demonstrate that, regardless of the sorbent, CCR, or engine rpm, the most significant impact on the engines occurs at 25 % of the engine load. However, this penalty decreases as the engine load increases, and the ORC system can even deliver excess power, as with MOF operation at a 70 % CCR.

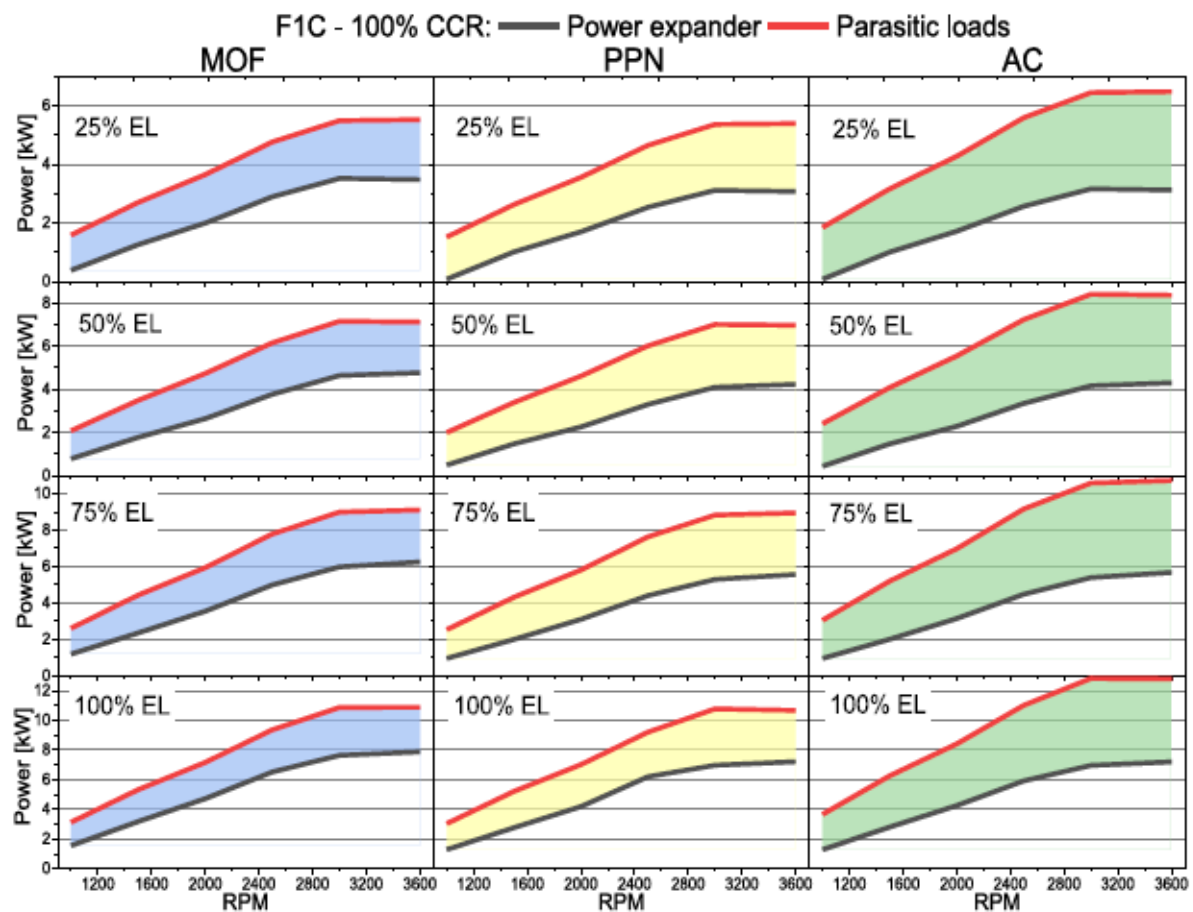


Fig. 6. Power production and parasitic loads in the CCS system with MOF-74-Mg and CCR of 100 % in the F1C engine.

As anticipated, the penalty percentage of the CCS-ORC system on the engine follows the AC operation > PPN operation > MOF operation sequence. The main reason for this is the reduced need for heating and desorption heat in MOF operation compared to other sorbents. The penalty percentage values of the CCS-ORC system on the F1C engine, at a 70 % CCR, range from 0 % with MOF operation to 10.8 % with AC operation. At a 100 % CCR, these values range from 2.2 % with MOF operation to 23.5 % with AC operation.

Likewise, for the M936G engine, at a 70 % CCR, the penalty percentage values range from 0 % with MOF operation to 7.1 % with AC operation. At a 100 % CCR, the penalty percentage values range from 1.9 % with MOF operation to 13.1 % with AC operation.

The values in the above figures show that the CCS system has a more significant penalty on the smaller engine size, irrespective of the sorbent used. In addition, at 25 % of the engine load, the highest penalty percentage values are obtained regardless of the sorbent since all the engines' power output is at its lowest point during this load condition, thereby amplifying the penalty percentage of the CCS system on the engines.

3.4. Weight and volume of the CCS-ORC system

The limited space within an ICEV poses a significant challenge for installing a CCS-ORC system. Hence, it is crucial to determine the mass

and area needed to incorporate a CCS-ORC system into the vehicle. This estimation involves calculating the mass and volume of the sorbent within the CCS-ORC system. The calculation procedure assumes a CCR of 100 % for both engines, an 8-h operation with 48 cycles of desorption and adsorption (each lasting 10 min), and an engine load of 75 % at the maximum torque RPM. The results of these calculations are presented in Table 8.

Finally, the mass and volume of the CCS-ORC system are estimated. The weight and volume of commercial compressors that meet the mass flow of CO₂ obtained in both engines are taken for this [56]. Concurrently, the weight and volume of a screw expander operating in the power ranges obtained in the simulations are taken from the literature [57]. Subsequently, the volume of the heat exchangers is obtained considering an area density (β) of 100 m²/m³ and the corresponding weight is extrapolated from analogous studies [58]. Finally, the tanks and ancillary systems' weight of the CCS-ORC system is estimated at 200 kg for the M936G engine and 120 kg for the F1C engine.

Based on the results, the CO₂ mass captured from the exhaust gases during an 8-h operation weighs 710 kg and 373 kg for the M936G and F1C engines, respectively. In its liquid state, the storage of this captured CO₂ requires 0.93 m³ and 0.49 m³ of volume for the M936G and F1C engines, respectively. The sorbent mass needed to capture CO₂ in the M936G engine amounts to 53.2 kg, 62.9 kg, and 112.1 kg for MOF, PPN, and AC operation, respectively, which translates to a sorbent volume

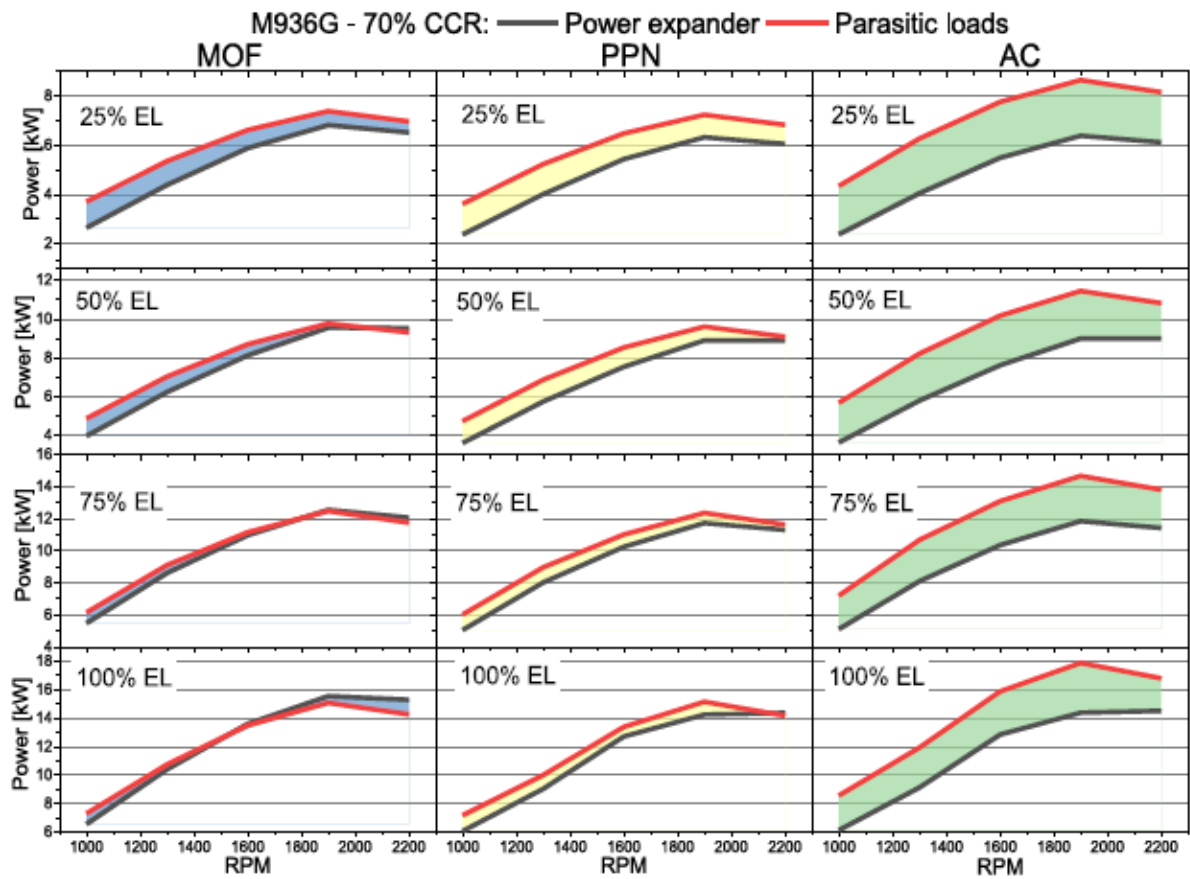


Fig. 7. Power production and parasitic loads in the CCS system with PPN-6-CH₂-DETA and CCR of 70 % in the M936G engine.

(RWA volume) of 0.116 m³, 0.156 m³, and 0.224 m³. For the FIC engine, the required sorbent mass is 28 kg, 33 kg, and 58 kg for MOF, PPN, and AC operation, respectively. The corresponding sorbent volumes are 0.061 m³, 0.082 m³, and 0.118 m³ for MOF, PPN, and AC operation, respectively. These results indicate that the selectivity parameter has the most significant impact on the weight of the CCS-ORC system. Consequently, the operation with AC, which has the lowest selectivity among the chosen sorbents, resulted in the highest weight for the CCS-ORC system.

The average weight and volume of the CCS-ORC system obtained are 1200 kg and 2.11 m³ for the M936G engine vehicle and 695 kg and 1.12 m³ for the FIC engine vehicle. Fig. 11 depicts the weight distribution of components within the CCS-ORC system. There, it can be seen that the CO₂ compressor is the equipment exerting the greatest influence on the total weight of the CCS-ORC system in both ICEVs, with its values ranging between 39.7 % and 45.4 % of the overall weight. Conversely, the heat exchangers, the RWA, and the tanks and auxiliaries exhibit comparable weight contributions across both engines, averaging 19.8 %, 17 %, and 6 %, respectively. Notably, the ORC-E exhibits a higher proportional weight in the FIC engine than the M936G; this disparity arises from using the same expander for both cases. The decision to use the same ORC-E in both ICEVs is due to its volume barely representing 2.7 % of the total volume of the CCS-ORC system, and it has a good performance with the mass flows of the WF obtained in both engines [58].

4. Analyses

The results show that the volume obtained for the CCS-ORC system with a CCR of 100 % represents scarcely 3.4 % of the total volume of a bus that uses the M936G engine and the space that the CCS-ORC system would occupy of a vehicle using an FIC engine represents 10.2 % of the total volume of the vehicle. These values can be diminished through a thorough design process for the heat exchangers. Although the values in the present research coincide with those reported in the literature [25, 57]. This process would consider factors such as the type of heat exchanger, geometric configuration, construction material, β , and other design parameters. Therefore, installing the CCS-ORC system in a heavy-duty vehicle is technically feasible since it barely affects its workspace. These values are even 15.6 % lower than the volume occupied by an electric battery of a heavy vehicle [59]. Regarding the CCS-ORC system weight, this could lead to an increase in fuel consumption. However, this extra weight in a heavy-duty vehicle would not imply a significant increase in fuel consumption [60]; consequently, the operation cost of the vehicle would hardly be affected by this variable.

However, the engine must augment fuel consumption to offset the parasitic loads the ORC fails to address. This is despite the crucial role played by the ORC in mitigating the penalty of the CCS system over the engine, which can be up to 11 % higher in the absence of the ORC. For this reason, it is necessary to quantify the extra fuel mass that the engine needs to cover the difference between the parasitic loads (PL) caused by the CCS system and the power produced by the ORC-E (PE); equation (8)

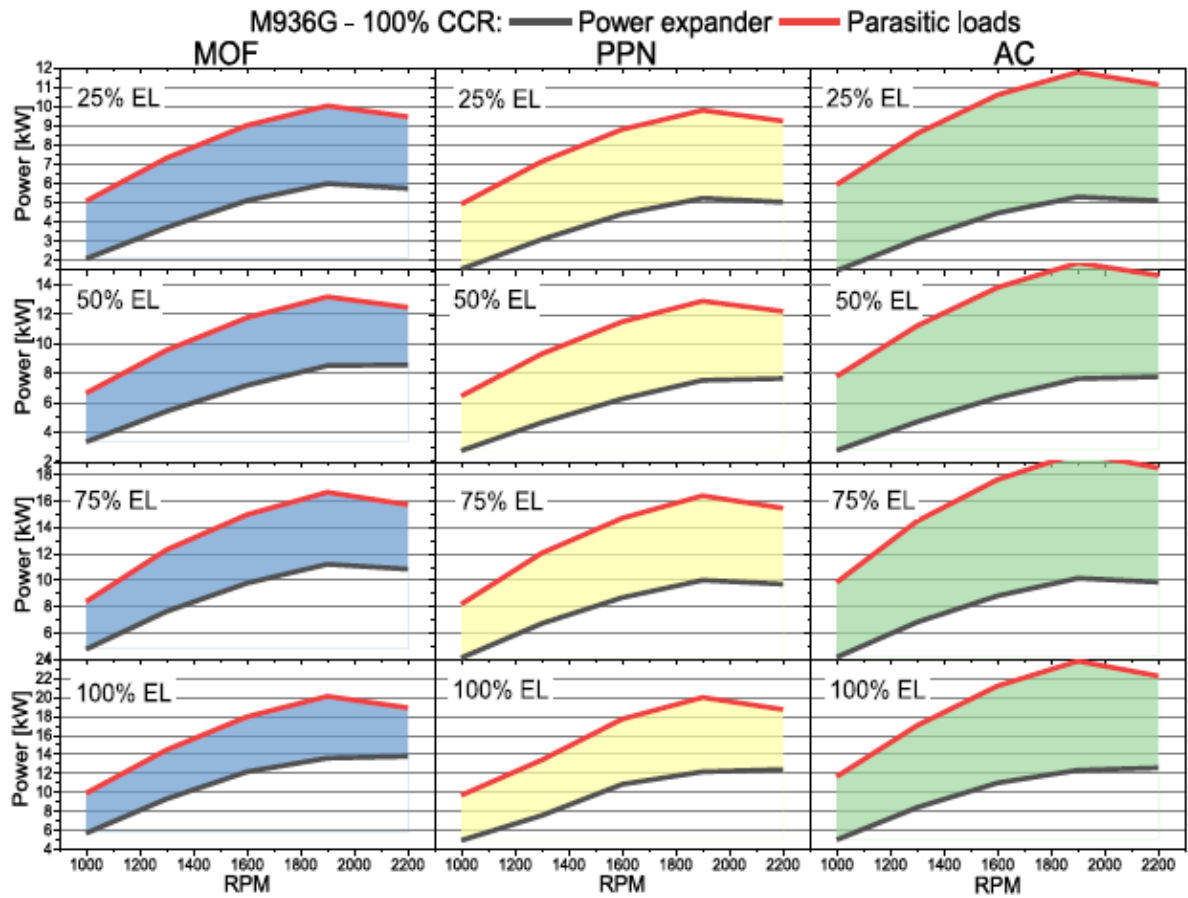


Fig. 8. Power production and parasitic loads in the CCS system with MOF-74-Mg and CCR of 100 % in the M936G engine.

is used. In this equation, the η_{comb} is the combustion efficiency and η_{eng} is the engine's thermal efficiency. These parameters are obtained from the engine simulations, whose values are listed in Appendix G and H. The assumptions for the calculations are the same as for the mass and volume calculation made in section 3.5 (75 % of engine load, at maximum torque and 8-h of operation). The results obtained are reported in Table 9.

$$m_{\text{fuel}} = \frac{28800(PL - PE)}{\eta_{\text{comb}} \eta_{\text{th}} LHV} \quad (8)$$

As seen in this table and as expected, the highest increase in the fuel mass is at 100 % of CCR and in AC operation, with values of 7.5 % in the M936G engine and 6.14 % in the F1C engine. However, at 70 % of CCR, the rise in the fuel mass with the MOF and PPN sorbents is almost marginal, with values less than 0.52 %. Even the fuel mass increase at 100 % of CCR could be covered if the transport sector must pay a carbon emission tax.

In the present research, the detail of the CCS-ORC system in the simulations was improved. Also, the WF mass flow calculation was changed and the U in the heat exchangers was updated (to get a more realistic process). As a result of these changes, the value obtained of the ORC efficiency was 11.7 %, which continues to coincide with the reported ORC efficiency in the literature [61,62]. In addition, as can be seen in Fig. 12, it was achieved that the size of the engine does not have a significant interference in the operation of the CCS-ORC system since the

percentage of the power of the parasitic loads covered by the ORC vary only with the type of sorbent used. The main difference between one engine and another at 70 % of CCR is 1.3 %, and 5.8 % at 100 % of CCR. Finally, it is observed that at 100 % CCR, the ORC can cover 42 % of the parasitic loads with AC and with MOF up to 60 %, while at 70 % CCR, this percentage goes from 73 % with AC to 92 % with MOF.

Fig. 13 shows the energy consumption of the capture process. As can be seen in this figure, the maximum energy consumption is obtained with CCR of 100 % in the F1C engine at 25 % of engine load and the lowest rpm engine, whose maximum value is 631 kJ/kgCO₂ in AC operation; with PPN operation, the value is close to 510 kJ/kgCO₂ and with MOF operation 429 kJ/kgCO₂. With the same CCR, these values are nearly 12 % lower in the M936G engine. These values coincide with the values reported by Kim et al. [63], who simulated an onboard CO₂ capture system with TVSA in diesel heavy-duty. Additionally in the literature, the energy consumption values for TSA, PSA and VSA are higher than 700 kJ/kgCO₂ at 90 % of CCR [64,65] and, with amine-scrubbing, are higher than 2500 kJ/kgCO₂ [66,67]. Therefore, the energy consumption of the CCS-ORC system is observed to be lower than the values reported in existing literature. This reduction is due to the taking advantage of waste heat from exhaust gases through the ORC. So, the findings reported herein and, in the literature, suggest that this kind of system, which is still in its design and simulation phase, has good prospects for its experimental development.

In analysing the behaviour of engines, the CCS-ORC system can

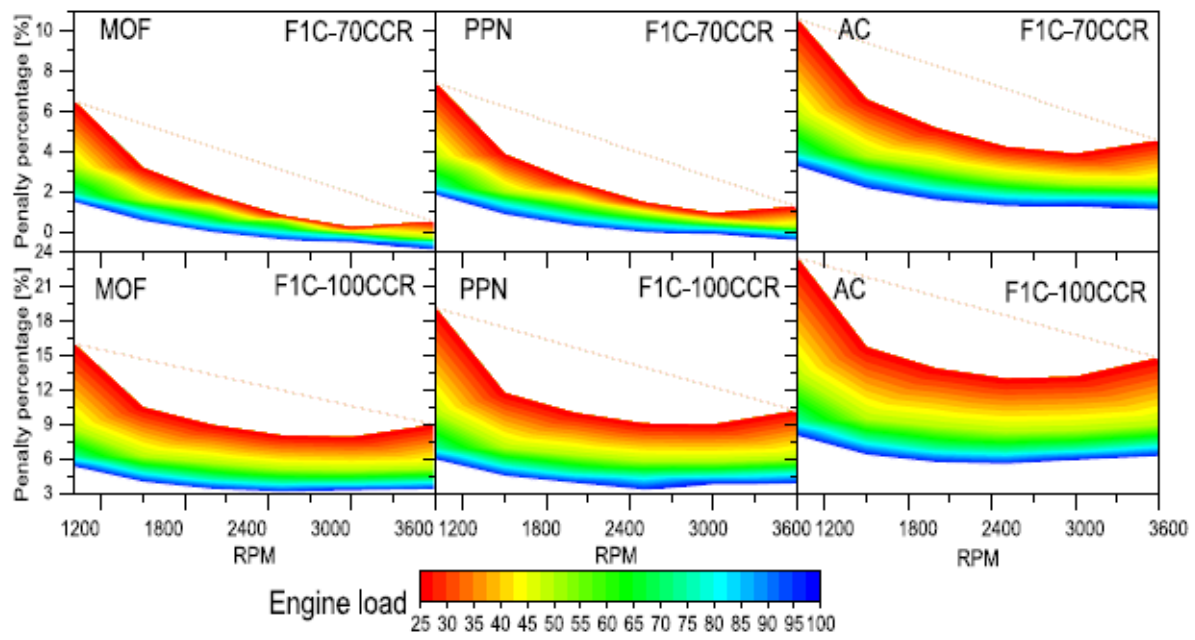


Fig. 9. Power percentage consumed by the CCS system operating in the M936G engine.

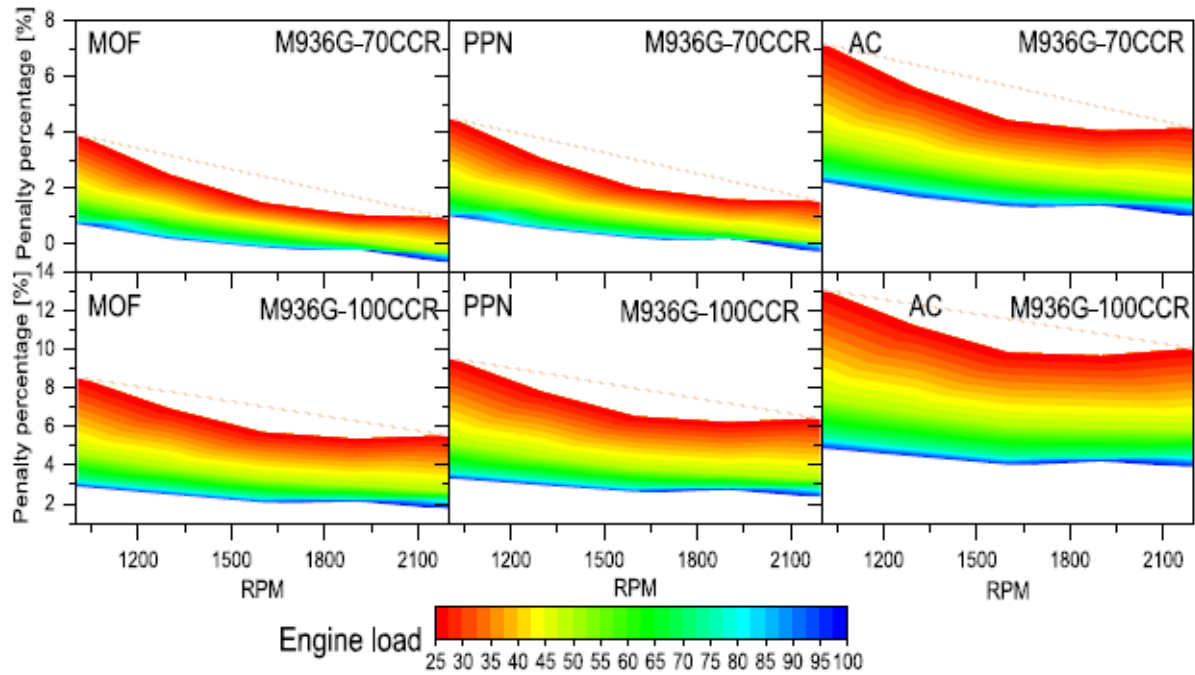


Fig. 10. Power percentage consumed by the CCS system operating in the F1C engine.

operate when there are engine accelerations (rise of load or rpm engine or both). Since the exhaust gas temperature increases due to the fuel enrichment in the engine charge (fuel-air mixture). This behaviour benefits the CO_2 desorption and the correct functioning of the ORC since

there is more waste heat in the exhaust gases available to take advantage of. On the contrary, when there are engine decelerations (reduction in load or rpm of the engine or both), the CCS-ORC system operation could be affected since there is a decrease in the fuel in the engine charge,

Table 8

Mass and volume of sorbent for 30 min of operation at 25 % of EL at the RPM of maximum torque.

Engine	M936G			F1C		
Sorbent	MOF	PPN	AC	MOF	PPN	AC
Exhaust mass [kg]	4610.07			2417.76		
CO ₂ mass captured [kg]	710.13			373.16		
CO ₂ volume [m ³]	0.93			0.49		
Sorbent mass (RWA weight) [kg]	53.2	62.9	112.1	28	33.0	58.9
^a Sorbent Volume (RWA volume) [m ³]	0.116	0.156	0.224	0.061	0.082	0.118
CO ₂ compressor weight [kg] [56]	540			276		
CO ₂ compressor volume [m ³] [56]	0.366			0.183		
ORC-E weight [kg] [57]	127.8					
ORC-E volume [m ³] [57]	0.03					
Heat exchangers volume [m ³] [58]	0.66	0.62	0.61	0.35	0.34	0.32
Heat exchangers weight [kg] [58]	257	241.8	238.5	135.7	132.1	126.2
^b Weight of CCS-ORC system [kg]	1178	1172.5	1218.4	687.4	688.9	708.9
Total Volume of CCS-ORC system [m ³]	2.11	2.11	2.17	1.11	1.12	1.14

^a Calculated with 50 % of the crystallographic density.^b Without the CO₂ mass.

reducing the exhaust gas temperature. This condition limits the desorption of CO₂ by not achieving the minimum desorption temperature, and in the ORC, there would be less waste heat available to take advantage of.

5. Conclusions

This paper introduces an innovative CCS-ORC system to mitigate CO₂ emissions from heavy-duty vehicles. The proposed system involves harnessing waste heat from the exhaust gases coming from an ICE to desorption of CO₂ and produce power into an ORC to supply the power demand in the CO₂ compression stage and cooling of all systems (see Fig. 1). The study within the framework of an energy analysis encompasses different case scenarios, wherein the sorbent is changed (PPN-6-CH₂-DETA, MOF-74-Mg, and activated carbon) and engine size (M936G

and F1C). The evaluation is carried out at four partial engine loads, the whole rpm range, and with two CCRs (70 and 100 %). The results provide valuable information on the energy requirement and size of the different components of the CCS-ORC system and the energy consumption by the CCS-ORC system to capture CO₂.

Based on the results, no significant difference was observed between the values obtained from the volume and weight of the CCS-ORC system when operating with the selected sorbents. This similitude is attributed to the fact that the RWA contributes merely 6 %, on average, to the weight and volume of the CCS-ORC system.

The study further revealed that the engine's size does not drastically influence the CCS-ORC system operation since the parasitic loads provoked by the CCS-ORC system remain almost constant between engines with average values of 2.9 % at 70 % of CCR and 9 % at 100 % CCR. The CCS-ORC system exhibited similar behaviour during PPN and MOF operations. However, when operating with AC, the CCS-ORC system exhibits increased parasitic loads and energy consumption to capture the CO₂, averaging 15 % across all engine loads and rpm ranges. This increase is due to the low selectivity of AC, leading to a higher

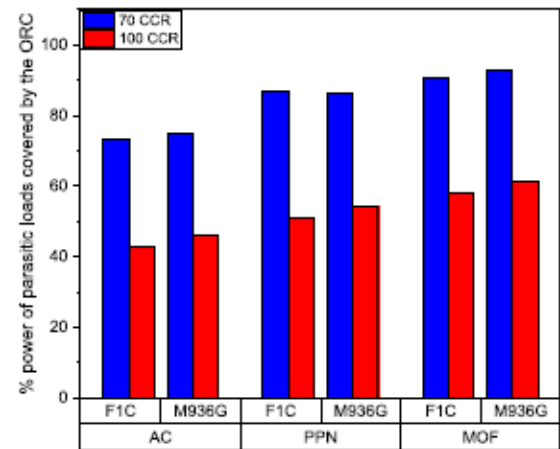


Fig. 12. Percentage of power of parasitic loads covered by the ORC.

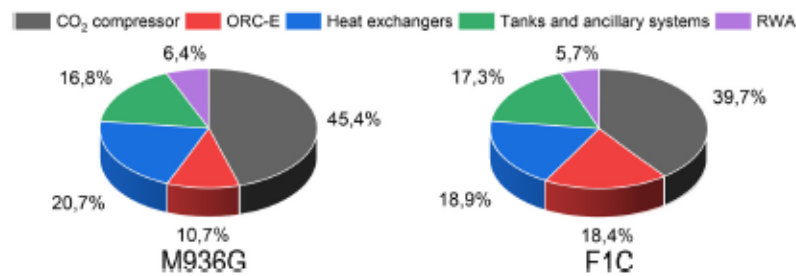
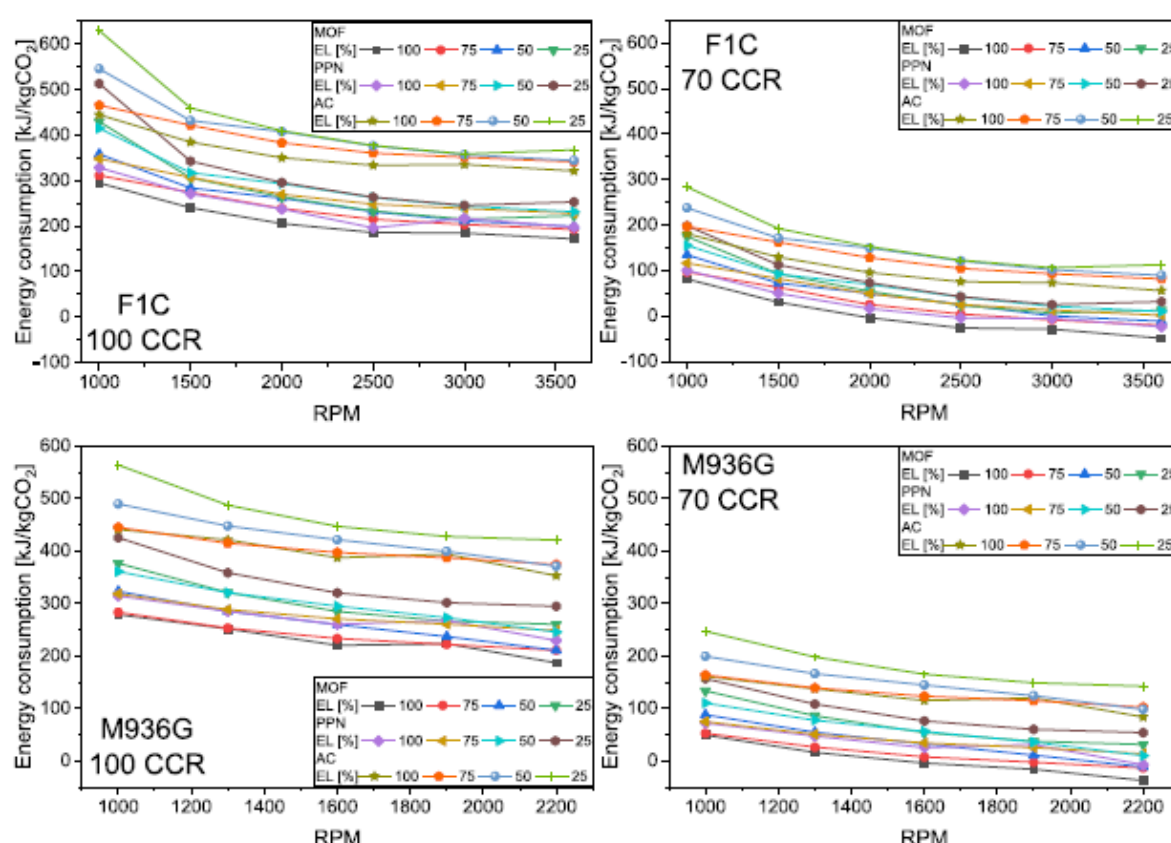


Fig. 11. Average weight of the several components of the CCS-ORC system.

Table 9

Total and percentage fuel mass increase in the engines to cover the CCS-ORC system operation at 75 % of engine load, 8 h of operation and maximum torque.

Engine	mass fuel [kg]	CCR [%]	PPN		MOF		AC	
			mass fuel [kg]	Increase mass fuel [%]	mass fuel [kg]	Increase mass fuel [%]	mass fuel [kg]	Increase mass fuel [%]
M936G	136.30	70	0.71	0.52	0.13	0.09	2.96	2.17
		100	7.04	5.17	6.09	4.47	10.22	7.5
F1C	259.54	70	1.38	0.53	0.31	0.12	4.95	1.91
		100	10.87	4.19	9.37	3.61	15.94	6.14

Fig. 13. Energy consumption of the CO₂ capture process.

concentration of N₂ impurities in the captured CO₂. Consequently, this necessitates greater compression power for liquefying the CO₂ and increases the energy consumption value to CO₂ capture regarding the MOF and PPN sorbents.

The information about the system's performance, weight, volume, and energy consumption obtained in this research suggests that applying this CCS-ORC technology is feasible in various sectors that utilise heavy-duty engines. Therefore, future research endeavours should focus on experimental validation of all the information provided by the simulations. Putting a particular focus on the complex operation of the RWA, the potential increase in fuel consumption of the ICE due to the additional weight of the vehicle caused by the CCS-ORC system, the sensitivity operation of the CCS-ORC system under the weather seasons and the evaluation of the adsorption and desorption times of the CO₂ of the sorbent. These areas will be the subject of further investigation by the current research team and contribute to their ongoing and future research.

CRediT authorship contribution statement

Alexander García-Marlaça: Conceptualization, Data curation, Formal analysis, Investigation, Methodology, Software, Writing – original draft, Writing – review & editing. Eva Llera-Sastres: Conceptualization, Funding acquisition, Investigation, Methodology, Supervision, Writing – original draft, Writing – review & editing. Francisco Moreno: Conceptualization, Data curation, Formal analysis, Software, Supervision, Writing – review & editing.

Declaration of Competing Interest

We wish to confirm no known conflicts of interest associated with this publication. There has been no significant financial support for this work that could have influenced its outcome.

We confirm that the manuscript has been read and approved by all named authors and that there are no other persons who satisfied the criteria for authorship but are not listed. We further confirm that the order of authors listed in the manuscript has been approved by all of us.

We confirm that we have given due consideration to the protection of intellectual property associated with this work and that there are no impediments to publication, including the timing of publication, concerning intellectual property. In so doing, we confirm that we have followed the regulations of our institutions concerning intellectual property.

We understand that the Corresponding Author is the sole contact for the Editorial process (including Editorial Manager and direct communications with the office). He is responsible for communicating with the other authors about progress, submissions of revisions and final approval of proofs. We confirm that we have provided a current, correct email address accessible by the Corresponding Author.

Data availability

Data will be made available on request.

Acknowledgements

funded by MCIN/AEI/10.13039/501100011033/ and by "ERDF A way of making Europe".

This paper is part of the R&D project PID2021-125137OB-I00,

Appendix A. Temperature, pressure, mass flow, and composition of the exhaust gases (Input parameters in the CCS-ORC simulations) obtained with the M936G engine model

Load	rpm	T_{EG} [°C]	\dot{m}_{EG} [kg/s]	\dot{m}_{CO2} [kg/s]	\dot{m}_{H2O} [kg/s]	\dot{m}_{N2} [kg/s]	Pressure [bar]
100	1000	565.45	0.1084	0.01670	0.01370	0.07800	1.09
100	1300	595.00	0.1470	0.02270	0.01860	0.10570	
100	1600	622.35	0.18925	0.02920	0.02390	0.13610	
100	1900	637.75	0.2096	0.03240	0.02650	0.15080	
100	2200	663.15	0.1969	0.03040	0.02490	0.14170	
75	1000	559.65	0.09203	0.01420	0.01160	0.06626	1.09
75	1300	588.9	0.13321	0.02050	0.01679	0.09590	
75	1600	607.75	0.16007	0.02470	0.02017	0.11524	
75	1900	618.65	0.17691	0.02725	0.02230	0.12736	
75	2200	626.75	0.16704	0.02573	0.02105	0.12026	
50	1000	523.65	0.07441	0.01138	0.00931	0.05373	1.09
50	1300	556.5	0.10554	0.01614	0.01320	0.07621	
50	1600	579.85	0.12860	0.01966	0.01609	0.09285	
50	1900	599.95	0.14275	0.02182	0.01786	0.10307	
50	2200	620.95	0.13467	0.02059	0.01684	0.09724	
25	1000	481.25	0.05788	0.00880	0.00720	0.04187	1.09
25	1300	524.00	0.08212	0.01249	0.01022	0.05941	
25	1600	554.35	0.10012	0.01523	0.01246	0.07244	
25	1900	570.35	0.11068	0.01683	0.01377	0.08007	
25	2200	574.95	0.10445	0.01589	0.01300	0.07557	

Appendix B. Temperature, pressure, mass flow, and composition of the exhaust gases (Input parameters in the CCS-ORC simulations) obtained with the F1C engine model

Load	rpm	T_{EG} [°C]	\dot{m}_{EG} [kg/s]	\dot{m}_{CO2} [kg/s]	\dot{m}_{H2O} [kg/s]	\dot{m}_{N2} [kg/s]	Pressure [bar]
100	1000	523.15	0.03464	0.00534	0.00437	0.02493	1.09
100	1500	575.00	0.05806	0.00897	0.00734	0.04176	
100	2000	610.00	0.07688	0.01187	0.00971	0.05529	
100	2500	630.50	0.09893	0.01528	0.01250	0.07115	
100	3000	656.95	0.11314	0.01746	0.01429	0.08139	
100	3600	673.95	0.11258	0.01742	0.01425	0.08092	1.09
75	1000	505.95	0.02922	0.00450	0.00368	0.02103	
75	1500	540.00	0.04900	0.00755	0.00617	0.03528	
75	2000	580.00	0.06489	0.01000	0.00818	0.04671	
75	2500	600.00	0.08395	0.01296	0.01060	0.06039	
75	3000	611.85	0.09609	0.01476	0.01208	0.06926	1.09
75	3600	621.45	0.09709	0.01477	0.01208	0.07024	
50	1000	467.95	0.02373	0.00361	0.00295	0.01716	
50	1500	528.00	0.03900	0.00602	0.00495	0.02860	
50	2000	550.50	0.05250	0.00800	0.00660	0.03800	
50	2500	575.00	0.06750	0.01030	0.00845	0.04880	1.09
50	3000	599.70	0.07775	0.01185	0.00970	0.05620	
50	3600	610.75	0.07720	0.01179	0.00965	0.05577	
25	1000	428.55	0.01859	0.00280	0.00229	0.01349	
25	1500	504.00	0.03070	0.00470	0.00385	0.02250	
25	2000	542.00	0.04100	0.00625	0.00513	0.02980	1.09
25	2500	572.00	0.05300	0.00800	0.00660	0.03860	
25	3000	589.65	0.06073	0.00915	0.00749	0.04409	
25	3600	582.95	0.06113	0.00914	0.00748	0.04451	

Appendix C. Adsorption and desorption heat at 100 % of CCR in the M936G engine

Load	rpm	PPN		MOF		AC	
		Q_{ads} [kW]	Q_{des} [kW]	Q_{ads} [kW]	Q_{des} [kW]	Q_{ads} [kW]	Q_{des} [kW]
100	1000	-27.3251	25.6312	-22.3638	20.6699	-27.3466	25.6527
100	1300	-37.0679	34.7701	-30.3376	28.0398	-37.0971	34.7992
100	1600	-47.7225	44.7642	-39.0577	36.0994	-47.7600	44.8017
100	1900	-52.8597	49.5829	-43.2622	39.9854	-52.9013	49.6245

(continued on next page)

(continued)

Load	rpm	PPN		MOF		AC	
		Q _{ads} [kW]	Q _{des} [kW]	Q _{ads} [kW]	Q _{des} [kW]	Q _{ads} [kW]	Q _{des} [kW]
100	2200	-49.6584	46.5800	-40.6421	37.5638	-49.6974	46.6191
75	1000	-23.1591	21.7234	-18.9542	17.5185	-23.1773	21.7416
75	1300	-33.5220	31.4439	-27.4355	25.3575	-33.5483	31.4703
75	1600	-40.2806	37.7836	-32.9671	30.4701	-40.3123	37.8153
75	1900	-44.5168	41.7572	-36.4341	33.6745	-44.5519	41.7923
75	2200	-42.0343	39.4286	-34.4023	31.7966	-42.0673	39.4616
50	1000	-18.5845	17.4324	-15.2102	14.0581	-18.5991	17.4471
50	1300	-26.3587	24.7248	-21.5729	19.9389	-26.3795	24.7455
50	1600	-32.1167	30.1258	-26.2854	24.2945	-32.1420	30.1511
50	1900	-35.6516	33.4416	-29.1785	26.9685	-35.6797	33.4696
50	2200	-33.6330	31.5481	-27.5264	25.4415	-33.6594	31.5745
25	1000	-14.3795	13.4881	-11.7686	10.8773	-14.3908	13.4994
25	1300	-20.4039	19.1391	-16.6993	15.4344	-20.4200	19.1551
25	1600	-24.8755	23.3335	-20.3590	18.8170	-24.8951	23.3531
25	1900	-27.4984	25.7938	-22.5056	20.8010	-27.5200	25.8154
25	2200	-25.9618	24.3431	-21.2399	19.6311	-25.9722	24.3635

Appendix D. Adsorption and desorption heat at 70 % of CCR in the M936G engine

Load	rpm	PPN		MOF		AC	
		Q _{ads} [kW]	Q _{des} [kW]	Q _{ads} [kW]	Q _{des} [kW]	Q _{ads} [kW]	Q _{des} [kW]
100	1000	-19.1276	17.9418	-15.6546	14.4689	-19.1426	17.9569
100	1300	-25.9475	24.3390	-21.2363	19.6279	-25.9679	24.3595
100	1600	-33.4057	31.3349	-27.3404	25.2696	-33.4320	31.3612
100	1900	-37.0018	34.7081	-30.2835	27.9898	-37.0309	34.7372
100	2200	-34.7608	32.6060	-28.4495	26.2946	-34.7882	32.6334
75	1000	-16.2113	15.2064	-13.2679	12.2630	-16.2241	15.2192
75	1300	-23.4654	22.0108	-19.2049	17.7502	-23.4838	22.0292
75	1600	-28.1964	26.4486	-23.0769	21.3290	-28.2186	26.4707
75	1900	-31.1618	29.2301	-25.5039	23.5722	-31.1863	29.2546
75	2200	-29.4240	27.6000	-24.0816	22.2576	-29.4471	27.6231
50	1000	-13.0091	12.2027	-10.6471	9.8407	-13.0194	12.2129
50	1300	-18.4511	17.3073	-15.1010	13.9572	-18.4656	17.3218
50	1600	-22.4817	21.0881	-18.3998	17.0062	-22.4994	21.1058
50	1900	-24.9561	23.4091	-20.4250	18.8779	-24.9758	23.4287
50	2200	-23.5431	22.0837	-19.2685	17.8090	-23.5616	22.1022
25	1000	-10.0656	9.4417	-8.2381	7.6141	-10.0735	9.4496
25	1300	-14.2828	13.3974	-11.6895	10.8041	-14.2940	13.4086
25	1600	-17.4129	16.3335	-14.2513	13.1719	-17.4266	16.3472
25	1900	-19.2489	18.0557	-15.7540	14.5607	-19.2640	18.0708
25	2200	-18.1663	17.0402	-14.8679	13.7418	-18.1806	17.0544

Appendix E. Adsorption and desorption heat at 100 % of CCR in the FIC engine

Load	rpm	PPN		MOF		AC	
		Q _{ads} [kW]	Q _{des} [kW]	Q _{ads} [kW]	Q _{des} [kW]	Q _{ads} [kW]	Q _{des} [kW]
100	1000	-8.7208	8.1802	-7.1374	6.5968	-8.7277	8.1871
100	1500	-14.6488	13.7407	-11.9891	11.0810	-14.6603	13.7522
100	2000	-19.3949	18.1926	-15.8734	14.6711	-19.4101	18.2078
100	2500	-24.9579	23.4107	-20.4264	18.8792	-24.9775	23.4304
100	3000	-28.5223	26.7542	-23.3437	21.5756	-28.5448	26.7767
100	3600	-28.4511	26.6874	-23.2854	21.5217	-28.4735	26.7098
75	1000	-7.3543	6.8984	-6.0190	5.5631	-7.3601	6.9042
75	1500	-12.3270	11.5628	-10.0888	9.3247	-12.3367	11.5725
75	2000	-16.3365	15.3238	-13.3703	12.3576	-16.3493	15.3366
75	2500	-21.1665	19.8544	-17.3234	16.0113	-21.1831	19.8710
75	3000	-24.1111	22.6165	-19.7334	18.2387	-24.1301	22.6354
75	3600	-24.1294	22.6336	-19.7483	18.2525	-24.1484	22.6526
50	1000	-5.8999	5.5341	-4.8287	4.4629	-5.9045	5.5388
50	1500	-9.8344	9.2248	-8.0488	7.4392	-9.8421	9.2325
50	2000	-13.0690	12.2588	-10.6961	9.8859	-13.0792	12.2691
50	2500	-16.8263	15.7832	-13.7712	12.7281	-16.8395	15.7965
50	3000	-19.3605	18.1603	-15.8453	14.6451	-19.3757	18.1756
50	3600	-19.2598	18.0659	-15.7629	14.5690	-19.2750	18.0811
25	1000	-4.5741	4.2906	-3.7436	3.4601	-4.5777	4.2942
25	1500	-7.6780	7.2021	-6.2839	5.8080	-7.6841	7.2081

(continued on next page)

(continued)

Load	rpm	PPN		MOF		AC	
		Q_{ads} [kW]	Q_{des} [kW]	Q_{ads} [kW]	Q_{des} [kW]	Q_{ads} [kW]	Q_{des} [kW]
25	2000	-10.2101	9.5772	-8.3563	7.7234	-10.2182	9.5852
25	2500	-13.0690	12.2588	-10.6961	9.8859	-13.0792	12.2691
25	3000	-14.9470	14.0204	-12.2331	11.3066	-14.9588	14.0322
25	3600	-14.9340	14.0083	-12.2225	11.2968	-14.9458	14.0200

Appendix F. Adsorption and desorption heat at 70 % of CCR in the FIC engine

Load	rpm	PPN		MOF		AC	
		Q_{ads} [kW]	Q_{des} [kW]	Q_{ads} [kW]	Q_{des} [kW]	Q_{ads} [kW]	Q_{des} [kW]
100	1000	-6.1046	5.7262	-4.9962	4.6178	-6.1094	5.7310
100	1500	-10.2541	9.6185	-8.3923	7.7567	-10.2622	9.6265
100	2000	-13.5764	12.7348	-11.1114	10.2698	-13.5871	12.7455
100	2500	-17.4705	16.3875	-14.2985	13.2155	-17.4843	16.4013
100	3000	-19.9656	18.7280	-16.3406	15.1029	-19.9813	18.7437
100	3600	-19.9158	18.6812	-16.2997	15.0652	-19.9314	18.6969
75	1000	-5.1480	4.8289	-4.2133	3.8942	-5.1521	4.8329
75	1500	-8.6289	8.0940	-7.0622	6.5273	-8.6357	8.1008
75	2000	-11.4355	10.7267	-9.3592	8.6504	-11.4445	10.7356
75	2500	-14.8165	13.8981	-12.1264	11.2079	-14.8282	13.9097
75	3000	-16.8778	15.8315	-13.8134	12.7671	-16.8911	15.8448
75	3600	-16.8906	15.8435	-13.8238	12.7768	-16.9038	15.8568
50	1000	-4.1299	3.8739	-3.3801	3.1240	-4.1332	3.8771
50	1500	-6.8841	6.4573	-5.6342	5.2074	-6.8895	6.4627
50	2000	-9.1483	8.5812	-7.4873	6.9202	-9.1555	8.5884
50	2500	-11.7784	11.0483	-9.6398	8.9097	-11.7877	11.0575
50	3000	-13.5523	12.7122	-11.0917	10.2516	-13.5630	12.7229
50	3600	-13.4819	12.6461	-11.0340	10.1983	-13.4925	12.6567
25	1000	-3.2019	3.0034	-2.6205	2.4220	-3.2044	3.0059
25	1500	-5.3746	5.0414	-4.3988	4.0656	-5.3788	5.0457
25	2000	-7.1471	6.7040	-5.8494	5.4064	-7.1527	6.7097
25	2500	-9.1483	8.5812	-7.4873	6.9202	-9.1555	8.5884
25	3000	-10.4629	9.8143	-8.5632	7.9146	-10.4711	9.8225
25	3600	-10.4538	9.8058	-8.5558	7.9077	-10.4621	9.8140

Appendix G. Thermal and combustion efficiencies in the M936G engine

Load	rpm	η_{th} [%]	η_{com} [%]
100	1000	38.81	98.53
100	1300	41.14	98.55
100	1600	39.82	98.54
100	1900	38.04	98.56
100	2200	35.35	98.58
75	1000	31.72	98.58
75	1300	34.16	98.58
75	1600	33.39	98.59
75	1900	31.76	98.59
75	2200	28.91	98.62
50	1000	22.25	98.66
50	1300	25.88	98.62
50	1600	25.09	98.62
50	1900	23.57	98.64
50	2200	20.87	98.63
25	1000	10.58	98.75
25	1300	12.18	98.71
25	1600	12.00	98.70
25	1900	10.95	98.70
25	2200	8.83	98.73

Appendix H. Thermal and combustion efficiencies in the FIC engine

Load	rpm	η_{is} [%]	η_{comb} [%]
100	1000	32.58	97.83
100	1500	34.50	97.82
100	2000	35.01	97.82
100	2500	33.60	97.86
100	3000	30.86	97.84
100	3600	27.35	97.88
75	1000	27.85	97.87
75	1500	29.10	97.84
75	2000	29.44	97.84
75	2500	27.80	97.90
75	3000	25.17	97.92
75	3600	20.36	98.01
50	1000	20.26	98.01
50	1500	22.10	97.98
50	2000	22.58	97.94
50	2500	21.05	97.94
50	3000	18.47	98.00
50	3600	15.56	98.04
25	1000	8.80	98.28
25	1500	10.24	98.18
25	2000	10.61	98.14
25	2500	10.12	98.12
25	3000	8.75	98.14
25	3600	5.67	98.25

References

- [1] Li Z, Khajepour A, Song J. A comprehensive review of the key technologies for pure electric vehicles. *Energy* 2019;182:824–39. <https://doi.org/10.1016/j.energy.2019.06.077>.
- [2] Li S, Djilali N, Rosen MA, Crawford G, Sul PC. Transition of heavy-duty trucks from diesel to hydrogen fuel cells: Opportunities, challenges, and recommendations. *Int J Energy Res* 2022;46:11718–29. <https://doi.org/10.1002/er.8066>.
- [3] Bireselloglu ME, Demirbag Kaplan M, Yilmaz BK. Electric mobility in Europe: a comprehensive review of motivators and barriers in decision making processes. *Transp Res Part A Policy Pract* 2018;109:1–13. <https://doi.org/10.1016/j.trra.2018.01.017>.
- [4] Rose L, Hussain M, Ahmed S, Malek K, Costanzo R, Kjeang E. A comparative life cycle assessment of diesel and compressed natural gas powered refuse collection vehicles in a Canadian city. *Energy Pol* 2013;52:453–61. <https://doi.org/10.1016/j.enpol.2012.09.064>.
- [5] Quiros DC, Smith J, Thiruvengadam A, Huai T, Hu S. Greenhouse gas emissions from heavy-duty natural gas, hybrid, and conventional diesel on-road trucks during freight transport. *Atmos Environ* 2017;168:36–45. <https://doi.org/10.1016/j.atmosenv.2017.08.066>.
- [6] European Commission. Amending Delegated Regulation (EU) 2021/2139 as regards economic activities in certain energy sectors and Delegated Regulation (EU) 2021/2178 as regards specific public disclosures for those economic activities. 2022. Brussels.
- [7] Pasini G, Lutzemberger G, Ferrari L. Renewable Electricity for Decarbonisation of road transport: Batteries or E-fuels? *Batteries* 2023;9. <https://doi.org/10.3390/batteries9020135>.
- [8] Budinis S, Krevor S, Dowell N Mac, Brandon N, Hawkes A. An assessment of CCS costs, barriers and potential. *Energy Strategy Rev* 2018;22:61–81. <https://doi.org/10.1016/j.esr.2018.08.003>.
- [9] Feenstra M, Monteiro J, van den Akker JT, Abu-Zahra MRM, Gilling E, Goetheer E. Ship-based carbon capture onboard of diesel or LNG-fuelled ships. *Int J Greenh Gas Control* 2019;85:1–10. <https://doi.org/10.1016/j.ijggc.2019.03.008>.
- [10] Ozaki M, Nakazawa N, Omata A, Komatsu M, Manabe H. Ship-Based carbon dioxide capture and storage for enhanced oil recovery. *Proceedings of the Annual Offshore Technology Conference* 2015;4:2412–25. <https://doi.org/10.4043/25861-ms>.
- [11] Ros JA, Skylogianni E, Doodé V, van den Akker JT, Vredevelde AW, Linders MJG, et al. Advancements in ship-based carbon capture technology on board of LNG-fuelled ships. *Int J Greenh Gas Control* 2022;114:103575. <https://doi.org/10.1016/j.ijggc.2021.103575>.
- [12] Francisco ARL. Ship-based transport of CO₂. *J Chem Inf Model* 2013;53:1689–99. <https://doi.org/10.1017/CBO9781107415324.004>.
- [13] Saravanan S, Kumar R. Experimental investigations on CO₂ recovery from engine exhaust using adsorption technology. *SAE Technical Paper* 2019. <https://doi.org/10.4271/2019-28-2577>.
- [14] Kumar P, Rathod V, Parwani AK. Experimental investigation on performance of adsorbents for carbon dioxide capture from diesel engine exhaust. *Environ Prog Sustain Energy* 2021;40. <https://doi.org/10.1002/ep.13651>.
- [15] Rajdurai MS, Rao AHS, Kamalakannan K. CO₂ capture using activated Alumina in gasoline passenger vehicles. *Int J Eng Res Appl* 2016;6:73–7.
- [16] García-Mariaca A, Llera-Sastres E. Energy and economic analysis feasibility of CO₂ capture on a natural gas internal combustion engine. *Greenhouse Gases: Sci Technol* 2022. <https://doi.org/10.1002/GHG.2176>.
- [17] Awoyomi A, Patchigolla K, Anthony EJ. Process and economic evaluation of an onboard capture system for LNG-Fueled CO₂ carriers. *Ind Eng Chem Res* 2020;59:6951–60. <https://doi.org/10.1021/acs.iecr.9b04659>.
- [18] Horvath S, Fasihi M, Breyer C. Techno-economic analysis of a decarbonized shipping sector: technology suggestions for a fleet in 2030 and 2040. *Energy Convers Manag* 2018;164:230–41. <https://doi.org/10.1016/j.enconman.2018.02.098>.
- [19] Fang S, Xu Y, Li Z, Ding Z, Liu L, Wang H. Optimal sizing of shipboard carbon capture system for maritime greenhouse emission control. *IEEE Trans Ind Appl* 2019;55. <https://doi.org/10.1109/tia.2019.2934088>.
- [20] Aramco. Capturing carbon on the move. 2019. <https://www.aramco.com/en/creating-value/technology-development/transport-technologies/mobile-carbon-capture#>. [Accessed 19 February 2023].
- [21] Al-Meshari AA, Mubalsh FI, Aleidan AA. Carbon capture: Saudi aramco's carbon management program. *J Petrol Technol* 2014;66:72–4. <https://doi.org/10.2118/0614-0072-jpt>.
- [22] Voice A, Hamad E. Mobile carbon capture for long-haul commercial transport: design, integration and results. *SSRN Electron J* 2022. <https://doi.org/10.2139/ssrn.4280720>.
- [23] Omata A, Hattori K. Preliminary feasibility study on CO₂ carrier for ship-based CCS. *Global CCS Institute*; 2011. p. 1–180.
- [24] Larkin C, Lampri K, Mazzone S, Oliva F, Li K, García-García FR. Retrofitting hollow fibre carbon capture systems to decarbonise surface transport. *J CO₂ Util* 2023;67. <https://doi.org/10.1016/j.jcou.2022.102336>.
- [25] Sharma S, Maréchal P. Carbon dioxide capture from internal combustion engine exhaust using temperature swing adsorption. *Front Energy Res* 2019;7:1–12. <https://doi.org/10.3389/fenrg.2019.00143>.
- [26] García-Mariaca A, Llera-Sastres E. Review on carbon capture in ICE driven transport. *Energies* 2021;14:6865. <https://doi.org/10.3390/en14216865>.
- [27] García-Mariaca A, Llera-Sastres E, Moreno F. Application of ORC to reduce the energy penalty of carbon capture in non-stationary ICE. *Energy Convers Manag* 2022;268:116029. <https://doi.org/10.1016/j.enconman.2022.116029>.
- [28] Hoffmann Kai, Benz Michael, Marko Weirich. The new mercedes-benz medium duty commercial natural gas engine. *MTZ Worldw* 2014;75:4–11. <https://doi.org/10.1007/s38313-014-0251-4>.
- [29] Iveco company. IVECO DAILY technical information. 2015. p. 1–39. https://www.iveco.com/Denmark/Documents/Configurator/Brochure/Dailyvan_DK.pdf. [Accessed 8 February 2023].
- [30] Mercedes-Benz. Citaro NGT technical information 2017;16. <https://www.mercedes-benz-bus.com/content/dam/mbo/markets/common/buy/services-online/download-technical-brochures/images/content/regular-service-buses/citaro-ngt/MB-NGT-2-ES-09-17.pdf> (accessed March 8, 2023).
- [31] Iveco company. IVECO change your business perspective 2021;1–44. <https://view.rjpaper.io/iveco-hq/uk/Daily-Van/?page=6> (accessed April 22, 2023).
- [32] Obols J, Soleri D, Dioc N, Moreau M. Potential of concomitant injection of CNG and gasoline on a 1.6L gasoline direct injection turbocharged engine. *SAE Technical Papers* 2011. <https://doi.org/10.4271/2011-01-1995>.
- [33] Yontar AA, Doğu Y. Effects of equivalence ratio and CNG addition on engine performance and emissions in a dual sequential ignition engine. *Int J Engine Res* 2020;21:1067–82. <https://doi.org/10.1177/1468087419834190>.

- [34] López JJ, Novella R, Gomez-Soriano J, Martinez-Hernandez PJ, Rampanarivo F, Libert C, et al. Advantages of the unscavenged pre-chamber ignition system in turbocharged natural gas engines for automotive applications. *Energy* 2021;218: 119466. <https://doi.org/10.1016/j.energy.2020.119466>.
- [35] Hovington P, Ghaffari-Nik O, Mariac L, Liu A, Henkel B, Marx S. Rapid cycle temperature swing adsorption process using solid structured sorbent for CO₂ capture from cement flue gas. *SSRN Electron J* 2021. <https://doi.org/10.2139/ssrn.3814414>.
- [36] Peris B, Navarro-Esbrí J, Molés F. Bottoming organic Rankine cycle configurations to increase Internal Combustion Engines power output from cooling water waste heat recovery. *Appl Therm Eng* 2013;61:364–71. <https://doi.org/10.1016/j.applthermaleng.2013.08.016>.
- [37] Invernizzi CM, Iora P, Manzolini G, Lasala S. Thermal stability of n-pentane, cyclopentane and toluene as working fluids in organic Rankine engines. *Appl Therm Eng* 2017;121:172–9. <https://doi.org/10.1016/j.applthermaleng.2017.04.038>.
- [38] Shu G, Li X, Tian H, Liang X, Wei H, Wang X. Alkanes as working fluids for high-temperature exhaust heat recovery of diesel engine using organic Rankine cycle. *Appl Energy* 2014;119:204–17. <https://doi.org/10.1016/j.apenergy.2013.12.056>.
- [39] Scaccabarozzi R, Tavano M, Invernizzi CM. Comparison of working fluids and cycle optimization for heat recovery ORCs from large internal combustion engines. *Energy* 2018. <https://doi.org/10.1016/j.energy.2018.06.017>.
- [40] Invernizzi CM, Bonalumi D. Thermal stability of organic fluids for Organic Rankine Cycle systems. In: *Organic Rankine cycle (ORC) power systems*. Woodhead Publishing; 2017. p. 121–51. <https://doi.org/10.1016/B978-0-08-100510-1.00005-3>.
- [41] Fatigati F, di Battista D, Cipollone R. Permeability effects assessment on recovery performances of small-scale ORC plant. *Appl Therm Eng* 2021;196:117331. <https://doi.org/10.1016/j.applthermaleng.2021.117331>.
- [42] Fatigati F, Di Bartolomeo M, Di Battista D, Cipollone R. Experimental and numerical characterization of the sliding rotary vane expander intake pressure in order to develop a novel control-diagnostic procedure. *Energies* 2019;12:1970. <https://doi.org/10.3390/en12101970>.
- [43] Fatigati F, di Bartolomeo M, di Battista D, Cipollone R. Experimental characterization of a hermetic scroll expander operating in an ORC-based power unit bottoming an internal combustion engine. In: *AIP conf proc*. American Institute of Physics Inc; 2019. <https://doi.org/10.1063/1.5138802>. 2191.
- [44] Kind Matthias, Martin Holger. *VDI heat atlas*. Second. Berlin: Springer; 2010. <https://doi.org/10.1007/978-3-540-77877-6>.
- [45] Yakah Noah. Heat exchanger design for a solar gas-turbine power plant. Master of science Thesis. KTH School of Industrial Engineering and Management; 2012.
- [46] Ping X, Yang F, Zhang H, Zhang J, Zhang W, Song G. Introducing machine learning and hybrid algorithm for prediction and optimization of multistage centrifugal pump in an ORC system. *Energy* 2021;222. <https://doi.org/10.1016/j.energy.2021.120007>.
- [47] Vodicka V, Novotny V, Mascuch J, Kolovratnik M. Impact of major leakages on characteristics of a rotary vane expander for ORC. *Energy Proc* 2017;129:387–94. <https://doi.org/10.1016/j.egypro.2017.09.249>. Elsevier Ltd.
- [48] Perry RH, Green DW, Maloney JO. *Perry's chemical engineers' handbook*. McGraw-Hill; 1997.
- [49] Gibson JAA, Mangano E, Shilko E, Greenaway AG, Gromov AV, Lozinska MM, et al. Adsorption materials and processes for carbon capture from gas-fired power plants: AMPGas. *Ind Eng Chem Res* 2016;55:3840–51. <https://doi.org/10.1021/acs.iecr.5b05015>.
- [50] Huck JM, Lin LC, Berger AH, Shahrak MN, Martin RL, Bhowan AS, et al. Supporting Information: Evaluating different classes of porous materials for carbon capture. *Energy Environ Sci* 2014;7:4132–46. <https://doi.org/10.1039/c4ee02636e>.
- [51] Verdegem WM, Wang K, Sculley JP, Wriedt M, Zhou HC. Evaluation of metal-organic frameworks and porous Polymer Networks for CO₂-capture applications. *ChemSusChem* 2016;9:636–43. <https://doi.org/10.1002/cssc.201501464>.
- [52] Lu C, Bai H, Wu B, Su F, Hwang JF. Comparative study of CO₂ capture by carbon nanotubes, activated carbons, and zeolites. *Energy Fuel* 2008;22:3050–6. <https://doi.org/10.1021/ef8000086>.
- [53] Himeno S, Komatsu T, Fujita S. High-pressure adsorption equilibria of methane and carbon dioxide on several activated carbons. *J Chem Eng Data* 2005;50:369–76. <https://doi.org/10.1021/je049786a>.
- [54] Plaza MG, García S, Rubiera F, Pis JJ, Pevida C. Post-combustion CO₂ capture with a commercial activated carbon: comparison of different regeneration strategies. *Chem Eng J* 2010;163:41–7. <https://doi.org/10.1016/j.cej.2010.07.030>.
- [55] You YY, Liu XJ. Modeling of CO₂ adsorption and recovery from wet flue gas by using activated carbon. *Chem Eng J* 2019;369:672–85. <https://doi.org/10.1016/j.cej.2019.03.118>.
- [56] Emerson Climate Technologies. Copeland TM Stream Semi-Hermetic Compressors for Use with CO₂ in Transcritical & Subcritical Applications Application Guidelines. 2019. p. 1–47. <https://www.copeland.com/documents/copeland-stream-co2-semi-hermetic-compressors-for-use-co2-in-transcritical-subcritical-applications-4mtl-05-to-4mtl-50-4mtl-03-to-4mtl-15-application-guidelines-en-gb-4218052.pdf>. [Accessed 29 December 2023].
- [57] Yang K, Zhang H, Song S, Zhang J, Wu Y, Zhang Y, et al. Performance analysis of the vehicle diesel engine-ORC combined system based on a screw expander. *Energies* 2014;7:3400–19. <https://doi.org/10.3390/en7053400>.
- [58] Zhang YQ, Wu YT, Xia GD, Ma CF, Ji WN, Liu SW, et al. Development and experimental study on organic Rankine cycle system with single-screw expander for waste heat recovery from exhaust of diesel engine. *Energy* 2014;77:499–508. <https://doi.org/10.1016/j.energy.2014.09.034>.
- [59] Pezzella G, Bhatt PM, AlHaji A, Ramirez A, Grande CA, Gascon J, et al. Onboard capture and storage system using metal-organic frameworks for reduced carbon dioxide emissions from vehicles. *Cell Rep Phys Sci* 2023;4:101467. <https://doi.org/10.1016/j.xcrp.2023.101467>.
- [60] Casadei A, Broda R, Ricardo Inc. Impact of vehicle weight reduction on fuel economy for various vehicle architectures. The Aluminum Association, Inc; 2008. p. 1–60. copy obtained from: https://www.b3xed.com/blogmedia/Ricardo_FR_MPG_Study.pdf. [Accessed 7 January 2024].
- [61] Shu G, Zhao M, Tian H, Wei H, Liang X, Huo Y, et al. Experimental investigation on thermal OS/ORC (Oil Storage/Organic Rankine Cycle) system for waste heat recovery from diesel engine. *Energy* 2016;107:693–706. <https://doi.org/10.1016/j.energy.2016.04.062>.
- [62] Lin S, Zhao L, Deng S, Ni J, Zhang Y, Ma M. Dynamic performance investigation for two types of ORC system driven by waste heat of automotive internal combustion engine. *Energy* 2019;169:958–71. <https://doi.org/10.1016/j.energy.2018.12.092>.
- [63] Kim J, Yoo Y, Kim S, Beak J, Oh S-D, Lee J, et al. Design and assessment of a novel mobile carbon capture system: energy and exergy analyses. *Energy Convers Manag* 2024;300:117934. <https://doi.org/10.1016/j.enconman.2023.117934>.
- [64] Jiang N, Shen Y, Liu B, Zhang D, Tang Z, Li G, et al. CO₂ capture from dry flue gas by means of VPSA, TSA and TVSA. *J CO₂ Util* 2020;35:153–68. <https://doi.org/10.1016/j.jcou.2019.09.012>.
- [65] Wu K, Deng S, Li S, Zhao R, Yuan X, Zhao L. Preliminary experimental study on the performance of CO₂ capture prototype based on temperature swing adsorption (TSA). *Carbon Capture Science and Technology* 2022;2. <https://doi.org/10.1016/j.cst.2022.100035>.
- [66] Li H, Guo H, Shen S. Low-energy-consumption CO₂ capture by liquid-solid phase change absorption using water-lean blends of amino acid salts and 2-alkoxyethanols. *ACS Sustain Chem Eng* 2020;8:12956–67. <https://doi.org/10.1021/acssuschemeng.0c03525>.
- [67] Tian W, Ma K, Ji J, Tang S, Zhong S, Liu C, et al. Nonaqueous MEA/PBG200 absorbent with high efficiency and low energy consumption for CO₂ capture. *Ind Eng Chem Res* 2021;60:3871–80. <https://doi.org/10.1021/acs.iecr.0c05294>.

5. SIZING AND TECHNO-ECONOMIC ASSESSMENT OF A CCS-ORC SYSTEM BY ADSORPTION

Techno-economic assessment represents the ultimate phase in gauging the viability of incorporating a CCS-ORC system into a natural gas-powered HD-ICEV. This chapter thoroughly explains the techno-economic assessment of the CCS-ORC system designed in the previous chapter. This assessment will be executed with the CCS-ORC system operating with the same selected ICEVs, sorbents and CCRs and under the same operative parameters as in the previous chapter.

5.1 METHODOLOGY

5.1.1 Description of CCS-ORC system and assessment conditions

Figure 31 depicts the schematic representation of the CCS-ORC system developed in the prior chapter. This Figure shows that the RWA was changed to a shell-and-tubes system to perform the TSA processes. This change is because the diameter that the RWA needed to house the mass sorbent is very high, which did not make it feasible to install it in a vehicle. The computation and design of this novel TSA system will be expounded upon in a subsequent section.

5.1.2 Heat exchanger sizing

As illustrated in Figure 31, the CCS-ORC system comprises seven heat exchangers, whose areas were determined through energy modelling conducted in

ASPEN+. Nonetheless, a meticulous design process is essential to validate the findings from ASPEN+ and thus ascertain the heat exchangers' cost. The assumptions for the calculations include: i) heat exchangers operating in cross-flow, ii) consideration of fully developed fluids, iii) the heat exchangers operating in steady-state conditions, iv) The fluids' inlet and outlet temperatures and mass flows of each fluid in the heat exchanger are taken at maximum power and engine load (refer to values for each heat exchanger, sorbent, and engine in Annexes G, H, and I).

Figure 31. CCS-ORC system schematic layout.

$$Re = \frac{\rho u D}{\mu} \quad (21)$$

Table 19. Correlation to obtain the Nusselt number in the shell side.

Table 20. Correlation to obtain the Nusselt number in the annular section.

Heat exchanger	Fluid	Nusselt Correlation	Constraints	Source
ORC-H	C ₅ H ₁₀	$Nu = \frac{f/8(Re - 1000) Pr}{(1 + 12.7(f/8)^{0.5} (Pr^{2/3} - 1))} \quad (24)$	$0.5 \leq Pr \leq 2000$ $3000 < Re$ $\leq 5 \times 10^6$	[158]
HE-CO ₂ -C	CO ₂			
HE-EG1	EG			
HE-EG2	EG			
ORC-C	C ₅ H ₁₀	$Nu = 0.85 Re_v^{0.11} Re_l^{0.45} Ja^{-0.12} Sc^{-0.45} \quad (25)$	$0.07 \leq Ja \leq 0.34$ $0.7 \leq Sc \leq 2.2$ $Re > 35000$	[159]

$$h = \frac{Nuk}{D} \quad (26)$$

The evaporative process of C₅H₁₀ conducted in the ORE-E is calculated using Equation 27 [160]. As this equation delineates, h hinges on various factors: the stratification parameter $f(Pr)$ [161], the surface-fluid combination ($G_{s,f}$) set at 1.5 (for copper pipes with different refrigerants) [106], the mean vapour mass fraction (\bar{X}) calculated using Equation 28, assuming x is half the pipe length, and the nucleate boiling heat (q_s) determined through Rohsenow's correlation (Equation 29) [162]. The coefficients C_{sf} and the exponent n , in Equation 29, depend on the specific surface and fluid combination, with assigned values of 0.0154 and 1.7, respectively, for the n-pentane-copper polished configuration [163]. Lastly, h_{sp} is computed using Equation 24, with fluid properties evaluated at the saturation temperature of C₅H₁₀.

$$h_{eva} = \left[0.6683 \left(\frac{\rho_{C_5H_{10},l}}{\rho_{C_5H_{10},v}} \right)^{0.1} \bar{X}^{0.16} (1 - \bar{X})^{0.64} f(Pr) + 1058 \left(\frac{A_c q_s}{\dot{m}_{C_5H_{10}} h_f} \right)^{0.7} (1 - \bar{X})^{0.8} G_{s,f} \right] h_{sp} \quad (27)$$

$$\bar{X} = \frac{q_s \pi D x}{\dot{m}_{C_5H_{10}} h_{fg}} \quad (28)$$

$$q_s = \mu_{C_5H_{10},l} h_{fg} \left[\frac{g (\rho_{C_5H_{10},l} - \rho_{C_5H_{10},v})}{\sigma} \right]^{0.5} \left(\frac{c_{p,l} \Delta T_e}{C_{sf} Pr_l^n} \right)^3 \quad (29)$$

The CO₂ liquefaction process in the CO₂-Con exhibits a low Re. A correlation found in the literature allows calculation h directly (Equation 30) [164], where the latent heat of vaporization (h'_{fg}) is modified as is shown in Equation 31. Finally, U is determined using a fouling factor outside and inside the heat exchanger of 4×10^{-4} and 2×10^{-4} m²K/W, corresponding to air and WF values [165], respectively. The heat of each heat exchanger is calculated using equation 32, where the ΔT_{ln} is the mean temperature logarithm.

$$h_{c,CO_2} = 0.555 \left[\frac{g \rho_{CO_2,l} (\rho_{CO_2,l} - \rho_{CO_2,v}) k_{CO_2,l}^3 h'_{fg}}{\mu_{CO_2,l} (T_{CO_2,out} - T_s) D} \right]^{1/4} \quad Re < 35000 \quad (30)$$

$$h'_{fg} = h_{fg} + \frac{3 c_{p,l} (T_{sat} - T_s)}{8} \quad (31)$$

$$\dot{Q} = U A \Delta T_{ln} \quad (32)$$

The β calculation for the heat exchangers is performed with a restriction on tube length, which must not exceed 0.6 m for the CCS-ORC system heat

exchangers intended for vehicles with M936G engines and 0.5 m for those with F1C engines. All these calculations are carried out using EES software, where the U values for each heat exchanger must have a maximum variation of $\pm 2\%$ compared to the results obtained in the previous chapter.

5.1.3 Design of the TSA device

The proposed TSA device utilizes a shell-and-tube heat exchanger design. The sorbent bed is placed inside the tubes while the hot exhaust gases or cooling air circulate through the shell. Figure 32 presents a cross-sectional view of the TSA device. The sizing process for the TSA device begins by determining the maximum radius of a cylindrical sorbent bed using a transient heat transfer model simplified in the radial direction (Equation 33). This model is applied at the sorbent bed outlet, where the exhaust gas temperature is known and represents the lowest temperature during desorption (Table 21). If the required desorption temperature (150 °C [107]) is achieved at the centre of the sorbent, it ensures the entire bed reaches the desired temperature within the specified timeframe. The boundary conditions governing the resolution of this equation involve a specular image at the centre (Equation 34) and a convection boundary condition at the surface (Equation 35). Finally, the initial condition stipulated is a sorbent temperature of 25 °C. The discretization of these equations is explained in Annex J.

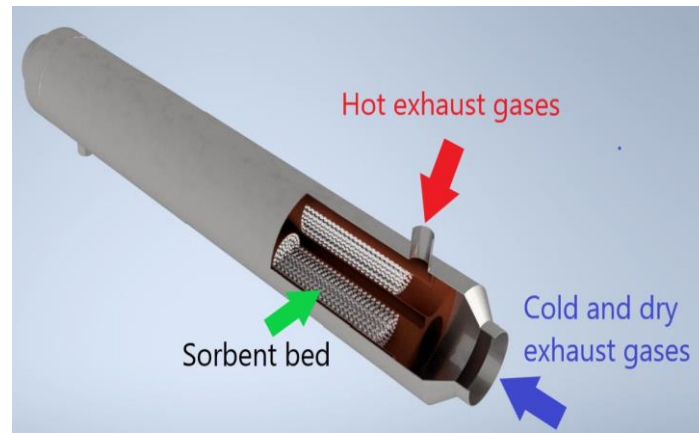


Figure 32. Cross-sectional view of TSA device

Table 21. Sorbent properties and temperature conditions used in the heat transfer mathematical model.

Engine	F1C	M936G	F1C	M936G	F1C	M936G
Sorbents	AC		MOF		PPN	
T_i at 25 % EL [°C]	428.55	481.25	428.55	481.25	428.55	481.25
T_o at 25% EL and 100 CCR [°C]	221.85	275.53	260.33	313.85	222.02	275.70
T_o at 25% EL and 70 CCR [°C]	285.01	338.42	311.57	364.85	285.13	338.53
c_p [J/kgK] [107]	1062		985		896	
k [W/mK]	0.36 [166]		0.52 [167]		0.3 [168]	
CO ₂ loading [kgCO ₂ /kg _{sor}] [107]	0.132		0.278		0.235	
ρ [kg/m ³] [107]	1140		812.88		805	

$$\frac{k}{r} \left(\frac{\partial}{\partial r} r \frac{\partial T}{\partial r} \right) = \rho C_p \frac{\partial T}{\partial t} \quad (33)$$

$$2 k \frac{\partial^2 T}{\partial r^2} = \rho C_p \frac{\partial T}{\partial t} \quad (34)$$

$$-k \frac{\partial T(r, t)}{\partial t} = h (T_{inf} - T(r, t)) \quad (35)$$

The heat transfer model presupposes a constant thermal conductivity and specific heat for the sorbent. Additionally, the density utilized is half of each sorbent's crystallographic density. The Nu is computed by following the procedure outlined in section 5.1.2 but utilizing equations 36 to 39 [169], where (B), (C), (Pt) and (D_e) are the baffles in the shell, the clearance between tubes, the tube pitch, and the equivalent diameter, respectively. Ultimately, the h value is ascertained using Equation 26.

$$A = \frac{D_{shell} C' B}{P_t} \quad (36)$$

$$D_e = \frac{4 (P_t^2 - 0.25 \pi d_o^2)}{\pi d_o} \quad (37)$$

$$Re = \frac{D_e \dot{m}_{EG}}{A \mu} \quad (38)$$

$$Nu = 0.027 Re^{0.8} Pr^{\frac{1}{3}} (\mu/\mu_w)^{0.14} \quad (39)$$

The mass flow and temperature values are selected at the lowest engine rpm and load. At these points, the exhaust gas mass flow is 66.9 kg/h for the F1C engine and 208.4 kg/h for the M936G engine, while the corresponding temperature values are provided in Table 21. The sorbent mass is calculated based on the CO₂ mass flow at the average operational points of the engines during the WHTC (see section 3.6). The CO₂ mass flow values are 45 kg/h for the M936G engine and 22.3 kg/h for the F1C engine. Based on the acquired results, the TSA device's geometry is determined, and its surface area is used to estimate the cost of the TSA device, treating it as if it were a heat exchanger. This process is repeated for each CCR condition and sorbent.

5.1.4 Economic assessment

The economic analysis aims to determine the capital expenditure (CAPEX) and the Operating Expenditure (OPEX) of the CCS-ORC system. The CAPEX is the sum of the costs of all components and the sum of the direct and indirect costs of the CCS-ORC system (equation 40) [170,171]. The correlations utilised to ascertain the CAPEX of the CCS-ORC system are delineated in Table 22. The OPEX variables considered in this research are maintenance, sorbent renovation cost, and the rise in engine fuel consumption resulting from CCS-ORC system

operation, as summarized in Table 23. The calculation of the latter is contingent upon the compressed natural gas (CNG) price, which is 1.017 €/kg (average consumer price in Spain in March of 2024 tax included) [172,173], the power penalty over the engine provoked by the CCS-ORC system (PP), the LHV, whose value is 48351 kJ/kg [128], and the combustion and engine efficiencies of the average operational points of the engines within the WHTC. It also assumes vehicle operation is 350 days and 16 hours per day. All these variable's values are listed in Annexes E and F.

$$CAPEX = \sum Cost_{Equipment} + \sum Cost_{direct} + \sum Cost_{indirect} \quad (40)$$

Table 22. CAPEX cost correlations and parameters

Process	Equipment	Cost correlation	Parameter (A)	Ref.
TSA	TSA-Device	$3397A^{0.86}$	Area (m ²)	[174–176]
Waste heat recovery (ORC)	ORC-expander	$10^{[2.2476+1.4965\log_{10}(A)+0.1618[\log_{10}(A)]^2]}$	Volume (m ³)	[177]
	ORC-pump	$900(A/300)^{0.25}$	Power (kW)	
	ORC-C ₅ H ₁₀ tank	31.5+16A	Volume (L)	
	ORC-Evaporator	190+310A	Area (m ²)	
	ORC-heater	190+310A	Area (m ²)	[178]
	ORC-condenser	190+310A	Area (m ²)	
Exhaust gases condition (EGC)	HE-EG1	190+310A	Area (m ²)	
	HE-EG2	190+310A	Area (m ²)	
	Cyclone	1776.22A	Volume (m ³)	[179]
	Fan	$900(A/300)^{0.25}$	Power (kW)	
CO ₂ storage system (CSS)	Condenser	190+310A	Area (m ²)	[178]
	Compressor	$267000(A/445)^{0.67}$	Power (kW)	[180]
	CO ₂ tank	31.5+16A	Volume (L)	[178]
Direct cost	Installing	8%A	TSA+ORC+EGC+CSS	[181]
	Instrumentation	5%A		
	Piping	1.5%A		
	Electric installing	1%A		
Indirect cost	Engineering	7%A	TSA+ORC+EGC+CSS + direct cost	[182,183]

Table 23. OPEX cost correlations and parameters

Concept	Cost correlation	Parameters A, B, C, D, E, F and G	Ref.
Sorbent renovation	2%A for PPN and MOF and 1%A for AC	Total CAPEX	Own criterion
Increased fuel consumption	$\frac{3.6ABCD}{EFG}$	Power penalty (kW), CNG cost (€/kg), hour operation, operation days, LHV (kJ/kg), Combustion efficiency, engine efficiency	Own criterion
O&M	1%A	Total CAPEX	[182,183]

5.2 SIZING AND TECHNO-ECONOMIC ASSESSMENT RESULTS

5.2.1 Heat exchanger sizing

Tables 24 and 25 display the results for the number and length of tubes and β for each heat exchanger. These tables show that the heat exchangers of the CCS-ORC system operating with the F1C engine generally exhibit a higher β than those operating with the M936G engine. This difference is attributed to the lower mass flows of the substances within the heat exchangers, which allows for a more

compact tube bank arrangement. Consequently, this leads to an increase in the Re number, ensuring compliance with the values of U and resulting in higher β values for the F1C engine.

Table 24. β , number and length of tubes for the heat exchangers operating in the CCS-ORC system in the M936G engine

Equipment	Number of tubes						Tube length [m]						β [m ² /m ³]					
	100 CCR			70 CCR			100 CCR			70 CCR			100 CCR			70 CCR		
	PPN	AC	MOF	PPN	AC	MOF	PPN	AC	MOF	PPN	AC	MOF	PPN	AC	MOF	PPN	AC	MOF
ORC-H		36			25		0.320	0.349	0.332	0.364	0.398	0.372	104.0	97.7	102.2		100.6	
ORC-E		256			256		0.472	0.446	0.477	0.508	0.494	0.508	124.5	123.7	124.5	124.9	124.5	124.6
ORC-C	375	372	420		450	480	0.584	0.598	0.592	0.585	0.591	0.593	107.0	99.3	125.2	115.2		106.9
HE-CO ₂ -C	28	36	16		25		0.543	0.463	0.498	0.425	0.466	0.424	97.2	93.5	97.9		97.3	
CO ₂ -Con	66	81	70		64		0.593	0.519	0.577	0.453	0.486	0.465	92.4	90.2	88.8	90.2	88.7	93.1
HE-EG1		675			510	480	0.597	0.597	0.598	0.585	0.596	0.589	126.6	114.6	116.0	102.3	109.4	132.7
HE-EG2	300		360	276	276	315	0.594	0.600	0.576	0.587	0.591	0.585	91.0	93.5	102.0	94.8	98.6	111.2

Table 25. β , number and length of tubes for the heat exchangers operating in the CCS-ORC system in the F1C engine

Equipment	Number of tubes						Tube length [m]						β [m ² /m ³]					
	100 CCR			70 CCR			100 CCR			70 CCR			100 CCR			70 CCR		
	PPN	AC	MOF	PPN	AC	MOF	PPN	AC	MOF	PPN	AC	MOF	PPN	AC	MOF	PPN	AC	MOF
ORC-H		25		15	16		0.329	0.352	0.335	0.425	0.436	0.407	134.9		134.6	125.7	125.9	126.1
ORC-E	176	169	187		196		0.484	0.475	0.456	0.462	0.451	0.463	167.2	164.7	166.9	166.4	166.4	167.2
ORC-C	338	330	372		380	418	0.497	0.483	0.477	0.494	0.499	0.485	105	109	110.9	105.1	105.1	106.3
HE-CO ₂ -C		25			24*		0.423	0.465	0.423	0.385	0.423	0.384	101.6		100.2	141.4	145.1	141.4
CO ₂ -Con		64			49		0.431	0.459	0.441	0.414	0.444	0.424	98.1	96.2	99.36	100.1	102.7	104.1
HE-EG1	570	540	570	420	400	408	0.497	0.5	0.495	0.496	0.499	0.500	152.1	139.9	139.5	103.8	101.2	104.3
HE-EG2	276	260	300	240	250	260	0.492	0.489	0.487	0.487	0.460	0.499	109.2	110.3	107.9	124.9	126.0	121.7

*Calculated with a diameter of 12 mm.

5.2.2 TSA device design

The high temperature and velocity of the exhaust gases within the TSA device enhance the heat transfer parameters (Re , h), allowing for obtaining a sorbent heating time of 180 seconds. This finding aligns with experimental results documented in the literature [184]. Tables 26 and 27 show that the smallest size of the TSA device is achieved with the MOF sorbent; this is because the MOF sorbent has higher thermal conductivity than the PPN and AC sorbents, facilitating the MOF sorbent's more expeditious reach of the required desorption temperature. Consequently, the TSA device incorporating the MOF sorbent can accommodate a greater sorbent mass and needs fewer tubes than its counterparts.

Table 26. Sizing of the TSA device operating in the CCS-ORC system at 100% of CCR.

Variable	M936G			F1C		
	AC	MOF	PPN	AC	MOF	PPN
Sorbent mass [kg]	17.03	8.09	9.56	8.44	4.01	4.73
Tube diameter [m]	0.078	0.122	0.09	0.046	0.09	0.062
Sorbent bed diameter [m]	0.074	0.118	0.086	0.042	0.086	0.058
Sorbent bed length [m]	6.95	1.62	4.08	10.69	1.51	4.45
Tube length [m]	1	1	1	1	1	1
Number of tubes	7	2	5	11	2	5
h [W/m ² K]	126.8	114.9	109.9	65.69	60.87	63.58
Re number	25465	36949	25462	6337	12967	8851
Shell diameter[m]	0.2496	0.2562	0.288	0.2024	0.189	0.1953
Heat transfer area [m ²]	1.72	0.77	1.41	1.59	0.57	0.97

Table 27. Sizing of the TSA device operating in the CCS-ORC system at 70% of CCR.

Variable	M936G			F1C		
	AC	MOF	PPN	AC	MOF	PPN
Sorbent mass [kg]	11.92	5.66	6.69	5.91	2.81	3.31
Tube diameter [m]	0.092	0.142	0.106	0.064	0.114	0.082
Sorbent bed diameter [m]	0.088	0.138	0.102	0.06	0.11	0.078
Sorbent bed length [m]	3.44	0.83	2.03	3.67	0.65	1.72
Tube length [m]	0.90	0.90	0.90	0.70	0.70	0.70
Number of tubes	4	1	3	6	1	3
h [W/m ² K]	148.1	178.7	141.8	61.32	75.72	62.33
Re number	36321	77594	41056	8385	22016	11665
Shell diameter[m]	0.2392	0.1704	0.2438	0.2048	0.1368	0.1886
Heat transfer area [m ²]	1.04	0.4	0.9	0.84	0.25	0.4

5.2.3 Tecno-economic assessment

CAPEX results are summarized in Tables 28 and 29. For all sorbents, the CAPEX mean value of the CCS-ORC system integrated within the M936G engine at 100% of CCR is 68.2 k€, and at 70% of CCR presents a reduction of 15.3%. Similarly, in the F1C engine, the CAPEX mean value of the CCS-ORC system at 100% CCR stands at 39.9 k€, decreasing by 17.3% its value at 70% CCR.

Table 28. CAPEX results of the CCS-ORC system operating in the m936G engine.

Process	Equipment	Parameter [A]						Cost [k€]					
		100 CCR			70 CCR			100 CCR			70 CCR		
		PPN	MOF	AC	PPN	MOF	AC	PPN	MOF	AC	PPN	MOF	AC
TSA	TSA device	1.41	0.77	1.72	0.9	0.4	1.04	4.56	2.71	5.42	3.10	1.54	3.51
Waste heat recovery (ORC)	ORC-E	12.45	13.81	12.6	14.38	15.55	14.52	4.93	5.54	4.99	5.80	6.33	5.86
	ORC-P	1.08	1.13	1	1.17	1.24	1.18	0.22	0.22	0.22	0.23	0.23	0.23
	ORC-C ₅ H ₁₀ tank	0.01	0.01	0.01	0.01	0.01	0.01	0.19	0.19	0.19	0.19	0.19	0.19
	ORC-E	7.59	7.66	7.17	8.16	8.17	7.95	2.54	2.56	2.41	2.72	2.72	2.65
	ORC-H	0.72	0.75	0.79	0.57	0.59	0.63	0.41	0.42	0.43	0.37	0.37	0.39
Exhaust gases condition	ORC-C	13.77	15.61	13.97	16.53	17.9	16.71	4.46	5.03	4.52	5.31	5.74	5.37
	HE-EG1	25.3	25.37	24.23	18.74	18.36	17.99	8.03	8.05	7.7	6.00	5.88	5.77
	HE-EG2	11.2	13.02	11.31	10.18	11.58	10.25	3.66	4.23	3.7	3.35	3.78	3.37
	Cyclone	0.3	0.3	0.3	0.21	0.21	0.21	0.53	0.53	0.53	0.37	0.37	0.37
CO ₂ storage system	Fan	0.99	0.7	1.05	1.282	0.834	1.35	0.22	0.2	0.22	0.23	0.21	0.23
	Condenser	2.46	2.54	2.64	1.82	1.87	1.96	0.95	0.98	1.01	0.75	0.77	0.80
	Cooling	0.95	0.75	1.05	0.67	0.67	0.73	0.48	0.42	0.52	0.40	0.40	0.42
	Compressor	17.93	18.33	21.76	12.7	13.03	15.28	11.64	11.86	13.65	8.78	8.96	10.21
Direct cost	CO ₂ tank	0.47	0.47	0.47	0.33	0.33	0.33	7.58	7.55	7.55	5.31	5.31	5.31
	Installing							4.03	4.04	4.24	3.43	3.42	3.57
	Instrumentation	50.43	50.50	53.06	42.91	42.81	44.68	2.52	2.53	2.65	2.15	2.14	2.23
	Piping							0.76	0.76	0.8	0.64	0.64	0.67
Indirect cost	Electric installing							0.5	0.51	0.53	0.43	0.43	0.45
	Engineering	58.24	58.33	61.28	50.72	50.65	52.90	4.08	4.08	4.29	3.47	3.46	3.61
	Contingency							4.66	4.67	4.9	3.96	3.96	4.13
Total CAPEX								66.95	67.08	70.47	56.99	56.86	59.35

Table 29. CAPEX results of the CCS-ORC system operating in the F1C engine.

Process	Equipment	Parameter [A]						Cost [k€]					
		100 CCR			70 CCR			100 CCR			70 CCR		
		PPN	MOF	AC	PPN	MOF	AC	PPN	MOF	AC	PPN	MOF	AC
TSA	TSA device	0.97	0.57	1.59	0.54	0.25	0.84	3.31	2.09	5.06	2.00	1.03	2.92
Waste heat recovery (ORC)	ORC-E	7.22	7.89	7.20	8.17	8.73	8.28	2.59	2.88	2.58	3.01	3.25	3.06
	ORC-P	0.61	0.69	0.59	0.70	0.73	0.66	0.19	0.20	0.19	0.20	0.20	0.19
	ORC-C ₅ H ₁₀ tank	0.01	0.01	0.01	0.01	0.01	0.01	0.19	0.19	0.19	0.19	0.19	0.19
	ORC-E	4.01	4.02	3.79	4.27	4.27	4.16	1.43	1.44	1.36	1.51	1.51	1.48
	ORC-H	0.39	0.39	0.42	0.30	0.31	0.33	0.31	0.31	0.32	0.28	0.29	0.29
HE-EG1	ORC-C	7.92	8.36	7.51	8.84	9.56	8.93	2.65	2.78	2.52	2.93	3.15	2.96
	HE-EG1	13.34	13.30	12.72	9.81	9.61	9.41	4.33	4.31	4.13	3.23	3.17	3.11

Exhaust gases condition (EGC)	HE-EG2	6.40	6.88	5.99	5.38	6.12	5.42	2.17	2.32	2.05	1.86	2.09	1.87
	Cyclone	0.15	0.15	0.15	0.11	0.11	0.11	0.27	0.27	0.27	0.19	0.19	0.19
	Fan	0.46	0.32	0.48	0.31	0.23	0.32	0.18	0.16	0.18	0.16	0.15	0.16
CO ₂ storage system (CSS)	Condenser	1.30	1.33	1.38	0.96	0.98	1.02	0.59	0.60	0.62	0.49	0.49	0.51
	Cooling	0.50	0.50	0.55	0.35	0.35	0.38	0.35	0.35	0.36	0.30	0.30	0.31
	Compressor	9.71	9.92	11.78	6.88	7.03	8.34	7.04	7.17	8.25	5.31	5.40	6.22
	CO ₂ tank	0.24	0.24	0.24	0.17	0.17	0.17	3.81	3.81	3.81	2.67	2.67	2.67
Direct cost	Installing							2.35	2.31	2.55	1.95	1.93	2.09
	Instrumentation	29.40	28.88	31.89	24.33	24.09	26.13	1.47	1.44	1.59	1.22	1.20	1.31
	Piping							0.44	0.43	0.48	0.36	0.36	0.39
	Electric installing							0.29	0.29	0.32	0.24	0.24	0.26
Indirect cost	Engineering	34	33.4	36.8	28.88	28.57	31.07	2.38	2.34	2.58	1.97	1.95	2.11
	Contingency							2.72	2.67	2.95	2.25	2.23	2.41
Total CAPEX								39.05	38.36	42.35	32.31	32.00	34.71

The CAPEX results derived from the CCS-ORC systems add to the original purchase cost of a CNG vehicle, allowing for the calculation of the increase in the initial purchase price of CNG vehicles equipped with CCS-ORC systems. The baseline initial purchase values are obtained from a 75 m³, 19 t bus employing the M936G engine [111], and a 5.2 t, 12 m³ van utilizing the F1C engine [185]. These values are then compared with those of other vehicles adopting zero CO₂ emissions technologies, such as electric battery (EB) vehicles and those equipped with hydrogen fuel cell batteries (HFCB), as detailed in Table 30.

Table 30 CAPEX including the initial purchase of the vehicle.

Vehicle	Technology	Purchase [€]	Difference from baseline [%]	Reference
Bus with an M936G engine of 19 t and 75 m ³ [111]	CNG	374600	0.0	[186,187]
	HFCB	650000	-73.5	[188]
	EB	604000	-61.2	[189]
	CNG+CCS-ORC at 100% of CCR	442767	-18.2	Own study
	CNG+CCS-ORC at 70% of CCR	432333	-15.4	Own Study
VAN with an F1C engine (or similar Va) 5.2 t and 12 m ³ [185]	CNG	40000	0.0	[190]
	EB	60000	50.0	[191,192]
	CNG+CCS-ORC at 100% of CCR	79922	-99.8	Own study
	CNG+CCS-ORC at 70% of CCR	73008	-82.5	Own Study

As depicted in Table 30, vehicles employing zero-emission technologies are priced 61% and 73% higher than baseline CNG vehicles lacking the CCS-ORC system. However, introducing the CCS-ORC system in the CNG bus resulted in an 18.2% increase in its initial price at 100% CCR and 15.4% at 70% CCR. Conversely, the van with 100% CCR experiences a 33.2% price hike, while at 70% CCR, it rises by 21.7% compared to the EB van. These findings suggest that while the increased cost is manageable for bus owners, it may pose feasibility challenges for smaller vehicle owners.

Table 31 presents the OPEX findings from the four case studies. The calculated OPEX for the CCS-ORS system, using the M936G engine, stands at an average of 10.91 k€ at 100% CCR and 4.4 k€ at 70% CCR. For the F1C engine, the figures are 6.05 k€ and 2.24 k€ at 100 and 70% CCR, respectively. Additionally, it is noted that despite AC having a 50% lower sorbent renewal cost in OPEX calculations due to its commercial nature, the operating expenses of the CCS-ORC

system in both engines employing AC are, on average, 27 and 43% higher at 100 and 70% CCR, respectively, compared to OPEX values obtained with MOF. This discrepancy is attributed to the greater impact of the CCS-ORC system with AC operation on the engines, leading to increased fuel consumption.

Table 31. OPEX [k€/year] for the CCS-ORC systems

Concept	M936G						F1C					
	100 CCR			70 CCR			100 CCR			70 CCR		
	PPN	MOF	AC	PPN	MOF	AC	PPN	MOF	AC	PPN	MOF	AC
Sorbent renovation	1.34	1.34	0.70	0.85	0.85	0.59	0.59	0.58	0.42	0.48	0.48	0.35
Fuel consumption increase	8.39	7.51	11.40	2.53	2.01	4.63	4.69	4.18	6.49	1.16	0.86	2.42
O&M	0.67	0.67	0.7	0.57	0.57	0.59	0.39	0.38	0.38	0.32	0.32	0.35
Total OPEX	10.40	9.52	12.81	3.95	3.43	5.82	5.66	5.14	7.33	1.97	1.66	3.11

Previously found results suggest that integrating a CCS-ORC system into heavy-duty vehicles may lack economic feasibility unless accompanying benefits or tax exemptions. This section will provide an economic assessment, taking 2027 as the starting point, when stricter emissions regulations in the transport sector will be enforced through the emission trading system 'ETS2' [193]. In this system, the EU has set a CO₂ emission rights price for the transport sector at 45 €/tCO₂ [193,194]. Transportation costs will rise in this situation unless the sector adopts more technologies to reduce CO₂ emissions.

The initial assessment aims to determine the period required for the integrated CCS-ORC system to pay for itself considering the annual net profit (Table 32). The payback time of the CCS-ORC system is ascertained by obtaining the benefits' net present value (NPV), which is calculated using an interest rate of 4% and deducted this value from the CAPEX for each year. Figure 33 provides the results obtained for 10 years, which, according to the literature, mirrors the typical useful lifespan of heavy transport vehicles [195].

Table 32. Incomes and Profits obtained for integrating a CCS-ORC system in a heavy-duty vehicle.

Concept	M936G						F1C					
	100			70			100			70		
	PPN	MOF	AC	PPN	MOF	AC	PPN	MOF	AC	PPN	MOF	AC
OPEX [k€/year]	10.40	9.52	12.81	3.95	3.43	5.82	5.66	5.14	7.33	1.97	1.66	3.11
Income [k€/year]		11.33			7.93			5.67			3.97	
Profits [k€/year]	0.93	1.81	-1.48	3.98	4.50	2.11	0.01	0.53	-1.66	2.00	2.31	0.86

The values obtained from the payback indicate that the initial investment fails to be recouped under any evaluated condition over the vehicle's useful lifespan. With MOF, the recovery percentages stand at 22 and 64% at 100 and 70% CCR, respectively, in the M936G engine. While in the F1C engine, the recovery percentages stand at 11 and 59% at 100 and 70% CCR, respectively. Employing PPN yields recovery percentages of 11% and 57% at 100% and 70% CCR, respectively, for the M936G engine and 50% at 70% CCR for the F1C engine.

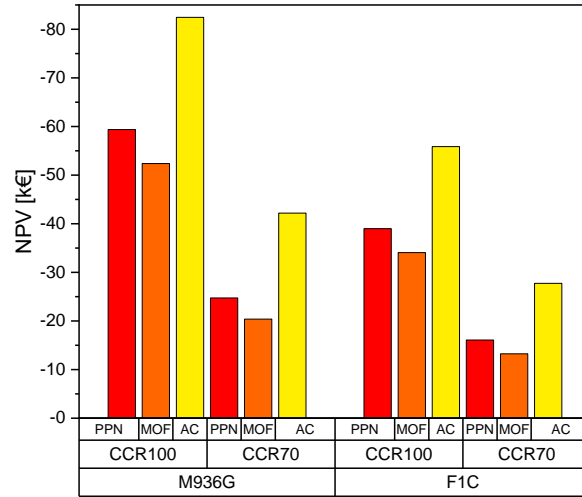


Figure 33. NPV calculated at 10 years of CCS-ORC system for the whole sorbent, CCR and engines.

It is highlighted to note that the carbon abatement costs (CAC) obtained for the CCS-ORC system proposed in this research, operating at 100% CCR, vary from 26.2 €/tCO₂ with MOF to 46.8 €/tCO₂ in the vehicle with the F1C engine and from 19.4 €/tCO₂ with MOF up to 33.9 €/tCO₂ with AC in the vehicle equipped with the M936G engine, as shown in Figure 34. These values are lower than those observed in other industries, such as glass and steel, whose CAC ranges are between 50 and 350 €/tCO₂ [196,197].

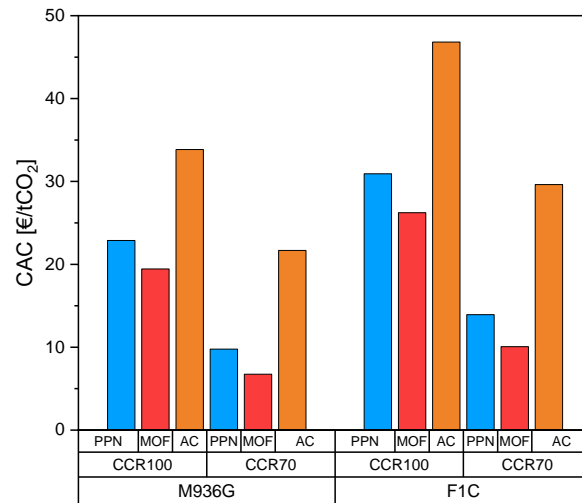


Figure 34. CCS-ORC system carbon abatement cost calculated for each sorbent, CCR, and engine.

5.3 SENSITIVITY ANALYSIS

This section presents two sensitivity analyses. The first determines the CO₂ emissions tax required to achieve payback on the initial investment within the 10-year lifespan of a heavy-duty vehicle. The second identifies the engine size that achieves a zero CAC, with a fixed CO₂ tax of 45 €/tCO₂. Figure 35 shows that for a 10-year payback with a CCR of 100%, the CO₂ tax must be 70.6, 74.4, and 85.4 €/tCO₂ for MOF, PPN, and AC operation in the M936G engine, respectively, and 78.3, 83.8, and 99.7 €/tCO₂ in the F1C engine. Lowering the CCR to 70% reduces the required CO₂ tax by 10 to 15 €/tCO₂ for all three sorbents in both engines.

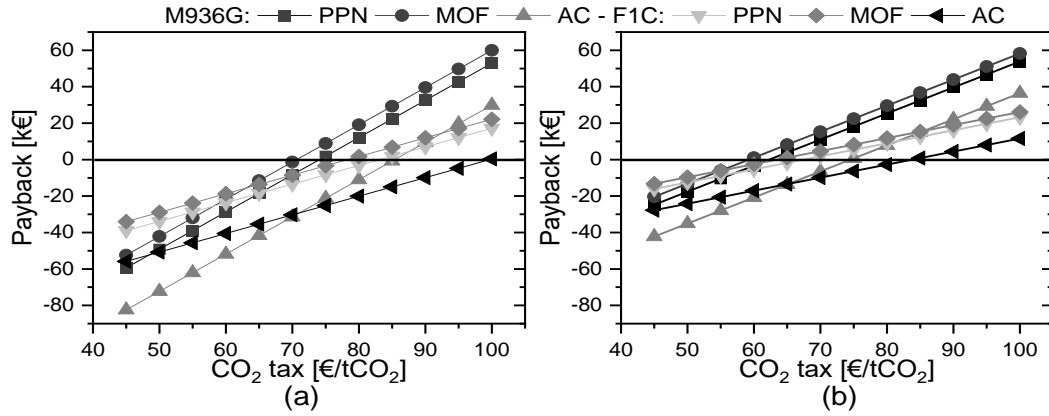


Figure 35. Payback sensitivity analysis: a) 100 CCR and b) 70 CCR

Figure 36 shows that achieving a zero or negative CAC at a 100% CCR requires an engine displacement volume (V_d) of over 20 L with AC and 22 L with MOF and PPN. This is due to the steeper slope of the CCS-ORC system's CAC between the F1C and M936G engines with AC. At a 70% CCR, a zero or negative CAC is achieved with a V_d of 18 L for MOF, 19 L for PPN, and 21 L for AC. Finally, regardless of the CCR rate, it is evident that a CCS-ORC system could yield a CAC of zero in engines with high V_d .

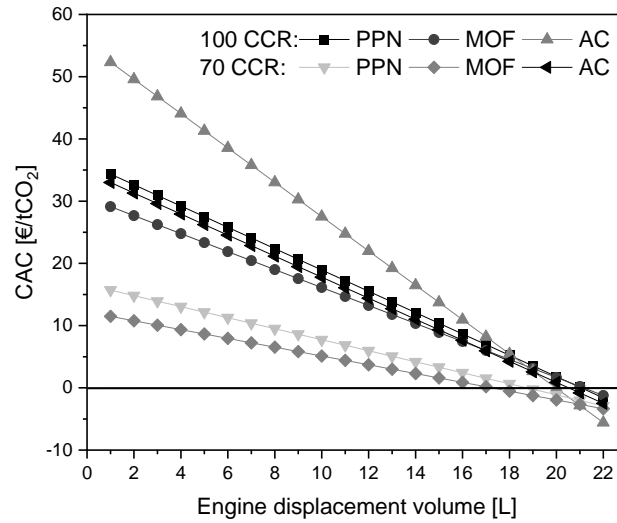


Figure 36. CAC sensitivity analysis for engine size

5.4 SUMMARY

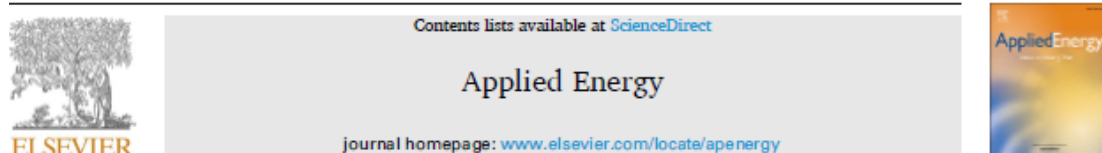
The techno-economic assessment conducted in this chapter shows that integrating the CCS-ORC system in vehicles used in heavy transport is feasible because the required volume of the devices hardly affects the vehicle's useful space and because it could be profitable in the medium term if the CO_2 tax value is above 65 €/t CO_2 . Hence, the proposed integration may mitigate CO_2 in the atmosphere at a low cost by the transport sector (if it is compared with other intensive energy sectors) and even would provide CO_2 for manufacturing e-fuels if they are used in the vehicles could reduce the time for recovery of the initial investment of the CCS-ORC system.

5.5 PUBLISHED PAPER

Finally, this study's details, findings, and conclusions have been included in an article published in the journal *Applied Energy*.

- García-Mariaca A, Llera Sastresa Eva. (2024). Techno-economic assessment for the practicability of on-board CO₂ capture in ICE vehicles. *Applied energy*, 376, Part B, 124167. <https://doi.org/10.1016/j.apenergy.2024.124167>

Applied Energy 376 (2024) 124167



Techno-economic assessment for the practicability of on-board CO₂ capture in ICE vehicles

Alexander García-Mariaca^{a,*}, Eva Llera-Sastresa^b

^a Energy and CO₂ Group, Department of Mechanical Engineering, Aragon Institute of Engineering Research (I3A), University of Zaragoza, Zaragoza 50018, Spain

^b Department of Mechanical Engineering and CIRCE Research Institute, University of Zaragoza, María de Luna s/n, Zaragoza 50018, Spain

HIGHLIGHTS

- Thermal study for dimensioning the CCS-ORC system operating in HD-ICEV.
- Techno-economic assessment of a novel CCS-ORC system for operation in HD-ICEV.
- CAC less than 35 €/tCO₂ for a carbon capture rate of 100 %.
- CCS-ORC system would be profitable with a CO₂ tax above of 80 €/tCO₂.

ARTICLE INFO

Keywords:
Carbon capture and storage
Temperature swing adsorption
Organic Rankine Cycle
Decarbonisation
Transport sector

ABSTRACT

The transport sector is a major energy-intensive and significant contributor to CO₂ emissions. With heavy-duty internal combustion engine vehicles (HD-ICEVs) set to remain a primary mode of transport for goods and passengers, the European Union plans to implement CO₂ emission rights starting in 2027 to address this issue. To mitigate CO₂ emissions, on-board carbon capture technologies can be an innovative solution, but a comprehensive analysis from several perspectives must be carried out. To tackle the existing knowledge gap on this subject, this paper presents the techno-economic assessment of a CO₂ capture and storage system hybridized with an organic Rankine cycle (CCS-ORC) integrated into an HD-ICEV whose technical ability has been previously demonstrated. In this paper, the capture installation based on temperature swing adsorption is designed for two engines with different displacement volumes, at varying carbon capture rates (CCR), and using three different sorbents. The size of the thermal devices is estimated as the determinant factor for the required space and the installation costs. The results show that the heat exchangers can achieve a minimum area density of 100 m²/m³, while the most significant temperature swing adsorption device obtained is scarcely 0.26 m³. The carbon abatement cost (CAC) obtained for the CCS-ORC system is less than 35 €/tCO₂ at 100 % of CCR, and with an engine size greater than 18 and 21 L, the CAC of the CCS-ORC system is zero at 100 and 70 % of CCR, respectively. Furthermore, with a CO₂ emissions right price above 71 €/tCO₂, the projected payback of the initial investment of the CCS-ORC system is achieved in the lifespan of the HD-ICEV for all sorbents evaluated at 100 % of CCR.

1. Introduction

As the world addresses the pressing challenge of climate change, finding innovative solutions to reduce carbon emissions has become forefront. For this reason, in recent years, much research has been conducted to tackle this problem in several intensive energy sectors [1]. One of the sectors where great interest has been aroused in the development of carbon capture and storage (CCS) systems is the transport

sector, notably in ships and heavy-duty road vehicles. This heightened interest is primarily driven by the fact that this sector alone is accountable for generating 7.98 Gt of CO₂ in 2022, constituting 23 % of the global CO₂ emissions for this year [2].

Nonetheless, developing an on-board CCS system for vehicles in road freight transport propelled by internal combustion engines (ICE) confronts numerous challenges. These include the necessity for adaptability to diverse engine operations, encompassing variations in engine load (EL) and rpm. Moreover, such a system must meet stringent criteria; it

* Corresponding author.

E-mail address: alexander.garcia@unizar.es (A. García-Mariaca).

<https://doi.org/10.1016/j.apenergy.2024.124167>

Received 16 April 2024; Received in revised form 24 July 2024; Accepted 6 August 2024

Available online 27 August 2024

0306-2619/© 2024 The Authors. Published by Elsevier Ltd. This is an open access article under the CC BY-NC-ND license (<http://creativecommons.org/licenses/by-nc-nd/4.0/>).

Abbreviations			
β	Area density	LHV	Lower Heating Value
B	Baffles	\dot{m}	Mass flow
CAPEX	Capital expenditure	NPV	Net present value
CAC	Carbon abatement cost	q_b	Nucleate boiling heat
CCS	Carbon Capture and Storage	Nu	Nusselt number
CCR	Carbon Capture rate	ORC-C	ORC condenser
C'	Clearance between tubes	ORC-E	ORC evaporator
η_{com}	Combustion efficiency	ORC-H	ORC heater
CNG	Compressed natural gas	ORC-P	ORC pump
h	Convection heat transfer coefficient	ORC-X	ORC expander
HE-CO ₂ -C	CO ₂ cooling heat exchanger	ORC	Organic Rankine Cycle
CO ₂ -con	CO ₂ condenser	U	Overall heat coefficient
CO ₂ -com	CO ₂ compressor	PP	Power penalty
C ₅ H ₁₀	Cyclopentane	Pr	Prandtl number
f	Darcy friction factor	R	Radius
ρ	Density	Re	Reynolds number
S_D	Diagonal pitch	T_{sat}	Saturation temperature
D	Diameter	Sc	Schmidt number
V_d	Displacement volume	c_p	Specific heat
μ	Dynamic viscosity	G_{sf}	Surface-fluid combination
EB	Electric batteries	Σ	Liquid surface tension
η_{eng}	Engine efficiency	TSA	Temperature Swing Adsorption
EL	Engine load	K	Thermal conductivity
D_e	Equivalent diameter	T	Time
EG	Exhaust gases	S_T	Transverse pitch
HE-EG1	Exhaust gas cooling heat exchanger 1	P_t	Tube pitch
HE-EG2	Exhaust gas cooling heat exchanger 2	X	Vapour mass fraction
Fr	Froude number	WHTC	World Harmonized Transient Cycle
HD-ICEV	Heavy-duty internal combustion engine vehicles	Subscripts	
HFCB	Hydrogen fuel cell batteries	i	Inner or inlet
ICE	Internal Combustion Engine	l	Liquid
Ja	Jacob number	o	Outlet
h_{fg}	Latent heat of vaporization	s	Property evaluated at surface temperature
S_L	Longitudinal pitch	v	Vapour

should be practical, efficient, and reliable, and it must be seamlessly integrated into existing vehicles with minimal impact on their usable volume. Above all, the effects of its operation on the engine's performance should be as minimal as possible. Furthermore, any investment in a CCS system must demonstrate economic viability for vehicle owners, i. e., the additional investment incurred through system installation should have a payback at least over the vehicle's lifespan.

In this regard, numerous researchers have been developing innovative research works on this topic. Consequently, significant progress is being made in the concept design of CCS systems operating in heavy-duty internal combustion engine vehicles (HD-ICEV). These initial approaches have introduced well-established technologies, such as amine scrubbing [3,4], temperature, pressure, or vacuum swing adsorption (TSA, PSA, and VSA), for on-board CO₂ capture [5]. Moreover, specific research endeavours have implanted auxiliary systems primarily to offset the power demand in CO₂ compression, such as organic Rankine cycles (ORC) that take advantage of the waste heat in the exhaust gases [6,7]. From these research works, different configurations of the CCS system have been obtained [5,8], the performance of the CCS system operating with various sorbents has been evaluated. It has been determined that the operation of the CCS system at a carbon capture rate (CCR) of 100 % requires an average less than 10 % of the power produced by the engine [9]. However, in the literature, no study has performed an in-depth techno-economic analysis of a CCS system operating in an HD-ICEV.

In this sense and in pursuit of advancing the continuous development

of this technology, this research carries out the first techno-economic assessment of a CCS system operating in an HD-ICEV. The techno-economic evaluation is based on the energy assessment results from a previous investigation of a CCS system with an integrated ORC (CCS-ORC system onwards) capable of operating under different load and rpm conditions of heavy-duty engines [9]. The conceptual design is mainly based on knowing in detail the configuration of the heat exchangers (number of tubes and lengths and arrangement). Subsequently, the compaction of these exchangers is calculated, which must satisfy the heat transfer parameters found in the simulations done in the previous study.

The initial variable calculated in the techno-economic assessment of the CCS-ORC system is the capital expenditure (CAPEX), which is then compared with other zero-emission technologies available in heavy-duty vehicles, such as hydrogen fuel cell batteries (HFCB) and electric batteries (EB). Subsequently, the operational expenditures (OPEX), the income obtained by avoiding paying the CO₂ emission tax, the profits and the carbon abatement cost (CAC) by introducing a CCS-ORC in an HD-ICEV system are obtained. Finally, with these results, a sensitivity analysis is carried out to determine the suitable value of the CO₂ emissions rights and the engine size so that the CCS system investment recovers as soon as possible. The key indicators for this study are the CCR (100 and 70 %), the kind of sorbent (PPN-6-CH₂-DETA, MOF-74-Mg and activated carbon) and the engine size (engine volume displacement). The outcomes of this research endeavour are vital to continue closing the knowledge gap about CCS systems operating in HD-ICEV, thereby

advancing technologies conducive to achieving complete decarbonization of the transport sector in the medium term.

2. Methodology

The procedures described in this section show the steps for obtaining the conceptual design and economic assessment of an innovative CCS-ORC system designed to operate on-board a natural gas-fuelled HD-ICEV. The methodology begins with selecting the vehicles, followed by a comprehensive description of the CCS-ORC system, heat exchanger sizing, and design of the TSA device and concludes with economic considerations.

2.1. Vehicle selection

The vehicles selected for the present research are the Citaro bus and the IVECO Daily VAN, whose engines are the M936G and the F1C, respectively. Both engines are turbocharged natural gas internal combustion engines. The simulation of engine performance and emissions parameters was conducted using the AVL software. The outcomes of these simulations, along with the technical specifications of the engines, are presented herein [8].

2.2. Description of CCS-ORC system and assessment conditions

Fig. 1 depicts the schematic representation of the CCS-ORC system proposed. The system comprises four distinct zones. The first one is dedicated to the processes of adsorption and desorption of CO₂ through a temperature swing of the sorbent (TSA). In this zone, the exhaust gases' waste heat is harnessed to heat the sorbent and desorb CO₂. The second zone encompasses the ORC, which takes the remaining waste heat from the exhaust gases to generate power. This power is then utilized to meet the energy demands of the CO₂ compression. The ORC comprises three heat exchangers (condenser, heater and evaporator), a pump, an expander, and a tank. The working fluid in the ORC is cyclopentane (C₅H₁₀), which was chosen due to its outstanding performance in prior research on ORC in ICE [10,11]. The third zone involves conditioning exhaust gases by cooling them until dry, consisting of two heat exchangers and a cyclone. The final section is focused on CO₂ storage and encompasses two heat exchangers, a CO₂ compressor and a CO₂ tank for

its storage. All zones are cooling with air that is supplied by a fan.

The energy analysis of the proposed CCS-ORC system was carried out with three different sorbents: PPN-6-CH₂-DETA (PPN onward), MOF-74-Mg (MOF onwards), activated carbon (AC onward), and two CCR 70 and 100 %. The results of the energy analysis are available in a prior study [9], which serves as the foundation for the techno-economic assessment presented in this paper. On that basis, the CCRs are kept, as well as the sorbents, which have a low adsorption heat is low [12], that is imperative for this application. Additionally, PPN and MOF exhibit high CO₂ loadings and CO₂/N₂ selectivity compared to AC, which has lower CO₂/N₂ selectivity and CO₂ loadings [13]. This allows for a comprehensive mapping of the evaluated variables and enables the extrapolation of results to other sorbents whose range of selectivity and CO₂ loadings are in the range of the evaluated sorbents.

2.3. Heat exchanger sizing

As shown in Fig. 1, the CCS-ORC system features seven heat exchangers, the areas of which were determined through energy modelling conducted in ASPEN+ [9]. However, a detailed design process is imperative to validate the results obtained in ASPEN+ and, in this way, ascertain the heat exchangers' cost. The assumptions for the calculations include: i) heat exchangers operating in cross-flow, ii) consideration of fully developed fluids, iii) the heat exchangers operating in steady-state conditions, iv) The fluids' inlet and outlet temperatures and mass flows of each fluid in the heat exchanger are taken at maximum power and engine load (see values for each heat exchanger, sorbent and engine in Appendixes A, B and C) and v) states' properties are calculated with the pressure and temperature averages at the inlet and outlet of each heat exchanger.

First, the Reynolds number for each fluid is obtained using Eq. 1. Once the flow regime for each fluid is determined, appropriate correlations are chosen to calculate the Nusselt number. Zukauskas' correlations for external convection in a flow cross-tube bank heat exchanger with staggered tube arrangement are employed for the shell side. The disposition of pipes is illustrated in Fig. 2. Table 1 outlines the correlations for each heat exchanger and the corresponding operating fluid (Eqs. 2 and 3).

$$Re = \frac{\rho V D}{\mu} \quad (1)$$

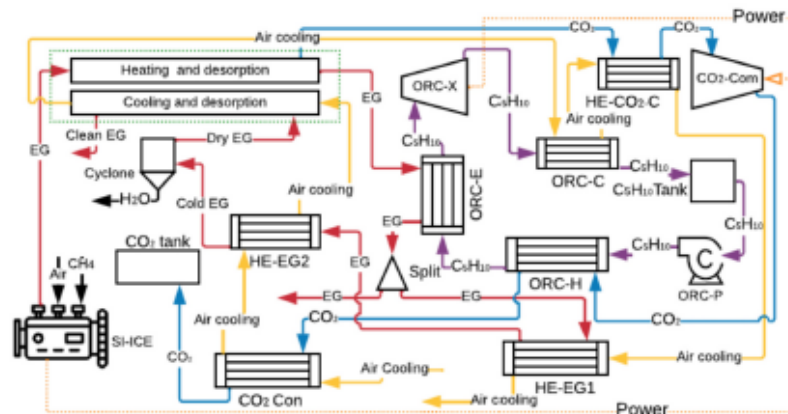


Fig. 1. CCS-ORC system schematic layout.

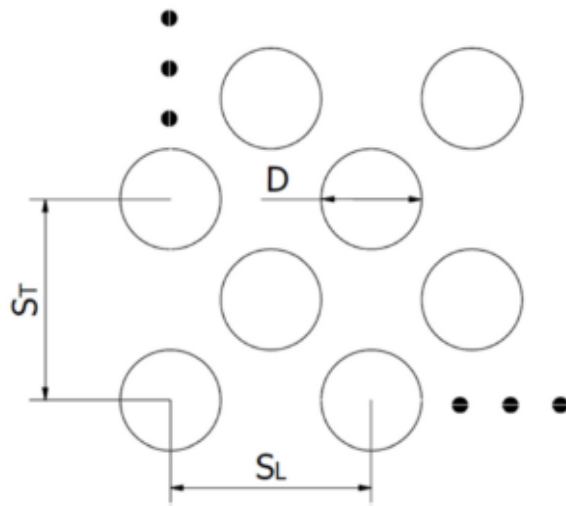


Fig. 2. Staggered disposition tube in the heat exchanger.

Within the annular section, the choice of correlation for Nusselt number computation is contingent upon the nature of the fluid process (heating, cooling, or condensing) and the fluid regime, which, in all instances, is turbulent. Table 2 delineates the selected correlation for each heat exchanger calculation (Eqs. 4 and 5). In each instance, a verification process was conducted to ensure that the constraints associated with each correlation were satisfied. Finally, for all cases enumerated in Table 2, the convection heat transfer coefficient (h) is obtained utilizing Eq. 6.

$$h = \frac{Nu k}{D} \quad (6)$$

The evaporative process of C_5H_{10} conducted within the ORC evaporator (ORE-E) exhibits a significantly elevated Reynolds number. The correlation identified in the literature to fit this condition is presented in Eq. 7 [17]. As delineated in the said equation, h is contingent upon the stratification parameter, $f(Fr)$, whose value is the unity for vertical tubes

and horizontal tubes with $Fr \geq 0.04$ [18], as is applicable in the present case. The surface-fluid combination ($G_{s,f}$) also influences h ; the value of this latter oscillates between 1 and 2 for copper pipes and various refrigerants [17]. Consequently, a value of 1.5 for the current procedure is taken. Also, h is contingent upon the mean vapour mass fraction (\bar{X}), computed using Eq. 8. The value of x taken is half the length of a pipe in the heat exchanger. The nucleate boiling heat (q_b) also affects the behaviour of h , which is determined through the correlation established by Rohsenow (Eq. 9) [19]. In this equation, the coefficients C_{sf} and the exponent n rely upon the surface and fluid combination, with assigned values of 0.0154 and 1.7, respectively, corresponding to the n-pentane-copper polished configuration [20]. Finally, the h_{sp} is calculated with Eq. 4 with the fluid properties evaluated with the C_5H_{10} saturation temperature.

$$h_{en} = \left[0.6683 \left(\frac{\rho_{C_5H_{10},l}}{\rho_{C_5H_{10},v}} \right)^{0.1} \bar{X}^{0.16} (1 - \bar{X})^{0.64} f(Fr) + 1058 \left(\frac{A_c q_b}{\dot{m}_{C_5H_{10}} h_{fg}} \right)^{0.7} (1 - \bar{X})^{0.8} G_{s,f} \right] h_p \quad (7)$$

$$\bar{X} = \frac{q_b \pi D x}{\dot{m}_{C_5H_{10}} h_{fg}} \quad (8)$$

$$q_b = \mu_{C_5H_{10},l} h_{fg} \left[\frac{g(\rho_{C_5H_{10},l} - \rho_{C_5H_{10},v})}{\sigma} \right]^{0.5} \left(\frac{c_{p,l} \Delta T_e}{C_{sf} Pr_l^1} \right)^3 \quad (9)$$

In contrast, the CO_2 liquefaction process in the CO_2 condenser (CO_2 -Con) exhibits a low Reynolds number. In response to this, a correlation found in the literature allows calculation h directly (Eq. 10) [21], where the latent heat of vaporization (h_{fg}) is modified as is shown in Eq. 11.

$$h_{c,CO_2} = 0.555 \left[\frac{g \rho_{CO_2,l} (\rho_{CO_2,l} - \rho_{CO_2,v}) k_{CO_2,l}^3 h_{fg}}{\mu_{CO_2,l} (T_{CO_2,sat} - T_s) D} \right]^{1/4} Re < 35000 \quad (10)$$

$$h'_{fg} = h_{fg} + \frac{3c_{p,l}(T_{sat} - T_s)}{8} \quad (11)$$

The determination of the overall heat transfer coefficient (U) is achieved through the application of Eq. 12; for this, it is used a fouling

Table 1
Correlation to obtain the Nusselt number in the shell side.

Heat exchanger	Fluid	Nusselt Correlation	Restriction	source
ORC-H	CO_2	$Nu = 0.35 \left(\frac{St}{SL} \right)^{0.2} Re^{0.6} Pr^{0.36} \left(\frac{Pr}{Pr_s} \right)^{0.25} \quad (2)$	$0.7 < Pr < 500$	[14]
ORC-E	EG		$1000 < Re < 2 \times 10^5$	
ORC-C	Air			
HE- CO_2 -C	Air			
HE-EG1	Air			
HE-EG2	Air	$Nu = 0.031 \left(\frac{St}{SL} \right)^{0.2} Re^{0.6} Pr^{0.36} \left(\frac{Pr}{Pr_s} \right)^{0.25} \quad (3)$	$0.7 < Pr < 500$	
CO_2 -Con	Air		$2 \times 10^5 < Re < 2 \times 10^6$	

Table 2
Correlation to obtain the Nusselt number in the annular section.

Heat exchanger	Process	Fluid	Nusselt Correlation	Constraints	Source
ORC-H	Heating	C_5H_{10}	$Nu = \frac{f/8(Re - 1000)Pr}{(1 + 12.7(f/8)^{0.5}(Pr^{2/3} - 1))} \quad (4)$	$0.5 \leq Pr \leq 2000$	[15]
HE- CO_2 -C	Cooling	CO_2		$3000 < Re \leq 5 \times 10^5$	
HE-EG1		FG			
HE-EG2		FG			
ORC-C	Condensing	C_5H_{10}	$Nu = 0.85 Re^{0.11} Re^{0.45} Ja^{-0.12} Sc^{-0.45} \quad (5)$	$0.07 \leq Ja \leq 0.34$ $0.7 \leq Sc \leq 2.2$ $Re > 35000$	[16]

factor is outside and inside in the heat exchanger of 4×10^{-4} and $2 \times 10^{-4} \text{ m}^2\text{K/W}$, corresponding to air and working fluid values [22], respectively. The heat of each heat exchanger is calculated using Eq. 13 where the ΔT_{lm} is the mean temperature logarithm.

$$U = \frac{1}{\frac{1}{h_i} + 2\pi r_i L R_i + \frac{1}{k} \ln\left(\frac{r_o}{r_i}\right) + 2\pi r_o L R_o + \frac{1}{h_o}} \quad (12)$$

$$\dot{Q} = UA\Delta T_{lm} \quad (13)$$

Finally, the area density (β) is determined. This variable represents the relation between the required area and volume of the heat exchanger to contain the tube arrangement. The determination of heat exchanger size encompasses design variables such as the number, diameter, and length of tubes for each heat exchanger and sorbent operating in the CCS-ORC system. Additionally, the calculation includes a restriction in the tube length; this must not exceed 0.6 and 0.5 m for the heat exchangers of the CCS-ORC system that will be integrated into vehicles equipped with M936G and F1C engines, respectively. All these calculations are conducted in EES software, in which the U values for each heat exchanger must be a maximum variation of $\pm 2\%$ with the results obtained in [9].

2.4. Design of the TSA device

Due to the lack of information about the cost of devices that carry out the TSA process in CO_2 capture, the design procedure of a TSA device is presented in this research, thereby facilitating the estimation of its manufacturing cost. The TSA device adopts a configuration reminiscent of a shell-and-tube heat exchanger. The bed sorbent is situated within the tubes, and the hot exhaust gases or the air-cooling flow in the shell (depending on the process developed). Fig. 3 shows a cross-sectional representation of the TSA device.

The sizing of the device begins with determining the maximum radius of the sorbent bed, whose geometry is cylindrical. A transient state heat transfer mathematical model is employed to achieve this. The model is made in the radial direction to simplify it (Eq. 14) and situated at the outlet of the bed sorbent due to it knowing the exhaust gases temperature at this point, which is the lowest temperature achieved in the desorption process (Table 3), so if the centre of the sorbent is obtained the desorption temperature required (150°C [12]) it is guaranteed that of sorbent bed have this or even exceeded the desired temperature within a specified timeframe.

The boundary conditions governing the resolution of this equation involve a specular image at the centre (Eq. 15) and a convection boundary condition at the surface (Eq. 16). Finally, the initial condition stipulated is a sorbent temperature of 25°C . The discretization of these equations is explained in Appendix D.

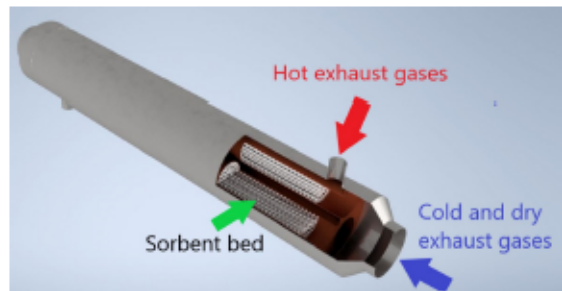


Fig. 3. Cross-sectional view of TSA device.

Table 3

Sorbent properties and temperature conditions used in the heat transfer mathematical model.

Engine	F1C	M936G	F1C	M936G	F1C	M936G
Sorbents	AC		MOF		PPN	
T_i at 25 % EL [$^\circ\text{C}$]	428.55	481.25	428.55	481.25	428.55	481.25
T_o at 25 % EL and 100 CCR [$^\circ\text{C}$]	221.85	275.53	260.33	313.85	222.02	275.70
T_o at 25 % EL and 70 CCR [$^\circ\text{C}$]	285.01	338.42	311.57	364.85	285.13	338.53
c_p [J/kgK] [12]	1062		985		896	
k [W/mK]	0.36 [23]		0.52 [24]		0.3 [25]	
CO_2 loading [kg CO_2 /kg SOx] [12]	0.132		0.278		0.235	
ρ [kg/m 3] [12]	1140		812.88		805	

$$\frac{k}{r} \left(\frac{\partial}{\partial r} r \frac{\partial T}{\partial r} \right) = \rho C_p \frac{\partial T}{\partial t} \quad (14)$$

$$2k \frac{\partial^2 T}{\partial r^2} = \rho C_p \frac{\partial T}{\partial t} \quad (15)$$

$$-k \frac{\partial T(r, t)}{\partial r} = h(T_{mf} - T(r, t)) \quad (16)$$

The heat transfer model assumes constant thermal conductivity and specific heat for the sorbent. Moreover, the density employed is half of each sorbent's crystallographic density. The Nusselt number is computed by following the procedure outlined in section 2.3 but utilizing Eqs. 17, 18, 19 and 20, which are used for a shell-tube heat exchanger on the shell side [26]. Ultimately, the h value is determined using Eq. 6.

$$A = \frac{D_{shell} C B}{P_t} \quad (17)$$

$$D_e = \frac{4(P_t^2 - 0.25\pi d_o^2)}{\pi d_o} \quad (18)$$

$$Re = \frac{D_e \dot{m}_{gas}}{A \mu} \quad (19)$$

$$Nu = 0.027 Re^{0.5} Pr^{\frac{1}{3}} (\mu/\mu_w)^{0.14} \quad (20)$$

As delineated in these equations, the ' h ' coefficient is contingent upon several parameters, including the distance between baffles in the shell (B), the clearance between tubes (C), the tube pitch (P_t), the equivalent diameter (D_e), and the mass flow rate of exhaust gases. To facilitate these computations and determine the viscosities and Prandtl numbers, the values of mass flow and temperature are selected at the critical operational condition of the engine, specifically at the lowest rpm and engine load. The exhaust gas mass flow at those points is 66.9 kg/h for the F1C engine and 208.4 kg/h for the M936G engine, while the corresponding temperature values are detailed in Table 3.

The sorbent mass is calculated based on the CO_2 mass flow at the average operational points of the engines within the World Harmonized Transient Cycle (WHTC) [27]. Precisely, these points correspond to 1300 rpm for the M936G engine and 2000 rpm for the F1C engine, both at 25 % of the engine load. The corresponding CO_2 mass flow values are 44.96 kg/h for the M936G engine and 22.29 kg/h for the F1C engine. Fig. 4 illustrates the step-by-step calculation process. Based on the acquired results, the TSA device's geometry is obtained, and its surface area is taken for the TSA device's cost as if it were a heat exchanger. This process is conducted for each condition of the CCR and sorbent.

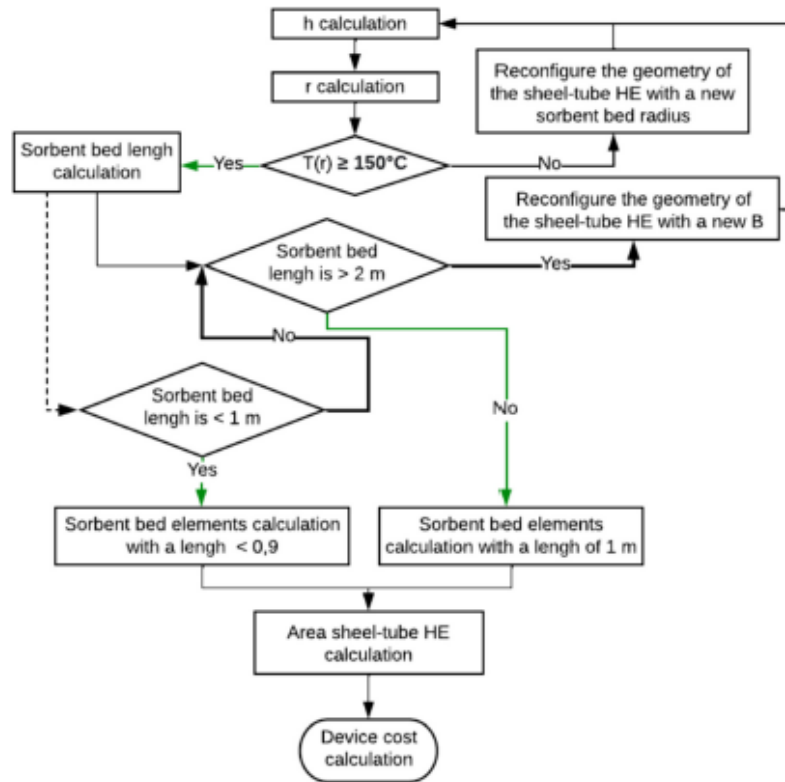


Fig. 4. Flowchart for calculation of the TSA device cost

2.5. Economical assessment

The economic analysis aims to determine the capital expenditure (CAPEX) of the CCS-ORC system. In this sense, the CAPEX is the sum of the costs of all components of the CCS-ORC system and the sum of direct and indirect costs (Eq. 21). The direct cost is associated with the installation, instrumentation, piping, and electric installation, and their value is a percentage of the sum of all equipment [28]. Subsequently, the indirect costs, which encompass engineering and contingency costs, are also computed as a percentage of the cumulative expenses incurred by

all devices and direct costs [29].

$$CAPEX = \sum Cost_{Equipment} + \sum Cost_{direct} + \sum Cost_{indirect} \quad (21)$$

Device costs are obtained through correlations, depending on key variables governing their operation or geometric parameters. In the case of the compressor, expander, pump and fan, the primary variable is the power consumed or produced. In the case of heat exchangers, the heat exchanger area is the primary variable, and in the case of tanks, the function is the tank volume. The correlations utilized to ascertain the CAPEX of the CCS-ORC system are delineated in Table 4, and each

Table 4
CAPEX cost correlations and parameters.

Process	Equipment	Cost correlation	Parameter (A)	Ref.
TSA	TSA-Device	$3397A^{0.36}$	Area (m ²)	[30–32]
	ORC-expander	$10[2.2476 + 1.4965 \log(A) + 0.1618 \log(A)^2]$	Volume (m ³)	[33]
	ORC-pump	$900(A/300)^{0.25}$	Power (kW)	
Waste heat recovery (ORC)	ORC-C ₂ H ₁₀ tank	$31.5 + 16A$	Volume (L)	
	ORC-Evaporator	$190 + 310A$	Area (m ²)	[34]
	ORC-heater	$190 + 310A$	Area (m ²)	
	ORC-condenser	$190 + 310A$	Area (m ²)	
	HE-EG1	$190 + 310A$	Area (m ²)	
Exhaust gases condition (EGC)	HE-EG2	$190 + 310A$	Area (m ²)	[35]
	Cyclone	$1776.22A$	Volume (m ³)	
	Fan	$900(A/300)^{0.25}$	Power (kW)	
	Condenser	$190 + 310A$	Area (m ²)	
CO ₂ storage system (CSS)	Compressor	$267,000(A/445)^{0.67}$	Power (kW)	[36]
	CO ₂ tank	$31.5 + 16A$	Volume (L)	[34]
	Installing	8 %A		
Direct cost	Instrumentation	5 %A		[37]
	Piping	1.5 %A		
	Electric installing	1 %A		
Indirect cost	Engineering	7 %A	TSA + ORC + EGC + CSS + direct cost	[38,39]

Table 5
OPEX cost correlations and parameters.

Concept	Cost correlation	Parameters A, B, C, D, E, F and G	Ref.
Sorbent renovation	2 %A for PPN and MOF and 1 %A for AC	Total CAPEX	Own criterion
Increased fuel consumption	$\frac{3.6ABCD}{EPG}$	Power penalty (kW), CNG cost (€/kg), hour operation, operation days, LHV (kJ/kg), Combustion efficiency, engine efficiency	Own criterion
O&M	1 %A	Total CAPEX	[38,39]

device's parameter A is obtained from the simulations performed in the energy analysis [9].

Operating Expenditure (OPEX) constitutes the ongoing costs the CCS-ORC system incurs. The variables considered for the OPEX in this research are maintenance, sorbent renovation cost, and increased engine fuel consumption resulting from CCS-ORC system operation, as summarized in Table 5. The calculation of the latter is contingent upon the compressed natural gas (CNG) price, which is 1.017€/kg (average consumer price in Spain in March of 2024 tax included) [40,41], the power penalty over the engine provoked by the CCS-ORC system (PP), lower heating value (LHV), whose value is 49,351 kJ/kg [42], and the combustion and engine efficiencies of the average operational points of the engines within the WHTC. It also assumes vehicle operation of 350 days and 16 h per day. The values of all of these variables are listed in Appendix E.

3. CCS-ORC system concept design

The following subsections present the outcomes obtained based on the methodology previously outlined concerning the sizing of the heat exchangers, the design of the TSA device, and the calculation of the CAPEX and OPEX of the CCS-ORC system. These findings provide new insights into the sizing of a CCS-ORC system and techno-economic considerations of integrating this system in an HD-ICEV.

Table 6
 β , number and length of tubes for the heat exchangers operating in the CCS-ORC system in the M936G engine.

Equipment	Number of tubes						Tube length [m]						β [m ² /m ³]					
	100 CCR			70 CCR			100 CCR			70 CCR			100 CCR			70 CCR		
	PPN	AC	MOF	PPN	AC	MOF	PPN	AC	MOF	PPN	AC	MOF	PPN	AC	MOF	PPN	AC	MOF
ORC-H	36			25			0.320	0.349	0.332	0.364	0.398	0.372	104.0	97.7	102.2	100.6		
ORC-E	256			256			0.472	0.446	0.477	0.508	0.494	0.508	124.5	123.7	124.5	124.9	124.5	124.6
ORC-C	375	372	420	450		480	0.584	0.598	0.592	0.585	0.591	0.593	107.0	99.3	125.2	115.2		106.9
HE-CO ₂ -C	28	36	16	25			0.543	0.463	0.498	0.425	0.466	0.424	97.2	93.5	97.9	97.3		
CO ₂ -Con	66	81	70	64			0.593	0.519	0.577	0.453	0.486	0.465	92.4	90.2	88.8	90.2	88.7	93.1
HE-EG1	675			510	480	496	0.597	0.597	0.598	0.585	0.596	0.589	126.6	114.6	116.0	102.3	109.4	132.7
HE-EG2	300		360	276	276	315	0.594	0.600	0.576	0.587	0.591	0.585	91.0	93.5	102.0	94.8	98.6	111.2

Table 7
 β , number and length of tubes for the heat exchangers operating in the CCS-ORC system in the F1C engine.

Equipment	Number of tubes						Tube length [m]						β [m ² /m ³]					
	100 CCR			70 CCR			100 CCR			70 CCR			100 CCR			70 CCR		
	PPN	AC	MOF	PPN	AC	MOF	PPN	AC	MOF	PPN	AC	MOF	PPN	AC	MOF	PPN	AC	MOF
ORC-H	25			15	16		0.329	0.352	0.335	0.425	0.436	0.407	134.9	134.6		125.7	125.9	126.1
ORC-E	176	169	187	196			0.484	0.475	0.456	0.462	0.451	0.463	167.2	164.7	166.9	166.4	166.4	167.2
ORC-C	338	330	372	380		418	0.497	0.483	0.477	0.494	0.499	0.485	105	109	110.9	105.1	105.1	106.3
HE-CO ₂ -C	25			24*			0.423	0.465	0.423	0.385	0.423	0.384	101.6		100.2	141.4	145.1	141.4
CO ₂ -Con	64			49			0.431	0.459	0.441	0.414	0.444	0.424	98.1	96.2	99.36	100.1	102.7	104.1
HE-EG1	570	540	570	420	400	408	0.497	0.5	0.495	0.496	0.499	0.500	152.1	139.9	139.5	103.8	101.2	104.3
HE-EG2	276	260	300	240	250	260	0.492	0.489	0.487	0.487	0.460	0.499	109.2	110.3	107.9	124.9	126	121.7

* Calculated with a diameter of 12 mm.

3.1. Heat exchanger sizing

Tables 6 and 7 list the results of the number and length of tubes and β for each heat exchanger, sorbent operating in the CCS-ORC system, and engine. These results are obtained by selecting two diameters of commercial copper tubes, 20 and 15 mm, intended for the heat exchangers of the CCS-ORC system that will be integrated into vehicles equipped with M936G and F1C engines, respectively.

These tables show that all heat exchangers' length restrictions were met. Consequently, many tubes are accommodated in the heat exchangers with more required area (HE-EG1, HE-EG2, ORC-C, ORC-E). As Fig. 5 shows, the lower the distance S_L , the greater the fluid speed and, therefore, the U value; this also allows greater compaction of the tubes and an increase in the β value. On the other hand, the heat exchangers of the CCS-ORC system operating with the F1C engine generally have a higher β than their counterpart, the M936G engine. This behaviour is caused by the

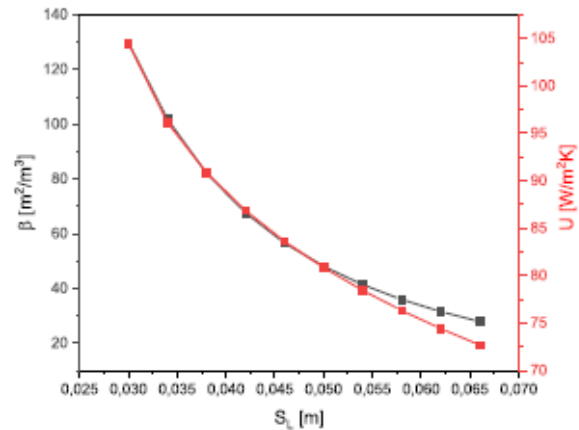


Fig. 5. β and U variation with the S_L distance in the heat exchanger arrangement

lower mass flows of the substances that interact in the heat exchangers, which allows greater compaction of the tube bank arrangement and, therefore, an increase in the Reynolds number that allows compliance with the values of U , triggering higher values for B in the FIC engine.

It is important to note that the heat exchangers in the proposed CCS-ORC system's compaction level, with β values close to $100 \text{ m}^2/\text{m}^3$, is significant, as observed in [9]. However, there is still a considerable margin for improvement through a detailed design of heat exchangers, as these values are 4 times below the β value of compact heat exchange with phase change and 7 times below the β value of compact heat exchangers without phase change [43].

3.2. TSA device design

The transient state heat transfer mathematical model indicates that a duration of 180 s is suitable for the sorbent bed to attain the desired temperature at its centre. This short period of sorbent heating is due to the high temperature and velocity of the exhaust gases within the TSA device, which enhances the heat transfer parameters (Re , h), consequently diminishing the sorbent's heating time. This finding aligns with experimental results documented in the literature [44]. This time also allows a decrease in sorbent mass, therefore reducing the cost of the TSA device operation.

Tables 8 and 9 show the sizing obtained for the TSA device corresponding to each sorbent. As can be seen there, the TSA device attains its smallest size with the MOF sorbent, mainly because the MOF sorbent necessitates a lesser quantity of sorbent to capture an equivalent amount of CO_2 compared to the other sorbents. Moreover, the MOF sorbent has

higher thermal conductivity when contrasted with the PPN and AC sorbents, facilitating the MOF sorbent in reaching the required desorption temperature more expeditiously. Consequently, the TSA device incorporating the MOF sorbent can accommodate a greater sorbent mass and, due to this, needs fewer tubes than the other TSA devices operating with the other sorbents.

4. Techno-economic assessment

4.1. CAPEX

Tables 10 and 11 show the values of parameter A , costs associated with individual devices, and the direct and indirect costs of CAPEX. As observed in these tables, no discernible impact exists on the CAPEX between different sorbents. Specifically, the CAPEX for the CCS-ORC system within the M936G engine at 100 % of CCR averages 68.17 k€, decreasing to 57.73 k€ at a 70 % CCR, denoting a reduction of 15.3 %. Similarly, in the FIC engine, the CAPEX at 100 % CCR stands at 39.92 k€, decreasing to 33.01 k€ at 70 % CCR, indicating a 17.3 % cost reduction. Notably, the disparity between sorbents at 100 % of CCR does not exceed 3.99 k€; at 70 % CCR, it remains within 2.7 k€ for both engines.

Fig. 6 shows the percentage weight in the CAPEX of each subsystem. The CSS system exerts the most significant influence on the CAPEX, constituting approximately 30 % of the initial investment, followed by the ORC system, which accounts for roughly 20 % of the initial investment at 100 % CCR. Notably, at 70 % CCR, an expected phenomenon unfolds: the CSS system reduces its weight over the total CAPEX while the ORC system increases its weight. This shift is attributed to the fact that it requires more robust equipment due to the high power production in this condition. Fig. 6 also shows that the TSA system with the MOF sorbent, for any engine and CCR, exhibits a weight in the CAPEX that is 40 % lower than with PPN and 60 % lower than with AC. However, the CAPEX of the ORC and EGC subsystems is higher with MOF compared to other sorbents. This, akin to the abovementioned observation, is attributed to the requirement for more robust equipment in MOF operation than other sorbents. The CCS subsystem in the M936G engine is directly correlated with the compression pressure of the compressor; hence, it manifests the following behaviour for this subsystem: $\text{PPN} < \text{AC} < \text{MOF}$. Nonetheless, MOF operation presents a higher value in the FIC engine at 100 % CCR due to the cumulative cost of heat exchangers and the compressor exceeding that of its AC operation counterpart.

The CAPEX obtained for the CCS-ORC systems is added to the initial purchase price of a CNG vehicle, allowing the increase in the initial purchase value of CNG vehicles that incorporate CCS-ORC systems to be calculated. The initial purchase values taken (baseline) are a bus of 75 m^3 and 19 t that uses the M936G engine [45] and a VAN of 5.2 t and 12 m^3 that uses the FIC engine [46]. Subsequently, these values are compared with other vehicles utilizing zero CO_2 emissions technologies, such as electric battery (EB) vehicles and those equipped with hydrogen-fuel-cell batteries (HFCB), as is shown in Table 12.

As can be seen in Table 12, vehicles that use zero-emission technologies are 61 % and 73 % more expensive than CNG vehicles without the CCS-ORC system (baseline). However, the CNG bus with the CCS-ORC system incorporated experiences only an increase of 18.2 % in its initial price for a 100 % CCR and 15.4 % for a 70 % CCR. On the other hand, installing the CCS-ORC system would increase its price to almost double the base case in the case of the VAN. The VAN with 100 % CCR turns out to be 33.2 % more expensive, and with 70 % CCR, it is 21.7 % more expensive than the EB VAN. These findings indicate that the initial cost is manageable for an owner in the case of the bus. Nevertheless, for smaller vehicles, the initial cost would not be feasible.

4.2. OPEX

Table 13 shows the OPEX results obtained for the four case studies. A

Table 8
Sizing of the TSA device operating in the CCS-ORC system at 100 % of CCR.

Variable	M936G			FIC		
	AC	MOF	PPN	AC	MOF	PPN
Sorbent mass [kg]	17.03	8.09	9.56	8.44	4.01	4.73
Tube diameter [m]	0.078	0.122	0.09	0.046	0.09	0.062
Sorbent bed diameter [m]	0.074	0.118	0.086	0.042	0.086	0.058
Sorbent bed length [m]	6.95	1.62	4.08	10.69	1.51	4.45
Tube length [m]	1	1	1	1	1	1
Number of tubes	7	2	5	11	2	5
h [$\text{W}/\text{m}^2\text{K}$]	126.8	114.9	109.9	65.69	60.87	63.58
Re number	25,465	36,949	25,462	6337	12,967	8851
Shell diameter [m]	0.2496	0.2562	0.288	0.2024	0.189	0.1953
Heat transfer area [m^2]	1.72	0.77	1.41	1.59	0.57	0.97

Table 9
Sizing of the TSA device operating in the CCS-ORC system at 70 % of CCR.

Variable	M936G			FIC		
	AC	MOF	PPN	AC	MOF	PPN
Sorbent mass [kg]	11.92	5.66	6.69	5.91	2.81	3.31
Tube diameter [m]	0.092	0.142	0.106	0.064	0.114	0.082
Sorbent bed diameter [m]	0.088	0.138	0.102	0.06	0.11	0.078
Sorbent bed length [m]	3.44	0.83	2.03	3.67	0.65	1.72
Tube length [m]	0.90	0.90	0.90	0.70	0.70	0.70
Number of tubes	4	1	3	6	1	3
h [$\text{W}/\text{m}^2\text{K}$]	148.1	178.7	141.8	61.32	75.72	62.33
Re number	36,321	77,594	41,056	8385	22,016	11,665
Shell diameter [m]	0.2392	0.1704	0.2438	0.2048	0.1368	0.1886
Heat transfer area [m^2]	1.04	0.4	0.9	0.84	0.25	0.4

Table 10
CAPEX results of the CCS-ORC system operating in the M936G engine.

Process	Equipment	Parameter [A]						Cost [k€]					
		100 CCR			70 CCR			100 CCR			70 CCR		
		PPN	MOF	AC	PPN	MOF	AC	PPN	MOF	AC	PPN	MOF	AC
TSA	TSA-Device	1.41	0.77	1.72	0.9	0.4	1.04	4.56	2.71	5.42	3.10	1.54	3.51
	ORC-expander	12.45	13.81	12.6	14.38	15.55	14.52	4.93	5.54	4.99	5.80	6.33	5.86
	ORC-pump	1.08	1.13	1	1.17	1.24	1.18	0.22	0.22	0.22	0.23	0.23	0.23
Waste heat recovery (ORC)	ORC-C ₆ H ₁₀ tank	0.01	0.01	0.01	0.01	0.01	0.01	0.19	0.19	0.19	0.19	0.19	0.19
	ORC-Evaporator	7.59	7.66	7.17	8.16	8.17	7.95	2.54	2.56	2.41	2.72	2.72	2.65
	ORC-heater	0.72	0.75	0.79	0.57	0.59	0.63	0.41	0.42	0.43	0.37	0.37	0.39
Exhaust gases condition	ORC-condenser	13.77	15.61	13.97	16.53	17.9	16.71	4.46	5.03	4.52	5.31	5.74	5.37
	FG1	25.3	25.37	24.23	18.74	18.36	17.99	8.03	8.05	7.7	6.00	5.88	5.77
	FG2	11.2	13.02	11.31	10.18	11.58	10.25	3.66	4.23	3.7	3.35	3.78	3.37
CO ₂ storage system	Cyclone	0.3	0.3	0.3	0.21	0.21	0.21	0.53	0.53	0.53	0.37	0.37	0.37
	Fan	0.99	0.7	1.05	1.282	0.834	1.35	0.22	0.2	0.22	0.23	0.21	0.23
	Condenser	2.46	2.54	2.64	1.82	1.87	1.96	0.95	0.98	1.01	0.75	0.77	0.80
Direct cost	Cooling	0.95	0.75	1.05	0.67	0.67	0.73	0.48	0.42	0.52	0.40	0.40	0.42
	Compressor	17.93	18.33	21.76	12.7	13.03	15.28	11.64	11.86	13.65	8.78	8.96	10.21
	CO ₂ tank	0.47	0.47	0.47	0.33	0.33	0.33	7.58	7.55	7.55	5.31	5.31	5.31
Indirect cost	Installing							4.03	4.04	4.24	3.43	3.42	3.57
	Instrumentation	50.43	50.50	53.06	42.91	42.81	44.68	2.52	2.53	2.65	2.15	2.14	2.23
	Piping							0.76	0.76	0.8	0.64	0.64	0.67
Total CAPEX	Electric installing							0.5	0.51	0.53	0.43	0.43	0.45
	Engineering	58.24	58.33	61.28	50.72	50.65	52.90	4.08	4.08	4.29	3.47	3.46	3.61
	Contingency							4.66	4.67	4.9	3.96	3.96	4.13
Total CAPEX								66.95	67.08	70.47	56.99	56.86	59.35

Table 11
CAPEX results of the CCS-ORC system operating in the F1C engine.

Process	Equipment	Parameter [A]						Cost [k€]					
		100 CCR			70 CCR			100 CCR			70 CCR		
		PPN	MOF	AC	PPN	MOF	AC	PPN	MOF	AC	PPN	MOF	AC
TSA	TSA-Device	0.97	0.57	1.59	0.54	0.25	0.84	3.31	2.09	5.06	2.00	1.03	2.92
	ORC-expander	7.22	7.89	7.20	8.17	8.73	8.28	2.59	2.88	2.58	3.01	3.25	3.06
	ORC-pump	0.61	0.69	0.59	0.70	0.73	0.66	0.19	0.20	0.19	0.20	0.20	0.19
Waste heat recovery (ORC)	ORC-C ₆ H ₁₀ tank	0.01	0.01	0.01	0.01	0.01	0.01	0.19	0.19	0.19	0.19	0.19	0.19
	ORC-Evaporator	4.01	4.02	3.79	4.27	4.27	4.16	1.43	1.44	1.36	1.51	1.51	1.48
	ORC-heater	0.39	0.39	0.42	0.30	0.31	0.33	0.31	0.31	0.32	0.28	0.29	0.29
Exhaust gases condition (EGC)	ORC-condenser	7.92	8.36	7.51	8.84	9.56	8.93	2.65	2.78	2.52	2.93	3.15	2.96
	FG1	13.34	13.30	12.72	9.81	9.61	9.41	4.33	4.31	4.13	3.23	3.17	3.11
	FG2	6.40	6.88	5.99	5.38	6.12	5.42	2.17	2.32	2.05	1.86	2.09	1.87
CO ₂ storage system (CSS)	Cyclone	0.15	0.15	0.15	0.11	0.11	0.11	0.27	0.27	0.27	0.19	0.19	0.19
	Fan	0.46	0.32	0.48	0.31	0.23	0.32	0.18	0.16	0.18	0.16	0.15	0.16
	Condenser	1.30	1.33	1.38	0.96	0.98	1.02	0.59	0.60	0.62	0.49	0.49	0.51
Direct cost	Cooling	0.50	0.50	0.55	0.35	0.35	0.38	0.35	0.35	0.36	0.30	0.30	0.31
	Compressor	9.71	9.92	11.78	6.88	7.03	8.34	7.04	7.17	8.25	5.31	5.40	6.22
	CO ₂ tank	0.24	0.24	0.24	0.17	0.17	0.17	3.81	3.81	3.81	2.67	2.67	2.67
Indirect cost	Installing							2.35	2.31	2.55	1.95	1.93	2.09
	Instrumentation	29.40	28.88	31.89	24.33	24.09	26.13	1.47	1.44	1.59	1.22	1.20	1.31
	Piping							0.44	0.43	0.48	0.36	0.36	0.39
Total CAPEX	Electric installing							0.29	0.29	0.32	0.24	0.24	0.26
	Engineering	34	33.4	36.8	28.88	28.57	31.07	2.38	2.34	2.58	1.97	1.95	2.11
	Contingency							2.72	2.67	2.95	2.25	2.23	2.41
Total CAPEX								39.05	38.36	42.35	32.31	32.00	34.71

vehicle yearly operation of 350 days and 16 h per day is considered. The OPEX of the CCS-ORC system calculated for the M936G engine, at 100 % of CCR, is on average 10.91 k€ and 4.4 k€ for 70 % of CCR, and the F1C engine is 6.05 and 2.24 k€ for 100 and 70 % of CCR, respectively. Likewise, it is observed that although the AC has a 50 % lower sorbent renewal cost in the OPEX calculation because it is a commercial material, the operating expenses of the CCS-ORC system obtained in the two engines with AC are, on average, 27 % and 43 % higher than 100 % and 70 % CCR, respectively, compared to the OPEX values obtained with MOF. This behaviour is due to the greater penalty that the CCS-ORC system exerts on engines with AC operation, which increases fuel consumption.

4.3. Payback analysis

As observed in the results found, the initial cost of installing a CCS-ORC system operating in a vehicle with an M936G engine is between 15 and 18 % (depending on the capture rate), and in a vehicle with an F1C engine, the cost of the vehicle increases to almost double. Furthermore, both vehicles' average annual operational expenses are 15 and 7 % of the initial CCS-ORC system cost for 100 and 70 % CCR, respectively. These results suggest that integrating a CCS-ORC system into heavy-duty vehicles may lack economic feasibility unless accompanying benefits or exemptions from avoiding emissions-related taxes exist. Hence, this section will undertake an economic assessment as an entry point from 2027, when a package of stricter rules comes into force to reduce transport sector emissions through a specialized emission

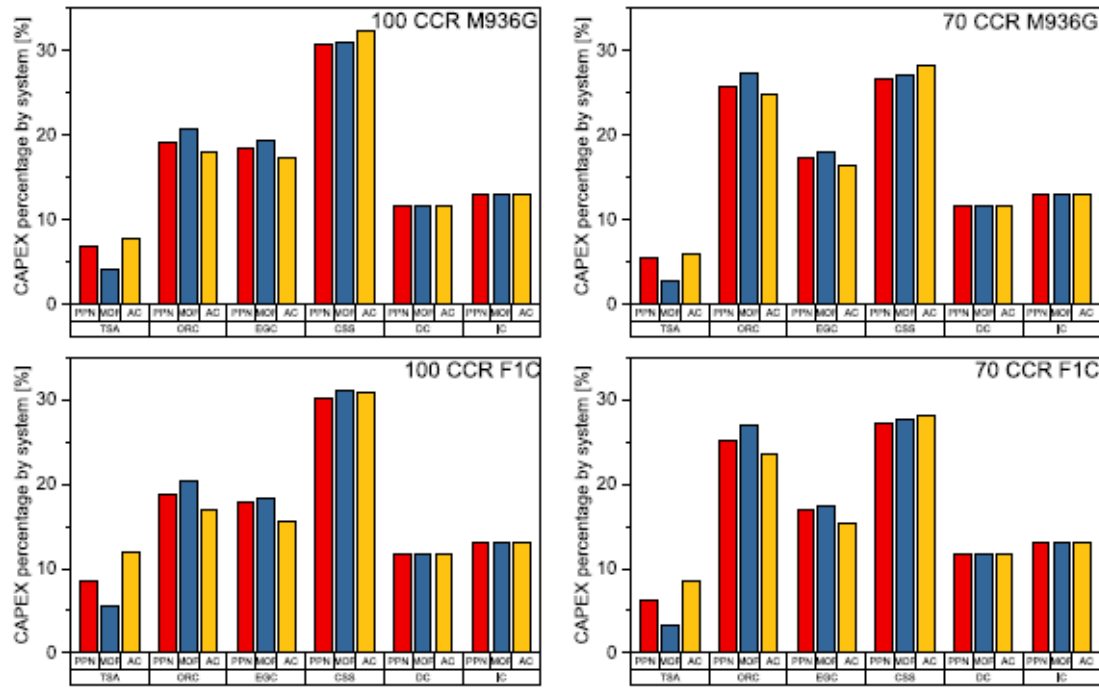


Fig. 6. CAPEX percentage by sub-system in the CCS-ORC system.

Table 12
CAPEX including the initial purchase of the vehicle.

Vehicle	Technology	Purchase [k€]	Difference from baseline [%]	Reference
Bus with a M936G engine (or similar V_d) and useful space of 75 m ³	CNG	374.6	0.0	[47,48]
	HFCB	650	-73.5	[49]
	EB	604	-61.2	[50]
	CNG + CCS-ORC at 100 % of CCR	442.	-18.2	Own study
	CNG + CCS-ORC at 70 % of CCR	432.3	-15.4	Own Study
VAN with a F1C engine (or similar V_d) and useful space of 12 m ³	CNG	40	0.0	[51]
	EB	60	50.0	[52,53]
	CNG + CCS-ORC at 100 % of CCR	79.9	-99.8	Own study
	CNG + CCS-ORC at 70 % of CCR	73	-82.5	Own Study

Table 13
OPEX for the CCS-ORC systems.

Concept	M936G						F1C					
	100 CCR			70 CCR			100 CCR			70 CCR		
	PPN	MOF	AC	PPN	MOF	AC	PPN	MOF	AC	PPN	MOF	AC
Sorbent renovation [k€/year]	1.34	1.34	0.70	0.85	0.85	0.59	0.59	0.58	0.42	0.48	0.48	0.35
Fuel consumption increase [k€/year]	8.39	7.51	11.40	2.53	2.01	4.63	4.69	4.18	6.49	1.16	0.86	2.42
O&M [k€/year]	0.67	0.67	0.7	0.57	0.57	0.59	0.39	0.38	0.38	0.32	0.32	0.35
Total OPEX [k€/year]	10.40	9.52	12.81	3.95	3.43	5.82	5.66	5.14	7.33	1.97	1.66	3.11

trading system often referred to as 'ETS2' [54]. In this, the European Union established the charge for CO₂ emission rights to the transport sector with an initial value of 45 €/tCO₂ [54,55]. This will increase the cost of goods transported if the transport sector does not have a broader range of technologies to reduce its CO₂ emissions by that date.

The initial analysis will determine the payback time for a CCS-ORC system integrated into a heavy-duty vehicle. Initially, the annual CO₂ emissions avoided for each engine are obtained utilizing the data provided in section 2.4. This data is multiplied by the established price of the CO₂ emission rights; thereby, the income is obtained for each case. Table 14 shows the values obtained from the income and the annual net profit, which is the difference between the OPEX and the income. Finally, the payback time of the CCS-ORC system is determined by calculating the net present value (NPV) using Eq. 22. In this calculation, i represents the interest rate, set at 4 %, t denotes the number of years, and n signifies a heavy transport vehicle's lifespan, typically 10 years, according to the literature [56]. Fig. 7 provides the result obtained for the NPV.

$$NPV = \sum_{t=0}^n \frac{Profit_t}{(1+i)^t} - CAPEX \quad (22)$$

Table 14
Incomes and Profits obtained for integrating a CCS-ORC system in a heavy-duty vehicle.

Concept	M936G						F1C					
	100			70			100			70		
OPEX [k€/year]	PPN	MOF	AC	PPN	MOF	AC	PPN	MOF	AC	PPN	MOF	AC
Income [k€/year]	10.40	9.52	12.81	3.95	3.43	5.82	5.66	5.14	7.33	1.97	1.66	3.11
Profits [k€/year]	11.33			7.93			5.67			3.97		
	0.93	1.81	-1.48	3.98	4.50	2.11	0.01	0.53	-1.66	2.00	2.31	0.86

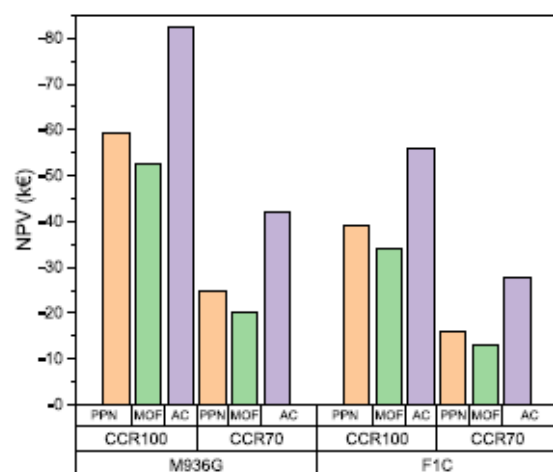


Fig. 7. NPV calculated at 10 years of CCS-ORC system for the whole sorbent, CCR and engines.

The values obtained from the payback time indicate that the capital expenditures (CAPEX, see Tables 10 and 11) fails to be recouped with any sorbent and with any under CCR conditions over the vehicles' useful lifespan. Notably, even with the AC in both engines and at 100 % of CCR, a reduction in CAPEX is not achieved. This behaviour is attributed to the fact that, under this CCR condition in both motors, no profits are obtained with the AC, but, on the contrary, additional expenses are incurred for the operation of the CCS-ORC system.

Conversely, with the other two sorbents at 100 % CCR, a partial recovery of the initial investment is achieved. Specifically, with MOF, the recovery percentages stand at 22 and 64 % at 100 and 70 % CCR, respectively, in the M936G engine, and 11 and 59 % at 100 and 70 % CCR, respectively, in the F1C engine. Employing PPN yields recovery percentages of 11 % and 57 % at 100 % and 70 % CCR, respectively, for the M936G engine and 50 % at 70 % CCR for the F1C engine.

As evidenced in the data previously shown, there is a more significant recovery on the initial investment of the CCS-ORC system in the M936G engine, especially at 70 % CCR, due to the lower initial investment and the more significant amount of CO₂ captured, which translates into a higher annual benefit compared to the operation of the CCS-ORC system in the vehicle with an F1C engine.

Despite not achieving the recovery of the investment within the established lifespan vehicle period, it is relevant to note that the carbon abatement costs (CAC) (calculated using Eq. 23) obtained for the CCS-ORC systems proposed in this research, operating at 100 % CCR, vary from 19.4 €/tCO₂ with MOF up to 33.9 €/tCO₂ with AC in the vehicle equipped with the M936G engine, and from 26.2 €/tCO₂ with MOF to 46.8 €/tCO₂ in the vehicle with the F1C engine, as shown in Fig. 8. These values are below those observed in other industries, such as glass and steel, whose CCS costs range between 50 and 350 €/tCO₂ [57,58]. As expected, Fig. 8 shows a decrease in CAC with the CCR reduction due to

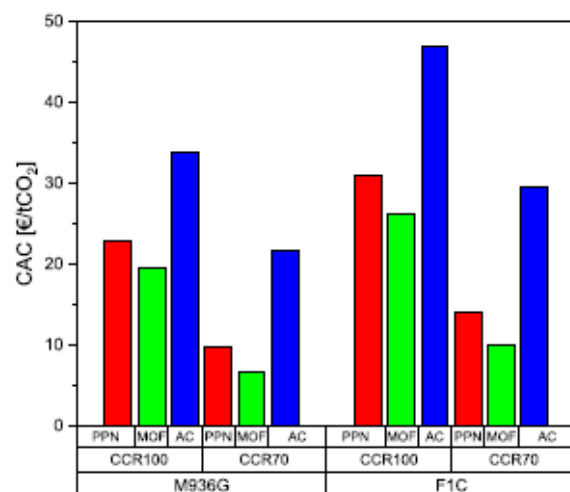


Fig. 8. CAC calculated of CCS-ORC system for the whole sorbent, CCR and engines.

the CCS-ORC system's lower CAPEX. Furthermore, a higher CAC is seen in both CCRs in the vehicle equipped with the F1C engine, which is attributed to the lower benefit obtained from the CCS-ORC system operating in this vehicle.

$$CAC = \frac{\frac{CAPEX}{\text{Sorbent}} - \text{Profits}}{\frac{CO_2}{\text{year avoided}}} \quad (23)$$

5. Sensitivity analysis

This section introduces two sensitivity analyses. The first seeks to establish the appropriate price of the CO₂ emissions tax to achieve the payback on the initial investment within the operational lifespan of a heavy-duty work vehicle (10 years). The second aims to identify the engine size (by varying the engine displacement volume) that achieves a CAC of zero. This latter analysis is made in the same period, and the price of the CO₂ emission tax remains fixed at 45 €/tCO₂.

Fig. 9 shows the results of the first analysis. It discloses that, to achieve a 10-year payback on investment with a CCR of 100 %, the required CO₂ emission rights prices are 70.6, 74.4 and 85.4 €/tCO₂ for the MOF sorbents, PPN and AC, respectively, in the M936G engine and the F1C engine, the value of the tax with MOF, PPN and AC must be 78.3, 83.8 and 99.7 €/tCO₂, respectively. On the other hand, by reducing the CCR to 70 %, a decrease is observed in the required value of the CO₂ tax to achieve the payback of the initial investment in the established period. Compared to the 100 % CCR scenario, this reduction amounts to 10 and 15 €/tCO₂ for all three sorbents in the M936G and F1C engines, respectively. Notably, the analysis indicates that smaller vehicles necessitate higher CO₂ tax payments to achieve the desired return on investment within the designated timeframe.

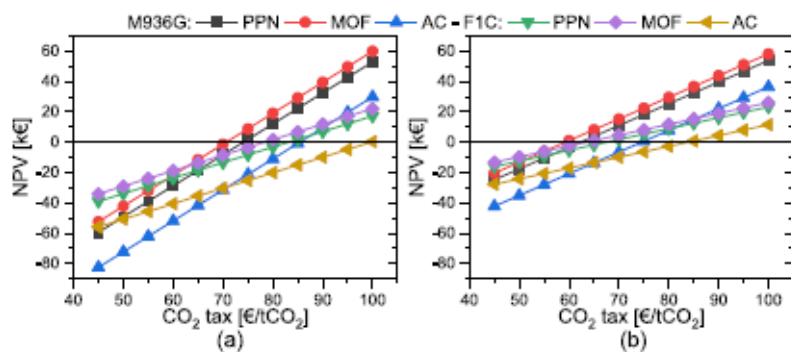


Fig. 9. Payback sensitivity analysis: a) 100 CCR and b) 70 CCR.

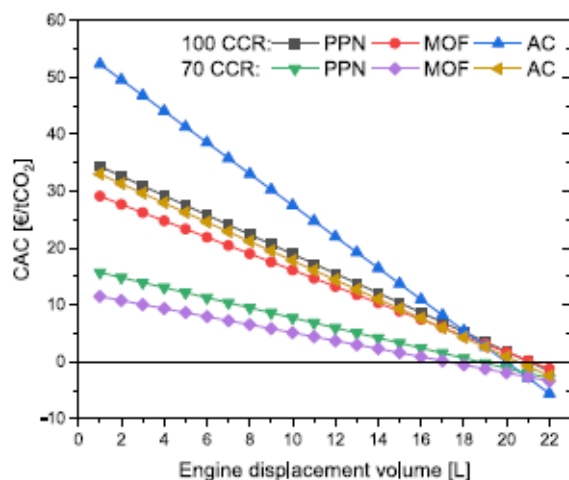


Fig. 10. CAC sensitivity analysis for engine size.

Fig. 10 reveals that achieving a CAC of zero or less at 100 % CCR requires an engine with a displacement volume (V_d) greater than 20 L with AC and 22 L with MOF and PPN. This specific finding is attributed to the steeper negative slope of the CAC of the CCS-ORC system between the F1C and M936G engines with AC. On the other hand, when moving to the CCR of 70 %, it is observed that the CAC of zero or less is obtained with a V_d of 18 L with MOF, 19 L with PPN and 21 L with AC. Although AC exhibits a higher negative slope in the latter scenario compared to other sorbents, this result aligns more closely with the trend observed in the preceding findings. Finally, regardless of the CCR rate, it is evident that a CCS-ORC system could yield a CAC of zero in engines with high V_d .

6. Conclusions

The present work constitutes the first sizing and techno-economic analysis of a CCS-ORC integrated into a heavy-duty vehicle. The CCS-ORC takes advantage of the waste heat in the exhaust gases to perform the TSA stages. Additionally, it integrates an ORC cycle to supply the power demand of the CO_2 compression stage. This is evaluated with two CCRs and three sorbents in two engines with different engine volume displacements. The heat exchangers and TSA device required for the correct operation of the CCS-ORC system are sizing, searching for the maximum compaction possible. A techno-economic analysis is conducted to determine the initial expenses of an HD-ICEV with an integrated CCS-ORC system and the operational cost of the latter. Finally, the economic feasibility of this integration, under the scenario when the

transport sector must pay for the CO_2 emissions rights, is evaluated.

The outcomes of the concept design conducted in the present research show that the volumes found for the TSA device, whose highest value is scarcely 0.26 m^3 , and the achieved compaction levels in the heat exchangers of the CCS-ORC system suggest that the CCS-ORC system can be installed in an HD-ICEV with minimal impact on the useful space. Nevertheless, in future research endeavours, a detailed design of the heat exchangers could achieve higher β values. This improvement would enhance the compaction of the CCS-ORC system, facilitating its integration into the HD-ICEV. Although, this does not mean a reduction in the cost since it is calculated with the heat exchanger area.

On the other hand, the CAPEX results show that the increase in the initial investment of a large vehicle with an integrated CCS-ORC system is barely higher than the baseline vehicle. Conversely, it is much lower than the initial investment for other zero-emissions technologies. It should be noted that the techno-economic analyses indicate that integrating a CCS-ORC system in a vehicle with a small engine is not feasible.

Although the NPV in the lifespan of a heavy-duty vehicle is far from zero, values between 19 and 47 €/tCO_2 of carbon abatement cost at 100 % CCR are obtained, which are low compared to other industries. So, the transport sector could incur this investment if it aims to meet the CO_2 reduction objectives established by the European Union for the year 2050. The payback of the initial investment can even be achieved with a CO_2 tax greater than 65 €/tCO_2 . The captured CO_2 could even be sold as raw material for producing e-fuels, which would compensate for the vehicle's operating cost and provide additional income that would increase the benefits obtained by integrating a CCS-ORC system. The captured CO_2 is also prevented from being stored underground, thus giving the CO_2 a productive value.

To sum up, this study shows that integrating the CCS-ORC system in vehicles used in heavy-duty transport is promising from the CO_2 mitigation perspective and a medium-term economic point of view. The proposed integration avoids the increase of CO_2 in the atmosphere provoked by the transport sector and provides CO_2 as raw material for manufacturing e-fuels. For this reason, future endeavours should encompass studies about life cycle assessments to determine the environmental and social impacts and experimental studies to validate the CCS-ORC system under actual conditions. In this way, the knowledge gap is closed, and thus, contributes to the development of a novel application that allows complete decarbonization of this energy-intensive sector.

CRediT authorship contribution statement

Alexander García-Marlaça: Writing – review & editing, Writing – original draft, Software, Methodology, Formal analysis, Data curation, Conceptualization. Eva Llera-Sastresa: Writing – review & editing, Project administration, Methodology, Investigation, Funding

acquisition, Formal analysis, Conceptualization.

Declaration of competing interest

None.

Data availability

Data will be made available on request.

Appendix A. Appendix

Area, temperature, pressure and mass flows of each heat exchanger with the CCS-ORC system operating with PPN.

Engine	OCR	Heat exchanger	Area [m ²]	$\dot{m}_{in,HP}$ [kg/h]	$T_{in,HP}$ [°C]	$T_{out,HP}$ [°C]	$\dot{m}_{in,CP}$ [kg/h]	$T_{in,CP}$ [°C]	$T_{out,CP}$ [°C]	$P_{in,HP}$ [bar]	$P_{out,HP}$ [bar]	$P_{in,CP}$ [bar]	$P_{out,CP}$ [bar]
M936G	100	ORC-H	0.72	104.60	573.87	119.49	527.52	50.93	99.49	75	75	24.9	22.9
		ORC-E	7.59	681.48	421.73	119.49	527.52	99.49	184.15	1.09	1.09	22.9	20.9
		ORC-C	13.77	527.52	121.02	48.87	43,529.61	30.00	35.99	1.5	1	1	1
		HE-CO ₂ -C	0.95	104.60	150.00	39.23	43,529.61	35.99	36.23	1	1	1	1
		CO ₂ -Con	2.46	104.60	119.49	29.30	43,529.61	25.00	25.58	75	75	1	1
		HE-EG1	25.30	681.48	119.49	39.23	43,529.61	36.23	41.05	1	1	1	1
		HE-EG2	11.20	681.48	39.23	30.00	43,529.61	25.58	26.31	1	1	1	1
		ORC-H	0.57	73.53	581.23	102.28	617.26	50.93	82.47	75	75	24.9	22.9
		ORC-E	8.16	681.48	483.01	102.47	617.26	82.47	184.15	1.09	1.09	22.9	20.9
		ORC-C	16.53	617.26	121.07	48.87	32,357.23	30.00	39.42	1.5	1	1	1
M936G	70	HE-CO ₂ -C	0.67	73.53	150.00	42.70	32,357.23	39.42	39.65	1	1	1	1
		CO ₂ -Con	1.82	73.53	102.28	29.30	32,357.23	25.00	25.50	75	75	1	1
		HE-EG1	18.74	477.04	102.47	42.65	32,357.23	39.65	43.55	1	1	1	1
		HE-EG2	10.18	477.04	42.65	30.00	32,357.23	25.50	26.52	1	1	1	1
		ORC-H	0.39	42.49	573.36	79.39	203.44	38.80	95.97	75	75	24.9	22.9
		ORC-E	4.01	276.75	408.58	115.97	203.44	95.97	184.15	1.09	1.09	22.9	20.9
		ORC-C	7.92	203.44	121.05	36.76	17,615.38	30.00	35.98	1.5	1	1	1
		HE-CO ₂ -C	0.50	42.49	150.00	38.98	17,615.38	35.98	36.22	1	1	1	1
		CO ₂ -Con	1.30	42.49	79.39	29.30	17,615.38	25.00	25.46	75	75	1	1
		HE-EG1	13.34	276.75	115.97	39.22	17,615.38	36.22	41.00	1	1	1	1
F1C	100	HE-EG2	6.40	276.75	39.22	30.00	17,615.38	25.46	26.29	1	1	1	1
		ORC-H	0.30	29.83	580.19	72.21	239.41	40.53	76.58	75	75	24.9	22.9
		ORC-E	4.27	276.75	470.12	96.58	239.41	76.58	184.15	1.09	1.09	22.9	20.9
		ORC-C	8.84	239.41	121.03	38.48	13,162.36	30.00	39.36	1.5	1	1	1
		HE-CO ₂ -C	0.35	29.83	150.00	42.36	13,162.36	39.36	39.58	1	1	1	1
		CO ₂ -Con	0.96	29.83	72.21	29.30	13,162.36	25.00	25.41	75	75	1	1
		HE-EG1	9.81	193.73	96.58	42.58	13,162.36	39.58	43.38	1	1	1	1
		HE-EG2	5.38	193.73	42.58	30.00	13,162.36	25.41	26.53	1	1	1	1

Appendix B. Appendix

Area, temperature, pressure and mass flows of each heat exchanger with the CCS-ORC system operating with MOF.

Engine	OCR	Heat exchanger	Area [m ²]	$\dot{m}_{in,HP}$ [kg/h]	$T_{in,HP}$ [°C]	$T_{out,HP}$ [°C]	$\dot{m}_{in,CP}$ [kg/h]	$T_{in,CP}$ [°C]	$T_{out,CP}$ [°C]	$P_{in,HP}$ [bar]	$P_{out,HP}$ [bar]	$P_{in,CP}$ [bar]	$P_{out,CP}$ [bar]
M936G	100	ORC-H	0.75	104.99	584.02	116.12	591.17	50.93	96.11	77.9	77.9	24.9	22.9
		ORC-E	7.66	681.48	458.93	116.13	591.17	96.11	184.15	1.09	1.09	22.9	20.9
		ORC-C	15.61	591.17	121.02	48.87	38,743.25	30.00	37.54	1.5	1	1	1
		HE-CO ₂ -C	0.95	104.99	150.00	40.80	38,743.25	37.54	37.81	1	1	1	1
		CO ₂ -Con	2.54	104.99	116.12	29.30	38,743.25	25.00	25.66	77.9	77.9	1	1
		HE-EG1	25.37	681.48	116.13	40.81	38,743.25	37.81	42.97	1	1	1	1
		HE-EG2	13.02	681.48	40.81	30.00	38,743.25	25.66	26.66	1	1	1	1
		ORC-H	0.59	73.67	591.15	101.33	659.74	50.93	81.33	77.9	77.9	24.9	22.9
		ORC-E	8.17	681.48	508.67	101.33	659.74	81.33	184.15	1.09	1.09	22.9	20.9
		ORC-C	17.90	659.74	121.02	48.87	29,315.32	30.00	41.12	1.5	1	1	1
M936G	70	HE-CO ₂ -C	0.67	73.67	150.00	44.35	29,315.32	41.12	41.36	1	1	1	1
		CO ₂ -Con	1.87	73.67	101.33	29.30	29,315.32	25.00	25.56	77.9	77.9	1	1
		HE-EG1	18.36	477.04	101.33	44.36	29,315.32	41.36	45.42	1	1	1	1
		HE-EG2	11.58	477.04	44.36	30.00	29,315.32	25.56	26.91	1	1	1	1
F1C	100	ORC-H	0.39	42.64	603.38	78.40	229.23	40.49	92.90	77.9	77.9	24.9	22.9

(continued on next page)

(continued)

Engine	CCR	Heat exchanger	Area [m ²]	$\dot{m}_{in,HP}$ [kg/h]	$T_{in,HP}$ [°C]	$T_{out,HP}$ [°C]	$\dot{m}_{in,CP}$ [kg/h]	$T_{in,CP}$ [°C]	$T_{out,CP}$ [°C]	$P_{in,HP}$ [bar]	$P_{out,HP}$ [bar]	$P_{in,CP}$ [bar]	$P_{out,CP}$ [bar]
F1C	70	ORC-E	4.02	276.75	445.94	112.90	229.23	92.90	184.15	1.09	1.09	22.9	20.9
		ORC-C	8.36	229.23	121.03	38.44	15,659.74	30.00	37.53	1.5	1	1	1
		HE-CO ₂ -C	0.50	42.64	150.00	40.53	15,659.74	37.53	37.80	1	1	1	1
		CO ₂ -Con	1.33	42.64	78.40	29.30	15,659.74	25.00	25.52	77.9	77.9	1	1
		HE-EG1	13.30	276.75	112.90	40.81	15,659.74	37.80	42.93	1	1	1	1
		HE-EG2	6.88	276.75	40.81	30.00	15,659.74	25.52	26.64	1	1	1	1
		ORC-H	0.31	29.92	590.55	71.49	256.24	40.64	75.40	77.9	77.9	24.9	22.9
		ORC-E	4.27	276.75	495.89	95.40	256.24	75.40	184.15	1.09	1.09	22.9	20.9
		ORC-C	9.56	256.24	121.04	38.59	11,909.73	30.00	41.06	1.5	1	1	1
		HE-CO ₂ -C	0.35	29.92	150.00	44.06	11,909.73	41.06	41.31	1	1	1	1
		CO ₂ -Con	0.98	29.92	71.49	29.30	11,909.73	25.00	25.46	77.9	77.9	1	1
		HE-EG1	9.61	193.73	95.40	44.31	11,909.73	41.31	45.27	1	1	1	1
		HE-EG2	6.12	193.73	44.31	30.00	11,909.73	25.46	26.91	1	1	1	1

Appendix C. Appendix

Area, temperature, pressure and mass flows of each heat exchanger with the CCS-ORC system operating with AC.

Engine	CCR	Heat exchanger	Area [m ²]	$\dot{m}_{in,HP}$ [kg/h]	$T_{in,HP}$ [°C]	$T_{out,HP}$ [°C]	$\dot{m}_{in,CP}$ [kg/h]	$T_{in,CP}$ [°C]	$T_{out,CP}$ [°C]	$P_{in,HP}$ [bar]	$P_{out,HP}$ [bar]	$P_{in,CP}$ [bar]	$P_{out,CP}$ [bar]
M936G	100	ORC-H	0.79	113.81	625.81	127.79	535.11	50.93	107.78	85.73	85.73	24.9	22.9
		ORC-E	7.17	681.48	421.58	127.91	535.11	107.78	184.15	1.09	1.09	22.9	20.9
		ORC-C	13.97	535.11	121.02	48.87	44,269.95	30.00	35.97	1.5	1	1	1
		HE-CO ₂ -C	1.05	113.81	150.00	39.24	44,269.95	35.97	36.24	1	1	1	1
		CO ₂ -Con	2.64	113.81	127.79	29.30	44,269.95	25.00	25.65	85.73	85.73	1	1
		HE-EG1	24.23	681.48	127.91	39.24	44,269.95	36.24	41.12	1	1	1	1
		HE-EG2	11.31	681.48	39.24	30.00	44,269.95	25.65	26.37	1	1	1	1
		ORC-H	0.63	79.90	633.15	108.01	623.90	50.93	88.02	85.73	85.73	24.9	22.9
		ORC-E	7.95	681.48	482.90	108.02	623.90	88.02	184.15	1.09	1.09	22.9	20.9
		ORC-C	16.71	623.90	121.02	48.87	32,794.40	30.00	39.40	1.5	1	1	1
M936G	70	HE-CO ₂ -C	0.73	79.90	149.98	42.65	32,794.40	39.40	39.64	1	1	1	1
		CO ₂ -Con	1.96	79.90	108.01	29.30	32,794.40	25.00	25.55	85.73	85.73	1	1
		HE-EG1	17.99	477.04	108.02	42.64	32,794.40	39.64	43.58	1	1	1	1
		HE-EG2	10.25	477.04	42.64	30.00	32,794.40	25.55	26.57	1	1	1	1
		ORC-H	0.42	46.22	625.21	87.26	206.70	40.30	106.17	85.73	85.73	24.9	22.9
		ORC-E	3.79	276.75	408.42	126.17	206.70	106.17	184.15	1.09	1.09	22.9	20.9
		ORC-C	7.51	206.70	121.05	38.26	17,843.54	30.00	35.96	1.5	1	1	1
		HE-CO ₂ -C	0.55	46.22	150.00	38.96	17,843.54	35.96	36.23	1	1	1	1
		CO ₂ -Con	1.38	46.22	87.26	29.30	17,843.54	25.00	25.52	85.73	85.73	1	1
		HE-EG1	12.72	276.75	126.17	39.23	17,843.54	36.23	41.13	1	1	1	1
F1C	100	HE-EG2	5.99	276.75	39.23	30.00	17,843.54	25.52	26.34	1	1	1	1
		ORC-H	0.33	32.45	632.61	71.79	242.05	40.57	83.19	85.73	85.73	24.9	22.9
		ORC-E	4.16	276.75	470.00	103.19	242.05	83.19	184.15	1.09	1.09	22.9	20.9
		ORC-C	8.93	242.05	121.04	38.52	13,247.07	30.00	39.40	1.5	1	1	1
		HE-CO ₂ -C	0.38	32.45	150.00	42.40	13,247.07	39.40	39.64	1	1	1	1
		CO ₂ -Con	1.02	32.45	71.79	29.30	13,247.07	25.00	25.43	85.73	85.73	1	1
		HE-EG1	9.41	193.73	103.19	42.64	13,247.07	39.64	43.53	1	1	1	1
		HE-EG2	5.42	193.73	42.64	30	13,247.07	25.43	26.55	1	1	1	1

Appendix D. Appendix

Discretization of the mathematical model used in the design of the TSA device:

Central nodes

$$k \frac{T_{m+1}^{i+1} - 2T_m^{i+1} + T_{m-1}^{i+1}}{\Delta r^2} + \frac{k}{i} \left(\frac{T_{m+1}^{i+1} - T_{m-1}^{i+1}}{2\Delta r^2} \right) = \rho C_p \frac{T_m^{i+1} - T_m^i}{\Delta t}$$

At $r = 0$ Eq. 14 is indeterminate, therefore the l'Hôpital's rule must be applied, obtaining:

$$2k \frac{\partial^2 T}{\partial r^2} = \rho C_p \frac{\partial T}{\partial t}$$

This latter equation is discretized by taking the mirror image and isolated boundary, obtaining the following discretization:

$$4k \frac{T_{m+1}^{i+1} - T_m^{i+1}}{\Delta r^2} = \rho C_p \frac{T_m^{i+1} - T_m^i}{\Delta t}$$

On the surface

$$\frac{2kT_{n-1}^{4+1}}{dr^2} - T_{n-1}^4 \left[\left(\frac{2k}{dr^2} + \frac{2h}{dr} + \frac{2h}{idr} + \frac{\rho C_p}{\Delta t} \right) + 1 \right] = -T_n^4 \left(\frac{\rho C_p}{\Delta t} \right) - \frac{2hT_{n-1}}{dr} - \frac{hT_{n-1}}{idr}$$

Appendix E. Appendix

Combustion and engine efficiencies at 1300 rpm and 25 of EL for the M936G engine and at 2000 rpm and 25 of EL for the F1C engine.

Engine	M936G	F1C
Engine efficiency (η_{eng}) [%]	20.65	17.05
Combustion efficiency (η_{comb}) [%]	98.71	98.14

References

- Bains P, Psarras P, Wilcox J. CO₂ capture from the industry sector. *Prog Energy Combust Sci* 2017;63:146–72. <https://doi.org/10.1016/j.pecs.2017.07.001>.
- International Energy agency. Global energy-related CO₂ emissions by sector – Charts – Data & Statistics – IEA. <https://www.iea.org/reports/co2-emissions-in-2022>; 2022 (accessed February 28, 2023).
- Voice A, Hamad E. Mobile carbon capture for long-haul commercial transport: design. *Integr Res SSRN Electron J* 2022. <https://doi.org/10.2139/ssrn.4280720>.
- García-Mariaca A, Llera-Saastrea E. Energy and economic analysis feasibility of CO₂ capture on a natural gas internal combustion engine. *Greenh Gas Sci Technol* 2022. <https://doi.org/10.1002/GHG.2176>.
- Kim J, Yoo Y, Kim S, Beak J, Oh S-D, Lee J, et al. Design and assessment of a novel mobile carbon capture system: energy and exergy analyses. *Energ Convers Manage* 2024;300:117934. <https://doi.org/10.1016/j.enconman.2023.117934>.
- Sharma S, Maréchal F. Carbon dioxide capture from internal combustion engine exhaust using temperature swing adsorption. *Front Energy Res* 2019;7:1–12. <https://doi.org/10.3389/fenrg.2019.00143>.
- García-Mariaca A, Llera-Saastrea E. Review on carbon capture in ICE driven transport. *Energies (Basel)* 2021;14:6865. <https://doi.org/10.3390/en14216865>.
- García-Mariaca A, Llera-Saastrea E, Moreno F. Application of ORC to reduce the energy penalty of carbon capture in non-stationary ICE. *Energ Convers Manage* 2022;268:116029. <https://doi.org/10.1016/j.enconman.2022.116029>.
- García-Mariaca A, Llera-Saastrea E, Moreno F. CO₂ capture feasibility by temperature swing adsorption in heavy-duty engines from an energy perspective. *Energ* 2024;292:130511. <https://doi.org/10.1016/j.energy.2024.130511>.
- Invernizzi CM, Iora P, Manzolini G, Lasala S. Thermal stability of n-pentane, cyclopentane and toluene as working fluids in organic Rankine engines. *Appl Therm Eng* 2017;121:172–9. <https://doi.org/10.1016/j.applthermaleng.2017.04.038>.
- Shu G, Li X, Tian H, Liang X, Wei H, Wang X. Alkanes as working fluids for high-temperature exhaust heat recovery of diesel engine using organic Rankine cycle. *Appl Energy* 2014;119:204–17. <https://doi.org/10.1016/j.apenergy.2013.12.056>.
- Verdegem WM, Wang K, Sculley JP, Wriedt M, Zhou HC. Evaluation of metal-organic frameworks and porous polymer networks for CO₂-capture applications. *ChemSusChem* 2016;9:636–43. <https://doi.org/10.1002/cssc.201501464>.
- Plaza MG, García S, Rubiera F, Pis JJ, Perida C. Post-combustion CO₂ capture with a commercial activated carbon: comparison of different regeneration strategies. *Chem Eng J* 2010;163:41–7. <https://doi.org/10.1016/j.cej.2010.07.030>.
- Žukauskas A. Heat transfer from tubes in crossflow. *Adv Heat Transf* 1972;8: 93–160. [https://doi.org/10.1016/S0065-2717\(08\)70038-8](https://doi.org/10.1016/S0065-2717(08)70038-8).
- Gnielinski V. New equations for heat and mass transfer in turbulent pipe and channel flow. *Int Chem Eng* 1976;16:359–67.
- Gu HF, Chen Q, Wang HJ, Zhang HQ. Condensation of a hydrocarbon in the presence of a non-condensable gas: heat and mass transfer. *Appl Therm Eng* 2015; 91:938–45. <https://doi.org/10.1016/j.applthermaleng.2015.08.092>.
- Kandlikar SG, Shoji M, Dhir VK. Handbook of phase change: Boiling and condensation. 1. Taylor & Francis; 1999.
- Incropera F, DeWitt D, Bergman T, Lavine A. Fundamentals of heat and mass transfer. 6. New York: Wiley; 1996.
- Rohsenow WM. A method of correlating heat-transfer data for surface boiling of liquids. *J Fluids Eng* 1952;74:969–75. <https://doi.org/10.1115/1.4015984>.
- Collier J, John Thome. Convective boiling and condensation. 3rd ed. New York: Oxford University Press; 1996.
- John Chato. Laminar condensation inside horizontal and inclined tubes (Doctoral dissertation, Massachusetts Institute of Technology). PhD Thesis. Massachusetts Institute of Technology; 1960.
- Holman JP. Heat transfer. 10th ed. New York: McGraw-Hill; 2010.
- Jin Z, Tian B, Wang L, Wang R. Comparison on thermal conductivity and permeability of granular and consolidated activated carbon for refrigeration. *Chin J Chem Eng* 2013;21:676–82. [https://doi.org/10.1016/S1004-9541\(13\)60525-X](https://doi.org/10.1016/S1004-9541(13)60525-X).
- Wang X, Guo R, Xu D, Chung J, Kivany M, Huang B. Anisotropic lattice thermal conductivity and suppressed acoustic phonons in MOF-74 from first principles. *J Phys Chem C* 2015;119:26000–8. <https://doi.org/10.1021/acs.jpcc.5b08675>.
- A. García-Mariaca and E. Llera-Saastrea
- Ally J, Pryor T. Life cycle costing of diesel, natural gas, hybrid and hydrogen fuel cell bus systems: an Australian case study. *Energy Policy* 2016;94:285–94. <https://doi.org/10.1016/j.enpol.2016.03.009>.
- Holland SP, Mansour ET, Müller NZ, Yates AJ. The environmental benefits of transportation electrification: urban buses. *Energy Policy* 2021;148. <https://doi.org/10.1016/j.enpol.2020.111921>.
- Spendlow J, Papageorgopoulos D, Satyapal S. Fuel cell technologies program record 12012: Fuel cell bus targets. 2012.
- Quarles N, Kockelman KM, Mohamed M. Costs and benefits of electrifying and automating bus transit fleets. *Sustainability* 2020;12:3977. <https://doi.org/10.3390/su12103977>.
- Fleet Owner. Pricing set for GM's CNG vans. <https://www.fleetowner.com/emissions-efficiency/article/21662580/pricing-set-for-gm-cng-vans>; 2010.
- Wątróbski J, Malecki K, Kijewska K, Iwan S, Karczmarczyk A, Thompson R. Multi-criteria analysis of electric vans for city logistics. *Sustainability* 2017;9:1453. <https://doi.org/10.3390/su9081453>.
- Jones J, Genovese A, Tob-Ogu A. Hydrogen vehicles in urban logistics: a total cost of ownership analysis and some policy implications. *Renew Sustain Energy Rev* 2020;119:109595. <https://doi.org/10.1016/j.rser.2019.109595>.
- Yu H, Zhang H, Zhao J, Liu J, Xia X, Wu X. The thermal conductivity of micro/nano-porous polymers: Prediction models and applications. n.d., 2024.
- Flynn Ann Marie, Akashige Toshihiro, Theodore Louis. Kern's process heat transfer. 2nd ed. New Jersey: Wiley; 2018.
- García-Mariaca A, Llera E. Dynamic CO₂ capture in a natural gas engine used in road freight transport. *SSRN Electron J* 2022. <https://doi.org/10.2139/ssrn.4272013>.
- Hofmann E, Maucher D, Homstein J, den Ouden R. Capital equipment purchasing. 2. Berlin, Heidelberg: Springer Berlin Heidelberg; 2012. <https://doi.org/10.1007/978-3-642-25737-7>.
- Wang N, Verzijlbergh RA, Heijnen FW, Herder PM. Incorporating indirect costs into energy system optimization models: application to the Dutch national program regional energy strategies. *Energ* 2023;276:127558. <https://doi.org/10.1016/j.energy.2023.127558>.
- Chang C, Liao Z, Costa ALH, Bagajewicz MJ. Globally optimal design of intensified shell and tube heat exchangers using complete set trimming. *Comput Chem Eng* 2022;158:107644. <https://doi.org/10.1016/j.compchemeng.2021.107644>.
- Robin Smith. Chemical process: Design and Integration. West Sussex: John Wiley & Sons; 2005.
- Shamouhaki M, Niknam PH, Talluri L, Manfrida G, Fiaschi D. Development of cost correlations for the economic assessment of power plant equipment. *Energies (Basel)* 2021;14:2665. <https://doi.org/10.3390/en14092665>.
- Astolfi M. Techno-economic optimization of low temperature CSP systems based on ORC with screw expanders. *Energ Procedia* 2015. <https://doi.org/10.1016/j.egypro.2015.03.220>.
- Quillin S, Declaye S, Tchanche BF, Lemort V. Thermo-economic optimization of waste heat recovery organic Rankine cycles. *Appl Therm Eng* 2011;31:2885–93. <https://doi.org/10.1016/j.applthermaleng.2011.05.014>.
- Cox B, Innis S, Steen J, Kunz N. The environmental and economic case for valuing water recovery and its relationship with tailings storage conservation. *Miner Eng* 2023;201:108157. <https://doi.org/10.1016/j.mineng.2023.108157>.
- De Saint Jean M, Baurens P, Bouallou C, Couturier K. Economic assessment of a power-to-substitute-natural-gas process including high-temperature steam electrolysis. *Int J Hydrogen Energ* 2015;40:6487–500. <https://doi.org/10.1016/j.ijhydene.2015.03.066>.
- Peters Max Stone, Timmerhaus Klaus D. Plant design and economics for chemical engineers. McGraw-Hill Companies; 1990.
- Abu-Zahra MRM, Niederer JPM, Feron PHM, Versteeg GF. CO₂ capture from power plants. Part II. A parametric study of the economical performance based on monoethanolamine. *Int J Greenh Gas Control* 2007;1:135–42. [https://doi.org/10.1016/S1750-5836\(07\)00032-1](https://doi.org/10.1016/S1750-5836(07)00032-1).
- Bailera M, Espatolero S, Lisbona P, Romeo LM. Power to gas-electrochemical industry hybrid systems: a case study. *Appl Energy* 2017;202:435–46. <https://doi.org/10.1016/j.apenergy.2017.05.177>.
- Gasolinera GNC. Guía de Precios actualizada a diario. <https://www.gasolinera.gnc.com/>; 2024.
- Alshammari F, Karvountzis-Kontakiotis A, Pseyridis A, Usman M. Expander technologies for automotive engine Organic Rankine cycle applications. *Energies (Basel)* 2018;11:1905. <https://doi.org/10.3390/en11071905>.
- López JJ, Novella R, Gomez-Soriano J, Martínez-Hernández PJ, Rampanarivo F, Libert C, et al. Advantages of the unscavenged pre-chamber ignition system in turbocharged natural gas engines for automotive applications. *Energ* 2021;218: 119466. <https://doi.org/10.1016/j.energy.2020.119466>.
- Cengel Yunus A. Heat and transfer: A practical approach. 2nd ed. McGraw-Hill Education; 2004.
- Tilli N, Gréville G, Vallières C. Carbon dioxide capture and recovery by means of TSA and/or VSA. *Int J Greenh Gas Control* 2009;3:519–27. <https://doi.org/10.1016/j.jggc.2009.04.005>.
- Mercedes-Benz. Citaro NGT technical information. 2017. p. 1–16.
- Iveco company. IVECO DAILY technical information. https://www.iveco.com/Denmark/Documents/Configurator/Brochure/Dailyvan_DK.pdf; 2015 (accessed February 8, 2023).
- Haywood I, Jakob M. The role of the emissions trading scheme 2 in the policy mix to decarbonize road transport in the European Union. *Transp Policy (Oxf)* 2023; 139:99–108. <https://doi.org/10.1016/j.transpol.2023.06.003>.
- Cerrera Iñaki. El transporte por carretera pagará por sus emisiones de carbono a partir de 2027. <https://elmercantil.com/2022/12/22/el-transporte-por-carretera-pagará-por-sus-emisiones-de-carbono-a-partir-de-2027/>; 2022 (accessed March 30, 2024).
- Zhou T, Roorda MJ, MacLean HL, Luk J. Life cycle GHG emissions and lifetime costs of medium-duty diesel and battery electric trucks in Toronto, Canada. *Transp Res D Transp Environ* 2017;55:91–8. <https://doi.org/10.1016/j.trd.2017.06.019>.
- Perpiñán J, Bailera M, Peña B, Romeo LM, Evely V. Technical and economic assessment of iron and steelmaking decarbonization via power to gas and amine scrubbing. *Energ* 2023;276:127616. <https://doi.org/10.1016/j.energy.2023.127616>.
- Barón C, Perpiñán J, Bailera M, Peña B. Techno-economic assessment of glassmaking decarbonization through integration of calcium looping carbon capture and power-to-gas technologies. *Sustain Prod Consum* 2023;41:121–33. <https://doi.org/10.1016/j.spc.2023.07.029>.

6 CARBON CAPTURE IN HD-ICEV BY ABSORPTION

Once the path of adsorption as a CO₂ capture technique has been explored, the final step of this thesis is to address CO₂ capture by absorption. This chapter objectively evaluates the energy consumption, operating costs, and economic viability of using absorption as a CO₂ capture technique in HD-ICEV. One of the engines previously used in the adsorption process is employed to ensure a comprehensive and accurate comparison between the two capture techniques. Additionally, a comparison between the CCS-ORC system and other CO₂ reduction technologies available on the market is made.

The aim is to thoroughly understand each method's advantages and disadvantages, addressing key questions such as i) is the intended heat integration of the exhaust gases with the CCS systems and ORC thermally feasible? ii) what is the maximum CCR with amine-scrubbing? iii) what is the purchase cost of a vehicle with a CCS system installed? iv) what is the power penalty of the CCS on engine performance? All of this enables the identification of the most viable and efficient option for CO₂ capture in HD-ICEV.

6.1 SIMULATION DESCRIPTION OF THE CCS-ORC SYSTEM

The amine scrubbing, CO₂ compression, and ORC facilities were designed and modelled in Aspen Plus. These systems have been integrated to use the EG waste heat from an ICEV in the stripper for the desorption process and the ORC for power production that supplies the power demand of the auxiliaries such as pumps and compressors.

Figure 37 displays the layout elaborated in the simulations of the CCS-ORC system proposed. There, the EG from the ICE is used to regenerate the solvent in the stripper (1). The desorption temperature is set to 120 °C to avoid corrosion

problems and high solvent degradation [198–200]. A pinch delta temperature of 10 °C is adopted; consequently, the EG outlet temperature in the stripper is set at 130 °C (2). After releasing heat in the ORC, the EG is cooled down and dried to 40 °C before entering the bottom of the absorber unit (4) [201]. The lean solvent enters at the top of the absorber unit (24), and it, in a countercurrent, reacts with the EG; the clean exhaust gas leaves the absorber at the top (5). Rich solvent leaves the column at the bottom (18) and is pumped to the heat exchanger (19), where its temperature is raised to 87 °C before entering the top of the stripper (20). The lean solvent abandons the stripper at 101 °C, then goes to the heat exchanger to reduce its temperature to 84 °C and transfer heat to the rich solvent (21-22). After, the lean solvent is cooled down to 40 °C in a cooler before entering the absorber again. On the other hand, the water content in the CO₂ stream is removed in the condenser, and the high-purity CO₂ stream goes to the compression stage (11). The CO₂ is stored in a tank as a liquid, gaseous CO₂ is compressed from 1 to 75 bar (11-12) with two cooling stages up to 29 °C. In the first cooling stage, the CO₂ releases heat to the ORC (12-13), and in the second stage, the CO₂ is cooled with atmospheric air under standard conditions (13-14). The ORC was designed following the procedure described in the previous chapter. However, the operation parameters vary due to the lower heat available in the EG after the desorption process in the stripper. Therefore, less pressure was obtained at the inlet expander than the CCS system working with adsorption. Table 33 summarises all pressure and temperature values for each set point in the simulations.

Table 33. Thermodynamic conditions of the fluids in the simulations

Point	Fluid	Quality	Pressure [bar]	Temperature [°C]
1, 2, 3	EG	1	1.09	$f(\text{Engine load, rpm})$
4	EG	1	1.09	40
5	EG	1	1.09	$f(\text{absorber process})$
6	C ₅ H ₁₀	1	6.8	≥ 120
7	C ₅ H ₁₀	$f(\text{Engine load, rpm})$	1.2	$f(\text{C}_5\text{H}_{10} \text{ mass Flow})$
8	C ₅ H ₁₀	0	1	49
9	C ₅ H ₁₀	0	9	49
10	C ₅ H ₁₀	$f(\text{exhaust gases mass flow})$	7.9	122
11	CO ₂	1	1	40
12	CO ₂	1	75	565
13	CO ₂	1	75	≥ 120
14	CO ₂	0	75	29.3
15	Air	1	1	25
16	Air	1	1	$f(\text{CO}_2 \text{ mass flow})$
17	Air	1	1	$f(\text{C}_5\text{H}_{10} \text{ mass Flow})$
18	Rich solvent	1	1	$f(\text{absorber process})$
19	Rich solvent	1	1.1	$f(\text{absorber process})$
20	Rich solvent	1	1.1	87
21	Lean solvent	1	1	118
22, 23, 24	Lean solvent	1	1.1	$f(\text{stripper process})$

constant reaction, which is significantly higher with MEA than with DMEA. Consequently, despite MEA's lower solvent mass flow, its higher reaction rate constant enables more efficient CO₂ absorption from the EG in the absorber. This results in a higher CCR and requires less regeneration heat than DMEA.

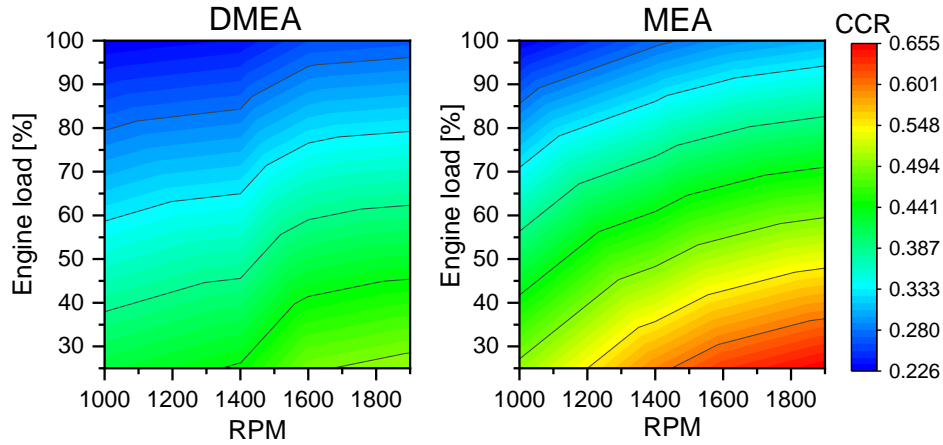


Figure 38. CCRs for MEA and MDEA over the entire rpm range and at partial engine loads.

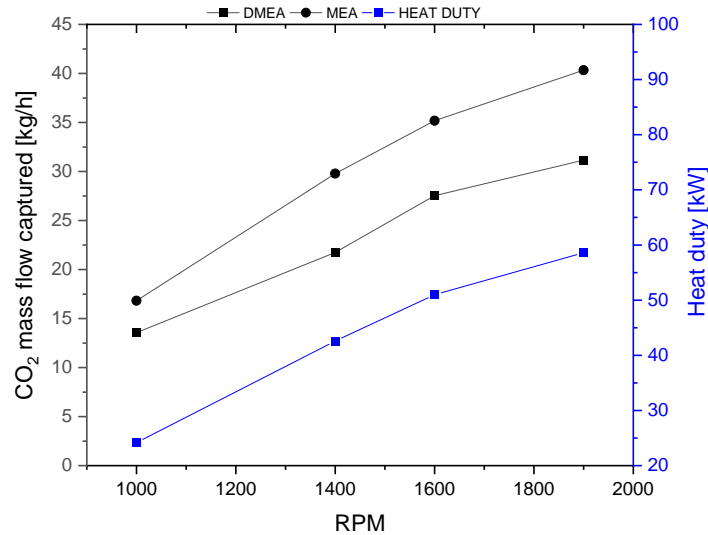


Figure 39. Heat duty in stripper and CO₂ mass captured with the amine selected

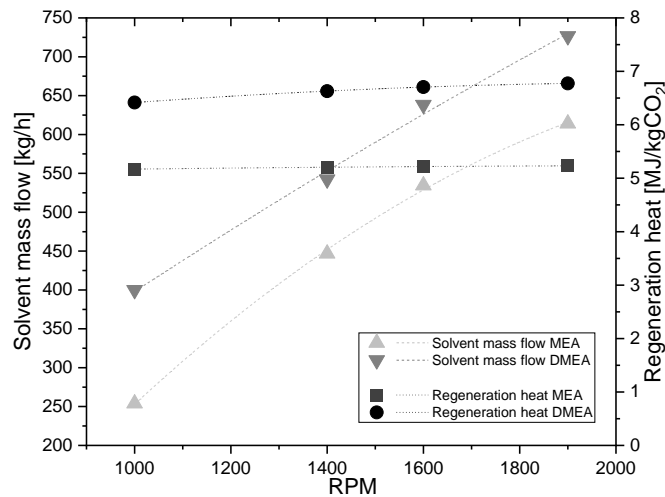


Figure 40. Solvent mass flow and regeneration.

6.3 ORC AND ENERGY ANALYSIS

Table 35 presents the areas of the ORC heat exchangers obtained from the simulations conducted with each solvent. As can be seen, the total sum of ORC heat exchanger areas is 0.741 m² with the MEA and 0.509 m² with MDEA. This difference is because there is less WF mass flow in the ORC with MDEA than MEA due to the less CO₂ captured with DMEA (see Figures 40 and 41); thus, less heat is transferred to the ORC. This situation produces less demand for cooling, whereby the CCS system operating with MDEA requires less air mass flow of cooling than with MEA.

Table 35. Heat exchangers areas obtained in the simulations

Amine	Heat exchanger	rpm	EL [%]	EG mass flow [kg/h]	Area [m ²]
MEA	Evaporator 1	1000	25	208.4	0.195
	Evaporator 2	1000	25	208.4	0.041
	ORC condenser	1900	100	754.7	0.361
	CO ₂ condenser	1900	100	754.7	0.144
MDEA	Evaporator 1	1000	25	208.4	0.143
	Evaporator 2	1000	25	208.4	0.033
	ORC condenser	1900	100	754.7	0.284
	CO ₂ condenser	1900	100	754.7	0.109

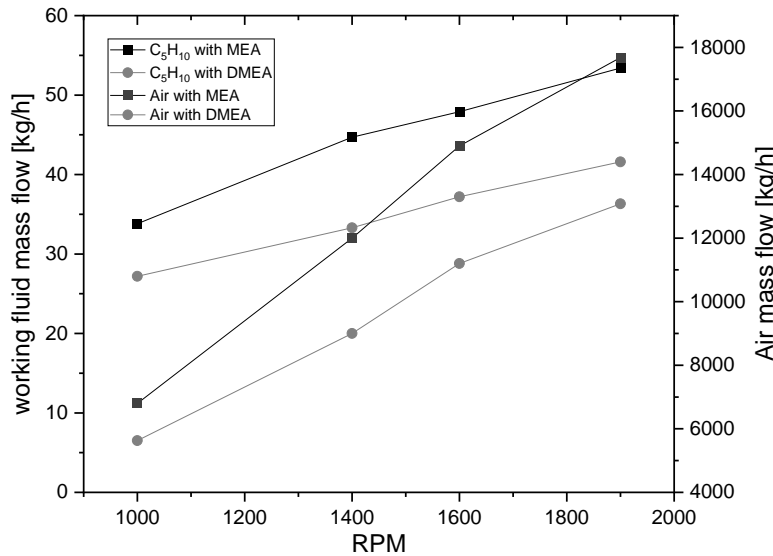


Figure 41. Air and working fluid mass flows in the ORC

Figure 42 shows that the ORC thermal efficiency peaks at 11% for both solvents at 1900 rpm and 25% engine load while reaching a minimum of 8.6% at 1000 rpm and full engine load. Figure 43 shows that the CCS-ORC system with MEA and working with the ORC has a penalisation over the engine at the critical juncture of 10.1%, whereas with MDEA, the penalty is 8%. This discrepancy arises from the higher CO₂ capture rate achieved with MEA, necessitating increased CO₂ compression power. However, simulations reveal that the CCS system without ORC produces a penalisation on average over the engine power of 1.5% higher

than the CCS system with ORC for both solvents. Conversely, the impact on engine power is scarcely discernible at the nadir.

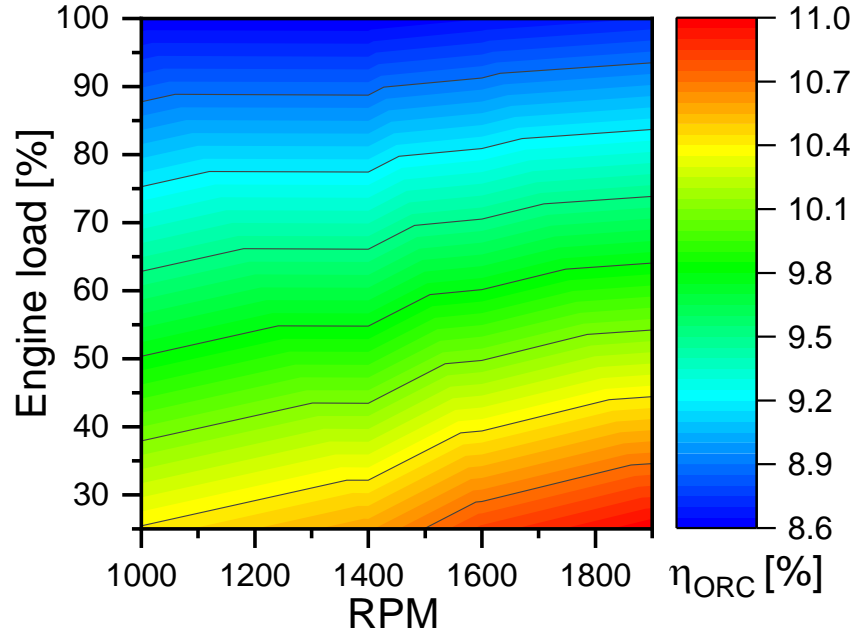


Figure 42. ORC efficiency over the entire engine rpm range and engine load conditions.

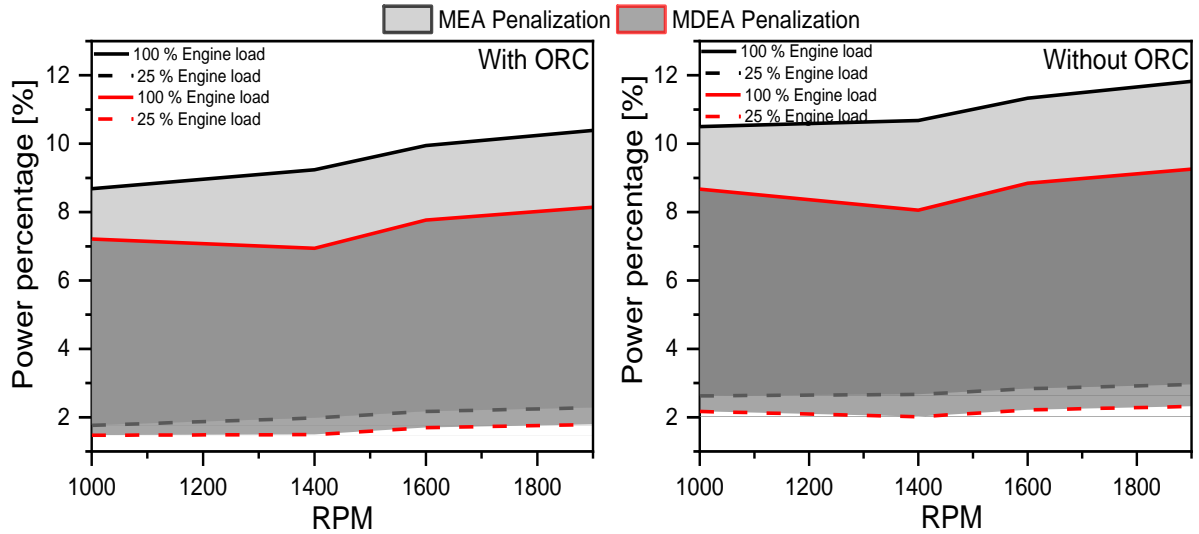


Figure 43. Percentage of power penalized of the engine by the CCS system with and without ORC.

6.4 ECONOMIC ANALYSIS

The economic evaluation of the complete CCS-ORC involves two scenarios: one with and without ORC for MEA and another solely with ORC for MDEA. Table 36 shows equipment costs that are determined using established equations from literature sources. Then, each result obtained is added to the initial investment price of CNG-fueled bus and compared against other commercial buses featuring CO₂ reduction technologies, such as hydrogen fuel cell buses (HFCB) and electric battery (EB) buses.

Table 36. CO₂ capture equipment installation costs CAPEX

Process	Equipment	Cost equation	Parameter (A)	Ref.
Amine plant	All equipment's	$26.094 \times 106(A/408)^{0.65}$	CO ₂ captured (t/h)	[182,183]
ORC	ORC-expander	$1.5(225+170A)$	Volume (m ³)	[177]
	ORC-pump	$900(A/300)0.25$	Power (kW)	
	ORC-fan	$900(A/300)0.25$	Power (kW)	
	ORC-C ₅ H ₁₀ tank	$31.5+16A$	Volume (L)	
	ORC-Evaporator	$190+310A$	Area (m ²)	
	ORC-heater	$190+310A$	Area (m ²)	
CO ₂ storage system	ORC-condenser	$190+310A$	Area (m ²)	[178]
	Condenser	$190+310A$	Area (m ²)	
	Compressor	$267000(A/445)0.67$	Power (kW)	
	CO ₂ tank	$31.5+16A$	Volume (L)	
Direct cost	Installing	8%A	Amineplant+ORC+CO ₂ storage system	[181]
	Instrumentation	5%A		
	Piping	1.5%A		
	Electric installing	1%A		
Indirect cost	Engineering	7%A	Amineplant+ORC+CO ₂ storage system+ direct cost	[182]
	Contingency	8%A		

Figure 44 shows the percentage of the different items considered in the CAPEX and the total investment of the CCS-ORC system. Notably, the cost of the amine plant constitutes over 50% of the total expenditure across all scenarios. Meanwhile, the contribution of ORC costs to the total investment ranges from 9.5% to 10.7%, contingent upon the amine utilized in the plant. This discrepancy is attributed to the dimensions of the heat exchangers and the CO₂ compressor.

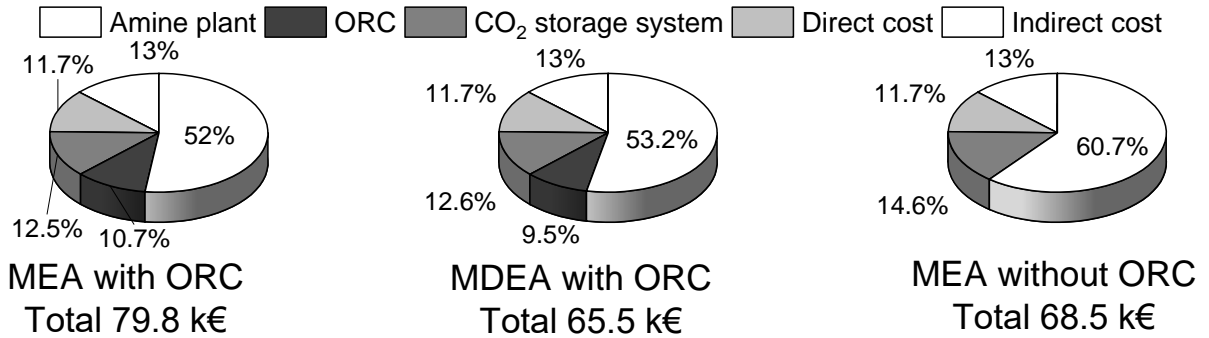


Figure 44. Total and percentage weight of each item included in the CAPEX

The findings reveal that employing MEA leads to a CAPEX increase of 14.3 k€ compared to MDEA. This difference is because the CCS-ORC system with MEA has a higher CCR than MDEA, requiring larger devices, which increases its cost. Conversely, opting for MEA in the CCS system without ORC results in a 14.1% reduction in CAPEX relative to the base case. Referring to the bus prices outlined in Table 37, diesel buses remain the most cost-effective option, 8.5% cheaper than the base case. However, it is well known that high pollutant emissions, mainly particulate matter and nitrogen oxide emissions, are the Achilles heel of these vehicles. On the other hand, it is observed that the price of buses equipped with a

CCS-ORC system is approximately 40% more economical than HFCB and EB buses.

Table 37. Initial purchase value of a bus

Technology or fuel	Value [k€]	Difference from the base case [%]	Reference
CNG	374.6	0.0	[186,187]
Diesel	342.9	8.5	[187]
HFCB	650	-73.5	[188]
EB	604	-61.2	[189]
CNG+CCS+ORC	454.4	-21.3	Own study
CNG+CCS	443.1	-18.3	Own Study

The obtained data show that installing a CCS-ORC system increases the cost of a CNG-fueled bus by 18.3 to 21.3%. Even under the conditions set out in this study, installing a CCS-ORC system with a 1 m³ storage tank could give the vehicle autonomy up to 600 km (calculated with a fuel consumption of 0.68 kg/km [205]), which is 2.4 times longer than the current maximum range of commercial electric vehicles, which is 250 km on average [206]. Nevertheless, it is essential to note that the maximum CCR achieved with MEA is 66%, meaning that the integrated CCS-ORC system does not achieve CO₂ neutrality, unlike electric and hydrogen cell vehicles. From an economic perspective, the captured CO₂ could serve as a raw material for producing fuels (e-fuels), thus adding value to the CO₂ captured. This added value could offset the initial investment, and operational costs of a bus equipped with an integrated CCS-ORC system. Furthermore, the transport sector will avoid paying the CO₂ tax, which will be implemented in this sector from 2025. Thus, it would obtain an income for selling the CO₂ captured, making the proposed CCS-ORC systems integrated into an ICEV could be competitive with their counterparts, such as HFCB and EB buses.

6.5 SUMMARY AND COMPARISON

According to the results, the amine with the highest potential for CO₂ capture is MEA, which has a higher CO₂ capture rate than MDEA under the whole range of engine operating conditions. However, the thermal integration of the exhaust gases between the CCS and ORC systems is not techno-economic feasible. Since the remaining waste thermal energy in the exhaust gases after the CO₂ desorption is insufficient to produce power in the ORC. Hence, incorporating an ORC into the CCS system does not offer a real benefit. On the contrary, it would add weight and volume to the vehicle, increasing its operating and maintenance costs. Even so, a CCS by amine-scrubbing with MEA and without ORC can become a competitive alternative to other technologies such as BEV and FCV, particularly in HD-ICEV.

Comparing the two CO₂ capture techniques studied in this thesis, it is clear that adsorption has better energy results than absorption. This is due to a lower heat requirement for sorbent regeneration than the heat required for amine regeneration. This behaviour in the absorption process causes that there is less available heat in the exhaust gases to be transformed into power by the ORC,

which results in low power production to meet the energy requirements of the CCS system, preventing achieve CO₂ capture rates above 70%, with average power penalties over the ICE less than 10%. On the other hand, as seen in Figure 34, the weight of the TSA device in the CAPEX value is less than 10%, while, as shown in Figure 44, the required amine plant represents more than 50% of the CAPEX value. This makes an approximately 50% more economical a CCS system with adsorption than a CCS system with amine-scrubbing. Therefore, energy and techno-economic studies addressed in this thesis demonstrate that adsorption is the technique with the greatest potential to be used in a CCS system in HD-ICEV.

6.6 PUBLISHED PAPER

Finally, all the details, findings, and conclusions of this study have been included in an article published in the journal "Greenhouse Gases: Science and Technology", which has the following reference:

- García-Mariaca, A., & Llera-Sastresa, E. (2023). Energy and economic analysis feasibility of CO₂ capture on a natural gas internal combustion engine. *Greenhouse Gases: Science and Technology*, 13(2), 144-159. <https://doi.org/10.1002/ghg.2176>

Original Research Article



Energy and economic analysis feasibility of CO₂ capture on a natural gas internal combustion engine

Alexander García-Mariaca and Eva Llera-Sastresa, University of Zaragoza, Zaragoza, Spain

Abstract: CO₂ capture by amine scrubbing is a widely developed technology in its most advanced stage of evolution. However, it has never been used to capture CO₂ from mobile sources. The present study performs an energy and economic analysis of an amine scrubbing CO₂ capture storage (CCS) system, which takes for the amine regeneration process the waste heat from the exhaust gases of a turbocharged natural gas internal combustion engine (mobile source). The selected engine for the study is an M936G, widely used in freight and passenger transport. A primary and a tertiary amine were chosen for the simulations. In order to reduce volume and increase autonomy, captured CO₂ is stored as a liquid, therefore, a specific installation is planned. The system is hybridised with an organic rankine cycle (ORC) to reduce the energy penalty on the CCS system. Results show that a CCS system operating with Monoethanolamine (MEA) at 30 wt% achieved a maximum CO₂ capture rate of 66%, with a penalty over the power engine of only 10%. On the other hand, the economic analysis showed that the CCS system with MEA and without ORC is 31.8% cheaper than a hydrogen fuel cells bus and 26% cheaper than a battery-electric bus. © 2022 Society of Chemical Industry and John Wiley & Sons, Ltd.

Keywords: CO₂ capture; amine-scrubbing; internal combustion engines; organic Rankine cycle

Introduction

Currently, the transport sector contributes 25% of total CO₂ emissions and is gradually migrating towards electrification to reduce its CO₂ footprint.¹ However, in freight and passenger transport, battery electric vehicles (BEV) and fuel cell vehicles (FCV) can only be a supplement, but not an alternative, to classic combustion engines,² due to short autonomies. This sector is expected to continue operating with C-H chain fuels, and thus the challenge focuses on fuels such as natural gas or synthetic natural gas. If, as in this last case, CH₄ is elaborated with a CO₂

captured (in an onboard Internal combustion engine vehicle) as raw material and an energy surplus from renewable sources, it could close the gap and drive the transport sector towards zero CO₂ emissions.

CCS is a potential technology for sustainable energy production and reducing CO₂ emissions.^{3,4} The CCS systems allow CO₂ to be separated from a gas stream before or after a combustion process.⁵ These technologies have mainly been applied in the heat and power generation sector and industries, such as cement and steel production.⁶ In particular, CO₂ capture technologies in post-combustion have had significant advances in recent years. Whereby the use of these

technologies in the transport sector could be functional. Some authors suggest that amine scrubbing, adsorption and membranes could be adapted to operate on mobile sources.^{7,8}

So far, the research about CCS systems in mobile sources has been focused on absorption and adsorption. Engine-driven ships offer the most favourable scenario for an absorption installation because the internal combustion engine (ICE) operates almost at the same load condition in a journey, which is quite like the operating conditions of a power plant. Ship-based carbon capture (SBCC) research works have focused on amine scrubbing facilities. They have made economic analyses and evaluated several amines in different proportions, CO₂ capture rates (CCR) and the use of waste energy recovery systems.

For instance, Awoyomi *et al.*⁹ studied the effect of exhaust gas recirculation (EGR) on an liquefied natural gas (LNG)-fuelled ship. They obtained a CCR of 90% with a solvent of NH₃ in a concentration of 4 wt% and solvent flow close to 40 kg/s. Stec *et al.*¹⁰ evaluated in a diesel-fuelled ship an amine-scrubbing facility under three atmospheric conditions (arctic, ISO and tropical) using a solvent with Monoethanolamine (MEA) at 30 wt%. The best results were found under tropical conditions with values of CCR of 91.4%, 2.249 MW of heat duty and a regeneration heat of 3.61 MJ/kgCO₂. Güler and Ergin,¹¹ in several LNG-fuelled ships, evaluated an amine-scrubbing facility with a solvent concentration of 35 wt% of MEA. The average result of CCR obtained in their study was 33%. Ros *et al.*¹² evaluated SBCC on 12 LNG-fuelled engines (8 MW each) with a solvent of 30 wt% of MEA. The main results were a maximum CCR of 81% with an average price of 125 €/CO₂ton (depending on the storage pressure of CO₂). Luo and Wang,¹³ in a diesel-fuelled ship of 10.8 MW with a waste energy recovery system (WERS), made an economic analysis of an amine-scrubbing plant using MEA at 30 wt% as solvent. The results show a CCR of 73% and a CO₂ capture price of 77.5 €/CO₂ton without the WERS. With WERS, 90% of CCR is reached with a higher CO₂ capture price of 163 €/CO₂ton. Feenstra *et al.*¹⁴ evaluated two solvents, MEA and piperazine (PZ), for the CO₂ capture process on a 3 MW LNG-fuelled ship. The main conclusion of their study is that the cost of CO₂ capture is 120 €/CO₂ton using MEA and 98 €/CO₂ton using PZ.

In contrast, in ICE vehicles (ICEv), their rapid accelerations and decelerations and changes in the speed and load in the engine are the bottlenecks that do not allow the implementation of CCS systems in this sector. The research works found in the literature have evaluated the energy requirements of the CCS system and the most suitable sorbent or solvent. Sharma and Maréchal¹⁵ elaborated an energy analysis of a CCS system by temperature swing adsorption (TSA) on a diesel-fuelled engine of a truck. The main result obtained is that with a WERS taking the thermal energy exhaust gases in advantage and with PPN-6-CH₂-TETA as sorbent, the CCS system does not have penalisation over the ICE with a CCR of 90%. García and Llera⁵ presented an energy analysis of a CCS system with TSA operating with several sorbents. The CCS system is hybridised with an organic Rankine cycle (ORC) to supply the utilities of the CCS system. The main conclusion obtained is a 73% of CCR with MOF-74-Mg without penalisation over the engine.

Regarding absorption, Kumar *et al.*^{16,17} evaluated MEA, methyl diethanolamine (MDEA) and blends with NH₃ on a diesel-fuelled engine. The main result of these investigations is that MEA has a CO₂ reduction overcome 90% in any engine load condition. However, these research works do not describe how the regeneration process of the solvent in the CO₂ capture unit would be.

As shown above, CO₂ capture by absorption in ICEv has a few scientific developments, and this study aims to broaden the knowledge of this field. This research paper presents the first thermo-economic study of a CCS system onboard a natural gas (NG)-fuelled vehicle operating in the entire rpm operating range and under four engine load conditions. The CCS system proposed is subject to a sensitivity analysis using a primary and tertiary amine with 30 wt% in the solvent. Evaluations are carried out also with the hybridisation of an ORC that takes the exhaust gases' thermal energy to supply the amine-scrubbing and CO₂ compression utilities. The simulation of the different processes was carried out in Aspen Plus. The feasibility analysis aims at answering the following questions: (i) Is the intended heat integration of the exhaust gases with the CCS systems and ORC thermally feasible? (ii) What is the maximum CCR with the primary and tertiary amines? (iii) How much is the purchase cost of a vehicle with a CCS system installed? (iv) What is the power penalisation of the CCS over the engine performance?

Table 1. Technical specifications of the M936G engine.²⁰

Architecture	In-line 6-cylinder engine
Aspiration method	Turbocharged with Aftercooler
Injection	Multipoint
Valves per cylinder:	4
Bore [mm]	110
Stroke [mm]	135
Displacement volume [cm ³]	7700
Compression ratio	17
Brake Power [kW]	222 at 1950 rpm
Torque [Nm]	1200 at 1600 rpm

Methodology

The energy analysis of CO₂ capture on board an ICEv through amine scrubbing developed in this research involves integrating three systems: the ICE (CO₂ generator), the CCS system and the WERS. Ideally, the thermal energy required for CO₂ desorption should come from the exhaust gases of the vehicle's engine, and the electricity for the operation of the CCS system devices should come from the engine and from the WERS, which in the case of this study will be an ORC. After technical analysis, an economic analysis is performed. The evaluated total capital expenditure (CAPEX) will be used to establish whether the hybridisation of these three systems in an ICEv for CO₂ reduction is competitive with other CO₂ reduction technologies available in the market. Each component and procedure developed in the simulations are described below.

Engine selection and model

Engine selection

In the short and medium term, ICEvs will keep using carbon-based fuels while the transport sector migrates completely towards electrification. Gaseous fuels such as natural gas (mainly CH₄) will be one of the best choices because of the high lower heating value (LHV) and short carbon chain that produces less CO₂.^{18,19} On this basis, a heavy-duty turbocharged natural gas (NG) spark ignition (SI) engine of reference M936G has been selected to run the simulations. This engine is widely used in trucks and buses. The technical specifications of the engine are summarised in Table 1.

Engine simulation

The selected SI-ICE is simulated over AVL BOOST software to determine the pressure, temperature and concentration of the engine exhaust gases at the catalytic converter outlet. The simulations were performed at four engine load conditions (25, 50, 75 and 100%) in the rotational speed range of 1000–1900 rpm. The models used in the simulations are the Heywood, Patton and Nitschke model for the friction, the Woschni heat transfer model for the heat transfer in the cylinders, and the re-analogy for the heat transfer in the engine ducts. Finally, the air inlet is at standard conditions. The main input parameters to run the simulations are listed in Table 2.

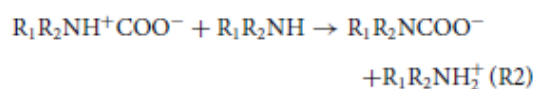
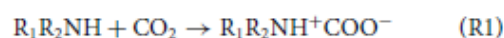
Engine model validation

The results of brake power (BP) and brake-specific fuel consumption (BSFC) obtained in the simulations are validated with the values given by the manufacturer for these variables.²⁰ As can be seen in Table 3, the maximum error between the simulation and the manufacturer values is 6.63%. Therefore, the results obtained in the engine simulation present an appropriate behaviour, considering that the pressure, temperature, concentration and exhaust gases mass flow are close to reality.

Model development of the amine-scrubbing and CO₂ compression facilities

Amine selection

Amines are organic compounds which have been used for CO₂ capture since the 1930s becoming a widely used effective method in the industry.²⁴ They are usually diluted in water in concentrations up to 30 wt%. Primary and secondary amines react with CO₂ to produce ammonium carbamates through the formation and deprotonation of zwitterion, as described in reactions 1 and 2.²⁵



Tertiary amine reaction does not form zwitterion. Tertiary amines produce an unstable carbamate, and an additional reaction leads to the generation of

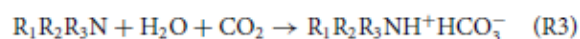
Table 2. Input parameters in AVL BOOST for the engine simulations.

Variable	Unit	M936G
Firing Order	NA	1,5,3,6,2,4
Star of combustion	CAD	−18
Combustion duration	CAD	57
A/F ratio	—	Stoichiometric combustion [16.75]
Maximum boost pressure ratio	—	2
Connecting Rod Length	mm	250
Lower heating value NG ^{21–23}	MJ/kg	48351

Table 3. Comparison engine results between the simulation and manufacturer chart.

Engine load [%]	rpm	Real ²⁰		Simulation		Error	
		BP [kW]	BSFC [g/kWh]	BP [kW]	BSFC [g/kWh]	BP [%]	BSFC [%]
100%	1000	110.0	200.00	110.17	192.04	−0.2%	4.0%
	1400	181.0	186.00	174.98	187.81	3.3%	−1.0%
	1600	204.0	188.00	197.27	188.33	3.3%	−0.2%
	1900	220.0	193.00	227.45	189.60	−3.39%	1.76%
75%	1000	82.5	225.00	82.91	221.52	−0.50%	1.54%
	1400	135.75	209.25	136	209.19	−0.18%	0.03%
	1600	153	211.50	153.6	211.57	−0.39%	−0.03%
	1900	165	217.13	166.3	217.29	−0.79%	−0.08%
50%	1000	55	270.00	55.26	269.47	−0.47%	0.19%
	1400	90.5	251.10	96.5	246.57	−6.63%	1.80%
	1600	102	253.80	104.36	253.61	−2.31%	0.07%
	1900	110	260.55	112.45	260.77	−2.23%	−0.09%
25%	1000	27.5	416.00	27.42	421.00	0.29%	−1.20%
	1400	45.25	386.88	45.26	387.11	−0.02%	−0.06%
	1600	51	391.04	50.69	391.21	0.61%	−0.04%
	1900	55	401.44	54.01	401.36	1.80%	0.02%

bicarbonate ions (reaction 3). This reaction increases theoretical CO₂ loading compared to primary and secondary amines.²⁶



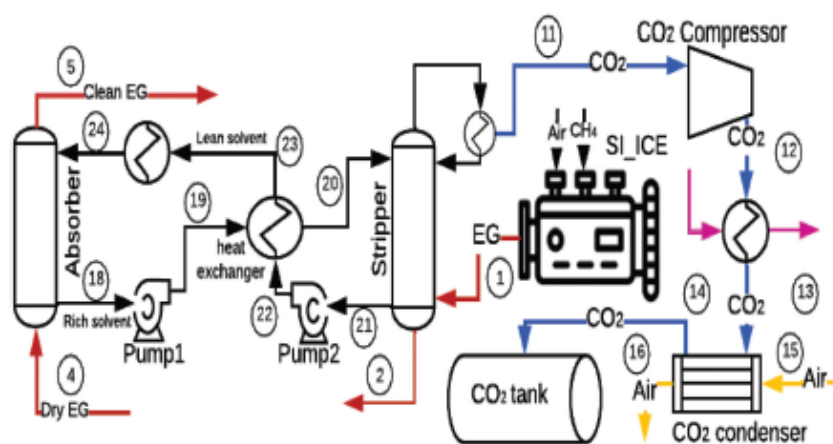
According to the literature, primary amines require more regeneration energy than tertiary amines.²⁷ The reported value for MEA is 5 MJ/kgCO₂, while MDEA presents values of 2.8 MJ/kgCO₂ with stripper temperatures between 100 and 120°C.²⁸ A similar behaviour presents the CO₂ loading capacity with values close to 0.6 molCO₂/mol_{amine} for amine

primaries²⁹ and 0.7 molCO₂/mol_{amine} for tertiary amines.³⁰ Despite this, primary and secondary amines are mainly used because carbamate formation exceeds those of bicarbonate. Several research works display that reaction constant can vary from 47740 m³/s/kmol for DETA³¹ to 8400 m³/s/kmol for MEA³² and 11.15 m³/s/kmol for MDEA.³⁰ Table 4 shows the main physical–chemical properties of the amines at a concentration of 30 wt%.

In the present research, a primary amine (MEA) and a tertiary amine (MDEA) have been selected to compare the maximum CO₂ capture rate (CCR).

Table 4. Amine properties at 30wt% and 313 K.

Solvent	Rate constant reaction [m ³ /kmol/s]	Absorption heat [kJ/kmol _{CO2}]	CO ₂ loading [molCO ₂ /mol _{amine}]	Reference
Ethanolamine (MEA)	8400	85.13	0.59	29, 33
Diethanolamine (DEA)	1340	74.24	0.61	29, 33, 34
Triethylamine (TEA)	16.8	66.59	0.38	29, 33, 34
Piperazine (Pz)	53700	80.58	0.91	35, 36
Aminomethyl propanol (AMP)	21000	80.91	0.78	29, 33, 34
Methyl diethanolamine (MDEA)	11.5	52.51	0.74	30, 37
Diethylenetriamine (DETA)	47000	89.48	1.414	38, 39, 40

Figure 1. Amine-scrubbing and CO₂ compression facilities diagram.

Capture rates are expected to depend on the variation of engine rotational speed and engine load conditions. The regeneration heat is obtained employing Eqn 1, which relates to the heat given up by the exhaust gases in the stripper (see Fig. 1) and the CO₂ mass captured.

$$Q_{\text{regeneration}} = \frac{Q_{\text{exhaust gases}}}{m_{\text{CO}_2\text{-storage}}} \quad (1)$$

CCS configuration

According to the literature, amine scrubbing has a great potential to be used as a technique of CO₂ capture onboard ICEv:⁷ Fig. 1 displays the amine scrubbing facility and the CO₂ compress process diagram. The exhaust gases from the ICE are used to heat the stripper and produce solvent regeneration (1, Fig. 1). The desorption temperature is set to 120°C to avoid corrosion problems and high solvent degradation. A pinch delta temperature of 10°C is assumed, whereby the exhaust gases at the stripper outlet are fixed to be

130°C (2, Fig. 1). After releasing heat in the ORC, the exhaust gases are cooled down and dried to 40°C before entering the bottom absorber (4, Fig. 1). The lean solvent enters at the top of the column (24, Fig. 1). The countercurrent flows of solvent and exhaust gases react in the absorber. The clean exhaust gas leaves the absorber at the top (5, Fig. 1). Rich solvent leaves the column at the bottom (18, Fig. 1), and it is pumped to the heat exchanger (19, Fig. 1), where the temperature is raised to 87°C before entering the top of the stripper (20, Fig. 1). Lean solvent abandons at 101°C and then goes to the heat exchanger and thus transfers thermal energy to the rich solvent (21-22, Fig. 1), reducing its temperature to 84°C. The lean solvent is cooled down until 40°C in a cooler before entering again in the absorber (23-24, Fig. 1). Finally, the water content in CO₂ flow is removed in the condenser, and high purity CO₂ gas flow goes to the compression stage (11, Fig. 1). Table 5 summarised the parameters assumed in the

Table 5. Parameters of the amine-scrubbing and CO₂ compression devices assumed in the simulations.

Device	Parameter	Value	Reference
Stripper	Operating temperature	120°C	41
Absorber	Operating temperature	40°C	42
Pumps 1 and 2	Isentropic efficiency	0.55	43
CO ₂ Compressor	Isentropic efficiency	0.65	43

Table 6. Parameter values for the calculation of the inlet pressure to the expander.

Variable	Value	Unit
Compressibility factor (Z)	0.73	NA
R	0.1186	kJ/kg·K
T _{sat} at 25% of engine load (6.8 bar)	395.13	K
ΔT _{SH} at 25% engine load (6.8 bar)	0	K
ΔT _{SH} at 50% engine load (6.8 bar)	10	K
ΔT _{SH} at 75% engine load (6.8 bar)	23	K
ΔT _{SH} at 100% engine load (6.8 bar)	39	K
ρ _{pump,in} at 1 bar (saturated liquid)	735.3	kg/m ³
η _{vol,exp}	0.45 ⁴³	NA
η _{vol,pump}	0.8 ⁴³	NA
β _{TV}	0.36	NA
β _{Vol}	0.5 ⁴³	NA
β _ω	0.2 ⁴³	NA

simulations for the devices in the amine-scrubbing and CO₂ compression facilities.

CO₂ compression stage

The CO₂ is stored as a liquid to reduce its volume. To achieve this condition, the CO₂ will be compressed from 1 bar to 75 bar (11-12, Fig. 1) with two cooling stages until it reaches 29°C. In the first cooling stage, the CO₂ releases heat to the ORC (12-13, Fig. 1), and in the second stage, the CO₂ is cooled with atmospheric air under standard conditions (13-14-15-16 Fig. 1). Finally, the CO₂ is stored in a tank, as seen in Fig. 1.

Organic cycle Rankine

Working fluid selection

Cyclopentane (C₅H₁₀) has been selected as a working fluid in the ORC. This working fluid (WF) has had excellent results in previous ORC research on ICEs.⁴⁴ Also, it is thermally stable at temperatures up to 350°C.⁴⁵ Another extensive factor for its selection is

that C₅H₁₀ has a limited environmental impact, low toxicity and is noncorrosive.⁴⁶

ORC configuration

The configuration of the ORC was made following the procedure developed by Fatigati *et al.*^{43,47} This procedure calculates the maximum inlet pressure in the expander using Eqn 2.

$$P_{\text{in,ex}} = ZR(T_{\text{sat}} + \Delta T_{\text{SH}}) \rho_{\text{pmp,in}} \beta_{\eta V} \beta_{\text{Vol}} \beta_{\omega} \quad (2)$$

This equation relates the inlet condition in the expander and pump of the ORC through dimensionless variables: $\beta_{\eta V}$ is the product of the volumetric efficiencies of the expander and pump; β_{Vol} is the ratio between the displacement volume of the pump and expander; and β_{ω} is the ratio between the rotational speed of the pump and the expander. Maximum inlet pressure also depends on the superheating temperature difference (ΔT_{SH}) that increases with the engine load. The rest of the parameters in Eqn 1 are summarised in Table 6.

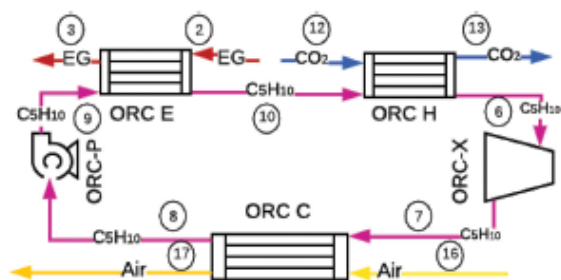


Figure 2. ORC layout used in the simulation.

For a pump inlet pressure of 1 bar, the maximum pressure obtained at the expander inlet is 9.05 bar. However, with the available heat in the exhaust gases after the stripper, the maximum saturation pressure achieved for the ORC cannot overcome 6.8 bar, whose value is less than the maximum allowed obtained with Eqn 2. So, the permeability value with 6.8 bar of expander inlet is 0.013 kg/MPa/s, which is a suitable permeability value according to the literature.⁴⁸

With the values of low and high pressure found above, the ORC operation is under subcritical conditions. As there are two sources of heat (from the exhaust gases (2-3) and from the CO₂ after the compression process (12-13), Fig. 2), the ORC will have two evaporators (9-10-6, Fig. 2). The pressure

drop value in the evaporators is 1.1 bar for each one, which is taken from the literature.⁴⁷ Finally, the ORC condenser cooling down the WF with air (7-8 and 16-17, Fig. 2), whose pressure drop is 0.2 bar.⁴⁷ This kind of ORC is called basic ORC (BORC).⁴⁹ Figure 2 displays the final configuration of the ORC, and Table 7 shows the values of the pressures and parameters considered for each device in the simulations.

Simulation of the hybridisation of the SI-ICE, CCS system and ORC

The amine scrubbing, CO₂ compression and ORC facilities were designed and modelled in Aspen plus. These systems have been integrated to use the residual heat in the exhaust gases in the desorption process and power production. Thus, to supply the power demand of the auxiliaries such as pumps and compressors considered in the simulations.

Figure 3 shows the hybridisation of the four systems mentioned above. Additional parameters are taken into account for the simulations: (i) concentration of the amine in the solvent is set to 30 wt%, (ii) mass fraction of the exhaust gases after the cooling down process is 17.9% CO₂, 3% H₂O and 79.1% N₂, and (iii) the full line pressure of the amine-scrubbing facility is maintained between 1 and 1.1 bar. Table 8 summarises

Table 7. Equipment conditions for ORC simulations.

Equipment	Parameter	Unit	Value	State	Fluid
ORC-C	Inlet pressure	bar	1.2	Vapour	C ₅ H ₁₀
	Overall heat transfer coefficient ⁵⁰	W/m ² K	500	NA	Air- C ₅ H ₁₀
ORC-P	Inlet pressure	bar	1	Saturated liquid	C ₅ H ₁₀
	Isentropic efficiency	NA	0.55	NA	
ORC-H	Inlet pressure	bar	9	Compressed liquid	C ₅ H ₁₀
	Overall heat transfer coefficient ⁵⁰	W/m ² K	150 Liquid-Gas	NA	C ₅ H ₁₀ -CO ₂
ORC-E	Inlet pressure	bar	7.9	Compressed liquid	C ₅ H ₁₀
	Overall heat transfer coefficient ⁵⁰	W/m ² K	70 Liquid-Gas 3000 Phase change 35 Gas-Gas	NA	C ₅ H ₁₀ -exhaust gas
ORC-X	Inlet pressure	bar	6.8	Vapour	C ₅ H ₁₀
	Isentropic efficiency	NA	0.65	NA	

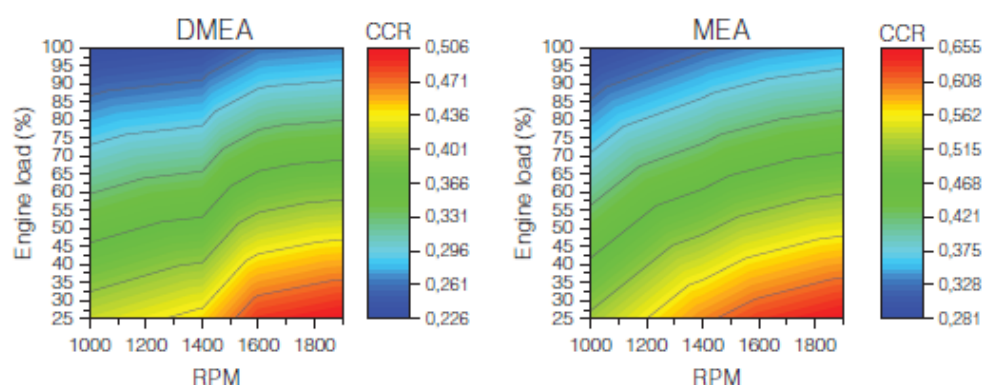


Figure 4. CCRs for MEA and MDEA over the entire rpm range and at partial engine loads.

all pressure and temperature values for each set point in the simulations. Since these parameters are established in the simulations, it proceeds to obtain the maximum CCR, the mass flow of solvent, WF and cooling air, as well as the power and thermal energy consumption of each device.

Results

Amine capture

Figure 4 shows the CCRs obtained in the amine-scrubbing facility with the two amines selected at partial engine load in the entire rpm range. There, it can be observed that the highest CCRs occur at the lower engine load conditions and highest rpm, with values of 0.506 and 0.655 for MDEA and MEA, respectively. The lowest values of the CCRs are presented, at high engine load and lower rpm, with values of 0.226 for MDEA and 0.281 for MEA.

Comparing the two amines, the solvent with MEA captures 14.9% more than MDEA at its best operating condition (25% engine load and 1900 rpm) and 5.5% more at the worst working condition (100% engine load and 1000 rpm). The tendency with both amines is similar; they present a high CCR at low engine loads and higher rpm and a lower CCR at high engine loads and lower rpm. The reason is that the mass of CO₂ captured, and the heat duty are the same for every engine load at a specific rotational speed (despite the increase in the exhaust gases' mass flow related to the engine load). These only increase with engine rotational speed and not with the engine load.

The heat duty for each rpm was always set up at 25 % of engine load with the aim that the stripper could

operate in the other engine load conditions. For this reason, the heat duty in the stripper is kept constant for both amines. Thus, the reaction rate constant controls the CO₂ capture. MEA has a higher reaction rate coefficient than MDEA and can react with more CO₂ in the absorber resulting in a higher solvent mass flow and CCR than MDEA. Regeneration heat is directly affected, as a lower mass of CO₂ is captured for the same heat duty with MDEA, producing a regeneration heat 33% higher than with MEA in the entire rpm range. This behaviour is because the CO₂ mass captured and the heat duty increase with the same slope. Figures 5 and 6 show the behaviours described above.

ORC heat exchanger areas

In order to be sure that the ORC can operate under all engine rpm and load conditions, the areas of the ORC and CO₂ compression system heat exchangers were obtained at the extreme points. Maximum engine load and 1900 rpm for the condensers and minimum load condition and 1000 rpm for the areas of the evaporators were set. Table 9 shows the resulting areas in the simulations with each solvent.

As is shown in the previous results, the total heat exchanger area in the ORC is 0.741 m² with the MEA solution and 0.509 m² with MDEA. This difference is since there is less WF mass flow in the ORC with MDEA than MEA because there is less solvent in the amine-scrubbing facility. This situation produces less demand for cooling, whereby the CCS system operating with MDEA requires less air mass flow of cooling than with MEA. This behaviour can be seen in Fig. 7.

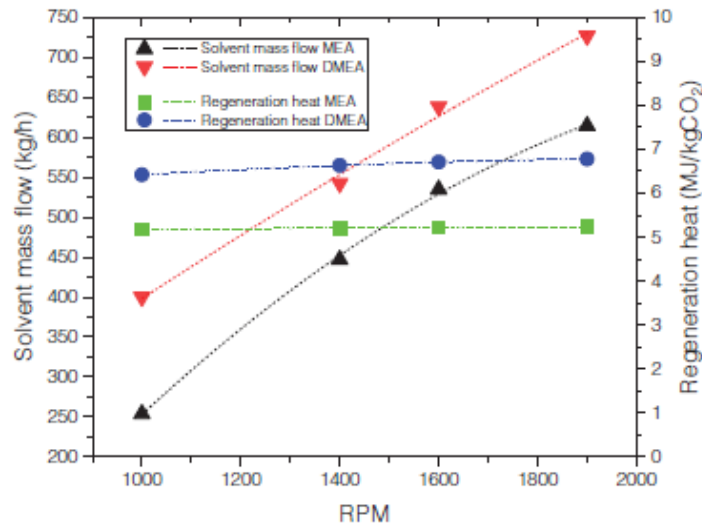
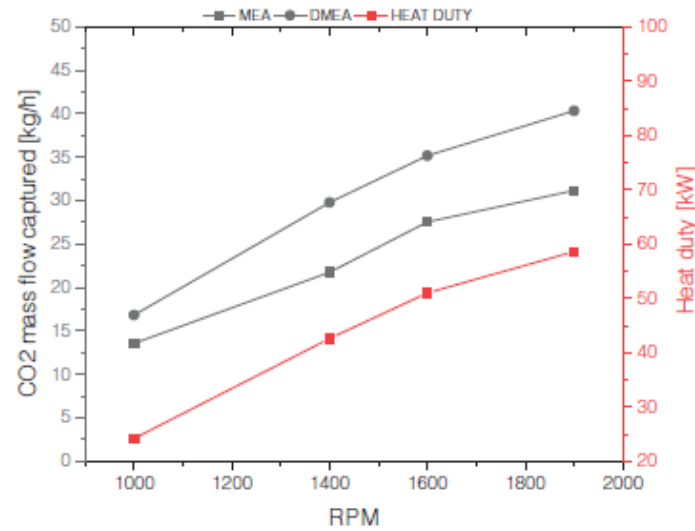


Figure 5. Solvent mass flow and regeneration heat for loading conditions.

Figure 6. Heat duty in stripper and CO₂ mass capturer with the amine selected.

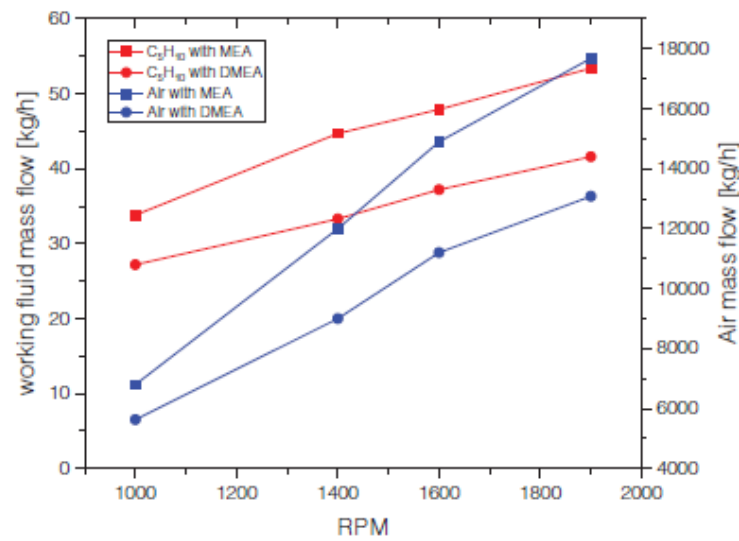
Energy analysis

The hybridisation of the ORC with the amine-scrubbing facility is done to further exploit the thermal energy available in the exhaust gases after the solvent regeneration process. This configuration tries to minimise the energy requirements of CO₂ storage, associated mainly with CO₂ compression. Figure 8 shows that the ORC thermal efficiency reaches a

maximum of 11% at 1900 rpm and 25% engine load and a minimum of 8.6% at 1000 rpm and full engine load. This behaviour is the same with both solvents in the ORC, as it only depends on the available heat from the exhaust gases after the stripper. Values agree with those reported in the literature for the simulation of internal combustion engines operating with ORC.^{48,51–53}

Table 9. Heat exchangers areas obtained in the simulations.

Amine	Heat exchanger	rpm	Engine load (%)	Exhaust gases mass flow (kg/h)	Area (m ²)	Variation (m ²)
MEA	Evaporator 1	1000	25	208.4	0.195	0.003
	Evaporator 2	1000	25	208.4	0.041	0.001
	ORC condenser	1900	100	754.7	0.361	0.0001
	CO ₂ condenser	1900	100	754.7	0.144	0.002
MDEA	Evaporator 1	1000	25	208.4	0.143	0.004
	Evaporator 2	1000	25	208.4	0.033	0.002
	ORC condenser	1900	100	754.7	0.284	0.001
	CO ₂ condenser	1900	100	754.7	0.109	0.003

**Figure 7. Working fluid and air mass flows in the ORC.**

The penalisation power percentage on the engine performance is calculated by adding the power ORC expander, the CO₂ compression power and the powers of the ORC and CCS pumps and dividing all this by the engine power (Eqn 3).

Power percentage

$$= \frac{-\dot{W}_{\text{ORC-X}} + \dot{W}_{\text{ORC-P}} + \dot{W}_{\text{Pump1}} + \dot{W}_{\text{Pump2}} + \dot{W}_{\text{CO}_2\text{-compressor}}}{\text{BP}} \quad (3)$$

Figure 9 shows that the CCS system with MEA and working with the ORC has a penalisation on the engine at its most critical point of 10.1%, while with MDEA, it

is 8%. The difference is that more CO₂ is captured with MEA, so more CO₂ compression power is required.

However, the simulations of the CCS system without ORC produce a penalisation on the engine power on average 1.5% higher than the CCS system with ORC for both solvents. In contrast, at the lowest point, the penalisation of the engine power is hardly noticeable.

Economic analysis

The economic analysis of the entire CCS is carried out with and without ORC for MEA and only with ORC for MDEA. Devices costs are obtained through equations found in the literature. The total capital investment (CAPEX) is completed after including the direct and

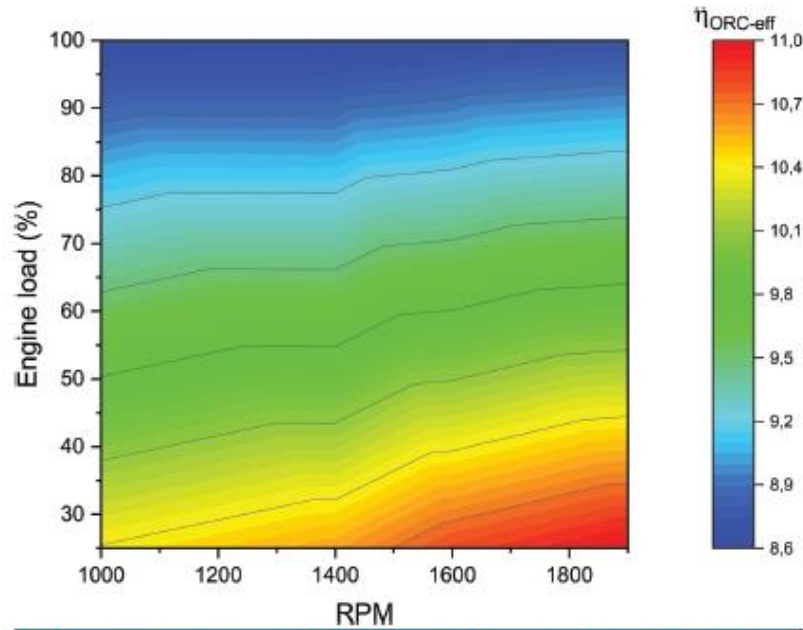


Figure 8. ORC efficiency over the entire engine rpm range and engine load conditions.

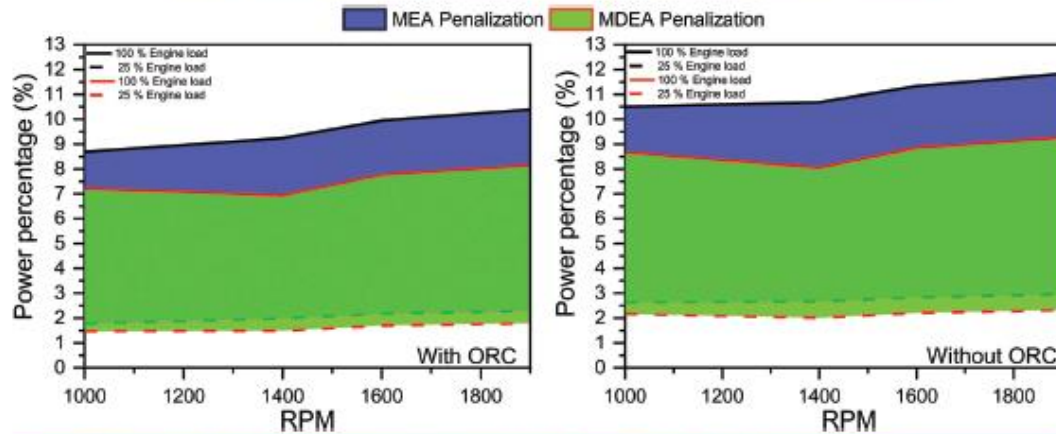


Figure 9. Percentage of power penalised of the engine by the CCS system with and without ORC.

indirect costs. Table 10 shows the equations used to calculate the CAPEX of the CCS system with the unit of waste heat recovery. The result is added to the value of an NG-fuelled bus, and they are compared with other commercial buses with CO₂ reduction technologies.

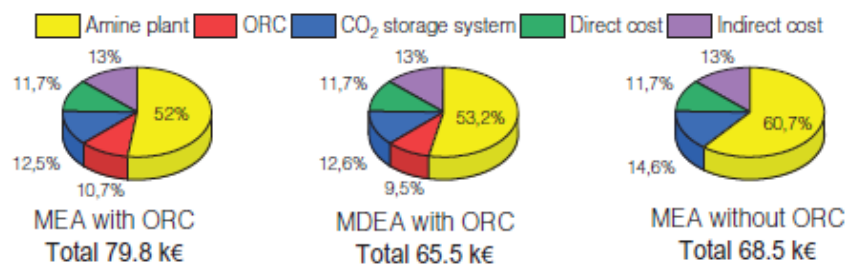
Figure 10 shows the percentage of the different items taken into account in the CAPEX and the total investment of the CCS system. It can be seen that amine plant cost has a weight greater than 50% in the

three cases, while the importance of the ORC cost over the total is between 9.5 and 10.7%, depending on the amine used in the amine plant. As mentioned above, this is due to the size of the heat exchangers and compressor of CO₂.

The results show that with MEA, the CAPEX is 14.3 k€ higher than with MDEA. This difference is because the CCS system with MEA has a higher CCR than MDEA, requiring larger devices, which increases its

Table 10. CO₂ capture equipment installation costs CAPEX.

Process	Equipment	Cost equation	Parameter (A)	Ref.
Amine plant	All equipment's	$26.094 \times 106(A/408)^{0.65}$	CO ₂ captured (t/h)	54, 55
ORC	ORC-X	$1.5(225+170A)$	Volume (m ³)	56
	ORC-P	$900(A/300)^{0.25}$	Power (kW)	57
	ORC-fan	$900(A/300)^{0.25}$	Power (kW)	
	ORC-C ₆ H ₁₀ tank	$31.5+16A$	Volume (L)	
	ORC-Evaporator	$190+310A$	Area (m ²)	
	ORC-H	$190+310A$	Area (m ²)	
	ORC-C	$190+310A$	Area (m ²)	
CO ₂ storage system	Condenser	$190+310A$	Area (m ²)	57
	Compressor	$267000(A/445)^{0.67}$	Power (kW)	58
	CO ₂ tank	$31.5+16A$	Volume (L)	57
Direct cost	Installing	8%A	Amineplant+ORC+CO ₂ storage system	Own criterion
	Instrumentation	5%A		
	Piping	1.5%A		
	Electric installing	1%A		
Indirect cost	Engineering	7%A	Amineplant+ORC+CO ₂ storage system+ direct cost	54
	Contingency	8%A		

**Figure 10. Total CAPEX and percentage weight of each item included in the CAPEX.**

cost. The CAPEX of the capture system without ORC using MEA is 14.1% lower regarding the base case. To conclude the economic viability of a bus with a CCS system, a search of bus prices that using different CO₂ reduction technologies such as hydrogen fuel cell buss (HFCB) and electric battery (EB) bus has been done. Table 11 shows the bus prices found.

According to the bus prices shown in Table 11, diesel bus is still the best alternative when it comes to the initial investment, as they are 8.5% cheaper than the base case. However, it is well known that high pollutant emissions, mainly particulate matter and nitrogen oxide emissions, are the Achilles heel of diesel buses. On the other hand, it is observed that the price of a bus with a CCS is about 40 percentage points below that of

hydrogen fuel cell and battery-electric buses.

From the obtained data, installing a capture system increases the cost of the CNG-fuelled bus by 18.3–21.3%. However, when the transport sector must pay for carbon Permits, the CCS in ICEv and the fuel cell system will be the best choice for the conventional vehicle. Based on the above, the fuel cell bus becomes more relevant because it does not emit CO₂. In the second place, it would be the vehicle with a capture system as it would achieve a CO₂ reduction of up to 66%, making it much more competitive than its conventional diesel counterpart. However, CCR is not enough to reach a totally CO₂-neutral system, unlike electric and hydrogen cell vehicles. Nevertheless, a bus

Table 11. Purchase of passenger transport buses in euros.

Technology or fuel	Value (k€)	Difference from the base case (%)	Reference
Compressed NG (CNG)	374.6	0.0	59, 60
Diesel	342.9	8.5	60
HFCB	650	-73.5	61
EB	604	-61.2	62
CNG+CCS+ORC	454.4	-21.3	This study
CNG+CCS	443.1	-18.3	This study

with a CCS system with a 1 m³ storage tank at the conditions set out in this study could have autonomy up to 600 km (calculated with fuel consumption of 0.68 kg/km⁶³), which is 2.4 times longer than the current maximum range of commercial electric vehicles, which is 250 km on average.⁶⁴

Conclusions

A thermo-economic study of onboard CO₂ capture using amine scrubbing of a vehicle powered by a spark-ignition turbocharged internal combustion engine operating on natural gas has been carried out. According to the obtained results, the amine with the highest potential for CO₂ capture is MEA, having a higher CO₂ capture rate than MDEA under the whole range of engine operating conditions. However, the thermal integration of the exhaust gases with the CCS systems and ORC is technically feasible only for the CCS system. Because the exhaust gases can cover the desorption process of the CO₂ captured, but with the thermal energy remaining in the exhaust gases after the stripper, the ORC cannot produce enough power to reduce the penalisation on the performance engine. Also, incorporating an ORC into the capture system does not offer a real benefit in terms of energy and economy. On the contrary, it would add weight and volume to the bus, increasing the vehicle's operating and maintenance costs.

The present study provides a first approximation to the use of amines in onboard capture. It would also be necessary to conduct detailed research on the reaction of amines with other pollutants in the exhaust gases, absorber and stripper sizing and engine operation problems due to the resistance offered by the systems to the exhaust gases detrimental to engine performance.

Although this type of application in the transport sector is still in its initial research phase, the

thermo-economic results obtained in this research show that a CCS by amine scrubbing with MEA and without ORC can become a competitive alternative to BEV and FCV, in particular in long distances. These capture-equipped vehicles will bring the transport sector closer to meeting the CO₂ reduction targets set by the European Union.

References

1. Kouridis C, Vlachokostas C. Towards decarbonising road transport: Environmental and social benefit of vehicle fleet electrification in urban areas of Greece. *Renewable Sustainable Energy Rev.* 2022;153:111775.
2. Auer M, Ganzer G, Müller-Baum P, Stiesch G. Synthetic fuels in large engines - how internal combustion engines become CO₂-neutral. *MTZ Worldwide.* 2019;80(3):48-51.
3. L'Orange Seigo S, Dohle S, Siegrist M. Public perception of carbon capture and storage (CCS): a review. *Renewable Sustainable Energy Rev.* 2014;38:848-63.
4. Rubin ES. Understanding the pitfalls of CCS cost estimates. *Int J Greenhouse Gas Control.* 2012;10:181-90.
5. García-Mariaca A, Llera-Sastresa E. Review on carbon capture in ICE driven transport. *Energies.* 2021;14:6865.
6. Leeson D, Mac Dowell N, Shah N, Petit C, Fennell PS. A Techno-economic analysis and systematic review of carbon capture and storage (CCS) applied to the iron and steel, cement, oil refining and pulp and paper industries, as well as other high purity sources. *Int J Greenhouse Gas Control.* 2017;61:71-84.
7. Sullivan JM, Sivak M. Carbon capture in vehicles: a review of general support, available mechanisms, and consumer acceptance issues [Internet]. University of Michigan Transportation Research Institute; 2012. Available from: <http://deepblue.lib.umich.edu/handle/2027.42/90951>
8. Schmauss TA, Barnett SA. Viability of vehicles utilising on-board CO₂ capture. *ACS Energy Letters.* 2021;6:3180-4.
9. Awoyomi A, Patchigolla K, Anthony EJ. CO₂/SO₂ emission reduction in CO₂ shipping infrastructure. *Int J Greenhouse Gas Control.* 2019;88:57-70.
10. Stec M, Tatarczuk A, Iluk T, Szul M. Reducing the energy efficiency design index for ships through a post-combustion carbon capture process. *Int J Greenhouse Gas Control.* 2021;108(May 2020).
11. Güler E, Ergin S. An investigation on the solvent based carbon capture and storage system by process modeling and

- comparisons with another carbon control methods for different ships. *Int J Greenhouse Gas Control*. 2021;110:103438.
12. Ros JA, Skylogianni E, Doedée V, van den Akker JT, Vredevelde AW, Linders MJG, et al. Advancements in ship-based carbon capture technology on board of LNG-fuelled ships. *Int J Greenhouse Gas Control*. 2022;114:103575.
 13. Luo X, Wang M. Study of solvent-based carbon capture for cargo ships through process modelling and simulation. *Appl Energy*. 2017;195:402–13.
 14. Feenstra M, Monteiro J, van den Akker JT, Abu-Zahra MRM, Gilling E, Goetheer E. Ship-based carbon capture onboard of diesel or LNG-fuelled ships. *Int J Greenhouse Gas Control*. 2019;85(March):1–10.
 15. Sharma S, Maréchal F. Carbon dioxide capture from internal combustion engine exhaust using temperature swing adsorption. *Front Energy Res*. 2019;7(December):1–12.
 16. Kumar P, Rathod V, Parwani AK. Experimental investigation on performance of absorbents for carbon dioxide capture from diesel engine exhaust. *Environ Prog Sustainable Energy*. 2021;e13651.
 17. Saravanan S, Kumar R. Experimental investigations on CO₂ recovery from engine exhaust using adsorption technology. *SAE Technical Paper*. 2019;28:2577.
 18. Osorio-Tejada JL, Llera-Sastresa E, Scarpellini S. Liquefied natural gas: Could it be a reliable option for road freight transport in the EU? *Renewable Sustainable Energy Rev*. 2017;71:785–95.
 19. Mottschall M, Kasten P, Rodriguez F. Decarbonization of on-road freight transport and the role of LNG from a German perspective. *Öko-institut eV, International 2020*, Berlin.
 20. Mercedes-Benz. Citaro NGT technical information [Internet]. 2017 [cited 2020 Feb 8]. Available from: https://www.mercedes-benz-bus.com/content/dam/mbo/markets/common/buy/services-online/download-technical-brochures/images/content/regular-service-buses/citaro-ngt/MB-NGT-2-ES-09_17.pdf
 21. Obiols J, Soler D, Dioc N, Moreau M. Potential of concomitant injection of CNG and gasoline on a 1.6L gasoline direct injection turbocharged engine. *SAE Technical Papers*. 2011.
 22. López JJ, Novella R, Gomez-Soriano J, Martínez-Hernández PJ, Rampanarivo F, Libert C, et al. Advantages of the unscavenged pre-chamber ignition system in turbocharged natural gas engines for automotive applications. *Energy*. 2021;218:119466.
 23. Yontar AA, Doğu Y. Effects of equivalence ratio and CNG addition on engine performance and emissions in a dual sequential ignition engine. *Int J Engine Res*. 2020;21(6):1067–82.
 24. Wu Y, Xu J, Mumford K, Stevens GW, Fei W, Wang Y. Recent advances in carbon dioxide capture and utilisation with amines and ionic liquids. *Green Chemical Engineering*. 2020;1(1):16–32.
 25. Gouedard C, Picq D, Launay F, Carrette PL. Amine degradation in CO₂ capture. I. A review. *Int J Greenhouse Gas Control*. 2012;10:244–70.
 26. Chowdhury FA, Yamada H, Higashii T, Goto K, Onoda M. CO₂ capture by tertiary amine absorbents: A performance comparison study. *Ind Eng Chem Res*. 2013;52(24):8323–31.
 27. Romeo LM, Minguel D, Shirmohammadi R, Andrés JM. Comparative analysis of the efficiency penalty in power plants of different amine-based solvents for CO₂ capture. *Ind Eng Chem Res*. 2020;59(21):10082–92.
 28. Cuccia L, Dugay J, Bontemps D, Louis-Louis M, Vial J. Analytical methods for the monitoring of post-combustion CO₂ capture process using amine solvents: A review. *Int J Greenhouse Gas Control*. 2018;72:138–51.
 29. Sada E, Hidehiro K, Butt MA. Gas absorption with consecutive chemical reaction: absorption of carbon dioxide into aqueous amine solutions chemical absorption mechanism. *Can J Chem Eng*. 1976;54(5):421–4.
 30. Ali BS, Aroua MK. Effect of piperazine on CO₂ loading in aqueous solutions of MDEA at low pressure. *Int J Thermophys*. 2004;25(8):1863–70.
 31. Hartono A, da Silva EF, Svendsen HF. Kinetics of carbon dioxide absorption in aqueous solution of diethylenetriamine (DETA). *Chem Eng Sci*. 2009;64(14):3205–13.
 32. Hikita H, Asai S, Katsu Y, Ikuno S. Absorption of carbon dioxide into aqueous monoethanolamine solutions. *AIChE J*. 1979;25(5):793–800.
 33. el Hadri N, Quang DV, Goetheer ELV, Abu Zahra MRM. Aqueous amine solution characterisation for post-combustion CO₂ capture process. *Appl Energy*. 2017;185:1433–49.
 34. Kim YE, Lim JA, Jeong SK, Yoon Y, Il, Bae ST, Nam SC. Comparison of carbon dioxide absorption in aqueous MEA, DEA, TEA, and AMP solutions. *Bull Korean Chem Soc*. 2013;34(3):783–7.
 35. Chen X, Rochelle GT. Aqueous piperazine derivatives for CO₂ capture: accurate screening by a wetted wall column. *Chem Eng Res Des*. 2011;89(9):1693–710.
 36. Bishnoi S, Rochelle GT. Absorption of carbon dioxide into aqueous piperazine: Reaction kinetics, mass transfer and solubility. *Chem Eng Sci*. 2000;55(22):5531–43.
 37. Wang Y, Zhao L, Otto A, Robinus M, Stolten D. A review of post-combustion CO₂ capture technologies from coal-fired power plants. *Energy Procedia*. 2017;114(November 2016):650–65.
 38. Derks PWJ, Versteeg GF. Kinetics of absorption of carbon dioxide in aqueous ammonia solutions. *Energy Procedia*. 2009;1(1):1139–46.
 39. Fu K, Sema T, Liang Z, Liu H, Na Y, Shi H, et al. Investigation of mass-transfer performance for CO₂ absorption into diethylenetriamine (DETA) in a randomly packed column. *Ind Eng Chem Res*. 2012;51(37):12058–64.
 40. Kim YE, Moon SJ, Yoon Y II, Jeong SK, Park KT, Bae ST, et al. Heat of absorption and absorption capacity of CO₂ in aqueous solutions of amine containing multiple amino groups. *Sep Purif Technol*. 2014;122:112–8.
 41. Nakagaki T, Yamabe R, Furukawa Y, Sato H, Yamanaka Y. Experimental evaluation of temperature and concentration effects on heat of dissociation of CO₂-loaded MEA solution in strippers. *Energy Procedia*. 2017;114:1910–8.
 42. Sonderby TL, Carlsen KB, Fosbel PL, Kierboe LG, von Solms N. A new pilot absorber for CO₂ capture from flue gases: measuring and modelling capture with MEA solution. *Int J Greenhouse Gas Control*. 2013;12:181–92.
 43. Fatigati F, di Battista D, Cipollone R. Permeability effects assessment on recovery performances of small-scale ORC plant. *Appl Therm Eng*. 2021;196:117331.
 44. Invernizzi CM, Iora P, Manzolini G, Lasala S. Thermal stability of n-pentane, cyclo-pentane and toluene as working fluids in organic Rankine engines. *Appl Therm Eng*. 2017;121:172–9.

45. Invernizzi CM, Bonalumi D. Thermal stability of organic fluids for organic Rankine cycle systems. *Organic Rankine cycle (ORC) power systems: technologies and applications*. Elsevier; 2017. p. 121–51.
46. Scaccabarozzi R, Tavano M, Invernizzi CM. Comparison of working fluids and cycle optimisation for heat recovery ORCs from large internal combustion engines. *Energy*. 2018;158:396–416.
47. Fatigati F, di Bartolomeo M, di Battista D, Cipollone R. Experimental and numerical characterization of the sliding rotary vane expander intake pressure in order to develop a novel control-diagnostic procedure. *Energies (Basel)*. 2019;12(10):1970.
48. Fatigati F, di Bartolomeo M, di Battista D, Cipollone R. Experimental characterisation of a hermetic scroll expander operating in an ORC-based power unit bottoming an internal combustion engine. In: *AIP Conference Proceedings*. American Institute of Physics Inc.; 2019.
49. Peris B, Navarro-Esbri J, Molés F. Bottoming organic Rankine cycle configurations to increase internal combustion engines power output from cooling water waste heat recovery. *Appl Therm Eng*. 2013;61(2):364–71.
50. Kind M, Martin H. *VDI Heat atlas*. Second. Berlin: Springer; 2010. p. 1–1609.
51. Badescu V, Aboaltaboq MHK, Pop H, Apostol V, Prisecaru M, Prisecaru T. Design and operational procedures for ORC-based systems coupled with internal combustion engines driving electrical generators at full and partial load. *Energy Convers Manage*. 2017;139:206–21.
52. Shu G, Zhao M, Tian H, Wei H, Liang X, Huo Y, et al. Experimental investigation on thermal OS/ORC (Oil Storage/Organic Rankine Cycle) system for waste heat recovery from diesel engine. *Energy*. 2016;107:693–706.
53. Hoang AT. Waste heat recovery from diesel engines based on organic Rankine cycle. *Appl Energy*. 2018;231(March):138–66.
54. Abu-Zahra MRM, Niederer JPM, Feron PHM, Versteeg GF. CO₂ capture from power plants. Part II. A parametric study of the economical performance based on mono-ethanolamine. *Int J Greenhouse Gas Control*. 2007;1(2):135–42.
55. Bailera M, Espatolero S, Lisbona P, Romeo LM. Power to gas-electrochemical industry hybrid systems: A case study. *Appl Energy*. 2017;202:435–46.
56. Astolfi M. Techno-economic optimization of low temperature CSP systems based on ORC with screw expanders. *Energy procedia*; 2015:1100–12.
57. Quoilin S, Declaye S, Tchanche BF, Lemort V. Thermo-economic optimisation of waste heat recovery organic Rankine cycles. *Appl Therm Eng*. 2011;31(14–15):2885–93.
58. De Saint Jean M, Baurens P, Bouallou C, Couturier K. Economic assessment of a power-to-substitute-natural-gas process including high-temperature steam electrolysis. *Int J Hydrogen Energy*. 2015;40(20):6487–500.
59. Ally J, Pryor T. Life cycle costing of diesel, natural gas, hybrid and hydrogen fuel cell bus systems: an Australian case study. *Energy Policy*. 2016;94:285–94.
60. Holland SP, Mansur ET, Muller NZ, Yates AJ. The environmental benefits of transportation electrification: urban buses. *Energy Policy*. 2021;148.
61. Spindel J, Papageorgopoulos D, Satyapal S. *Fuel Cell Technologies Program Record 12012: Fuel Cell Bus Targets*. 2012.
62. Quarles N, Kockelman KM, Mohamed M. Costs and benefits of electrifying and automating bus transit fleets. *Sustainability*. 2020;12(10):3977.
63. Stempien JP, Chan SH. Comparative study of fuel cell, battery and hybrid buses for renewable energy constrained areas. *J Power Sources*. 2017;340:347–55.
64. Wenz KP, Serrano-Guerrero X, Barragán-Escandón A, González LG, Clairand JM. Route prioritisation of urban public transportation from conventional to electric buses: A new methodology and a study of case in an intermediate city of Ecuador. *Renewable Sustainable Energy Rev*. 2021;148:111215.

7 CONCLUSIONS, SCIENTIFIC CONTRIBUTIONS AND FUTURE RESEARCH AND ENDEAVOURS

7.1 CONCLUSIONS

The transportation sector's electrification is advancing steadily. However, despite ongoing progress and the various alternatives available on the market, the persistent increase in CO₂ emissions from heavy transport continues to pose a significant challenge. This issue requires a different approach to meet the objectives set by the European Union. Consequently, exploring alternatives to reduce the carbon footprint in the transportation sector is imperative. To offer solutions for reducing CO₂ emissions in this sector, this thesis proposes and analyses an innovative CO₂ capture and storage (CCS) system designed to adapt to the various operating conditions of heavy-duty internal combustion engine vehicles (HD-ICEVs).

According to the bibliographic review conducted, a higher level of research is observed in the maritime sector compared to road transport. It is also evident the exhaust gases can be used for CO₂ desorption. In particular, on ships, the ICE regularly operates in a constant regime, which implies less variation in the EG mass flow. This behaviour along with the ample space on ships to install additional equipment makes the amine-scrubbing process more suitable for these characteristics. In contrast, HD-ICEVs operate with frequent accelerations and decelerations, causing continuous variations in the EG mass flow. Additionally,

the limited space in these vehicles poses a challenge when installing the necessary equipment for a CAC system. In this context, adsorption emerges as the most viable option, as it operates with fixed beds that can be regenerated using the EG waste heat. Being a cyclic process, desorption times and equipment sizes can be tailored to the specific operating conditions of the vehicle.

The results confirmed that the waste heat contained in the EG can cover all the thermal energy demands in the CCS system operating with temperature swing adsorption (TSA). Furthermore, hybridising the organic Rankine cycle (ORC) is advantageous since, depending on the sorbent used, the penalty imposed by the CCS system on the engine power varies between 1.9% and 23.5% at a 100% CO₂ capture rate (CCR). These results corroborate that implementing an ORC as a complement to a CCS system is theoretically feasible from an energy point of view. Additionally, a dynamic analysis revealed that the CCS-ORC system produces a slight increase in engine power of 4.93%, which leads to an increase in fuel consumption of 10%. Likewise, it was found that the energy consumption for CO₂ capture is, on average, 450 kJ/kgCO₂ at 100% of CCR and 150 kJ/kgCO₂ at 70% of CCR, which is almost 50% less than reported in the literature. These promising results are mainly due to the integration of the ORC and the thermal configuration of the devices proposed in this thesis.

On the other hand, no significant difference was observed in the values obtained from the volume and weight of the CAC-COR system when operating with the sorbents selected for the study. This similarity is attributed to the fact that the TSA device merely contributes, on average, 6% to the weight and volume of the CAC-COR system. The study further revealed that the engine size does not substantially influence the operation of the CCS-ORC system as the parasitic loads caused by the CCS-ORC system remain almost constant, with average values of 2.9% at 70% of CCR and 9% at 100% of CCR. In contrast, the type of sorbent is a predominant factor in the performance behaviour of the CAC-COR system. The CCS-ORC system exhibited a suitable performance with the PPN and MOF sorbents, and both displayed similar energy behaviour. However, when carbon active was used, the CCS-ORC system incurred higher parasitic loads and energy consumption to capture CO₂, with an average of 15% across all engine loads and rpm ranges. This increase is due to the low selectivity of activated carbon, leading to a higher concentration of N₂ impurities in the captured CO₂. Consequently, this requires higher compression power to liquefy CO₂ and escalates energy consumption for CO₂ capture compared to MOF and PPN sorbents. Therefore, ideal sorbent properties should include low heat of adsorption, high selectivity and the ability to tolerate small fractions of water if complete drying of the EG is not achieved. Based on these criteria, the sorbent that most closely aligns with these characteristics is PPN. However, this type of

sorbent is still in laboratory production, so it would not yet be a viable option for immediate implementation.

As previously mentioned, no significant differences are observed in the energy behaviour results attributed to the engine's size. However, concerning the available space for integrating the CCS-ORC system and in the economic analysis carried out in this thesis, significant differences related to the engine size were found. For large engine, analysed in a bus, the impact vehicle's usable volume is only 3.4%. In contrast, in the vehicle with the smallest engine (VAN), the required volume to install the CCS-ORC system is 10.2%. Furthermore, CAPEX results show that the increase in initial investment for a bus with an integrated CCS-ORC system is barely higher than that of the base bus and is 29% lower compared to other existing zero-emission technologies for buses. Conversely, the initial investment for VAN with an integrated CCS-ORC system is not feasible as its cost increases by 25% compared to electrical technologies and almost 50% compared to the base VAN.

On the other hand, it is observed that the payback on investment of a system like the one proposed in this thesis, evaluated throughout the lifespan of an HD-ICEV (10 years), is significantly impacted by the increase in the fuel consumption necessary to cover the parasitic loads, as well as of the cost of the equipment and the maintenance and operation of the CCS-ORC system. However, the carbon abatement cost (CAC) values obtained are between 19 and 47 €/tCO₂ at 100% of CCR, which is up to 50% lower than other proposals for CCS systems developed for different industries. Based on these results, the transport sector could consider this investment, which is not very high, if it is to meet the CO₂ reduction objectives established by the European Union for the year 2050.

According to the sensitivity analyses carried out in the techno-economic assessment, the value of the CO₂ tax that the transport sector would need to pay to recover the initial investment in the vehicle lifespan must be greater than 65 €/tCO₂. Furthermore, if the CO₂ captured is sold as a raw material for the production of synthetic fuels, this could offset the vehicle's operating cost and provide additional income, thereby increasing the benefits derived from integrating a CCS-ORC system. This would reduce the payback time or the price of the CO₂ tax. Likewise, it would prevent the CO₂ captured from being stored underground, giving a productive value to this emission.

In the case of absorption, the results show that the MEA has the highest CO₂ capture potential, surpassing the MDEA in the entire range of engine operating conditions. However, the thermal integration of EG waste heat with CCS and ORC systems is technically feasible only for the CCS system. This is because the waste heat from the EG can cover only the thermal demand of the CO₂ desorption process. Therefore, hybridising an ORC with the CCS system is not feasible since

it increases the weight, volume and cost of the CCS-ORC system. These increases are not compensated since the ORC cannot generate enough power to cover the parasitic loads generated by the CCS system using the EG waste heat available after passing through the stripper.

In summary, this study reveals that integrating the CCS-ORC system into an HD-ICEV holds considerable promise from both the absorption and adsorption processes from the perspective of CO₂ mitigation and a medium-term techno-economic approach. The proposed integration has the potential to reduce CO₂ emissions from the transport sector and supply CO₂ for the production of synthetic fuels. For this to be fully functional, the ICEs of these vehicles should operate on natural gas, as it yields lower CO₂ emissions compared to those powered by diesel or gasoline, thus allowing for greater CO₂ storage capacity. Furthermore, using synthetic fuels from captured CO₂ opens the opportunity for a circular and sustainable transportation system focused on ICEs, a widely recognised and established technology. Therefore, it is necessary to carry out experimental studies to validate the CCS-ORC system under real world conditions and address the existing knowledge gap. Such measures will enable the development of a feasible solution that supports the complete decarbonisation of this energy-intensive sector

7.2 SCIENTIFIC CONTRIBUTIONS

The main contributions of this thesis are related to innovative proposals and explorations of the technical issues involved in developing CO₂ capture and storage technologies in heavy transport vehicles. In this case, the problems addressed were the adaptability of the capture and storage system to operate at different load conditions and engine rpms and the need for knowledge of the economic impact that integrating this type of system in a vehicle would entail. This perspective differs entirely from previous works found in the literature and patents that address the issue of configuring the CO₂ capture and storage system but with the engine operating under a single operating condition [64,74]. The main contributions of this thesis are summarized below:

- First energy validation of integrating an ORC that takes the EG waste heat coming from an ICE to produce power and thus supply the power demand of a CCS system integrated into a heavy-duty vehicle.
- First thermal design and energy analysis of a CCS system operating by TSA and another by amine-scrubbing, able to work under different operating conditions of an ICE
- First energy evaluation of three different sorbents and two amines operating in a CCS system on board a heavy transport vehicle
- First conceptual design, sizing, and thermal modelling of a CCS system and its CO₂ capture unit operating with TSA.

- First techno-economic analysis of a CCS system, obtaining variables such as initial investment costs, carbon abatement costs, and investment payback.
- First calculation of performance penalties on the engine due to the integration of a CCS system operating by TSA working under the dynamic conditions of an ICE was obtained.

Other complementary contributions resulting from this thesis are:

- Elaboration of the first bibliographic review of CO₂ capture and storage systems for mobile sources was conducted, classifying them by CO₂ capture method and technique.
- Participation in the national research project titled: Decarbonisation of energy-intensive sectors. CO₂ capture in gas engines for the circularisation of sustainable synthetic fuels and viability of the storage of pollutants (CAPTICES) 2022-2025.
- Application of research project to regional call, titled: Techno-economic study of the adsorption capture with zeolites for closing the CO₂ cycle in the road transport sector (Z-CAT)

The scientific contributions presented at international conferences during the development of the thesis are:

- García Mariaca, Alexander and Llera, Eva, Dynamic CO₂ Capture in a Natural Gas Engine Used in Road Freight Transport. Proceedings of the 16th Greenhouse Gas Control Technologies Conference (GHGT-16), 23-24 Oct 2022, Lyon France.
- García Mariaca, Alexander, Llera, Eva and Francisco Moreno, Energy Analysis of a Mobile CCS-ORC System Operating in a Heavy-Duty Engine. Proceedings of the International Conference on Efficiency, Cost, Optimization, Simulation and Environmental Impact of Energy Systems (ECOS 2024), 30 June - 5 July, 2024, Rhodes, Greece.
- Alexander García Mariaca, Jorge Perpiñan, Manuel Bailera, Eva Llera-Sastresa, Begoña Peña, Techno-Economic analysis of the Integration of Mobile-CCS and PTG in a Heavy Vehicle Fleet. Proceedings of the 19th Conference on Sustainable Development of Energy, Water and Environment Systems (SDEWES-19), 8 – 12 September 2024. Rome, Italy
- Alexander García-Mariaca, Eva Llera-Sastresa, Francisco Moreno, Luis M Romeo, Energy Efficiency Evaluation of a Mobile CCS-ORC System in Operation with a Heavy-Duty Engine. Proceedings of the 17th International Conference on Greenhouse Gas Control Technologies (GHGT-17), 20 -24 October 2024, Calgary Canada

Finally, the thesis has contributed to training in human resources for science, technology and innovation through the preparation of three final degree projects titled:

- Development of a simplified model for the analysis of the operation of a natural gas spark engine. Rosana Blecua Arilla, 2020.
- Thermal modeling of a zeolite bed for CO₂ capture by temperature swing adsorption. Alejandro Aparacio, (in progress).
- Design of the evaporator of an organic Rankine cycle to drive a CO₂ capture system in engines. Raúl Alvira, (in progress).

7.3 FUTURE RESEARCH ENDEAVOURS

Integrating CCS-ORC systems in heavy-duty vehicles involves complex activities that must be addressed from an interdisciplinary approach to address all the concepts necessary for real implementation. Based on this, future works should focus in the following directions:

- Experimental validation with the engine operating at partial loads and in a transient state to know:
 - The increase in engine back pressure, caused by the installation of additional systems in the exhaust gases duct.
 - The operation of the TSA device, including sorbent regeneration times and maximum CCRs.
 - The sorbent's or solvent's degradation due to their interaction with other polluting emissions such as nitrogen oxides, carbon dioxide, and unburned hydrocarbons.
 - The behaviour of the CCS-ORC system considering the thermal inertia.
 - The increase in the engine fuel consumption to fulfil the parasitic loads provoked by the operation of the CCS system.
- Life cycle analysis to conclude the feasibility of installing a CAC system in mobile sources.
- Theoretical and experimental evaluation of the CCS-ORC system under various climatic conditions.
- Detailed design of the CCS-ORC system, which includes the selection of materials, sizing, possible location in the vehicle, structural loads, maintenance, operation and control in the system's operation.
- Optimization of the cooling systems of the CCS-ORC system
 - In the case of the CCS-ORC absorption system, the sizing of the absorber and scrubber

CONCLUSIONES, APORTACIONES CIENTIFICAS Y TRABAJOS FUTUROS

CONCLUSIONES

La electrificación en el sector del transporte avanza paulatinamente. No obstante, a pesar de los continuos progresos y de las diversas alternativas disponibles en el mercado, el incremento persistente de las emisiones de CO₂ originadas por el transporte pesado sigue representando un desafío significativo. Este problema requiere un enfoque distinto para cumplir con los objetivos establecidos por la Unión Europea. En consecuencia, resulta imperativo explorar alternativas para reducir la huella de carbono en el sector del transporte. Con el propósito de ofrecer soluciones para la reducción de emisiones de CO₂, esta tesis propone y analiza un innovador sistema de captura y almacenamiento de CO₂ (CAC), diseñado para adaptarse a las diversas condiciones operativas de los vehículos de trabajo pesado con motores de combustión interna.

Según la revisión bibliográfica realizada, se observa un mayor nivel de investigación en el sector marítimo en comparación con el transporte por carretera. Se evidencia también que el calor residual de los gases de escape se puede utilizar para la desorción del CO₂. En particular, en los barcos, los motores de combustión interna operan regularmente a un régimen constante, lo que implica una menor variación en el flujo másico de los gases de escape. Este comportamiento, junto con el amplio espacio disponible en los barcos para instalar equipos adicionales hace que el proceso de lavado con aminas sea más adecuado

para estas características. En contraste, los vehículos de trabajo pesado con motor de combustión interna operan con frecuentes aceleraciones y desaceleraciones, lo que provoca variaciones continuas en el flujo másico de los gases de escape. Además, el espacio limitado disponible en estos vehículos dificulta la instalación del equipamiento necesario para un sistema CAC. En este contexto, la adsorción se presenta como la opción más viable, ya que opera con lechos fijos que pueden regenerarse utilizando el calor residual de los gases de escape. Al ser un proceso cíclico, los tiempos de desorción y los tamaños de los equipos pueden ajustarse a las condiciones operativas específicas del vehículo.

Los resultados confirman que el calor residual contenido en los gases de escape puede cubrir todas las demandas de energía térmica en el sistema CAC operando con adsorción por oscilación de temperatura. Además, la hibridación del ciclo orgánico de Rankine (COR) es ventajosa, ya que, dependiendo del sorbente utilizado, la penalización que impone el CAC sobre la potencia del motor apenas varía entre un 1.9% y un 23.5% a una tasa de captura de CO_2 de 100%. Estos resultados corroboran que implementar un COR como complemento a un sistema CAC es teóricamente factible desde el punto de vista energético. Adicionalmente, un análisis dinámico reveló que el sistema CAC-COR produce un aumento de la potencia del motor del 4.93%, lo que conlleva un incremento del consumo de combustible del 10%. Asimismo, se encontró que el consumo de energía para la captura de CO_2 es, en promedio, de 450 kJ/kg CO_2 a una tasa de captura de CO_2 de 100% y de 150 kJ/kg CO_2 a una tasa de captura de CO_2 de 70%, lo cual es casi un 50% menos de lo reportado en la literatura. Estos prometedores resultados se deben principalmente a la integración del COR y a la configuración térmica de los dispositivos propuesta en esta tesis.

Por otro lado, no se observó ninguna diferencia significativa en los valores obtenidos del volumen y peso del sistema CAC-COR al operar con los sorbentes seleccionados para el estudio. Esta similitud se atribuye al hecho de que el dispositivo de adsorción por oscilación de temperatura apenas contribuye, en promedio, con un 6% al peso y volumen del sistema CAC-COR. El estudio reveló además que el tamaño del motor no influye drásticamente en el funcionamiento del sistema CAC-COR, ya que las cargas parásitas provocadas por el sistema CAC-COR se mantienen casi constantes, con valores promedio de 2.9% con un 70% de tasa de captura de CO_2 y de 9% con un 100% de tasa de captura de CO_2 . En contraste, el tipo de sorbente sí es un factor predominante en el desempeño del sistema CAC-COR. El sistema CAC-COR mostró un rendimiento adecuado con los sorbentes PPN y MOF y ambos mostraron un comportamiento energético similar. Sin embargo, cuando se utilizó carbón activo, el sistema CAC-COR tuvo mayores cargas parásitas y consumo de energía para capturar CO_2 , con un promedio del 15% en todas las cargas del motor y rangos de rpm. Este aumento se debe a la baja selectividad del carbón activo, lo que lleva a una mayor concentración de

impurezas de N_2 en el CO_2 capturado. En consecuencia, esto requiere una mayor potencia de compresión para licuar el CO_2 y aumenta el consumo de energía para la captura de CO_2 en comparación con los sorbentes MOF y PPN. Por lo tanto, las propiedades ideales del sorbente deben incluir un bajo calor de adsorción y una alta selectividad, además de la capacidad de tolerar pequeñas fracciones de agua en caso de que no se logre el secado completo de los gases de escape. Basado en estos criterios, el sorbente que más se acerca a estas características es el PPN. No obstante, este tipo de sorbente aún se encuentra en producción a nivel de laboratorio, por lo que aún no sería una opción viable para su implementación inmediata.

Como se mencionó anteriormente, a nivel energético no se observan grandes diferencias en los resultados debido al tamaño del motor. Sin embargo, en lo que respecta al espacio útil para la integración del sistema CAC-COR y en el análisis tecno-económico realizado en esta tesis, sí se encontraron diferencias significativas relacionadas con el tamaño del motor. Para el caso del motor grande cuyo, cuyo vehículo de análisis fue un bus, la afectación en el volumen de trabajo del vehículo es de apenas un 3.4%, mientras que en el vehículo que opera con el motor más pequeño (VAN), el volumen útil requerido para la instalación del sistema CAC-COR es del 10.2%. Además, los resultados de CAPEX muestran que el incremento de la inversión inicial para bus con un sistema CCS-ORC integrado es apenas superior al del bus base y es un 29% menor en comparación con otras tecnologías de cero emisiones existentes para buses. Por el contrario, la inversión inicial para VAN con un sistema CAC-COR integrado no es viable, ya que su coste se incrementa en un 25% respecto a las tecnologías eléctricas y casi un 50% respecto a la VAN base.

Por otro lado, se observa que el retorno de la inversión de un sistema como el propuesto en esta tesis, evaluado a lo largo de la vida útil de un vehículo pesado (10 años), está lejos de ser cero debido al incremento en el consumo de combustible necesario para cubrir las cargas parásitas, así como al coste de los equipos y al mantenimiento y operación del sistema CAC-COR. Sin embargo, los valores de costos de abatimiento de carbono obtenidos se encuentran entre 19 y 47 €/t CO_2 a una tasa de captura de CO_2 de 100%, lo cual es hasta un 50% más bajo en comparación con otras propuestas de sistemas de captura y almacenamiento de CO_2 desarrollados para otras industrias. Basado en estos resultados, el sector del transporte podría considerar esta inversión, que no es muy alta, si se pretende cumplir con los objetivos de reducción de CO_2 establecidos por la Unión Europea para el año 2050.

Según los análisis de sensibilidad realizados en la evaluación tecno-económica, el valor del impuesto de CO_2 que el sector del transporte debería pagar, una vez implementado, para recuperar la inversión inicial en la vida útil de los vehículos,

debe ser superior a 65 €/tCO₂. Además, si el CO₂ capturado se vende como materia prima para la producción de combustibles sintéticos, esto podría compensar el coste operativo del vehículo y proporcionar ingresos adicionales, aumentando así los beneficios obtenidos al integrar un sistema CAC-COR. Esto reduciría el tiempo de recuperación de la inversión o el coste del impuesto de CO₂. Asimismo, evitaría que el CO₂ capturado se almacene bajo tierra, otorgándole un valor productivo a esta emisión.

En el caso de la absorción, los resultados obtenidos muestran que la MEA tiene el mayor potencial de captura de CO₂, superando a la MDEA en todo el rango de condiciones de operación del motor. Sin embargo, la integración térmica del calor residual de los gases de escape con los sistemas CAC y COR solo es técnicamente viable para el sistema CAC. Esto se debe a que el calor residual de los gases de escape puede cubrir solo la demanda térmica del proceso de desorción del CO₂. Por lo tanto, la hibridación de un COR con el sistema CAC no es factible, ya que conlleva un aumento en el peso, volumen y costo del sistema CAC-COR. Este incremento no se compensa, dado que el COR no puede generar suficiente potencia para cubrir las cargas parásitas generadas por el CAC utilizando el calor residual de los gases de escape disponible después de pasar por el stripper.

En resumen, este estudio evidencia que la integración del sistema CAC-COR en los vehículos de trabajo pesado con motor de combustión interna es prometedora tanto en el proceso de absorción como en el de adsorción, desde la perspectiva de la mitigación del CO₂ y desde un enfoque tecno-económico a medio plazo. La integración propuesta puede reducir las emisiones de CO₂ del sector del transporte y proporcionar CO₂ para la producción de combustibles sintéticos. Para que esto sea completamente funcional, los motores de combustión interna de estos vehículos deberían operar con gas natural, ya que este produce menos emisiones de CO₂ en comparación con los motores de combustión interna alimentados con diésel o gasolina. Esto permitiría una mayor autonomía en términos de almacenamiento de CO₂. Además, el uso de combustibles sintéticos producidos a partir del CO₂ capturado abre la puerta a un sistema de transporte circular y sostenible centrado en los motores de combustión interna, la cual es una tecnología ampliamente conocida. Por consiguiente, es necesario llevar a cabo estudios experimentales para validar el sistema CAC-COR en condiciones reales y cerrar la brecha de conocimiento existente. Esto permitirá alcanzar una aplicación viable que posibilite la descarbonización completa de este sector intensivo en energía.

CONTRIBUCIONES CIENTÍFICAS

Las principales contribuciones de esta tesis están relacionadas con propuestas innovadoras y la exploración de los aspectos técnicos involucrados en el desarrollo de tecnologías de captura y almacenamiento de CO₂ en vehículos de transporte pesado. En particular, los problemas que se abordaron fueron la adaptabilidad del

sistema de captura y almacenamiento para operar en diferentes condiciones de carga y rpm del motor y el desconocimiento del impacto económico que supondría la integración de este tipo de sistemas en un vehículo. Esta perspectiva difiere completamente de los trabajos previos encontrados en la bibliografía y patentes que se centran en la configuración del sistema de captura y almacenamiento de CO₂ con el motor funcionando bajo una única condición de operación [64,74]. Así, las principales aportaciones de esta tesis se resumen a continuación:

- Primera validación energética de la integración de un COR que toma el calor residual de los gases de escape provenientes de un motor de combustión interna para producir potencia que satisfaga la demanda de potencia de un sistema CAC integrado en un vehículo pesado.
- Primer diseño térmico y análisis energético de un sistema CAC operado por adsorción por oscilación de temperatura y otro por lavado de aminas, capaz de trabajar bajo diferentes condiciones de operación de un motor de combustión interna.
- Primera evaluación energética de tres sorbentes diferentes y dos aminas funcionando en un sistema CAC a bordo de un vehículo de transporte pesado
- Primer diseño conceptual, dimensionamiento y modelado térmico de un sistema CAC y su unidad de captura de CO₂ operando con adsorción por oscilación de temperatura.
- Primer análisis tecno-económico de un sistema CAC, obteniendo variables como costos de inversión inicial, costos de abatimiento de carbono y retorno de la inversión.
- Primer cálculo de las penalizaciones sobre el rendimiento del motor por la integración de un sistema CAC operado por adsorción por oscilación de temperatura trabajando en las condiciones dinámicas de un motor de combustión interna.

Otras contribuciones complementarias producto de esta tesis son:

- Elaboración de la primera revisión bibliográfica de sistemas de captura y almacenamiento de CO₂ para fuentes móviles, clasificándolos por método y técnica de captura de CO₂.
- Participación en el proyecto de investigación nacional titulado: Decarbonisation of energy-intensive sectors. CO₂ capture in gas engines for the circularisation of sustainable synthetic fuels and viability of the storage of pollutants (CAPTICES) 2022-2025
- Postulación de proyecto de investigación a convocatoria autonómica, titulado: Estudio tecno-económico de la captura por adsorción con zeolitas para el cierre del ciclo de CO₂ en el sector del transporte por carretera (Z-CAT)., en caso de ser aprobado se ejecutará en los años 2025-2026

Las contribuciones científicas presentadas a conferencias internacionales durante el desarrollo de la tesis son:

- García Mariaca, Alexander and Llera, Eva, Dynamic CO₂ Capture in a Natural Gas Engine Used in Road Freight Transport. Proceedings of the 16th Greenhouse Gas Control Technologies Conference (GHGT-16), 23-24 Oct 2022, Lyon France.
- García Mariaca, Alexander, Llera, Eva and Francisco Moreno, Energy Analysis of a Mobile CCS-ORC System Operating in a Heavy-Duty Engine. Proceedings of the International Conference on Efficiency, Cost, Optimization, Simulation and Environmental Impact of Energy Systems (ECOS 2024), 30 June - 5 July 2024, Rhodes, Greece.
- Alexander García Mariaca, Jorge Perpiñan, Manuel Bailera, Eva Llera-Sastresa, Begoña Peña, Techno-Economic analysis of the Integration of Mobile-CCS and PTG in a Heavy Vehicle Fleet. Proceedings of the 19th Conference on Sustainable Development of Energy, Water and Environment Systems (SDEWES-19), 8 – 12 September 2024. Rome, Italy
- Alexander García-Mariaca, Eva Llera-Sastresa, Francisco Moreno, Luis M Romeo, Energy Efficiency Evaluation of a Mobile CCS-ORC System in Operation with a Heavy-Duty Engine. Proceedings of the 17th International Conference on Greenhouse Gas Control Technologies (GHGT-17), 20 -24 October 2024, Calgary Canada

Finalmente, la formación en recurso humano para la ciencia, la tecnología y la innovación también ha sido un componente importante de esta tesis a través de la elaboración de tres trabajos fin de grado titulados:

- Elaboración de un modelo simplificado para el análisis del funcionamiento de un motor de encendido provocado con gas natural. Rosana Blecua Arilla. 2020
- Modelado térmico de un lecho de zeolita para la captura de CO₂ mediante adsorción por oscilación de temperatura. Alejandro Aparacio, (en curso).
- Diseño del evaporador de un ciclo orgánico Rankine para el accionamiento de un sistema de captura de CO₂ en motores. Raúl Alvira, (en curso).

FUTUROS ESFUERZOS DE INVESTIGACIÓN

La integración de sistemas CCS-ORC en vehículos pesados implica actividades complejas que deben abordarse desde un enfoque interdisciplinar para abarcar todos los conceptos necesarios para su implementación real. En base a esto, los trabajos futuros deberían orientarse en las siguientes direcciones:

- Validación experimental con el motor funcionando a cargas parciales y en estado transitorio para conocer:

- El aumento de la contrapresión del motor, provocado por la instalación de sistemas adicionales en el conducto de gases de escape.
 - El funcionamiento del dispositivo de adsorción por oscilación de temperatura, incluidos los tiempos de regeneración del sorbente y la tasa de captura de CO₂ máxima.
 - La degradación del sorbente o solvente debido a su interacción con otras emisiones contaminantes como óxidos de nitrógeno, dióxido de carbono e hidrocarburos no quemados.
 - El comportamiento del sistema CAC-COR teniendo en cuenta la inercia térmica.
 - El aumento en el consumo de combustible del motor para satisfacer las cargas parásitas provocadas por el funcionamiento del sistema CAC.
- Análisis de ciclo de vida para concluir sobre la viabilidad de la instalación de un sistema CAC en fuentes móviles.
 - Evaluación teórica y experimental del sistema CCS-ORC bajo diversas condiciones climáticas.
 - Diseño detallado del sistema CCS-ORC, que incluye la selección de materiales, dimensionamiento, posible ubicación en el vehículo, cargas estructurales, mantenimiento, operación y control en la operación del sistema.
 - Optimización de los sistemas de refrigeración del sistema CCS-ORC.
 - En el caso del sistema de absorción CCS-ORC, el dimensionamiento del absorbente y del depurador

BIBLIOGRAPHY

- [1] IEA. Total final consumption (TFC) by sector, World 1990-2017. Total Final Consumption (TFC) by Sector, World 1990-2017 2019. [https://www.iea.org/data-and-statistics?country=WORLD&fuel=Energy consumption&indicator=Total final consumption \(TFC\) by sector](https://www.iea.org/data-and-statistics?country=WORLD&fuel=Energy%20consumption&indicator=Total%20final%20consumption%20(TFC)%20by%20sector) (accessed November 27, 2019).
- [2] Bellocchi S, De Falco M, Gambini M, Manno M, Stilo T, Vellini M. Opportunities for power-to-Gas and Power-to-liquid in CO₂-reduced energy scenarios: The Italian case. *Energy* 2019;175:847–61. <https://doi.org/10.1016/j.energy.2019.03.116>.
- [3] Lu J, Chen H, Cai X. From global to national scenarios: Exploring carbon emissions to 2050. *Energy Strategy Reviews* 2022;41:100860. <https://doi.org/10.1016/j.esr.2022.100860>.
- [4] Hof AF, den Elzen MGJ, Admiraal A, Roelfsema M, Gernaat DEHJ, van Vuuren DP. Global and regional abatement costs of Nationally Determined Contributions (NDCs) and of enhanced action to levels well below 2 °C and 1.5 °C. *Environ Sci Policy* 2017;71:30–40. <https://doi.org/10.1016/j.envsci.2017.02.008>.
- [5] European Commission. A Clean Planet for all. A European long-term strategic vision for a prosperous, modern, competitive and climate neutral economy. Com(2018) 773 2018:114.
- [6] Bains P, Psarras P, Wilcox J. CO₂ capture from the industry sector. *Prog Energy Combust Sci* 2017;63:146–72. <https://doi.org/10.1016/j.pecs.2017.07.001>.
- [7] Wang D, Li S, Liu F, Gao L, Sui J. Post combustion CO₂ capture in power plant using low temperature steam upgraded by double absorption heat transformer. *Appl Energy* 2018;227:603–12. <https://doi.org/10.1016/j.apenergy.2017.08.009>.
- [8] Budinis S, Krevor S, Dowell N Mac, Brandon N, Hawkes A. An assessment of CCS costs, barriers and potential. *Energy Strategy Reviews* 2018;22:61–81. <https://doi.org/10.1016/j.esr.2018.08.003>.
- [9] Leeson D, mac Dowell N, Shah N, Petit C, Fennell PS. A Techno-economic analysis and systematic review of carbon capture and storage (CCS) applied to the iron and steel, cement, oil refining and pulp and paper industries, as well as other high purity sources. *International Journal of Greenhouse Gas Control* 2017;61:71–84. <https://doi.org/10.1016/J.IJGGC.2017.03.020>.
- [10] Global CCS Institute. The Global Status of CCS: 2023. Australia: 2023.

- [11] L'Orange Seigo S, Dohle S, Siegrist M. Public perception of carbon capture and storage (CCS): A review. *Renewable and Sustainable Energy Reviews* 2014;38:848–63. <https://doi.org/10.1016/J.RSER.2014.07.017>.
- [12] Rubin ES. Understanding the pitfalls of CCS cost estimates. *International Journal of Greenhouse Gas Control* 2012;10:181–90. <https://doi.org/10.1016/J.IJGGC.2012.06.004>.
- [13] García-Mariaca A, Llera-Sastresa E. Review on Carbon Capture in ICE Driven Transport. *Energies* 2021, Vol 14, Page 6865 2021;14:6865. <https://doi.org/10.3390/EN14216865>.
- [14] Romeo LM, Bolea I, Escosa JM. Integration of power plant and amine scrubbing to reduce CO₂ capture costs. *Appl Therm Eng* 2008;28:1039–46. <https://doi.org/10.1016/J.APPLTHERMALENG.2007.06.036>.
- [15] Wu Y, Xu J, Mumford K, Stevens GW, Fei W, Wang Y. Recent advances in carbon dioxide capture and utilization with amines and ionic liquids. *Green Chemical Engineering* 2020;1:16–32. <https://doi.org/10.1016/J.GCE.2020.09.005>.
- [16] Demir H, Aksu GO, Gulbalkan HC, Keskin S. MOF Membranes for CO₂ Capture: Past, Present and Future. *Carbon Capture Science & Technology* 2022;2:100026. <https://doi.org/10.1016/J.CCST.2021.100026>.
- [17] Mdletshe Z, Msomi V, Nemraoui O. Experimental investigation of the adsorbents using pressure and thermal swing for adsorption and desorption. *Results in Engineering* 2022;15:100513. <https://doi.org/10.1016/J.RINENG.2022.100513>.
- [18] Zhao R, Liu L, Zhao L, Deng S, Li S, Zhang Y. A comprehensive performance evaluation of temperature swing adsorption for post-combustion carbon dioxide capture. *Renewable and Sustainable Energy Reviews* 2019;114:109285. <https://doi.org/10.1016/j.rser.2019.109285>.
- [19] Raganati F, Miccio F, Ammendola P. Adsorption of Carbon Dioxide for Post-combustion Capture: A Review. *Energy & Fuels* 2021;35:12845–68. <https://doi.org/10.1021/acs.energyfuels.1c01618>.
- [20] Liu F, Shafique M, Luo X. Literature review on life cycle assessment of transportation alternative fuels. *Environ Technol Innov* 2023;32:103343. <https://doi.org/10.1016/j.eti.2023.103343>.
- [21] Wanniarachchi S, Hewage K, Wirasinghe C, Chhipi-Shrestha G, Karunathilake H, Sadiq R. Transforming road freight transportation from fossils to hydrogen: Opportunities and challenges. *Int J Sustain Transp* 2023;17:552–72. <https://doi.org/10.1080/15568318.2022.2068389>.
- [22] Huang Y, Ng ECY, Zhou JL, Surawski NC, Chan EFC, Hong G. Eco-driving technology for sustainable road transport: A review. *Renewable and*

- [23] Panagiotis Fafoutellis, Eleni G. Mantouka, Eleni I. Vlahogianni. Eco-driving and its impacts on fuel efficiency An overview of technologies and data-driven methods. *Sustainability* 2021;13:226. <https://doi.org/10.3390/su13010226>.
- [24] Kühlwein J, Berlin B|, Brussels |, San |, Washington F|. *Driving Resistances of Light-Duty Vehicles In Europe: Present Situation, Trends, And Scenarios For 2025*. 2016.
- [25] Agudelo AF, García-Contreras R, Agudelo JR, Armas O. Potential for exhaust gas energy recovery in a diesel passenger car under European driving cycle. *Appl Energy* 2016;174:201–12. <https://doi.org/10.1016/j.apenergy.2016.04.092>.
- [26] Merkisz J, Fuc P, Lijewski P, Ziolkowski A, Wojciechowski KT. The Analysis of Exhaust Gas Thermal Energy Recovery Through a TEG Generator in City Traffic Conditions Reproduced on a Dynamic Engine Test Bed. *J Electron Mater* 2015;44:1704–15. <https://doi.org/10.1007/s11664-014-3522-6>.
- [27] Arsie I, Cricchio A, Pianese C, Ricciardi V, De Cesare M. Modeling analysis of waste heat recovery via thermo-electric generator and electric turbo-compound for CO₂ reduction in automotive SI engines. *Energy Procedia* 2015;82:81–8. <https://doi.org/10.1016/j.egypro.2015.11.886>.
- [28] Sprouse C, Depcik C. Review of organic Rankine cycles for internal combustion engine exhaust waste heat recovery. *Appl Therm Eng* 2013;51:711–22. <https://doi.org/10.1016/j.applthermaleng.2012.10.017>.
- [29] Sanguesa JA, Torres-Sanz V, Garrido P, Martinez FJ, Marquez-Barja JM. A Review on Electric Vehicles: Technologies and Challenges. *Smart Cities* 2021;4:372–404. <https://doi.org/10.3390/smartcities4010022>.
- [30] Cremades L V., Oller L. Techno-environmental feasibility of synthetic fuels in ground transportation. Application to the Spanish automobile fleet in 2035. *Energy Reports* 2024;11:5466–74. <https://doi.org/10.1016/j.egyr.2024.05.032>.
- [31] International Energy agency. Global energy-related CO₂ emissions by sector – Charts – Data & Statistics - IEA 2022. <https://www.iea.org/reports/co2-emissions-in-2022> (accessed February 28, 2023).
- [32] International Energy Agency. Electric vehicles 2024. <https://www.iea.org/energy-system/transport/electric-vehicles> (accessed June 19, 2024).
- [33] Li Z, Khajepour A, Song J. A comprehensive review of the key technologies for pure electric vehicles. *Energy* 2019;182:824–39. <https://doi.org/10.1016/j.energy.2019.06.077>.

- [34] Auer M, Ganzer G, Müller-Baum P, Stiesch G. Synthetic Fuels in Large Engines - How Internal Combustion Engines Become CO₂-neutral. *MTZ Worldwide* 2019;80:48–51. <https://doi.org/10.1007/s38313-018-0160-z>.
- [35] Statista. Global transport CO₂ emissions breakdown 2020 | Statista 2020. <https://www.statista.com/statistics/1185535/transport-carbon-dioxide-emissions-breakdown/> (accessed November 14, 2021).
- [36] EV-Volumes. EV-Volumes - The Electric Vehicle World Sales Database. The Electric Vehicle World Sales Database 2019. <https://www.ev-volumes.com/news/global-bev-phev-sales-for-2019/%0Ahttp://www.ev-volumes.com/country/total-euefta-plug-in-vehicle-volumes-2/> (accessed November 29, 2019).
- [37] Majhi RC, Ranjitkar P, Sheng M, Covic GA, Wilson DJ. A systematic review of charging infrastructure location problem for electric vehicles. *Transp Rev* 2021;41:432–55. <https://doi.org/10.1080/01441647.2020.1854365>.
- [38] Skeete J-P, Wells P, Dong X, Heidrich O, Harper G. Beyond the Event horizon: Battery waste, recycling, and sustainability in the United Kingdom electric vehicle transition. *Energy Res Soc Sci* 2020;69:101581. <https://doi.org/10.1016/j.erss.2020.101581>.
- [39] Amarakoon, S., Smith, J., & Segal B. Li-ion Batteries and Nanotechnology for Electric Vehicles: LCA Study. vol. EPA 744-R-. 2012.
- [40] Kalghatgi G. Is it really the end of internal combustion engines and petroleum in transport? *Appl Energy* 2018;225:965–74. <https://doi.org/10.1016/j.apenergy.2018.05.076>.
- [41] Schmauss TA, Barnett SA. Viability of Vehicles Utilizing On-Board CO₂ Capture. *ACS Energy Lett* 2021;6:3180–4. <https://doi.org/10.1021/acsenergylett.1c01426>.
- [42] Eveloy V, Gebreegziabher T. A Review of Projected Power-to-Gas Deployment Scenarios. *Energies (Basel)* 2018;11. <https://doi.org/10.3390/en11071824>.
- [43] Llera E, Romeo LM, Bailera M, Osorio JL. Exploring the integration of the power to gas technologies and the sustainable transport. *International Journal of Energy Production and Management* 2018;3:1–9. <https://doi.org/10.2495/EQ-V3-N1-1-9>.
- [44] Streibel M, Nakaten N, Kempka T, Kühn M. Analysis of an integrated carbon cycle for storage of renewables. *Energy Procedia* 2013;40:202–11. <https://doi.org/10.1016/j.egypro.2013.08.024>.
- [45] Kühn M, Nakaten N, Streibel M, Kempka T. CO₂ geological storage and utilization for a carbon neutral “power-to-gas-to-power” cycle to even out fluctuations of renewable energy provision. *Energy Procedia* 2014;63:8044–9. <https://doi.org/10.1016/j.egypro.2014.11.841>.

- [46] Götz M, Lefebvre J, Mörs F, McDaniel Koch A, Graf F, Bajohr S, et al. Renewable Power-to-Gas: A technological and economic review. *Renew Energy* 2016;85:1371–90. <https://doi.org/10.1016/j.renene.2015.07.066>.
- [47] Rönsch S, Schneider J, Matthischke S, Schlüter M, Götz M, Lefebvre J, et al. Review on methanation - From fundamentals to current projects. *Fuel* 2016;166:276–96. <https://doi.org/10.1016/j.fuel.2015.10.111>.
- [48] Pasini G, Lutzemberger G, Ferrari L. Renewable Electricity for Decarbonisation of Road Transport: Batteries or E-Fuels? *Batteries* 2023;9. <https://doi.org/10.3390/batteries9020135>.
- [49] Hagos DA, Ahlgren E. A state-of-the art review on the development of CNG/LNG infrastructure and natural gas vehicles (NGVs). Chalmers University of Technology 2017.
- [50] Osorio-Tejada JL, Llera-Sastresa E, Scarpellini S. Liquefied natural gas: Could it be a reliable option for road freight transport in the EU? *Renewable and Sustainable Energy Reviews* 2017;71:785–95. <https://doi.org/10.1016/j.rser.2016.12.104>.
- [51] Kalghatgi G, Levinsky H, Colket M. Future transportation fuels. *Prog Energy Combust Sci* 2018;69:103–5. <https://doi.org/10.1016/j.pecs.2018.06.003>.
- [52] Mikulčić H, Ridjan Skov I, Dominković DF, Wan Alwi SR, Manan ZA, Tan R, et al. Flexible Carbon Capture and Utilization technologies in future energy systems and the utilization pathways of captured CO₂. *Renewable and Sustainable Energy Reviews* 2019;114. <https://doi.org/10.1016/j.rser.2019.109338>.
- [53] Ramirez A, Sarathy SM, Gascon J. CO₂ Derived E-Fuels: Research Trends, Misconceptions, and Future Directions. *Trends Chem* 2020;2:785–95. <https://doi.org/10.1016/J.TRECHM.2020.07.005>.
- [54] Feenstra M, Monteiro J, van den Akker JT, Abu-Zahra MRM, Gilling E, Goetheer E. Ship-based carbon capture onboard of diesel or LNG-fuelled ships. *International Journal of Greenhouse Gas Control* 2019;85:1–10. <https://doi.org/10.1016/j.ijggc.2019.03.008>.
- [55] Ozaki M, Nakazawa N, Omata A, Komatsu M, Manabe H. Ship-Based carbon dioxide capture and storage for enhanced oil recovery. *Proceedings of the Annual Offshore Technology Conference* 2015;4:2412–25. <https://doi.org/10.4043/25861-ms>.
- [56] Ros JA, Skylogianni E, Doedée V, van den Akker JT, Vredeveltdt AW, Linders MJG, et al. Advancements in ship-based carbon capture technology on board of LNG-fuelled ships. *International Journal of Greenhouse Gas Control* 2022;114:103575. <https://doi.org/10.1016/J.IJGGC.2021.103575>.

- [57] Barrio M, Aspelund A, Weydahl T, Sandvik T, Wongraven L, Krogstad H, et al. Ship-based transport of CO₂. *Greenhouse Gas Control Technologies* 7, vol. 53, Elsevier; 2005, p. 1655–60. <https://doi.org/10.1016/B978-008044704-9/50193-2>.
- [58] Saravanan S, Kumar R. Experimental Investigations on CO₂ Recovery from Engine Exhaust Using Adsorption Technology. *SAE Technical Paper* 2019;2019-28–2577. <https://doi.org/10.4271/2019-28-2577.Abstract>.
- [59] Rajdurai MS, Rao AHS, Kamalakkannan K. CO₂ Capture Using Activated Alumina in Gasoline Passenger Vehicles. *Int J Eng Res Appl* 2016;6:73–7.
- [60] Awoyomi A, Patchigolla K, Anthony EJ. CO₂/SO₂ emission reduction in CO₂ shipping infrastructure. *International Journal of Greenhouse Gas Control* 2019;88:57–70. <https://doi.org/10.1016/j.ijggc.2019.05.011>.
- [61] Stec M, Tatarczuk A, Iluk T, Szul M. Reducing the energy efficiency design index for ships through a post-combustion carbon capture process. *International Journal of Greenhouse Gas Control* 2021;108. <https://doi.org/10.1016/j.ijggc.2021.103333>.
- [62] Luo X, Wang M. Study of solvent-based carbon capture for cargo ships through process modelling and simulation. *Appl Energy* 2017;195:402–13. <https://doi.org/10.1016/j.apenergy.2017.03.027>.
- [63] Kumar P, Rathod V, Parwani AK. Experimental investigation on performance of absorbents for carbon dioxide capture from diesel engine exhaust. *Environ Prog Sustain Energy* 2021:e13651. <https://doi.org/10.1002/ep.13651>.
- [64] Kim J, Yoo Y, Kim S, Beak J, Oh S-D, Lee J, et al. Design and assessment of a novel mobile carbon capture system: Energy and exergy analyses. *Energy Convers Manag* 2024;300:117934. <https://doi.org/10.1016/j.enconman.2023.117934>.
- [65] Awoyomi A, Patchigolla K, Anthony EJ. Process and Economic Evaluation of an Onboard Capture System for LNG-Fueled CO₂ Carriers. *Ind Eng Chem Res* 2020;59:6951–60. <https://doi.org/10.1021/acs.iecr.9b04659>.
- [66] Horvath S, Fasihi M, Breyer C. Techno-economic analysis of a decarbonized shipping sector: Technology suggestions for a fleet in 2030 and 2040. *Energy Convers Manag* 2018;164:230–41. <https://doi.org/10.1016/j.enconman.2018.02.098>.
- [67] Fang S, Xu Y, Li Z, Ding Z, Liu L, Wang H. Optimal Sizing of Shipboard Carbon Capture System for Maritime Greenhouse Emission Control. *IEEE Trans Ind Appl* 2019;55:1–1. <https://doi.org/10.1109/tia.2019.2934088>.
- [68] Aramco. Capturing carbon on the move 2019. <https://www.aramco.com/en/creating-value/technology->

development/transport-technologies/mobile-carbon-capture# (accessed February 19, 2023).

- [69] Al-Meshari AA, Muhaish FI, Aleidan AA. Carbon Capture: Saudi Aramco's Carbon Management Program. *Journal of Petroleum Technology* 2014;66:72–4. <https://doi.org/10.2118/0614-0072-jpt>.
- [70] Voice A, Hamad E. Mobile Carbon Capture for Long-Haul Commercial Transport: Design, Integration and Results. *SSRN Electronic Journal* 2022. <https://doi.org/10.2139/ssrn.4280720>.
- [71] Larkin C, Lampri K, Mazzone S, Oliva F, Li K, García-García FR. Retrofitting hollow fibre carbon capture systems to decarbonise surface transport. *Journal of CO₂ Utilization* 2023;67. <https://doi.org/10.1016/j.jcou.2022.102336>.
- [72] Saravanan S, Kumar CR. Carbon dioxide capture using Adsorption Technology in Diesel Engines. *International Journal of Renewable Energy Research* 2020;10:1614–20. <https://doi.org/10.20508/ijrer.v10i4.11450.g8046>.
- [73] Subramanian T, Sonthalia A, Varuvel EG. Environmental Effects Effect of calcite / activated carbon-based post- combustion CO₂ capture system in a biodiesel- fueled CI engine — An experimental study. *Energy Sources, Part A: Recovery, Utilization, and Environmental Effects* 2018;41:1972–82. <https://doi.org/10.1080/15567036.2018.1548525>.
- [74] Sharma S, Maréchal F. Carbon Dioxide Capture From Internal Combustion Engine Exhaust Using Temperature Swing Adsorption. *Front Energy Res* 2019;7:1–12. <https://doi.org/10.3389/fenrg.2019.00143>.
- [75] Güler E, Ergin S. An investigation on the solvent based carbon capture and storage system by process modeling and comparisons with another carbon control methods for different ships. *International Journal of Greenhouse Gas Control* 2021;110:103438. <https://doi.org/10.1016/J.IJGGC.2021.103438>.
- [76] Di Battista D, Mauriello M, Cipollone R. Waste heat recovery of an ORC-based power unit in a turbocharged diesel engine propelling a light duty vehicle. *Appl Energy* 2015;152:109–20. <https://doi.org/10.1016/J.APENERGY.2015.04.088>.
- [77] Zhang YQ, Wu YT, Xia GD, Ma CF, Ji WN, Liu SW, et al. Development and experimental study on organic Rankine cycle system with single-screw expander for waste heat recovery from exhaust of diesel engine. *Energy* 2014;77:499–508. <https://doi.org/10.1016/J.ENERGY.2014.09.034>.
- [78] Fatigati F, Di Battista D, Cipollone R. Permeability effects assessment on recovery performances of small-scale ORC plant. *Appl Therm Eng* 2021;196:117331. <https://doi.org/10.1016/J.APPLTHERMALENG.2021.117331>.

- [79] Badescu V, Aboaltabooq MHK, Pop H, Apostol V, Prisecaru M, Prisecaru T. Design and operational procedures for ORC-based systems coupled with internal combustion engines driving electrical generators at full and partial load. *Energy Convers Manag* 2017;139:206–21. <https://doi.org/10.1016/j.enconman.2017.02.046>.
- [80] Fatigati F, Di Bartolomeo M, Di Battista D, Cipollone R. Experimental and Numerical Characterization of the Sliding Rotary Vane Expander Intake Pressure in Order to Develop a Novel Control-Diagnostic Procedure. *Energies (Basel)* 2019;12:1970. <https://doi.org/10.3390/en12101970>.
- [81] Lin S, Zhao L, Deng S, Ni J, Zhang Y, Ma M. Dynamic performance investigation for two types of ORC system driven by waste heat of automotive internal combustion engine. *Energy* 2019;169:958–71. <https://doi.org/10.1016/j.energy.2018.12.092>.
- [82] Scaccabarozzi R, Tavano M, Invernizzi CM, Martelli E. Comparison of working fluids and cycle optimization for heat recovery ORCs from large internal combustion engines. *Energy* 2018;158:396–416. <https://doi.org/10.1016/j.energy.2018.06.017>.
- [83] Bombarda P, Invernizzi CM, Pietra C. Heat recovery from Diesel engines: A thermodynamic comparison between Kalina and ORC cycles. *Appl Therm Eng* 2010;30:212–9. <https://doi.org/10.1016/j.applthermaleng.2009.08.006>.
- [84] Di Battista D, Di Bartolomeo M, Villante C, Cipollone R. On the limiting factors of the waste heat recovery via ORC-based power units for on-the-road transportation sector. *Energy Convers Manag* 2018;155:68–77. <https://doi.org/10.1016/J.ENCONMAN.2017.10.091>.
- [85] Grelet V, Reiche T, Lemort V, Nadri M, Dufour P. Transient performance evaluation of waste heat recovery rankine cycle based system for heavy duty trucks. *Appl Energy* 2016;165:878–92. <https://doi.org/10.1016/J.APENERGY.2015.11.004>.
- [86] Carraro G, Pili R, Lazzaretto A, Haglind F. Effect of the evaporator design parameters on the dynamic response of organic Rankine cycle units for waste heat recovery on heavy-duty vehicles. *Appl Therm Eng* 2021;198:117496. <https://doi.org/10.1016/J.APPLTHERMALENG.2021.117496>.
- [87] Feng Y, Hung TC, Zhang Y, Li B, Yang J, Shi Y. Performance comparison of low-grade ORCs (organic Rankine cycles) using R245fa, pentane and their mixtures based on the thermoeconomic multi-objective optimization and decision makings. *Energy* 2015;93:2018–29. <https://doi.org/10.1016/j.energy.2015.10.065>.
- [88] Christodoulou A, Gonzalez-Aregall M, Linde T, Vierth I, Cullinane K. Targeting the reduction of shipping emissions to air. *Maritime Business Review* 2019;4:16–30. <https://doi.org/10.1108/mabr-08-2018-0030>.

- [89] Roussanaly S, Jakobsen JP, Hognes EH, Brunsvold AL. Benchmarking of CO₂ transport technologies: Part I-Onshore pipeline and shipping between two onshore areas. *International Journal of Greenhouse Gas Control* 2013;19:584–94. <https://doi.org/10.1016/j.ijggc.2013.05.031>.
- [90] International Maritime Organization. Energy efficiency and the reduction of GHG emissions from ships. 2023 IMO Strategy on Reduction of GHG Emissions from Ships 2023. <https://www.imo.org/en/OurWork/Environment/Pages/2023-IMO-Strategy-on-Reduction-of-GHG-Emissions-from-Ships.aspx> (accessed June 10, 2024).
- [91] Comer B, Chen C, Rutherford D. Relating short-term measures to IMO's minimum 2050 emissions reduction target. 2018.
- [92] van den Akker J. Carbon capture onboard LNG-fueled vessels. Delft University of Technology, 2017.
- [93] Fang S, Xu Y, Li Z. Joint generation and demand-side management for shipboard carbon capture and storage system. *Conference Record - Industrial and Commercial Power Systems Technical Conference 2019;2019-May:1–8*. <https://doi.org/10.1109/ICPS.2019.8733353>.
- [94] Sullivan JM, Sivak M. Carbon capture in vehicles: a review of general support, available mechanisms, and consumer acceptance issues. 2012.
- [95] Pera-Titus M, Alshebani A, Nicolas CH, Roumégoux JP, Miachon S, Dalmon JA. Nanocomposite MFI-alumina membranes: High-flux hollow fibers for CO₂ capture from internal combustion vehicles. *Ind Eng Chem Res* 2009;48:9215–23. <https://doi.org/10.1021/ie9004018>.
- [96] Van Blarigan A, Kozarac D, Seiser R, Chen JY, Cattolica R, Dibble R. Spark-ignited engine NO_x emissions in a low-nitrogen oxycombustion environment. *Appl Energy* 2014;118:22–31. <https://doi.org/10.1016/j.apenergy.2013.12.007>.
- [97] Van Blarigan AC, Seiser R, Chen JY, Cattolica R, Dibble RW. Working fluid composition effects on methane oxycombustion in an SI-engine: EGR vs. CO₂. *Proceedings of the Combustion Institute* 2013;34:2951–8. <https://doi.org/10.1016/j.proci.2012.05.012>.
- [98] Van Blarigan A, Kozarac D, Seiser R, Cattolica R, Chen J-Y, Dibble R. Experimental Study of Methane Fuel Oxycombustion in a Spark-Ignited Engine. *J Energy Resour Technol* 2014;136. <https://doi.org/10.1115/1.4024974>.
- [99] US9222480B2. Integrated method of driving a CO₂ compressor of a CO₂-capture system using waste heat from an internal combustion engine on board a mobile source, 2015.
- [100] US8480798B1. Vehicle System to Separate and Store Carbon Dioxide From Engine Exhaust, 2013.

- [101] US10280877B2. Heat Exchanger Equipped with Thermal Electric Device for Engine Exhaust Carbon Dioxide Collection System, 2016.
- [102] Thiagarajan S, Varuvel EG, Martin LJ, Beddhanan N. Mitigation of carbon footprints through a blend of biofuels and oxygenates, combined with post-combustion capture system in a single cylinder CI engine. *Renew Energy* 2019;130:1067–81. <https://doi.org/10.1016/j.renene.2018.07.010>.
- [103] Thiagarajan S, Edwin Geo V, Martin LJ, Nagalingam B. Carbon dioxide (CO₂) capture and sequestration using biofuels and an exhaust catalytic carbon capture system in a single-cylinder CI engine: an experimental study. *Biofuels* 2018;9:659–68. <https://doi.org/10.1080/17597269.2017.1292019>.
- [104] Thiagarajan S, Geo VE, Martin LJ, Nagalingam B. Combined effect of fuel-design and after-treatment system on reduction of local and global emissions from CI engine. *Environmental Technology (United Kingdom)* 2019;40:2802–12. <https://doi.org/10.1080/09593330.2018.1453871>.
- [105] Ajith Kumar PS, Varghese A, Vaishanth SS, Balaji G. Development and test of a new carbon capture system using Zeolite with addition of Activated carbon and Monoethanolamine for IC engines. *IOP Conf Ser Mater Sci Eng* 2020;912. <https://doi.org/10.1088/1757-899X/912/4/042037>.
- [106] Kaushal A, Ahirwar R, Vardhan A. Investigation of CO₂ Capturing Capacity of Solid Adsorbents (PEIs) Polyethylenimines from Automotive Vehicle Exhausts System for 4-Stroke SI Engine. *Bonfring International Journal of Industrial Engineering and Management Science* 2018;08:31–5. <https://doi.org/10.9756/bijiems.8400>.
- [107] Verdegaal WM, Wang K, Sculley JP, Wriedt M, Zhou HC. Evaluation of Metal-Organic Frameworks and Porous Polymer Networks for CO₂-Capture Applications. *ChemSusChem* 2016;9:636–43. <https://doi.org/10.1002/cssc.201501464>.
- [108] Kim YE, Lim JA, Jeong SK, Yoon Y Il, Bae ST, Nam SC. Comparison of carbon dioxide absorption in aqueous MEA, DEA, TEA, and AMP solutions. *Bull Korean Chem Soc* 2013;34:783–7. <https://doi.org/10.5012/bkcs.2013.34.3.783>.
- [109] Einewall P, Tunestal P, Johansson B. Lean burn natural gas operation vs. stoichiometric operation with egr and a three way catalyst. *SAE Technical Papers* 2005. <https://doi.org/10.4271/2005-01-0250>.
- [110] Zhang Q, Xu Z, Li M, Shao S. Combustion and emissions of a Euro VI heavy-duty natural gas engine using EGR and TWC. *J Nat Gas Sci Eng* 2016;28:660–71. <https://doi.org/10.1016/j.jngse.2015.12.015>.
- [111] Mercedes-Benz. Citaro NGT technical information 2017:1–16.
- [112] Wartsila Marine Solutions. Wärtsilä 46DF Product Guide 2019:242.

- [113] Jiang N, Shen Y, Liu B, Zhang D, Tang Z, Li G, et al. CO₂ capture from dry flue gas by means of VPSA, TSA and TVSA. *Journal of CO₂ Utilization* 2020;35:153–68. <https://doi.org/10.1016/j.jcou.2019.09.012>.
- [114] You YY, Liu XJ. Modeling of CO₂ adsorption and recovery from wet flue gas by using activated carbon. *Chemical Engineering Journal* 2019;369:672–85. <https://doi.org/10.1016/j.cej.2019.03.118>.
- [115] Himeno S, Komatsu T, Fujita S. High-pressure adsorption equilibria of methane and carbon dioxide on several activated carbons. *J Chem Eng Data* 2005;50:369–76. <https://doi.org/10.1021/je049786x>.
- [116] Plaza MG, García S, Rubiera F, Pis JJ, Pevida C. Post-combustion CO₂ capture with a commercial activated carbon: Comparison of different regeneration strategies. *Chemical Engineering Journal* 2010;163:41–7. <https://doi.org/10.1016/j.cej.2010.07.030>.
- [117] Won W, Lee S, Lee KS. Modeling and parameter estimation for a fixed-bed adsorption process for CO₂ capture using zeolite 13X. *Sep Purif Technol* 2012;85:120–9. <https://doi.org/10.1016/j.seppur.2011.09.056>.
- [118] Huck JM, Lin LC, Berger AH, Shahrak MN, Martin RL, Bhowan AS, et al. Supporting Information: Evaluating different classes of porous materials for carbon capture. *Energy Environ Sci* 2014;7:4132–46. <https://doi.org/10.1039/c4ee02636e>.
- [119] Shu G, Li X, Tian H, Liang X, Wei H, Wang X. Alkanes as working fluids for high-temperature exhaust heat recovery of diesel engine using organic Rankine cycle. *Appl Energy* 2014;119:204–17. <https://doi.org/10.1016/j.apenergy.2013.12.056>.
- [120] Payri, F., Desantes JM. Motores de combustión interna alternativos. Universitat politècnica de Valencia; 2011.
- [121] Hoang AT. Waste heat recovery from diesel engines based on Organic Rankine Cycle. *Appl Energy* 2018;231:138–66. <https://doi.org/10.1016/j.apenergy.2018.09.022>.
- [122] J. Ringler, M. Seifert, v. Guyotot, W. Hübner. Rankine Cycle for Waste Heat Recovery of IC Engines. *SAE Int J Engines* 2009;1:67–76.
- [123] Shi L, Shu G, Tian H, Deng S. A review of modified Organic Rankine cycles (ORCs) for internal combustion engine waste heat recovery (ICE-WHR). *Renewable and Sustainable Energy Reviews* 2018;92:95–110. <https://doi.org/10.1016/J.RSER.2018.04.023>.
- [124] Hoffmann Kai, Benz Michael, Weirich Marko. The New Mercedes-Benz Medium Duty Commercial Natural Gas Engine. *MTZ Worldw* 2014;75:4–11. <https://doi.org/10.1007/s38313-014-0251-4>.

- [125] FPT Industrial. Powertrains for industrial vehicles 2024. <https://www.fptindustrial.com/en/engines/Onroad/Light-Commercial-Vehicles/F1C-NG> (accessed April 22, 2024).
- [126] Obiols J, Soleri D, Dioc N, Moreau M. Potential of concomitant injection of CNG and gasoline on a 1.6L gasoline direct injection turbocharged engine. SAE Technical Papers 2011. <https://doi.org/10.4271/2011-01-1995>.
- [127] Yontar AA, Doğu Y. Effects of equivalence ratio and CNG addition on engine performance and emissions in a dual sequential ignition engine. International Journal of Engine Research 2020;21:1067–82. <https://doi.org/10.1177/1468087419834190>.
- [128] López JJ, Novella R, Gomez-Soriano J, Martinez-Hernandiz PJ, Rampanarivo F, Libert C, et al. Advantages of the unscavenged pre-chamber ignition system in turbocharged natural gas engines for automotive applications. Energy 2021;218:119466. <https://doi.org/10.1016/j.energy.2020.119466>.
- [129] Nikzadfar K, Shamekhi AH. Investigating the relative contribution of operational parameters on performance and emissions of a common-rail diesel engine using neural network. Fuel 2014;125:116–28. <https://doi.org/10.1016/j.fuel.2014.02.021>.
- [130] Heywood JB. Internal combustion engine fundamentals. vol. 1. McGraw-Hill Book Company; 1988. [https://doi.org/10.1016/s1350-4789\(10\)70041-6](https://doi.org/10.1016/s1350-4789(10)70041-6).
- [131] Peris B, Navarro-Esbrí J, Molés F. Bottoming organic Rankine cycle configurations to increase Internal Combustion Engines power output from cooling water waste heat recovery. Appl Therm Eng 2013;61:364–71. <https://doi.org/10.1016/j.applthermaleng.2013.08.016>.
- [132] Invernizzi CM, Bonalumi D. Thermal stability of organic fluids for Organic Rankine Cycle systems. Elsevier Ltd; 2017. <https://doi.org/10.1016/B978-0-08-100510-1.00005-3>.
- [133] Invernizzi CM, Iora P, Manzolini G, Lasala S. Thermal stability of n-pentane, cyclo-pentane and toluene as working fluids in organic Rankine engines. Appl Therm Eng 2017;121:172–9. <https://doi.org/10.1016/j.applthermaleng.2017.04.038>.
- [134] Fatigati F, Di Bartolomeo M, Di Battista D, Cipollone R. Experimental characterization of a hermetic scroll expander operating in an ORC-based power unit bottoming an internal combustion engine. AIP Conf Proc, vol. 2191, American Institute of Physics Inc.; 2019. <https://doi.org/10.1063/1.5138802>.
- [135] Matthias Kind and Holger Martin. VDI Heat Atlas. Second. Berlin: Springer ; 2010. <https://doi.org/10.1007/978-3-540-77877-6>.

- [136] Coker A.K. Ludwig's Applied Process Design for Chemical and Petrochemical Plants. 4th ed. 2015. <https://doi.org/10.1016/B978-0-7506-8524-5.00017-3>.
- [137] Badescu V, Aboaltabooq MHK, Pop H, Apostol V, Prisecaru M, Prisecaru T. Avoiding malfunction of ORC-based systems for heat recovery from internal combustion engines under multiple operation conditions. *Appl Therm Eng* 2019;150:977–86. <https://doi.org/10.1016/j.applthermaleng.2019.01.046>.
- [138] Capata R, Piras G. Condenser Design for On-Board ORC Recovery System. *Applied Sciences* 2021;11:6356. <https://doi.org/10.3390/app11146356>.
- [139] Shu G, Zhao M, Tian H, Wei H, Liang X, Huo Y, et al. Experimental investigation on thermal OS/ORC (Oil Storage/Organic Rankine Cycle) system for waste heat recovery from diesel engine. *Energy* 2016;107:693–706. <https://doi.org/10.1016/J.ENERGY.2016.04.062>.
- [140] Yu G, Shu G, Tian H, Wei H, Liu L. Simulation and thermodynamic analysis of a bottoming Organic Rankine Cycle (ORC) of diesel engine (DE). *Energy* 2013;51:281–90. <https://doi.org/10.1016/J.ENERGY.2012.10.054>.
- [141] Cornelis Havenith, Stein J. WHDC Worldwide Heavy-Duty Certification Validation Results Executive Summary, Informal document No. 12 (43rd GRPE session). Dübendorf: 2002.
- [142] Escudero AI, Espatolero S, Romeo LM, Lara Y, Paufigue C, Lesort AL, et al. Minimization of CO₂ capture energy penalty in second generation oxy-fuel power plants. *Appl Therm Eng* 2016;103:274–81. <https://doi.org/10.1016/j.applthermaleng.2016.04.116>.
- [143] Gibson JAA, Mangano E, Shiko E, Greenaway AG, Gromov A V., Lozinska MM, et al. Adsorption Materials and Processes for Carbon Capture from Gas-Fired Power Plants: AMPGas. *Ind Eng Chem Res* 2016;55:3840–51. <https://doi.org/10.1021/acs.iecr.5b05015>.
- [144] Hovington P, Ghaffari-Nik O, Mariac L, Liu A, Henkel B, Marx S. Rapid Cycle Temperature Swing Adsorption Process Using Solid Structured Sorbent for CO₂ capture from Cement Flue Gas. *SSRN Electronic Journal* 2021. <https://doi.org/10.2139/ssrn.3814414>.
- [145] Ping X, Yang F, Zhang H, Zhang J, Zhang W, Song G. Introducing machine learning and hybrid algorithm for prediction and optimization of multistage centrifugal pump in an ORC system. *Energy* 2021;222. <https://doi.org/10.1016/j.energy.2021.120007>.
- [146] Noah Yakah. Heat Exchanger Design for a Solar Gas-Turbine Power Plant. Master of Science Thesis. KTH School of Industrial Engineering and Management, 2012.
- [147] Vodicka V, Novotny V, Mascuch J, Kolovratnik M. Impact of major leakages on characteristics of a rotary vane expander for ORC. *Energy Procedia*, vol.

- 129, Elsevier Ltd; 2017, p. 387–94. <https://doi.org/10.1016/j.egypro.2017.09.249>.
- [148] Perry RH, Green DW, Maloney JO. Perry's chemical engineers' handbook. McGraw-Hill; 1997.
- [149] Lu C, Bai H, Wu B, Su F, Hwang JF. Comparative study of CO₂ capture by carbon nanotubes, activated carbons, and zeolites. *Energy and Fuels* 2008;22:3050–6. <https://doi.org/10.1021/ef8000086>.
- [150] Emerson Climate Technologies. Copeland™ Stream Semi-Hermetic Compressors for Use with CO₂ in Transcritical & Subcritical Applications Application Guidelines 2019:1–47. <https://www.copeland.com/documents/copeland-stream-co2-semi-hermetic-compressors-for-use-co2-in-transcritical-subcritical-applications-4mtl-05-to-4mtl-50-4msl-03-to-4msl-15-application-guidelines-en-gb-4218052.pdf> (accessed December 29, 2023).
- [151] Yang K, Zhang H, Song S, Zhang J, Wu Y, Zhang Y, et al. Performance Analysis of the Vehicle Diesel Engine-ORC Combined System Based on a Screw Expander. *Energies* (Basel) 2014;7:3400–19. <https://doi.org/10.3390/en7053400>.
- [152] Pezzella G, Bhatt PM, AlHaji A, Ramirez A, Grande CA, Gascon J, et al. Onboard capture and storage system using metal-organic frameworks for reduced carbon dioxide emissions from vehicles. *Cell Rep Phys Sci* 2023;4:101467. <https://doi.org/10.1016/j.xcrp.2023.101467>.
- [153] Casadei A, Broda R, Ricardo Inc. Impact of Vehicle Weight Reduction on Fuel Economy for Various Vehicle Architectures. The Aluminum Association, Inc 2008:1–60. copy obtained from https://www.h3xed.com/blogmedia/Ricardo_FE_MPG_Study.pdf (accessed January 7, 2024).
- [154] Wu K, Deng S, Li S, Zhao R, Yuan X, Zhao L. Preliminary experimental study on the performance of CO₂ capture prototype based on temperature swing adsorption (TSA). *Carbon Capture Science and Technology* 2022;2. <https://doi.org/10.1016/j.ccst.2022.100035>.
- [155] Li H, Guo H, Shen S. Low-Energy-Consumption CO₂ Capture by Liquid-Solid Phase Change Absorption Using Water-Lean Blends of Amino Acid Salts and 2-Alkoxyethanols. *ACS Sustain Chem Eng* 2020;8:12956–67. <https://doi.org/10.1021/acssuschemeng.0c03525>.
- [156] Tian W, Ma K, Ji J, Tang S, Zhong S, Liu C, et al. Nonaqueous MEA/PEG200 absorbent with high efficiency and low energy consumption for CO₂ capture. *Ind Eng Chem Res* 2021;60:3871–80. <https://doi.org/10.1021/acs.iecr.0c05294>.
- [157] Žukauskas A. Heat Transfer from Tubes in Crossflow. *Adv Heat Transf* 1972;8:93–160. [https://doi.org/10.1016/S0065-2717\(08\)70038-8](https://doi.org/10.1016/S0065-2717(08)70038-8).

- [158] Gnielinski V. New Equations for Heat and Mass Transfer in Turbulent Pipe and Channel Flow. *International Chemical Engineering* 1976;16:359–68.
- [159] Gu HF, Chen Q, Wang HJ, Zhang HQ. Condensation of a hydrocarbon in the presence of a non-condensable gas: Heat and mass transfer. *Appl Therm Eng* 2015;91:938–45. <https://doi.org/10.1016/j.applthermaleng.2015.08.092>.
- [160] Kandlikar SG (Satish G), Shoji M, Dhir VK. *Handbook of phase change : boiling and condensation*. vol. 1. Taylor & Francis; 1999.
- [161] Incropera F, DeWitt D, Bergman T, Lavine A. *Fundamentals of Heat and Mass Transfer*. vol. 6. New York: Wiley; 1996.
- [162] Rohsenow WM. A Method of Correlating Heat-Transfer Data for Surface Boiling of Liquids. *J Fluids Eng* 1952;74:969–75. <https://doi.org/10.1115/1.4015984>.
- [163] Collier J, Thome John. *Convective Boiling and Condensation*. 3rd ed. New York: Oxford University Press; 1996.
- [164] Chato John. Chato, J. C. (1960). *Laminar condensation inside horizontal and inclined tubes* (Doctoral dissertation, Massachusetts Institute of Technology). PhD Thesis. Massachusetts Institute of Technology, 1960.
- [165] Holman JP. *Heat Transfer*. 10th ed. New York: McGraw-Hill; 2010.
- [166] Jin Z, Tian B, Wang L, Wang R. Comparison on thermal conductivity and permeability of granular and consolidated activated carbon for refrigeration. *Chin J Chem Eng* 2013;21:676–82. [https://doi.org/10.1016/S1004-9541\(13\)60525-X](https://doi.org/10.1016/S1004-9541(13)60525-X).
- [167] Wang X, Guo R, Xu D, Chung J, Kaviani M, Huang B. Anisotropic Lattice Thermal Conductivity and Suppressed Acoustic Phonons in MOF-74 from First Principles. *Journal of Physical Chemistry C* 2015;119:26000–8. <https://doi.org/10.1021/acs.jpcc.5b08675>.
- [168] Yu H, Zhang H, Zhao J, Liu J, Xia X, Wu X. Thermal conductivity of micro/nano-porous polymers: Prediction models and applications. *Front Phys (Beijing)* 2022;17:23202. <https://doi.org/10.1007/s11467-021-1107-4>.
- [169] Ann Marie Flynn, Toshihiro Akashige, Louis Theodore. *Kern's Process Heat Transfer*. 2nd ed. New Jersey: Wiley; 2018.
- [170] Hofmann E, Maucher D, Hornstein J, den Ouden R. *Capital Equipment Purchasing*. vol. 2. Berlin, Heidelberg: Springer Berlin Heidelberg; 2012. <https://doi.org/10.1007/978-3-642-25737-7>.
- [171] Wang N, Verzijlbergh RA, Heijnen PW, Herder PM. Incorporating indirect costs into energy system optimization models: Application to the Dutch national program Regional Energy Strategies. *Energy* 2023;276:127558. <https://doi.org/10.1016/j.energy.2023.127558>.

- [172] Gasolineras GNC. Guía de Precios actualizada a diario 2024. <https://www.gasolinerasgnc.com/> (accessed July 9, 2024).
- [173] Alshammari F, Karvountzis-Kontakiotis A, Pesyridis A, Usman M. Expander Technologies for Automotive Engine Organic Rankine Cycle Applications. *Energies* (Basel) 2018;11:1905. <https://doi.org/10.3390/en11071905>.
- [174] Chang C, Liao Z, Costa ALH, Bagajewicz MJ. Globally optimal design of intensified shell and tube heat exchangers using complete set trimming. *Comput Chem Eng* 2022;158:107644. <https://doi.org/10.1016/j.compchemeng.2021.107644>.
- [175] Smith Robin. *Chemical Process: Design and Integration*. West Sussex: John Wiley & Sons; 2005.
- [176] Shamoushaki M, Niknam PH, Talluri L, Manfrida G, Fiaschi D. Development of Cost Correlations for the Economic Assessment of Power Plant Equipment. *Energies* (Basel) 2021;14:2665. <https://doi.org/10.3390/en14092665>.
- [177] Astolfi M. Techno-economic Optimization of Low Temperature CSP Systems Based on ORC with Screw Expanders. *Energy Procedia*, vol. 69, Elsevier Ltd; 2015, p. 1100–12. <https://doi.org/10.1016/j.egypro.2015.03.220>.
- [178] Quoilin S, Declaye S, Tchanché BF, Lemort V. Thermo-economic optimization of waste heat recovery Organic Rankine Cycles. *Appl Therm Eng* 2011;31:2885–93. <https://doi.org/10.1016/j.applthermaleng.2011.05.014>.
- [179] Cox B, Innis S, Steen J, Kunz N. The environmental and economic case for valuing water recovery and its relationship with tailings storage conservation. *Miner Eng* 2023;201:108157. <https://doi.org/10.1016/j.mineng.2023.108157>.
- [180] De Saint Jean M, Baurens P, Bouallou C, Couturier K. Economic assessment of a power-to-substitute-natural-gas process including high-temperature steam electrolysis. *Int J Hydrogen Energy* 2015;40:6487–500. <https://doi.org/10.1016/j.ijhydene.2015.03.066>.
- [181] Max Stone Peters, Klaus D. Timmerhaus. *Plant Design and Economics for Chemical Engineers*. McGraw-Hill Companies; 1990.
- [182] Abu-Zahra MRM, Niederer JPM, Feron PHM, Versteeg GF. CO₂ capture from power plants. Part II. A parametric study of the economical performance based on mono-ethanolamine. *International Journal of Greenhouse Gas Control* 2007;1:135–42. [https://doi.org/10.1016/S1750-5836\(07\)00032-1](https://doi.org/10.1016/S1750-5836(07)00032-1).
- [183] Bailera M, Espatolero S, Lisbona P, Romeo LM. Power to gas-electrochemical industry hybrid systems: A case study. *Appl Energy* 2017;202:435–46. <https://doi.org/10.1016/j.apenergy.2017.05.177>.

- [184] Tlili N, Grévilot G, Vallières C. Carbon dioxide capture and recovery by means of TSA and/or VSA. *International Journal of Greenhouse Gas Control* 2009;3:519–27. <https://doi.org/10.1016/j.ijggc.2009.04.005>.
- [185] Iveco company. IVECO DAILY technical information 2015. https://www.iveco.com/Denmark/Documents/Configurator/Brochure/Dailyvan_DK.pdf (accessed February 8, 2023).
- [186] Ally J, Pryor T. Life cycle costing of diesel, natural gas, hybrid and hydrogen fuel cell bus systems: An Australian case study. *Energy Policy* 2016;94:285–94. <https://doi.org/10.1016/j.enpol.2016.03.039>.
- [187] Holland SP, Mansur ET, Muller NZ, Yates AJ. The environmental benefits of transportation electrification: Urban buses. *Energy Policy* 2021;148. <https://doi.org/10.1016/j.enpol.2020.111921>.
- [188] Spendelow J, Papageorgopoulos D, Satyapal S. Fuel Cell Technologies Program Record 12012: Fuel Cell Bus Targets. 2012.
- [189] Quarles N, Kockelman KM, Mohamed M. Costs and Benefits of Electrifying and Automating Bus Transit Fleets. *Sustainability* 2020;12:3977. <https://doi.org/10.3390/su12103977>.
- [190] Fleet Owner. Pricing set for GM's CNG vans 2010. <https://www.fleetowner.com/emissions-efficiency/article/21662580/pricing-set-for-gms-cng-vans> (accessed February 28, 2024).
- [191] Wątróbski J, Małecki K, Kijewska K, Iwan S, Karczmarczyk A, Thompson R. Multi-Criteria Analysis of Electric Vans for City Logistics. *Sustainability* 2017;9:1453. <https://doi.org/10.3390/su9081453>.
- [192] Jones J, Genovese A, Tob-Ogu A. Hydrogen vehicles in urban logistics: A total cost of ownership analysis and some policy implications. *Renewable and Sustainable Energy Reviews* 2020;119:109595. <https://doi.org/10.1016/j.rser.2019.109595>.
- [193] Haywood L, Jakob M. The role of the emissions trading scheme 2 in the policy mix to decarbonize road transport in the European Union. *Transp Policy (Oxf)* 2023;139:99–108. <https://doi.org/10.1016/j.tranpol.2023.06.003>.
- [194] Cerrera Iñaki. El transporte por carretera pagará por sus emisiones de carbono a partir de 2027 2022. <https://elmercantil.com/2022/12/22/el-transporte-por-carretera-pagara-por-sus-emisiones-de-carbono-a-partir-de-2027/> (accessed March 30, 2024).
- [195] Zhou T, Roorda MJ, MacLean HL, Luk J. Life cycle GHG emissions and lifetime costs of medium-duty diesel and battery electric trucks in Toronto, Canada. *Transp Res D Transp Environ* 2017;55:91–8. <https://doi.org/10.1016/j.trd.2017.06.019>.

- [196] Perpiñán J, Bailera M, Peña B, Romeo LM, Eveloy V. Technical and economic assessment of iron and steelmaking decarbonization via power to gas and amine scrubbing. *Energy* 2023;276:127616. <https://doi.org/10.1016/j.energy.2023.127616>.
- [197] Barón C, Perpiñán J, Bailera M, Peña B. Techno-economic assessment of glassmaking decarbonization through integration of calcium looping carbon capture and power-to-gas technologies. *Sustain Prod Consum* 2023;41:121–33. <https://doi.org/10.1016/j.spc.2023.07.029>.
- [198] Romeo LM, Minguell D, Shirmohammadi R, Andrés JM. Comparative Analysis of the Efficiency Penalty in Power Plants of Different Amine-Based Solvents for CO₂ Capture. *Ind Eng Chem Res* 2020;59:10082–92. <https://doi.org/10.1021/acs.iecr.0c01483>.
- [199] Cuccia L, Dugay J, Bontemps D, Louis-Louisy M, Vial J. Analytical methods for the monitoring of post-combustion CO₂ capture process using amine solvents: A review. *International Journal of Greenhouse Gas Control* 2018;72:138–51. <https://doi.org/10.1016/J.IJGGC.2018.03.014>.
- [200] Sada E, Hidehiro K, Butt MA. Gas Absorption with Consecutive Chemical Reaction: Absorption of Carbon Dioxide into Aqueous Amine Solutions Chemical absorption mechanism. *Can J Chem Eng* 1976;54:421–4. <https://doi.org/10.1002/cjce.5450540507>.
- [201] Sønderby TL, Carlsen KB, Fosbøl PL, Kiørboe LG, von Solms N. A new pilot absorber for CO₂ capture from flue gases: Measuring and modelling capture with MEA solution. *International Journal of Greenhouse Gas Control* 2013;12:181–92. <https://doi.org/10.1016/J.IJGGC.2012.10.010>.
- [202] el Hadri N, Quang DV, Goetheer ELV, Abu Zahra MRM. Aqueous amine solution characterization for post-combustion CO₂ capture process. *Appl Energy* 2017;185:1433–49. <https://doi.org/10.1016/j.apenergy.2016.03.043>.
- [203] Ali BS, Aroua MK. Effect of piperazine on CO₂ loading in aqueous solutions of MDEA at low pressure. *Int J Thermophys* 2004;25:1863–70. <https://doi.org/10.1007/s10765-004-7740-7>.
- [204] Wang Y, Zhao L, Otto A, Robinius M, Stolten D. A Review of Post-combustion CO₂ Capture Technologies from Coal-fired Power Plants. *Energy Procedia* 2017;114:650–65. <https://doi.org/10.1016/j.egypro.2017.03.1209>.
- [205] Stempien JP, Chan SH. Comparative study of fuel cell, battery and hybrid buses for renewable energy constrained areas. *J Power Sources* 2017;340:347–55. <https://doi.org/10.1016/J.JPOWSOUR.2016.11.089>.
- [206] Wenz KP, Serrano-Guerrero X, Barragán-Escandón A, González LG, Clairand JM. Route prioritization of urban public transportation from conventional to electric buses: A new methodology and a study of case in an

intermediate city of Ecuador. *Renewable and Sustainable Energy Reviews* 2021;148:111215. <https://doi.org/10.1016/J.RSER.2021.111215>.

ANNEXES

Annex A

Adsorption and desorption heat at 100% of CCR in the M936G engine

Load	rpm	PPN		MOF		AC	
		Qads [kW]	Qdes [kW]	Qads [kW]	Qdes [kW]	Qads [kW]	Qdes [kW]
100	1000	-27.3251	25.6312	-22.3638	20.6699	-27.3466	25.6527
100	1300	-37.0679	34.7701	-30.3376	28.0398	-37.0971	34.7992
100	1600	-47.7225	44.7642	-39.0577	36.0994	-47.7600	44.8017
100	1900	-52.8597	49.5829	-43.2622	39.9854	-52.9013	49.6245
100	2200	-49.6584	46.5800	-40.6421	37.5638	-49.6974	46.6191
75	1000	-23.1591	21.7234	-18.9542	17.5185	-23.1773	21.7416
75	1300	-33.5220	31.4439	-27.4355	25.3575	-33.5483	31.4703
75	1600	-40.2806	37.7836	-32.9671	30.4701	-40.3123	37.8153
75	1900	-44.5168	41.7572	-36.4341	33.6745	-44.5519	41.7923
75	2200	-42.0343	39.4286	-34.4023	31.7966	-42.0673	39.4616
50	1000	-18.5845	17.4324	-15.2102	14.0581	-18.5991	17.4471
50	1300	-26.3587	24.7248	-21.5729	19.9389	-26.3795	24.7455
50	1600	-32.1167	30.1258	-26.2854	24.2945	-32.1420	30.1511
50	1900	-35.6516	33.4416	-29.1785	26.9685	-35.6797	33.4696
50	2200	-33.6330	31.5481	-27.5264	25.4415	-33.6594	31.5745
25	1000	-14.3795	13.4881	-11.7686	10.8773	-14.3908	13.4994
25	1300	-20.4039	19.1391	-16.6993	15.4344	-20.4200	19.1551
25	1600	-24.8755	23.3335	-20.3590	18.8170	-24.8951	23.3531
25	1900	-27.4984	25.7938	-22.5056	20.8010	-27.5200	25.8154
25	2200	-25.9518	24.3431	-21.2399	19.6311	-25.9722	24.3635

Annex B

Adsorption and desorption heat at 70% of CCR in the M936G engine

Load	rpm	PPN		MOF		AC	
		Q_{ads} [kW]	Q_{des} [kW]	Q_{ads} [kW]	Q_{ads} [kW]	Q_{des} [kW]	Q_{ads} [kW]
100	1000	-19.1276	17.9418	-15.6546	14.4689	-19.1426	17.9569
100	1300	-25.9475	24.3390	-21.2363	19.6279	-25.9679	24.3595
100	1600	-33.4057	31.3349	-27.3404	25.2696	-33.4320	31.3612
100	1900	-37.0018	34.7081	-30.2835	27.9898	-37.0309	34.7372
100	2200	-34.7608	32.6060	-28.4495	26.2946	-34.7882	32.6334
75	1000	-16.2113	15.2064	-13.2679	12.2630	-16.2241	15.2192
75	1300	-23.4654	22.0108	-19.2049	17.7502	-23.4838	22.0292
75	1600	-28.1964	26.4486	-23.0769	21.3290	-28.2186	26.4707
75	1900	-31.1618	29.2301	-25.5039	23.5722	-31.1863	29.2546
75	2200	-29.4240	27.6000	-24.0816	22.2576	-29.4471	27.6231
50	1000	-13.0091	12.2027	-10.6471	9.8407	-13.0194	12.2129
50	1300	-18.4511	17.3073	-15.1010	13.9572	-18.4656	17.3218
50	1600	-22.4817	21.0881	-18.3998	17.0062	-22.4994	21.1058
50	1900	-24.9561	23.4091	-20.4250	18.8779	-24.9758	23.4287
50	2200	-23.5431	22.0837	-19.2685	17.8090	-23.5616	22.1022
25	1000	-10.0656	9.4417	-8.2381	7.6141	-10.0735	9.4496
25	1300	-14.2828	13.3974	-11.6895	10.8041	-14.2940	13.4086
25	1600	-17.4129	16.3335	-14.2513	13.1719	-17.4266	16.3472
25	1900	-19.2489	18.0557	-15.7540	14.5607	-19.2640	18.0708
25	2200	-18.1663	17.0402	-14.8679	13.7418	-18.1806	17.0544

Annex C

Adsorption and desorption heat at 100% of CCR in the F1C engine

Load	rpm	PPN		MOF		AC	
		Q_{ads} [kW]	Q_{des} [kW]	Q_{ads} [kW]	Q_{ads} [kW]	Q_{des} [kW]	Q_{ads} [kW]
100	1000	-8.7208	8.1802	-7.1374	6.5968	-8.7277	8.1871
100	1500	-14.6488	13.7407	-11.9891	11.0810	-14.6603	13.7522
100	2000	-19.3949	18.1926	-15.8734	14.6711	-19.4101	18.2078
100	2500	-24.9579	23.4107	-20.4264	18.8792	-24.9775	23.4304
100	3000	-28.5223	26.7542	-23.3437	21.5756	-28.5448	26.7767
100	3600	-28.4511	26.6874	-23.2854	21.5217	-28.4735	26.7098
75	1000	-7.3543	6.8984	-6.0190	5.5631	-7.3601	6.9042
75	1500	-12.3270	11.5628	-10.0888	9.3247	-12.3367	11.5725
75	2000	-16.3365	15.3238	-13.3703	12.3576	-16.3493	15.3366
75	2500	-21.1665	19.8544	-17.3234	16.0113	-21.1831	19.8710
75	3000	-24.1111	22.6165	-19.7334	18.2387	-24.1301	22.6354
75	3600	-24.1294	22.6336	-19.7483	18.2525	-24.1484	22.6526
50	1000	-5.8999	5.5341	-4.8287	4.4629	-5.9045	5.5388
50	1500	-9.8344	9.2248	-8.0488	7.4392	-9.8421	9.2325
50	2000	-13.0690	12.2588	-10.6961	9.8859	-13.0792	12.2691
50	2500	-16.8263	15.7832	-13.7712	12.7281	-16.8395	15.7965
50	3000	-19.3605	18.1603	-15.8453	14.6451	-19.3757	18.1756
50	3600	-19.2598	18.0659	-15.7629	14.5690	-19.2750	18.0811
25	1000	-4.5741	4.2906	-3.7436	3.4601	-4.5777	4.2942
25	1500	-7.6780	7.2021	-6.2839	5.8080	-7.6841	7.2081
25	2000	-10.2101	9.5772	-8.3563	7.7234	-10.2182	9.5852
25	2500	-13.0690	12.2588	-10.6961	9.8859	-13.0792	12.2691
25	3000	-14.9470	14.0204	-12.2331	11.3066	-14.9588	14.0322
25	3600	-14.9340	14.0083	-12.2225	11.2968	-14.9458	14.0200

Annex D

Adsorption and desorption heat at 70% of CCR in the F1C engine

Load	rpm	PPN		MOF		AC	
		Q_{ads} [kW]	Q_{des} [kW]	Q_{ads} [kW]	Q_{ads} [kW]	Q_{des} [kW]	Q_{ads} [kW]
100	1000	-6.1046	5.7262	-4.9962	4.6178	-6.1094	5.7310
100	1500	-10.2541	9.6185	-8.3923	7.7567	-10.2622	9.6265
100	2000	-13.5764	12.7348	-11.1114	10.2698	-13.5871	12.7455
100	2500	-17.4705	16.3875	-14.2985	13.2155	-17.4843	16.4013
100	3000	-19.9656	18.7280	-16.3406	15.1029	-19.9813	18.7437
100	3600	-19.9158	18.6812	-16.2997	15.0652	-19.9314	18.6969
75	1000	-5.1480	4.8289	-4.2133	3.8942	-5.1521	4.8329
75	1500	-8.6289	8.0940	-7.0622	6.5273	-8.6357	8.1008
75	2000	-11.4355	10.7267	-9.3592	8.6504	-11.4445	10.7356
75	2500	-14.8165	13.8981	-12.1264	11.2079	-14.8282	13.9097
75	3000	-16.8778	15.8315	-13.8134	12.7671	-16.8911	15.8448
75	3600	-16.8906	15.8435	-13.8238	12.7768	-16.9038	15.8568
50	1000	-4.1299	3.8739	-3.3801	3.1240	-4.1332	3.8771
50	1500	-6.8841	6.4573	-5.6342	5.2074	-6.8895	6.4627
50	2000	-9.1483	8.5812	-7.4873	6.9202	-9.1555	8.5884
50	2500	-11.7784	11.0483	-9.6398	8.9097	-11.7877	11.0575
50	3000	-13.5523	12.7122	-11.0917	10.2516	-13.5630	12.7229
50	3600	-13.4819	12.6461	-11.0340	10.1983	-13.4925	12.6567
25	1000	-3.2019	3.0034	-2.6205	2.4220	-3.2044	3.0059
25	1500	-5.3746	5.0414	-4.3988	4.0656	-5.3788	5.0457
25	2000	-7.1471	6.7040	-5.8494	5.4064	-7.1527	6.7097
25	2500	-9.1483	8.5812	-7.4873	6.9202	-9.1555	8.5884
25	3000	-10.4629	9.8143	-8.5632	7.9146	-10.4711	9.8225
25	3600	-10.4538	9.8058	-8.5558	7.9077	-10.4621	9.8140

Annex E

Thermal and combustion efficiencies in the M936G engine

Load	rpm	η_{th} [%]	η_{com} [%]
100	1000	38.81	98.53
100	1300	41.14	98.55
100	1600	39.82	98.54
100	1900	38.04	98.56
100	2200	35.35	98.58
75	1000	31.72	98.58
75	1300	34.16	98.58
75	1600	33.39	98.59
75	1900	31.76	98.59
75	2200	28.91	98.62
50	1000	22.25	98.66
50	1300	25.88	98.62
50	1600	25.09	98.62
50	1900	23.57	98.64
50	2200	20.87	98.63
25	1000	10.58	98.75
25	1300	12.18	98.71
25	1600	12.00	98.70
25	1900	10.95	98.70
25	2200	8.83	98.73

Annex F

Thermal and combustion efficiencies in the F1C engine

Load	rpm	η_{th} [%]	η_{com} [%]
100	1000	32.58	97.83
100	1500	34.50	97.82
100	2000	35.01	97.82
100	2500	33.60	97.86
100	3000	30.86	97.84
100	3600	27.35	97.88
75	1000	27.85	97.87
75	1500	29.10	97.84
75	2000	29.44	97.84
75	2500	27.80	97.90
75	3000	25.17	97.92
75	3600	20.36	98.01
50	1000	20.26	98.01
50	1500	22.10	97.98
50	2000	22.58	97.94
50	2500	21.05	97.94
50	3000	18.47	98.00
50	3600	15.56	98.04
25	1000	8.80	98.28
25	1500	10.24	98.18
25	2000	10.61	98.14
25	2500	10.12	98.12
25	3000	8.75	98.14
25	3600	5.67	98.25

Annex G

Area, temperature, pressure and mass flows of each heat exchanger with the CCS-ORC system operating with PPN.

Engine	CCR	Heat exchanger	Area [m ²]	\dot{m}_{in_HF} [kg/h]	T _{in_HF} [°C]	T _{out_HF} [°C]	\dot{m}_{in_CF} [kg/h]	T _{in_CF} [°C]	T _{out_CF} [°C]	P _{in_HF} [bar]	P _{out_HF} [bar]	P _{in_CF} [bar]	P _{out_CF} [bar]
M936G	100	ORC-H	0.72	104.60	573.87	119.49	527.52	50.93	99.49	75	75	24.9	22.9
		ORC-E	7.59	681.48	421.73	119.49	527.52	99.49	184.15	1.09	1.09	22.9	20.9
		ORC-C	13.77	527.52	121.02	48.87	43529.61	30.00	35.99	1.5	1	1	1
		HE-CO ₂ -C	0.95	104.60	150.00	39.23	43529.61	35.99	36.23	1	1	1	1
		CO ₂ -Con	2.46	104.60	119.49	29.30	43529.61	25.00	25.58	75	75	1	1
		HE-EG1	25.30	681.48	119.49	39.23	43529.61	36.23	41.05	1	1	1	1
		HE-EG2	11.20	681.48	39.23	30.00	43529.61	25.58	26.31	1	1	1	1
		ORC-H	0.57	73.53	581.23	102.28	617.26	50.93	82.47	75	75	24.9	22.9
M936G	70	ORC-E	8.16	681.48	483.01	102.47	617.26	82.47	184.15	1.09	1.09	22.9	20.9
		ORC-C	16.53	617.26	121.07	48.87	32357.23	30.00	39.42	1.5	1	1	1
		HE-CO ₂ -C	0.67	73.53	150.00	42.70	32357.23	39.42	39.65	1	1	1	1
		CO ₂ -Con	1.82	73.53	102.28	29.30	32357.23	25.00	25.50	75	75	1	1
		HE-EG1	18.74	477.04	102.47	42.65	32357.23	39.65	43.55	1	1	1	1
		HE-EG2	10.18	477.04	42.65	30.00	32357.23	25.50	26.52	1	1	1	1
		ORC-H	0.39	42.49	573.36	79.39	203.44	38.80	95.97	75	75	24.9	22.9
		ORC-E	4.01	276.75	408.58	115.97	203.44	95.97	184.15	1.09	1.09	22.9	20.9
F1C	100	ORC-C	7.92	203.44	121.05	36.76	17615.38	30.00	35.98	1.5	1	1	1
		HE-CO ₂ -C	0.50	42.49	150.00	38.98	17615.38	35.98	36.22	1	1	1	1
		CO ₂ -Con	1.30	42.49	79.39	29.30	17615.38	25.00	25.46	75	75	1	1
		HE-EG1	13.34	276.75	115.97	39.22	17615.38	36.22	41.00	1	1	1	1
		HE-EG2	6.40	276.75	39.22	30.00	17615.38	25.46	26.29	1	1	1	1
		ORC-H	0.30	29.83	580.19	72.21	239.41	40.53	76.58	75	75	24.9	22.9
		ORC-E	4.27	276.75	470.12	96.58	239.41	76.58	184.15	1.09	1.09	22.9	20.9
		ORC-C	8.84	239.41	121.03	38.48	13162.36	30.00	39.36	1.5	1	1	1
F1C	70	HE-CO ₂ -C	0.35	29.83	150.00	42.36	13162.36	39.36	39.58	1	1	1	1
		CO ₂ -Con	0.96	29.83	72.21	29.30	13162.36	25.00	25.41	75	75	1	1
		HE-EG1	9.81	193.73	96.58	42.58	13162.36	39.58	43.38	1	1	1	1
		HE-EG2	5.38	193.73	42.58	30.00	13162.36	25.41	26.53	1	1	1	1

Annex H.

Area, temperature, pressure and mass flows of each heat exchanger with the CCS-ORC system operating with MOF.

Engine	CCR	Heat exchanger	Area [m ²]	\dot{m}_{in_HF} [kg/h]	T _{in_HF} [°C]	T _{out_HF} [°C]	\dot{m}_{in_CF} [kg/h]	T _{in_CF} [°C]	T _{out_CF} [°C]	P _{in_HF} [bar]	P _{out_HF} [bar]	P _{in_CF} [bar]	P _{out_CF} [bar]
M936G	100	ORC-H	0.75	104.99	584.02	116.12	591.17	50.93	96.11	77.9	77.9	24.9	22.9
		ORC-E	7.66	681.48	458.93	116.13	591.17	96.11	184.15	1.09	1.09	22.9	20.9
		ORC-C	15.61	591.17	121.02	48.87	38743.25	30.00	37.54	1.5	1	1	1
		HE-CO ₂ -C	0.95	104.99	150.00	40.80	38743.25	37.54	37.81	1	1	1	1
		CO ₂ -Con	2.54	104.99	116.12	29.30	38743.25	25.00	25.66	77.9	77.9	1	1
		HE-EG1	25.37	681.48	116.13	40.81	38743.25	37.81	42.97	1	1	1	1
		HE-EG2	13.02	681.48	40.81	30.00	38743.25	25.66	26.66	1	1	1	1
M936G	70	ORC-H	0.59	73.67	591.15	101.33	659.74	50.93	81.33	77.9	77.9	24.9	22.9
		ORC-E	8.17	681.48	508.67	101.33	659.74	81.33	184.15	1.09	1.09	22.9	20.9
		ORC-C	17.90	659.74	121.02	48.87	29315.32	30.00	41.12	1.5	1	1	1
		HE-CO ₂ -C	0.67	73.67	150.00	44.35	29315.32	41.12	41.36	1	1	1	1
		CO ₂ -Con	1.87	73.67	101.33	29.30	29315.32	25.00	25.56	77.9	77.9	1	1
		HE-EG1	18.36	477.04	101.33	44.36	29315.32	41.36	45.42	1	1	1	1
		HE-EG2	11.58	477.04	44.36	30.00	29315.32	25.56	26.91	1	1	1	1
F1C	100	ORC-H	0.39	42.64	603.38	78.40	229.23	40.49	92.90	77.9	77.9	24.9	22.9
		ORC-E	4.02	276.75	445.94	112.90	229.23	92.90	184.15	1.09	1.09	22.9	20.9
		ORC-C	8.36	229.23	121.03	38.44	15659.74	30.00	37.53	1.5	1	1	1
		HE-CO ₂ -C	0.50	42.64	150.00	40.53	15659.74	37.53	37.80	1	1	1	1
		CO ₂ -Con	1.33	42.64	78.40	29.30	15659.74	25.00	25.52	77.9	77.9	1	1
		HE-EG1	13.30	276.75	112.90	40.81	15659.74	37.80	42.93	1	1	1	1
		HE-EG2	6.88	276.75	40.81	30.00	15659.74	25.52	26.64	1	1	1	1
F1C	70	ORC-H	0.31	29.92	590.55	71.49	256.24	40.64	75.40	77.9	77.9	24.9	22.9
		ORC-E	4.27	276.75	495.89	95.40	256.24	75.40	184.15	1.09	1.09	22.9	20.9
		ORC-C	9.56	256.24	121.04	38.59	11909.73	30.00	41.06	1.5	1	1	1
		HE-CO ₂ -C	0.35	29.92	150.00	44.06	11909.73	41.06	41.31	1	1	1	1
		CO ₂ -Con	0.98	29.92	71.49	29.30	11909.73	25.00	25.46	77.9	77.9	1	1
		HE-EG1	9.61	193.73	95.40	44.31	11909.73	41.31	45.27	1	1	1	1
		HE-EG2	6.12	193.73	44.31	30.00	11909.73	25.46	26.91	1	1	1	1

Annex I.

Area, temperature, pressure and mass flows of each heat exchanger with the CCS-ORC system operating with AC.

Engine	CCR	Heat exchanger	Area [m ²]	\dot{m}_{in_HF} [kg/h]	T _{in_HF} [°C]	T _{out_HF} [°C]	\dot{m}_{in_CF} [kg/h]	T _{in_CF} [°C]	T _{out_CF} [°C]	P _{in_HF} [bar]	P _{out_HF} [bar]	P _{in_CF} [bar]	P _{out_CF} [bar]
M936G	100	ORC-H	0.79	113.81	625.81	127.79	535.11	50.93	107.78	85.73	85.73	24.9	22.9
		ORC-E	7.17	681.48	421.58	127.91	535.11	107.78	184.15	1.09	1.09	22.9	20.9
		ORC-C	13.97	535.11	121.02	48.87	44269.95	30.00	35.97	1.5	1	1	1
		HE-CO ₂ -C	1.05	113.81	150.00	39.24	44269.95	35.97	36.24	1	1	1	1
		CO ₂ -Con	2.64	113.81	127.79	29.30	44269.95	25.00	25.65	85.73	85.73	1	1
		HE-EG1	24.23	681.48	127.91	39.24	44269.95	36.24	41.12	1	1	1	1
		HE-EG2	11.31	681.48	39.24	30.00	44269.95	25.65	26.37	1	1	1	1
M936G	70	ORC-H	0.63	79.90	633.15	108.01	623.90	50.93	88.02	85.73	85.73	24.9	22.9
		ORC-E	7.95	681.48	482.90	108.02	623.90	88.02	184.15	1.09	1.09	22.9	20.9
		ORC-C	16.71	623.90	121.02	48.87	32794.40	30.00	39.40	1.5	1	1	1
		HE-CO ₂ -C	0.73	79.90	149.98	42.65	32794.40	39.40	39.64	1	1	1	1
		CO ₂ -Con	1.96	79.90	108.01	29.30	32794.40	25.00	25.55	85.73	85.73	1	1
		HE-EG1	17.99	477.04	108.02	42.64	32794.40	39.64	43.58	1	1	1	1
		HE-EG2	10.25	477.04	42.64	30.00	32794.40	25.55	26.57	1	1	1	1
F1C	100	ORC-H	0.42	46.22	625.21	87.26	206.70	40.30	106.17	85.73	85.73	24.9	22.9
		ORC-E	3.79	276.75	408.42	126.17	206.70	106.17	184.15	1.09	1.09	22.9	20.9
		ORC-C	7.51	206.70	121.05	38.26	17843.54	30.00	35.96	1.5	1	1	1
		HE-CO ₂ -C	0.55	46.22	150.00	38.96	17843.54	35.96	36.23	1	1	1	1
		CO ₂ -Con	1.38	46.22	87.26	29.30	17843.54	25.00	25.52	85.73	85.73	1	1
		HE-EG1	12.72	276.75	126.17	39.23	17843.54	36.23	41.13	1	1	1	1
		HE-EG2	5.99	276.75	39.23	30.00	17843.54	25.52	26.34	1	1	1	1
F1C	70	ORC-H	0.33	32.45	632.61	71.79	242.05	40.57	83.19	85.73	85.73	24.9	22.9
		ORC-E	4.16	276.75	470.00	103.19	242.05	83.19	184.15	1.09	1.09	22.9	20.9
		ORC-C	8.93	242.05	121.04	38.52	13247.07	30.00	39.40	1.5	1	1	1
		HE-CO ₂ -C	0.38	32.45	150.00	42.40	13247.07	39.40	39.64	1	1	1	1
		CO ₂ -Con	1.02	32.45	71.79	29.30	13247.07	25.00	25.43	85.73	85.73	1	1
		HE-EG1	9.41	193.73	103.19	42.64	13247.07	39.64	43.53	1	1	1	1
		HE-EG2	5.42	193.73	42.64	30	13247.07	25.43	26.55	1	1	1	1

Annex J

Discretization of the mathematical model used in the design of the TSA device:

Central nodes

$$k \frac{T_{m+1}^{i+1} - 2T_m^{i+1} + T_{m-1}^{i+1}}{\Delta r^2} + \frac{k}{i} \left(\frac{T_{m+1}^{i+1} - T_{m-1}^{i+1}}{2\Delta r^2} \right) = \rho C_p \frac{T_m^{i+1} - T_m^i}{\Delta t}$$

At $r = 0$ equation 14 is indeterminate, therefore the l'Hôpital's rule must be applied, obtaining:

$$2k \frac{\partial^2 T}{\partial r^2} = \rho C_p \frac{\partial T}{\partial t}$$

This latter equation is discretized by taking the mirror image and isolated boundary, obtaining the following discretization:

$$4k \frac{T_{m+1}^{i+1} - T_m^{i+1}}{\Delta r^2} = \rho C_p \frac{T_m^{i+1} - T_m^i}{\Delta t}$$

On the surface

$$\frac{2kT_{m-1}^{i+1}}{dr^2} - T_m^{i+1} \left[\left(\frac{2k}{dr^2} + \frac{2h}{dr} + \frac{2h}{idr} + \frac{\rho C_p}{\Delta t} \right) + 1 \right] = -T_m^i \left(\frac{\rho C_p}{\Delta t} \right) - \frac{2hT_\infty}{dr} - \frac{hT_\infty}{idr}$$


Annex K

Impact factor and category of the journals of the articles published in this thesis.

1. García-Mariaca, A. Llera-Sastresa, E. Review on Carbon Capture in ICE Driven Transport. *Energies* (2021), 14, 6865. <https://doi.org/10.3390/en14216865>

Journal: Energies; Q3 in 2021

2023 Journal Performance Data for: Energies

 Open Access since 2008

ISSN	EISSN	
N/A	1996-1073	
JCR ABBREVIATION	ISO ABBREVIATION	
ENERGIES	Energies	
Journal Information		
EDITION	CATEGORY	
Science Citation Index Expanded (SCIE)	ENERGY & FUELS	
LANGUAGES	REGION	1ST ELECTRONIC JCR YEAR
English	SWITZERLAND	2010
Publisher Information		
PUBLISHER	ADDRESS	PUBLICATION FREQUENCY
MDPI	ST ALBAN-ANLAGE 66, CH-4052 BASEL, SWITZERLAND	24 issues/year

Journal's Performance

Journal Impact Factor

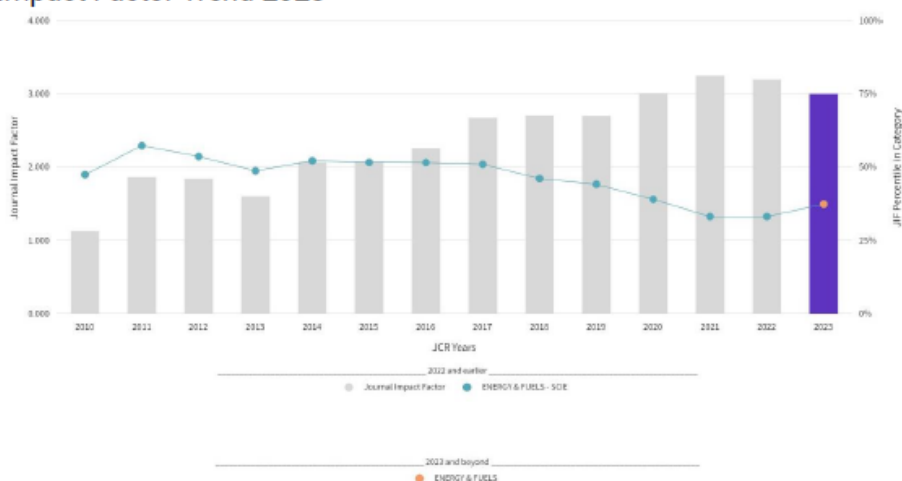
2023 JOURNAL IMPACT FACTOR

3.0

2023 JOURNAL IMPACT FACTOR WITHOUT SELF CITATIONS

2.4

Journal Impact Factor Trend 2023



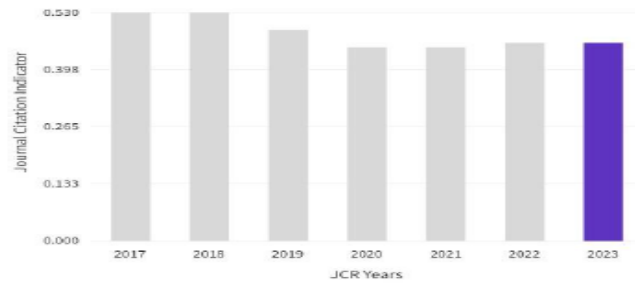
Journal Impact Factor is calculated using the following metrics

Citations in 2023 to items published in 2021 (26,303) - 2022 (27,160)	=	53,463	=	3.0
Number of citable items in 2021 (8,530) + 2022 (9,399)	=	17,929		

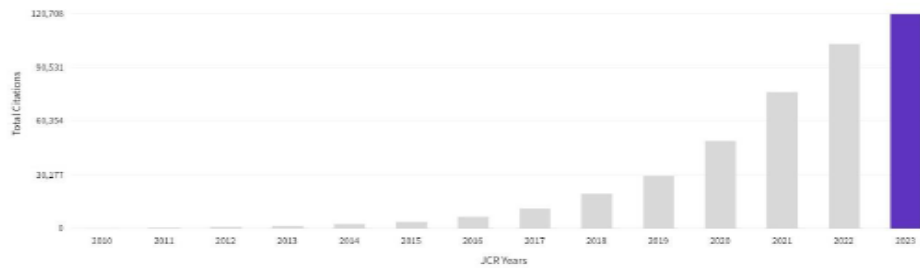
Journal Impact Factor without self cites is calculated using the following metrics

Citations in 2023 to items published in 2021 (26,303) + 2022 (27,160) - Self Citations in 2023 to items published in 2021 (4,723) + 2022 (6,295)	=	53,463 - 11,018	=	2.4
Number of citable items in 2021 (8,530) + 2022 (9,399)	=	17,929		

Journal Citation Indicator (JCI) 0.46



Total Citations 20,708



Rank by Journal Impact factor

CATEGORY
ENERGY & FUELS

107/170

JCR YEAR	JIF RANK	QUART JIF PERCENTILE ILE	
2023	107/170	Q3 37.4	<div><div></div></div>

Rank by JIF before 2023 for ENERGY & FUELS

EDITION

Science Citation Index Expanded (SCIE)

JCR YEAR	JIF RANK	QUART JIF PERCENTILE ILE	
2022	80/119	Q3 33.2	<div><div></div></div>
2021	80/119	Q3 33.19	<div><div></div></div>
2020	70/114	Q3 39.04	<div><div></div></div>
2019	63/112	Q3 44.20	<div><div></div></div>
2018	56/103	Q3 46.12	<div><div></div></div>
2017	48/97	Q2 51.03	<div><div></div></div>

Rank by Journal Citation Indicator (JCI)

CATEGORY
ENERGY & FUELS

115/173

JCR YEAR	JCI RANK	QUART JCI PERCENTILE ILE	
2023	115/173	Q3 33.82	<div><div></div></div>
2022	99/155	Q3 36.45	<div><div></div></div>
2021	93/145	Q3 36.21	<div><div></div></div>
2020	81/133	Q3 39.47	<div><div></div></div>
2019	73/132	Q3 45.08	<div><div></div></div>
2018	70/131	Q3 46.95	<div><div></div></div>
2017	68/126	Q3 46.43	<div><div></div></div>

2. García-Mariaca, A., Llera-Sastresa, E., & Moreno, F. (2022). Application of ORC to reduce the energy penalty of carbon capture in non-stationary ICE. Energy Conversion and Management, 268, 116029. <https://doi.org/10.1016/j.enconman.2022.116029>

Journal: Energy Conversion and Management; Q1 in 2022

2023 Journal Performance Data for: ENERGY CONVERSION AND MANAGEMENT

ISSN	EISSN	
0196-8904	1879-2227	
JCR ABBREVIATION	ISO ABBREVIATION	
ENERG CONVERS MANAGE	Energy Conv. Manag.	
Journal Information		
EDITION	CATEGORY	
Science Citation Index Expanded (SCIE)	MECHANICS ENERGY & FUELS THERMODYNAMICS	
LANGUAGES	REGION	1ST ELECTRONIC JCR YEAR
English	ENGLAND	1997
Publisher Information		
PUBLISHER	ADDRESS	PUBLICATION FREQUENCY
PERGAMON-ELSEVIER SCIENCE LTD	THE BOULEVARD, LANGFORD LANE, KIDLINGTON, OXFORD OX5 1GB, ENGLAND	24 issues/year

Journal's Performance

Journal Impact Factor

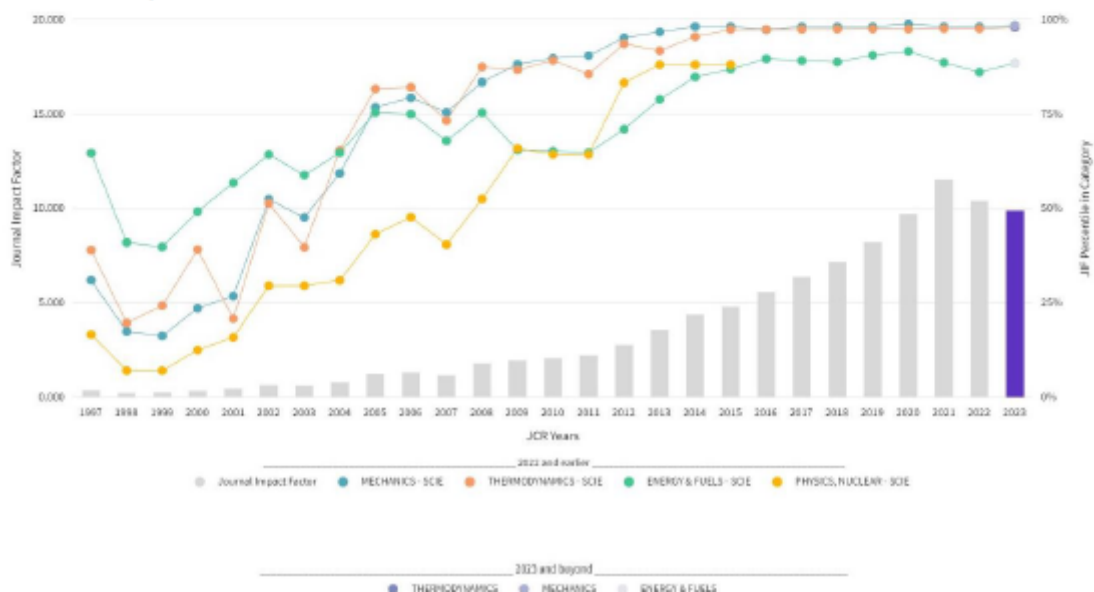
2023 JOURNAL IMPACT FACTOR

9.9

2023 JOURNAL IMPACT FACTOR WITHOUT SELF CITATIONS

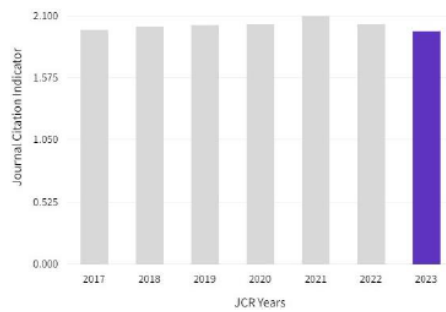
8.7

Journal Impact Factor Trend 2023

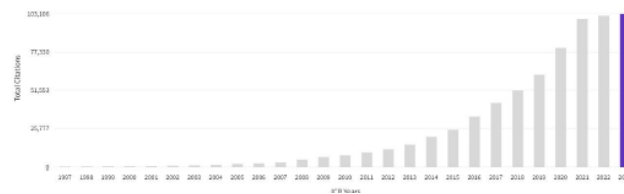


Journal Impact Factor is calculated using the following metrics			
Citations in 2023 to items published in 2021 (13,702) - 2022 (11,784)		25,486	
<hr/>			
Number of citable items in 2021 (1,298) + 2022 (1,278)		2,576	= 9.9
<hr/>			
Journal Impact Factor without self cites is calculated using the following metrics			
Citations in 2023 to items published in 2021 (13,702) + 2022 (11,784) - Self Citations in 2023 to items published in 2021 (1,300) + 2022 (1,670)		25,486 - 2,970	
<hr/>			
Number of citable items in 2021 (1,298) + 2022 (1,278)		2,576	= 8.7

Journal Citation Indicator (JCI) 1.97



Total Citations 103,106



Rank by Journal Impact factor

CATEGORY **ENERGY & FUELS 20/170**

EDITION

Science Citation Index Expanded (SCIE)

JCR YEAR	JIF RANK	QUART JIF PERCENTILE	ILE
2023	20/170	Q1 88.5	
2022	17/119	Q1 86.1	
2021	14/119	Q1 88.66	
2020	10/114	Q1 91.67	
2019	11/112	Q1 90.63	
2018	12/103	Q1 88.83	
2017	11/97	Q1 89.18	

CATEGORY **MECHANICS 3/170**

EDITION

Science Citation Index Expanded (SCIE)

JCR YEAR	JIF RANK	QUART JIF PERCENTILE	ILE
2023	3/170	Q1 98.5	
2022	3/137	Q1 98.2	
2021	3/138	Q1 98.19	
2020	2/135	Q1 98.89	
2019	3/136	Q1 98.16	
2018	3/134	Q1 98.13	
2017	3/134	Q1 98.13	

CATEGORY **THERMODYNAMICS 2/76**

EDITION

Science Citation Index Expanded (SCIE)

JCR YEAR	JIF RANK	QUART JIF PERCENTILE	ILE
2023	2/76	Q1 98.0	
2022	2/63	Q1 97.6	
2021	2/63	Q1 97.62	
2020	2/60	Q1 97.50	
2019	2/61	Q1 97.54	
2018	2/60	Q1 97.50	
2017	2/59	Q1 97.46	

Rank by Journal Citation Indicator (JCI)

CATEGORY **ENERGY**

& FUELS 13/173

JCR YEAR	JCI RANK	QUART JCI PERCENTILE	ILE
2023	13/173	Q1 92.77	
2022	8/155	Q1 95.16	
2021	8/145	Q1 94.83	
2020	7/133	Q1 95.11	
2019	7/132	Q1 95.08	
2018	7/131	Q1 95.04	
2017	7/126	Q1 94.84	

CATEGORY

MECHANICS 4/170

JCR YEAR	JCI RANK	QUART JCI PERCENTILE	ILE
2023	4/170	Q1 97.94	
2022	4/164	Q1 97.87	
2021	3/163	Q1 98.47	
2020	3/156	Q1 98.40	
2019	3/156	Q1 98.40	
2018	3/154	Q1 98.38	
2017	3/154	Q1 98.38	

CATEGORY

THERMODYNAMICS 2/76

JCR YEAR	JCI RANK	QUART JCI PERCENTILE	ILE
2023	2/76	Q1 98.03	
2022	2/78	Q1 98.08	
2021	2/77	Q1 98.05	
2020	2/73	Q1 97.95	
2019	2/73	Q1 97.95	
2018	2/73	Q1 97.95	
2017	2/73	Q1 97.95	

3. García-Mariaca, A., & Llera-Sastresa, E. (2022). Energy and economic analysis feasibility of CO₂ capture on a natural gas internal combustion engine. *Greenhouse Gases: Science and Technology*, 13(2), 144-159. <https://doi.org/10.1002/ghg.2176>

Journal: Greenhouse Gases: Science and Technology; Q3 in 2023

2023 Journal Performance Data for: Greenhouse Gases-Science and Technology

ISSN	EISSN	
2152-3878	2152-3878	
JCR ABBREVIATION	ISO ABBREVIATION	
GREENH GASES	Greenh. Gases	
Journal Information		
EDITION	CATEGORY	
Science Citation Index Expanded (SCIE)	ENVIRONMENTAL SCIENCES ENERGY & FUELS ENGINEERING, ENVIRONMENTAL	
LANGUAGES	REGION	1ST ELECTRONIC JCR YEAR
English	ENGLAND	2012

Publisher Information	ADDRESS	PUBLICATION FREQUENCY
PUBLISHER	ONE MONTGOMERY ST, SUITE 1200, SAN	6 issues/year
WILEY PERIODICALS, INC	FRANCISCO, CA 94104	

Journal's Performance

Journal Impact Factor

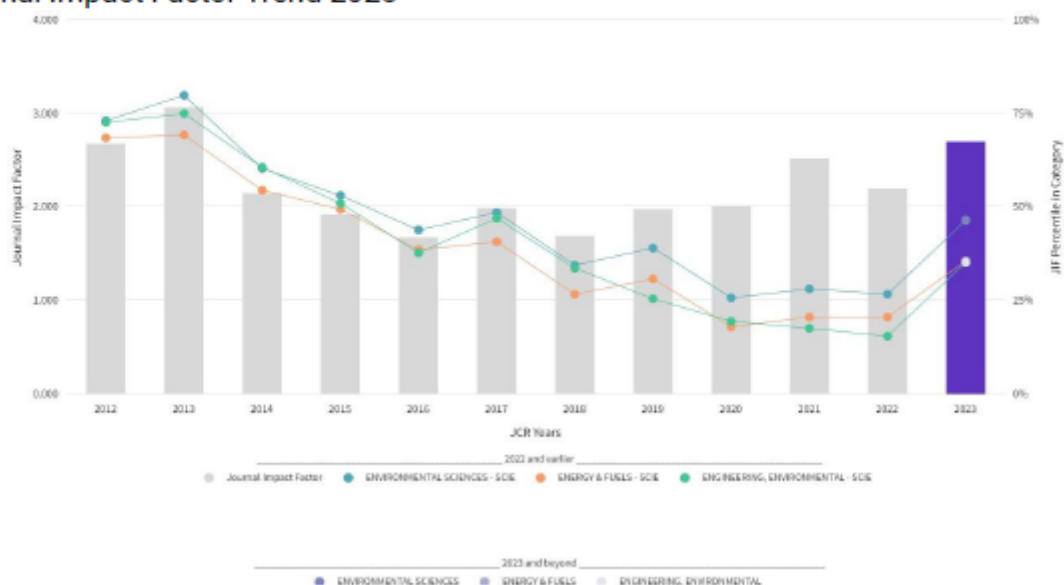
2023 JOURNAL IMPACT FACTOR

2.7

2023 JOURNAL IMPACT FACTOR WITHOUT SELF CITATIONS

2.6

Journal Impact Factor Trend 2023



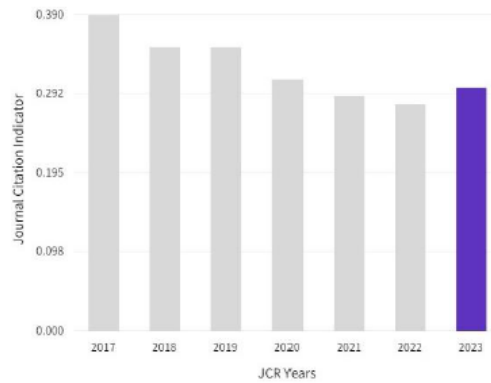
Journal Impact Factor is calculated using the following metrics

Citations in 2023 to items published in 2021 (235) - 2022 (113)	=	348	=	2.7
Number of citable items in 2021 (78) + 2022 (49)	=	127		

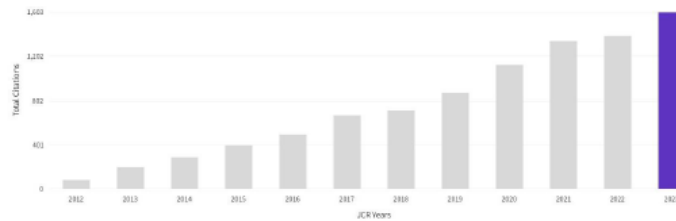
Journal Impact Factor without self cites is calculated using the following metrics

Citations in 2023 to items published in 2021 (235) + 2022 (113) - Self Citations in 2023 to items published in 2021 (10) + 2022 (10)	=	348 - 20	=	2.6
Number of citable items in 2021 (78) + 2022 (49)	=	127		

Journal Citation Indicator (JCI) 0.3



Total Citations 1,603



Rank by Journal Impact factor

CATEGORY **ENERGY & FUELS 110/170**

EDITION

Science Citation Index Expanded (SCIE)

JCR YEAR	JIF RANK	QUART JIF PERCENTILE ILE
2023	110/170	Q3 35.6
2022	95/119	Q4 20.6
2021	95/119	Q4 20.59
2020	94/114	Q4 17.98
2019	78/112	Q3 30.80
2018	76/103	Q3 26.70
2017	58/97	Q3 40.72

CATEGORY

ENGINEERING, ENVIRONMENTAL 53/8

Rank by JIF before 2023 for

ENGINEERING, ENVIRONMENTAL

EDITION

Science Citation Index Expanded (SCIE)

JCR YEAR	JIF RANK	QUART JIF PERCENTILE ILE
2023	53/81	Q3 35.2
2022	47/55	Q4 15.5
2021	45/54	Q4 17.59
2020	44/54	Q4 19.44
2019	40/53	Q4 25.47
2018	35/52	Q3 33.65
2017	27/50	Q3 47.00

CATEGORY

ENVIRONMENTAL SCIENCES 192/358

Rank by JIF before 2023 for

ENVIRONMENTAL SCIENCES

EDITION

Science Citation Index Expanded (SCIE)

JCR YEAR	JIF RANK	QUART JIF PERCENTILE ILE
2023	192/358	Q3 46.5
2022	202/275	Q3 26.7
2021	201/279	Q3 28.14
2020	204/274	Q3 25.73
2019	162/265	Q3 39.06
2018	165/251	Q3 34.46
2017	125/242	Q3 48.55

Rank by Journal Citation Indicator (JCI)

CATEGORY **ENERGY & FUELS 147/173**

EDITION

Science Citation Index Expanded (SCIE)

JCR YEAR	JCI RANK	QUART JCI PERCENTILE ILE
2023	147/173	Q4 15.32
2022	127/155	Q4 18.39
2021	116/145	Q4 20.34
2020	99/133	Q3 25.94
2019	89/132	Q3 32.95
2018	88/131	Q3 33.21
2017	79/126	Q3 37.70

CATEGORY

ENVIRONMENTAL SCIENCES

301/359

Science Citation Index Expanded (SCIE)

JCR YEAR	JCI RANK	QUART JCI PERCENTILE ILE
2023	301/359	Q4 16.30
2022	291/334	Q4 13.02
2021	277/325	Q4 14.92
2020	256/306	Q4 16.50
2019	234/302	Q4 22.68
2018	225/297	Q4 24.41
2017	202/286	Q3 29.55

CATEGORY

ENGINEERING, ENVIRONMENTAL 62/81

Science Citation Index Expanded (SCIE)

JCR YEAR	JCI RANK	QUART JCI PERCENTILE ILE
2023	62/81	Q4 24.07
2022	58/75	Q4 23.33
2021	51/71	Q3 28.87
2020	48/67	Q3 29.10
2019	41/66	Q3 38.64
2018	41/65	Q3 37.69
2017	37/62	Q3 41.13

4. García-Mariaca, A., Llera-Sastresa, E., & Moreno, F. (2024). CO₂ capture feasibility by Temperature Swing Adsorption in heavy-duty engines from an energy perspective. *Energy*, 292, 130511. <https://doi.org/10.1016/j.energy.2024.130511>
Journal: Energy; Q1 in 2023

2023 Journal Performance Data for: Energy

ISSN
0360-5442
JCR ABBREVIATION
ENERGY

EISSN
1873-6785
ISO ABBREVIATION
Energy

Journal Information
EDITION

Science Citation Index Expanded (SCIE)
LANGUAGES
English

CATEGORY

ENERGY & FUELS THERMODYNAMICS
REGION
ENGLAND

1ST ELECTRONIC JCR YEAR
1997

Publisher Information

PUBLISHER
PERGAMON-ELSEVIER SCIENCE LTD

ADDRESS
THE BOULEVARD, LANGFORD LANE,
KIDLINGTON, OXFORD OX5 1GB, ENGLAND

PUBLICATION FREQUENCY
11 issues/year

Journal's Performance

Journal Impact Factor

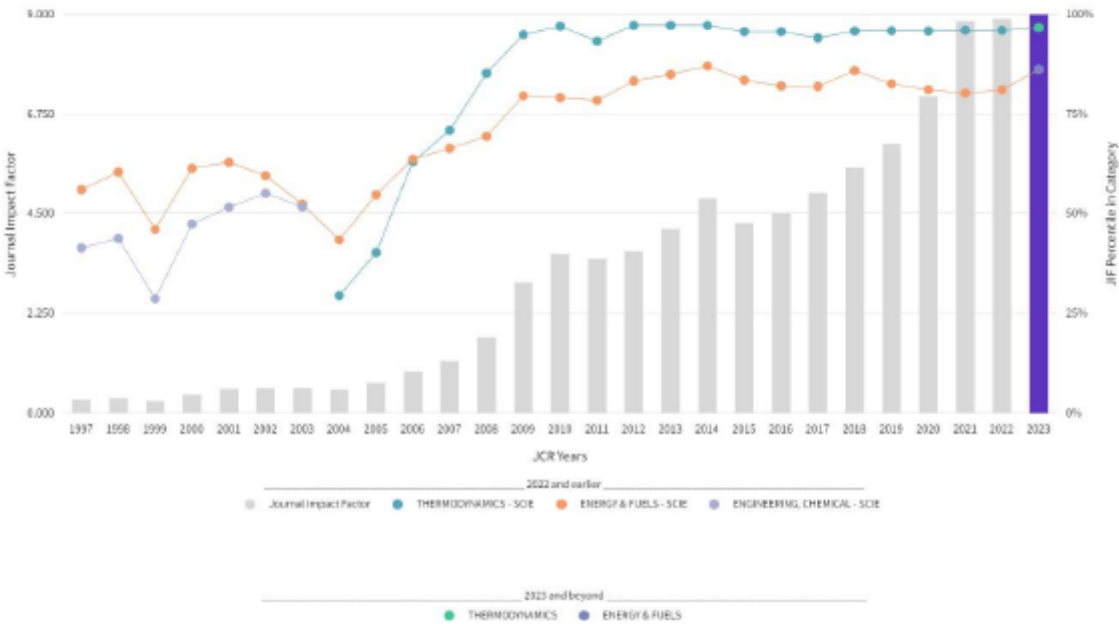
2023 JOURNAL IMPACT FACTOR

9.0

2023 JOURNAL IMPACT FACTOR WITHOUT SELF CITATIONS

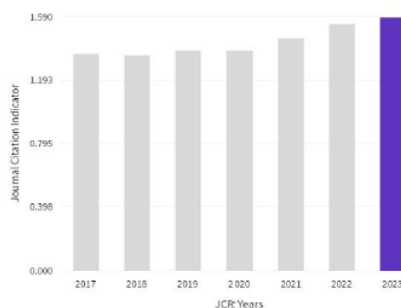
7.5

Journal Impact Factor Trend 2023

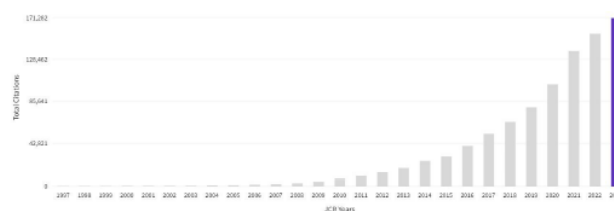


Journal Impact Factor is calculated using the following metrics			
Citations in 2023 to items published in 2021 (33,204) - 2022 (28,199)			
	=	61,403	
Number of citable items in 2021 (3,480) + 2022 (3,372)			
	=	6,852	
	=	9.0	
Journal Impact Factor without self cites is calculated using the following metrics			
Citations in 2023 to items published in 2021 (33,204) + 2022 (28,199) - Self Citations in 2023 to items published in 2021 (4,407) + 2022 (5,319)			
	=	61,403 - 9,726	
Number of citable items in 2021 (3,480) + 2022 (3,372)			
	=	6,852	
	=	7.5	

Journal Citation Indicator (JCI) 1.59



Total Citations 171,282



Rank by Journal Impact factor

CATEGORY ENERGY & FUELS 24/170

EDITION

Science Citation Index Expanded (SCIE)

JCR YEAR	JIF RANK	QUART JIF PERCENTILE	ILE
2023	24/170	Q1 86.2	
2022	23/119	Q1 81.1	
2021	24/119	Q1 80.25	
2020	22/114	Q1 81.14	
2019	20/112	Q1 82.59	
2018	15/103	Q1 85.92	
2017	18/97	Q1 81.96	

CATEGORY THERMODYNAMICS 4/76

JCR YEAR JCI RANK QUART JCI PERCENTILE ILE

2023	4/76	Q1 95.39	
2022	4/78	Q1 95.51	
2021	4/77	Q1 95.45	
2020	4/73	Q1 95.21	
2019	4/73	Q1 95.21	
2018	5/73	Q1 93.84	
2017	8/73	Q1 89.73	

CATEGORY THERMODYNAMICS 3/76

EDITION

Science Citation Index Expanded (SCIE)

JCR YEAR	JIF RANK	QUART JIF PERCENTILE	ILE
2023	3/76	Q1 96.7	
2022	3/63	Q1 96.0	
2021	3/63	Q1 96.03	
2020	3/60	Q1 95.83	
2019	3/61	Q1 95.90	
2018	3/60	Q1 95.83	
2017	4/59	Q1 94.07	

Rank by Journal Citation Indicator (JCI)

CATEGORY ENERGY & FUELS 23/173

JCR YEAR	JCI RANK	QUART JCI PERCENTILE	ILE
2023	23/173	Q1 86.99	
2022	21/155	Q1 86.77	
2021	20/145	Q1 86.55	
2020	18/133	Q1 86.84	
2019	18/132	Q1 86.74	
2018	18/131	Q1 86.64	
2017	19/126	Q1 85.32	

5. García-Mariaca A, Llera Sastresa Eva. (2024). Techno-economic assessment for the practicability of on-board CO₂ capture in ICE vehicles. Applied energy, 376, Part B, 124167. <https://doi.org/10.1016/j.apenergy.2024.124167>

Journal: Applied Energy; Q1in 2023

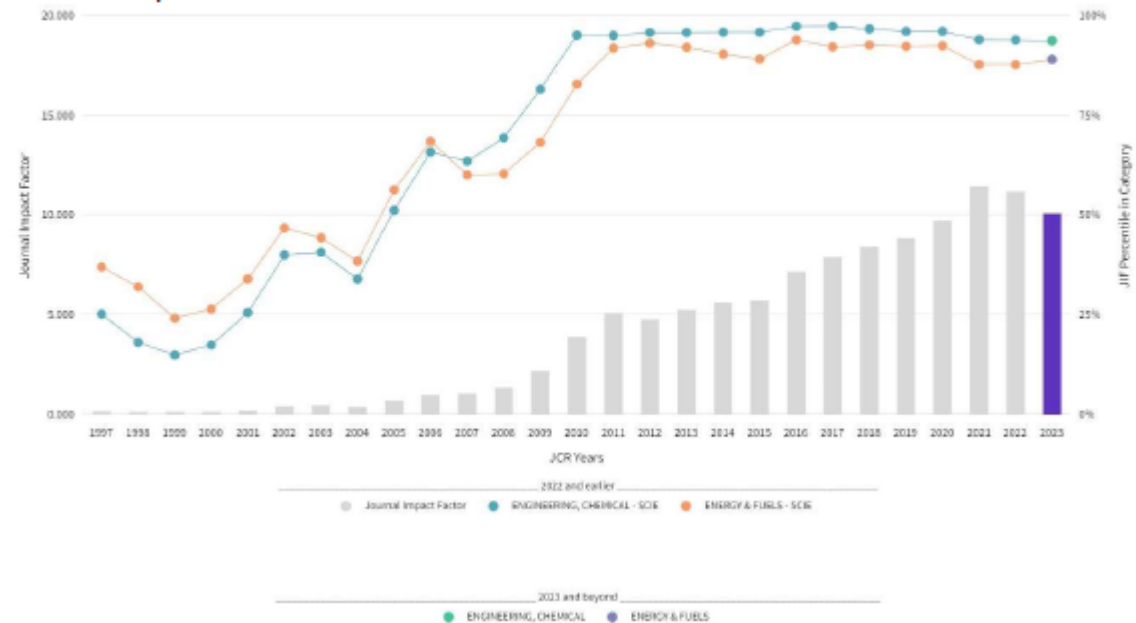
2023 Journal Performance Data for: APPLIED ENERGY

ISSN	EISSN	
0306-2619	1872-9118	
JCR ABBREVIATION	ISO ABBREVIATION	
APPL ENERG	Appl. Energy	
Journal Information		
EDITION	CATEGORY	
Science Citation Index Expanded (SCIE)	ENGINEERING, CHEMICAL ENERGY & FUELS	
LANGUAGES	REGION	1ST ELECTRONIC JCR YEAR
Multi-Language	ENGLAND	1997
Publisher Information		
PUBLISHER	ADDRESS	PUBLICATION FREQUENCY
ELSEVIER SCI LTD	125 London Wall, London EC2Y 5AS, ENGLAND	24 issues/year

Journal's Performance Journal Impact Factor

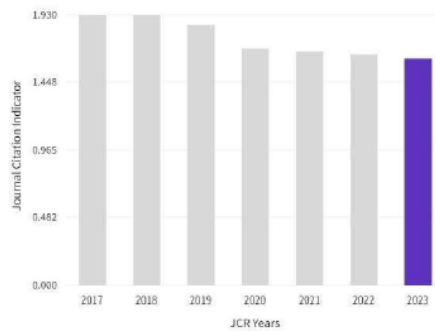
2023 JOURNAL IMPACT FACTOR 10.1
2023 JOURNAL IMPACT FACTOR WITHOUT SELF CITATIONS 9.1

Journal Impact Factor Trend 2023

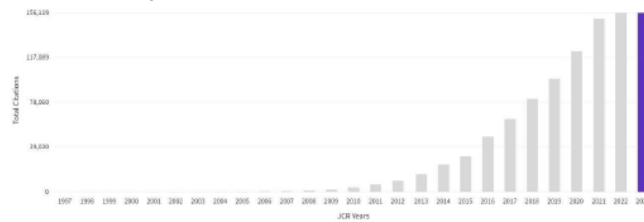


Journal Impact Factor is calculated using the following metrics			
Citations in 2023 to items published in 2021 (17,426) - 2022 (16,686)		34,112	
		=	
Number of citable items in 2021 (1,518) + 2022 (1,854)		3,372	10.1
Journal Impact Factor without self cites is calculated using the following metrics			
Citations in 2023 to items published in 2021 (17,426) + 2022 (16,686) - Self Citations in 2023 to items published in 2021 (1,519) + 2022 (1,815)		34,112 - 3,334	
		=	
Number of citable items in 2021 (1,518) + 2022 (1,854)		3,372	9.1

Journal Citation Indicator (JCI) 1.62



Total Citations 156,119



Rank by Journal Impact factor

CATEGORY

ENERGY & FUELS

19/170

JCR JIF RANK QUART JIF PERCENTILE

YEAR ILE

2023 19/170 Q1 89.1

Rank by JIF before 2023 for

ENERGY & FUELS

EDITION

Science Citation Index

Expanded (SCIE)

JCR JIF RANK QUART JIF PERCENTILE

YEAR ILE

2022 15/119 Q1 87.8

2021 15/119 Q1 87.82

2020 9/114 Q1 92.54

2019 9/112 Q1 92.41

2018 8/103 Q1 92.72

2017 8/97 Q1 92.27

ENGINEERING, CHEMICAL

11/170

JCR JIF RANK QUART JIF PERCENTILE

YEAR ILE

2023 11/170 Q1 93.8

Rank by JIF before 2023 for

ENGINEERING, CHEMICAL

EDITION

Science Citation Index

Expanded (SCIE)

JCR JIF RANK QUART JIF PERCENTILE

YEAR ILE

2022 9/142 Q1 94.0

2021 9/143 Q1 94.06

2020 6/143 Q1 96.15

2019 6/143 Q1 96.15

2018 5/138 Q1 96.74

2017 4/137 Q1 97.45

Rank by Journal Citation Indicator (JCI)

CATEGORY

ENERGY & FUELS

21/173

JCR JCI RANK QUART JCI PERCENTILE

YEAR ILE

2023 21/173 Q1 88.15

2022 20/155 Q1 87.42

2021 14/145 Q1 90.69

2020 11/133 Q1 92.11

2019 11/132 Q1 92.05

2018 9/131 Q1 93.51

2017 8/126 Q1 94.05

CATEGORY

ENGINEERING, CHEMICAL

11/171

JCR JCI RANK QUART JCI PERCENTILE

YEAR ILE

2023 11/171 Q1 93.86

2022 11/160 Q1 93.44

2021 9/160 Q1 94.69

2020 7/157 Q1 95.86

2019 6/156 Q1 96.47

2018 6/155 Q1 96.45

2017 5/154 Q1 97.08

Annex L

Contribución a las publicaciones

Dña. Eva María Llera Sastresa profesora titular del Área de Máquinas y motores térmicos del departamento de Ingeniería Mecánica de la Universidad de Zaragoza:

CERTIFICA:

Que la contribución de D. Alexander García Mariaca ha sido fundamental en las tareas de conceptualización y diseño de ideas, simulaciones, análisis de resultados y redacción de manuscritos para las siguientes publicaciones:

1. García-Mariaca A, Llera Sastresa Eva. (2024). Techno-economic assessment for the practicability of on-board CO₂ capture in ICE vehicles.
García-Mariaca, A. Conceptualization, Data curation, Formal analysis, Investigation, Methodology, Software, Writing – original draft, Writing – review & editing.
Llera-Sastresa, E. Project administration, Conceptualization, Funding acquisition, Investigation, Methodology, Writing – original draft, Writing – review & editing.
2. CO₂ capture feasibility by Temperature Swing Adsorption in heavy-duty engines from an energy perspective.
García-Mariaca, A. Conceptualization, Data curation, Formal analysis, Investigation, Methodology, Software, Writing – original draft, Writing – review & editing.
Llera-Sastresa, E. Conceptualization, Funding acquisition, Investigation, Methodology, Supervision, Writing – original draft, Writing – review & editing.
Moreno, F. Conceptualization, Data curation, Formal analysis, Software, Supervision, Writing – review & editing.
3. Energy and economic analysis feasibility of CO₂ capture on a natural gas internal combustion engine.
García-Mariaca, A. Conceptualization, Data curation, Formal analysis, Investigation, Methodology, Software, Writing – original draft, Writing – review & editing.
Llera-Sastresa, E. Conceptualization, Investigation, Methodology, Supervision, Writing – original draft, Writing – review & editing.
4. Application of ORC to reduce the energy penalty of carbon capture in non-stationary ICE.
García-Mariaca, A. Conceptualization, Methodology, Software, Writing – review & editing
Llera-Sastresa, E. Methodology, Writing – original draft, Supervision, Writing – review & editing
Moreno, F. Supervision, Software, Validation, Writing – review & editing.

5. Dynamic CO₂ Capture in a Natural Gas Engine Used in Road Freight Transport

García-Mariaca, A. Conceptualization, Data curation, Formal analysis, Investigation, Methodology, Software, Writing – original draft, Writing – review & editing.

Llera-Sastresa, E. Conceptualization, Funding acquisition, Investigation, Supervision, Writing – original draft, Writing – review & editing.

6. Review on Carbon Capture in ICE Driven Transport.

García-Mariaca, A. Conceptualization, Methodology, Software, Validation, Formal analysis, Investigation, Data curation, Writing – original draft, Writing – review & editing.

Llera-Sastresa, E. Conceptualization, Methodology, Validation, Formal analysis, Investigation, Sources, Investigation, Supervision, Writing – review & editing, supervision.

Zaragoza 27 de agosto de 2024

Eva María Llera Sastresa